UNIVERSITY OF OKLAHOMA

GRADUATE COLLEGE

LABORATORY AND MODEL PREDICTION OF RUTTING IN ASPHALT CONCRETE

A Dissertation

SUBMITTED TO THE GRADUATE FACULTY

in partial fulfillment of the requirements for the

degree of

DOCTOR OF PHILOSOPHY

By

RAFIQUL ALAM TAREFDER

Norman, Oklahoma

2003

UMI Number: 3104294

UMI Microform 3104294

ProQuest Information and Learning Company
300 North Zeeb Road
P.O. Box 1346
Ann Arbor, MI 48106-1346

LABORATORY AND MODEL PREDICTION OF RUTTING IN
ASPHALT CONCRETE

A Dissertation APPROVED FOR THE
SCHOOL OF CIVIL ENGINEERING AND ENVIRONMENTAL SCIENCE

BY

Chair: Md. Musharrafuzzaman 10/31/2003
Dr. Musharraf Zaman

Member: K.K. M
Dr. Kanthasamy Muraleetharan

Member: Gerald A. Miller
Dr. Gerald Miller

Member: Luther White
Dr. Luther White

Member: Thurman E Scott
Dr. Thurman Scott, Jr.

DEDICATION

This dissertation is dedicated to my parents.

ACKNOWLEDGEMENTS

I would like to express my deepest gratitude and appreciation towards my supervisor Dr. Musharraf Zaman, for his relentless support and guidance throughout my Ph.D. program. His guidance and expectations have led me to work harder than I thought I could. Without his active involvement, encouragement, and thoughtful suggestions this work could not have been completed.

I would like to acknowledge and thank Dr. Luther White for the long hours he put into assisting me in much of the modeling work involved. His knowledge and expertise have been a guiding light for me.

Sincere appreciation is also in order for the assistance and cooperation provided by the other members of my dissertation committee, Dr. Gerald Miller, Dr. Kanthasamy Muraleetharan, and Dr. Thurman Scott, Jr.

The Oklahoma Department of Transportation (ODOT) in cooperation with the Federal Highway Administration (FHWA) has provided notable financial support and other services, for which I am also deeply grateful.

My dissertation work would not be in its current stage if it were not for the constant understanding, patience, and encouragements provided by my wife. I am forever grateful towards her.

I am greatly indebted towards my parents, without whose compassion and prayers I would certainly not have come this far.

In addition, I would like to thank the faculty and staff of the School of Civil Engineering, University of Oklahoma, for their invaluable support. Others who are greatly appreciated are my fellow colleagues who worked with me at the Broce lab.

TABLE OF CONTENTS

LIST OF TABLES

LIST OF FIGURES

LIST OF SYMBOLS AND ABBREVIATIONS

LIST OF SYMBOLS

ν	Poisson's Ratio
ξ	Performance Function or Cost Function
λ	Eigenvalue
$\in$	Belongs to
ε_γ	Resilient Strain or Recoverable Strain
$\varphi(.)$	Activation Function
$\sigma(x)$	Standard Deviation of the Feature x
σ_1	Axial Stress Applied to The Specimen
σ_3	Confining Pressure
σ_d	Cyclic Deviatoric Stress
δ	Phase Angle between Load and Deformation Response
Δ_h	Deformation in Horizontal Direction
$\mu(x)$	Mean Value of the Feature x
$^\circ$	Degree
A(q)	Network Architecture, A Initialized with q Parameters
b_j	Bias Applied at Neuron j
df_{err}	Degrees Freedom of Error
df_x	Degrees of Freedom of Factor x

E	Young's Modulus
e	Error (difference between actual and model value)
F	Fisher's Statistic
$f(q)$	Average Performance of a Neural Network of q Parameters
g	Gradient Vector
G^*	Shear Modulus of Binder
G_{mb}	Bulk Specific Gravity of Asphalt Concrete Sample
G_{mm}	Theoretical Maximum Specific Gravity of Asphalt Mixture
G_{sb}	Bulk Specific Gravity of The Aggregate
$h(q)$	Performance of a neural network with q Parameter
h_1	Hidden Layer 1
h_2	Hidden Layer 2
J	Jacobian Matrix
L_{1x}	Level Sum For Factor x at Level 1
L_{2x}	Level Sum For Factor x at Level 2
L_s	Level Sum of Significant Factor, s
M_r	Resilient Modulus
$N(w)$	Network, N Initialized with Synaptic Weights, w
N_d	Design Number of Gyration
n_{h1}	Number of Neurons in Hidden Layer 1
N_{max}	Maximum Number of Gyration
o_i	Neural Network Output
P	Applied Load

P_b	Percentage of Bituminous Binder
P_{ba}	Percentage Absorbed Asphalt
P_w	Probability Statistic of Weight, w
q	Architecture Parameter (Neurons, Layers etc.)
R_v	Viscosity of Asphalt Binder
R^2	Coefficient of Determination
S	Covariance Matrix
SS_x	Sum of Squares of Factor x
t_i	Target Output
T_n	Data Sets Consists of n Input-Output Pairs
V_a	Volume of Air Voids
V_b	Volume of Asphalt
V_{ba}	Volume of Absorbed Asphalt
V_{be}	Volume of Effective Asphalt
V_{err}	Variance of Error
v_j	Sum of Effects of Neurons Connected to j Neuron
V_s	Volume of Aggregate or Stone
V_{sa}	Apparent Volume of Aggregate
V_{se}	Effective Volume of Aggregate
V_x	Variance of Factor, x
w_{jk}	Synaptic Weight from Neuron k to Neuron j
x_i	Input No. I of a Neural Network
y_j	Output of the Neuron j

LIST OF ABBREVIATIONS

APA	Asphalt Pavement Analyzer
ARZ	Above the Restricted Zone
AVC	Asphalt Vibratory Compactor
AVE	Average Relative Error
BRZ	Below the Restricted Zone
DSR	Dynamic Shear Rheometer
FAA	Fine Aggregate Angularity
FF	Fractured Face
HMA	Hot Mix Asphalt
LMA	Levenberg-Marquardt Algorithm
LVDT	Linear Variable Differential Transducer
MSE	Mean Square Error
NN	Neural Network
PG	Performance Grade
RAP	Recycled Asphalt Pavement
RD	Rut Depth
RTFO	Rolling Thin Film Oven
SGC	Superpave Gyratory Compactor
TRZ	Through the Restricted Zone
VFA	Voids Filled with Asphalt
VMA	Voids in Mineral Aggregate

ABSTRACT

Rutting is one of the major distresses of flexible pavement. It is defined as the formation of longitudinal depressions under the wheel paths caused by the progressive movement of materials under traffic loading in the asphalt pavement layer, or in the underlying base, through consolidation or plastic flow. A safeguard is needed to protect asphalt pavements against rutting after opening roadways to traffic. Traditionally, predicting rutting performance of Hot Mix Asphalt (HMA) in the field has been a complicated task. In this study, a simpler method of determining rutting potential of HMA is employed that uses an Asphalt Pavement Analyzer (APA) in the laboratory. In the APA, rutting susceptibility is evaluated by subjecting HMA samples to moving wheel loads and measuring permanent deformation at selected points along the wheel path as a function of the number of loading cycles. The APA can simulate the field conditions (traffic load, temperature, etc.) of flexible pavements in the laboratory. Using the APA, a series of rut tests are performed on HMA mixes and these mixes are ranked based on their rut potentials. Pertinent mix properties (binder content, air voids), aggregate properties (angularity, size), asphalt binder properties (viscosity, grade), loading (wheel loads, hose pressure), and environment (temperature, wet/dry condition) that lead to differential rutting are identified. The factors affecting rutting are ranked based on their type and magnitude. Also, the correlation between resilient modulus and HMA rutting is examined. To this end, a comprehensive rut database containing APA rut values and factors affecting rutting potential of hundreds of HMA mixes is developed. Using this database, a neural network model is developed to predict rutting in HMA. The

proposed neural network represents a mapping associating rutting potential of HMA with rut factors. Preprocessing and principal component analyses are applied to examine the significance of each rut-influencing parameter, and the network is trained using the Levenberg-Marquardt algorithm. Using randomly generated weight factors to initialize the training algorithm, histograms are compiled and outputs are estimated using statistical estimators. An excellent agreement is achieved between test data and simulations based on maximum likelihood estimator. The developed neural network is used to simulate the optimum asphalt content of a Superpave mix. It is expected that this method will be a useful tool for mix design for new pavements, as well as for rehabilitation of existing ones.

CHAPTER 1

INTRODUCTION

1.1 Background

Rutting is defined as the formation of longitudinal depressions under the wheel paths caused by the progressive movement of materials under traffic loading in the asphalt pavement layers (asphalt concrete) or in the underlying base through consolidation or plastic flow. Depending on the magnitude of the traffic load and the relative strength of the pavement layers, rutting can occur in the subgrade, base, or upper hot-mix asphalt layers. Recent studies indicate that the rutting generally occurs in the top 75 to 100 mm (3 to 4 in.) of asphalt pavement (Stuart et al., 2001; Witczak et al., 2000; Monismith et al., 2000, Kandhal et al., 1993; Brown et al., 1992). The present study focuses on the rutting of top 75 to 100 mm (asphalt concrete) of the flexible pavement system.

Asphalt concrete, also known as Hot Mix Asphalt (HMA), combines bituminous binder and aggregate to give a pavement structure that is flexible over a wide range of climatic conditions. Asphalt concrete can be produced from a wide variety of local aggregates. Asphalt concrete is relatively inexpensive and can be constructed rather quickly. Asphalt concrete is the pavement of choice throughout the United States and the whole world (Hall, 2003). Annually, about 500 million tons of asphalt concrete or HMA is laid in the United States at a cost of 20 billion. Ninety-three percent of all paved roads and streets in the United States (about 3.9 million miles) are surfaced with asphalt (Carlson, 2002). The vehicular miles traveled in the country have increased approximately 75% in the past 20 years (PTI, 2002). In the last decade, loads on the nation's highways have increased more than 60% (Brock et al., 1999). In addition to the increased loads, the increased use of radial tires and high tire pressures are leading causes of increased rutting in some asphalt roads.

Rutting is a national problem now. Excessive rutting has been reported in Florida, Georgia, Illinois, Pennsylvania, Tennessee, and Virginia (Christensen, 2001; Barksdale, 1993). Rutting is a prevailing concern in Oklahoma today. Rutting is of concern for at least two reasons: (i) if the surface is impervious, rut traps water causing hydroplaning, which is a potential threat to road vehicles, (ii) with increasing rut depth, steering becomes increasingly difficult and sometimes dangerous. Rutting can significantly reduce both structural and functional performance of a pavement. Sometimes the rutting magnitude may not be alarming for structural performance, but is important from the safety point of view (Roberts et al., 1996). Rutting can provide useful information in selecting rehabilitation methods if it is quantified and categorized (Choubane et al., 1998; Gramling et al., 1991). In case of consolidation (volume of asphalt concrete changes due to contraction of air voids in it) and shear (material flows as the rounded particles slide and roll and flat particles bend) rutting, a thicker overlay can be used to improve serviceability. In case of shear rutting, rehabilitation strategies can involve milling or leveling with a new wearing course, or recycling of the surface course (Cooley et al., 2001; Gramling et al., 1991). For these and other reasons, it is important to predict rutting in asphalt concrete.

Traditionally, prediction of field rutting potential of asphalt concrete has been a complicated task. A safeguard is needed to protect against making substantial investments in asphalt pavement only to discover, after opening to traffic, that pavement will not meet expectations (NCHRP, 2001). It is important to identify practical laboratory test methods to predict HMA rutting. With the evaluation of mix designs from conventional Marshall design to the Superpave (Superior Performing Pavement) design, researchers have sought for a simple and yet reliable testing procedure to assess rutting potential of HMA for more than a decade. Currently, the most common type of laboratory equipment of this nature is a loaded wheel tester (LWT). Several LWTs are currently being used in the United States. They include the Georgia Loaded Wheel Tester (GLWT), Asphalt Pavement Analyzer (APA), Hamburg Wheel Tracking Device (HWTD), LCPC (French) Wheel Tracker, Purdue University Laboratory Wheel Tracking Device (PURWheel), and one-third scale Model Mobile Load Simulator (MMLS3) (Colley et al., 2001). Among these, the APA has received the most attention in recent years (Jackson and Ownby, 1998). In this equipment, rutting susceptibility is evaluated by subjecting HMA samples to moving wheel loads and measuring rutting (permanent deformation) at selected points along the wheel path as a function of the number of loading cycle. In this study, the APA is employed to determine the rutting potential of HMA in the laboratory.

Rutting is influenced mainly by loading, environment and time-dependent material behavior under loading. An element of HMA layer subjected to traffic loading transfers the load from the surface to underlying layers through intergranular contact and resistance to flow of the binder matrix. The stress pattern induced in a three-dimensional pavement structure due to traffic loading is complex. The stresses are transient and change with time as the wheel passes. When the response also depends on the time or rate of loading and temperature, material characterization becomes even more difficult. The properties of the individual components of HMA and how they react with each other affect its behavior. There are occasions when the asphalt binder and aggregate are adequate but the mix fails to exhibit desired performance because of poor compaction, use of incorrect binder content, poor adhesion or some other problems associated with the mixture. The mixture properties alone are not sufficient to ensure satisfactory performance. No rational model to predict rutting has been developed yet that would encompass all field variables. In this study, a neural network model is proposed to predict rutting encompassing most of the rut influencing parameters.

1.2 Hypotheses and Objectives

Hypothesis One

Aggregate gradation, binder's grade, and mix parameters (air voids, binder content) can significantly affect the extent of rutting. Influences of mix temperature, axle load, and tire pressure can be examined meaningfully using an asphalt pavement analyzer. These factors can be investigated in the laboratory.

Objectives

The objectives are to

- Evaluate and analyze aggregate, asphalt, and pertinent mix properties that lead to differential rutting potentials of HMA specimens.
- Conduct a series of the APA rut tests on selected mixes and rank the mixes based on their rutting performance.

- Perform statistical analysis to identify the significant rut influencing parameters.
- Examine the correlation of resilient modulus with the APA rutting.

Hypothesis Two

An appropriate neural network model can be developed to predict rutting by training the model with laboratory data incorporating the rut influencing parameters.

Objectives

The objectives are to

- Design a neural network for rutting potential of HMA.
- Apply the resulting neural networks to predict optimum asphalt content of HMA mixes.

1.3 Dissertation Outline

This dissertation is composed of seven chapters. Chapter 1 provides a brief statement of rutting problems, including specific goals and objectives. Chapter 2 focuses on the experimental aspects of rutting, particularly on evaluation of rutting potential using the APA. A particular emphasis is placed on the repeatability and reproducibility of rut tests. The concept of volumetrics of HMA is introduced there as well. Chapter 3 presents binder's contribution to rut potential of HMA. The mechanical and rheological properties of different binders are correlated with their rutting performance in a mix. A statistical evaluation of parameters that affect rutting is presented in Chapter 4. The details of the statistical procedure to rank a number of rut factors is presented. Chapter 5 describes the correlation of resilient modulus with the APA rutting. Also, the variability and complexity of modulus test is also focused from the pavement design point of view. Chapter 6 presents the use of neural networks for pavement rutting. The design, training and application of neural networks for mapping asphalt design and testing factors of HMA samples to their rutting performance are presented. Finally, in Chapter 7, a summary and conclusion of this study are presented, followed by recommendations.

CHAPTER 2

LABORATORY RUT TESTING

2.1 Introduction

In this chapter, laboratory rut testing equipment, namely the APA, testing procedure, rutting mechanisms, mixture volumetrics, aggregate testing, and sample preparation are introduced. The APA is evaluated primarily to determine if it readily distinguishes between differing properties of HMA. In essence, three controlled mixes are chosen for laboratory rut test. Also, ten different plant produced HMA mixes are tested and ranked based on their rut potentials. Mix properties are correlated with their rutting potential. Also, there needs to be an acceptable repeatability in the APA test results in order to use APA with confidence. Consequently, the repeatability and reproducibility of laboratory rut testing are discussed in this chapter.

2.2 Background

During the past three decades, a wide variety of equipment and procedures have been developed and used to assess rutting characteristics of HMA mixes in the laboratory (Lai, 1996). The adoption of Superpave (Superior Performing Pavement) methods by governmental agencies has attracted worldwide attention to seek for advanced laboratory equipment to examine rutting performance of asphalt concrete. While the HMA industry has moved from Hveem or Marshall to Superpave design, traditional test methods for quantifying HMA performance are found to be inapplicable for Superpave (e.g., Texas gyratory compactor is not applicable to mix having aggregate size of 25.4 mm or 1 in.). Thus, materials engineers have struggled with exactly how to evaluate performance in the practical manner to which they have become accustomed.

As full Superpave implementation nears, the industry has been naturally drawn towards relatively new types of empirical tests to fill the consequential performance evaluation void. A common class of device popular with many practicing engineers is known as the performance test device, which finds its name in the fact that no basic material property can be computed from its results. Typically, this class of test involves the application of scaled-down load events that are applied to small laboratory samples based upon the assumption that field pavements will respond to full-scale traffic loadings in some related manner.

One of the most recent and promising performance tests currently commercially available is the APA. The significant changes in the rut testing procedure occurred when the Pavement Technology Inc. (PTI) started a commercial development of the APA. The APA applies repetitive loadings on laboratory samples through a pressure regulated rubber tube and rut depths are measured as a function of loading cycles. The APA features an automated data acquisition system that obtains all rutting measurements and plots them in a graphical and numeric format.

The APA is a multi-functional loaded wheel tester that can be successfully used for evaluating permanent deformation (rutting), fatigue cracking, and moisture susceptibility of both hot and cold asphalt mixes. Although the APA can be used to conduct fatigue testing and moisture sensitivity analyses, the vast majority of published literature indicates that rutting susceptibility studies are its most popular application

(Brock et al., 1998). Currently, the APA is the most widely used piece of laboratory equipment designed to determine the rutting susceptibility of HMA mixes.

In the development of the APA, numerous studies are conducted to compare results of APA testing to actual field performance. Most of these studies are to relate APA rut depths to actual field rutting (Collins et al., 1995). A joint study by the FHWA evaluated the APA to predict rutting performance on mixtures placed at the full-scale pavement study WesTrack (Williams et al., 1999). Data of 10 test sections from WesTrack shows a strong relationship ($R^2 = 0.91$) between APA and field rutting.

2.3 Asphalt Pavement Analyzer

An APA has three chambers as shown in Figure 2.1(a). These are the top control system, the middle wheel tracking, and the bottom sample holding assembly. The middle wheel-tracking chamber is shown in Figure 2.1(b). The basic component of an APA consists of the following items:

- Wheel Tracking or Loading System: consists of drive, loading, and valve assemblies and three special rubber hoses. The wheel tracking system applies wheel loading on repetitive linear wheel tracking actions that control magnitude and contact pressure on beam and cylindrical samples for rut testing.
- Sampling Holding Assembly: consists of sample tray and molds, holds the asphalt concrete samples directly underneath the rubber hoses to allow the samples to be subjected to the wheel tracking actions during rut testing. The sliding tray design allows the samples to be pulled out from inside the machine,

making it easier to perform rut depth measurements and for installation of the sample.

- Temperature Control System: controls and maintains the temperature of the APA chamber. The test and conditioning chamber temperatures are set at any point between 40.6°C to 64°C (105°F to 147.2°F) within ± 33.8°F (1°C).
- Water Submersion System: consists of water tank, water tray and pneumatic cylinder. This system allows the water to cover the test sample during the submerged-in-water test and automatically drains the water upon completing the test before the sample tray is pulled out.
- Operating Controls: operate the machine and are mounted on the control panel located in the front of the machine. The magnitude of wheel load, hose pressure, temperature, number of cycles, and wet or dry conditions are changed or varied using the controls.
- Sample Temperature Conditioning Shelf: is located inside the lower front doors. It can hold extra beams or cylindrical samples to allow heat soaking.

2.4 APA Rut Testing

The APA has the capability of testing both rectangular and cylindrical specimens. A typical APA rut test uses either a three-beam specimens, each 75 mm x 125 mm x 300 mm (3 in x 5 in x 12 in) or six-cylindrical specimens, each 150 mm diameter x 75 mm height (6 in x 3 in). Laboratory mixed specimens, including those prepared by a gyratory compactor, Marshall samples, or roadway cores can be tested. In testing procedure, the compacted specimens are placed in the molds and preconditioned at testing temperature (typically 64°C for Oklahoma mix) for a minimum of 10 hours. However, the specimens should not be held at this temperature for more than 24 hours prior to testing. Once the chamber temperature is stabilized, the molded specimens are tested in the APA. Typically, the vertical wheel load is kept at 445 N (100 lbs), and the hose pressure at 700 kPa (100 psi). The APA is run for 8000 loading cycles. The rut depth is measured as a function of load cycle. An automated rut-depth measuring system plots the cycles or time with respect to rutting.

2.5 Rut Specimen Compaction

The compaction method used to prepare rut specimens can significantly affect rutting potential of a HMA sample. Recently, Superpave Gyratory Compactor (SGC) and Asphalt Vibratory Compactor (AVC) have received much more attention within the asphalt industry. Both of theses compactors are used in this study.

2.5.1 Superpave Gyratory Compactor

The Superpave gyratory compactor is a laboratory device used in Superpave mix design. The SGC can orient the aggregate particles in a way that is similar to that observed in the field and has the capability to accommodate larger aggregates (up to 50 mm) in the mix (Roberts et al., 1996). A photographic view of the SGC is shown in Figure 2.2. It consists of a rigid reaction frame, loading system, and specimen height measurement system. It compacts asphalt mixture specimens at a constant pressure of 600 kPa. The mixture is compacted by a gyratory kneading action using a compaction angle of 1.25 degrees and operating at 30 rpm. By knowing the mass of the specimen being compacted and the height of the specimen, specimen density can be estimated during the compaction process. This is accomplished by dividing the specimen mass by the specimen volume. To estimate volume, the specimen is assumed at any point to be a smooth-sided cylinder of 150 mm in diameter and measured height. From the laboratory experience, the SGC is found to be very consistent to prepare samples. It is also found that the gyratory compacted samples show equal compaction in the top and the bottom of samples and significantly more compaction in the middle (Tarefder et al., 2003).

2.5.2 Asphalt Vibratory Compactor

A photographic view of the AVC (model no. AVC II) used in this study is shown in Figure 2.3. The AVC, developed by PTI, can be used to prepare beam or cylindrical samples. The AVC compacts asphalt at the same amplitude, same frequency, and same relative weight that are found in the roadway pavement compactors. In AVC, the forward pressure is typically kept at 14.5 psi (100 kPa) and the backpressure at 5.8 psi (40 kPa). The time to compact beam specimens can be varied 25 to 40 seconds. In AVC, compaction is achieved through vibration. Vibratory compaction tends to result in more compaction at top and less compaction at the bottom of samples. This is generally true for both beam and cylindrical samples. In AVC, it is difficult to reach the desired level of compaction (Tarefder et al., 2003).

2.6 Rutting Mechanisms

Permanent deformation is generally considered to be the result of two mechanisms: shear deformation and consolidation (Lekarp et al., 1996). Figure 2.4(a) shows a typical cross section of a conventional flexible pavement. It consists of surface course, base course, and compacted subgrade layer. With repeated loading, rutting may occur at different layers based on the rutting mechanism and layer stiffness.

2.6.1 Deformation

Bending of flat particles, sliding and rolling of rounded grains are considered to be distortion. HMA materials flow laterally due to loss of interlocking of contracting particles, rather than densification (Gramling et al., 1991). This type of rutting is mainly caused when an asphalt mixture with very low shear strength is subjected to repeated heavy loads as shown in Figure 2.4(b). This figure shows that the pavement has very strong base and subgrade. Rutting occur in the surface layer due to plastic deformation of HMA materials. This study focuses on rutting of asphalt HMA mix only.

2.6.2 Consolidation

The change in shape and compressibility of particle assemblies is considered consolidation. Volume changes due to changes in grain arrangements, particle orientation, and generalized contraction of the assembly without modification of the aggregate structure. Rutting caused by densification of asphalt mixtures having high air voids is usually not considered during the initial mix design. Consolidation type of rutting normally occurs in subgrade, subbase, or base below the asphalt layer as shown in Figure 2.4(c). Although stiffer paving materials can partially reduce this type of rutting, it is normally considered more of a structural problem rather than materials problem. Rutting in the base and subgrade are not focused in this study.

2.7 Asphalt Mixture Volumetrics

A hot mix asphalt material comprises three material components:

- Air Voids
- Mineral Aggregate
- Bituminous Binder

In production, the latter two materials are proportioned by mass (weight). It has long been acknowledged that the performance of HMA mixtures is more significantly influenced by the relative volumetric proportions of the three components. The use of the volumetric proportioning of HMA mixtures is called volumetrics. This section does not investigate nor justify the critical design values assigned to any of these, or other, volumetric parameters, but to explain their meanings and interrelationships. The nomenclature used throughout this study is based on the modified Asphalt Institute system adopted by the Superpave system.

2.7.1 Primary Volumetric Parameters

The primary volumetric parameters are those relating directly to the relative volumes of the individual components:

- Air Voids, V_v - the volume of air voids
- Binder Volume, V_b - the volume of the bituminous binder
- Aggregate Volume, V_s - the volume of the mineral aggregate

Due to the phenomenon of absorption, some of the bituminous binder is absorbed into the external pore structure of the aggregate. This leads to the situation wherein a portion of the aggregate and binder share a common space that is, the sum of the individual volumes ($V_b + V_s$) is greater than their combined volume (V_{b+s}). This leads to further sub-division of the primary volumetric parameters as described below:

- Effective Binder Volume, V_{be} - the volume of bituminous binder external to the aggregate particles, i.e., that volume not absorbed into the aggregate.
- Absorbed Binder Volume, V_{ba} - the volume of bituminous binder absorbed into the external pore structure of the aggregate.
- Bulk Aggregate Volume, V_{sb} - the total volume of the aggregate, comprising the "solid" aggregate volume, the volume of the pore structure permeable to water but not to bituminous binder and the volume of the pore structure permeable to the bituminous binder.
- Effective Aggregate Volume, V_{se} - the volume of the aggregate comprising the "solid" aggregate volume and the volume of the pore structure permeable to water but not to bituminous binder.
- Apparent Aggregate Volume, V_{sa} - the volume of the "solid" aggregate, i.e., that volume permeable to neither water nor bituminous binder.

These various volumetric components are conventionally represented by a "phase diagram" shown in Figure 2.5.

2.7.2 Secondary Volumetric Parameters

For many years, three additional volumetric parameters are widely used, and at various times, have formed critical design thresholds (Patrick, 2003). These are the percent air voids (V_a), Voids in the Mineral Aggregate (VMA), and Voids Filled with Asphalt (VFA). These three parameters are described below:

- Percent Air Voids, V_a - the volume of the air voids, V_v, expressed as a percentage of the total volume, V_T of the mixture. With reference to Figure 2.5, the following relationship can be derived: $V_a = V_v/V_T \times 100$.
- Voids in the Mineral Aggregate, VMA - the sum of the air voids, V_v, and the effective binder volume, V_{be}, expressed as a percentage of the total volume of the mixture. This parameter is directly analogous to "porosity" in soil mechanics. Similarly, it can be shown, $VMA = (V_v + V_{be})/V_T \times 100$.
- Voids Filled with Asphalt, VFA - the degree to which the VMA are filled with the bituminous binder, expressed as a percentage. This is directly analogous to the “degree of saturation” in soil mechanics. Similarly, VFA can be derived as: $VFA = V_{be}/(V_v+V_{be}) \times 100$.

In practice, two of these parameters (V_a and VMA) are obtained from measurements of various specific gravities (G_{mb} - the bulk specific gravity of the compacted mixture, G_{mm}, - the maximum theoretical (void-free) specific gravity of the mixture, and G_{sb} - the bulk specific gravity of the blended aggregate) and knowledge of the mass percentage of bituminous binder in the mixture, P_b. The tests methods followed in this study for determination of specific gravities are ASTM D 2726 (AASHTO T 166), AASHTO T 209 (ASTM D 2041), AASHTO T 84, and AASHTO T 85. The secondary volumetric parameters are calculated from the weight-volume relationships as follows:

- For a compacted specimen (SGC or AVC), the bulk specific gravity (G_{mb}) and Rice Specific gravity (G_{mm}) are used to calculate the percent air void:

$$V_a = \left(1 - \frac{G_{mb}}{G_{mm}}\right) \times 100 \qquad (2.1)$$

- Using the bulk specific gravity of the aggregate (G_{sb}), the bulk specific gravity of the compacted specimen (G_{mb}), and the asphalt content (P_b), the VMA is calculated as follows:

$$\mathrm{VMA} = \left(1 - \frac{G_{mb}(1 - P_b)}{G_{sb}}\right) \times 100 \tag{2.2}$$

- The VFA for each specimen is calculated using V_a and VMA as follows:

$$\mathrm{VFA} = \left(\frac{\mathrm{VMA} - V_a}{\mathrm{VMA}}\right) \times 100 \tag{2.3}$$

2.8 Aggregate Testing

Prior to mixing the aggregate with asphalt binder, aggregates are tested for gradation, Los Angeles abrasion values, sand equivalent, durability, fractured faces, fine aggregate angularity, and bulk and effective specific gravities.

Gradation tests are performed for plant produced and control mixes. Gradation is perhaps the most important property of an aggregate. It affects almost all the important properties of a HMA, including stiffness, stability, durability, permeability, workability, fatigue resistance, frictional resistance, and resistance to moisture damage. Therefore, gradation is a primary consideration in asphalt mix design, and the specifications used by most states limit the gradations that can be used in HMA. Figure 2.6 shows the gradation of control mixes, which is a straight line on the 0.45-power-chart. In this figure, a gradation passing Though the Restricted Zone (TRZ) (Figure 2.6) is believed to have high rut potential. Also, gradation passing Above the Restricted Zone (ARZ) is believed to have low VMA and fails to meet Superpave design criteria. Aggregate gradation Passing Below the Restricted zone(BRZ) is most common and widely used for HMA design. Gradation tests are performed using AASHTO T 27.

The Los Angeles (L.A.) abrasion test is frequently used to obtain an indication of desired toughness and abrasion characteristics of aggregate. The test method ASTM C 131 or AASHTO T 96 is a measure of degradation of mineral aggregates. It gives a combination of actions including abrasion or attrition, impact, and grinding for a prescribed number of revolutions in a rotating steel drum containing a specific number of steel spheres. Another method of evaluating aggregate abrasion and durability is Micro-Deval (Appendix I). This test is performed with soaked aggregate under water. This is widely used as an indicator of the relative quality or competency of various sources of aggregate having similar mineral compositions.

The Sand Equivalent Test is performed to determine the relative proportions of plastic fines and dust in a fine aggregate mix. Dust especially, clay adhering to aggregate, prevents good bond between the asphalt binder and aggregate. In this test, the amount of clay is measured (ASTM D 2419 or AASHTO T 176). The sand equivalent is the ratio of the height of sand to the height of clay expressed in percentage.

Aggregate particles with more fractured faces exhibit greater interlock and internal friction, and hence result in greater mechanical stability and resistance to rutting than do the rounded particles. Currently, there is no ASTM or AASHTO standard test procedure for measuring the percentage of fractured faces for an aggregate. In this study, a sample of coarse aggregate (retained on sieve no. 8) is divided into 3 stacks. The particles that had none, one, and two or more fractured faces are counted.

The first stack contained all the particles with zero fractured faces. The second stack contained all particles with one fractured face, and the third stack contains all particles with two or more fractured faces. The percentage by weight of each stack with one or more fractured faces and with two or more fractured faces is then determined (OHD Designation: L 18).

Aggregates are tested for bulk specific gravity, G_{sb} (ASTM C 127 and C 128 or AASHTO T 85 and T 84). The specific gravity of coarse aggregate is useful in making weight-volume conversions (Equation 2.2) and in calculating the VMA and VFA in a compacted mix.

2.9 Mixing, Compacting and Rut Testing

Aggregates are dried at 110 ± 2°C for about 10 to 12 hours and sieved into different sizes (preferably individual sizes) and about 3 percent moisture is added to the materials passing sieve no. 10. Adding of such small amount of water to the fines helps to prevent segregation during mixing. Usually, two or three aggregates of different size are combined and heated to a mixing temperature of 163°C (325°F). Asphalt cement is heated for one hour at the same temperature. The hot asphalt and aggregates are then mixed together. A complete mix design procedure can be found in Appendix II. The mixes are compacted to contain a target air voids of 7.0±1 percent using the SGC and AVC. Rice specific gravities (G_{mm}) of the loose HMA mix samples are measured in accordance with the AASHTO T 209 (ASTM D2041), where as the bulk specific gravity (G_{mb}) of compacted specimen are determined in accordance with the ASTM D 2726 (AASHTO T 166) and the CoreLok^{TM} (OHD L 42) method (Appendix III). The compacted specimens are conditioned for at least 10 hours at testing temperature (i.e., 60°C or 64°C). The conditioned samples are then tested for rutting in the APA.

2.10 Controlled Mix: Test Results

Three mixes (limestone mix ID: 3012-OAPA-99037, gravel mix ID: 3011-OK99-63070, gravel mix ID: 3011-OK99-63071) were selected for rut testing in co-operation with the Oklahoma Department of Transportation (ODOT). Aggregates and asphalt binders were supplied by ODOT. The contractors supplied the source of materials and the proportions used for batching and mixing. Aggregate, mix and specimen tests as discussed above were conducted for each mix. The HMA mix information is given in Table 2.1 to Table 2.3. It can be seen that one of the mixes is limestone and the other two gravel mixes.

Figure 2.7 shows a typical rut versus number of cycle curve. This figure represents rut results of six cylindrical samples of Mix ID 3011-OK99-63071. There are three curves each representing average rut for two samples. A small difference in rut values is observed between the left and the middle samples. However, the rut depth varies by about 1 mm between the left and the right samples. This is most likely due to the difference in air voids. The testing parameters are listed in Table 2.3. Initially, the AVC is used to prepare samples for rut testing. The asphalt content varies from test to test.

From Figure 2.8 (for Mix ID: 3012-OAPA-99037), it can be seen that the rut depths at 64°C are more than the double of the rut depths at 60^{0}C. A small increase in temperature changes the rut performance of the mix drastically. This can be explained from the stiffness and temperature relationship of HMA. Figure 2.9 shows a simplified diagram illustrating the temperature dependence of HMA stiffness at a particular loading (Roberts et at., 1996). At a temperature below 60°C (140°F), stiffness is essentially temperature-independent. In this case, the stiffness approaches the elastic modulus (most asphalt cements exhibit non-Newtonian or viscoelastic flow). At a temperature above 60°C (140°F), the stiffness decreases with an increase in temperature. The slope of the line at temperatures below 60°C (140°F) is very small. Whereas, a sharp change in the slope of the line occurs at temperatures above 60°C (140°F) (Bahia and Anderson, 1995). Therefore, a significant difference in rut performance can be justified when the HMA temperature is increased from 60°C to 64°C.

Figure 2.10 shows the correlation between rut depth and air voids for (Mix ID: 3012-OAPA-99037). Significant trend between rut depth and air voids is not evident. For samples with air voids more than 5%, rut depth generally increases with increase in air voids. In this case, rut occurs due to consolidation. As the air voids of a sample increase, more empty space inside the sample is available for consolidation. For samples with air voids less than 4%, rut depth increases with a decrease of air voids. In this case, rutting occurs due to shear flow. As the air voids decrease, a sample becomes denser and more materials flow due to shearing action (Chen and Lin, 1998).

Figure 2.11 shows air voids, percent asphalt content and rut depth for Mix ID: 3011-OK99-63070. The percent asphalt content is in the design range. Therefore, the rut depth did not vary significantly from one sample to another. The AVC samples show higher rut depths when compared to those of the SGC samples. A total of 20 samples' data are plotted in Figure 2.11.

A total of 26 samples' data (Mix ID: 3011-OK99-63070) are plotted in the form of a bar graph in Figure 2.12 (Mix ID: 3011-OK99-63071). The maximum rut depth at 60°C is about 4.5 mm. The corresponding rut depth at 64°C is about 6 mm. The rut depth for the gravel mix is higher than that for the exploratory mix. Once again, the air void is not in the range of 6-8%. However, this data are useful for developing neural network model.

Figure 2.13 (Mix ID: 3011-OK99-63071) shows the correlation of rut depth with air voids. This plot illustrates that there is no apparent pattern in the APA rut depth data with respect to air voids. The very poor correlation of the data, as evidenced by the nearly flat regression line and extremely low coefficient of determination value (R^2-value) confirms that air voids in this range have very little effect on the observed rut depth in the APA. It is to be noted that a few data points plotted are available at certain percentage asphalt content. Linear regression analysis is performed at a constant percentage asphalt contents.

Figure 2.14 shows the effect of gradation on rut depth for all three mixes. It can be seen that the mix (3011-OK99-63070) whose gradation passes through the restricted zone, showed maximum rut depth. Of the two mixes passing above the maximum density line, the lime stone mix (3012-OAPA-99037) show less rut potential compared to the base gravel mix (3011-OK99-63071). A possible explanation can be the grave mix has 79.1% of aggregate fractured faces, where as the limestone mix has 83% fractured faces (Table 2.1).

2.11 Plant Mix: Test Results

This section deals with the rutting susceptibility of 10 selected HMA mixes. Mix information and rut test results are shown in Tables 2.4 to 2.8. The proportions of the aggregate used in HMA mixes are listed in Table 2.5. Typically, three to four aggregates of different gradations are blended to achieve certain desirable gradation required for HMA mixes. Table 2.5 also shows that Mix 1, Mix 5 and Mix 7 have used 37.5 mm (1½ in.) rocks; therefore, the nominal maximum size is 25.0 mm (1 in.). Mixes were collected in sufficient amounts for rut testing. Each mix is burned to determine the asphalt content using the National Center for Asphalt Technology (NCAT) ignition oven. Aggregate gradation is determined as discussed above. The gradation test results for all mixes are listed in Table 2.6. The binder's Performance Grade (PG), aggregate properties and mix volumetric properties are listed in Table 2.7. An asphalt cement grade of PG 64-22 is used for Mix 1, Mix 2, Mix 3, and Mix 8, while PG 76-28 type asphalt is used for Mix 6. An asphalt cement grade, PG 70-28 is used for the other mixes. The percent of asphalt cement used in the design mix varied from 4.4% to 6.3%.

2.11.1 Plant Mix Ranking

Figure 2.15 is a histogram showing all mixes with increasing rut values for cylindrical samples. Mixes have been labeled E (Excellent), G (Good), F (Fair) and P (Poor) on the basis of rut value in millimeter. Four mixes exhibited rut values below 2 mm (0.079 in.) and are labeled as excellent. Three mixes exhibited rut depth more than 2 mm (0.079 in.) and less than 3 mm (0.118 in.) and are classified as good. Mixes with rut potential of 3 mm to 4 mm (0.118 in. to 0.16 in.) have been characterized as fair. Mix 3 showed a rut depth of more 4 mm (0.16 in.) and is classified as poor. Figure 2.16 is a histogram which ranks the mixes based on beam specimen's rut values. For all cases, beam specimens rutted more than the cylindrical specimens. The ranking criteria for beam samples are fixed by increasing the rut depth criteria for cylindrical samples by 1 mm. Based on this criterion, two mixes are excellent, one is good and others are poor performing mixes of the seven mixes. It can be seen that Mix 3 is poor performing in both cases.

2.11.2 Effect of HMA Type on Rutting

Table 2.8 shows rut depth versus asphalt mix type for the cylindrical samples. Three of the ten mixes used in this study are Type A mixes (with Recycled Asphalt Pavement, RAP), six mixes are Type B insoluble and one is a C insoluble. Type A mixes exhibited a mean rut of about 2.3 mm (0.09 in.) with a standard deviation of 0.45, while the Type B mixes exhibited a mean rut depth of 2.5 mm (0.098 in.) with a standard deviation of 1.1. Type C mix exhibited rut depth of 3.2 mm (0.12 in.). This is because the Type A mixes combine larger aggregates (nominal maximum size of aggregate 19.0 mm) compared to the Type B mixes (nominal maximum size of aggregate 12.5 mm) or the Type C mixes (nominal maximum size of aggregate 9.5 mm). The coarse aggregate provides the shear strength to resist rutting where as the fines are used to fill the voids in coarse aggregates.

2.11.3 Effects of Asphalt Content and Grade on Rutting

It can be seen from Table 2.8 that for Type A mixes, Mix 7 with a percent asphalt content of 4.1 of PG 70-28 had the lowest rut depth, where as Mix 1 with a percent asphalt content of 4.6 of PG 64-22 had the highest rut depth of 2.8 mm. By comparing Mix 7 with Mix 5, it can be seen that the higher asphalt content of Mix 5 had lower rut depth than the lower asphalt content Mix 7. Therefore, the coarse mix, larger nominal maximum size (19.0 mm) is more sensitive to binder's performance grade as well as percent asphalt content. For Type M mix, asphalt content is not a sensitive parameter.

2.11.4 Effect of Materials Passing No. 200 Sieve on Rutting

Table 2.8 shows that the maximum rut depth for mix Type B is 4.3 mm with a minimum of 1.4 mm. The rut depth for type B mixes increases (Mix 3 and Mix 9 show higher ruts compared to other B mixes) as the percent passing no. 200 sieve increased. Mix 2 and Mix 4 had less materials passing no. 200 sieve (4.2 and 4.7 percent, respectively) as compared to Mix 9 and Mix 3 (5.4 and 5.7 percent respectively). Mix 2 and Mix 4 have less rut value compared to Mix 9 and Mix 3. Therefore, the mixes with smaller nominal maximum size (12.5 mm) are more sensitive to materials passing no. 200 sieve.

2.11.5 Effect of Gradation on Rutting

Mix gradations passing BRZ are coarser (i.e., the size of the aggregate particles are bigger) than that of mix gradations passing ARZ. Table 2.8 shows that ARZ mixes have higher rut values compared to the BRZ and TRZ mixes. Again, TRZ mixes have higher rut depths compared to the BRZ. The same is very clear when comparing the Type B insoluble mixes of different gradations. For example, Mix 2 with BRZ had the lowest rut depth (1.4mm) compared to the TRZ and ARZ mixes. Mix 4 with TRZ had the second lowest rut when comparing the rut values of the Type B mixes. It is evident from Table 2.8 that the aggregate gradations passing through the restricted zone are not susceptible to high rutting.

2.12 Repeatability and Reproducibility

An identical result cannot be obtained from the tests performed using the APA under presumably identical circumstances. The differences in results are due to unavoidable random errors or factors inherent in every test procedure. In other words, the factors that influence the outcome of a test cannot be completely controlled. For practical interpretation of test results, this inherent variability must be accounted for. Therefore, an inter-laboratory study is undertaken to determine whether the data collected are adequately consistent and verify data precision. The primary factor of concern is the sample preparation at a target air voids. Other factors such as temperature, wheel load, and tire pressure could be controlled by proper calibration.

A measure of the greatest difference between two test results is considered acceptable when properly conducted repetitive determination is made on the same material by a competent operator. This is defined as repeatability or within laboratory precision (ASTM 670). It is the square root of the pooled average of within laboratory variances. Reproducibility is a measure of the greatest difference between two tests. The tests are usually conducted by two different operators in different laboratories on portions of a material that are identical, or as nearly identical as possible. Repeatability would be considered acceptable when the difference in test results is negligible. The reproducibility is the square root of the pooled average of between laboratory variances. The fundamental statistics underlying repeatability and reproducibility is the standard deviation (one sigma limit, 1s or difference two-sigma limit, d2s) of the population of measurements. In some cases, it is appropriate to use the coefficient of variation in place of the standard deviation as the fundamental statistic. The results of two properly conducted tests from two different laboratories on samples of same material should not change the value obtained from multiplying 1s or d2s by 2.828 (ASTM C 670).

An outlier can be defined as discarding individual test results that appear to differ by suspiciously large amounts from the others. However, discarding of suspicious test results should be avoided unless there is a clear physical evidence to consider the result faulty. Sometimes if a test really went wrong, it is better to discard the results and repeat the test. Tests should not be repeated, however, just because the results do not look good. A consistency statistics generated through the method may assist in the detection of outlying data (ASTM E691). For a single APA rut test, there are 3 sets of rut results from six samples. An outlier is imposed to these 3 sets according to OHD L-43 method. If the difference between any set and average of the set divided by the standard deviation of that set exceeds 1.155, the result of that particular set is rejected.

2.12.1 Experimental Program and Testing

A limestone aggregate (T. J. Campbell Co. materials) is used for the variability analysis. Aggregate batching is performed at the University of Oklahoma (OU) Broce laboratory.

The optimum asphalt content of 5.1% is found from the mix design information. Binder mixing is performed in both the OU laboratory as well as the ODOT laboratory. It is decided not to perform batching in both laboratories in order to keep the number of variables limited. A total of 24 samples are prepared; half of these samples are prepared in the OU laboratory and half of them are prepared in ODOT laboratory. A sample prepared at OU and tested at ODOT is represented by OU-ODOT. Similarly, four combinations of samples are tested, namely, OU-ODOT, OU-OU, ODOT-OU, ODOT-ODOT. A total of 6 samples prepared at OU are tested at ODOT (OU-ODOT). Also, 6 samples prepared at OU are tested at OU (OU-OU). Similarly, half of the samples prepared at ODOT are tested at OU (ODOT-OU) and ODOT (ODOT-ODOT).

2.12.2 Interpretation of Test Results

The test results are plotted in Figure 2.17(a)-2.17(d). From Figure 2.17(a), (OU-OU) sample with air voids of 6.7% shows a rut depth slightly higher and lower than that of samples with 6.9% air voids. Again, in Figure 2.17 (c), (ODOT-ODOT) samples with air void of 7.5 % showed higher rut depth compared to that of samples with air voids of 6.9% and 7.4%. Clearly, the trend of rut depth with air voids cannot be established from these results. Therefore, an outlier approach is employed to throw a sample test result if it deviates significantly from the average of three curves as in each of figures. An outlier calculation is explained in Table 2.9. The critical value for student test (t-statistic) is taken to be 1.155. If the calculated t-statistic (or t-calculated) value is greater or equal to this value (1.155), then one chance in one hundred the value is from the same population (OHD L-43, 2001). According to this procedure, no data set is rejected as an outlier. Therefore, all the data are considered to be good.

Table 2.10 shows that the results between and within analysis for the various samples tested. The table shows the average and standard deviation for each combination tested. It is evident that the results of samples prepared at OU and tested at ODOT (combination, OU-ODOT) differ radically when compared to the other combinations. The combination OU-ODOT had 10 times the second highest variance. Therefore, the data obtained from this combination is excluded.

Table 2.10 also shows one sigma limit (1s) or coefficient of variation, which is an indication of variability. The value of repeatability (1s%) within laboratory ranges from 2.6 to 5.5. Therefore, results of two properly conducted tests by the same operator on the same material should not differ by more than 7% to 15% (second to last column in Table 7.2). The multi-laboratory coefficient of variation had been found to be 15% to 45%. The results of two different laboratories differ from each other by more than 45% of the average.

Based on the above interpretation, it evident that the actual variability of rut values is due to the variability in air voids. Results found from the APA testing are consistent if the specimens are compacted to uniform air voids. Essentially, there is no significant difference in final rut depths obtained from the OU and the ODOT laboratory. Therefore, the test results can be considered repeatable and reproducible.

2.13 Total Data

A total of 744 data sets have been reported in this study (Appendix IV). Each data set represents an average of two HMA specimens rut values. For each data set (each row), the HMA mix design identification number (mix ID), type of HMA, the name of the highway where the HMA used, the average daily traffic capacity (in million) of the highway, aggregate gradation, binder properties, mix properties, testing temperature, wheel load, hose pressure and rut depths at different cycles are listed in Appendix IV. A correlation of rutting with binder's PG, air voids, and asphalt content, and materials passing 19.0 mm sieve are plotted in Figures 2.18 to 2.21. Overall, the modified binders (PG 70-28 and PG 76-28) have low rut potential compared to those of unmodified binder (PG 64-22) as shown in Figure 2.18. However, the correlations of rutting with air voids, asphalt content, and gradation are poor. This is an interpretation of data from the linear regression results. Consequently, detail investigations of the factors that affect rutting are performed in the subsequent chapters.

Table 2.1 Selected Mix Information

Selected Mix Design No.	3012-OAPA -99037	3011-OK99 -63070	3011-OK99 -63071
Asphalt Concrete	B Insoluble	A	A
Project Number	NHY-8N (005)-10088(13)	NHY-8N (005)-10088(13)	NHY-8N (005) -10088(13)
Highway	US54	US54	US54
Avg. Daily Traffic	3M+	3M+	3M+
Contractor	Duit Const.	Duit Const.	Duit Const.
<u>Blended Materials</u>		% Used	
1-1/2" Rock	00	15	15
3/4" Chips	25	20	30
3/8" Chips	30	00	00
Crushed Gravel	00	38	20
Screenings	30	27	35
Sand	15	00	00
<u>Asphalt Information</u>			
Asphalt Type	PG 70-28	PG 64-22	PG 64-22
Asphalt Content	5.0 - 6.0	4.5 - 5.5	4.3 - 5.3
Asphalt Source	Royal Trading Tulsa, OK	Total Petroleum Ardmore, OK	Total Petroleum Ardmore, OK
Asphalt Specific Gravity	1.0177	1.0078	1.0078
<u>Aggregate Property</u>			
Sand Equivalent	48	61	46
L.A. Abrasion % Wear	29.5	28.9	28.9
Durability	76	78	78
IOC	0.34	0.42	0.53
Insoluble Residue (Ca)	80	0.0	0.0
Fractured Faces	83	83	79.1
ESG	2.657	2.636	2.649
<u>Mixture Property</u>			
% Compaction	94.5	95.5	95.0
VMA (%)	15	13	13
Retained Strength (%)	85	90	91
Hveem Stability	57	52	55

Note: IOC = Ignition Oven Correction factor, ESG = Effective Specific Gravity, VMA = Voids in the Mineral Aggregate, and PG = Performance Grade.

Table 2.2 Mixing and Testing Temperature

Procedure	Temperature (°F)			Time
	3012-OAPA -99037	3011-OK99 -63070	3011-OK99 -63071	
Oven drying of Aggregate	230	230	230	Over-night
Gradation Test	77	77	77	> 2 hr
Preheating Aggregate	325±10	325±10	325±10	>1.5 hr
Mixing	325±10	325±10	325±10	3 minutes
Short-Term Aging	305±10	290±10	305±10	>2 < 4 hr
Compaction	305±10	290±10	305±10	35 sec
Cooling	77	77	77	>4 hr
Density and G_{mm} Test	77	77	77	0.5 hr
Sample Conditioning	147.2	147.2	147.2	>10 hr
Testing	147.2	147.2	147.2	2.5 hr

Table 2.3 Rut Parameters of Mix: 3012-OAPA-99037

Parameter Name	Parameter value		
Sample Position in the APA	Left	Middle	Right
Asphalt content	5.75	5.75	5.25
Bulk Specific Gravity	2.333	2.364	2.372
Maximum Specific Gravity	2.432	2.432	2.450
% Air Voids	4.1	2.8	3.2
% Material Passing No. 200 Sieve	6	6	6
% Material Passing No. 10 Sieve	40	40	40
Test Temperature (°C)	64	64	64
% Fractured Face	75	75	75
% Natural Sand	15	15	15
Binder Specific Gravity at 23 °C	1.0177	1.0177	1.0177

Note: APA = Asphalt Pavement Analyzer

Table 2.4 Plant Mix Design Information

Mix ID	Project ID	Design ID	County	Highway	AC Type	A.D.T
1	STP-55B(957)AG	3011-56875	Oklahoma	City Street	A Rec	0.3M+
2	CIP-132B(11)IP	3012-OAPA-99048	Hughes	US75	B Ins	0.3M+
3	SAP-151C(58)	3012-OAPA-20095	Muskogee	Lake Road	B ins	0.3M+
4	STP-RES-49B(280)	3012-APAC-99018	Mayes	SH-20	B ins	3M+
5	IMY-40-4(366)138	3011-OAPA-20048	Canadian	I40	A Rec	3M+
6	IMY-40-4(366)138	3012-OAPA-20049	Canadian	I40	B ins	3M+
7	CIP-155N(114)IP	3011-OAPA-20090	Oklahoma	City Street	A Rec	3M+
8	MC-116B(16)Pt.1-3	3013-OAPA-20225	Cimarron	City Street	C Ins	0.3M+
9	CIP-155N(114)IP	3012-OAPA-20095	Oklahoma	City Street	B ins	3M+
10	CIP-175N(11)IP	3012-OAPA-20033	Oklahoma	US183	B ins	3M+

Note: AC= Asphalt Concrete; A.D.T = Average Daily Traffic; Rec= Recycled; Ins= Insoluble, and ID = Identification Number

Table 2.5 Types of Aggregate and Percentage Used

Mix ID	1-1/2" Rock (%)	3/4" Chips (%)	5/8" Chips (%)	5/8" Mill Run (%)	3/8" Screen -ings (%)	1/4" Chips (%)	Shot (%)	Stone Sand (%)	Chat (%)	No.4 Screen -ing (%)	Screen -ings (%)	RAP (%)	Sand (%)
1	22	-	-	-	-	-	20	-	-	-	22	25	11
2	-	-	30	34	-	28	-	-	-	-	-	-	8
3	-	17	35	-	-	-	-	-	-	-	33	-	15
4	-	26	-	-	-	-	-	-	36	-	23	-	15
5	39	-	-	-	13	-	-	15	-	-	-	23	10
6		-	42	-	18	-		25	-	-	-	-	15
7	24	-	-	-	-	-	18	-	-	-	21	25	12
8	-	25	30	-	-	-	-	-	-	-	30	-	15
9	-		28	-	-	-	-	10	-	-	47	-	15
10	-	12	30	-	-	-	-	-	-	26	20	-	12

Note: RAP = Recycled Asphalt Pavement, '-' = No value

Table 2.6 Mix Aggregate Gradations

Mix ID	% Materials Passing Through									
Sieve Sizes	1½ in.	1 in.	¾ in.	½ in.	3/8 in.	No. 4	No.10	No. 40	No.80	No. 200
(mm)	(37.5)	(25.4)	(19.5)	(12.5)	(9.5)	(4.75)	(2.0)	(0.425)	(0.18)	(0.075)
1	100	99	-	84	-	60	35	20	9	4.5
2	-	-	100	98	85	54	30	17	7	4.2
3	-	-	100	90	75	50	37	22	12	5.7
4	-	-	100	95	86	50	32	20	8	4.7
5	100	98	-	76	-	54	40	20	9	4.7
6	-	-	100	99	86	60	45	22	9	4.6
7	100	99	-	82	-	61	36	23	11	4.7
8	-	-	-	100	95	66	44	18	10	5.7
9	-	-	100	99	89	62	44	25	12	5.4
10	-	-	100	89	73	57	40	20	10	5.3

Note: '-' = No value

Table 2.7 HMA Mix Properties

Mix ID	Binder Properties			Aggregate Properties						Mix Properties		
	PG	Source	Sp. Gr.	S.E.	L.A.	Dura-bility	IOC	IR	FF	P_b	VMA	Hveem Stability
1	PG64-22OK	a	1.0100	70	23.5	69	0.22	87.4	100	4.6	13.7	41
2	PG64-22	d	1.0201	70	27.3	83	0.14	87.4	100	4.8	15.4	48
3	PG64-22OK	e	1.0119	56	34.7	58	1.04	90.0	100	5.6	15	49
4	PG70-28OK	c	1.0198	71	23.4	73	0.22	40.4	100	4.9	16	45
5	PG70-28OK	b	1.0100	77	23.2	73	0.10	87.4	100	3.8	13.7	59
6	PG76-28OK	b	1.0232	79	26.4	77	0.23	40.0	100	4.7	15.7	50
7	PG70-28OK	a	1.0100	62	20.7	72	0.22	79.3	100	4.1	14.5	62
8	PG64-22OK	f	0.9943	75	20.0	84	0.3	80.9	100	6.3	15.5	51
9	PG70-28OK	a	1.0128	59	20.9	77	0.78	70.5	100	5.2	17.2	59
10	PG70-28	c	1.0245	68	25.2	84	0.12	63.5	100	4.5	16.2	53

Note: S.E = Sand Equivalent; L.A. =Los Angeles Abrasion, P_b = Percent Asphalt Content; IOC = Ignition Oven Calibration Factor, IR = Insoluble Residue; FF = Fractured Face; VMA = Voids in Mineral Aggregate

Table 2.8 Effect of Asphalt Concrete Type

Mix ID	AC Type	Gradation	Nominal Maximum Size (mm)	% Passing No. 200 Sieve	% Asphalt Content	DAR	Rut Depth (mm)
7	A rec	ARZ	19.0	4.7	4.1	1.15	1.9
5	A rec	ARZ	19.0	4.7	3.8	1.24	2.3
1	A rec	ARZ	19.0	4.5	4.6	0.98	2.8
2	B ins	BRZ	12.5	4.2	4.8	0.88	1.4
4	B ins	TRZ	12.5	4.7	4.9	0.96	1.9
10	B ins	ARZ	12.5	5.3	4.5	1.18	2.0
6	B ins	ARZ	12.5	4.6	4.7	0.98	2.1
9	B ins	ARZ	12.5	5.4	5.2	1.04	3.5
3	B ins	ARZ	12.5	5.7	5.6	1.02	4.3
8	C ins	TRZ	9.5	5.7	6.3	0.90	3.2

Note: rec =Recycled aggregate, ins = insoluble aggregate, DAR = Dust to Asphalt Ratio

Table 2.9 Outlier for Rut Depth Calculation

Sample	Rut (mm)	m-Values	Outlier	Average Rut (mm)
1	8.5033	1.124	8.5033	
2	7.1522	0.791	7.152	7.71
3	7.4755	0.333	7.4755	
Average	7.710			
Stdev	0.705	If m> 1.155 then throw		

Note: stdev = standard deviation; Note: m= (x-average)/stdev; Stdev = Standard Deviation

Table 2.10 Between and Within Analysis for Rut Tests

Within Laboratory	Specimen No			Average	Stdev	Var.	1s% Limit	1s%
	No. 1	No. 2	No. 3					
OU-OU	7.503	7.152	7.475	7.377	0.195	0.038	7.484	2.644
ODOT-ODOT	6.371	5.699	6.074	6.048	0.337	0.113	15.757	5.568
ODOT-OU	7.012	7.265	6.596	6.958	0.338	0.114	13.740	4.855
OU-ODOT	6.162	7.92	5.961	6.681	1.078	1.161	45.650	16.131

Note: OU-OU means sample prepared at OU and tested at OU; OU-ODOT means sample prepared at OU but tested at ODOT; Average = sum of n tests results for a particular combination divided by the specimen number; Var. = means variance, the sum of the squares of n test results for a particular combination minus n times; the square of the average for that combination, divided by one less than the number of replicate test results; 1s% = (Standard Deviation x 100)/Average

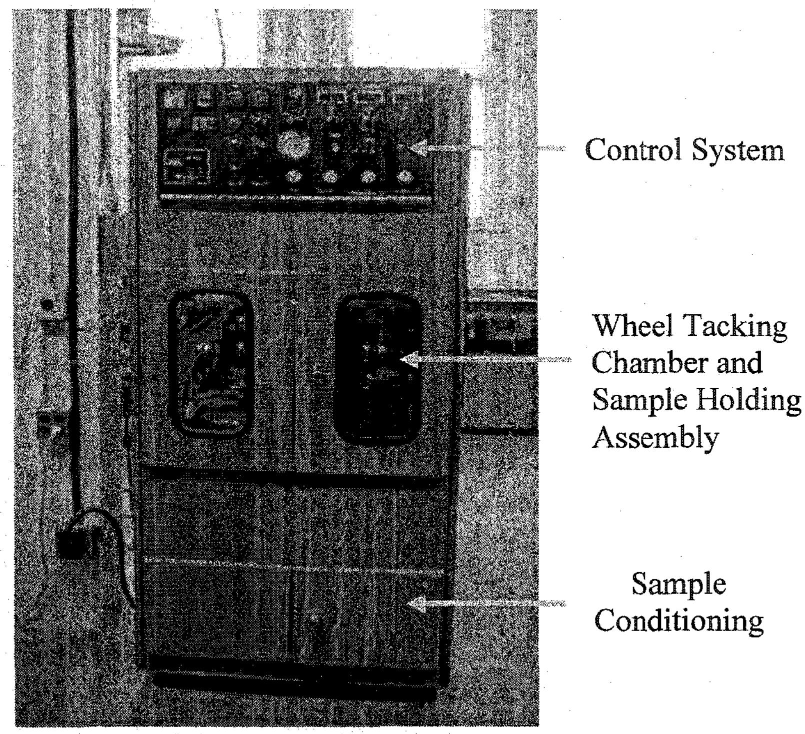

(a) Asphalt Pavement Analyzer (APA)

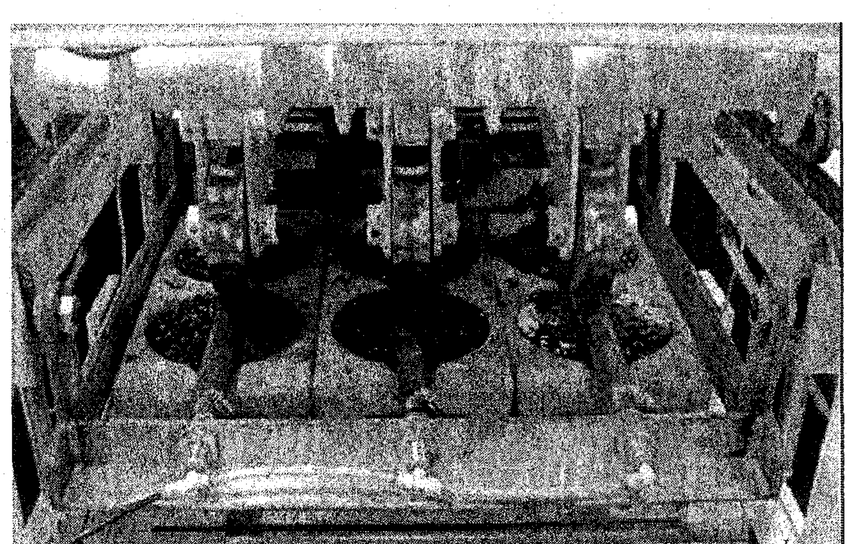

(b) Inside View of APA Chamber

Figure 2.1 Photographic view of Asphalt Pavement Analyzer (APA)

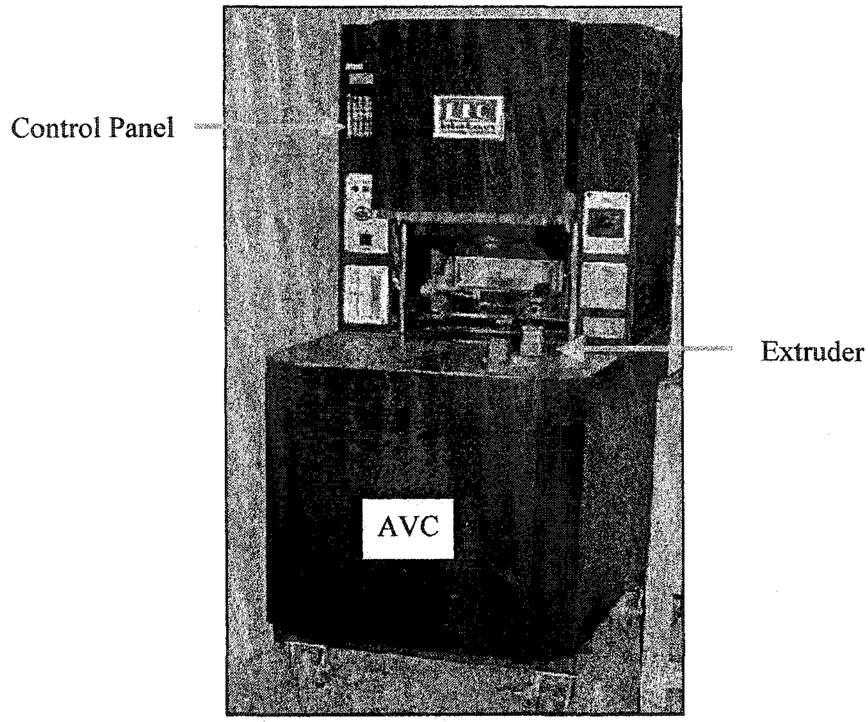

Figure 2.2 Photographic View of Superpave Gyratory Compactor (SGC)

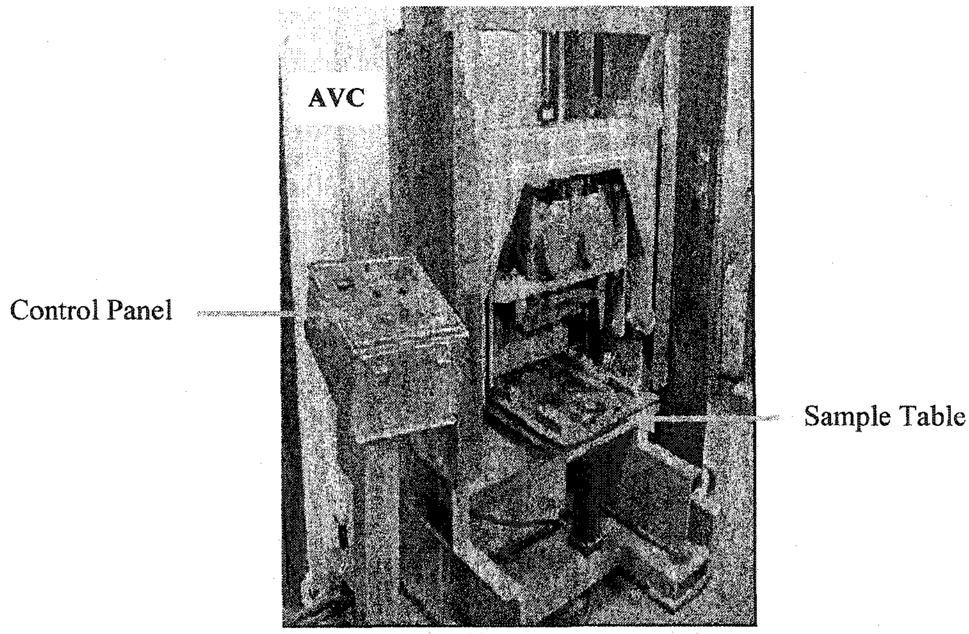

Figure 2.3 Photographic View of Asphalt Vibratory Compactor (AVC)

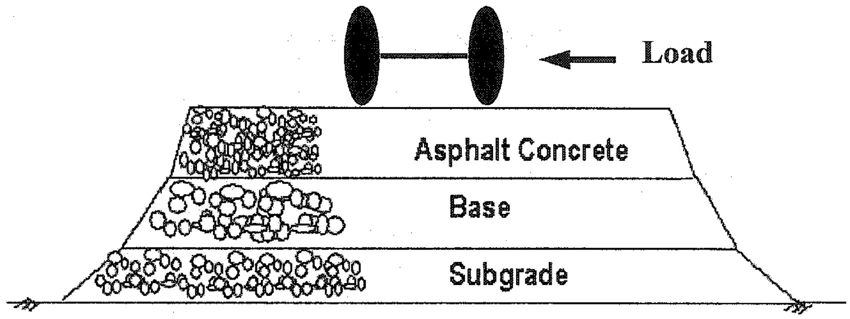

(a) A Typical Pavement Section

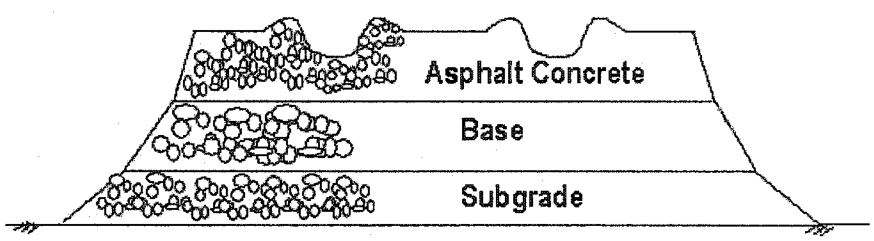

(b) Rutting from a Weak HMA

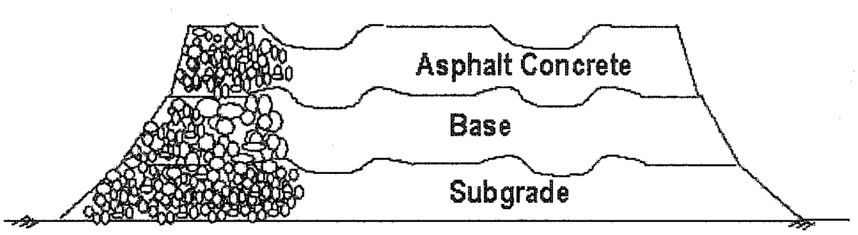

(c) Rutting from a Weak Subgrade

Figure 2.4 Pavement Cross-Section and Rutting

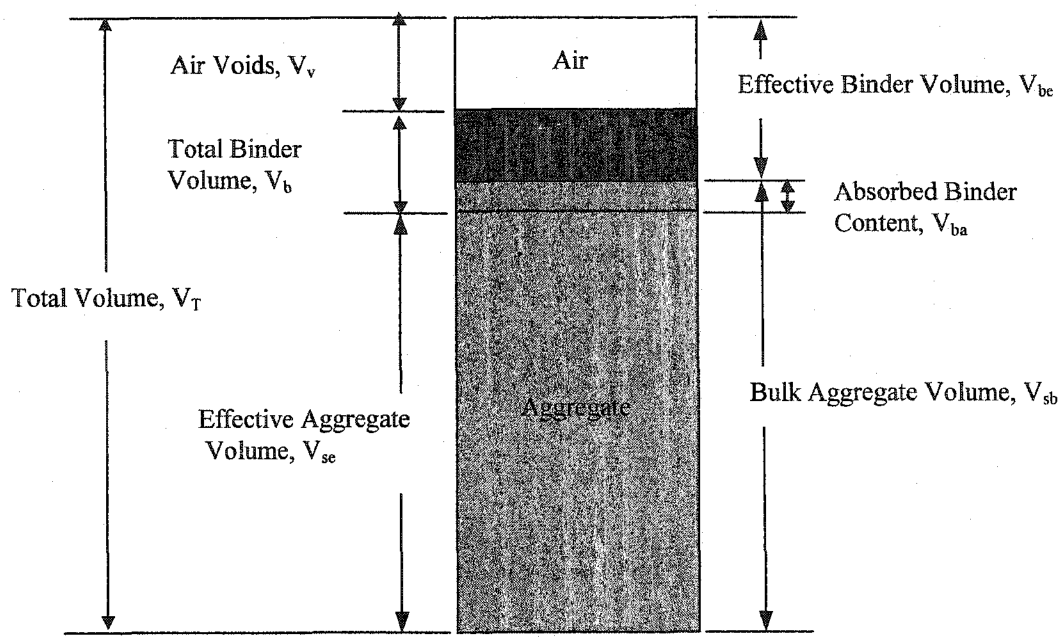

Figure 2.5 Phase Relationships of Hot Mix Asphalt

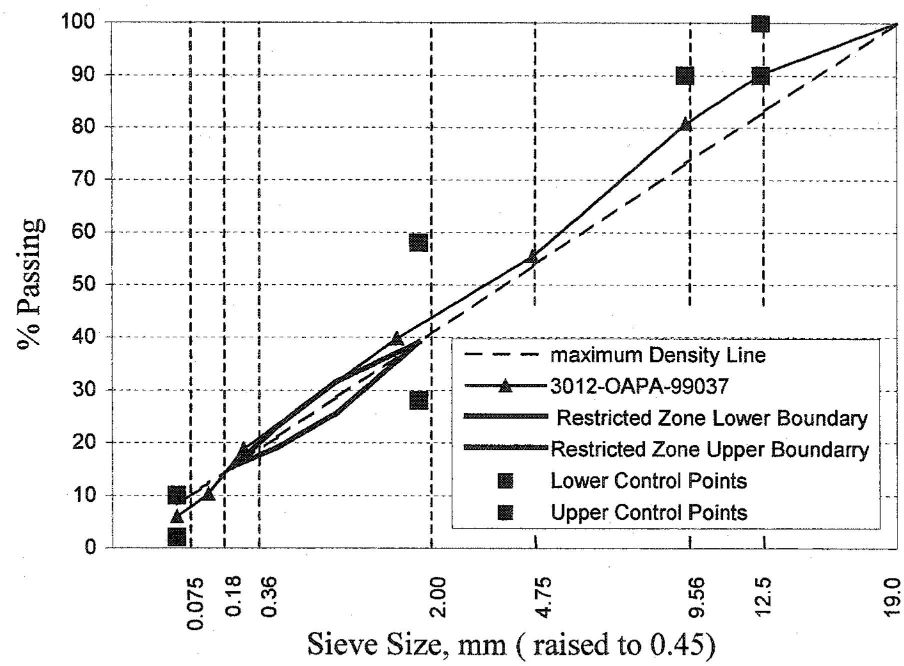

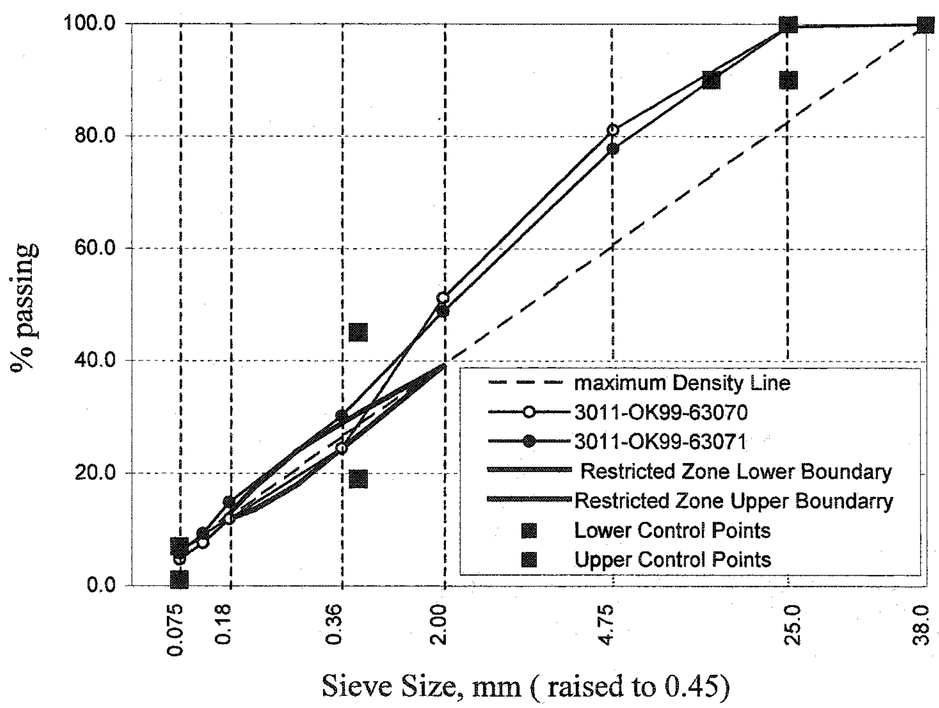

Figure 2.6 Gradation Plot of Controlled Mixes on 0.45-Power Chart

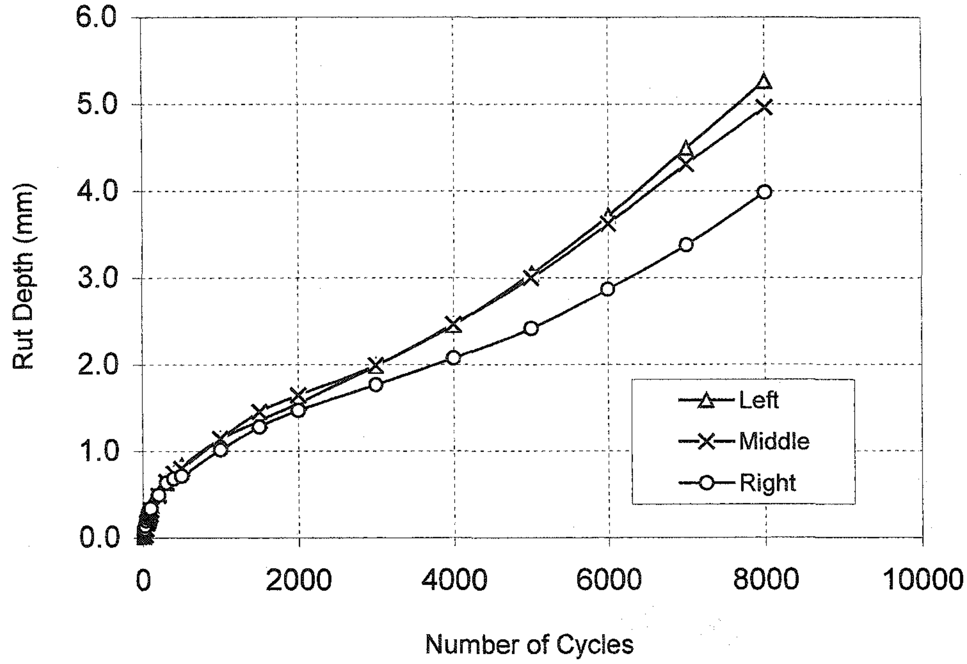

Figure 2.7 Typical Rut Plot of Mix ID: 3011-OK99-99037

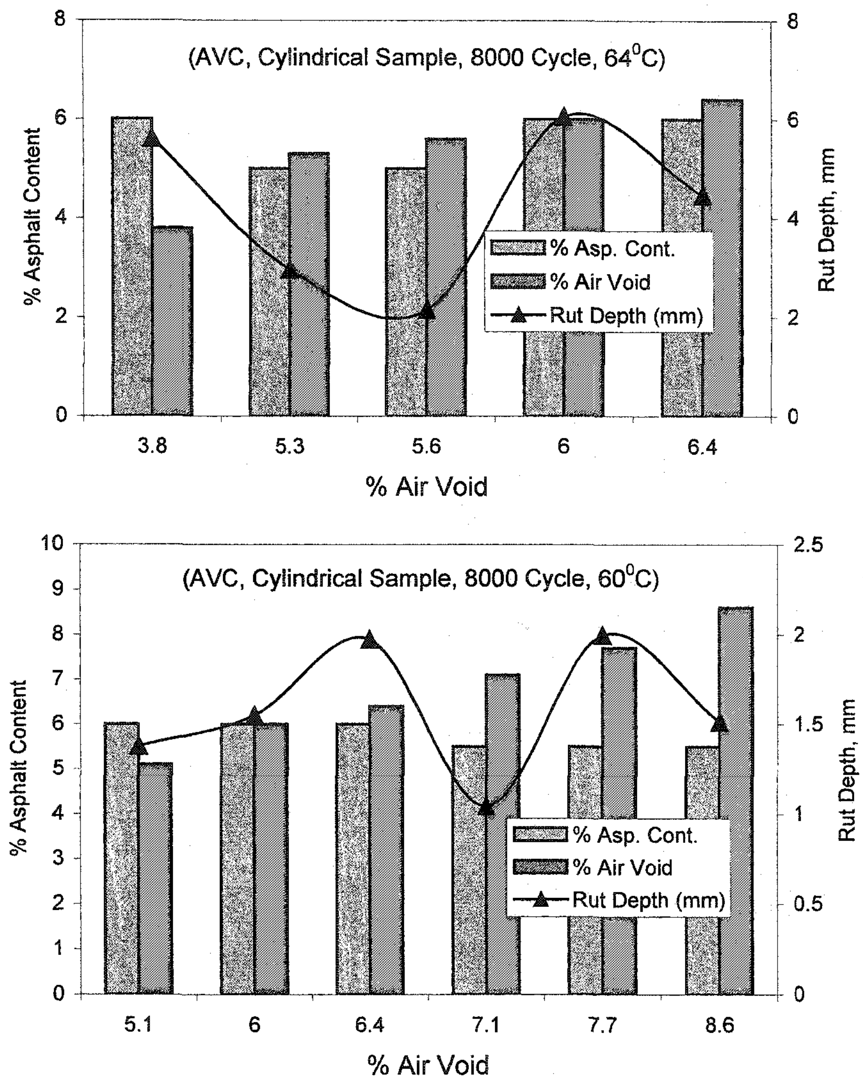

Figure 2.8 Rut Plot of Mix ID: (3012-OAPA-99037)

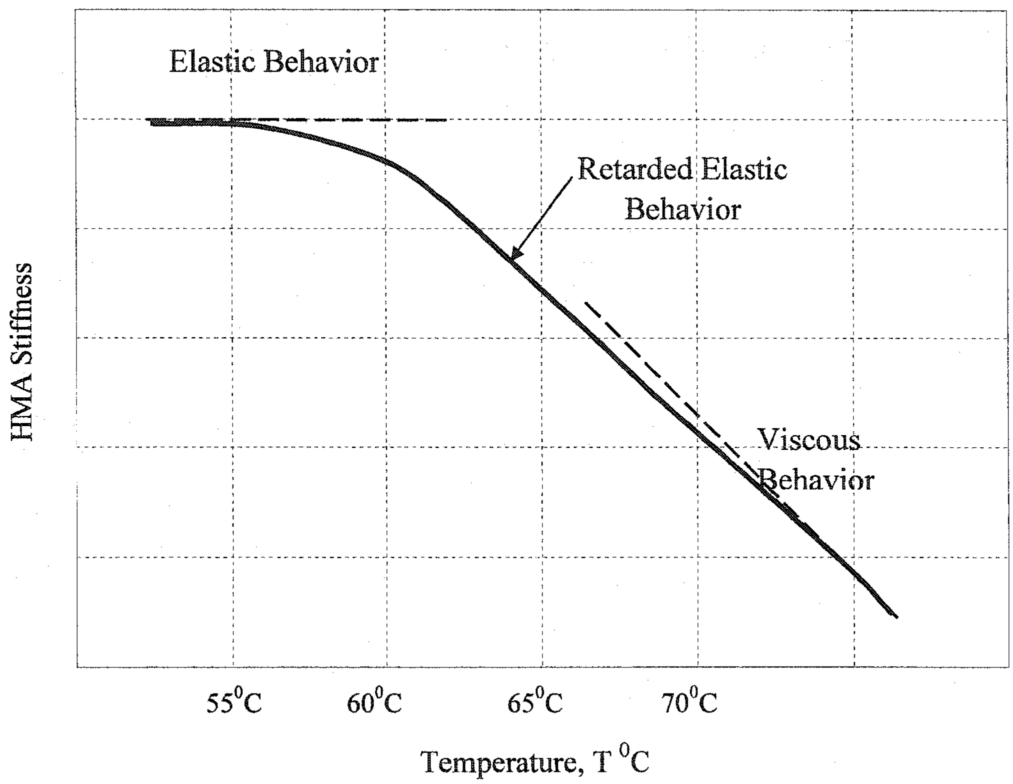

Figure 2.9 Idealized Temperature Dependence of the Stiffness of Asphalt Concrete (Roberts et al., 1996)

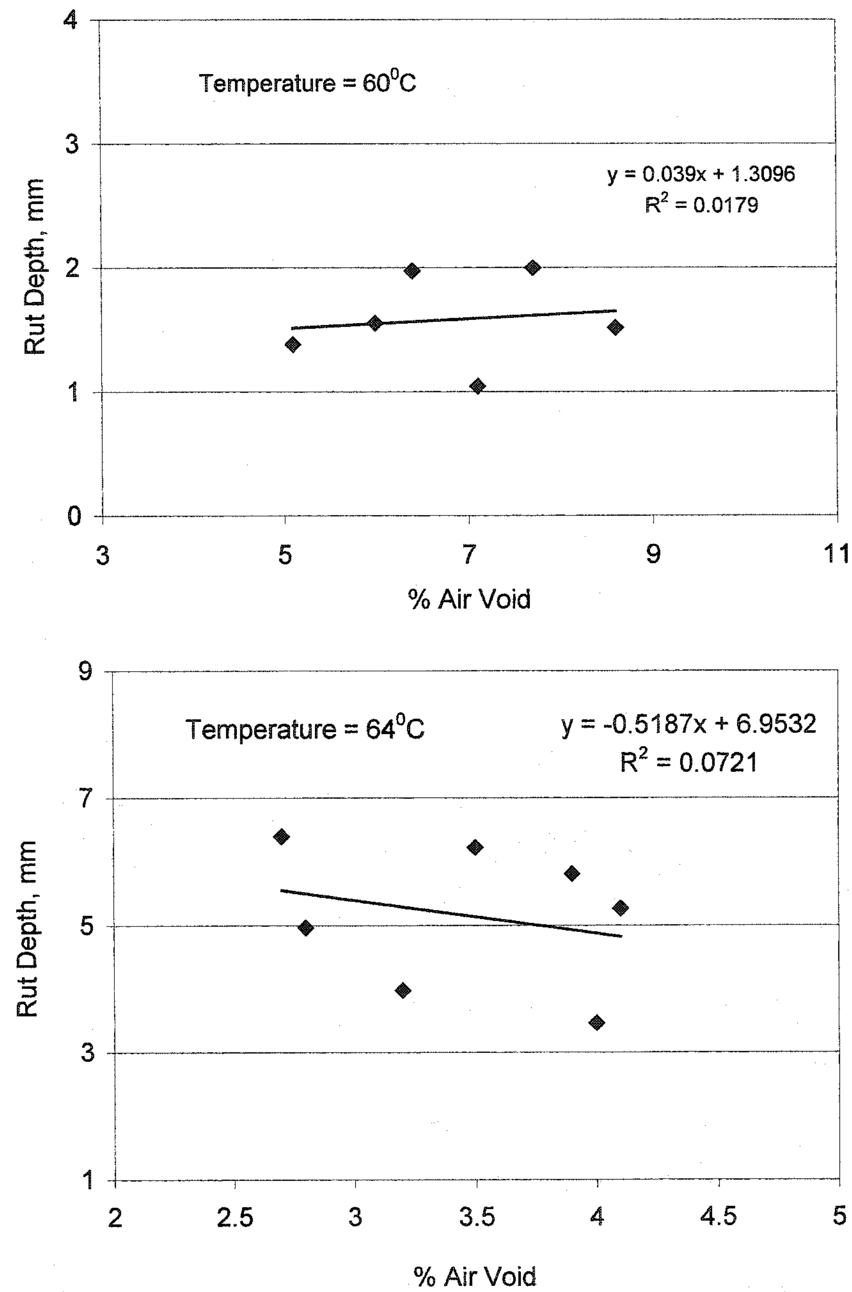

Figure 2.10 Correlation Between Rut Depth and Air Voids (3012-OAPA-99037)

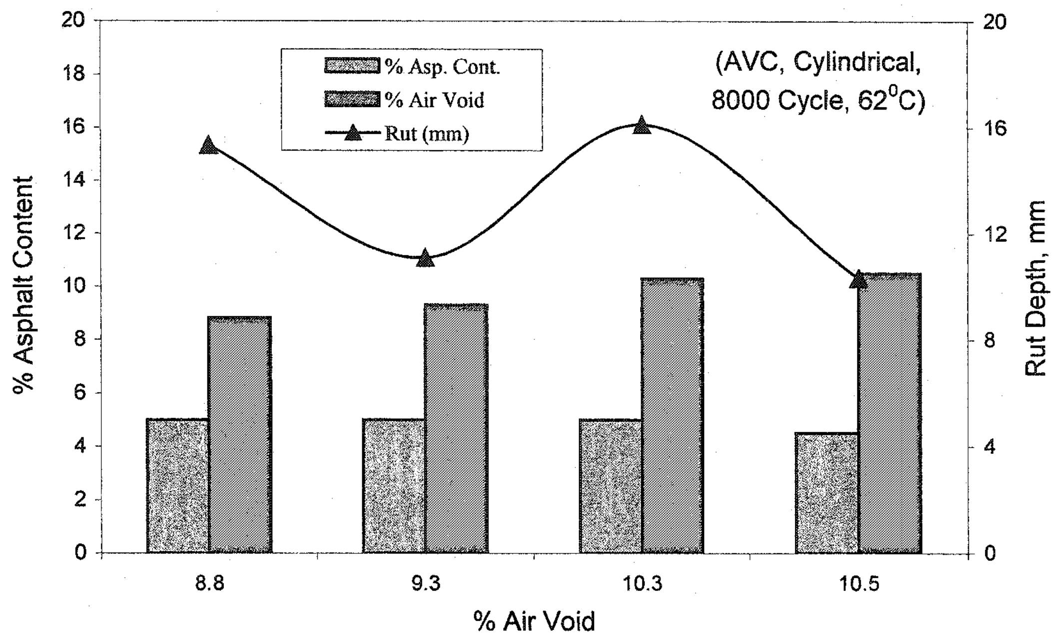

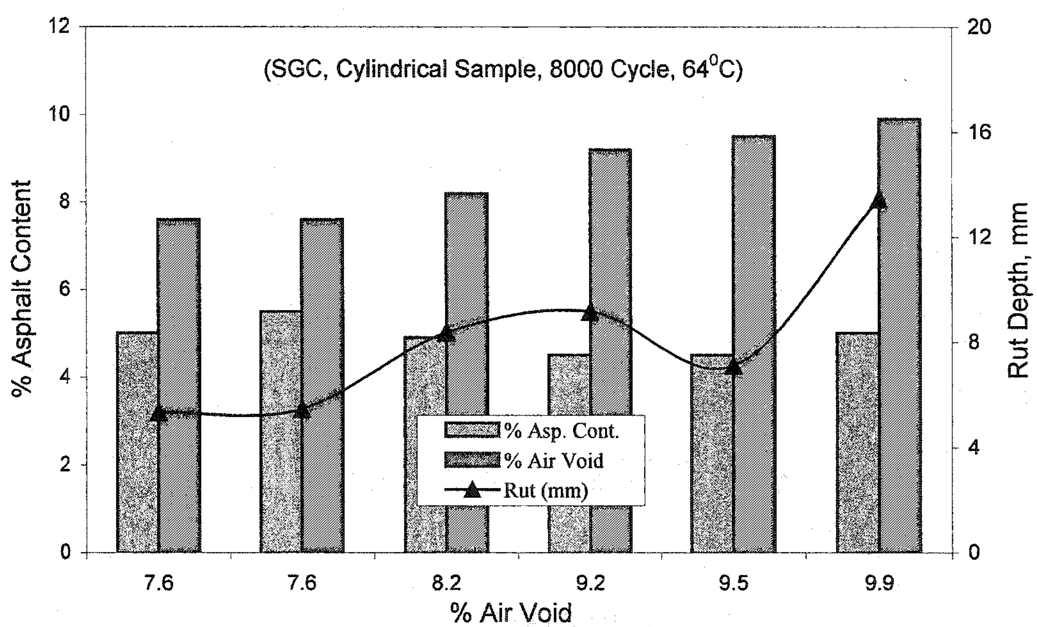

Figure 2.11 Rut Plot of Mix (ID: 3011-OK99- 63070)

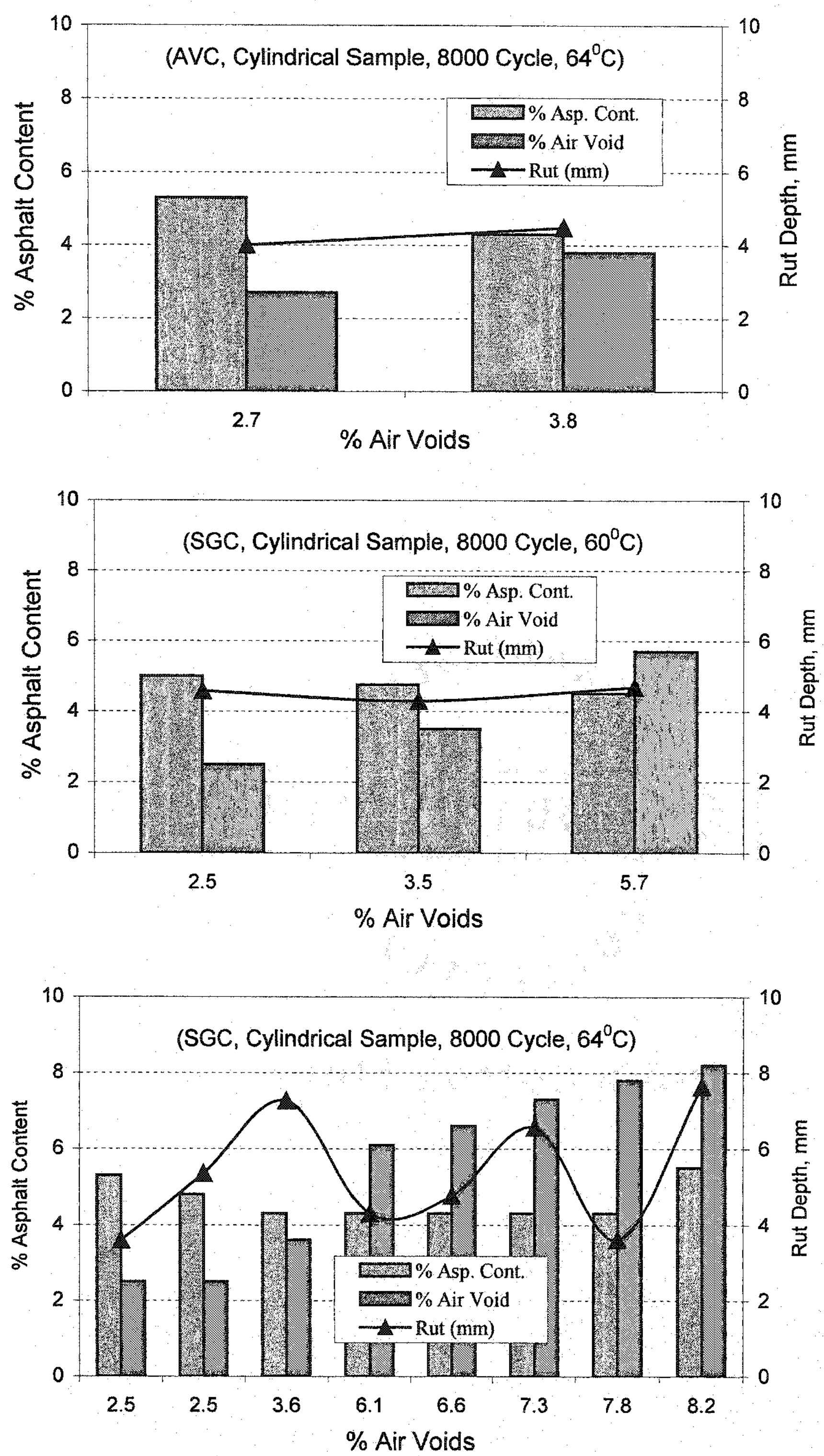

Figure 2.12 Rut plot of Mix (ID: 3011-OK99- 63071)

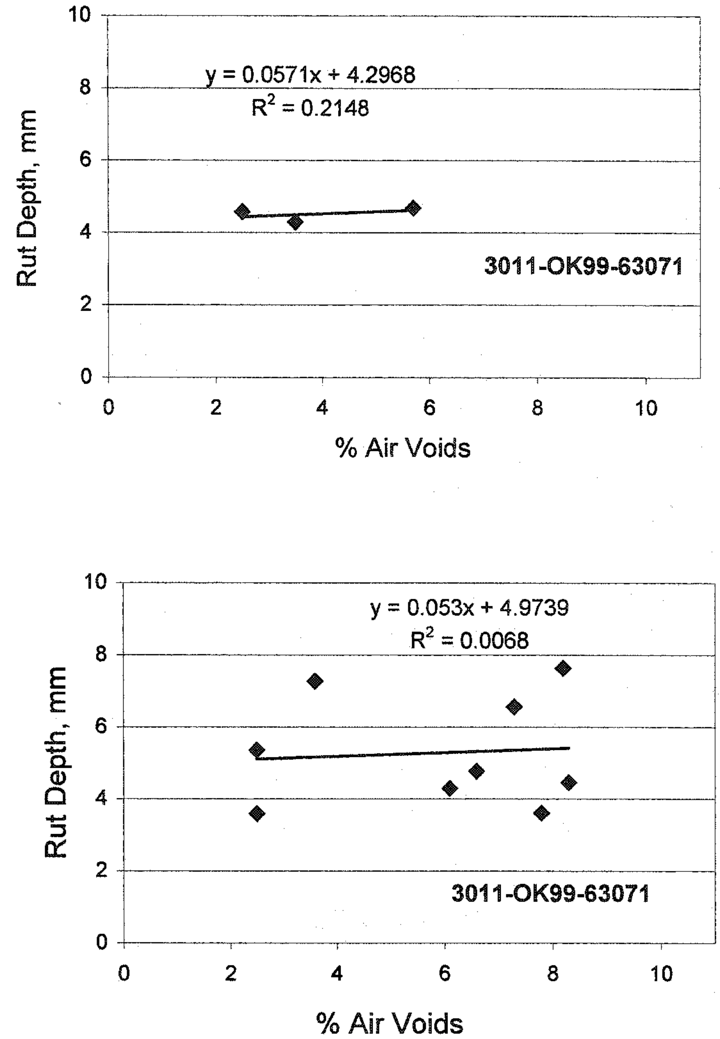

Figure 2.13 Correlation of Rut with Air Voids (Mix ID: 3011-OK99-63071)

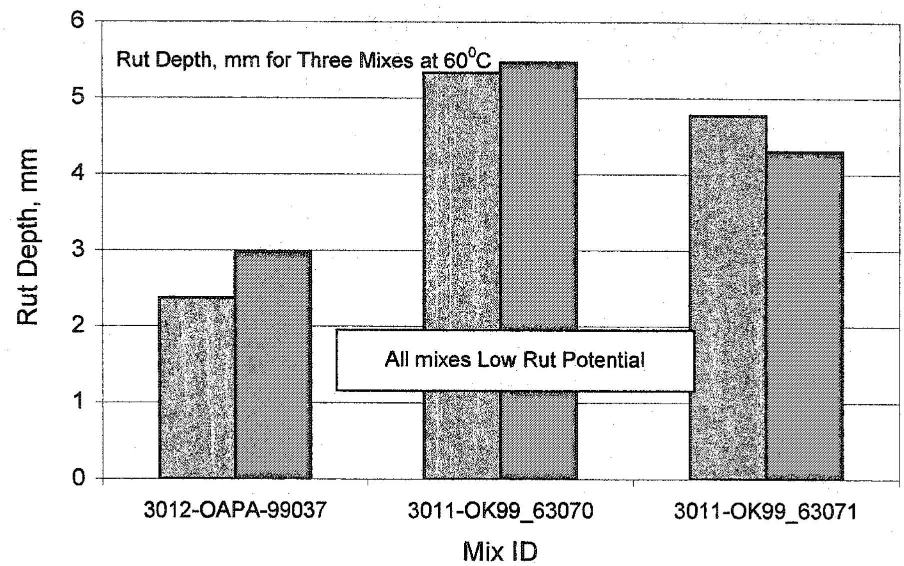

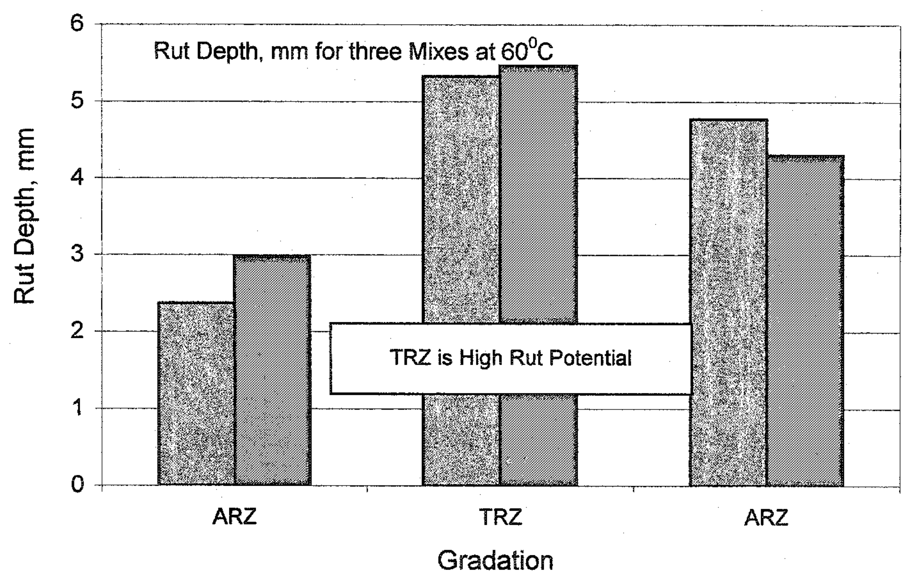

Figure 2.14 Comparison of Rut Potential of Controlled Mixes

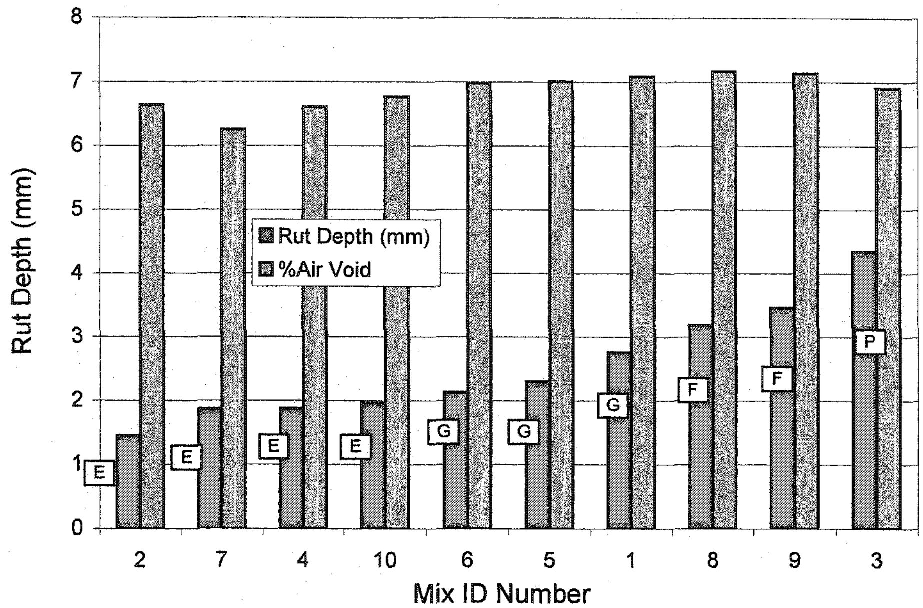

Figure 2.15 Plant Mix Ranking Based on Rutting Potential of Cylindrical Specimen

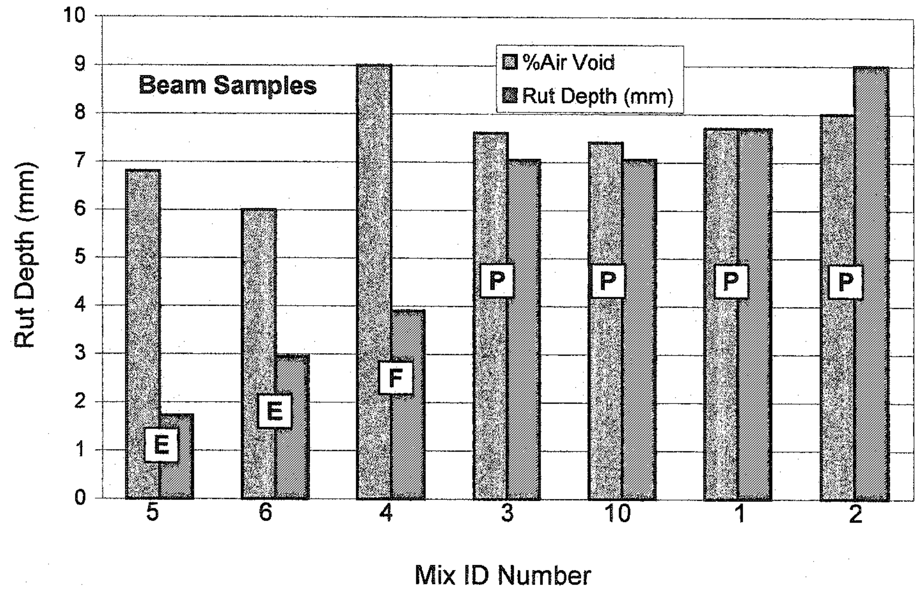

Figure 2.16 Plan Mix Ranking Based on Rutting Potential of Beam Specimen

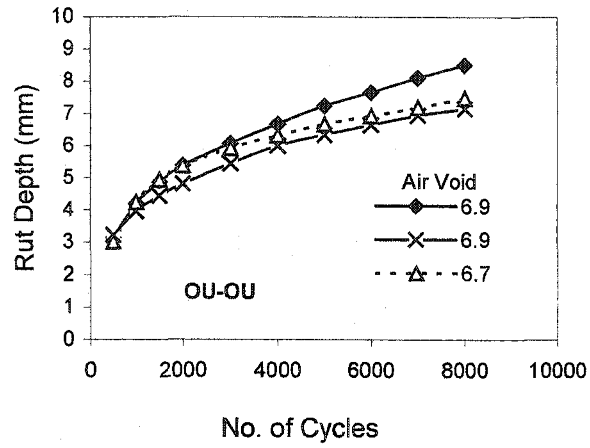

(a) OU-OU

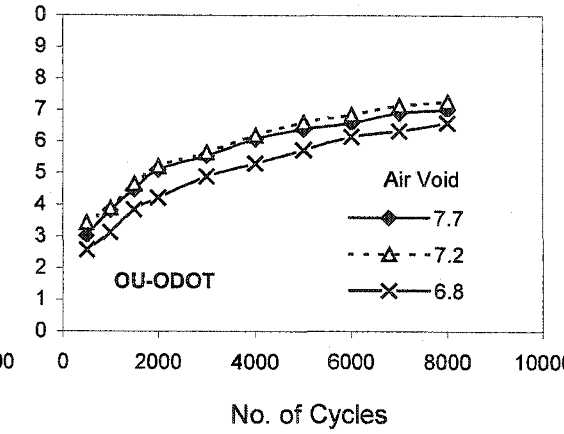

(b) OU-ODOT

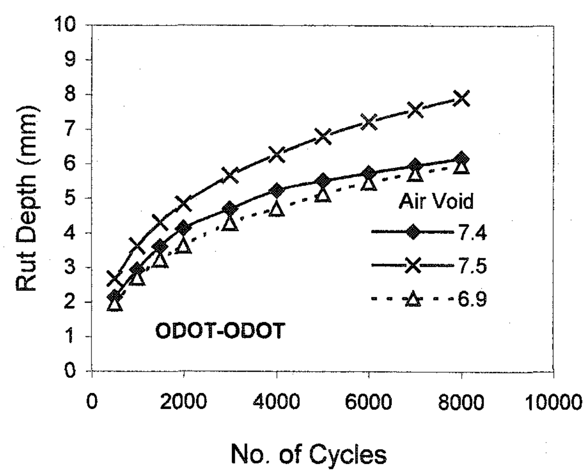

(c) ODOT-ODOT

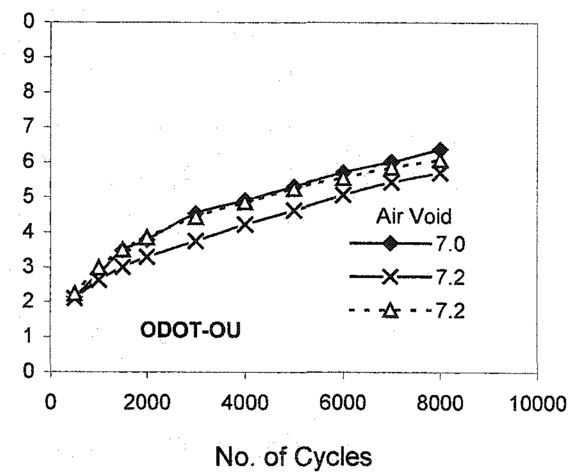

(d) ODOT-OU

Figure 2.17 Rut Depth Versus Number of Cycles

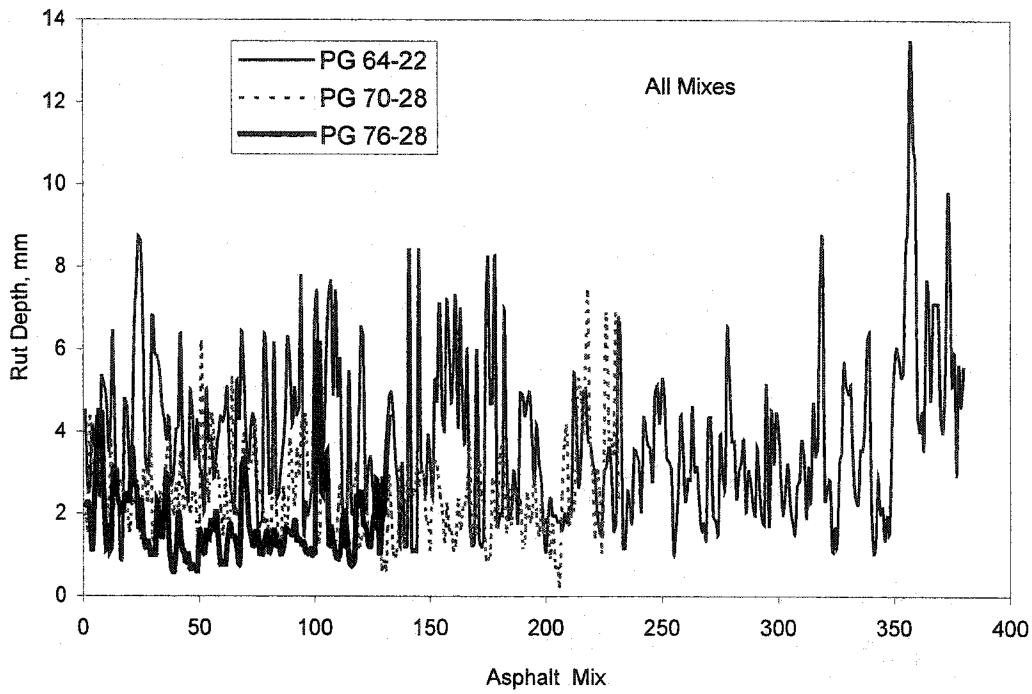

Figure 2.18 Overall Effect of Binder Performance Grade on Rutting

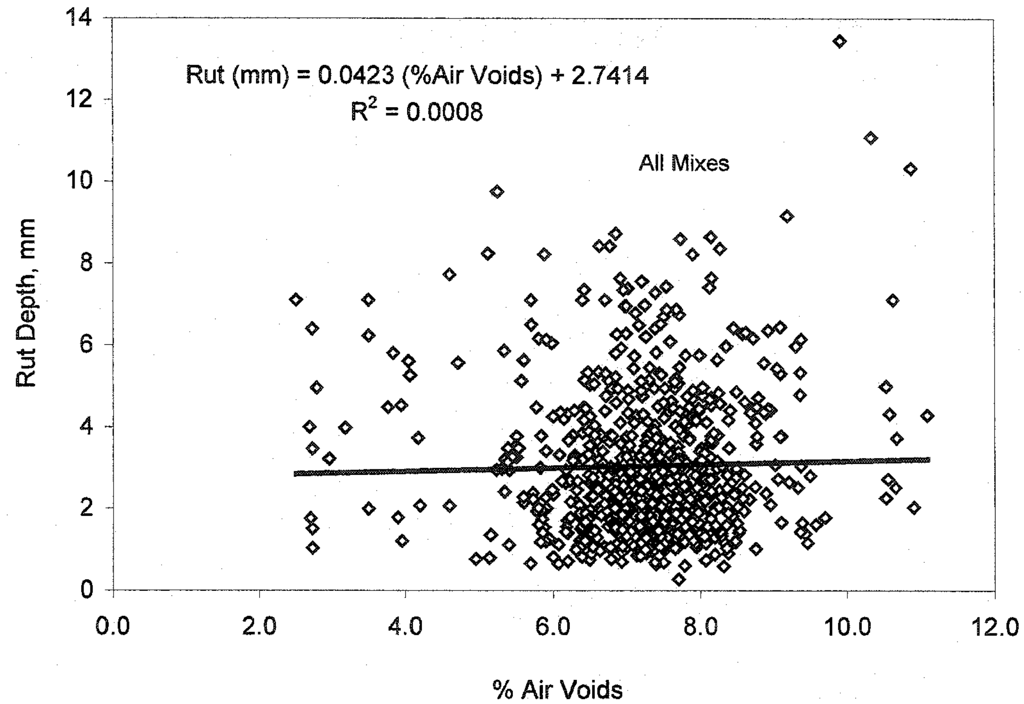

Figure 2.19 Overall Effect of Air Voids on Rutting

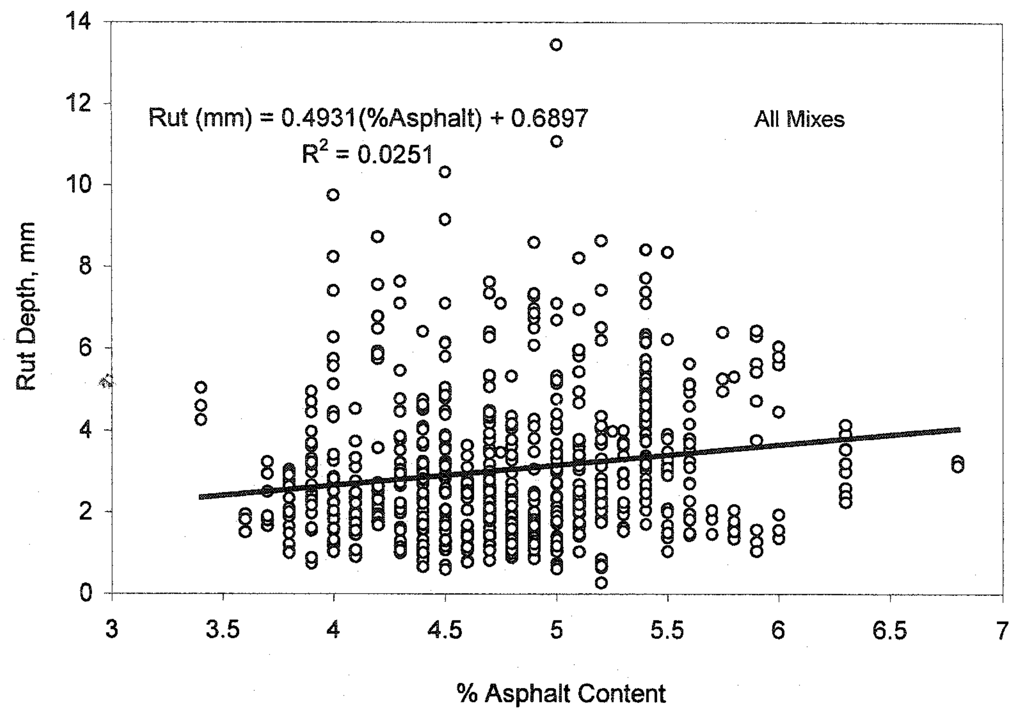

Figure 2.20 Overall Effect of Asphalt Content on Rutting

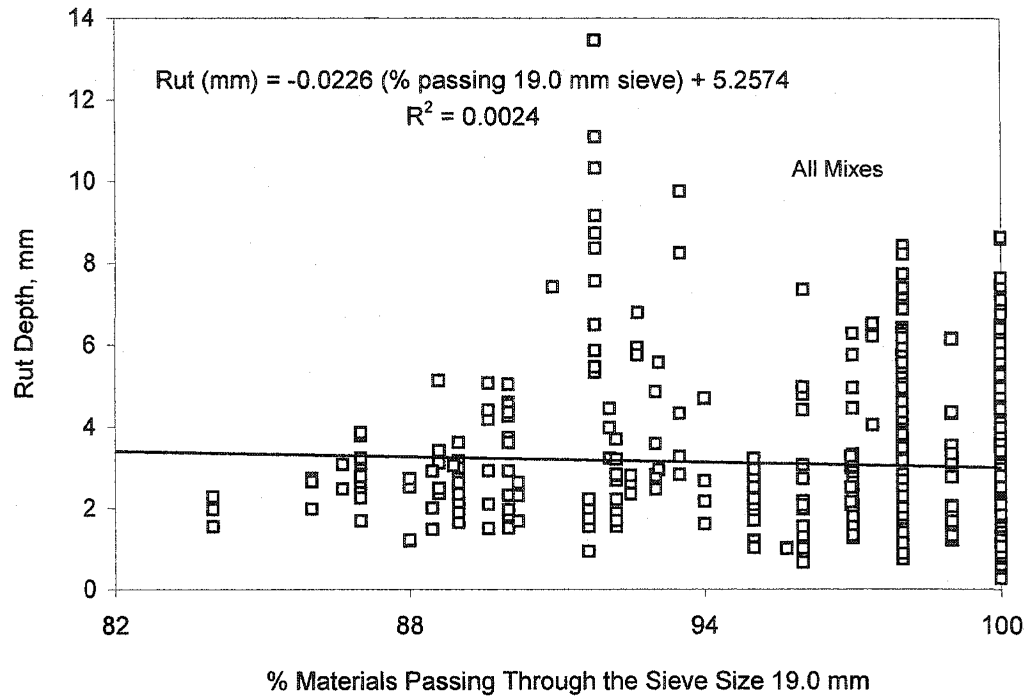

Figure 2.21 Overall Effect of Gradation on Rutting

CHAPTER 3

AN ASSESSMENT OF BINDERS' CONTRIBUTION TO RUTTING SUSCEPTIBILITY

3.1 Introduction

The relationship between rheological and mechanical properties for various binders based on the asphalt mixture's rutting performance is studied. The rutting performance of a mixture is determined from the laboratory test results. The test results are analyzed and interpreted to examine whether binder's Performance Grade (PG) affects rutting. Both modified binders and unmodified binders (base crudes) are examined. Moreover, linear and nonlinear regression models are developed to predict Rut Depth (RD). In particular, the effect of two parameters (binder's viscosity, R_v and rut factor, $G^*/\sin\delta$; where G^* is the shear modulus of binder and δ is the phase difference between applied load and the corresponding shear deformation) to rutting is investigated.

3.2 Background

The concept of creating HMA concrete with increased resistance to permanent deformation or rutting is a major driving force behind much of the asphalt-related research performed under the Strategic Highway Research Program (SHRP). The provisional binder specification AASHTO MP1-98 (better known as the SHRP or the Superpave binder specification) represents a historic and logical steppingstone on the path to a performance-related specification for binders (AASHTO MP1-98, 2000). In the 40's and 50's, the penetration grading system, ASTM D 946 was primarily used for specifying binders (ASTM D 946, 1998). However, the penetration value does not describe pavement distress, as it is not a fundamental property of a binder.

The next evolutionary step is the viscosity grading system, ASTM D 3381 (ASTM D 3381, 1998). The performance of pavements built with viscosity-graded asphalt binders were thought to be controlled by their viscosity-temperature susceptibility (Anderson et al., 1991). However, asphalt cements classified on the basis of viscosity does not adequately reflect the rheology of the binder. Viscosity does not provide a true indication of how asphalt cement performs within a pavement over its yearly temperature range. A binder can be non-Newtonian (and visco-elastic); therefore, it requires further characterization in addition to the viscosity.

In the late 80's and early 90's, a new specification, called Performance-Based Asphalt (PBA), attempted to include regional climatic variations and long-term aging in the field (Reese et al., 1993). The Superpave binder specification adopted many of the concepts in PBA specifications. The most significant advancement in the Superpave Binder (SB) specification is the move from empirical testing to advanced performance-based testing. With Superpave specifications, a binder can be characterized at a controlled rate and temperature to obtain engineering properties of that binder. In the Superpave binder specification, the Dynamic Shear Rheometer (DSR), Bending Beam Rheometer (BBR) and Direct Tension (DT) replaced such tests as the viscosity, penetration and ductility. Nine-binder grade-classifications are used under the asphalt grading system (AASHTO TP5-98, AASHTO TP1-98, AASHTO TP3-00).

The Oklahoma Department of Transportation (ODOT) adopted the PG binder specification in July 1997. The ODOT supplemented the AASHTO MP1 (AASHTO MP1-98, 2000) specifications in 1999 (ODOT, 1999). The new grading system, AASHTO MP1 (AASHTO MP1-98, 2000) more appropriately relates the grade of the asphalt binder to the pavement temperature and traffic loading for a construction project than the previous grading systems. Under a true PG grading system, binders classified the same should have similar performance characteristics. Mixes containing these binders should show similar performance characteristics. PG binders of the same grade, produced from different crudes and manufacturing process and meeting the specification requirements of MP1-98 may show different performance in HMA mixes. If different binders of the same PG grade do not perform similarly, then the binder specification may lose its significance. It should be noted that the PG system is a purchase specification. A real attempt is made by the SHRP researchers to relate the various PG grades to actual performance (Natu et al., 1999). No binder grading system may fully identify the full mixture performance when binder characteristics alone are considered.

Rutting and fatigue failure models are developed during the SHRP research (Asphalt Institute, 2001). These models continue to be refined. The Superpave Shear Test (SST) (AASHTO TP9, 2000) and Indirect Tensile Test (IDT) (AASHTO TP7, 2000) machines are expensive. Only five Superpave centers had these machines in the early 1990's. The cost of these machines has made full use of the SHRP research using the SST and IDT cost and time prohibitive. Full implementation of Superpave, by state and local agencies, using these machines may be delayed.

Superpave testing equipment and procedures, for a full evaluation of the permanent deformation resistance for a given mixture, are still under development. Recently, the APA has become increasingly popular in evaluating rutting potential of HMA mixes (Kandhal et al., 1999). Accordingly, many state agencies have started using the APA to evaluate rutting potential. The present study has employed the APA to investigate the performance of different binders based on HMA rut potential. The main objective of this study is to evaluate and compare the performance of these binders in the context of rut potential of mixes with these binders. A subsequent objective is to examine the performance of binders with the same high temperature PG grade (unmodified binders or modified binders) and the performances of binders with different high temperature PG grade (comparison modified and unmodified binders). The primary goals of this study are to develop rutting prediction equations of HMA mixes and to examine whether MP1-98 specified binders could produce a low rut potential mix.

3.3 Binders Description

This section describes HMA produced from thirteen different unmodified and modified binders from different sources and PG grades HMA. These binders are currently being used in different projects in Oklahoma. The unmodified binders referred to as PG1 are PG 64-22 or PG 64-22 OK and they are refined from eight different sources. The unmodified binders are known as base asphalt. The modified binders referred to as PG2 are PG 70-28 and PG 70-28 OK, typically contains 2% styrene-butadiene-styrene (SB) polymer. These two binders used in samples of this study are obtained from two different sources. The modified binder PG3 is a PG 76-28 OK from one of the PG2 sources. It contains 5% SB polymer with 0.05% chemical anti-strip additive. Although the modified binders are produced from the same base asphalts, they contain relatively low amount of asphaltenes. The PG 64-22 OK, PG 70-28 OK and PG 76-28 all meet the requirements for PG 64-22, PG 70-28 and PG 76-28 in accordance with AASHTO MP1, as well as the additional requirements of ODOT specifications (ODOT, 1999).

3.4 Binders Properties

Tests are conducted by ODOT to determine the complex shear modulus, G^* and phase angle, δ values using a DSR at the high PG temperature (e.g, for PG 64-22 at 64°C, for PG 70-28 at 70°C) and at 10 radian per sec frequency of loading. The DSR tests are performed on the original and Rolling Thin Film Oven (RTFO) samples. The Superpave binder specification uses a factor called rutting factor, $G^*/\sin\delta$ to characterize binder stiffness or rut resistance at high pavement service temperature. The rutting factor reflects the total resistance of a binder to deform under repeated loading (G^*), and the relative energy dissipated into non-recoverable deformation ($\sin\delta$) during the loading cycle (Roberts et al., 1996). A higher value of $G^*/\sin\delta$ implies that the binder behaves more like an elastic material, which is desirable for rutting resistance. As the binder ages, the G^* increases and the δ decreases and binders increasingly become less viscous. The SHRP rutting factor $G^*/\sin\delta$ for unaged and aged binders are listed in Table 3.1.

From Table 3.1, it can be seen that all binders are within the Superpave specification for the rutting factor, $G^*/\sin\delta$. The value of $G^*/\sin\delta$ should be 1.00 kPa

(0.145 psi) minimum for unaged binders, and 2.20 kPa (0.319 psi) for RTFO aged binders. The mean rutting factor for the unmodified binder is 1.40, whereas for the modified binders the corresponding value is 1.57 for unaged condition. The mean rutting factor of 3.3 for the unmodified binder and 3.10 for the modified binder indicates that there is no significant improvement in the rutting factor due to modification. The rutting factor can be compared at the same temperature assuming linear behavior. For example, rutting factors for modified binder (i.e. PG 2) of 3.10 at 70°C would be 6.2 at 64°C (Summers, 2001). Therefore, all the modified binders have high rutting factors compared to the unmodified binders at 64°C. A study by Bahia et al. (1999) showed that polymer modification increases the elastic responses and dynamic modulus of bitumen at intermediate and high temperatures, and it influences complex and stiffness modulus at high temperature. Polymer can also reduce the temperature susceptibility, the glass transition and limiting stiffness temperatures of a bitumen (Bahia et al., 1999).

The binders have also been tested by DOT for viscosity at 135^{0}C (275^{0}F) using a rotational viscometer (AASHTO TP48-97) and the values are listed in Table 3.1. Although the viscosity tests are usually conducted for mixing and handling performance, this study investigates the correlation of viscosity with rutting performance. The higher viscosity values for modified binders, as shown in Table 3.1, indicates that polymer modification makes binders more resistance to disturbance. Table 3.1 also shows that the viscosity is different for various modified binders depending on the source. The degree of improvement in binder quality generally increases with polymer content, but varies with base bitumen, bitumen source, PG grade and polymer type (Isacsson, 1999)

3.5 Aggregate and Mix Design

Four mineral aggregates consisting 16.0 mm (5/8 in.) chips, screenings, shot and sand are incorporated into the Superpave method of mix design to produce asphalt concrete. Aggregate information is listed in Table 3.2. In the experimental procedure one, aggregates are evaluated, and gradation tests are performed to obtain a blend that met all of the Superpave gradation criteria. The final blend gradation plotted on the 0.45-power-chart, as shown in Figure 3.1, passes below the maximum density line with a Nominal Maximum Size (NMS) of 12.5 mm (½ in.). The blended aggregate properties are summarized in Table 3.3. Mix designs are performed using a traffic level of more than 3 and less than 30 million Equivalent Single Axle Loads (ESALs). Although the binder grades of PG 64-22 and PG 64-22 OK are recommended for less than 3 million ESALs in ODOT specification, this study has considered 3 million ESALs as the design criteria for volumetric properties.

The maximum gyration, N_{max} is 160 and the design gyration, N_{design} is 100. Design mixes are mixed at 163°C (325°F), aged at 149°C (300°F) for 3 hours and compacted at 149°C (300°F) using a Superpave Gyratory Compactor (SGC). The SGC is set at a vertical pressure of 600 kPa (87 psi) and a gyratory angle of 1.25°. The optimum asphalt content is determined at 4% air voids at N_d (number of gyration for a specific design). Figure 3.2 and Table 3.4 represents optimum asphalt content of four binders and volumetric properties as well as Superpave volumetric criteria. After each mix design is completed, the mix is tested for water susceptibility (AASHTO T 283). Only mixes with a Tensile Strength Ratio (TSR) more than 0.80 are used in the final mix design. In addition, some binders are mixed at lower and higher optimum asphalt contents to examine the effect of asphalt binder on rutting performance of mixes.

3.6 Rut Testing

Cylindrical specimens of 75 mm (3 in.) height are compacted in the SGC at a target air void of 6 to 8%. It is to be noted that HMA are usually designed with a target air voids of 4% (laboratory), however, constructed with a target air voids of 6 to 8% (field). Specimens are preconditioned at 64°C (147.3°F) for 10 hours before rut testing. In the APA testing procedure, the cylindrical samples are subjected to repeated passes of a 445 N (100 lb) loaded wheel through a 690 kPa (100 psi) pressurized hose. Specimens are tested at 64°C (147.3°F) temperature. The rut depth is measured in millimeters as a function of number of wheel passes. A total of ninety specimens are prepared and tested for rut depth at 8000 loading cycles. Figure 3.3 shows the typical variations of rut depth in millimeters with the number of load cycle for mixes containing various modified and unmodified binders. Three modified binders out of four showed rut depths of less than 3 mm. Others showed more than 4.5 mm rut depth at 8000 cycles of loading. From Figure 3.3, it can be seen that more than 50% of the final rutting occurs within 1000 loading cycles for all mixes.

The initial higher rate of rutting can be attributed to the initial densification or compaction of materials. After completion of initial densification, the rate of rutting (slope of rutting curve) decreases with the increase in loading cycles for each mixture.

The slope of rutting curves in the range of 2000 cycle to 8000 cycles is nearly equal for all mixes (except for S4-PG 64-22). Therefore, it can be concluded that the major difference in final rut depth is primarily due to densification of materials and not by plastic flow at higher cycles.

3.7 Analysis of Test Results

In this section, the binders are ranked based on their rutting performances in mix testing. An interpretation of the factors affecting rut is also presented.

3.7.1 Overall Ranking

Figure 3.4 is a histogram showing all binders with increasing rut depth for samples with 6 to 8 percent air voids. A threshold value of rut depth for classifying a mix as good or poor performing has yet to be developed by ODOT. Currently, Oklahoma DOT is considering a limiting rut depth of 6.0 mm for mixes with ESALs in the range of 0.3-3.0 millions (OHD L 43, 2002). This study considers a rut depth of 6 mm as a threshold between excellent-good mixes and poor mixes. Accordingly, in Figure 3.4, the binders are classified as E (excellent), G (good) and P (poor) on the basis of the threshold value associated with rutting performance. It is evident that 3 mixes fall in the category of excellent, 6 mixes are in the good category and 4 exhibit poor rutting performance. These are the rating of 13 mixes prepared with various modified and unmodified Superpave binders. From this ranking procedure, it is evident that the asphalt pavement analyzer can be used for screening of poor mixtures. That is, the APA can be used as proof tester for HMA mix.

3.7.2 Effect of Binder's Performance Grade

Figure 3.5 shows that most PG2 and PG3 (modified binders) mixes have lower rut potential (excellent) compared to the rutting performance of PG1 (unmodified binders). The mean rut depth for the modified binders is 3.4 mm with a standard deviation of 1.8 mm. The unmodified binders show a mean rut depth of 5.8 mm with a standard deviation of 0.78 mm. The higher standard deviation for the case of modified binders is due to the poor performance of S8-PG 70-28 OK. From the binder's PG point of view, it can be shown that the overall performance of the modified binders is much better than that of the unmodified binders. This agrees with what is expected from the Superpave binder's specification point of view. However, there is no significant difference when the performance of the modified binder S8-PG 70-28 OK mixture is compared with the performance of unmodified binders. The rutting performance of S7-PG3 does not differ when compared with the performance of the S7-PG2 binder mixture. From the test results, it is evident that the binder's higher performing grade is not a sufficient criterion to conclude that the mixture will perform well. A polymer-modified binders' performance should be evaluated by the rut performance of the mix in an APA.

3.7.3 Effect of Source

One of the objectives of the present study is to examine whether the performance of mixes with same PG binder grade differs with the source. For the PG1 binder, the following source ranking is S6>S5>S3>S1>S8>S4>S7>S2, based on the low to high rutting potential. From Figure 3.5, it can be seen that the rut potential for PG1 binders differs very little (varies from 5 mm to 7 mm) by source. But, in the case of the PG2 binder the performance of S8 is worse compared to the source S7. Based on the APA test results, it is evident that the APA is sensitive to a binder's PG grade and source. A simple APA rut test can facilitate the prediction of binder's actual behavior in a HMA mix. Therefore, binders meeting the specification requirements of MP1-98 should also be evaluated by the APA rut testing.

3.7.4 Effect of Rut Factor

Figure 3.6 shows that the rut depth of mixes prepared with modified binders generally increases with decreasing rut factor, $G^*/\sin\delta$. However, for the case of unmodified binders, rut depth generally decreases with the decreasing value of rutting factor. The overall ranking based on rutting factor, as shown in Figure 3.7, does not comply with the overall rank based on rutting performance as noted. Basically, the binder's DSR test properties cannot reflect the mix performance. It can also be seen that the S8-G1 has the lowest rutting factor and S5-G1 has the highest, but their rutting performance dose not differ significantly. Figure 3.8 shows that the rut depth at 500 cycles plotted with percentage increases in the binder's rutting factor due to RTFO aging. There is no significant effect of aging on rut depth at 500 cycles for both the modified and unmodified binders.

3.7.5 Effect of Viscosity

Figure 3.9 shows a bar plot of viscosity and rut depth for all the binders. It shows that the modified binders have higher viscosities or resistance to flow. Mixes containing these binders show low rut potential. The unmodified binders have low viscosity and exhibit higher rut potential. Therefore, the viscosity of binders at 135^0 C (275^0 F) can be a good performance-based binder evaluation parameter

3.8 Statistical Analysis

Many independent variables affect rutting. This study deals only with the variables that cover laboratory mix design, binder properties, rut specimen preparation and the APA rut testing. The following nine variables are identified for data analysis: mixture binder content (P_b), air void (V_a), Void in Mineral Aggregate (VMA), Void Filled with Asphalt (VFA), absorbed asphalt (P_{ba}), viscosity (R_v), unaged $G^*/\sin\delta$ (DSR_u) and aged $G^*/\sin\delta$ (DSR_a), and the APA load cycles. A single independent variable, when used to predict rut potential, is shown to give very poor prediction. For example, the amount of air void is likely to be the most important physical property of asphalt mixes that relates to rutting (Brown et al., 1989). The correlation of air voids to rutting, as shown in Figure 3.10, is very poor. Brown et al. (1989) reported that total air voids might actually increase with additional traffic once rutting starts.

According to many engineers, plastic flow is likely to begin once the air void is reduced to approximately 3 percent (Ford, 1988). However, these analyses are performed at an air void of 6 to 7 percent that changes with load cycle. Therefore, air voids cannot reflect the actual correlation with rutting. Two rut prediction models are developed using Linear Multiple Regression (LMR) analysis and Nonlinear Regression (NR) analysis. A total of 45 sets of data, each with an average of 2 specimens are used for model development considering the above-mentioned parameters. The final prediction model includes only significant variables that affect rutting.

3.8.1 Linear Multiple Regression Model

The stepwise method is employed for LMR model development. In step one, the independent variable that best correlated with the dependent variable (rutting) is included in the equation. In the second step, the remaining independent variables with the highest partial correlation with the dependent are entered. This process is repeated until the addition of a remaining independent does not increase the R^2 value by a significant amount (or until all variables are entered). The dependent variable (rut depth, RD in millimeter) is multiplied by 1000 and transferred to a logarithmic scale prior to incorporation into the linear model. The loading cycle is also transferred to logarithmic scale. The established terminal simplified expression for the linear model is given below:

$$\mathrm{Ln}(\mathrm{RD} \times 1000) = -2.51 - 0.20(R_v) + 5.29(P_b) - 4.92(P_{be}) - 0.59\left(\frac{G^*}{\sin\delta}\right)_{unaged} + 0.608\,\mathrm{Ln}(\mathrm{cycle}) \qquad (3.1)$$

where

RD = 8000-cycle Rut Depth

$(G^*/\sin\delta)_{unaged}$ = rut factor of unaged binder (G^* = shear modulus and δ = phase angle)

R_v = viscosity, kPa.s

P_b = asphalt content, %

P_{be} = Effective asphalt content.

A summary of relevant statistics for the LMR model is reported in Table 3.5. The sample multiple correlation coefficient (R = 0.951) measured the degree of relationship between the actual Ln (RD x 1000) and the predicted Ln (RD x 1000). The value indicates that the relationship between Ln (RD x 1000) and the five independent variables is quite strong and positive. The sample coefficient of determination, R^2-value measures the goodness-of-fit of the estimated sample regression equation. It explains the proportion of the variation in the dependent variable predicted by the fitted the Simple Regression Plane (SRP). The value of $R^2 = 0.905$ simply means that about 90% of the variation in Ln (RD x 1000) can be explained or accounted for by the estimated SRP that uses Ln (cycle), R_v, P_b, P_{ba}, DSR_{unaged} as the independent variables. Adjusted R^2 is the sample coefficient of determination after adjusting for the degrees-of-freedom lost in the process of estimating the regression parameters. In this case, adjusted $R^2 = 0.904$ is a better measure of the goodness-of-fit of the estimated SRP than its nominal/unadjusted counterpart. Standard Error of Estimate $S_e = 0.507$ means that, on an average, the predicted values of the Ln (RD x 1000) can vary by ±0.507 about the estimated regression equation for each value of independent variables during the sample period and by a much larger amount outside the sample period.

3.8.2 Nonlinear Regression Model

The present study also employs the iterative estimation of Levenberg-Marquardt method for nonlinear model development. A regression model is called nonlinear, if the derivatives of the model with respect to the model parameters depend on one or more parameters. The specific advantages such as the parameters of a nonlinear model usually have direct interpretation in terms of the process or mechanism under considerations. In the modeling procedure, trials are made to fit a nonlinear equation to observed rutting, giving initial values of parameters. The adjustment of all parameters is considered in one iteration. In the next iteration, the program attempts to improve on the fit by modifying the parameters. If any further improvement is not possible, the fit (model relation or equation) is considered converged. Iterations are stopped when the relative reduction between successive residual sums of squares is, at most, 1.000E-08. Several models with different parameters are examined. A model (for example, one with more parameters) is satisfactory, if the relative increase in sum-of-squares (going from one to another model) is greater than the relative increase in the degrees-of-freedom of that model, i.e. $(SS1-SS2)/SS2>(DF1-DF2)/DF2$, where, SS = regression Sum of Square and DF = Degrees-of-Freedom.

In a linear regression model, the quality of fit of a model is expressed in terms of the R^2-value. In nonlinear regression, such a measure is unfortunately not readily defined. One of the problems with the R^2-value definition is that it requires the presence of an intercept, which most nonlinear models do not have. A measure, relatively closely corresponding to R^2-value in the nonlinear case is Pseudo-R^2=1–SS (residual) /SS ($Total_{Corrected}$). The final form of the nonlinear model with a pseudo coefficient of determination, Pseudo-R^2 =0.807 can be expressed as follows:

$$RD=-2.57-1.09(R_v)+1.68(P_b)+0.35(V_a)-0.14(VMA)-0.71\left(\frac{G^*}{\sin\delta}\right)_{unaged}$$

$$+0.2442\,Ln\,(cycle)^{0.3359} \qquad (3.2)$$

where

V_a = percentage air voids

VMA = voids in the mineral aggregate.

Table 3.6 contains the partitioning of the total sum of squares for the model and data into a regression sum of squares explained by the model and a residual sum of squares. The mean square error of this fit ($R^2 = 0.5697$) is the estimate of variability in the data when adjusted for the nonlinear model.

3.9 Comparison of Measured Rut Depth with Model Predictions

Figure 3.11 is a plot of measured rut versus model predicted rut depth for unmodified binder, S8-PG1-OK. The nonlinear prediction is closer to the measured rut depth and better than the linear prediction. The linear prediction is 3.0 mm more than both the measured rut depth and the nonlinear prediction. The nonlinear prediction for binder, S2-PG1 is shown in Figure 3.12. It follows the previous trend but the predicted values are about 2 mm less than the measured. The linear predictions are higher than nonlinear predictions. Figures 3.13–3.14 are the plots for modified binders S7-PG2 and S7-PG3, respectively. Both these figures show that both nonlinear and linear predictions cannot explain the measured rut depth. The linear and nonlinear prediction equations include the viscosity and $G^*/\sin\delta$ (unaged), but these values do not vary significantly for modified binders. Although the final rut depth for linear prediction is better (representative to laboratory rut value) than the nonlinear prediction, the slope of the nonlinear prediction at higher load cycles is almost equal to measured rut depth.

3.10 Rut at 500-Cycle Versus Rut at 8000-Cycle

Often time, in cyclic tests, the performance of a material at a lower cycle is correlated with its performance at higher cycles. Therefore, the correlation of 500-cycle rutting with 8000-cycle rutting is attempted in this study. It believed that at lower cycles, rutting occurs due to consolidation and at higher cycle, rutting occurs due to plastic flow. The APA rut depth at 500-cycle can be a transition between consolidation and plastic flow of materials. Also, the preceding analyses indicate that the visco-elastic properties of a binder are significant at lower numbers of loading cycles. At higher loading cycles, binder properties are less significant and rate of rutting is almost equal for all binders. Therefore, trials are made to correlate 8000-cycle APA rut depth to 500-cycle rut depth. From the linear regression analysis, the following relationship is obtained with a $R^2 = 0.830$:

$$RD = 1.96 + 1.8(RD_{500}) + 0.93\left(\frac{G^*}{\sin\delta}\right)_{unaged} - 2.3\left(\frac{G^*}{\sin\delta}\right)_{aged} \tag{3.3}$$

where

RD_{500} = Rut depth at 500-cycle

$(G^*/\sin\delta)_{aged}$ = rut factor of aged binder.

A nonlinear analysis is found to give a better correlation with $R^2 = 0.89$ and the following equation:

$$RD = 15.76 - 0.17(R_v) + 2.67(P_b) + 0.53(V_a) - 0.8(VMA) - 2.16\left(\frac{G^*}{\sin\delta}\right)_{unaged}$$

$$+ 7.2(P_{be}) - 19.62(RD_{500})^{-0.17} \tag{3.4}$$

The predicted 8000-cycle rut depths for all mixes are plotted against measured rut depths in Figures 3.15 and 3.16 for linear and nonlinear prediction, respectively. These model predictions show that the nonlinear prediction has less scatter along a 45^0 line drawn between the measured and predicted rut values. One of the basic ideas behind establishing this kind of relationship is to distinguish rutting performance of a pavement at the end of pavement life from its early life. The 8000-cycle rut depth is correlated to 500-cycle rut depth as shown in Figure 5.17. The R2-value is found to be 0.7683 and the prediction equation is given below:

$$RD = 2.0557(RD_{500}) + 1.2759 \tag{3.5}$$

This equation can be useful (i.e., rule of thumb) for approximating final rut depth from the 500-cycle rut depth.

3.11 Concluding Remarks

The following points summarize the findings of this chapter:

- This study ranked 13 different binders based on mixes' performance and also on their properties. The binders' ranking based on their properties do not match with the mixture performance. A binder's PG grade does not ensure the performance of the mixture containing the binder. Therefore, a binder satisfying the Superpave specification requirements should be evaluated by the rutting performance of the corresponding HMA mix, determined by APA testing.
- The performance of modified binders having the same PG grade can vary significantly with the combining process or source. If the binders are unmodified or neat asphalts then the changing source will not vary in rutting depth by more than 1 mm, if the binders satisfy AASHTO MP1-98. As binders' source is always changing, the ranking of unmodified binders depending on the source become less significant.

- The higher the rutting factor the lower rut potential is not valid always. Rather, binder's viscosity and mix performance have to be considered with rutting factor. In this study, binder's viscosity has shown to have a good correlation with the mix performance.
- If a rut depth of 6.00 mm is the divider between good and poor mixes, then ODOT's restriction for using of unmodified binders in roads with 3M+ ESALs on some sources should be reinvestigated.
- If the air voids of laboratory-produced rut specimens are kept within 6 to 8%, then air voids plays an insignificant role in the contribution to rut potential.
- A 500-cycle APA rut depth can be used to predict 8000-cycle rut depth, both for modified and unmodified binders mix using linear and nonlinear regression models.
- The nonlinear model has higher R^2 value compared to that of linear prediction model developed in this study. Both models over predicted rut depth for mixes with modified binders
- Although rutting involves many parameters, mainly the binder properties are considerer in the model development in this study.

Table 3.1 Properties of Unaged and RTFO Aged Binder

Binder Type	Binder Source	Binder PG	Specific Gravity	Viscosity (R_v)	$G^*/\sin\delta\|_{unaged}$	$G^*/\sin\delta\|_{aged}$	% Increase $G^*/\sin\delta$
Un-modified	S1	PG 64-22	1.0152	0.47	1.58	3.60	128
	S2	PG 64-22	1.0315	0.45	1.55	3.33	115
	S3	PG 64-22	1.0254	0.61	1.74	3.59	106
	S4	PG 64-22	1.0159	0.63	1.27	3.33	162
	S5	PG 64-22OK	1.0103	0.64	1.25	3.48	178
	S6	PG 64-22	1.0076	0.59	1.27	2.62	106
	S7	PG 64-22	1.0151	0.60	1.29	3.21	149
	S8	PG 64-22	1.0110	0.60	1.23	3.53	187
	S8	PG 64-22OK	1.0160	0.56	1.41	3.35	138
Modified	S7	PG 70-28	1.0122	1.11	1.40	2.64	89
	S7	PG 70-28OK	1.0150	1.20	1.66	3.33	101
	S8	PG 70-28OK	1.0087	1.17	1.45	3.58	147
	S7	PG 76-28OK	1.0258	1.08	1.78	2.86	61

Note: R_v = viscosity is measured at 135 °C with a gyration of 10 radian/second;
$G^*/\sin\delta$ = rut factor is measured at high PG temperature (i.e. 64°C or 70°C)

Table 3.2 Aggregate Information

Material	Source	Type	% Used
16 mm (5/8 in.) Chips	Western Rock at Davis, Oklahoma	Rhyolite	35
Screening	Western Rock at Davis, Oklahoma	Rhyolite	35
Shot	Dolese Co. at Davis, Oklahoma	Limestone	20
Sand	Dolese Co. at Oklahoma City, Oklahoma	Quartz	10

Table 3.3 Blended Aggregate Properties

Properties	Measured	Required
L.A. Abrasion, % wear	23	40 Max.
Durability Index	74	40 Min.
Insoluble Residue (%)	68.7	40 Min.
Fractured Faces (%)	100	95/90 Min.
Sand Equivalent (%)	52	45 Min.
Fine Aggregate Angularity (%)	46	45 Min.
Specific Gravity (SSD)	2.639	
Absorption (%)	0.189	

Table 3.4 Volumetric Properties for Optimum Asphalt Content

Binder	Optimum AC	% V_a at N_d	% VMA at N_d	% VFA at N_d	% G_{mm} at N_i	% G_{mm} at N_d
S3-G1	5.4	4.0	14.2	72.0	88.8	96.0
S8-G2	5.4	4.1	14.7	72.3	88.5	95.9
S7-G2	5.1	4.0	13.9	70.9	88.2	96.0
S2-G1	5.1	4.1	14.0	70.7	89.0	95.9
Superpave Requirement		4.0	14 min	65-76	Less than 89	96.0

Table 3.5 Linear Regression Model Summary

Model	Independent Variables (Predictor)	R	R^2	Adjusted R^2	Std. Error of The Estimate
1	C, LNCY	0.931	0.867	0.867	0.5989
2	C, Ln (cycle), R_v	0.944	0.892	0.891	0.5409
3	C, Ln (cycle), R_v, P_b	0.948	0.899	0.899	0.5219
4	C, Ln (cycle), R_v, P_b P_{be}	0.950	0.902	0.902	0.5137
5	C, Ln (cycle), R_v, P_b P_{be} DSR_u	0.951	0.905	0.905	0.5068
6	C, Ln (cycle), P_b P_{be} DSR_u VFA	0.952	0.906	0.906	0.5038
7	C, Ln (cycle), R_v, P_b P_{be} DSR_u, VFA	0.952	0.906	0.906	0.5039
8	C, Ln (cycle), P_b P_{be} DSR_u VFA DSR_a	0.952	0.906	0.906	0.5031

Note: Dependent Variable = Ln (RD x 1000) , C=constant

Table 3.6 Non Linear Model Summary Statistics

Source	DF	Sum of Squares	Mean Square
Regression	8	6456.02	807.00
Residual	1522	867.09	0.5697
Uncorrected Total	1530	7323.11	
(Corrected Total)	1529	4473.71314	

R squared = 1 - Residual SS / Corrected SS = 0.80618

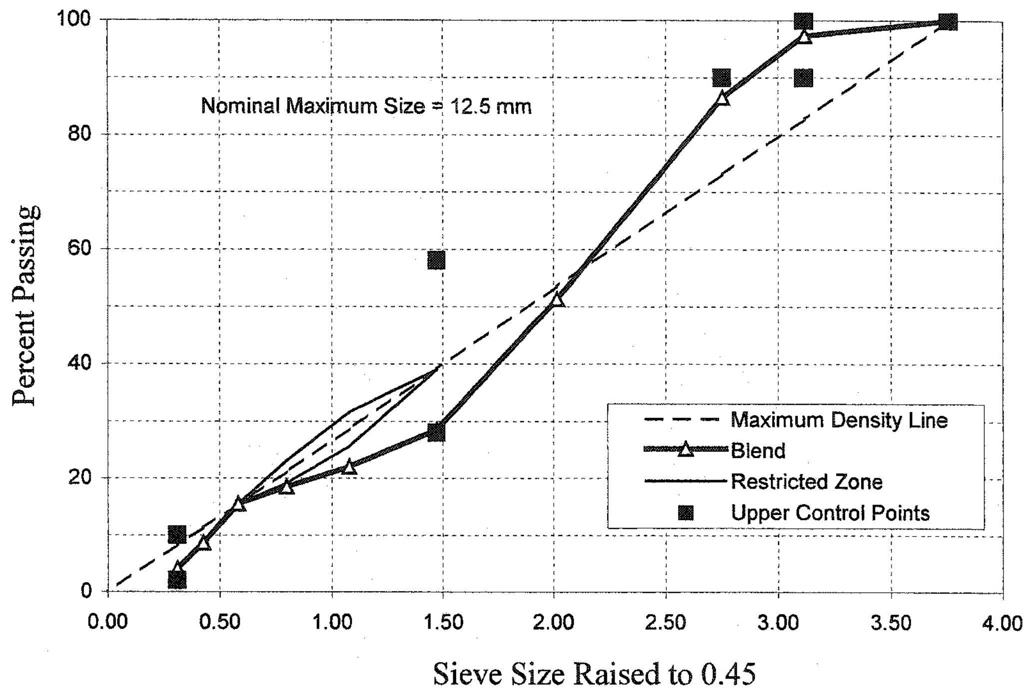

Figure 3.1 Blended Aggregate Gradation Used for Mix Design

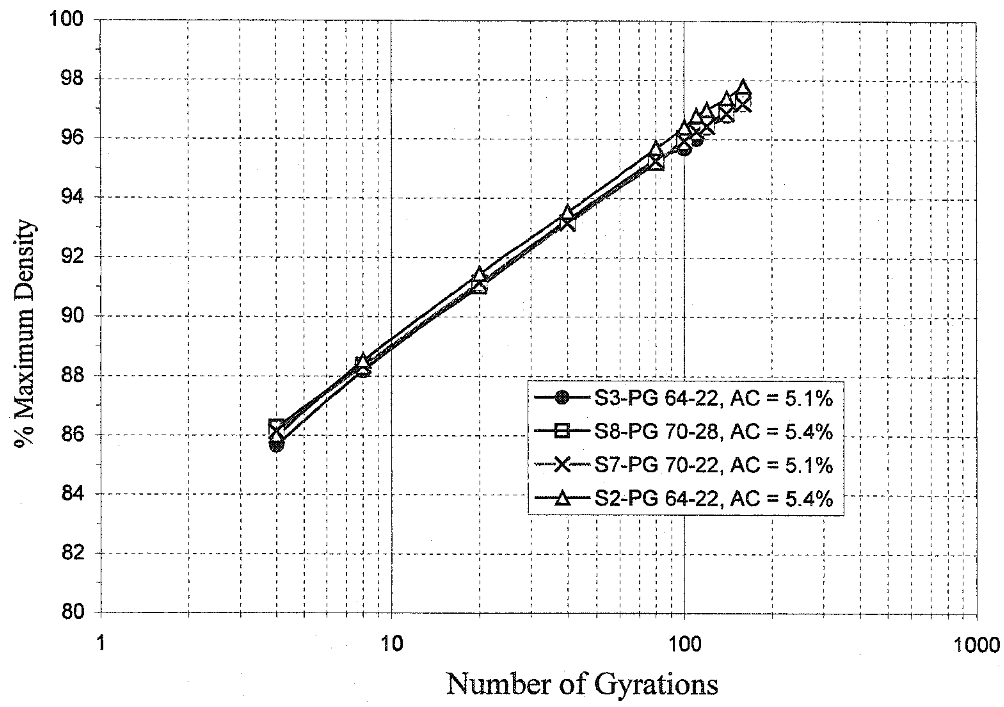

Figure 3.2 Average Densification Curve with Optimum Asphalt Content

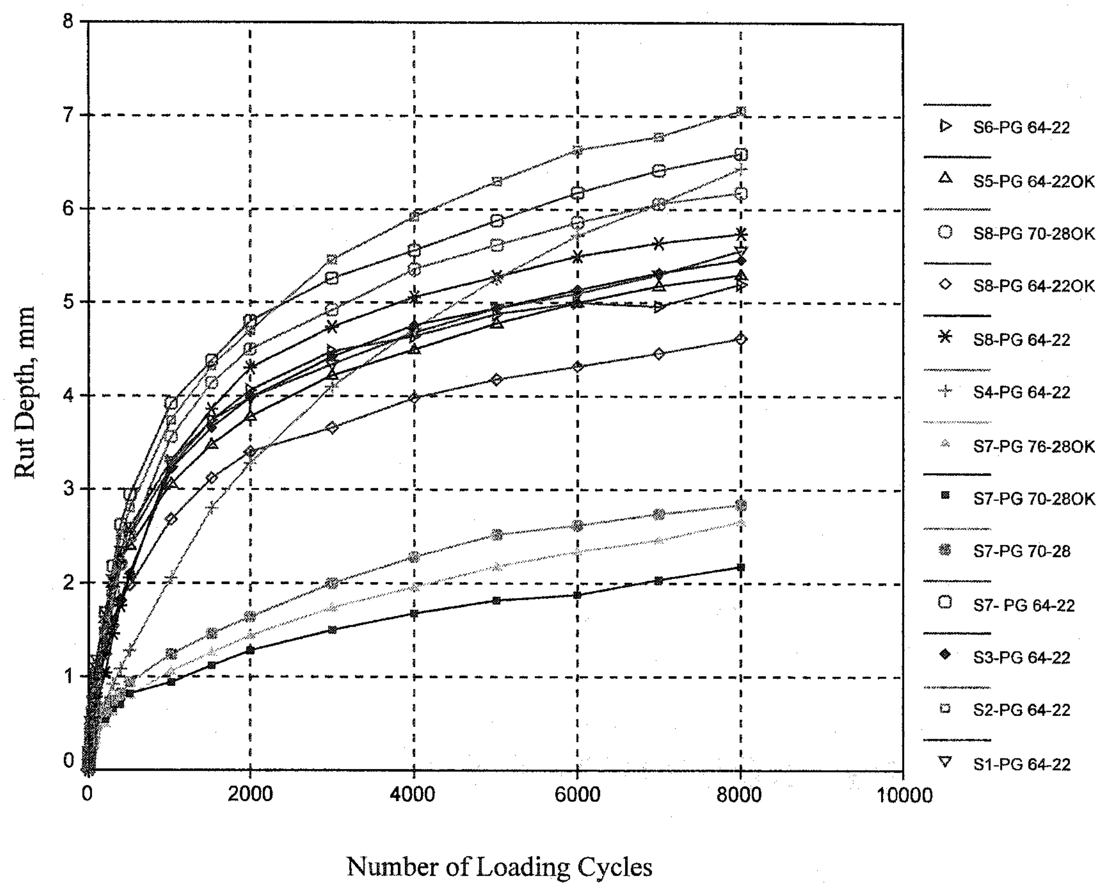

Figure 3.3 Typical Rut Depth Versus Load Cycle

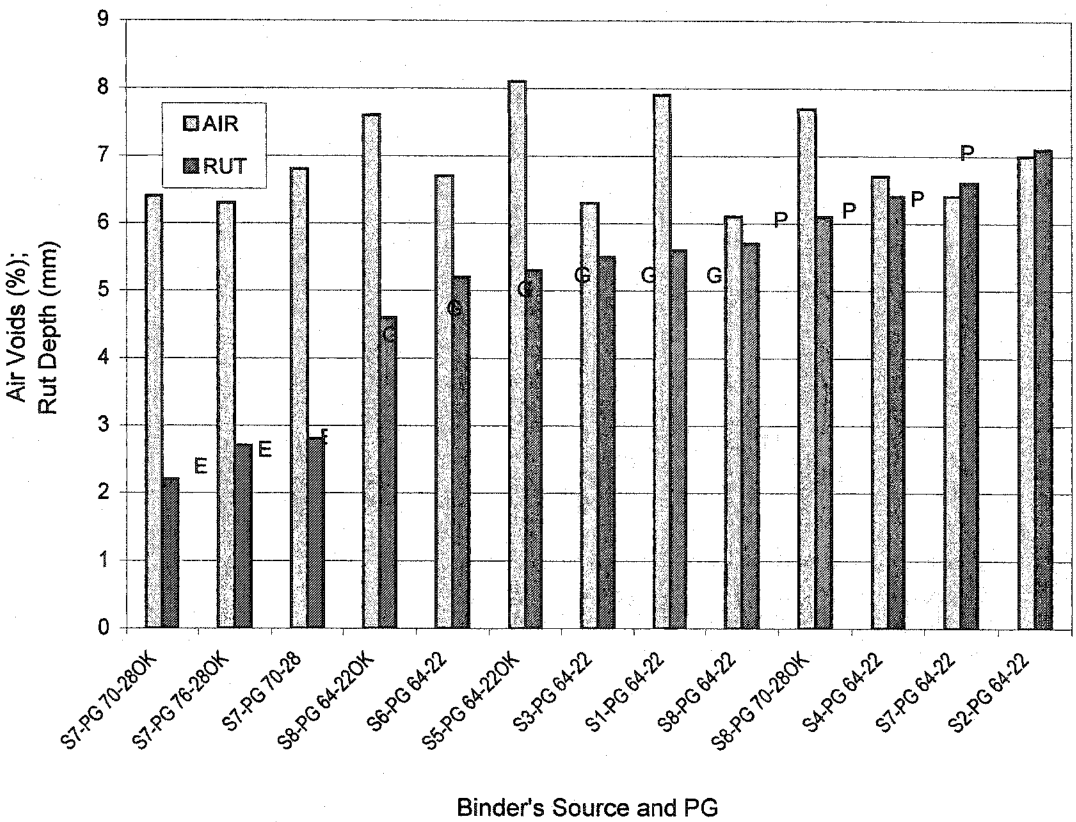

Figure 3.4 Overall Ranking of Mix

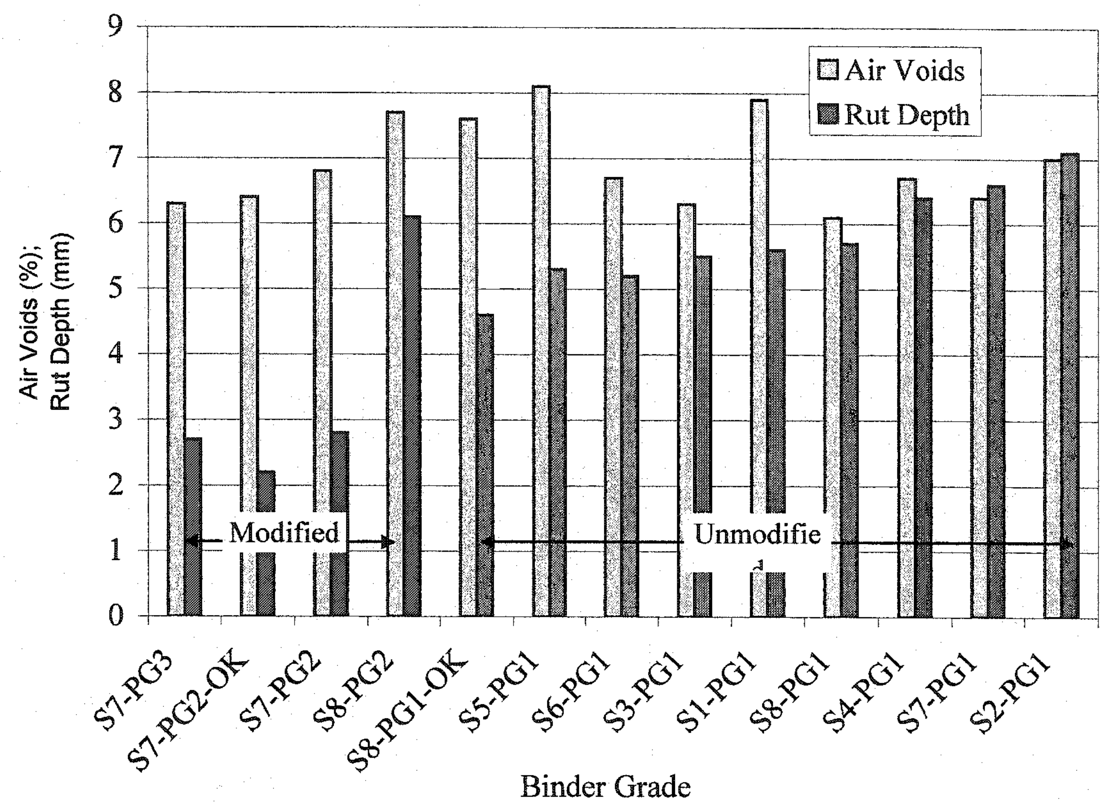

Figure 3.5 Modified and Unmodified Binders Performance

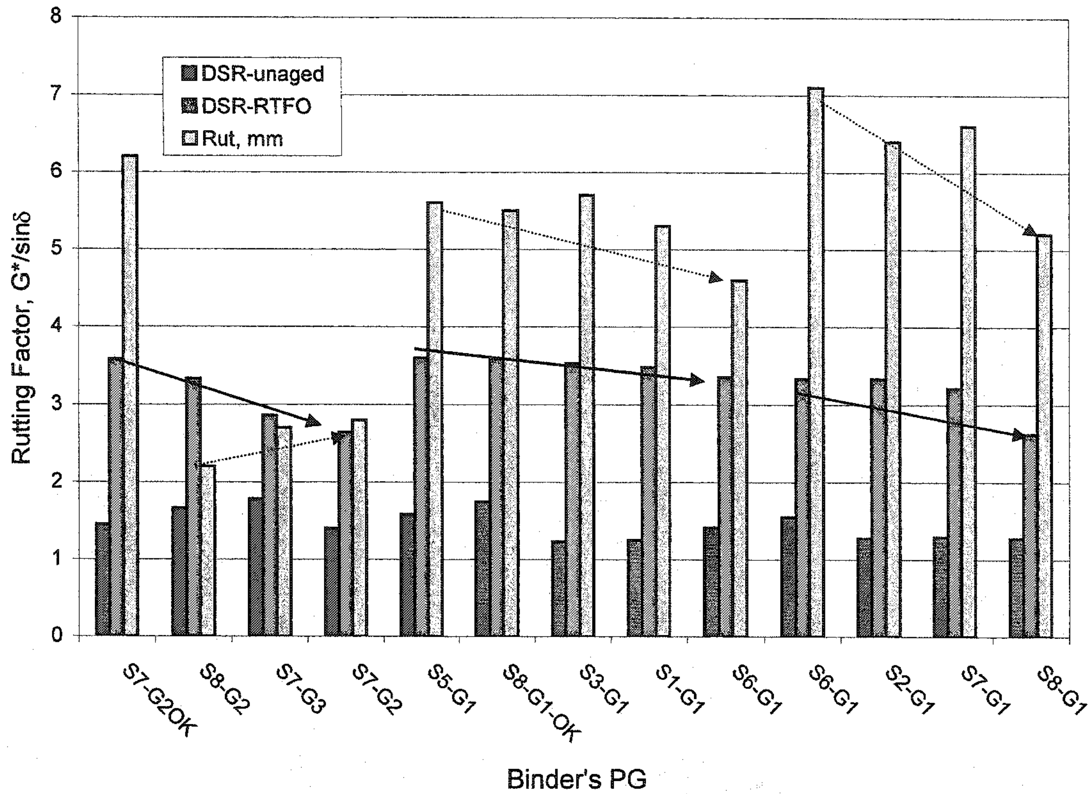

Figure 3.6 Effect of Rutting Factor on Rutting Performance

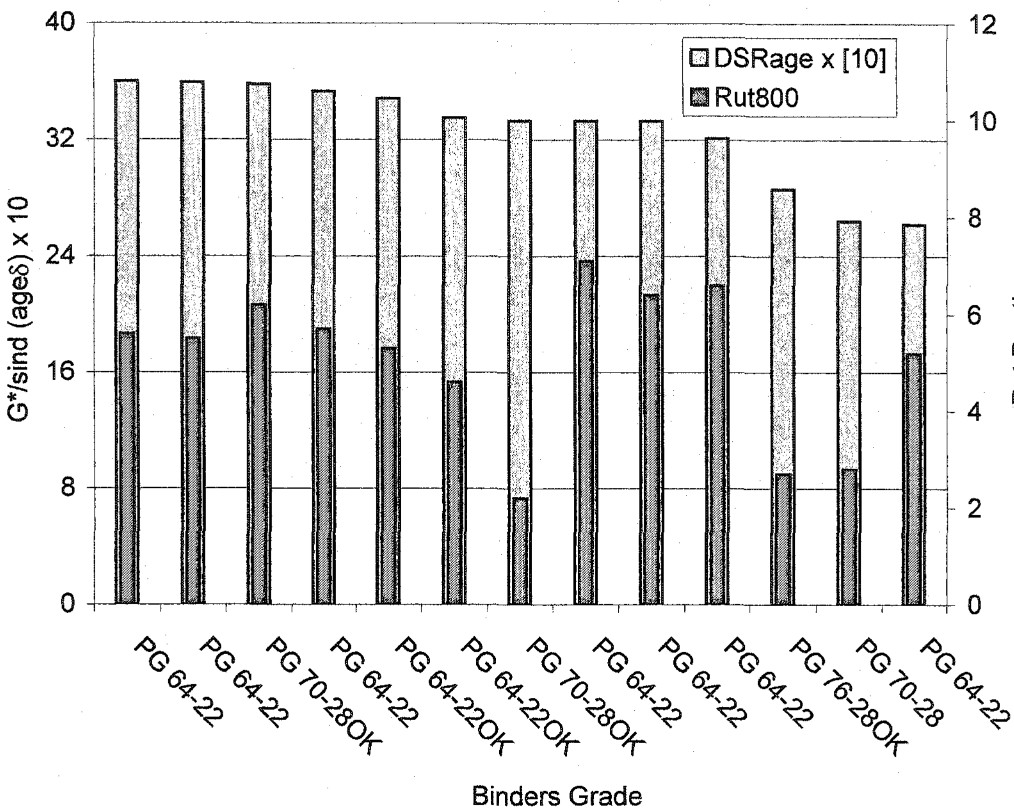

Figure 3.7 Overall Ranking of Binder Based on $G^*/\sin\delta$ (aged) Values

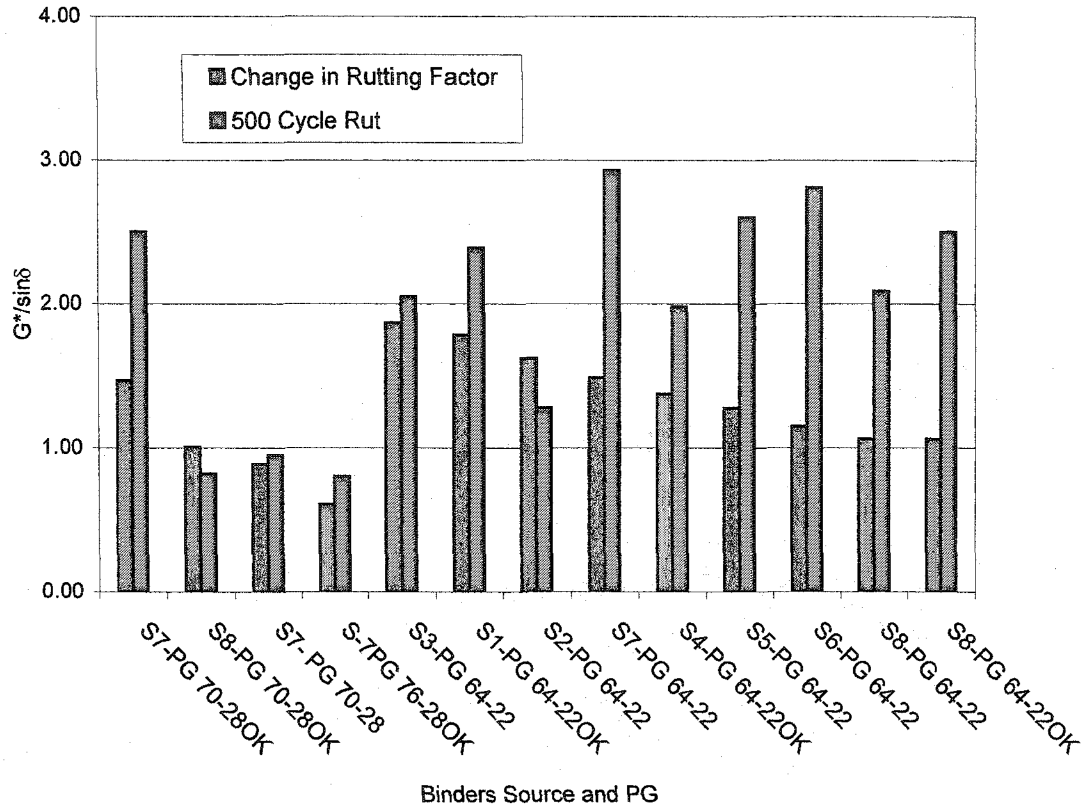

Figure 3.8 Effect of RTFO Aging on Binder's Performance

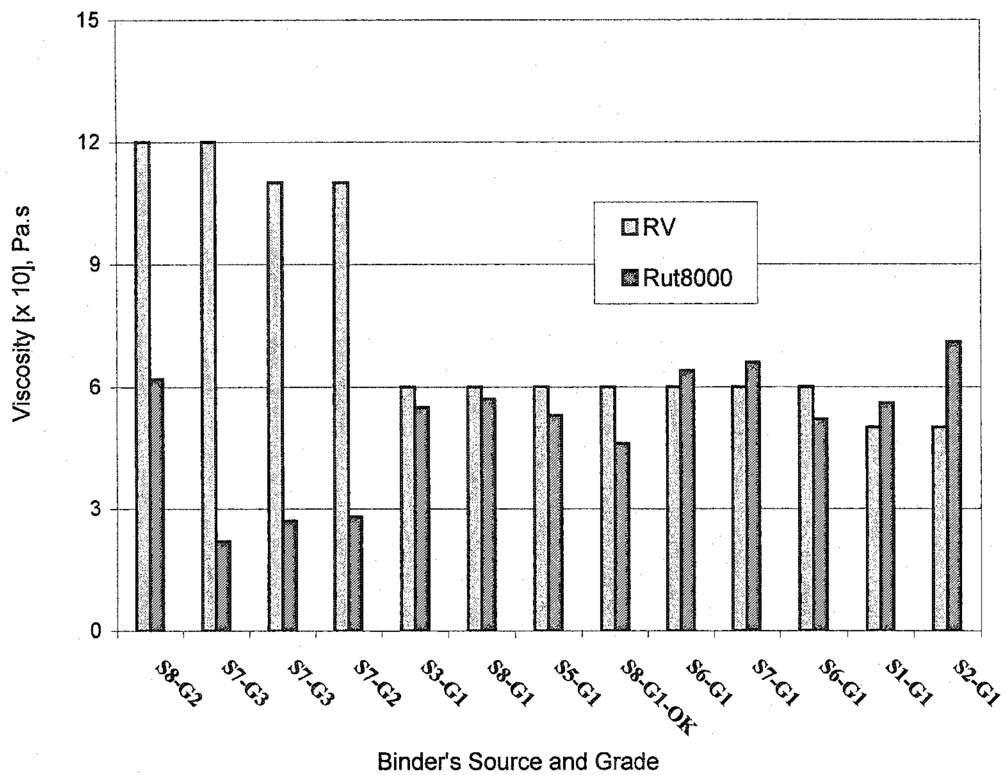

Figure 3.9 Effect of Viscosity on Rut Performance

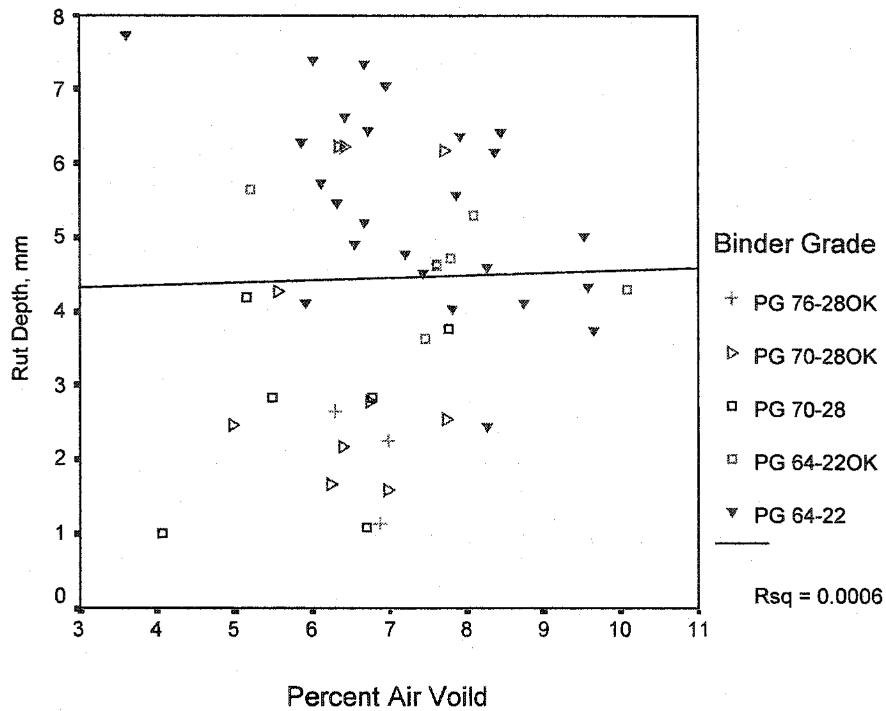

Figure 3.10 Correlation Between Rut Depth and Percent Air Void

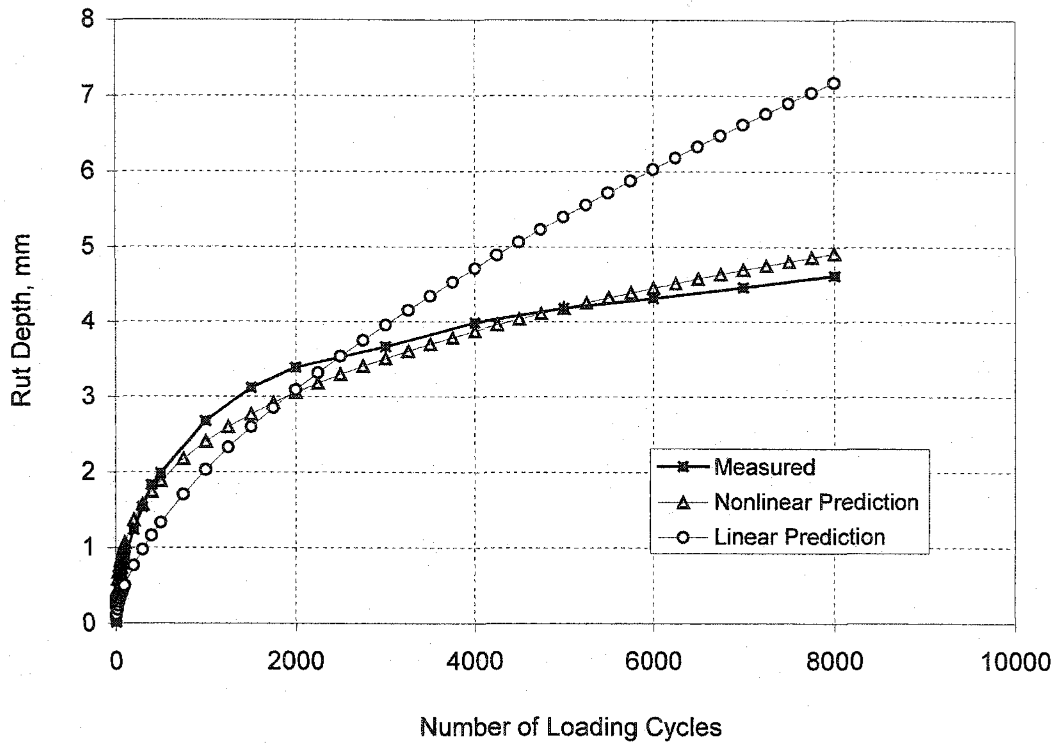

Figure 3.11 Prediction Versus Measured Rut Depth for Binder S8-PG 64-22OK

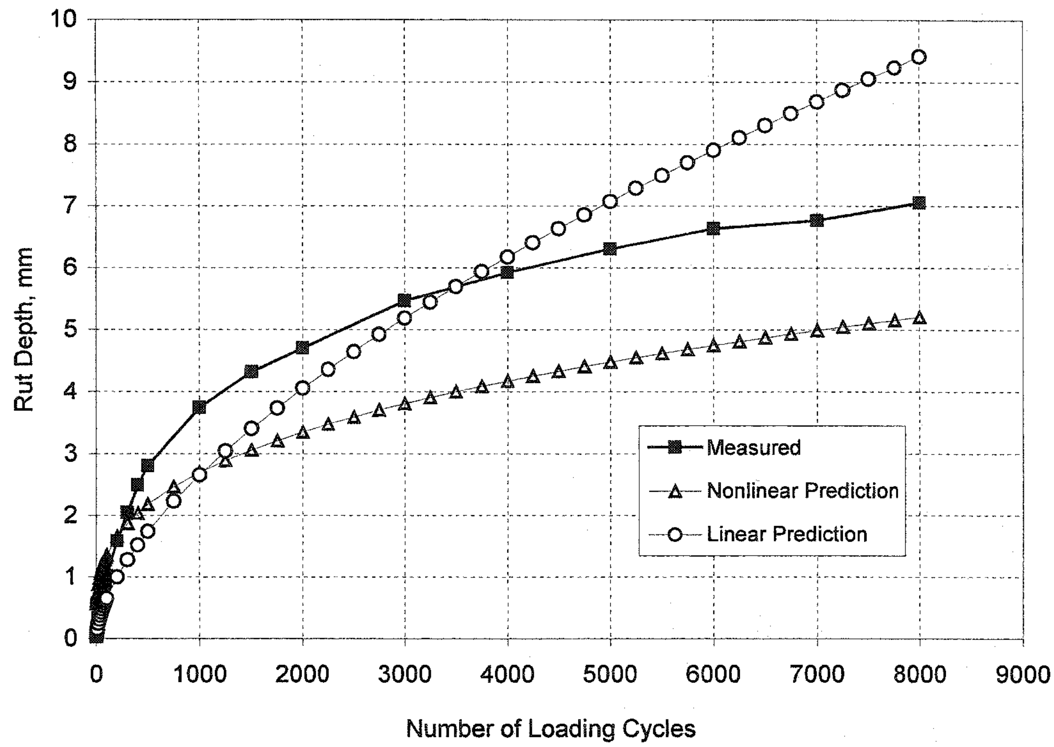

Figure 3.12 Prediction Versus Measured Rut Depth for Binder S2-PG 64-22OK

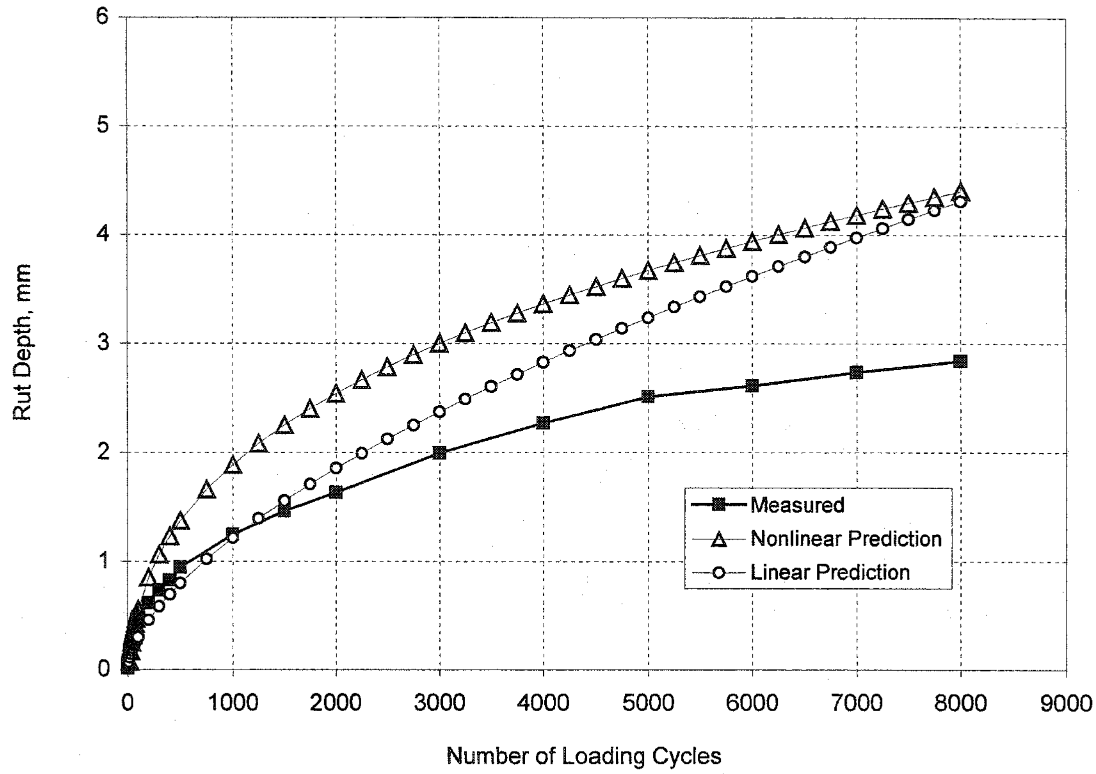

Figure 3.13 Prediction Versus Measured Rut Depth for Binder S7-PG 70-28

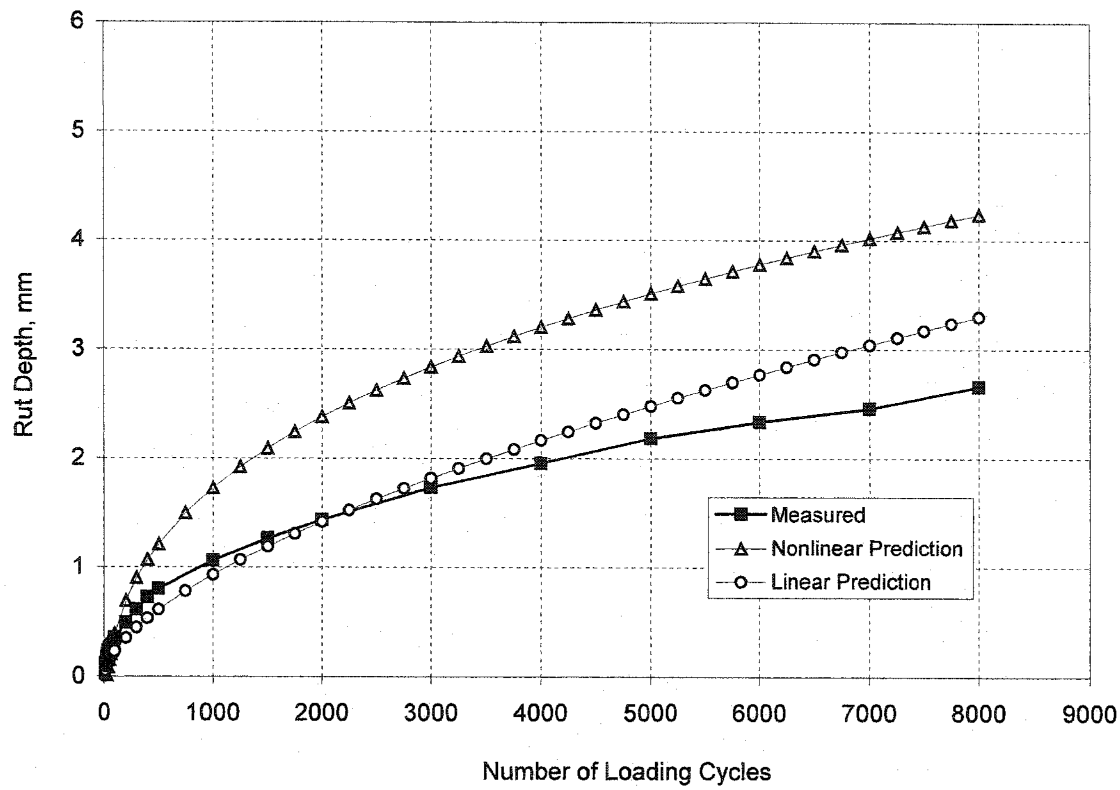

Figure 3.14 Prediction Versus Measured Rut Depth for Binder S7-PG 76-28OK

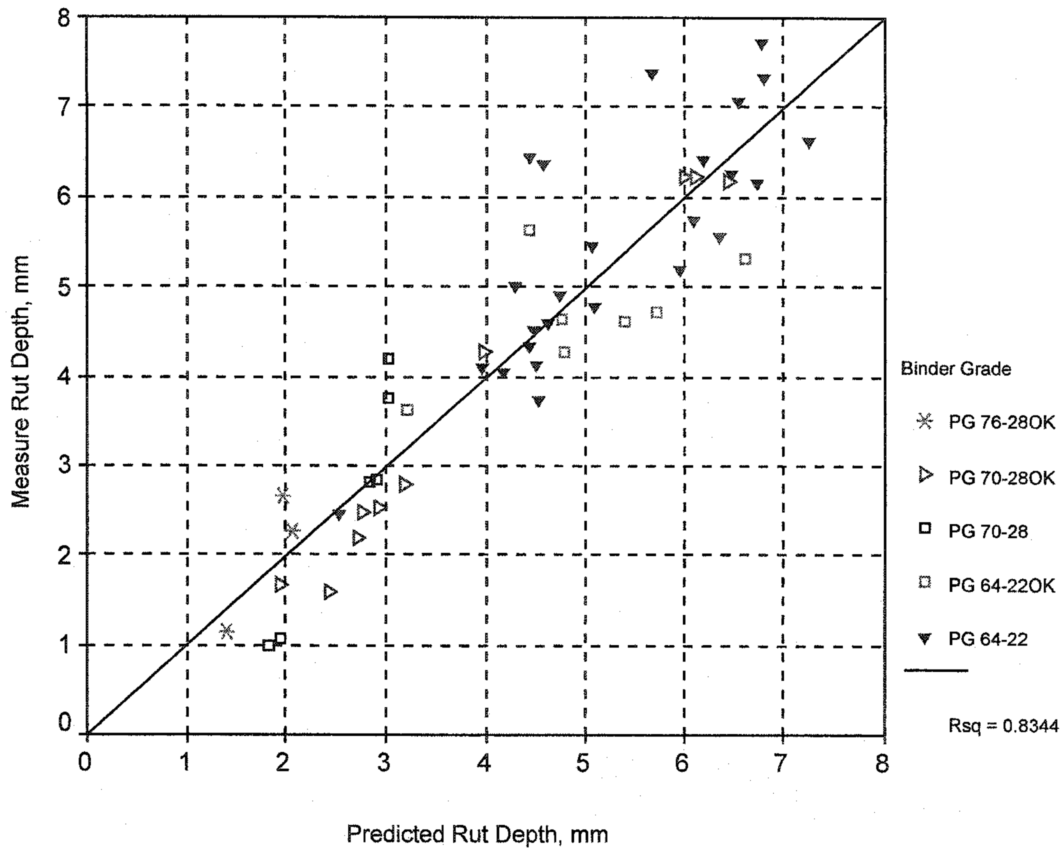

Figure 3.15 Linear Model Predicted 8000-Cycle Rut and Measured Rut

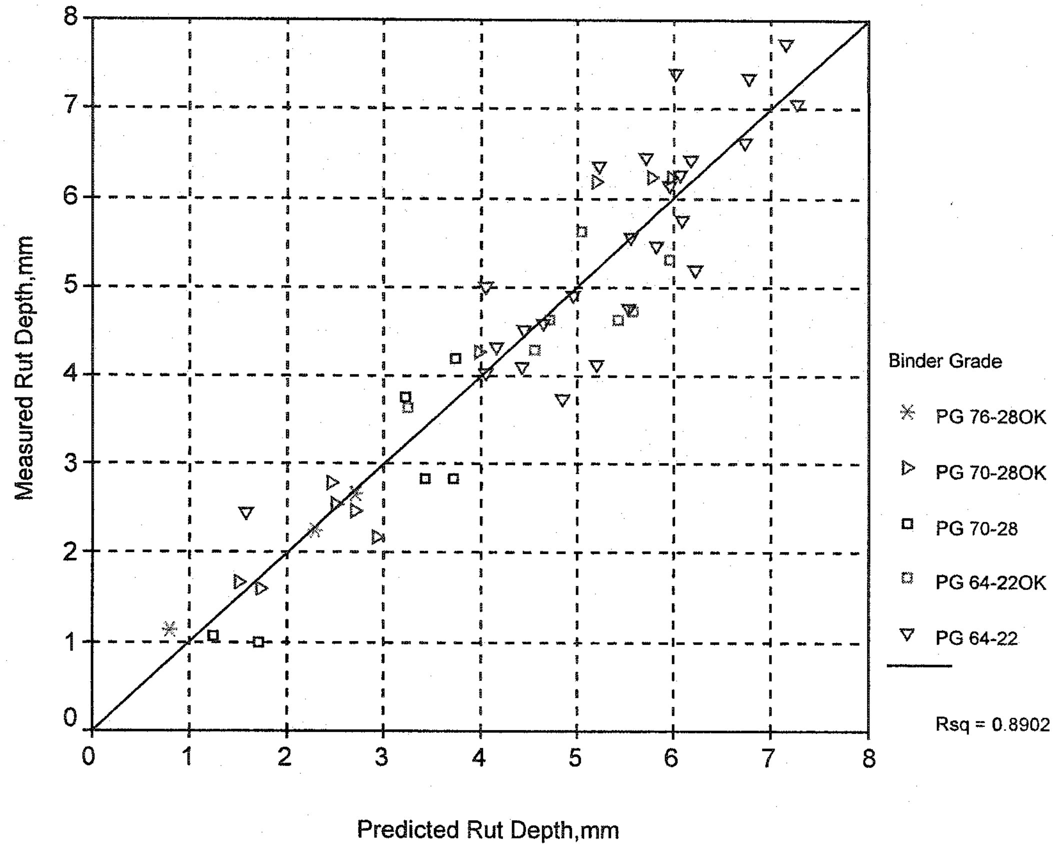

Figure 3.16 Nonlinear Regression Model Predicted 8000-Cycle Rut and Measured Rut

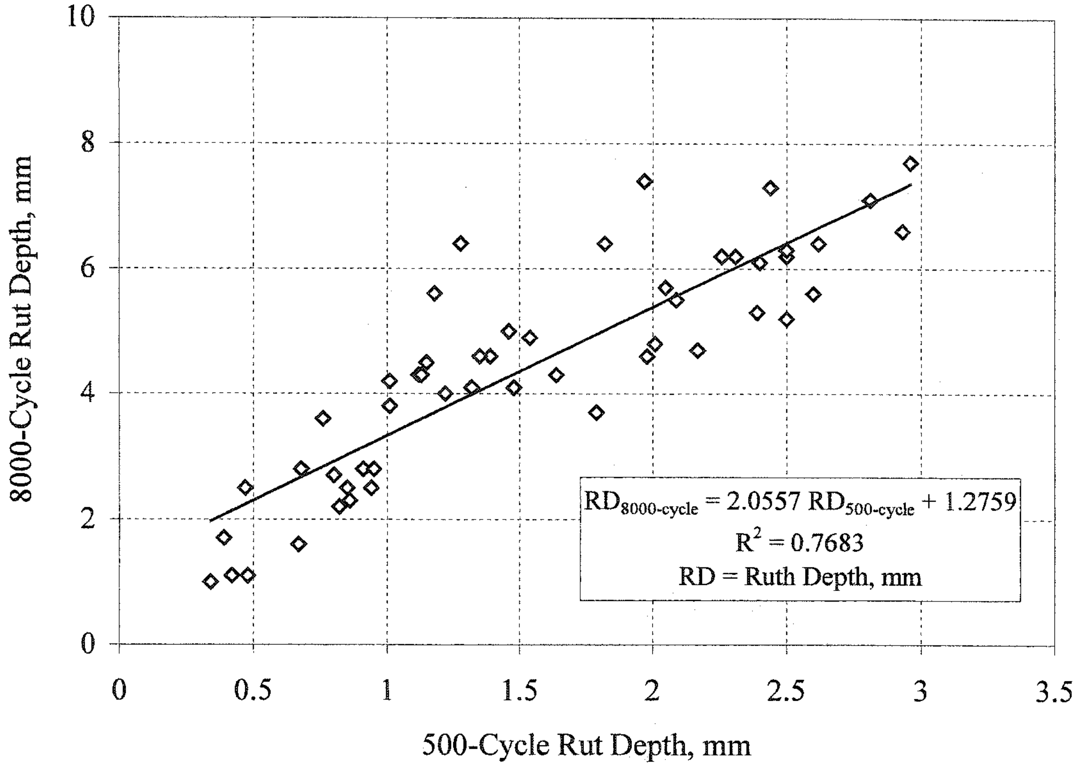

Figure 3.17 Relation Between 8000-Cycle Rut Depth and 500-Cycle Rut Depth

CHAPTER 4

A LABORATORY AND STATISTICAL EVALUATION OF FACTORS AFFECTING RUTTING

4.1 Introduction

The research presented in this chapter identifies the most significant factors from those factors evaluated, which affect rutting potential of HMA. The experimental program employed in this study consists of three sets of test, each set representing a matrix whose elements are rut parameters. In Set A, seven factors, each at two levels, are examined using a mixture of limestone aggregates designed in accordance with Superpave method. The test results are analyzed statistically. In Set B, six factors: aggregate gradation, temperature, moisture, asphalt content, load, and hose pressure are investigated using a Hveem designed mixture with gravel aggregates. One of the levels of asphalt content selected for Set B is at optimum, while the other at one percent more than the optimum. Also, an experimental Set C with five factors: temperature, gradation, moisture, load, and hose pressure is examined. In this chapter, a statistical procedure is developed and described to analyze a designed experimental program to interpret test results without the need for a full factorial approach.

4.2 Objective and Scope

The objective of this study is to quantify the effect of selected mix, load and environmental factors on HMA rutting based on APA data. A range is considered for each selected factor and tests are conducted using a combination of these factors. The test matrix is designed to minimize the total number of rut tests, while maximizing the interaction of the factors within the matrix. The objective is to obtain a set of factors for which rut is high, a set of factors for which rut is low, and a set of rut factors for which rut value lies within a certain range statistically.

4.3 Identification of Rut Factors

The mix factors include binder's performance grade, asphalt content (AC), and aggregate gradation. The load factors include wheel load and tire pressure, whereas the environmental factors include temperature and moisture.

Binder's performance grade is an important factor that influences rutting. According to the Superpave asphalt binder specification, the physical properties remain constant for all PG, but temperature at which these properties must be achieved varies from grade to grade (AASHTO MP1-93). That is, binder's viscosity (resistance to flow) at a specified temperature varies from one grade to another. The increased viscosity or resistance to flow of HMA materials can be achieved by using modified asphalt binders. In general, a HMA produced from a modified binder shows lower rut depth compared to the HMA produced from an unmodified binder (base or crudes). Also, use of excessive asphalt binder is a common cause of rutting. Shear forces developed due to repeated traffic loading in HMA is resisted by the bonding force of asphalt in asphalt film and by the frictional force acting on contacts between aggregates. If the amount of asphalt content exceeds the optimum asphalt content, there is a loss of internal friction at aggregate contacts, resulting in loads being carried by the asphalt binder rather than the aggregate. Barksdale (1993) reported that the permanent deformation in dense-graded asphalt concrete is directly related to the asphalt content. Aggregate gradation also affects rutting. A gradation having maximum density provides increased contacts and reduced air void space in the mineral aggregate. Gradation is determined by sieve analysis and is normally plotted as the total percent passing versus the sieve sizes raised to the power 0.45. Superpave method specifies a restricted zone in the 0.45-power-chart as a design guide to avoid too much natural sand in a mix. A HMA gradation passing through the restricted zone has excessive fines and thus more rut susceptibility than a HMA gradation passing below the restricted zone.

The stiffness of HMA varies with temperature due to the rheological behavior of asphalt binder in it. As the temperature increases, HMA stiffness decreases and therefore, its rut potential increases. Moisture is also an important factor influencing HMA rut potential. Moisture produces a loss of strength through weakening of the bond between asphalt cement and aggregate. The gradual loss of strength over a period of time can contribute to the development of lateral flow of HMA materials. The rate of rutting is accelerated by loss of cohesion due to moisture-induced damage in HMA. Tire pressure and wheel load can also affect rutting. An increase in tire pressure decreases the contact area between tire and pavement surface, therefore, increases the stress in HMA. As noted by Brock et al. (1999), increased stress due to vehicles having high tire pressures and heavier wheel loads can be the leading causes of increased rutting. Studies by Middleton et al. (1886) and Kim et al. (1988) have shown that truck tire pressures that increased substantially above the 482 kPa to 551 kPa (70 psi to 80 psi) levels are responsible for high rutting. In a separate study, Hudson et al. (1988)

showed that truck tire pressure is sometimes as high as 965 kPa (140 psi) and has become the primary cause of rutting. Laboratory prediction of rutting may vary depending on the type of specimens used in testing. Two specimens having identical air voids can have different orientation of aggregate (density gradient) in them, if prepared by different compaction methods. For the APA rut testing, a Superpave gyratory compactor is used to prepare cylindrical specimens, whereas an asphalt vibratory compactor is used to prepare beam specimen. Cooley et al. (1999) reported that vibratory compaction tends to result in high compaction at top and low compaction at the bottom of a specimen. Gyratory compacted specimens, on the other hand, show low compaction on the top and the bottom and significantly high compaction in the middle. Laboratory predicted rut can, therefore, vary with specimen type (cylinder or beam).

4.4 Selection of Factor Levels

All of the above mentioned factors are studied at two different levels in three sets of experiments. Table 4.1 is the list of factors and their levels used in the experimental program. There are three sets of test in this program. The test Set A consists of seven parameters. These parameters are used to prepare limestone mixes designed in accordance with Superpave method. Two different grades: an unmodified binder (PG 64-22) and a modified binder (PG 70-28) are used in preparing the HMA. Both of these binders are commonly used in Oklahoma and they meet the AASHTO MP1 (AASHTO MP1-93) requirements. The unmodified binder is produced from crude oil having a high level of asphaltenes and is known as base asphalt. The modified binder, on the other hand, typically contains 2% styrene-butadiene-styrene (SB) polymer with base asphalt.

The optimum asphalt content is 5.1% when using PG 64-22, the optimum asphalt content is 5.4% when using PG 70-28. Thus, two levels of asphalt contents chosen in this study are 5.1% and 5.4%. One of the testing temperatures is selected to be 64°C (147.2°F). This is the design pavement temperature during hot summer in Oklahoma. The other level of temperature is selected to be 60°C (140°F). This is a key temperature often used for aging of specimens for Hveem stability test (OHD L 16), retained strength test (OHD L 36) and indirect tensile strength test (AASHTO T 283). An APA rut test, conducted for 8000 cycles with 445 N (100 lb) wheel load and 690 kPa (100 psi) hose pressure, approximates the total load expected in the design life of an asphalt pavement. As noted by Brock et al. (1999), the tire pressure, which was 70 psi in the last decade, is now believed to be more than 100 psi. To reflect this trend, two wheel loads and hose pressures are selected 445 N (100 lb), 690 kPa (100 psi) and 489 N (110 lb), 760 kPa (110 psi). Moisture-induced damage especially stripping is now a concern within the pavement industry. To examine the influence of moisture, in this study, specimens are tested under both dry and wet conditions. Beam and cylindrical specimens are tested to investigate the effect of specimen type (method parameter) as well as compaction methods. Beams are excluded from subsequent testing due to the difficulty involved in the preparation of beam specimens of consistent quality using AVC. The test Set B consists of six factors namely, asphalt content, wheel load, hose pressure, test temperature, test condition, and gradation. Several designs of limestone aggregates of gradation passing through the restricted zone failed to meet the VMA required by Superpave specification. To this end gravel aggregates are chosen to meet VMA criteria required by Hveem method of mix design. It is to be noted that a

Superpave method of mix design requires its aggregate to have at least two fractured faces. A gravel aggregate has one fractured face and cannot produce a Superpave mix. Therefore, the factors in Set B and in subsequent set are from gravel mixes designed in accordance with Hveem method (OHD L 16). Two aggregate gradations: one passing BRZ and the other passing TRZ are considered. One of the levels of asphalt content is optimum asphalt content and the other level is one percent higher than the optimum asphalt content. The test Set C consists of five factors namely, wheel load, hose pressure, test temperature, moisture, and gradation. One of the levels of temperature is 66°C, which is selected to be higher than the temperature examined in Set A or Set B. The other level of temperature is chosen to be 62°C, which is the intermediate of the temperature between the levels examined in the Set A or the Set B.

4.5 Mix Information

The limestone mixture (for Set A) consists of 16 mm chips (5/8 in.), screenings, shot and sand. Mix gradation plotted on the 0.45-power-chart passes below the restricted zone, as shown in Figure 4.1. Its nominal maximum size (NMS) size is 12.5 mm (1/2 in.). The mixture is designed for serving roadway traffic levels of more than 10 million Equivalent Single Axle Loads (ESALs). The maximum number of gyrations, N_{max} is chosen to be 160 and the design number of gyrations, N_d is 100 (ODOT, 1999). Aggregates are mixed at a temperature of 163°C (325°F) and the resulting mix is aged at 149°C (300°F) for 3 hours. The gravel mixtures (for Set B and Set C) consist of 25 mm (1 in.) rock, 19.0 mm (3/4 in.) chips, screenings and crushed gravel using PG 64-22 graded binder. The gravel mix gradations (e.g., BRZ and TRZ) are also shown in Figure

4.1. The design criteria for ESALs is 0.3 to 3 million where as the mixing and aging temperatures are identical to those of limestone mixture.

4.6 Specimen Preparation

Cylindrical specimens of 75 mm (3 in.) height are compacted using a SGC at target air voids of 6 to 8%. Beam specimens of the same height are prepared using an AVC at the same target air voids. Specimen's air voids is calculated from its bulk specific gravity as determined by the CoreLok^{TM} method (OHD L 45) and mixture's theoretical maximum specific gravity (AASHTO T 209). Specimens are subjected to test temperature and moisture for 10 hours before rut testing. Specimens tested under water are subjected to vacuum saturation to a degree of 55% to 75% before preconditioning (OHD L43).

4.7 Experimental Program and Testing

Table 4.2 lists the combination of factors selected for different sets in the experimental program. The value in the row indicates the factor levels and each row represents a Trial. The vertical column represents the experimental factors. Each of the assigned columns contains each level of a factor for four times in eight Trials. The columns are said to be orthogonal or balanced, since the combination of the levels occurred the same number of times, when two or more columns of the matrix or set are formed. Each factor in the matrix is compared to all other factors in equal number of times (Taguchi, 1987). A total of 8 beam and 16 cylindrical specimens is tested under Set A. Average rut results from two beam and 4 cylinders is reported for each test. In Set B, a total of 32 cylindrical specimens are tested and average of 4 cylinders are reported for each test.

The samples in Set B are prepared with PG 64-22. Also, a total of 32 cylindrical specimens are tested to complete Set C. The samples in Set C are cylinders and contain optimum (5.1%) asphalt of type PG 62-22.

4.8 Interpreting Test Results

In Set A (Table 4.2) for limestone experiment, it can be easily seen that Trial 1 to Trial 4 with unmodified binders show higher rut values compared to those in Trial 5 to Trial 8 with modified binders. Beam specimens in Trial 2 and Trial 3 show higher rut susceptibility compared to the cylinders in Trial 1 and Trial 4. Overall rut depth of beam specimens is higher than that of cylindrical specimens. However, comparison between any of the Trial 1, Trial 2, Trial 7, or Trial 8 at 60°C (140°F) and any of the Trial 3, Trial 4, Trial 5, and Trial 6 at 64 °C (147.2°F) cannot explain the affect of temperature on rutting potential due to the interaction of other parameters. Similarly, one cannot report that wet specimens have higher rut potential over dried specimens from the Trial in Set B (Table 4.2) without a statistical analysis. Also, the effect of asphalt content, load, and pressure cannot be explained readily from the test result of Set A. Therefore, an analysis approach is necessary so that one can look at the overall trend instead of individual numbers (rut value). Again, in Set B (Table 4.2) for the gravel experiment, it is evident that mixture with gradation passing through the restricted zone has higher rut potential compared to that of the mixture with gradation passing below the restricted zone. If Trial 3 is compared to Trial 1, the asphalt content increases one percent and sample is run under water with 760 kPa (110 psi) hose pressure. The rutting increases from 6.0 mm to 7.6 mm; however, due not only to increase in asphalt content but also for changes in moisture and hose pressure. Also, from Set C (Table 4.2), it is evident that in overall, each of the trials (trials 2, 4, 6, 8) at the higher temperature, 66°C (150.8°F) shows higher rut values compared to those of mixtures at the lower temperature of 62°C (143.2°F). The effect of factors such as gradation, moisture, load, and pressure on rutting cannot be readily evaluated from the test results of Trials using Set C, as can be seen from Table 4.2.

4.9 Analysis Approach

From the above discussion, it is evident that the experimental results of this study are not enough to draw a meaningful conclusion on how the factors affect rutting. Experimental results can only make some general points about rutting contribution of some factors. A particular concern rises when attempting to evaluate and compare one factor with another, with respect to rutting contribution. Statistical analyses are useful to interpret experimental results and to demonstrate one factor's contribution to rutting compared to that of the other factor (Kyle, 1995). This study has employed a four-step statistical analysis approach for meaningful interpretation of factors' contribution to rutting from the experimental rut results presented in Table 4.2. Rut depth is considered to be the response or dependent variable. Its value depends on the rut factors, which are considered as independent variables. The important analysis steps are described below:

Step One

The sum of squares of rut depths for each factor is calculated and the factors are grouped depending on the values of the sum of squares. The higher the sum of squares for a factor the greater the influence of that factor on rutting. The sum of square values for each factor are calculated from the following formula,

$$SS_x = \left(\frac{L_{1x}^2 + L_{2x}^2}{n}\right) - \frac{\left(\sum R\right)^2}{N} \tag{4.1}$$

where

SS_x = sum of squares for factor x

L_{1x} = level sum for factor x at level 1

L_{2x} = Level sum for factor x at level 2

R = the final rut depth at 8000-cycles, mm

n = number of experiments used in calculating the level sums for level 1 or level 2

N = total number of test or experiments in a designed matrix.

Step Two

The degrees of freedom, variance and Fisher's statistic are calculated to investigate the statistical significance of a factor. Degrees of freedom are the number of independent comparisons available to evaluate rut data and used for variance calculation. The variance represents variability generally used to characterize the dispersion among the rut values. Fisher's statistic represents the significance of a factor involved in interactions with other factors (Frigon, 1997). The degrees of freedom and variance of each factor, and Fisher's statistic are calculated from the following equations:

$$df_x = n_x - 1 \tag{4.2}$$

$$V_x = \left(\frac{SS_x}{df_x}\right) \tag{4.3}$$

$$F(\text{statistic}) = \frac{V_x}{V_{err}} \tag{4.4}$$

where

df_x = degrees of freedom for factor x,

V_x = variance of factor x,

F = Fisher's statistic

V_{err} = variance of error

Step Three

The expected sums of squares are calculated to estimate the compensation for any experimental error that influences the calculation of the sum of squares. The percentage contribution is determined to estimate the portion of the variation that could be attributed to a factor (e.g., load, temperature) in the experiment. The factors are rated according to their rutting contribution at the end of this step. The expected sum of squares and the percent contribution are calculated from the following formulas,

$$SS'_x = SS_x - (V_{err} - df_x) \tag{4.5}$$

$$P_x = \left(\frac{SS'_x}{SS_t}\right) \times 100 \tag{4.6}$$

where

SS'_x = expected sum of squares for factor, x

V_{err} = variance of error

P_x = percent contribution of factor, x

SS_t = total sum of squares for all factors

Step Four

The mean rut depth for each set of factors is estimated. This is the expected result from a Trial consisting of a recommended number of factors, each at a specified level. The error of the estimate is also calculated to determine the spread that can be expected in the data. The predicted mean rut depth is calculated from the following equation,

$$RD_m = \frac{\sum RD}{N} + \sum_{i=1}^{n1}\left(L_{si} - \frac{\sum RD}{N}\right) \tag{4.7}$$

where

RD_m = predicted mean rut depth, mm

L_s = level sum for a significant factor s at its specified level

n1 = number of significant factors

RD = rut depth, mm

N = number of tests.

The estimation of the mean response is meaningful only if the spread in data is known. A range or spread in rut data is calculated by adding and subtracting the error with the predicted mean value. Sometimes, additional tests are conducted to check whether the test results are in the predicted or estimated range. The error of the estimate is calculated from the following formula,

$$R_{err} = \mathrm{sqrt}\left(\frac{F_{df_x:df_{err}} \cdot V_{err}}{n_{eff}}\right) \tag{4.8}$$

where

R_{err} = error in predicted rut depth

n_{eff} = effective number of d.o.f. for the error = N/(1+total d.o.f. for significant factors)

$F_{df_x:df_{err}}$ = F statistic associated with the specified risk level and the degrees of freedom (d.o.f.) for each factor in the experiment, df_x and the degrees of error term, df_{err}

4.10 Discussion of Results

Figure 4.2 shows rut depths as a function of loading cycles. A total of six trials (two trials from each set) are plotted. The rut depths at 8000-cycles are considered as the final rut potential of a mix. Only the final rut values (e.g., for Set-A in Trial-7, the final rut depth = 4.2 mm) are used in statistical calculation. The sums of squares, SS_x for each factor in Set A are calculated using Equation 4.1. The sums of squares are plotted in descending order of magnitude from the left to the right and points are connected by a solid line, as shown in Figure 4.3. The factors having higher sum of square values have greater effect on the rut potential compared to that of other factors. The factors along the steepest section of the graph are the more important ones and those along the flat portion or the bottom of the slope are the least important. From Figure 4.3, binder's grade is found to have the most significant effect on rutting followed by specimen type (cylindrical or beam), temperature and moisture. The remaining factors: hose pressure, percentage asphalt, and wheel load does not affect rutting significantly. Asphalt content does not show a significant effect on rutting probably because of the fact that their level used in Set A are either optimum or varies only 0.3%. In fact, a variation of asphalt content within 0.3%±optimum is allowed under Superpave mix design (ODOT, 2001). Figure 4.4 is the plot of level sum squares, SS_x against the factors involved in Set B. Temperature is the most significant factor. The gradation has the second highest effect on rutting among the parameters. From this plot, it can be seen that the effect of asphalt content is significant. This is due to an asphalt content relatively (e.g., 1%±optimum) higher than the optimum. A small variation in asphalt content, which is within ±0.3% from optimum AC, does not affect the rut value in limestone experiment of Set A. Therefore, asphalt content is even more significant than the moisture in case of gravel mix experiment of Set B. Using Equation 4.1, the sums of squares, SS_x, for each factor in Set C is also calculated. Figure 4.5 is the plot of sum of squares against the factors involved the Set C. It follows the similar trend found in Set B (Figure 4.4). Temperature is the most significant factor followed by gradation and moisture. From all plots (Figures 4.3–4.5), it is evident that the effect of wheel load and hose pressure can be neglected.

The factors that had little or no effect on rutting are grouped. The factor that resulted from the grouping of the insignificant factors is represented by error term. For Set A, three factors: wheel load, asphalt content, and hose pressure are grouped together as error term and its value is given in Table 4.3. The factor load and pressure are grouped as error in both test Set B and Set C. The total sum of squares is calculated by summing the individual factor's sums of squares. The degrees of freedom df_x, variance V_x, and Fisher's statistic F are calculated from the Equations 4.2, 4.3, and 4.4 respectively. The values of df_x, V_x, and F statistics are listed in Table 4.3. For Set A, the calculated F-statistics for the binder's grade, specimen type, temperature, and moisture are higher than the F-table values (calculated for 3 degrees of freedom for error and for 5% confidence level). Therefore, these parameters are statistically significant. For Set B and Set C, the F-statistics for temperature, gradation, AC, and moisture are higher than F-table values and therefore, the factors are statistically significant.

The expected sum of squares, SS'_x and the percent contribution, P_x are calculated from Equation 4.5 and Equation 4.6, respectively. These values are listed in Table 4.3. For Set A, it is evident that the significant factors: PG, specimen type, temperature, and moisture contributes about 88 % of rut depth for a specific trial. There are 12% of the percent contributions that could not be attributed to any of the factors examined in Set A. Similar results are found also for test Set B and Set C. This is due to interaction between factors or due to the effect of unknown factors. There are also situations where a factor may be determined to be statistically insignificant according to the F statistic, but that it may have a sizable percent contribution.

The significant factors of each test set are rated by assigning a number according to their level sums of square values. The smaller the assigned number to a factor, the higher the significance of that factor in contribution to rutting. The rating for each set is presented in Table 4.4. An overall rating for a combined set is also determined from the rating of factors in individual sets. Using the significant factor and their level for set A (Table 4.4), the predicted mean response is calculated to be 9.2 mm from Equation 4.7. The higher rut value is due to the combined effect of the significant factors (that affect rutting) in the mix. Based on this prediction, a beam specimen prepared using limestone aggregates and PG 64-22 binder exhibits a rut value of 9.2 mm tested under water at a temperature of 64° C (147.2° F) using APA. The error for the estimate is calculated to be ±1.1 mm from Equation 4.8. The spread in the rut data for significant factors is 9.2 ±1.1 mm. Therefore, the predicted rutting value can be expected to be within the range of 8.0 mm to 10.3 mm. The predicted mean rut depth, error in prediction, and expected spread of predicted rut is listed in Table 4.5. In a separate experiment, two beam specimens prepared using limestone aggregate combined by binder grade of 64-22 are tested under water at 64 ^{o} C temperature. The test results showed that rut depths of 9.3 mm and 9.7 mm are produced. These rut depths are within the predicted range listed in Table 5 for limestone experiment in Set A. This confirms the validity of the statistically predicted range of rut depth in Set A. Similarly, for Set B, the predicted rut range is 10.9 mm to 13.8 mm if the level of factors shown in Table 4.4 (for Set B) is used. The predicted rut value falls between 8.0 mm and 15.0 mm if the level of factors as shown in Table 4.4 (for Set C) is used.

4.11 Conclusions

The following is a summary of the contents of this chapter;

- Major factors that affect rut potential of HMA can be identified by using the statistical approach shown in this chapter.
- The mix factors that showed the most significant contribution to rutting for the three sets of tests examined with seven, six, and five factors respectively are:
    - Binder grade (PG 64-22 vs. PG 70-28) – This is the most significant.
    - Temperature (64°C vs. 60°C) –This is second most significant.
    - Gradation – TRZ in the gravel mixture has more rutting potential than that of BRZ.
    - Moisture or test specimens (wet vs. dry).

        - Binder content – When binder content exceeded one percent, it became a significant factor for the gravel mixture.
- The Specimen mold type (AVC Beam vs. SGC cylinder) – When included in a testing matrix, this factor becomes the second most significant factor in limestone mix. It is excluded from test sets due to difficulty in fabrication of beam specimen using the AVC.
- The rut depth and range of variation can be predicted for a matrix of factors as shown and verified for test Set A. Additional experiments should include significant factors as determined by the statistical analysis of the same matrix.
- The detailed statistical procedure such as one similar to the method developed and shown in this chapter can be applied to design and analysis of test sets involving numerous factors.

Table 4.1 Rut Factors and Levels

Factor	Set A		Set B		Set C	
	Level 1	Level 2	Level 1	Level 2	Level 1	Level 2
Binder's PG	PG64-22	PG70-28	-	-	-	-
Moisture	Dry	Wet	Dry	Wet	Dry	Wet
Temperature (°C)	60	64	60	64	62	66
Wheel Load (lb)	100	110	100	110	100	110
Hose Pressure (psi)	100	110	100	110	100	110
Specimen Type	Cylinder	Beam	-	-	-	-
Asphalt (%)	5.1	5.4	Opt.	Opt.+1	-	-
Gradation	-	-	BRZ	TRZ	BRZ	TRZ

Note: '-' means the corresponding factor (in the row) is not considered in the test matrix.

Table 4.2 Experimental Matrix of Rut Factors and Test Results

Set	Trial	PG	Gradation	Temperature (°C)	Load (N)	Pressure (kPa)	Asphalt (%)	Moisture	Specimen Type	Rut (mm)
Set A	1	PG 64-22	BRZ	60	489	760	5.1	Dry	Cylinder	5.0
	2	PG 64-22		60	449	690	5.4	Dry	Beam	6.8
	3	PG 64-22		64	489	760	5.4	Wet	Beam	9.4
	4	PG 64-22		64	449	690	5.1	Wet	Cylinder	7.0
	5	PG 70-28		64	489	690	5.4	Dry	Cylinder	2.7
	6	PG 70-28		64	449	760	5.1	Dry	Beam	5.2
	7	PG 70-28		60	489	690	5.1	Wet	Beam	4.2
	8	PG 70-28		60	449	760	5.4	Wet	Cylinder	3.2
Set B	1	PG 64-22	BRZ	60	449	690	4.5	Dry	Cylinder	6.0
	2		BRZ	64	489	760	4.5	Dry		7.1
	3		BRZ	60	449	760	5.5	Wet		7.6
	4		BRZ	64	489	690	5.5	Wet		11.4
	5		TRZ	60	489	690	4.3	Wet		8.3
	6		TRZ	64	449	760	4.3	Wet		11.3
	7		TRZ	60	489	760	5.3	Dry		10.1
	8		TRZ	64	449	690	5.3	Dry		9.9
Set C	1	PG 64-22	BRZ	62	449	690	5.1	Dry	Cylinder	4.8
	2		BRZ	66	489	760		Dry		10.6
	3		BRZ	62	449	760		Wet		5.3
	4		BRZ	66	489	690		Wet		9.1
	5		TRZ	62	489	690		Wet		7.6
	6		TRZ	66	449	760		Wet		10.5
	7		TRZ	62	489	760		Dry		10.5
	8		TRZ	66	449	690		Dry		13.2

Table 4.3 Variance, F Statistic and Percentage Contribution of Rut Factors

Test	Factors	$df_x = (n_x-1)$	SS_x	Variance, $V_x = \frac{SS_x}{df_x}$	$F_x = \frac{V_x}{V_{err}}$ (Statistics)	$F_{Table} =$ F (1,3) 0.05	SS'_x	% Contri-Bution, P_x
Set A	PG	1	20.9	20.7	102.6	10.1	20.3	58.5
	Specimen	1	7.3	7.3	36.1	10.1	6.7	19.4
	Temperature	1	2.9	2.9	14.1	10.1	2.3	6.5
	Moisture	1	1.9	1.9	9.5	10.1	1.3	3.8
	Error	3	0.6	0.2				
	Total	7	34.6	5.0				88.2
Set B	Temperature	1	7.4	7.4	21.5	10.1	7.1	25.2
	Gradation	1	7.0	7.0	20.4	10.1	6.7	23.8
	AC	1	5.0	5.0	14.4	10.1	4.6	16.4
	Moisture	1	3.8	3.8	11.0	10.1	3.4	12.2
	Error	2	0.7	0.4				
	Total	5	28.1	5.6				77.6
Set C	Temperature	1	28.9	28.8	22.1	18.5	27.6	47.6
	Gradation	1	18.0	18.0	13.8	18.5	16.7	28.8
	Moisture	1	5.5	5.5	4.2	18.5	4.1	7.2
	Error	2	2.6	1.3				
	Total	5	57.9	11.6				83.6

Note: SS_x =Sum of the Square, SS'_x = Modified Sum of the Square; df_x = Degrees of Freedom

Table 4.4 Statistical Rating of Significant Factors

Factor	Set A		Set B		Set C		Combined Rating
	Level	Rating	Level	Rating	Level	Rating	
PG	PG64-22	1	-	-	-	-	1
Specimen	Beam	2	-	-	-	-	6
Temperature	64°C	3	64°C	1	66°C	1	2
Moisture	Wet	4	Wet	4	Wet	3	4
Gradation	-	-	TRZ	2	TRZ	2	3
Asphalt (%)	-	-	Opt.+1	3	-	-	5

Note: "-" the factor (in the row) does not significantly affect rutting in the corresponding set; Opt =optimum asphalt content

Table 4.5 Statistically Predicted Mean, Error and Range of Rut

Factor	Set A	Set B	Set C
Predicted Mean (mm)	9.2	12.3	11.5
Predicted Error (mm)	1.1	1.5	3.5
Predicted Range (mm)	8.1 -10.3	10.8 -13.8	8.0 – 15.0

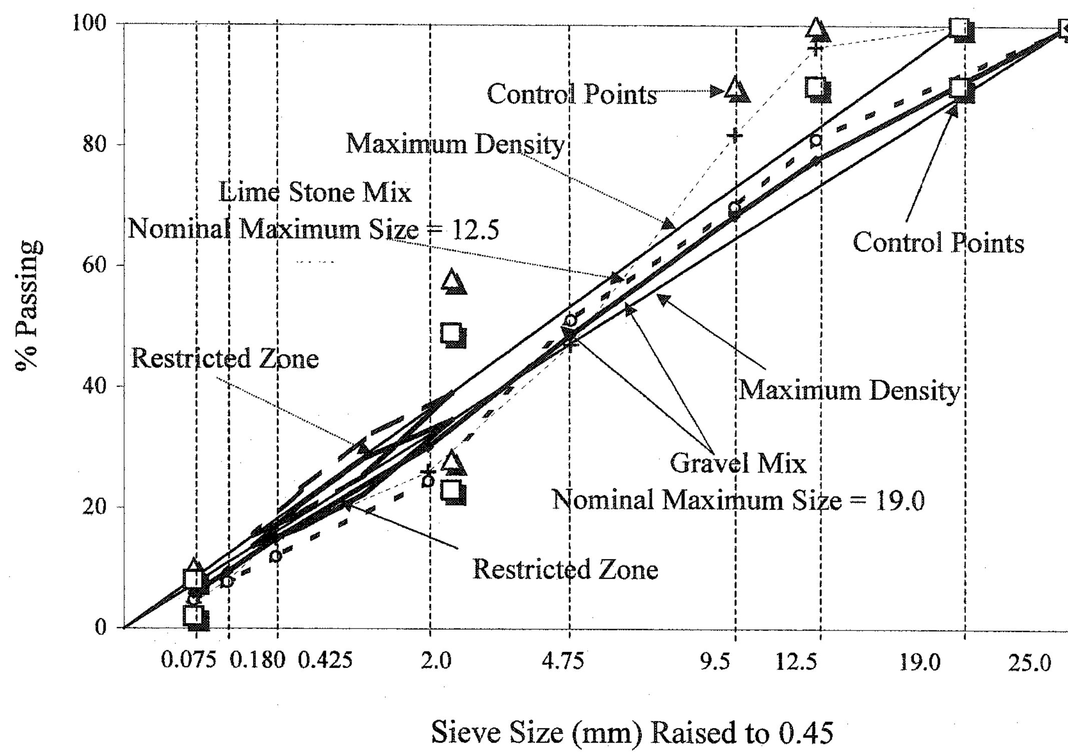

Figure 4.1 Gradation Plot for Limestone and Gravel Mixes

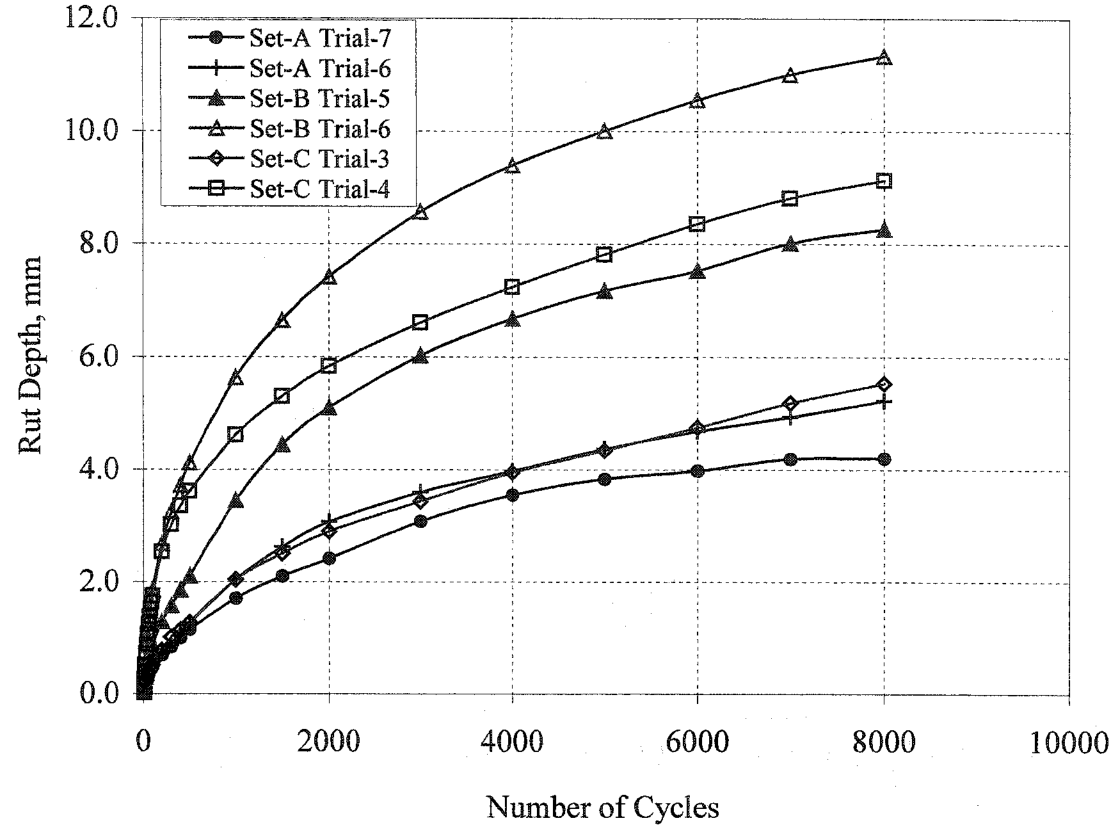

Figure 4.2 Rut Depths as a Function of Loading Cycle

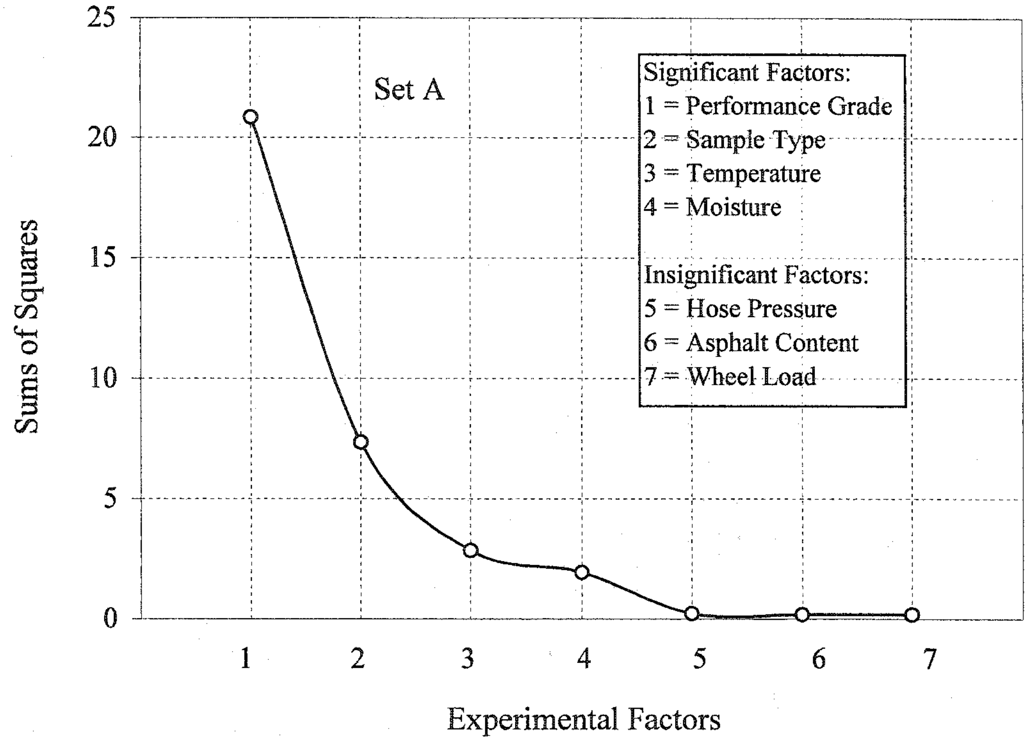

Figure 4.3 Sum of Square Versus Factor Plot for Set A

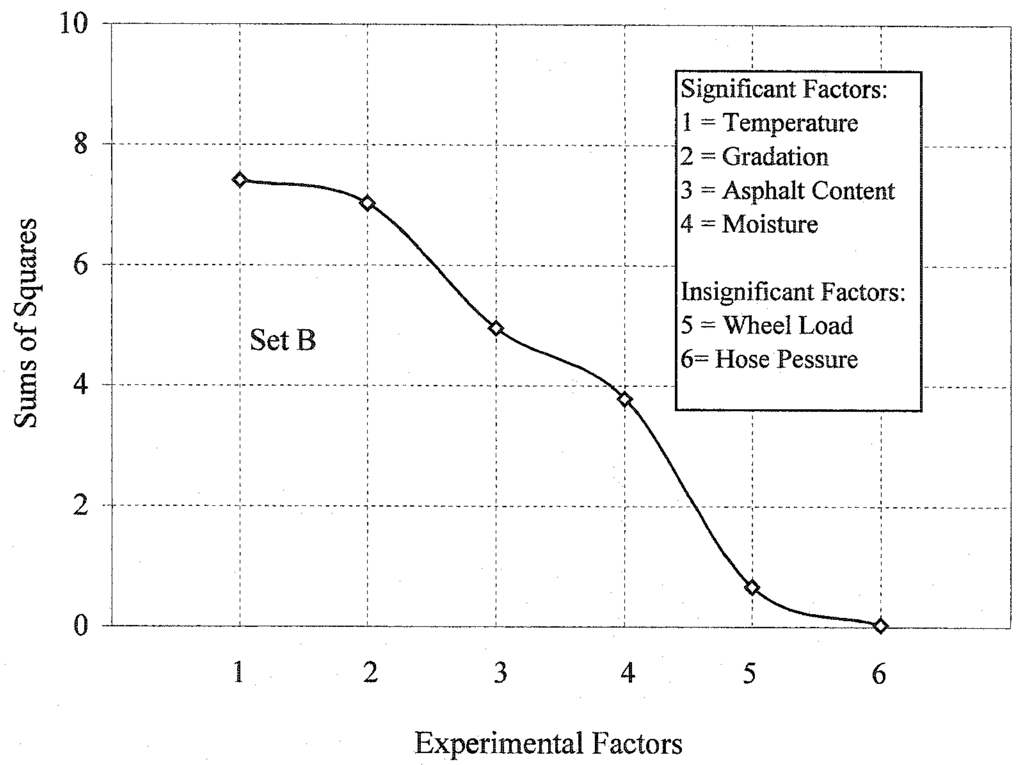

Figure 4.4 Sum of Square Versus Factor Plot for Set B

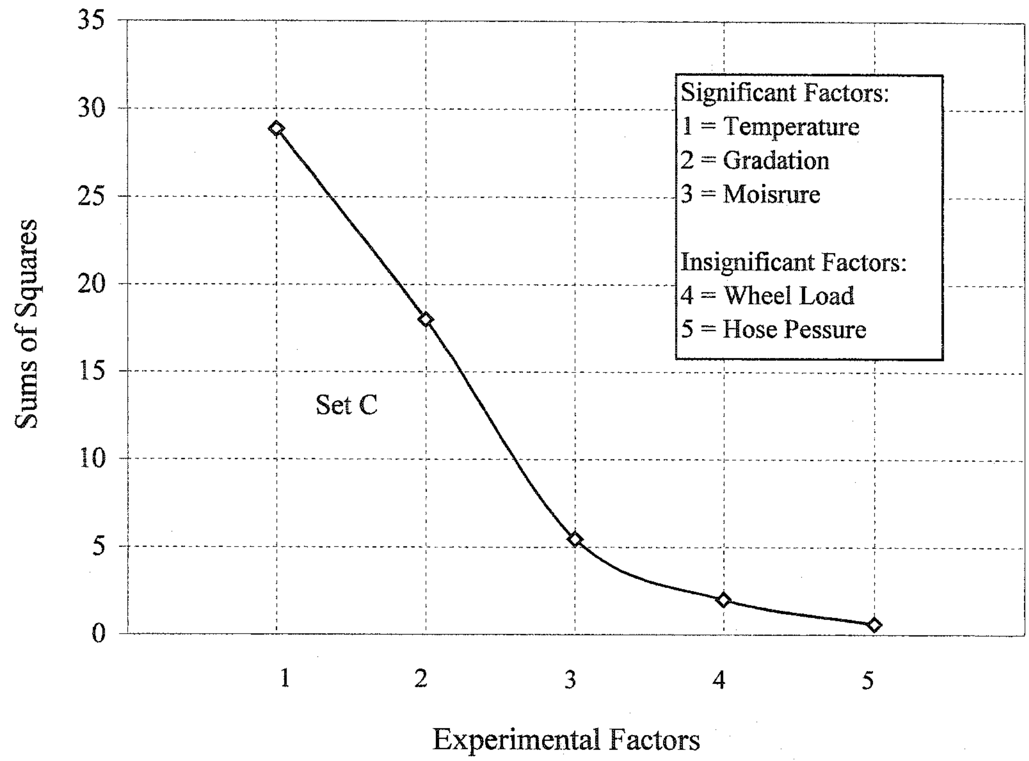

Figure 4.5 Sum of Square Versus Factor Plot for Set C

CHAPTER 5

CORRELATION OF RUTTING WITH RESILIENT MODULUS

5.1 Introduction

Resilient modulus (stiffness) is a material property and rutting is a manifestation of performance that depends on different properties and design factors. It is logical to question if an HMA mix with high resilient modulus exhibits low rut potential and vice versa. In a more broad sense, one may question if resilient modulus and APA rut potential could be correlated for HMA mixes. So far, no systematic studies are undertaken to answer these questions. This is partly because the field of resilient modulus testing of HMA specimens is largely unexplored so far. In this study, a series of modulus and rut tests are conducted to generate laboratory data to examine if resilient modulus could be correlated with the APA rutting.

Also, in recent years, there has been a change in philosophy in flexible pavement design from an empirical approach to a more mechanistic approach, based on elastic theory. According to the AASHTO 2002 guide for flexible pavement design, viscoelastic analysis is not required for asphalt concrete layer, provided the asphalt concrete's modulus (dynamic or resilient modulus) value used in design addresses appropriate loading rate (frequency) and temperature. Modulus value is used to calculate stress, strain and deflection (pavement response) in a pavement layer. The pavement responses are then correlated to the rutting and fatigue damages empirically. Thus, a pavement design procedure implicitly considers rutting and fatigue cracking.

However, this procedure does not explicitly consider mix properties and hence, provides no quantitative means for addressing the relative merits of different mixes. A performance test of asphalt concrete using the APA can close the large gap between the mix design and thickness design parameters. Therefore, the correlation of Superpave mix properties with resilient modulus and rutting is examined in this study. Laboratory resilient modulus of asphalt concrete is determined by repeated load triaxial compression tests and cyclic indirect tensile tests. However, the laboratory modulus testing of asphalt concrete is a rather complex and challenging area. It sometimes suffers from variability of results due to noise. A very small movement due to noise can change the resilient modulus of a sample by several orders. Therefore, the repeatability issue of laboratory resilient modulus testing of asphalt concrete is also addressed in this study.

5.2 Background

HMA pavement is a series of layers of aggregate and asphalt concrete. It is exposed to weather and is subjected to repeated traffic loads. The loads can be either static or dynamic. If the loading (dynamic) time is short, the viscous effect of viscoelastic materials such as asphalt concrete is small. That is, the material can be assumed to act elastically under short dynamic load. Therefore, under an individual loading cycle, pavement layers are assumed to behave essentially elastically (resilient strain), although plastic deformation (rutting) can accumulate with repeated cycles. Among the common methods to measure the elastic properties of asphalt concrete (Young's, shear, bulk, dynamic, complex, resilient, and Shell nomograph moduli), the resilient modulus is the most appropriate for use in multiplayer elastic theories (Huang, 1993). Resilient modulus is defined as the ratio of applied stress (transient stress within a layer) to the strain induced by the transient load (moving wheel load). Resilient modulus tests in the laboratory involve cyclic loading. Evaluation of rutting potential of HMA using an APA also involves cyclic loading. While the APA rut testing is considered to be a practical approach by the mix designer, resilient modulus testing is believed to be a rational approach by the pavement designer. Finding the correlation between rutting and modulus can have tremendous positive impacts on transportation community's continued effort to implement Superpave mix design with AASHTO 2002 pavement design.

Resilient modulus is an important material property in the mechanistic design of flexible pavements (NCHRP, 2002). It defines the relative efficiencies of different layers to distribute load-induced stresses within a pavement system. When used in a layered system analysis, it is an important property in predicting pavement thickness. If the design resilient modulus value is too high, the thickness of the pavement layer becomes insufficient. If, on the other hand, the design resilient modulus value is too low, the thickness is conservative but costly. It is, therefore, important to know the factors that influence the laboratory determination of resilient modulus of asphalt concrete. One important question whose answer would be very useful for AASHTO 2002 Guide for Pavement Design is: is it possible to determine resilient modulus of asphalt samples in the laboratory reliably? In the process of seeking an answer, this study addresses the issue of repeatability of resilient modulus testing in the laboratory.

Also, the variation of resilient modulus with temperature, mix properties and test methods are discussed.

5.3 Objectives And Scope

The primary objective of this study is to explore relationship(s) between resilient modulus (both triaxial and diametral), if any. The other objective is to examine the correlations of parameters such as: temperature, asphalt content, binder's PG and air voids with resilient modulus and rutting. Another objective is to address the issue of repeatability in laboratory resilient modulus testing of asphalt concrete. Because both rut values and resilient modulus values depend on various factors including temperature, compaction (air voids), asphalt content, and binder grade, only these factors are considered in this study to the extent allowed by the laboratory data. Two mixes: one is an unmodified binder mix with high rut potential and the other is a modified binder mix with low rut potential are included in this research.

5.4 Overview of Modulus Testing Protocol

A typical resilient modulus test using a cyclic triaxial apparatus involves application of various stress and loading sequences. For unbound materials such as aggregate and soil, the testing protocol is relatively well established (e.g., AASHTO T 307-99; ASTM D 5311-92). For such materials, the resilient modulus test is conducted by first placing a specimen in the triaxial cell (Witczak et al., 2002). The specimen is subject to an all-around confining pressure (σ_3), and a cyclic axial or deviatoric stress, σ_d ($\sigma_d = \sigma_1 - \sigma_3$); where, σ_1 represents the axial stress applied to the specimen. The resulting recoverable axial strain, ε_γ, is determined by measuring the recoverable deformation across a known gauge length or the total sample height. The resilient modulus is calculated by using the following expression:

$$M_r = \frac{\sigma_d}{\varepsilon_\gamma} \tag{5.1}$$

where

M_r = resilient modulus

σ_d = cyclic deviatoric stress

ε_γ = resilient strain.

For asphalt concrete, however, there is no widely accepted procedure within the framework of repeated load triaxial test methods. A protocol for cyclic triaxial testing is adopted based on the literature review, personal contacts and experience (Zaman and Zhu, 1999). The test is conducted applying a haversine wave shaped load pulse having duration of 0.1 sec and a rest period of 0.9 sec (loading frequency of 1 Hz). Depending on the loading characteristic, a triaxial modulus can be called dynamic modulus or triaxial resilient modulus. The difference between a triaxial resilient modulus test and a dynamic modulus test for asphalt concrete is that the former uses loading of any form with rest period, while the latter applies a sinusoidal or haversine loading with no rest period.

Another method commonly used to evaluate the resilient modulus of asphalt concrete samples involves application of cyclic loading diametrically (Figure 5.1), instead of axially (ASTM D 4123 or AASHTO TP31-96). Indirect or diametral tensile resilient modulus testing provides an insight into the ability of a material to function in an environment that produces tensile stresses. These tensile stresses may be load-induced or non-load-induced (e.g., environmental). In this testing procedure, diametral deformations along vertical and lateral directions, and vertical load are measured precisely. The lateral deformation is determined from the deviatoric stress and recoverable vertical strain. The Poisson's ratio is evaluated from the ratio of the lateral and vertical strains. According to Brown and Foo (1989), the ASTM D 4123 testing protocol suffers from the lack of accuracy and precision and some agencies have expressed lack of satisfaction. Barksdale et al. (1997) showed that the repeated load diametral test is the most practical and realistic method for evaluating resilient modulus of asphalt concrete (AASHTO TP31-96). The resilient modulus measured by indirect tensile test is selected by engineers (ASTM D 4123 or AASHTO TP 31-96), whereas the researchers have used resilient modulus measured by repeated load triaxial tests. The reason for selecting indirect tensile test is mainly because of the thin lifts of pavement. Cores or sample extracted from thin lifts cannot satisfy the sample criteria (height to diameter ratio of 1.5 to 2) for triaxial tests. Some researchers so use the cyclic indirect tensile test to measure resilient modulus. But this test method cannot accurately simulate the stress conditions encountered in real pavement systems. The diametral test, however, does reasonably simulate the stress conditions existing at the bottom of the asphalt concrete layer. While practical tests are needed to help today's engineers and to improve quality control and quality assurance, research to understand fundamental mechanisms are pursued in this study. Subsequent to these studies, both deformation and load measurement techniques and equipment (LVDTs, load cell) have improved considerably. Therefore, the reliability of the resilient modulus value obtained using this protocol is examined (AASHTO TP31-96 with surface gage-point-mounted LVDTs). The expression for calculating the diametral tensile resilient modulus is derived in the next paragraph.

If a plastic disk or cylinder is loaded diametrically (Figure 5.1), from the theory of elasticity and photoelastic analyses, it is possible to determine the elastic modulus of the material. It can be mathematically shown that this load gives rise to a uniform tensile stress along the horizontal diametral plane of the sample (Timoshenko and Goodier, 1951). The expressions for the total normal stress on the vertical plane, σ_x and the total normal stress on the horizontal plane, σ_y can be found in the literature as given below (Frocht, 1948):

$$\sigma_x = 2P/\pi t d \, [1 - 16 d^2 x^2/(d^2 + 4x^2)^2] \tag{5.2}$$

$$\sigma_y = 2P/\pi t d \, [1 - 4 d^4/(d^2 + 4x^2)^2] \tag{5.3}$$

where

x = the distance from the origin along the abscissa (horizontal)

y = the ordinate from the origin along the ordinate (vertical)

t = thickness of the disk (sample)

d = diameter of the disk (sample)

P = applied laod

Assuming plane stress condition and elastic behavior, the expression for the horizontal strain, ε_x can be given as:

$$\varepsilon_x = 1/E \, [\sigma_x - \nu(\sigma_y - \sigma_z^0)] \tag{5.4}$$

where

E = Young's modulus

σ_Z = plain stress, which is zero

ν = Poisson's ratio.

Under short-duration dynamic loads on a viscous materials (such as asphalt concrete), the viscous effects are small and the apparent Young's modulus, E, is frequently referred as the resilient modulus, M_r. By substituting σ_X and σ_Y from Equation (5.4), the following expression can be obtained:

$$\varepsilon_x = 2P/M_r \pi td[(4d^4\nu - 16d^2x^2)/(d^2+4x^2)^2 + (1-\nu)] \qquad (5.5)$$

The total horizontal deformation, Δ_h is given by,

$$\Delta_h = \int_{-d_g/2}^{d_g/2} \varepsilon_x dx \qquad (5.6)$$

where, d_g = gage length for the mounted horizontal LVDTs. By substituting ε_X and integrating between the limits $\pm$ d_g, the following equation can be shown:

$$M_r = 2P/\Delta_h \pi td[d^2 d_g^3 + \nu) + (1+\nu)\{d_g^3\ 2d(d^2+d_g^2)\tan^{-1}(d_g/d)\}]/(d^2+d_g^2) \qquad (5.7)$$

Equation (5.7) is used to calculate indirect tensile resilient modulus of asphalt concrete in this study.

5.5 Testing Plan

Both triaxial and diametral resilient modulus tests are conducted on two replicate specimens for each of the six mixtures (2 binders x 3 asphalt content) evaluated in this study. The aggregate source (limestone) and gradation of the mixes are conformed to the dense graded surface course mixture used by the Oklahoma DOT (ODOT, 2002).

For each mixture tested, a full factorial of test temperatures (0, 23, 40°C) and 1.0 Hz frequency are used. Each specimen is tested in an increasing order of temperature, that is, 0, 25, and 40°C. This temperature-frequency sequence is carried out to cause minimum damage to the specimen before the next sequential test. This is due to the fact that at cold temperatures, the material behaves stronger compared to warmer temperatures. A total of 72 (2 binders x 3 asphalt contents x 2 test methods x 3 temperatures x 2 replicates) resilient modulus tests are conducted. Mixes (asphalt samples) are designed according to the Superpave procedure (Roberts, et al., 1996). Also, a total of 48 (2 test methods x 3 temperatures x 8 tests) triaxial resilient modulus tests are conducted on one mix to address the issue of repeatability in resilient modulus testing. Thus, for two mixes a total of 120 modulus tests are conducted in this study. In fact, the actual test matrix included a number of exploratory tests in addition to the 120 tests. For example, some of the specimens are tested twice at different orientations (0° and 180°). The average of the two test results is reported as the final resilient modulus. Also, a total of 12 sets of APA rut tests are conducted. Rut value from each set represents an average of the rut of two specimens.

5.6 Sample Preparation

The triaxial resilient modulus specimens are prepared in a rather unique manner for this study. For a given mix type, a 150 mm (6 in.) diameter gyratory specimen is compacted at the specific design asphalt content. The compaction is achieved using the SGC at a wide range of air voids level (4 to 12%). The specimen is compacted to an approximate height of 175 mm (7 in.). Upon extrusion, the SGC specimens are measured for density and then cored using a heavy-duty asphalt-coring machine. The ends of the cored specimens are trimmed by a double bladed saw. Each core had a diameter of 100 mm (4 in.), an approximate height of 150 mm (6 in.) and therefore complied with a minimum height to diameter ratio of 1.5 for dynamic modulus evaluation (Witczak, 2002). For, indirect tensile resilient modulus test, the final triaxial sample is cut into two pieces with a double bladed saw. The final dimensions of the specimen for diametral tests are approximately 100 mm (4 in.) diameter and 75 mm (3 in.) height. Air voids of the specimens are determined using the CoreLok™ sealing method (InstroTek Inc., 2002). Other volumetric properties are also evaluated and used in statistical correlations and interpretations of test results.

5.7 Testing

A Material Testing Service (MTS) electro-hydraulic test system is used to load the specimens. The resilient modulus is measured by applying a computer-generated 1 Hz haversine load with a loading duration of 0.1 sec and a rest period of 0.9 sec on unconfined specimens (if the rest period is zero, the resilient modulus is equivalent to the dynamic modulus). The load is measured through the MTS load cell, whereas, the deformations are measured through two spring-loaded LVDTs (Linear Variable Differential Transformers) of 2.54 mm (0.1 in.) stroke length, connected to a 16-bit resolution analog-to-digital converter and a real time interface using LabVIEW (Laboratory Virtual Instrument Engineering Workbench). These LVDTs are clamped vertically on diametrically opposite specimen sides. Parallel clamps are placed approximately 100 mm (4 in) apart and located 2.54 mm (1 in.) from the top and bottom of the specimen used to secure the LVDTs in place.

Modulus tests are conducted within an environmental chamber throughout the testing sequence (i.e., temperature is held constant within the chamber to ±1°C throughout the test). After a test at a given temperature has been completed, the new temperature is adjusted in the chamber for the next test and specimens stored within the chamber to reach the new equilibrium temperature. This required a time period of generally 18 to 24 hours for the specimen to reach and maintain the required test temperature. As noted from this description, all triaxial resilient modulus tests are conducted in accordance with a procedure similar to AASTHO T 307-99; ASTM D 5311-92. For triaxial tests at room temperature (23°C), the range of resilient stress is 138.9 to 206.8 kPa (20 to 30 psi) for a cycle range of 50 to 100 cycles. For preconditioning, a stress in the range of 34.5 to 68.9 kPa (5 to 10 psi) is used for a total of 500 cycles. However, the applied loads and cycles differed from sample to sample along with temperatures.

Rut tests are conducted on specimens prepared with a dimension of 75 mm (3 in.) height by 150 mm (6 in.) diameter using the SGC. These specimens are preconditioned at testing temperature of 64°C for a minimum of 10 hours. The temperature of 64°C is found to be suitable for laboratory rut testing in Oklahoma's environment (Tarefder and Zaman, 2002). The preconditioned specimens are then tested for rut in accordance with the APA testing protocol (PTI, 1999). In this procedure, the rutting potential of an asphalt sample is determined by applying a vertical wheel load of 445 N (100 lbs) through pressurized hose with a pressure of 700 kPa (100 psi) for 8000 cycles. The rut depths are measured as a function of load cycles. The 8000-cycle rut depth is reported as final rut potential of asphalt concrete.

5.8 Results and Discussions

Table 5.1 shows mix parameters, test parameters, modulus and rut test results from the laboratory. The sample numbers are placed in ascending order in column 1. The column 2 shows two mixes of which one is modified binder (PG 70-28) and the other is unmodified binder (PG 64-22). Three asphalt contents, one at optimum, one at below 0.5% optimum, and the other at 0.5% above the optimum asphalt content are used in each case of the binders. The difference in air voids in replicate (by PG and % asphalt) samples are due to the tedious methods of long sample preparation for three different tests (rut, triaxial, diametral) methods. Results of a total of 36 cyclic resilient modulus tests and a total of 36 diametral resilient modulus tests, and 12 rut tests are shown in Table 5.1. Over all, the triaxial resilient modulus has higher value compared to those of diametral resilient tests. Also, modulus value at a lower temperature is higher than that at a higher temperature. Overall, the modified binder mix (PG 70-28) showed a lower rut potential and higher triaxial resilient modulus compared to those of unmodified mix (PG 64-22). Table 5.1 is discussed further subsequently. In the next section, the rut and modulus factors are interpreted using graphical method and statistical analysis.

5.9 Correlations of Mixture Properties

In Table 5.2, the correlations of mix properties, namely asphalt content, air voids, and percentage binder with resilient modulus and rut depth are shown. As always, the correlation matrix (Table 5.2) is a symmetric matrix. In a particular row, it can be seen that PG grade has the highest correlation (coefficient of correlation = - 0.438) with the diametral resilient modulus at 23°C. However, this correlation is very poor for interpretation. The negative correlation means that the use of unmodified binder has decreased resilient modulus values. The PG grade has a positive correlation with rutting, which means the use of unmodified binders has increased rutting. Similarly, from the third row, it can be seen that the correlation of binder with triaxial resilient modulus at 0°C is –0.443, which means increase in binder content has resulted in decreased triaxial resilient modulus. In general, it appears to be difficult to interpret the limited test results based on this correlation. Therefore, a graphical interpretation is pursued subsequently.

5.10 Asphalt Content, Performance Grade and Modulus

Figure 5.2 (a) shows that the modulus value is lower at higher temperature, as expected. At 40°C, if the diametral modulus values at different asphalt contents (5.1%, 5.6% for unmodified binders) are compared, it can be seen that the resilient modulus at optimum (5.1%) asphalt content is lower than those at an asphalt content of 5.6%. This may be due to the fact that the increased asphalt content increases the thickness of the binder film between aggregate particles, thereby, an increased proportion of asphalt acts to resist the applied tensile stress over a cross-section normal to the direction of applied load.

Tensile strains are concentrated in the asphalt binder (binder is much more compliant than the stiffer aggregate particles) and thicker films result in smaller binder strain when the added asphalt does not alter the overall mixture strain. Moreover, because tensile stresses must ultimately be transferred through the asphalt, more asphalt means more asphalt area in a cross-section and hence, less stress in the asphalt. However, the diametral modulus at 40°C and 4.6% asphalt is higher than that at 40°C and 5.1% asphalt. Thus, the effects of asphalt content can be further complicated by the related effects of asphalt content on mix stiffness and, as a result, on the stresses and strains.

5.11 Air Voids and Resilient Modulus

From Figure 5.2 (b), it can be seen that the samples (modified asphalt) with air voids of 12.1% and at 8.6% show slightly lower triaxial resilient modulus than those of the samples with 4.2% and 4.7% air voids. The modified asphalt samples with 5.5% and 7.4% air voids have the highest triaxial resilient modulus. Therefore, air voids have higher influence on the diametral resilient modulus values than that on triaxial resilient modulus values. Overall, a resilient modulus value changes with a change in air void. Therefore, resilient modulus testing sample should be cored from the 150 mm (6 in) sample to a 100 mm (4 in) to reduce the density gradient in the final core.

5.12 Asphalt Content and Rut Depth

Figure 5.3 illustrates that the rut potential of an asphalt concrete increases as the amount of binder content increases. If the rut depths of specimens containing modified binder are compared with the rut depths of specimens containing unmodified binder, it can be seen that modified binders have lower rut depth than the unmodified binders. Also, the modified binder mix is more sensitive to the percentage asphalt content.

5.13 Air Voids and Rut Depth

The plot in Figure 5.4 shows that rut depths do not vary significantly for the air voids within 6% to 8% for all cylindrical specimens. The regression line between the rut depth and air voids for the modified asphalt binder shows a good correlation. From Figure 5.4, it can be seen that rut depth is smaller at smaller air voids in the range of 5% to 12%. A smaller air void content affects rutting in mainly two ways. First, because air transmits little or no stress, replacing some of its volume with asphalt and aggregate reduces the stress level in these components. Second, a sample having smaller air voids creates a more homogenous asphalt-aggregate structure. Whereas, one with fewer or smaller air voids results in less stress concentration at solid and air interfaces. Reduced air voids can increased stiffness and decreased rut potential of asphalt materials.

5.14 Diametral and Triaxial Resilient Modulus Relationship

Figure 5.5 compares the repeated load triaxial resilient modulus to the repeated load diametral (or indirect tension) resilient modulus at three different temperatures. For all cases the correlation between the diametral resilient modulus and triaxial resilient modulus is very poor. The correlation coefficient between these two moduli at 40°C is better than that at other temperatures. The triaxial resilient modulus is about 5 to10 times higher than the diametral resilient modulus for most cases. The data is very scattered as shown in Figure 5.5. This is probably due to the complexity of resilient modulus testing (Monismith, 1989).

5.15 Repeatability of Modulus Testing

Several factors may contribute to the variability (or accuracy) associated with resilient testing. Experimental error may include operator, specimen preparation, equipment setup, equipment calibration, and the testing environment. In order to quantify the error due to operator, a sample of PG 64-22 mix (asphalt content = 4.6%, and air voids = 5.4%) is prepared and tested for 16 times by two operators (namely, Operator A and Operator B). The same sample is tested using a triaxial apparatus at 0°C. These test results are presented in Figure 5.6. It can be seen that the modulus test results at 0°C vary randomly for a particular operator. This may be due to the difference in test setup (load cell contact with the sample, signal conditioner adjustments, MTS operation) by a specific operator. For an example, the load cell used in this study has a resolution of 13.4 N (3 lb). Using this load cell, an operator may apply a target contact load of 44.4 N (10 lb) in one test, however, the same operator may be off from the target with an amount of ±13.4 N (3 lb) in another test. However, both of these tests are considered to be performed at the same testing condition. Therefore, several duplicate tests were conducted for a given testing conditions and test results having extreme deviation from the average, were rejected.

Triaxial modulus test results at 23°C and 40°C by operator A are plotted in Figure 5.6. It is evident that the variation in the test results is due to temperature. At higher test temperature, the random variation in test results is less than that at lower testing temperature. This may attribute to the measurement error due to smaller deformation (strain) at lower temperature. Also, results from a total of 42 tests are listed in Table 5.3 to compare the repeatability between triaxial and diametral tests. For each set of tests (number of observation) mean, standard deviation (stdev), % error (stdev/mean), and coefficient of variance are calculated. These values are listed in Table 5.3. The mean value is an indication of the average performance over all tests, while coefficient of variance is an indication of the variation in different test results. Overall, the coefficient of variance in diametral tests is smaller than that in triaxial resilient modulus tests. The variance in diametral resilient modulus test at a higher temperature is higher than that at a lower temperature. Therefore, a diametral resilient modulus can provide a better confidence level at lower temperature. However, the triaxial resilient modulus test shows a lower coefficient of variance at higher temperature. When comparing diametral modulus to triaxial modulus, the diametral modulus is more reliable at lower temperature, whereas the triaxial resilient modulus is more reliable at higher temperature.

5.16 Relationship Between Modulus and Rut

Figure 5.7 shows the correlation between resilient modulus and rut potential at different temperatures for both triaxial and diametral cases. The regression plots at 40°C and 0°C are linear plots, while the regression plot at 23°C is an exponential plot (the exponential plot has a better R^2-value compared to that of a linear plot). At 0°C, the diametral resilient shows a better correlation compared to those at the other two temperatures. The regression coefficient for triaxial modulus is lower than that for diametral resilient modulus. Over all, the correlations are very poor. The poor correlations can be explained due to the mechanistic differences (stress level, strain, temperature, loading cycle etc.) between modulus and rut tests. The applied stress for an APA rut test is in the range of 689.5 kPa to 758.5 kPa (100 psi to110 psi), whereas the applied stresses for resilient modulus tests (triaxial and diametral) are in the range of 138 kPa to 206 kPa (20-30 psi). The corresponding deformations in modulus tests are elastic (small). The deformation in rut test is elasto-plastic (high). The number of cycles in a laboratory rut test is 8000 preceded by a preconditioning for 50 cycles. The testing cycle for modulus is only 50 for triaxial test and 30 for diametral test. The preconditioning cycle is 500 for a triaxial test and 90 for a diametral test. Also, rut test is performed at 64°C with a preconditioning of the sample at 60°C for at least 10 hours. Modulus testing temperatures are much lower (0°C, 23°C, 40°C) than rut testing temperatures. The samples for modulus testing are preconditioned at testing temperatures for at least 10 hours. The loading time (number of cycles) for rutting is approximately 2½ hours (or 8000 cycles), whereas the loading time for modulus testing is less than 1 minute (30 to 50 cycles).

From the above statistics, it is evident that there are a number of differences between modulus and rut testing parameters. However, the choice of the combinations of temperatures and loading time for each test is appropriate and logical. Rutting is expected to occur at higher temperatures and with higher cycles of load applications, whereas modulus should represent stress-strain properties of HMA at intermediate temperatures and lower loading cycles. These differences in temperature, stress level, and loading cycles result in poor correlations between modulus and rutting for the same set of mixtures. A multiple linear regression analysis is also performed and regressions equations (as shown in Table 5.2) are developed to predict rutting using asphalt content, binder's PG, percentage air voids and resilient modulus at a specific temperature as descriptors. The regression equation relating diametral resilient modulus at 40°C has the highest coefficient of determination (R^2 = 0.267). The diametral resilient modulus at higher temperature may have better correlation with rutting. This would require further testing at higher temperatures, which was not performed in this study.

5.17 Concluding Remarks

- Overall, the modified binder mix (PG 70-28) showed a lower rut potential and higher triaxial resilient modulus compared to those of an unmodified binder mix (PG 64-22).
- Although rut potential of an asphalt concrete increases as the amount of binder increases, the correlation of modulus and asphalt content is poor.
- The correlations between air voids with rut and resilient modulus is not clear from this study. This may be due to relatively few tests (72 modulus tests) performed in this study.
- The triaxial resilient modulus shows higher values compared to those of diametral resilient modulus tests.
- Modulus value at lower temperatures is higher than that at higher temperatures.
- The coefficient of variance (%error) of diametral resilient modulus testing is smaller than that in repeated load triaxial resilient modulus tests. The diametral

resilient modulus test can provide a higher level of confidence, at least in an overall sense, compared to a triaxial resilient modulus test.

- Conducting the resilient modulus tests is complex and difficult. The end results can be influenced by several factors. A laboratory resilient modulus measurement may not always be repeatable and/or reliable, at least from a practical point view. One must be very cautious in using laboratory resilient modulus in level 1 pavement design according to AASHTO 2000 guide.
- A poor relationship exists between the laboratory triaxial resilient modulus and the APA rut values. When multiple regression analysis is performed based on selective descriptors (%air, asphalt content, binder's PG), it is found that the diametral resilient modulus at 40°C has a relatively good correlation with rut potential of an asphalt mix. If diametral resilient modulus tests at a higher temperature with several aggregate gradations and mixes are conducted, it would be interesting to see whether the correlation between resilient modulus and rut improves.

Table 5.1 Matrix of Laboratory Test Results

Sample No	Binder Grade	% Binder	% Air Voids	Triaxial Resilient Modulus, psi (10^5)			Diametral Resilient Modulus, psi (10^5)			Rut Depth (mm)
				0°C	23°C	40°C	0°C	23°C	40°C	
1	PG 64-22	5.1	7.6	51.6	2.91	1.48	7.63	6.00	1.24	5.2
2	PG 70-28	5.4	4.7	55.3	5.87	1.74	5.45	3.78	1.98	2.6
3	PG 70-28	4.9	5.5	55.0	6.77	3.59	8.53	4.02	1.99	1.7
4	PG 70-28	4.9	7.4	26.0	4.16	1.91	8.67	4.09	2.10	2.0
5	PG 64-22	4.6	6.5	55.7	17.4	2.12	6.02	5.79	2.28	4.8
6	PG 64-22	4.6	3.4	47.3	20.1	10.1	5.92	5.84	2.26	4.2
7	PG 64-22	5.6	3.1	57.3	9.13	5.13	4.50	3.51	3.30	6.0
8	PG 64-22	5.6	10.1	23.4	13.4	11.4	4.56	3.81	3.01	7.8
9	PG 70-28	5.9	12.1	6.01	3.02	2.02	6.79	5.20	0.951	6.3
10	PG 70-28	5.9	8.6	6.28	4.28	3.28	6.85	5.10	0.939	5.2
11	PG 70-28	5.4	4.2	2.52	15.2	12.2	6.14	4.08	2.04	2.3
12	PG 64-22	5.1	4.5	2.61	4.13	2.13	7.96	6.85	1.24	5.0

Note: 1 psi = 6.894 kPa

Table 5.2 Correlation Matrix and Multiple Linear Regression Results

Correlation Matrix	Triaxial RM, °C	PG Grade	% Binder	% Air Voids	Triaxial RM 23°C	Triaxial RM 40°C	Diametral RM 0°C	Diametr al RM 23°C	Diametral RM 40°C
Triaxial RM 0°C	1	-0.389	-0.6	-0.641	0.298	-0.112	0.496	-0.111	-0.164
PG-Grade	-0.389	1	0.345	0.228	-0.397	-0.164	-0.384	-0.438	0.36
% Binder	-0.6	0.345	1	0.477	-0.443	0.044	-0.19	-0.345	-0.333
% Air	-0.641	0.228	0.477	1	-0.375	-0.192	-0.39	0.039	0.114
Triaxial RM 23°C	0.298	-0.397	-0.443	-0.375	1	0.715	0.58	-0.023	-0.532
Triaxial RM 40°C	-0.112	-0.164	0.044	-0.192	0.715	1	0.503	-0.291	-0.514
Diametral RM 0°C	0.496	-0.384	-0.19	-0.39	0.58	0.503	1	-0.595	-0.618
Diametral RM 23°C	-0.111	-0.438	-0.345	0.039	-0.023	-0.291	-0.595	1	0.361
Diametral RM 40°C	-0.164	0.36	-0.333	0.114	-0.532	-0.514	-0.618		1

<u>Multiple Linear Regression Results</u>

Triaxial RM, 0°C	$Rut = -9.838 - 0.841\,(PG) + 3.202\,P_b - 0.32A_v + (RM_0)\,0.2155 \times 10^{-6}$	$R^2 = 0.457$
Triaxial RM, 23°C	$Rut = -9.0 - 0.787\,(PG) + 3.12\,P_b - 0.30A_v + (RM_{23})\,0.6317 \times 10^{-6}$	$R^2 = 0.464$
Triaxial RM, 40°C	$Rut = -6.703 - 0.876\,(PG) + 2.746\,P_b - 0.359A_v + (RM_{40})\,0.7373 \times 10^{-6}$	$R^2 = 0.457$
Diametral RM, 0°C	$Rut = -7.439 - 0.859\,(PG) + 2.858\,P_b - 0.362A_v + (RM_0)\,2.544 \times 10^{-6}$	$R^2 = 0.442$
Diametral RM, 23°C	$Rut = -5.179 - 1.117\,(PG) + 2.756\,P_b - 0.367A_v - (RM_{23})\,1.67 \times 10^{-6}$	$R^2 = 0.441$
Diametral RM, 40°C	$Rut = 3.006 - 0.184\,(PG) + 1.484\,P_b - 0.278A_v - (RM_{40})\,6.9 \times 10^{-6}$	$R^2 = 0.580$

Note: P_b = %asphalt content, A_v = % air voids, RM =resilient modulus, PG= performance grade

Table 5.3 Repeatability Statistics of Resilient Modulus

Modulus Test Method	Temperature (°C)	Number of Observation	Mean (psi)	Standard Deviation	% Error	% CV
Diametral Resilient Modulus	0	6	1766945	147425	8.3	3.04
	23	10	408119	38183	9.4	4.51
	40	6	204075	40098	19.6	8.02
Triaxial Resilient Modulus	0	12	5381300	800700	14.9	11.21
	23	12	303190	49800	16.4	9.8
	40	12	144190	2430	1.7	3.71

Note: CV = Coefficient of Variance

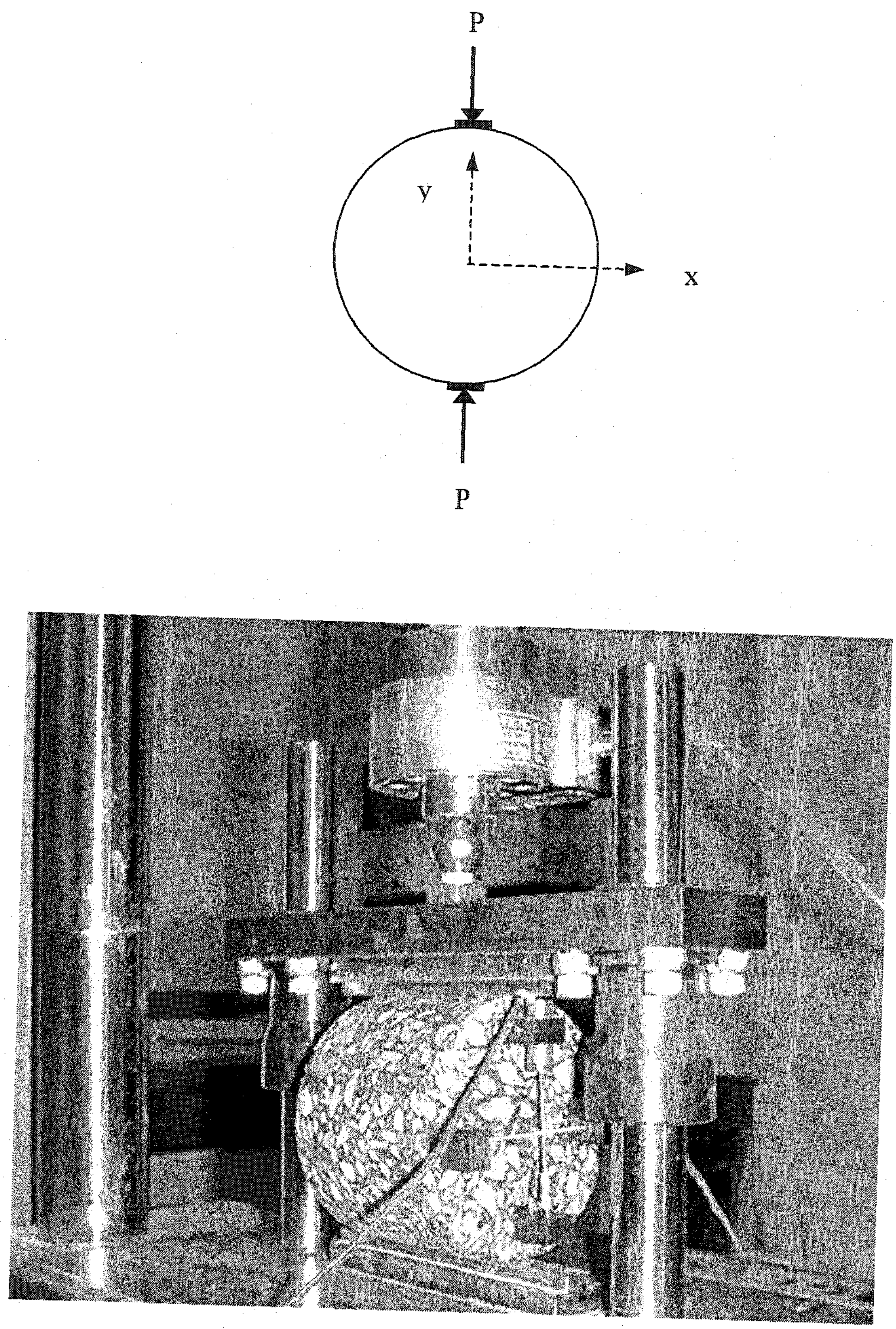

Figure 5.1 Diametrical Resilient Modulus Testing of Asphalt Concrete

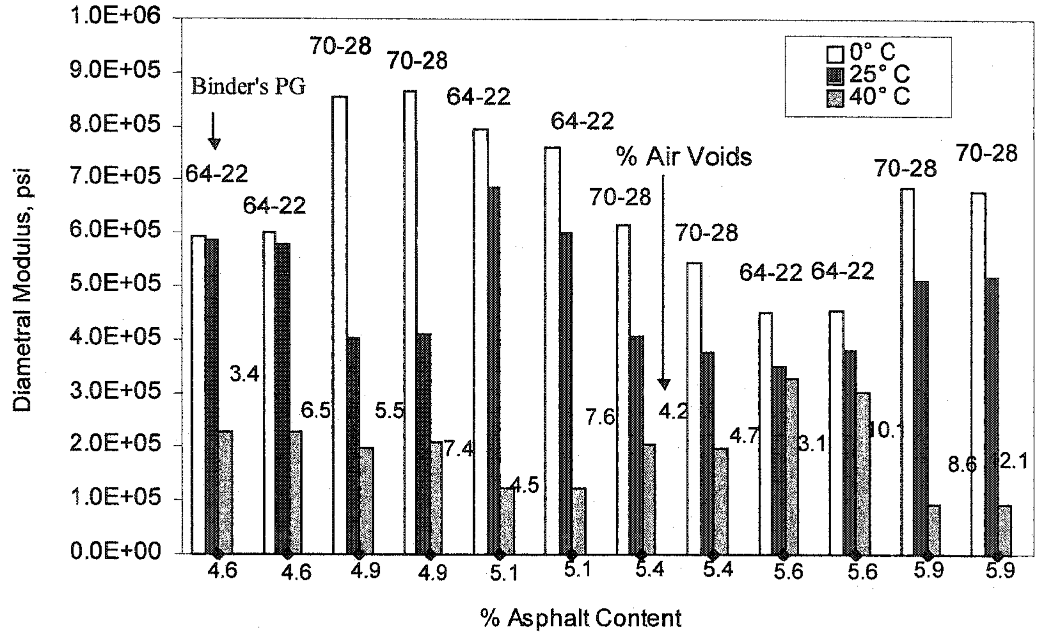

(a) Diametral Resilient Modulus

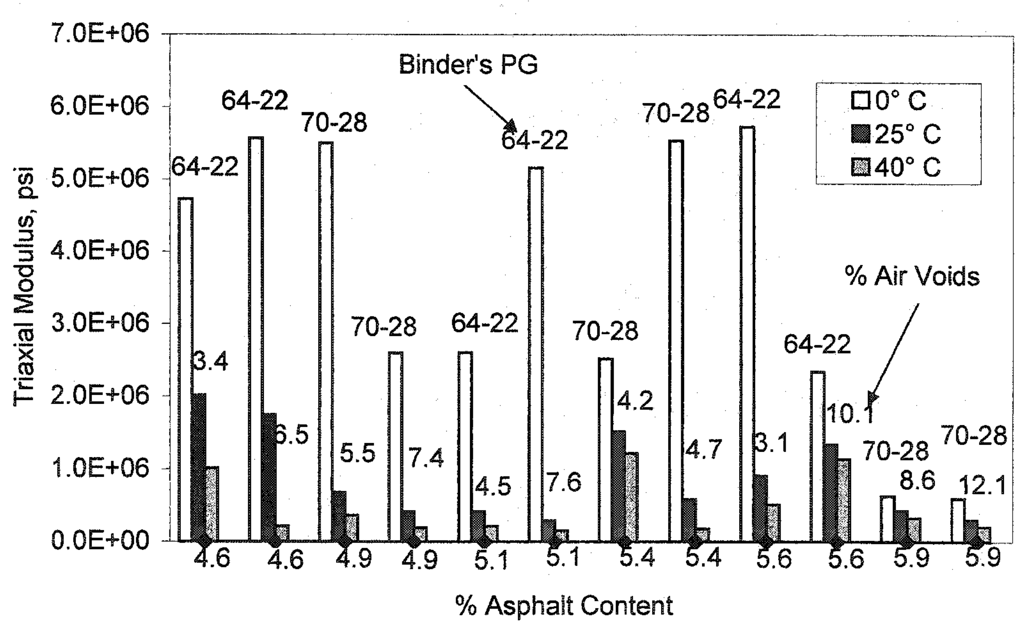

(b) Triaxial Resilient Modulus

Figure 5.2 Variations of Diametral and Triaxial Resilient Modulus with Binder's PG and Binder Content

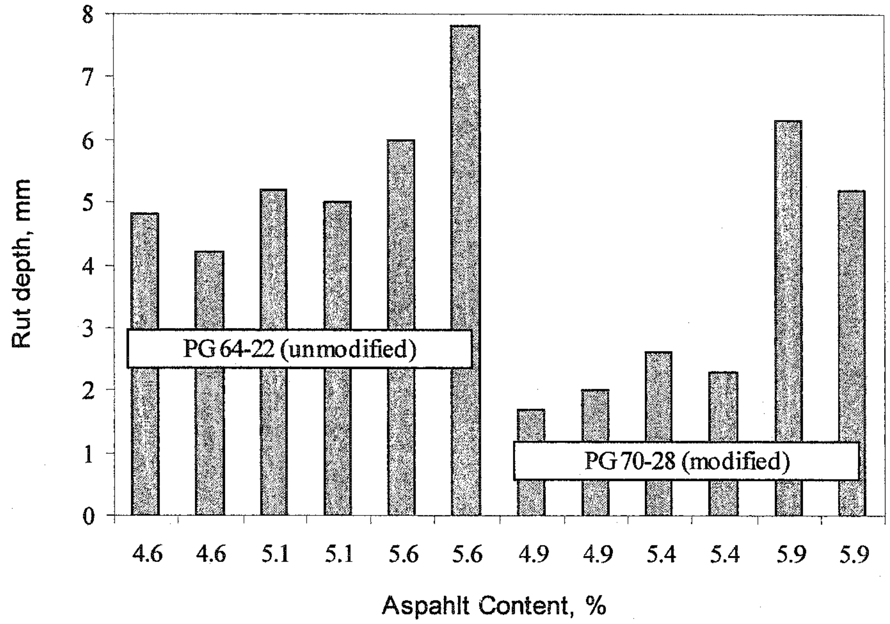

Figure 5.3 Rut Depth Versus Binder Content

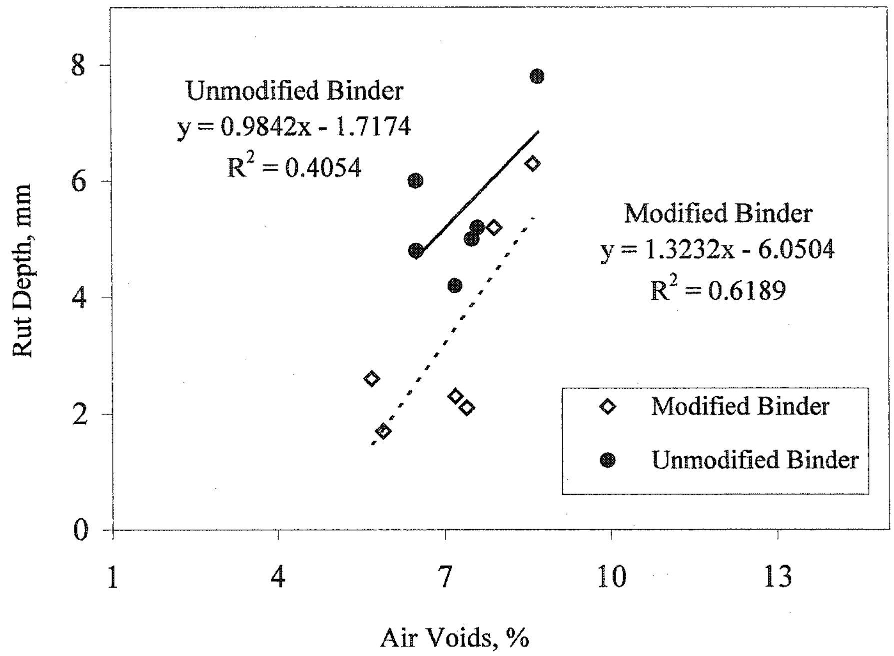

Figure 5.4 Air Voids and Rut Depth

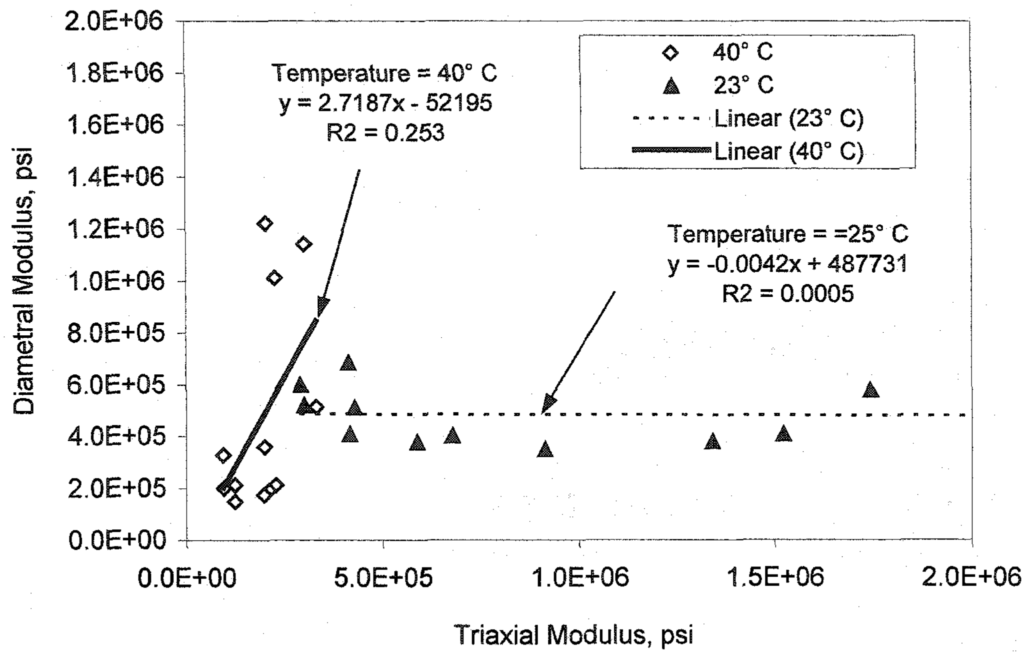

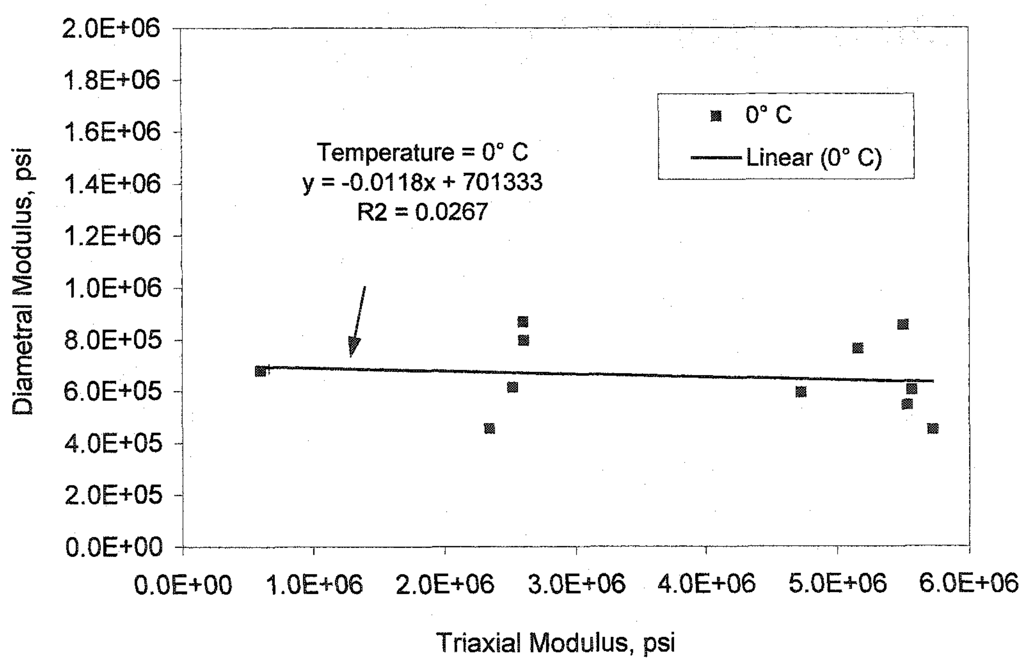

Figure 5.5 Correlation Between Diametral and Triaxial Resilient Modulus

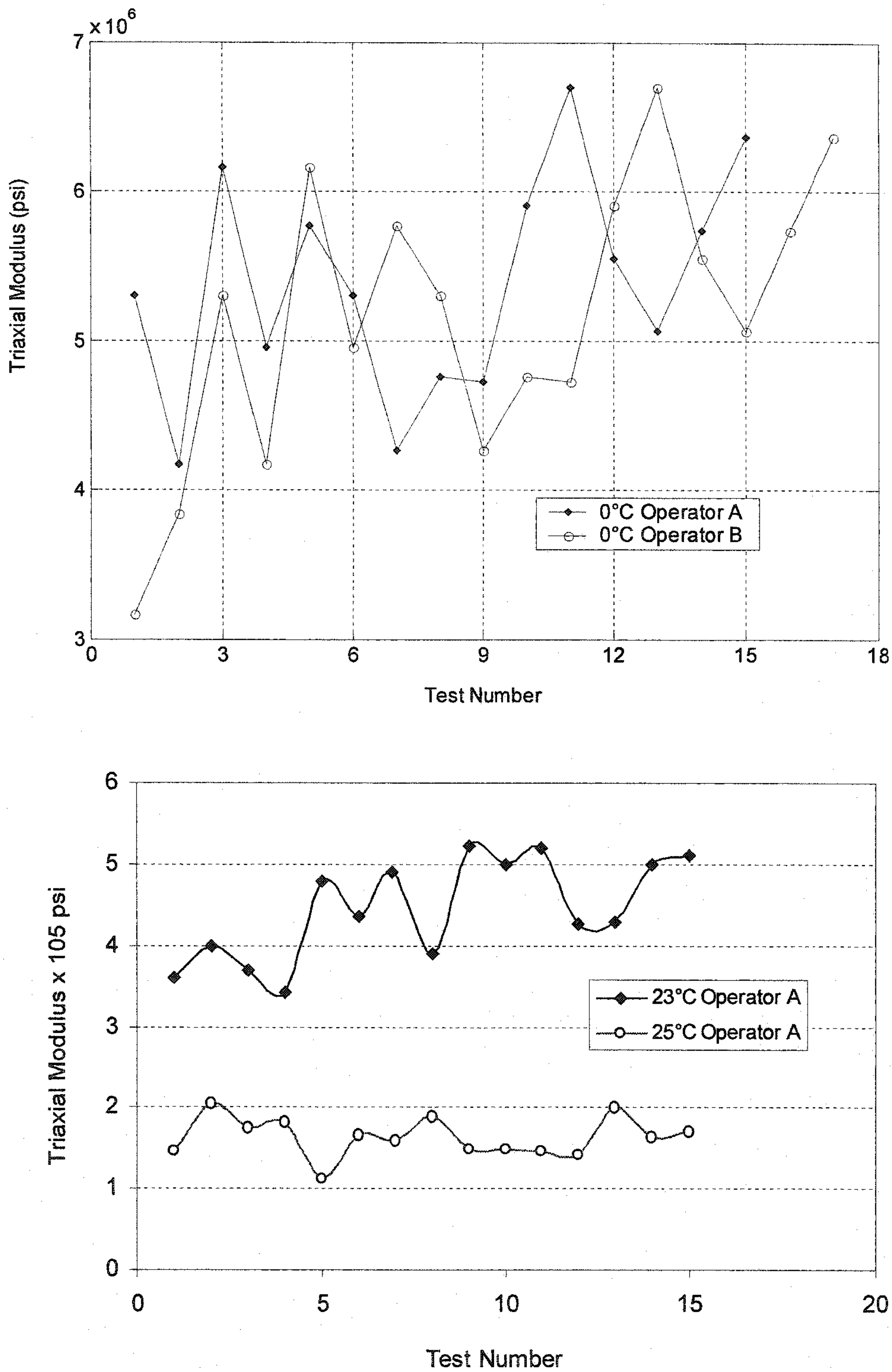

Figure 5.6 Triaxial Resilient Modulus of Asphalt Concrete

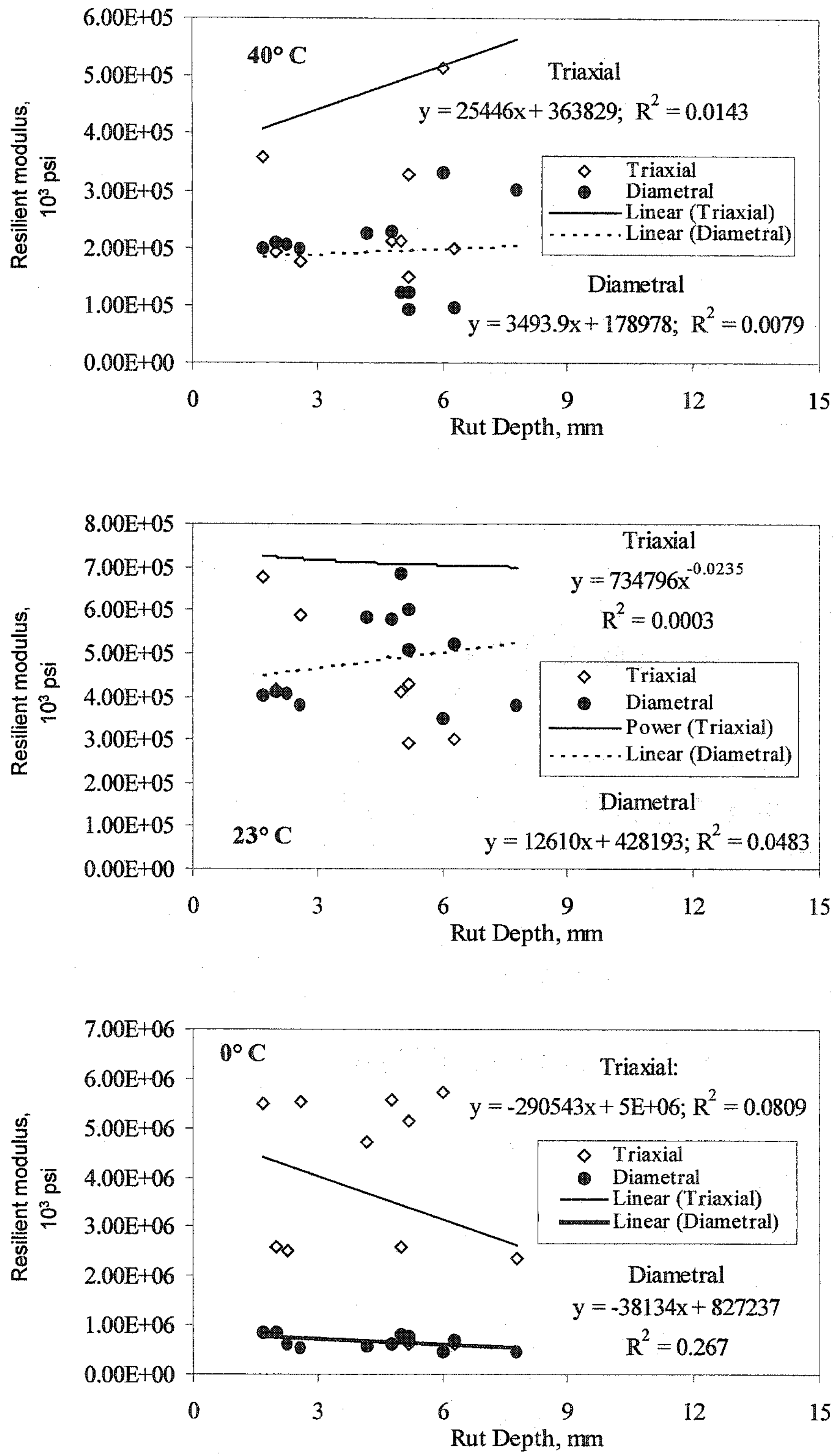

Figure 5.7 Relationships Between Modulus and Rutting

CHAPTER 6

NEURAL NETWORK MODELING OF RUTTING

6.1 Introduction

Although it is preferable to conduct the APA tests to predict the rutting potential of a mix, such tests are not always feasible for a project due to economic reasons. A rut prediction model can be a useful tool in such situations. Prediction of rutting using a model is a rather complex and challenging task. Traditional statistical models have often exhibited weaknesses in predicting reliable rut values (Fine, 1996; White et al., 1992). One of the main objectives of this study is to develop a neural network (NN) model to predict the rutting performance of asphalt concrete. The steps to be taken in the design, training, and performance evaluation of a neural network model are discussed in this chapter.

A neural network is a network of many simple processors (units, nodes, and neurons), each of which has a small amount of local memory (Fine, 1996). These processors are connected by unidirectional communication channels (connections) that carry numerical data. Neural networks are uniquely powerful tools that are used in applications where formal analysis would be difficult or impossible, such as pattern recognition and nonlinear system identification and control. Not only that, it often outperforms classical statistical methods in its ability to analyze incomplete, noisy data, to deal with problems that have no closed-form solutions (Hornik et al., 1989; Engelbrecht, 2001). Absence of close-form solutions and the inherent nonlinearity associated with the rutting factors in asphalt concrete makes the problem of rutting very suitable for modeling with NNs.

Neural networks have already been used successfully in pavement systems. Most of NN studies in the pavement area mainly concentrated on: planning, traffic control and operations, construction and maintenance, and facilities management (Faghri et al., 1997; Dougherty, 1995). In the past decade, there is a considerable interest in using NNs for geotechnical engineering applications, as well as pavement systems. The majority of NN-based models are for geomaterials, such as subgrade soils and aggregate, rather than for paving materials such as asphalt and concrete (Toll, 1996). The work presented here deals with mapping problems specifically in the area of pavement materials.

One of the drawbacks of a neural network model is that there is no established method for deciding which architecture is best for certain mappings (Bishop, 1995; Fine, 1998). In fact, the design of NN architecture is the main topic of this chapter. It is later shown that a three-layer neural network having tan-sigmoid transfer function is best capable of predicting rut potential of asphalt concrete.

6.2 Chapter Organization

The rest of this chapter is organized as follows. Following the introductory section, a basic description of NNs including a mathematical model of a neuron, activation function, and NN architecture is presented. This is followed by a discussion on learning rules, minimization algorithms and issues of global and local minima. Next, the architecture selection methodology and the issues pertaining to NN performance are discussed. After this, the neural network design methodology is presented, followed by a section for the prediction of NN. Finally, concluding remarks are included at the end of this chapter.

6.3 Neural Network Basics

In this section, the basic structural constituents of a NN model known as "neurons" as well as the type of NN used in this study are described.

6.3.1 Model of a Neuron

A neuron is an information processing unit that is fundamental to the operation of a NN. Figure 6.1 shows the model of a neuron. As illustrated, a neuron has three elements, which are synaptic weight, adder, and activation function. As shown in Figure 6.1, a typical neuron k, whose output is denoted by x_k, is connected to the neuron under construction j with an appropriate interconnection weight w_{jk}. The effect of neuron k to neuron j is described by the product $x_k w_{jk}$. If k is active and w_{jk} is positive (excitatory synapse), then neuron k affects neuron j positively. If, on the other hand, neuron k is active but w_{jk} is negative (inhibitory synapse), then neuron k affects neuron j negatively. It is important to note the manner in which the subscripts of the synaptic weight w_{jk} are written. The first subscript refers to the destination neuron, while the second subscript refers to the originating neuron for the synapse under consideration. The adder is to sum the input signals, weighted by the respective synapses of the neuron. The activation function is used for limiting the amplitude of the output of a neuron. Also, the neuron model as shown in Figure 6.1 includes an externally applied threshold, b_j (also referred to as bias). In mathematical terms, a neuron j is described in the form of Equation (6.1) and Equation (6.2) as follows (Bishop, 1995):

$$v_j = \sum_{k=1}^{K} w_{jk} x_k + b_j \tag{6.1}$$

$$y_j = \phi(v_j) \tag{6.2}$$

where, x_1, x_2,……, x_k are the input signals; w_{j1}, w_{j2},…..,w_{jk} are the synaptic weights converging to neuron j; v_j is the cumulative effect of all the neurons connected to neuron j and the internal threshold of neuron j; φ(.) is the activation function; b_j is the bias; and y_j is the output signal of the neuron.

6.3.2 Activation Function

The activation function, denoted by φ(.) in Equation (6.2), defines the output of a neuron in terms of the activity level at its input. Two activation functions are used in the study. The activation functions (also called transfer functions) are described below:

Sigmoid Transfer Function

A sigmoid function, whose graph is s-shaped, is the most common form of an activation function used in the construction of NNs. It is a strictly increasing function that saturates to the value of -1 (for very high negative v input values) and 1 (for very high positive v input values). The sigmoid function is differentiable everywhere. The sigmoid function used in this study is a 'tansig' (tan-sigmoid) named after the hyperbolic tangent, *tanh(v)*. Its shape is shown in Figure 6.2 and defined as follows:

$$\varphi(v) = \frac{2}{1+e^{-2v}} - 1 \qquad (6.3)$$

Linear Transfer Function

The linear transfer function can be expressed as:

$$\varphi(v) = v \qquad (6.4)$$

By varying the domain of input, active range of this function can be shown in the range of [-∞, +∞]. Using this function in the output layer with a sigmoid function in the inner layer of NN, it is possible to get the outputs in any range. This combination is very common in the NNs usually designed for function mapping (Hornik et al., 1994).

6.3.3 Neural Network Architectures

The manner in which the neurons of the NN described above are structured is called the NN architecture. Usually, neurons are organized in the form of layers. Depending on the number of layers, a NN can be classified as a single layered or multiple layered network.

Single-Layer Feed-Forward Networks

The simplest possible layered NN is the single-layer NN that consists of a layer of inputs (input layer) and a layer of output nodes (output layer). No synaptic weight connections are allowed amongst the nodes belonging to the same layer. Therefore, data is fed only in the forward direction. The architecture is called a single-layer feed-forward NN.

Multilayer Feed-Forward Networks

The extension of the single-layer feed-forward structure is obviously the multilayer feedforward structure as depicted in Figure 6.3. It can be seen from Figure 6.3, the NN has an input layer and an output layer as in the single-layer case, but now in between these two layers, there exists one or more layers of nodes, designated as hidden layers. All these layers of nodes are denoted by layer 0 (input layer), layer 1 (first hidden layer), layer 2 (second hidden layer), and so on until the layer M (output layer) is reached. Figure 6.3 shows a multilayered feedforward structure with an input layer of K nodes, an output layer of I nodes, and a single hidden layer of J nodes. As with the single-layer NN, weight connections are only allowed from a layer of certain index to a layer of higher index. No connections are permitted amongst the nodes belonging to the same layer or from a layer of higher index to a layer of lower index. Figure 6.3 shows weight connections from a layer of certain index to a layer of an immediately higher index. This type of weight connectivity is referred to as standard connectivity. Once again, data in the multilayered NN structure of Figure 6.3 propagates in the forward direction from the input layer (layer 0), towards the hidden layers (layer 1 in Figure 6.3), and finally to the output layer (layer 2 in Figure 6.3). This is why the multilayered NN structure is denoted as the multilayered feed forward NN. The multilayer NN as shown in Figure 6.3 is fully connected because every node in each layer of the network is connected to every node in the adjacent forward layer. If any of the communication links (synaptic weights) are missing, the network is called partially connected.

Multilayer NNs are more powerful than single layer ones, since multilayer NNs use a combination of transfer functions. Using a linear transfer function in the output layer and sigmoid functions in the hidden layers, a multilayer feedforward network can approximate any function with a finite number of discontinuities with arbitrary accuracy (Haykin, 1994). The only requirement is that enough neurons exist in the hidden layers. In principle, a NN consisting of just one hidden layer can be taught to approximate any continuous functional mapping (Fine, 1998; Hornik, et al., 1994). As is shown in this study (discussed later), the learning task of mapping is faster using multiple hidden layers even with fewer neurons. The NN learns the mapping from a collective set of input-output given to it. The learning process follows a set of algorithms, which are discussed in the next section.

6.4 Learning Algorithm

Neural network learns about the input-output mapping through an interactive process (training or learning) of adjustments applied to its synaptic weights and biases. A prescribed set of well-defined rules for the solution of a learning problem is called a learning algorithm. There are five commonly known learning rules: error-correction learning, memory-based learning, Hebbian learning, competitive learning, and Boltzmann learning. In this study, error-correction learning that is based on an optimization or error minimization technique is employed.

6.4.1 Error-Correction Learning Algorithm

A neural network learns from a given training set of examples, $T_n = \{(x_i, t_i) : i = 1{:}n\}$ consisting of n input-output pairs (x is the inputs, t is the target outputs). For a given m-dimensional input x (rut factors) and an associated target value t (rut), the goal is to design a neural network, NN (x_i, w) that generalizes (learns) well to new function values. The output of NN is denoted by y_i. This output is compared to the target output, t_i. The error is denoted by e_i and can be expressed as,

$$e_i = t_i - y_i \tag{6.5}$$

The error signal e_i actuates a mechanism, the purpose of which is to apply a sequence of corrective adjustments to the synaptic weights of neurons in the network. The corrective adjustments are designed to make the output signal y_i come close to the target response t_i, in a step-by-step manner. The objective is achieved by minimizing a cost function or index of performance, ξ.

6.4.2 Performance Function

The performance function or minimization function can be defined in terms of error, e_i as:

$$\xi = \frac{1}{n}\sum_{i=1}^{n} e_i^2 \tag{6.6}$$

where, ξ is the instantaneous value of the error energy. The adjustments to the synaptic weights of neurons are continued until the system reaches a steady state (i.e., the synaptic weights are essentially stabilized). At that point the learning is terminated. Having computed the synaptic adjustments Δw_k, the updated value of the synaptic weight w_{k+1} is determined from the following formula:

$$w_{k+1} = w_k + \Delta w_k \tag{6.7}$$

where, w_k is the current weight value. The manner in which the error, e_i is used to determine the Δw_k term is closely related to optimization or minimization algorithm.

6.4.3 Minimization Algorithm

For the cost function, ξ (w) defined by Equation (6.6) is minimized with respect to some unknown weight (parameter) vector w. An optimal solution w^* that satisfies the condition, $\xi(w^*) \leq \xi(w)$ is found. The necessary condition for optimality is $\nabla\xi(w^*)=0$, where, ∇ is the gradient operator and $g(w) = \nabla\xi(w)$ is the gradient vector of the cost function.

Typically, all optimization algorithms for feedforward neural network uses gradient of the cost function to determine how to adjust the weights. A class of optimization algorithms widely used today is based on the idea of local iterative descent. This algorithm starts with an initial guess denoted by w_0, and then generates a sequence of weight vectors $w_1, w_2, \ldots w_k$, such that the cost function, ξ (w) is reduced at each iteration of the algorithm by $\xi(w_{k+1}) < \xi(w_k)$, where w_k is the old value of the weight vector and w_{k+1} is its updated value. The hope is that the algorithm eventually converges to the optimal solution w^*.

However, the mean squared error, $\xi(w)$, is a relatively complex surface in the weight space, possibly with many local minima, flat sections, narrow irregular valleys, and saddle points (Wasserman, 1993). The complexity of the error surface is the main reason that the behavior of a minimization algorithm can be very complex, often with oscillations around a local minimum. The problem of minimization of a function of many variables (multi-variable function), $\xi(w)$, has been researched since the 17th century and its principles were formulated by people such as Kepler, Fermat, Newton, Leibnitz, and Gauss (Mehra, 1992). In practice, there are three types of optimization algorithms that are used to select network parameters to minimize $\xi(w)$, namely, steepest descent, Newton's method, and Gauss-Newton method. The behavior of these algorithms can be improved by making modifications to their parameters, or to the algorithm itself. Of them, the fastest and most popular is the Levenberg-Marquardt algorithm, which originates from the Gauss-Newton method (Hagan, 1996). A brief overview of these methods is presented below:

The Levenberg-Marquardt method expresses the cost function of Equation (6.6) in the form of:

$$\xi(w) = \frac{1}{2}\sum_{i=1}^{n} e_i^2 \tag{6.8}$$

where, the scaling factor of 1/2 is included to simplify expressions in the subsequent analysis. All the error terms in this formula are calculated on the basis of a weight vector w that is fixed over the entire observation interval $1 \le i \le n$. The error e_i is a function of the adjustable weight vector w. For a given operating point, w_k (k is the number of trial or iteration), the dependence of e_i on w can be written as:

$$e_i'(w_{k+1}) = e_i + J_{ij}(w_{k+1} - w_k),\ i = 1, 2, \ldots n, \text{ and } j = 1, 2, \ldots m \tag{6.9}$$

where, n is the number of training datasets, m the number of weights to be adjusted and $J_{ij} = \frac{\partial e_i}{\partial w_j}$ the n-by-m Jacobian matrix of error, e_i. The updated weight vector w_{k+1} is then defined by:

$$w_{k+1} = \arg\min_{w}\left\{\frac{1}{2}\left\|e_i(w_{k+1})\right\|^2\right\} \tag{6.10}$$

Using Equation (6.9) to evaluate the squared Euclidean norm of $e_i'(w_{k+1})$, the following relation can found:

$$\frac{1}{2}\| e_i(w_{k+1}) \|^2 = \frac{1}{2}\|e_i\|^2 + e_i^T J_{ij}(w_{k+1} - w_k) + \frac{1}{2}(w_{k+1} - w_k)^T J_{ij}^T J_{ij}(w_{k+1} - w_k)$$

Differentiating the above expression with respect to w_{k+1} and setting the result equal to zero, the following equation can be obtained:

$$w_{k+1} = w_k - (J_{ij}^T J_{ij})^{-1} J_{ij}^T e_i \tag{6.11}$$

This is known as the Gauss-Newton method. This requires the Jacobian matrix of the error vector e_i. However, for the Gauss-Newton iteration to be computable, the matrix product, J^TJ must be nonsingular. The J^TJ is always nonnegative definite. To ensure that it is nonsingular, the Jacobian J_{ij} must have the row rank n; that is, the n rows of J_{ij} must be linearly independent. Unfortunately, there is no guarantee that this condition will always hold.

To guard against the possibility that J is rank deficient, Levenberg-Marquardt method adds a simple positively scaled unit matrix, εI, to the matrix J^TJ. The parameter ε is a small positive constant chosen to ensure that $M_k = [J^TJ + \varepsilon I]$ is positive definite for all i. Therefore, the Levenberg-Marquardt Algorithm (LMA) can be expressed in the form of:

$$w_{k+1} = w_k - (J_{ij}^T J_{ij} + \varepsilon I)^{-1} J_{ij}^T e_i \tag{6.12}$$

The Jacobian matrix J can be computed through a standard backpropagation (of error) technique. The matrix J^TJ is automatically symmetric and non-negative definite. Typically, large size of J may require a careful memory management in evaluating the product of J^TJ. The performance of the algorithm depends on the choice of ε in Equation (6.12). When ε is large, the LMA becomes equivalent to the method of steepest descent. When the scalar ε is zero, the LMA is equivalent to the Newton's method. The

Newton's method is faster and more accurate as it approaches the error minima. The aim of decreasing ε is to shift towards the Newton's method. Thus, the value of ε is decreased after each successful step (reduction in performance) and is increased only when a tentative step increases the performance function. In this way, the performance function is always reduced at each iteration of the algorithm (Demuth, 1998).

6.4.4 Local and Multiple Minima

Although the preceding discussion has focused on identifying a minimum value of the cost function, $\xi(w)$, or training error, $\xi_T(w)$, the algorithms may fixate on to a local optimum without finding a global optimum. Using the above local optimizers to identify a single good neural network yielding a low value of cost function or training error (local minima), the algorithms themselves identify large sequences of networks. This is because the outcome of a minimization algorithm is strongly dependent on the initial choice of the starting point (initial weights). Hence, repeating (minimization) training with a different and randomly chosen initial condition, the same network performance, $\xi(w)$ is rarely obtained. Of course, it is always possible to construct instances in which one algorithm performs better than others. The lack of uniqueness of a neural network representation of a function establishes that some multiple minima occur due to the symmetries that cause the non-uniqueness; several parameter vectors give rise to the same function and hence to the same value of error (Auer et al., 1996). In many applications, it is possible to attain a satisfactory performance at many of the local minima and have little incentive to find a global minimum or explore all the local minima (Kearns, 1997). This study explores a variety of initial conditions to achieve a good minimum training error.

6.4.5 Global Optimization

In global optimization, the algorithm searches for the global optimum by employing mechanisms to search larger parts of the search space (error surface). Some of the global optimizers such as: simulated annealing, LeapFrog, and swarm algorithm are discussed below. These methods are applicable only when the dimension of the search space is small. If the dimension of the search space is high, then the search for global error is time consuming and in many cases, it is impossible to search the entire space (Engelbrecht, 2002). Search for global error is not pursued in this study because rutting problem requires a NN with a large number of weights. To develop intuition, the issue of global search in the case of rutting can be discussed as follows. A neural network designed with a minimum number of parameters requires at least nine inputs and seven outputs. For seven outputs, seven neurons in the output layer is required. If a one layer Feed Forward Neural (FFN) network with 2 neurons in the hidden layer is considered, the total number of parameters become, $q = ((9+1) \times 2 + (2+1) \times 7) = 41$, where q is the total number of weights to be adjusted. The goal is to seek for $q=\{w_1, w_2, \ldots w_{41}\}$ of minimum or lowest error, $\xi_T(q)$. Proceeding by evaluating ξ_T at a closely spaced (spacing s) grid points (the points in the plot of error function or error versus weights plot) and selecting the mapped point of lowest error, the number of required training grows exponentially in the dimension s of q. In this case, if 2 grid points are considered, the total number of search is 2^{49}. This becomes impossible for closer grid points or high dimension of error surface. For large networks an exhaustive search for global error is unrealistic.

6.5 Outline of the Proposed Approach to Architecture Selection

The abstract formulation of the architecture selection problem can be described as the minimization of a function ξ: $Q \rightarrow R^q$, where Q is the set of architecture parameter vectors. The architecture selection problem is to find a $q^* \in Q$ such that:

$$\xi(q^*) = \min_{q \in Q} \xi(q) \tag{6.13}$$

As discussed in the previous section, the minimization algorithm cannot be expected to converge to a global minimum. Convergence to a local minimum is even problematic for some minimization algorithms. The Levenberg-Marqardt algorithm generally converges to a local minimum. Therefore, it is not always obvious what is the best architecture. Indeed, one of the most challenging problems in neural network design is finding a suitable architecture.

In architecture selection procedure, a few networks of different architectures are trained first. Of them the one that results in the lowest generalization error is selected as final network. As a first step, two families of networks are trained in this study. The assumed number of hidden layers is one in the first family, while it is two in the second family. The total number of weight parameters defining the architecture in each family is varied. In particular, a NN starts with a small number of hidden neurons, and the hidden units are added to the NN incrementally based on the generalization performance defined in the next section. This is a trial-and-error approach in which, the training data is not fitted too closely assuming the convergence to a well-selected local minimum is satisfactory. Each trial network is trained for several times and the final performance is calculated from the linear combination of these training outputs. Finally, the NN with best performance is chosen. However, if several networks fit the training set equally well, then the simplest network (i.e. the network which has the smallest number of weights) is selected as the final NN.

6.6 Analysis of NN Performance

In this section, the various aspects that have an influence on the performance of NNs are discussed. These aspects include performance index, performance measure, and data manipulation.

6.6.1 Performance Index

Three indices are used in this study to design the NN. The most common measure of performance of NN is the Mean Squared Error (MSE), expressed as,

$$\mathrm{MSE} = \frac{\sum_{j=1}^{p}\sum_{i=1}^{n}(o_{i,j} - t_{i,j})^2}{n.p} \tag{6.14}$$

where

n = total number of data set

o = network output

p = number of outputs

t = target output.

Instead of mean square error, an Average Relative Error (ARE) can be used to measure the performance of a NN. The average relative error is calculated using the L_2-norm of error vector normalized by the L_2-norm of output vector, as shown below:

$$\xi_T = \frac{1}{n}\sum_{i=1}^{n}\left(\frac{1}{p}\sum_{j=1}^{p}\frac{(o_{j,i}-t_{j,i})^2}{t_{j,i}^2}\right) \tag{6.15}$$

Correlation Coefficient: Although the above two indices are the most common for measuring performance of a NN, an additional measure of NN performance, the correlation between the output and target values for all data sets, is useful in architecture selection. The measure of such performance, referred to as the correlation coefficient, R-value, is calculated as follows:

$$r = \frac{\sum_{p=1}^{P} o_{k,p}t_{k,p} - \frac{1}{P}\sum_{p=1}^{P} o_{k,p}\sum_{p=1}^{P} t_{k,p}}{\sqrt{\sum_{p=1}^{P} o_{k,p}^2 - \frac{1}{P}\left(\sum_{p=1}^{P} o_{k,p}\right)^2}\sqrt{\sum_{p=1}^{P} t_{k,p}^2 - \frac{1}{P}\left(\sum_{p=1}^{P} t_{k,p}\right)^2}} \tag{6.16}$$

6.6.2 Performance Measure

After the performance indices are defined, an accurate measurement of these indices is important to ensure that the resulting architecture works reasonably well for the entire family of initializations.

Consider a performance index, $\xi(.,.)$ described in the Section 6.6.1. Therefore, $\xi(q, w)$ is a measure of the performance of the neural network when the architecture, A(q) has q parameters and the network N(w), initialized with w. If Equation (6.14) or Equation (6.15) defines the performance function, then a lower value of ξ is preferred.

If it is defined by the Equation (6.16), then a higher value of the performance function is desired. The performance function can be defined as below:

$$g(q,w)=\xi[A(q),N(w)] \tag{6.17}$$

The aim is to define an object function of g (.,.) alone that quantifies the performance of the architecture A (q), so that by minimizing this object function with respect to q, the optimal architecture can be found. There are two choices, as discussed in the following.

6.6.2.1 Best Performance

The best performance or lowest error of a NN can be defined as:

$$h(q)=\min_{w\in W} g(q,w)=\min_{w\in W}\xi[A(q),N(w)] \tag{6.18}$$

Here, h(q) measures the best-case performance of an architecture A(q), as the initialization varies over $\{N(w),\ w\in W\}$. Such a choice of h(q) may not correspond to achieving the best possible (stable) performance. The NN thus designed is denoted as a "Best Net" in this study.

6.6.2.2 Likelihood Performance

The second choice is to settle for architectures that work satisfactorily "most of the time". One way to capture this idea in a mathematical framework is to introduce a probability measure P_w on the set W, that reflects that the best initialization N(w) is distributed in the set of possible initializations $\{N(w),\ w\in W\}$. In particular, $N(w_0)$ can be a most likely initialization for a fixed parameterized architecture and the probability measure P_w can be peaked around $N(w_0)$. After knowing the probability measure P_w, the objective function to be minimized can be defined as:

$$f(q) = E_{P_w}[g(q,w)] = E_{P_w}[\xi(A(q), N(w)] \tag{6.19}$$

Thus, f(q) is the expected or average performance of the architecture, E is the expectation, A(q) when the initialization is distributed according to the probability P_w.

While the best-case objective function as defined in Equation (6.18) is easy to understand and to interpret, the interpretation of the expected-value type of objective function defined in Equation (6.19) needs additional elaboration. Ideally, f(q) is computed for a given q and a finite number of initializations, $\{w = [w_1\ w_2 \ldots\ w_m]^t \in W^m\}$ and collection of m-trial initializations. For each A(q), the expected value is approximated by a mean or a maximum likelihood estimator described below.

Mean Estimator

The performance f(q) of an architecture A(q) is approximated by taking the mean of the performances of randomly initialized networks, $N(w_1)$, $N(w_2)$, ……$N(w_m)$. The mean can be defined, based on the multisampling w, as:

$$\hat{E}(g_q, W) := \frac{1}{m}\sum_{i=1}^{m} g_q(w_i) = \frac{1}{m}\sum_{i=1}^{m} g(w_i, q),\ q \in Q \tag{6.20}$$

Maximum likelihood Estimator

The principle behind the maximum likelihood method is the multisampling of w. If $g(w_1)$, $g(w_2)$, ……$g(w_m)$ are the m observed performances of the network, then the estimated performance of the NN is most likely to produce or represent these observed values. The probability density function of f(w) is determined. Then the one with maximum probability density is considered to be the final performance of that family

$\{f(w), w \subseteq W\}$. Then the one with maximum probability density is considered the final performance.

In this study, the selection of architecture in NN design is based only on its mean performance, and not on the best-case performance. Once the network architecture is selected, the neural network is used to map new data by the method of likelihood. The likelihood method is simply what is used to generate simulated data after the unknown parameters (weights) are guessed. The simulation performance of the designed NN is evaluated using the likelihood method (by mean estimator and by maximum likelihood estimator), as well as the best performance index. The best-case performance index is defined by mean square error or average relative error.

6.7 Neural Network Design and Performance Estimation

In this section, the input and rut date sets are described first. Next, the preprocessing of raw data and principle component analysis are described. The selection of neural network architecture is described in a step-by-step procedure. The training and validation performance of NN are described. Finally, the simulation results are presented followed by an illustration of the application of neural network in HMA design.

6.7.1 Input Factors

As a first step, a set of input factors or descriptors that affect the rutting performance of asphalt concrete under consideration is identified (Tarefder et al., 2002; 2003). Mainly two classes of factors affect laboratory rutting of asphalt concrete. One is mix design measured at design stage and the other is testing parameters measured during laboratory rut testing. The mix design factors include aggregate properties, asphalt cement properties and mixture properties. The volumetric parameters and their interrelationships (discussed in Chapter 2) can be found from these properties. Aggregate size, gradation, and angularity are the most important factors to affect rutting and therefore, the full series of sieve sizes used to define a Superpave mix are included to define the proposed NN. Binder's PG is one of the most important factors to affect rutting and included in the proposed NN. In many situations aggregate and binder's meet the Superpave design requirements but the mix performance is not satisfactory; thus, several mix properties, environmental factors, and loading factors are included in the proposed NN model. Specifically, the factors considered in this study are as follows:

1. Percentage of materials passing through no. 200 sieve
2. Percentage of materials passing through no. 100 sieve
3. Percentage of materials passing through no. 50 sieve
4. Percentage of materials passing through no. 30 sieve
5. Percentage of materials passing through no. 16 sieve
6. Percentage of materials passing through no. 8 sieve
7. Percentage of materials passing through no. 4 sieve
8. Percentage of materials passing through 9.5 mm sieve
9. Percentage of materials passing through 12.5 mm sieve
10. Percentage of materials passing through 19.0 mm sieve
11. Binder's Performance Grade (PG)
12. Percentage asphalt content (P_b)

13. Specific gravity of asphalt (G_b)

14. Maximum specific gravity of mix (G_{mm})

15. Bulk specific gravity of aggregate (G_{sb})

16. Bulk specific gravity of HMA (mix) sample (G_{mb})

17. Temperature

18. Wheel load

19. Tire pressure

20. Fine Aggregate Angularity (FAA)

21. Aggregate's Fractured Face (FF)

The ranges of the input factors are shown in Figures 6.4(a) to 6.4(c). The distribution of particle sizes expressed as a percent of the total weight (gradation) is plotted in vertical axis in Figure 6.4(a). Gradation is determined by sieve analysis and normally expressed as total percent passing various sieve sizes as shown in the horizontal axis. Gradation is a primary consideration in asphalt mix design and specifications. The mixes included in the design of neural network are currently being used in the State of Oklahoma and their gradation is shown in Table 6.1. The specific gravities of HMA components as well as the binder's performance grade (PG) are shown in Figure 6.4 (b). A basic understanding of weight-volume relationships of compacted HMA is important from both a mixture design standpoint and from a field construction standpoint. The input factors 11-16 shown in Figure 6.4(b) are the parameters required to understand mix design. These parameters are used to determine the volume of asphalt cement and aggregates required to produce a mixture with the desired properties. It is to be noted that the VMA and VFA can be calculated from the specific gravities and percentage asphalt content using Equation (2.2) and Equation (2.3). The range of the factors 17-21 is shown Figure 6.4 (c). Three of these factors (factors 17-19) are to simulate the field pavement conditions while the other two factors (factors 20-21) are aggregate properties.

6.7.2 Target Vector

The output data is obtained by means of cyclic rutting tests in which the deformations of samples are recorded over 8000 cycles. For the purpose of this study, it suffices to describe this time series of rut or deformations by an interpolation with piecewise linear elements using only a few deformation values. Consequently, the domain of the neural network to be constructed and trained is a vector space of input factors and whose range space consists of vectors obtained from a few values of deformation. Observations of deformations are made at eight selected cycles: 1, 500, 1000, 1500, 2000, 4000, 6000, and 8000. Since the deformation at cycle number 1 for all data is essentially the same (zero deformation), the target vector consists of 7 components. The range of 8000 cycle rut depth is 0.3 mm to 13.4 mm. The spread of the rut depths at different cycles are shown in Figure 6.5. Finally, a dataset consists of 21 inputs (described in the previous section) and 7 outputs (500, 1000, 1500, 2000, 4000, 6000, and 8000-cycle rut).

6.7.3 Data Preprocessing

One of the most important steps in using a NN is to define a data set and transform data into a form acceptable to the NN. Neural network training can be made efficient if the following preprocessing steps are performed on the network inputs and targets.

6.7.3.1 Removal of Missing Value Data

It is common that data sets have missing values for input parameters. NNs need a value for each of the input parameters. There are two options: one is to remove the data set and the other is to replace each missing value with the average value for that input parameter. In this study, the entire data sets are removed. Initially, there are 793 data sets (a total of 1586 samples, a total of two samples are tested to produce one data set), after removing the missing data, a total of 769 data sets are available for outlier analysis described in the next section.

6.7.3.2 Outlier Analysis

Very often, in large data sets, there exist samples that do not comply with the general behavior of the data model. Such samples, which are significantly different or inconsistent with the remaining set of data, are called outliers. Because of the large deviation from the norm, the outliers result in large errors, and consequently a NN is subjected to large weight updates. In this study, any data that deviates more than two times the standard deviation from the mean value of the corresponding data vectors are considered as outlier. A total of 23 data sets are removed based on the outlier criteria and finally, the database for the construction of NN model contains 746 data sets.

6.7.3.3 Transformation of Non-Numeric Data

All the input values to a NN must be numeric. Nominal values, therefore, are transformed to numerical values. This study encounters one non-numeric or nominal input parameter that is the PG of asphalt binder. The PG has 3 different values, which are coded as 3 different numeric input parameters. The PG that corresponds to a grade of PG 64-22 is assigned a value of 1, the grade of PG 70-28 is assigned a value of 2, and the PG 76-28 is assigned a value of 3.

6.7.3.4 Data Normalization

It is useful to scale and normalize the input and output data, so that, they always fall within the active range and domain of the activation function. From Figure 6.3, it can be shown that the active domain of tan-sigmoid function is [-1.73, 1.73]. Values near the asymptotic ends of this sigmoid function have a very small influence on weight updates. Changes in these values result in very small changes in output. Furthermore, the derivatives near the asymptotes are approximately zero, causing weight updates to be approximately zero. Therefore, no learning is achieved in these areas. Since, the weighted sums of the network inputs are mapped through an activation function, an efficient weight initialization can speed up the convergence process significantly, even by an order of magnitude. In normalization procedure, the mean value $\mu(x)$ and the standard deviation $\sigma(x)$ of a feature x_i, are computed for the entire data set. The feature value is transformed to x_{ni} using the Equation (6.21) as shown below:

$$x_{ni} = \frac{x_i - \mu}{\sigma} \qquad (6.21)$$

In this study, all of the 21 input vectors are normalized so that the mean value of each input factor, averaged over 746 data sets, is zero and the standard deviations is unity (using Equation 6.21). The deformation values at 500, 1000, 1500, 2000, 4000, 6000, and 8000 cycles over 746 data sets so that the normalized deformation has zero mean and unity variance. This is not necessary as a pure linear activation function is used in the output layer; however, this step is useful in case the network weights are updated based on MSE instead of ARE. Also, the Principal Component Analysis (PCA) of input factors requires normalized data.

6.7.3.5 Principal Component Analysis

The purpose of principal components analysis is to derive new variables (in decreasing order of importance) that are linear combinations of the original variables and are uncorrelated. Geometrically, principal components analysis can be thought of as a rotation of the axes of the original coordinate system to a new set of orthogonal axes that are ordered in terms of the amount of variation of the original data they account for (Kantardzic, 2003).

A set of n-dimensional vector samples $X = \{x_1, x_2, x_3, \ldots\ldots\ldots x_n\}$ is considered first. This vector is then transformed into another set $Y = \{y_1, y_2, y_3 \ldots y_m\}$ of reduced dimensionality, but the vector Y has the property that most of its information content is stored in the first dimension. The goal is to reduce the data set to a smaller number of dimensions with low information loss. A matrix A is determined, so that the computation, Y=A.X has the largest variance possible for a given data set. In practice, a covariance matrix is computed as given below:

$$S_{nxn} = \frac{1}{(n-1)}\left[\sum_{j}^{n}(x_j - \bar{x})^T (x_j - \bar{x})\right] \tag{6.22}$$

where, $\bar{x}$ is the mean of x_j. The eigenvalue of the covariance matrix S is calculated for given data. The eigenvalues of S_{nxn} are $\lambda_1, \lambda_2, \lambda_3, \ldots\ldots\ldots\ldots \lambda_n$, where $\lambda_1 \geq \lambda_2 \geq \lambda_3 \ldots . \geq$

$\lambda_n \geq 0$. Then, the proportion of variance is calculated. Dividing the sum of the first m eigenvalues by the sum of all the variances (all eigenvalues), the quality of the representation based on the first m principal components is measured. The result is expressed as a percentage. Typically, the projection that accounts for over 90% of the total variance is considered to be good. The ration is expressed as follow:

$$Re = \left(\sum_{i}^{m} \lambda_i \right) / \left(\sum_{i}^{n} \lambda_i \right) \tag{2.23}$$

By setting a threshold values for Re, the principal components that contribute less than the others to the total variation in a give dataset is eliminated.

In this study, a total of three principal component analyses are conducted in which factors accounting for 0.1%, 1% and 2% of the variation of the input vectors are used. Using a variance of 0.1% (Equation 2.23), the number of input factors remained the same. Whereas, using the variance of 1%, the number of input factors reduces from 21 to 15; that is, input factors accounting for 99.0% of variation in the total data set leads to a reduction in input dimension. Using 98% of variation in the total data set, the number of input factors reduced to 12 and is used to construct and train the neural network. Finally, a data set (training set) is designed to consist of data in the form of pairs of vectors composed of 12 input factors and associated 7 target vectors.

6.7.4 Neural Network Architecture and Training

The manner in which the neurons are structured in a NN is called architecture. Usually, neurons are organized in the form of layers. In this case, the NN architecture can be defined as follows: each of the 12-inputs is connected to each of the q-hidden neurons (either in one or two layers), and the outputs of the hidden neurons are fed into the 7-output neurons. The number of hidden neurons, q in the final NN is determined by trial and error method. It is a sequential algorithm in which at each step a new feed forward neural network designed by adding a neuron to a specific hidden layer, trained by the Levenberg-Marquardt minimization algorithm, validated, and tested for generalization performance (Demuth, 1998; Hagan, 1996). However, the architecture or topology of NN must be established before training. The network constructed and trained in this study has three processing layers (also called neuron layers) and denoted by 12-h_1-h_2-7 as shown in Figure 6.6.

In the training step, the first hidden layer takes a preconditioned input column of n_i=12 vectors and maps it to a column of n_{h1}=11 vectors by a tan-sigmoid transfer function (Equation 6.3). The resulting vectors are then taken as an input by the seconf hidden layer as inputs and mapped by a tan-sigmoid function to a column of n_{h2}=11. These vectors are then taken as input by the output layer neurons and mapped though a linear operation to an output consisting of a column vector with n_o=7 components. The network weights are randomly generated from a uniform distribution for the linear transfer function. For the tangent sigmoid transfer function, the random weights are processed in accordance with the algorithm developed by Nguyen and Widrow (MathWorks, 2002). The weights are continuously updated based on error (difference between the NN outputs and target vector) determined by the Levenberg-Marquardt minimization algorithm.

One of the problems that occur during the NN training phase is called overfitting. The error on the training set is driven to a very small value, but when new data is presented to the network the error is large. The network memorizes the training examples, but it does not learn to generalize to new situations. Overfitting occurs when the NN architecture is too large or NN is trained for too long. Overtraining may end up fitting the data with a more complex function, than the true relationship (e.g., a higher-degree polynomial can fit the same sample points as a lower-degree polynomial). Fitting too closely to the training set means fitting to the noise (experimental errors) as well and thereby doing less well on new inputs that will contain noise independent of that found in the training set.

In order to detect the point of overfitting, the original data set is divided into three sets: the training set, the validation set, and the test set. The training data set is used for computing the gradient and updating the network weights and biases. The error on the validation set is monitored during the training process. The test set is not used during training, but is used to compare different models (architectures). Figure 6.7 shows the training and generalization errors as a function of training epochs (presentation of the data sets to the NN). It can be seen that from the start of training, both the training and validation errors decrease usually exponentially. In the case of oversized NNs or too many epochs, there is a point at which the training error continues to decrease, while the validation error starts to increase. The epoch number of 25 is the point of overfitting. Training is stopped at epoch 25.

6.7.5 Data Set Division

Although there is no rule to divide the data set, a precise data division may yield good performance (Fine, 1998). The total of 746 data sets are divided into three parts arbitrarily, employed in the training procedure using training and validation data sets, and NN performance is investigated on test sets. The MSE, ARE, and R-values for different data divisions are summarized in Table 6.2. The difference between Set A and Set B is that the number of data in the validation Set B is higher than that in Set A. Obviously, the MSE performance of Set B is better (lower MSE value) than that of Set A for the validation set, whereas the training set MSE performance of Set B and Set A are almost equal. Due to an increased number of unknown data in the validation data set, the R-value of Set B (R = 0.8214) is less than that of Set A (R = 0.6692). There is a little difference between the MSE performances of Set A and Set B based on the test data. The R-value of Set C (R = 0.8125) is improved compared to that of Set A. Also, the Set D has highest R-value. This is because most of available data are used to train the network and the calculation of R- value involves all data. However, the Set D is rejected because the MSE and ARE errors are high. For similar reasons, the data division of Set E is rejected. From Table 2, it can be seen that the MSE, and ARE errors of Set C are smaller than those of the other data sets. Therefore, the data division of data Set C is chosen for designing the NN in this study.

6.7.6 Training, Validation and Test Performance

Figure 6.8 shows the MSE performance during the training process. Using the data set C as described above, the MSE performance on the training, validation and test data sets are determined and plotted as a function of epochs is shown in Figure 6.8. It can be seen that the error in the test set reaches a minimum at a similar iteration number as the validation set error. The result is reasonable. Since the test set error and the validation set error have similar characteristics, it does not appear that any significant overfitting is occurred. This also confirms that the selected Set C eliminates the dependence of NN performance on the training set and thereby, ensures that the division in the data sets is not affected the selection of network architecture in this study.

6.7.7 Trial Neural Networks

NNs with One Hidden Layer

First, a two layer feedforward network with one hidden neuron (12-1-7) is initialized and trained using a total of 469 training data sets and a total of 187 validation data sets. Before the training, the principle components that contributed less than 2% to the total variation in the data set are eliminated. As a result of this step, the dimension of the input space reduced from 21 to 12. A total of 100 trials are performed with different random initializations of network weight and bias values. In each trial, each of the subsets (training, validation, test data sets) is randomly chosen so that the sequence of data in an epoch differs from one trial to another. The average of MSE performance from 100 trials is then computed. To this end, a second NN with two neurons in the hidden layer (12-2-7) is selected, trained, evaluated for MSE performances. The procedure continued, designing and training up to 40 more NNs, before the average MSE performances on the test data sets are determined as shown in Figure 6.9. It is evident that as the number of neurons in hidden layer one increases the average MSE error decreases until it reaches 25 neurons. After 25 neurons, an increase in the hidden neurons of NNs does not improve NN performance, but rather the standard deviation of MSE increases. Therefore, a total of 25 hidden neurons are selected as the final NN (i.e., 12-25-7 NN). Also, the R-value (correlation coefficient) between the NN predicted rut and the actual rut along with the MSE and ARE are shown in Figure 6.9. The R-value increases as the hidden neurons are increased in the trial neural network. The nearly maximum R-value of 0.8264 with a standard deviation 0.0341 is found when the number of hidden neurons is 25 in the trial network (9-25-7).

NNs with Two Hidden Layers

The performance of a NN having one layer of hidden neurons can be improved to a certain extent by using two layers of hidden neurons. The number of hidden neurons in first hidden layer is increased, while the number of neurons in the other hidden layer of the NN remains constant. The input layer takes 12 inputs and the output layer has 7 neurons. The number of nodes in the first layer is arbitrarily chosen to vary from 1 to 20, whereas the number of nodes in the second layer is kept between 1 and 15. A total of 300 NNs had been trained to find a NN that shows better performance over the others. For a selected configuration, a network is trained 100 times and then a simulation is performed on the trained NN using the training, validation, test data and total data sets. Results are reported by average and standard deviation of MSE, as shown in Table 6.3. Column 2 and Column 3 show the number of hidden neurons in first and second hidden layers, respectively. The results are presented in ascending order of test sets MSE. The average performance of the first five NNs (first 5 rows) over all simulations are close to each other. The mean MSE error (value = 0.4006) on test data is the lowest in 12-12-11-7 NN, whereas the validation MSE (value = 0.5103) is minimum in 12-13-10-7 NN. However, it can be seen that 9-11-11-7 NN has lower variance in performance compared to that of any other NNs. Also, the variance or standard deviation is very important in selection of NNs. The network, 12-12-11-7 NN is selected as the final NN from the NN family with two hidden layers. The R-value for this network is 0.8129, which is slightly less than that of 12-25-7 NN. The total number of parameters to be adjusted in neural network, 12-25-7 NN is 507 (i.e. weights=25x12+7x25 and bias=25+7). This is higher than the total of parameters 383 (i.e., weights=12x12+12x11+7x11 and bias=12+11+7) to be adjusted in the neural network, 12-12-11-7 NN. It is evident that the increase in the total number of parameters of NN 12-25-7 improves the NN performance by a very little amount. The neural network (12-12-11-7 NN) with two hidden layers is used for prediction.

6.7.8 Neural Network Prediction

At this stage, the trained and tested (validated) network (12-12-11-7 NN) is used to map or simulate a new set of inputs. The difference between the testing and prediction is that the target output is known during testing, whereas in prediction steps, the tested NN is used to find the unknown (target) rutting. A final simulation output is obtained through the development of ensemble networks, where the aim is to optimize the NN outputs through a combination of a number of individual network outputs, trained on same data sets, using the architecture (12-12-11-7 NN) found above. A total of 20 data sets (prediction set), which are used in the architecture selection, are simulated using the 12-12-11-7 NN. The training and simulation procedure is carried out for several times and the resulting output vector is compiled. Figures 6.10(a) to 6.10(g) are the histograms of rut depths (RD) at 500, 1000, 1500, 2000, 4000, 6000, 8000 cycles for data set 5 (mix

ID: 3012-APAC-20117). Similarly, histograms of the rut depths, RD (1)-RD (7) for the each of these 20 data sets are compiled. Estimators of the deformations are calculated from the histograms. In particular, deformations are predicted based on estimators of the mean and maximum likelihood estimator as described earlier. Also, the NN that provides the minimum error (MSE or ARE) on the validation data sets 100 trials is used in simulation (i.e., prediction). In study, the estimation from a NN with the minimum MSE is termed "best MSE net" estimation, whereas the estimation by NN with lowest ARE is termed as "best ARE net" estimation.

The deformations based on mean, maximum likelihood, best net ARE, and best net ARE estimations for data set number 5 using 12-12-11-7 NN are depicted in Figure 6.11. An excellent agreement is observed between the predicted and the actual rut depths. Deformation responses obtained from a single best net, based on the minimum MSE and ARE, are also shown. It can be seen that the maximum likelihood prediction is close to the mean prediction; where as the best net simulation does not show a good generalization capability of the designed NN. Similarly, the predicted and laboratory rut values for the data set number 7 is shown Figure 6.12. A regression analysis of the networks predicted deformations are performed. The entire test data set is applied to the neural network and performed a linear regression between the network outputs and the corresponding targets. In this case, there are 7 outputs and therefore, seven regressions are performed. The results for 8000-cycle rut depth for a test data set 12 using 12-12-11-7 NN are shown in Figures 6.13(a) to 6.13(g). The best linear fit is indicated by dash line. The perfect fit (output equal to target) is indicated by the solid line. As the best linear fit line approaches close to the perfect fit line, the NN simulation is evaluated as better. It can be seen that 8000-cycle (Figure 6.13(g)) rut depth has the highest correlation coefficient among the rut depths at other cycles (Figure 6.13(a)). Also, the maximum likelihood and mean prediction has higher correlation that of a single neural network. The regression coefficient for the validation and training data sets are listed in Table 6.4. From the regression coefficients shown in Table 6.4 and Figure 6.13(a)-(g), it is evident that the use of families of networks trained on different initial conditions can improve the network performance. Better performance can be achieved through the linear combination of the trained networks instead of simply choosing the single best network. A possible explanation of this can be that the linear combination of network results in a new, more complex network that can explain the improved fit to the training data. The total error from simulation over the test data sets is determined to be:

Total relative error of mean estimator = 0.2394

Total relative error of the maximum likelihood estimator = 0.2456

Total relative error of best net by the minimum MSE = 0.2451

Total relative error of best net by the minimum ARE = 0.2775

6.7.9 Neural Networks Application

As mentioned before, one of the major goals of this study is to use the designed NN as a performance-based mix design tool. Consequently, the validated NN model, found above, is applied to design Superpave mixes to examine HMA rutting potential. It is know that the Superpave method of mix design requires three parameters for the determination of optimum asphalt content. These are percentage air voids, VMA, and VFA. According to the Superpave method of mix design, HMA is designed based on the volumetric properties only. Currently, the Superpave method does not include a performance test to check whether a mix having the optimum asphalt content will perform satisfactorily. This study proposes rut as a performance test for the Superpave method of mix design. The rut value can be obtained from laboratory testing or using the NN developed in this study. In essence, two Superpave mixes (Mix 3037-OAPA-25089 and Mix 3012-OK-02156) are tested for rutting using NN simulations. Both of these mixes are currently being used in the state of Oklahoma. From the mix design information, it is known that Mix 3037-OAPA-25089 contains an optimum asphalt content of 4.8%. In a neural network simulation procedure, the mix information such as gradation, aggregate properties, and binder PG is kept constant, whereas the amount of binder is varied. The simulation results using the developed NN model are shown in Figure 6.14 for Mix 3037-OAPA-25089. It can be seen that for asphalt content in the range of 4 to 4.8 %, rut depth (mm) increases as binder content increases. Then in the range of 4.8 to 5.5%, rut depth slightly decreases as the asphalt content of the mix increases. Beyond 5.5%, rut depth increases exponentially as the asphalt content increases. Clearly, there is an inflection point at 5.5% asphalt content. Therefore, the optimum asphalt content of Mix 3037-OAPA-25089 is 5.5% based on the rut criteria. The HMA mixes prepared with asphalt contents below 4.5% satisfy the low rut criteria, but fail to meet the moisture-induced damage criteria (indirect tensile test). Similarly, the simulation results for Mix 3012-OK-02156 are plotted in Figure 6.15. It can be seen that for asphalt content in the range of 3.5 to 4.3%, rut depth (mm) increases with increasing binder content. For asphalt content in the range of 4.3 to 4.49%, rut depth slightly decreases as the asphalt content of the mix increases. Beyond that (4.49%-

5.5%), rut depth increases exponentially with increasing asphalt content. Clearly, there is an inflection point at 4.49% asphalt content, which is considered the optimum asphalt content for this mix. Simulations are not performed beyond 5.5% asphalt content because with higher amount of asphalt, the mix will flow. Also, it is impractical to fabricate HMA samples at very high asphalt contents. Again, below 3.5% asphalt content, mixes fail due to moisture-induced damage. Although this study finds the inflection points (Figures 6.14-6.15) for each case of the Mix 3037-OAPA-25089 and Mix 3012-OK-02156, further investigations would be helpful to conclude that such an inflection point always occurs. There may occur situations in which a mix will not show any inflection point. In such cases, this study recommends selecting the optimum asphalt content based on air voids, VMA, VFA, and moisture-induced damage criteria. Of course, rut performance can be a secondary check for such mixes. Thus, the developed neural network in this study can be used to examine new designs (HMA) prior to implementation. It is to be noted that finding the optimum amount of asphalt in these example mixes is very inexpensive and time-efficient. In addition, by changing model inputs and observing the resulting outputs, it is possible to study the important variables, and how variables interact with each other. Also, a neural network model can be used to estimate the performance (non-destructive performance) of existing pavements. In a neural network simulation, a broader range of experimental conditions can be covered, than would generally be possible through laboratory testing.

6.8 Conclusions

In this study, a 3-layer feedforward neural network model is designed and applied to determine a mapping that associates asphalt mix design factors and testing parameters of HMA samples with their rutting performance. The developed network uses 12 neurons in the first hidden layer, 11 hidden neurons in the second hidden layer, whereas the output layer uses a total of 7 neurons. Using a total of 21 mix factors as input, the developed model produces rut depths at 7 different cycles. The time series (cycle) of rutting are recorded over 8000 cycles by an interpolation with piecewise linear elements, using these few outputs. A total of 746 sets of data obtained from mix design information and laboratory tests are used for developing this NN model. Preprocessing and principal component analyses are applied, and the network trained using the Levenberg-Marquardt algorithm. Using randomly generated weight factors to initialize the training algorithm, histograms are compiled and outputs estimated using statistical estimators. An excellent agreement is observed between test data and simulations. To this end, the developed NN is used to estimate (based on the rut performance) the optimum asphalt content for a Superpave mix. The results are satisfactory. It is believed that the proposed NN model will be a useful tool in the study of asphalt mix design and performance evaluation.

Table 6.1 Mix Properties Used in Neural Network Design

Properties	Mix Type	S2	S3	S3-rec	S4	S6
Sieve Size, mm (in)	37.5 (1 ½ in.)	100	-	-	-	-
	25.0 (1 in.)	90-100	100	100	-	-
	19.0 (3/4 in.)	-	90-100	90-100	100	-
	12.5 (1/2in.)	-	90max	90max	90-100	-
	9.5 (3/8 in.)	-	-	-	90 max	100
	4.75 (No.4)	40-40	-	-	-	80-100
	2.36 (No.8)	19-45	23-49	23-49	28-58	54-90
	2.00 (No.10)	-	-	-	-	-
	1.18 (N0.16)	18-24	22-28	22-28	26-32	39-39
	0.60 (No.30)	14-18	17-21	17-21	19-23	26-32
	0.425 (No.40)	-	-	-	-	-
	0.30 (No.50)	11-11	14-14	14-14	16-16	19-23
	0.15 (N.100)	-	-	-	-	16-16
	0.075 (No.200)	0.6 –1.2 P_{eff}	0.6 –1.2 P_{eff}	0.6 –1.2 P_{eff}	0.6 –1.2 P_{eff}	5-15
Design Method		Superpave	Superpave	Superpave	Superpave	Superpave
Nominal Maximum Size (NMS), mm		25	19	19	12.5	4.75
Lift Thickness, mm		56-112	56-112	56-112	37.5-75	12.5-25
Compaction Method		SGC/field	SGC/field	SGC/field	SGC/field	SGC/field
Asphalt to Dust Ratio		1.2	0.9	1.1	1.1	0.9

Note: P_{eff} = Effective Percentage Binder, SGC = Superpave Gyratory Compactor, '-' = N/A value, and S2 = Superpave mix type 2

Table 6.2 Neural Network Performances on Different Data Divisions

Data Set		Mean Square Error (MSE)			Average Relative Error			R-value
		Training	Validation	Test	Training	Validation	Test	All Data
A	$D_T = 273$ $D_V = 187$ $D_G = 187$	0.3616	0.5731	0.5012	0.2579	0.3729	0.3764	0.6692
B	$D_T = 373$ $D_V = 283$ $D_G = 90$	0.3006	0.5146	0.5044	0.2846	0.2982	0.2815	0.8214
C	$D_T = 469$ $D_V = 187$ $D_G = 90$	0.3019	0.5018	0.4111	0.2519	0.2781	0.2618	0.8125
D	$D_T = 567$ $D_V = 90$ $D_G = 90$	0.3580	0.6172	0.596	0.2907	0.3450	0.3339	0.8537
E	$D_T = 90$ $D_V = 567$ $D_G = 90$	0.4013	0.7861	0.7402	0.2741	0.5126	0.3941	0.4587

Note: D_T = Training Data Sets, D_V = Validation Data Sets, D_G = Test Data Sets.

Table 6.3 Training Performances of NNs with Two Hidden Layers

Trial NN No.	Neurons in h_1 layer	Neurons in h_2 layer	Training Data Set		Validation Data Set		Test Data Set		Total Data Set	
			Mean	Std dev.	Mean	Std Dev.	Mean	Std Dev.	Mean	Std Dev.
1	12	11	0.3120	0.0314	0.5251	0.0649	0.4006	0.0413	0.3081	0.0236
2	18	10	0.3018	0.0375	0.5526	0.1028	0.4271	0.1446	0.3205	0.0326
3	10	12	0.3053	0.0209	0.5704	0.0550	0.4524	0.0829	0.3293	0.0173
4	13	10	0.2980	0.0200	0.5103	0.0668	0.4532	0.0957	0.3175	0.0167
5	10	12	0.3198	0.0500	0.6022	0.1478	0.4858	0.1931	0.3379	0.0449
6	16	9	0.3232	0.0279	0.6008	0.1007	0.5077	0.1139	0.3412	0.0265
7	12	10	0.3305	0.0249	0.6419	0.0554	0.5663	0.0655	0.3446	0.0216
8	14	12	0.3132	0.0483	0.6194	0.1311	0.6006	0.1539	0.3561	0.0444
9	11	10	0.3578	0.0183	0.7281	0.0993	0.6623	0.1143	0.3682	0.0179
10	9	9	0.3645	0.0344	0.7341	0.0540	0.6425	0.1604	0.3881	0.0456

Note: h_1 = hidden layer 1; h_2 = hidden layer 2; Std Dev. = standard deviation

Table 6.4 R-value for the Linear Regression Fit of Simulated and Actual Rut Depths

NN Output (Rut-Cycle)	R-value			
	Maximum Likelihood	Mean Estimator	Best Net (MSE)	Best Net (ARE)
Using Training Data				
RD-0500-cycle	0.7454	0.7846	0.7785	0.7039
RD-1000-cycle	0.8047	0.8324	0.8219	0.7639
RD-1500-cycle	0.8053	0.8398	0.8322	0.7763
RD-2000-cycle	0.8238	0.8431	0.8365	0.7834
RD-4000-cycle	0.8295	0.8491	0.8455	0.7967
RD-6000-cycle	0.8249	0.8456	0.8440	0.8001
RD-8000-cycle	0.8155	0.8401	0.8403	0.8028
Using Validation Data				
RD-0500-cycle	0.8902	0.8981	0.9041	0.9065
RD-1000-cycle	0.9035	0.9167	0.9202	0.9221
RD-1500-cycle	0.9166	0.9275	0.9305	0.9308
RD-2000-cycle	0.9222	0.9307	0.9323	0.9327
RD-4000-cycle	0.9320	0.9355	0.9354	0.9337
RD-6000-cycle	0.9286	0.9334	0.9329	0.9297
RD-8000-cycle	0.9258	0.9285	0.9267	0.9230
Using Total Data				
RD-0500-cycle	0.8577	0.8719	0.8716	0.8581
RD-1000-cycle	0.8796	0.8955	0.8933	0.8820
RD-1500-cycle	0.8892	0.9054	0.9041	0.8911
RD-2000-cycle	0.8973	0.9082	0.9067	0.8935
RD-4000-cycle	0.9055	0.9127	0.9113	0.8968
RD-6000-cycle	0.9021	0.9110	0.9096	0.8951
RD-8000-cycle	0.8989	0.9066	0.9047	0.8915

Note: MSE=Mean Square Error, ARE= Average Relative Error, R=Regression Coefficient
NN = neural network, RD =Rut Depth, Total Data = (Training+Testin+validation) data

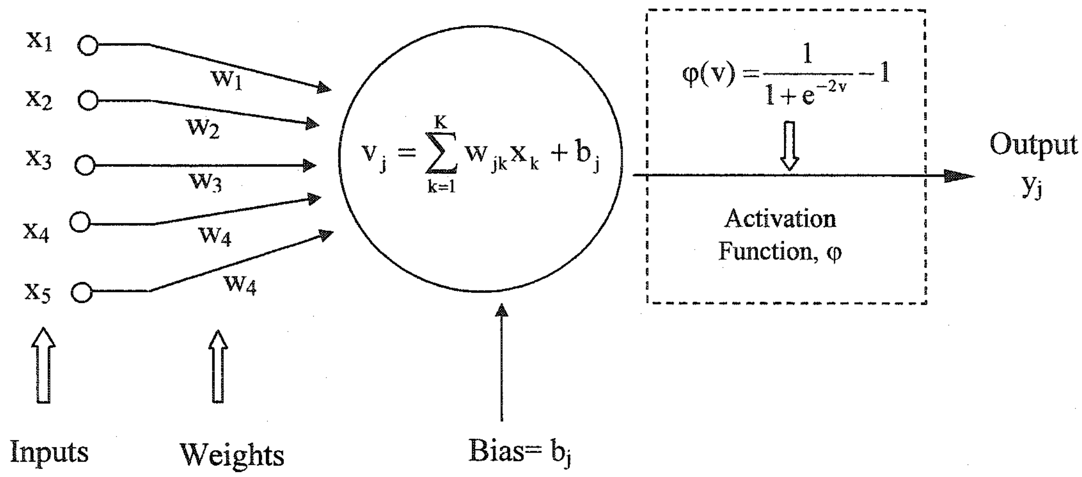

Figure 6.1 Nonlinear Model of a Neuron

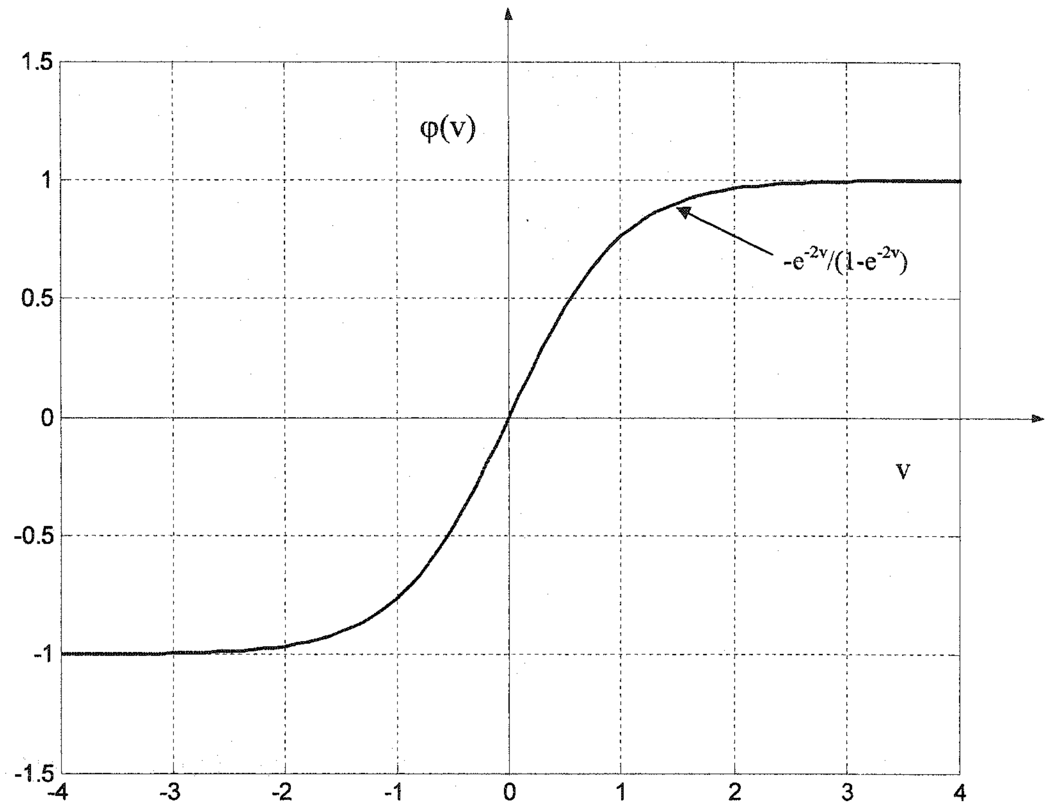

Figure 6.2 Tan-Sigmoid Transfer Function

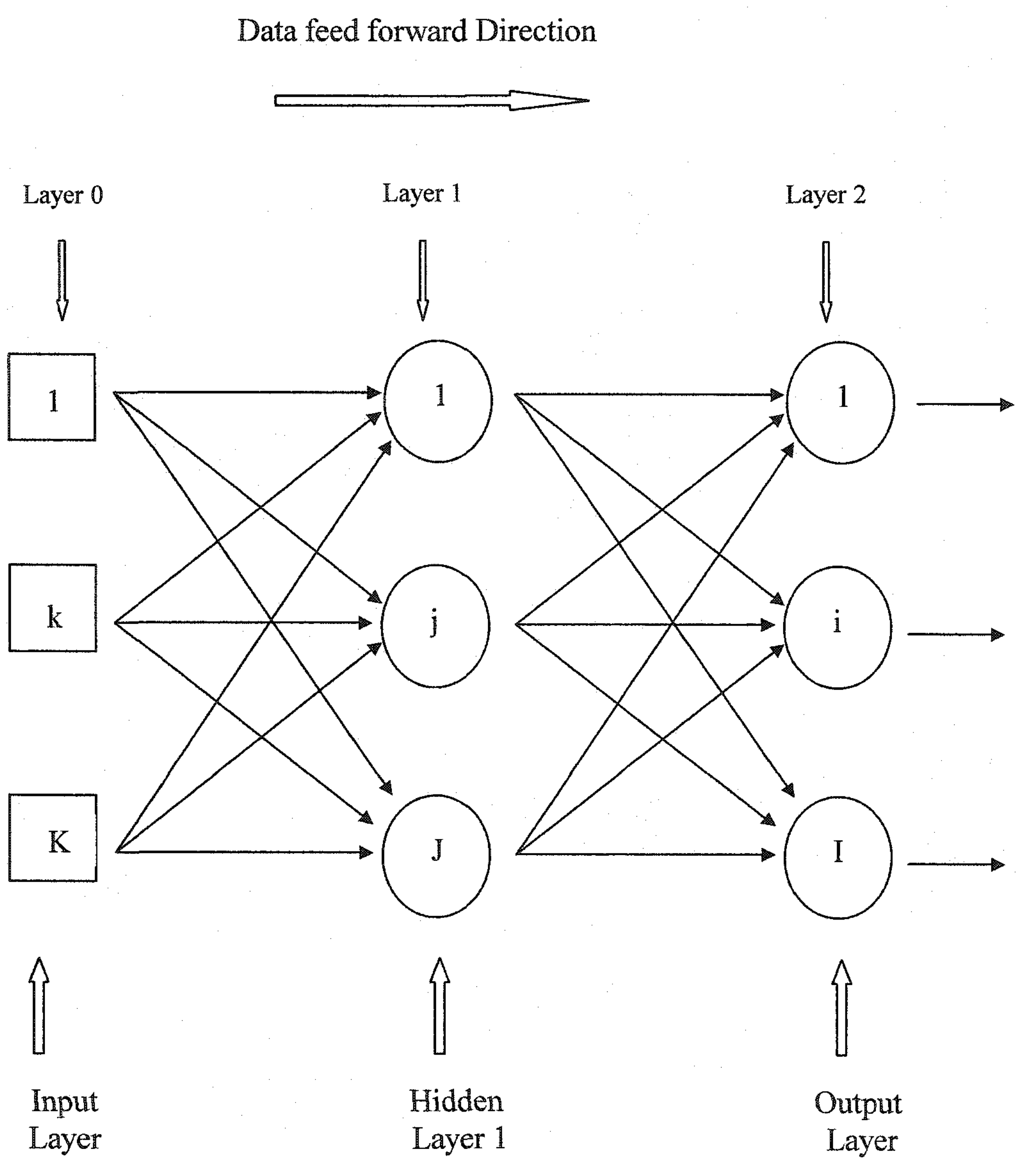

Figure 6.3 Multilayer Feedforward NN Architecture

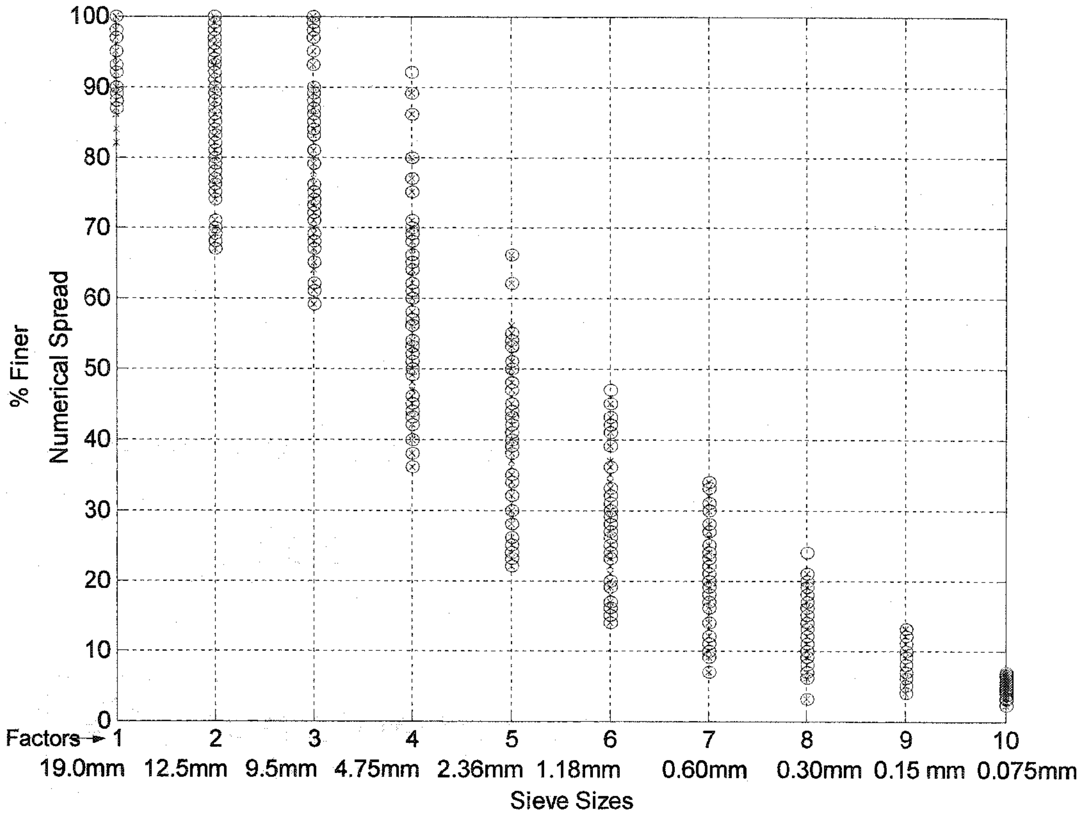

Figure 6.4 (a) Numerical Spread of the Input Factors 1-10

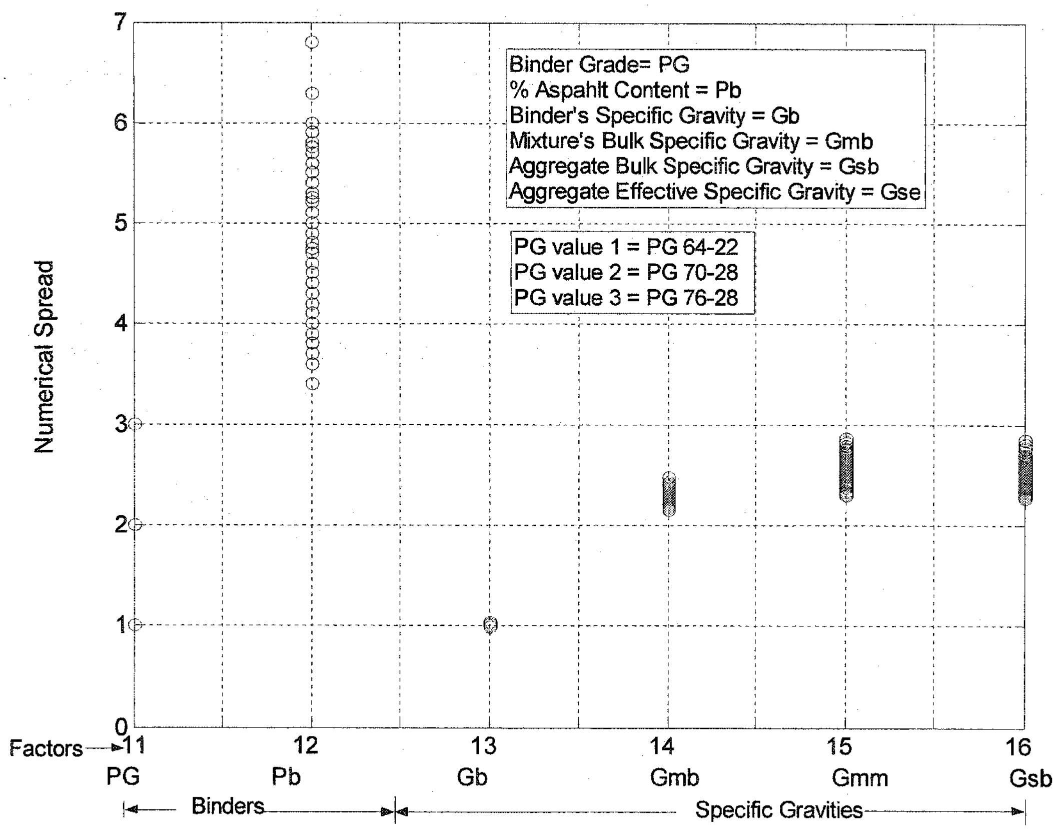

Figure 6.4 (b) Numerical Spread of the Input Factors 11-16

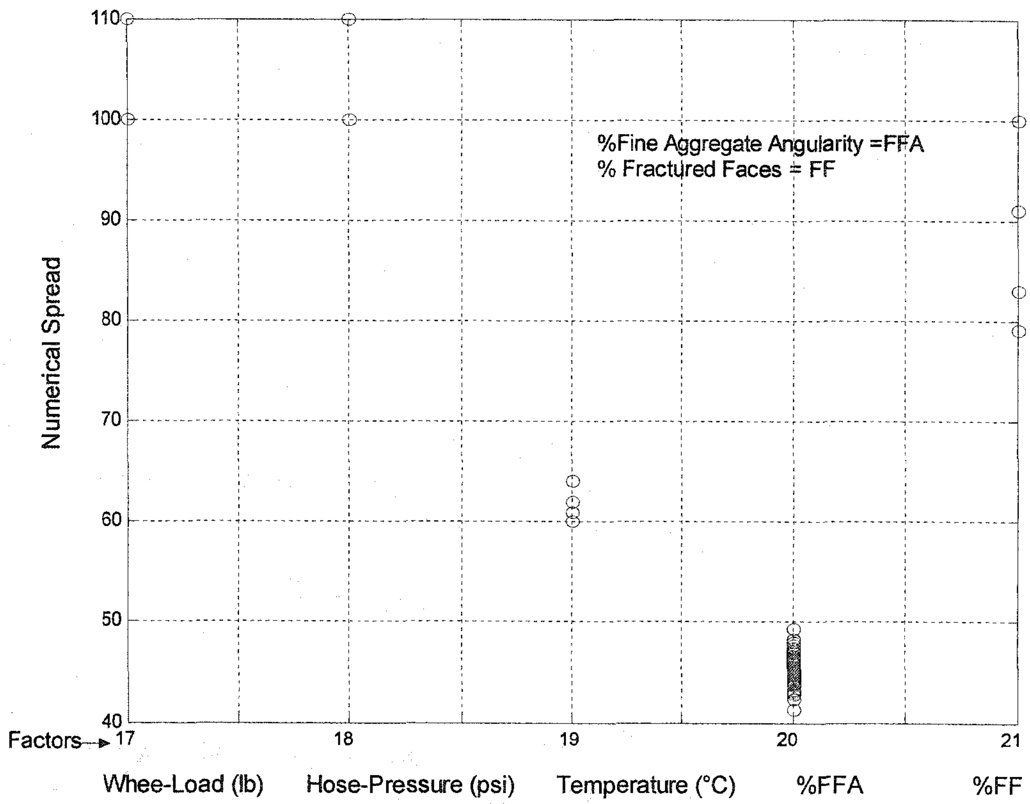

Figure 6.4 (c) Numerical Spread of the Input Factors 17-21

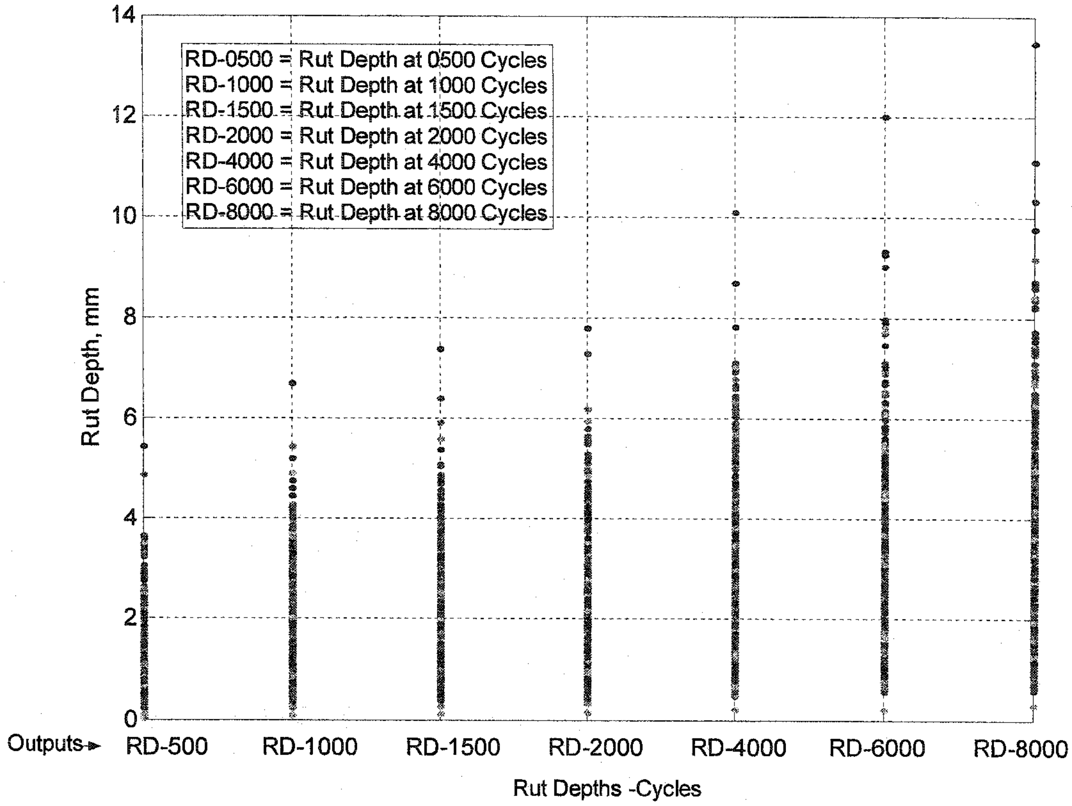

Figure 6.5 Numerical Spread of the Output Vector (1-7)

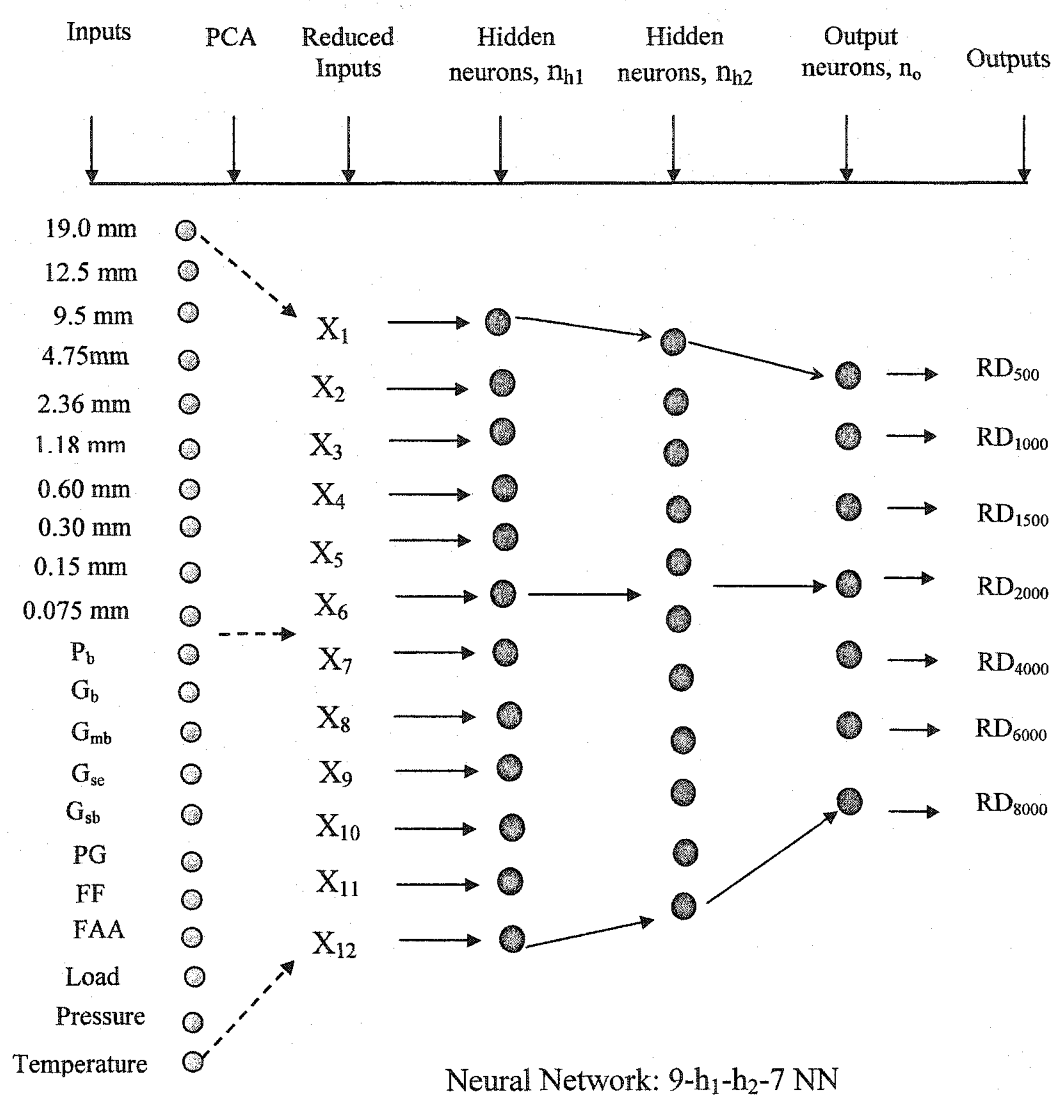

Figure 6.6 Neural Network for Predicting Asphalt Rutting

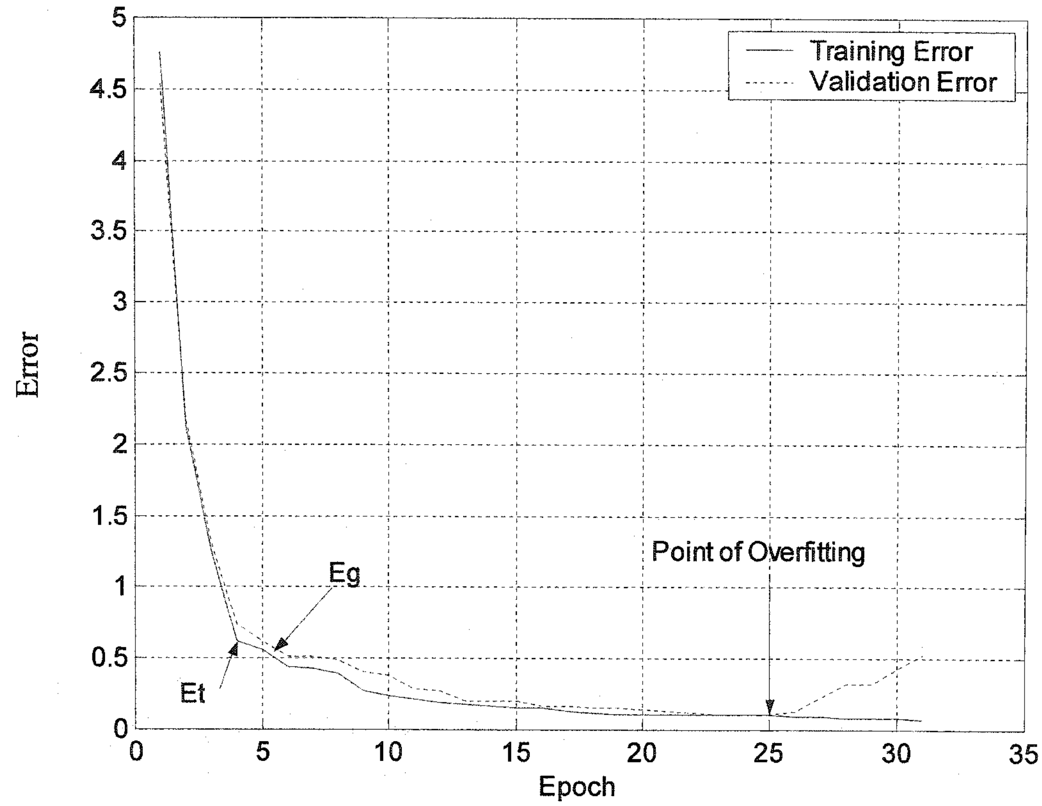

Figure 6.7 Overfitting of Neural Network

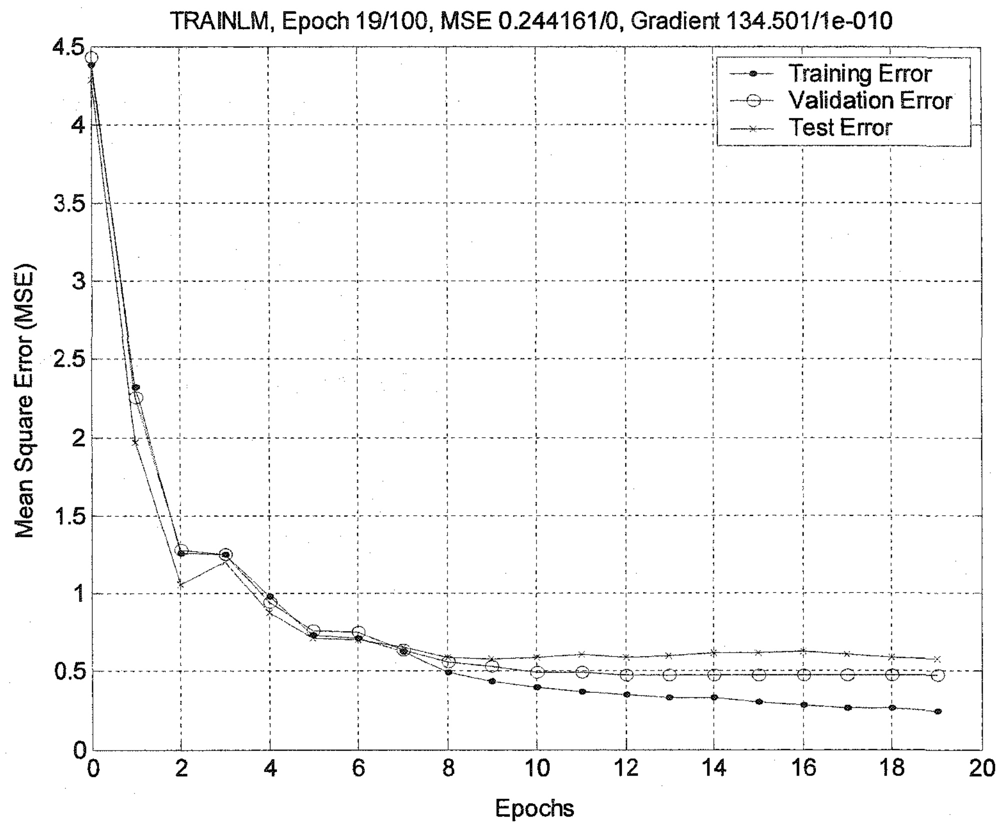

Figure 6.8 Training Performance of Neural Network

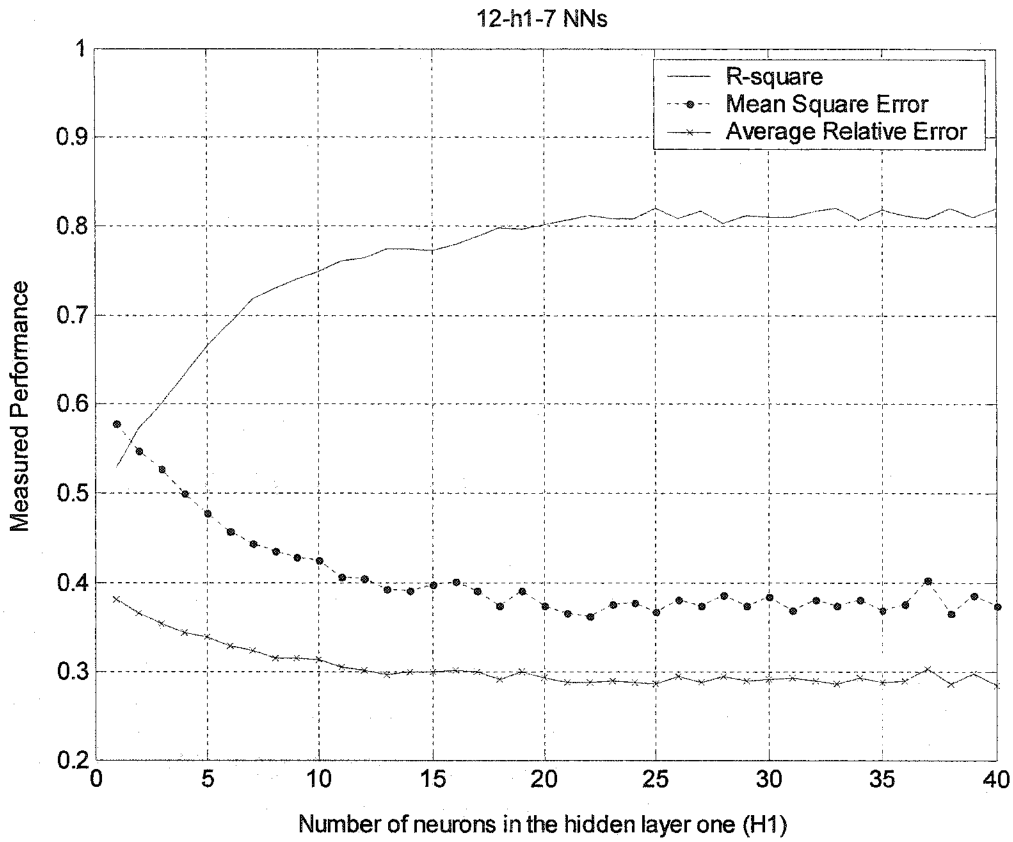

Figure 6.9 Performance of NNs with One Hidden Layer

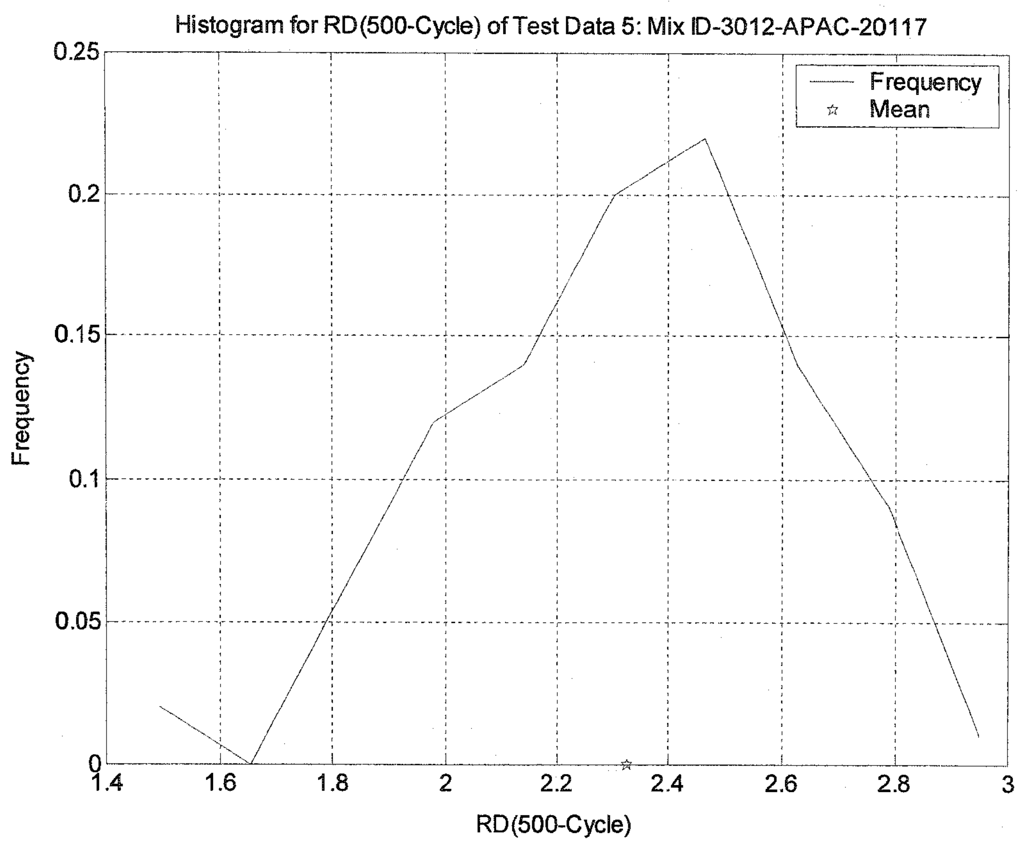

Figure 6.10(a) Histogram for RD (1) of Test Data 5

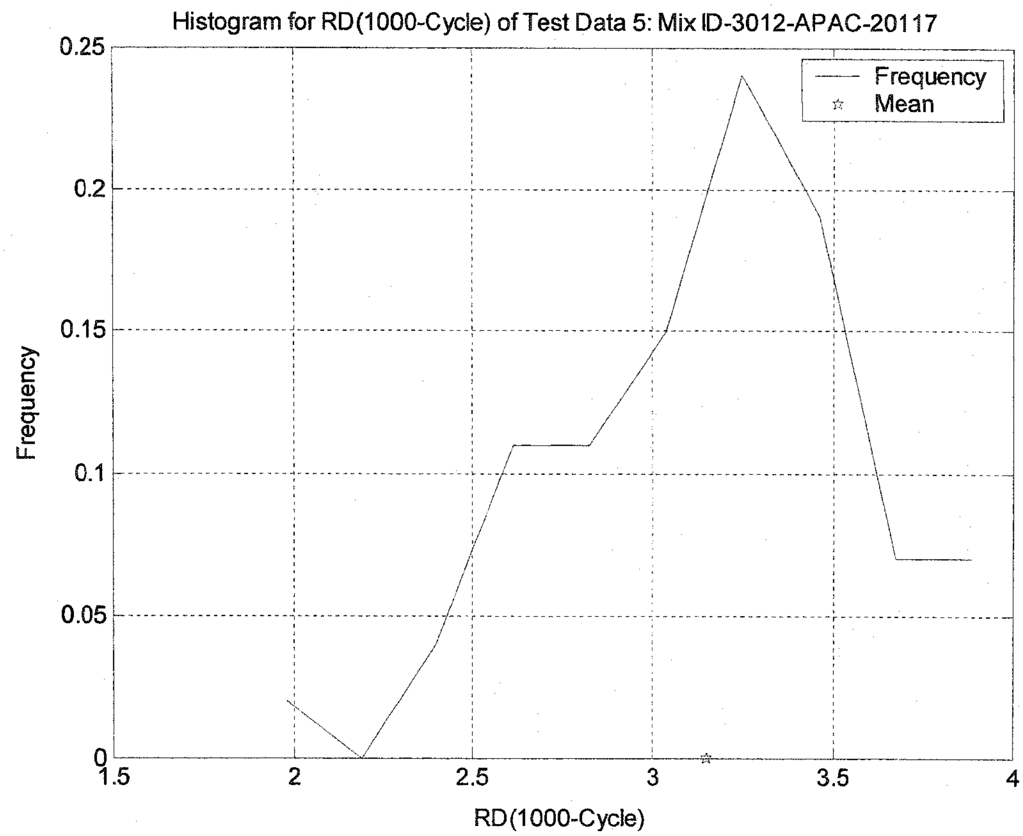

Figure 6.10(b) Histogram for RD (2) of Test Data 5

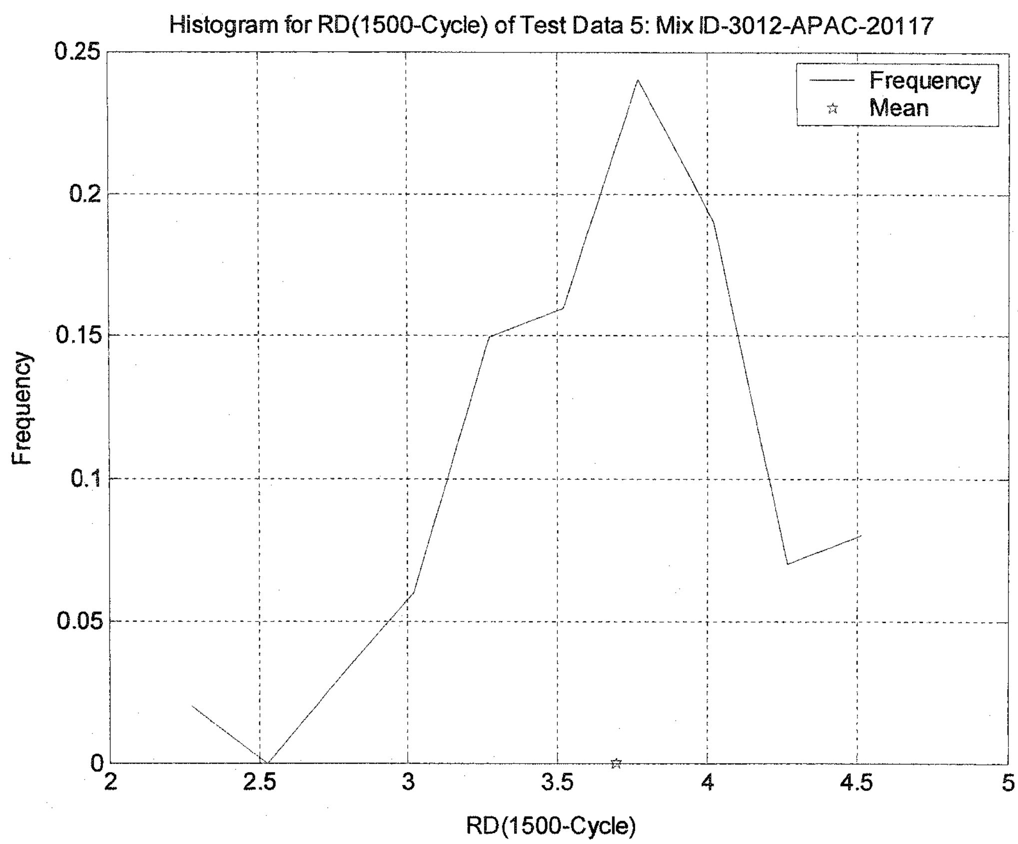

Figure 6.10(c) Histogram for RD (3) of Test Data 5

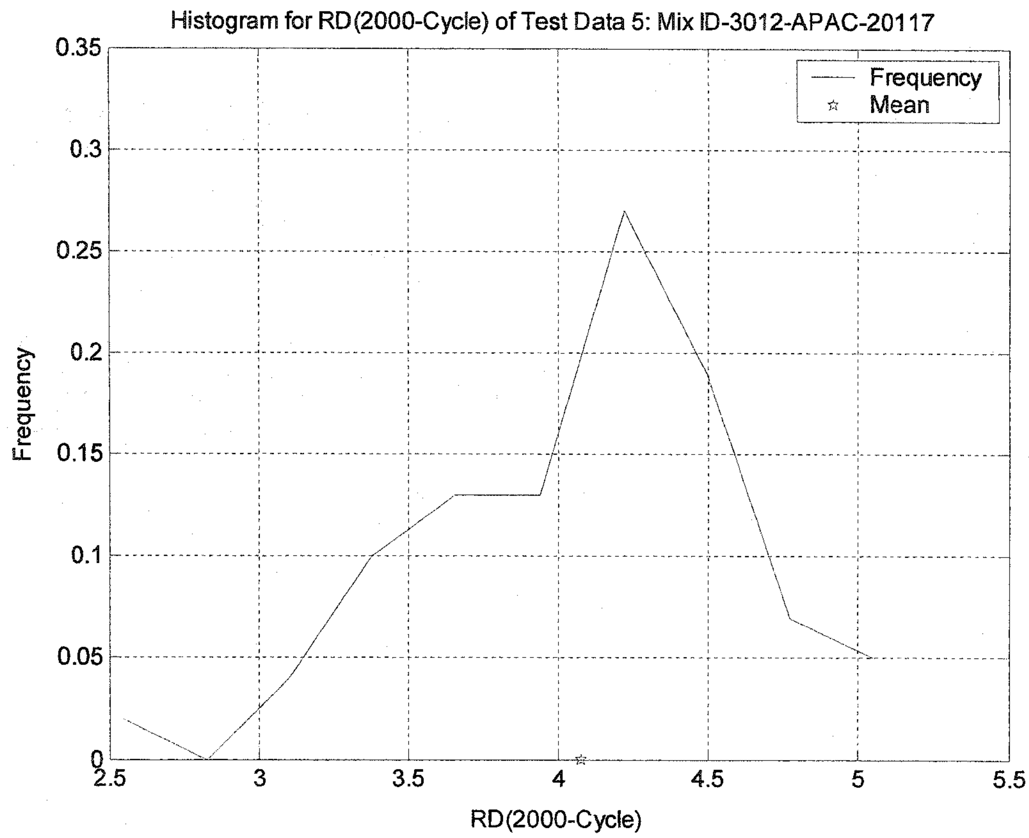

Figure 6.10(d) Histogram for RD (4) of Test Data 5

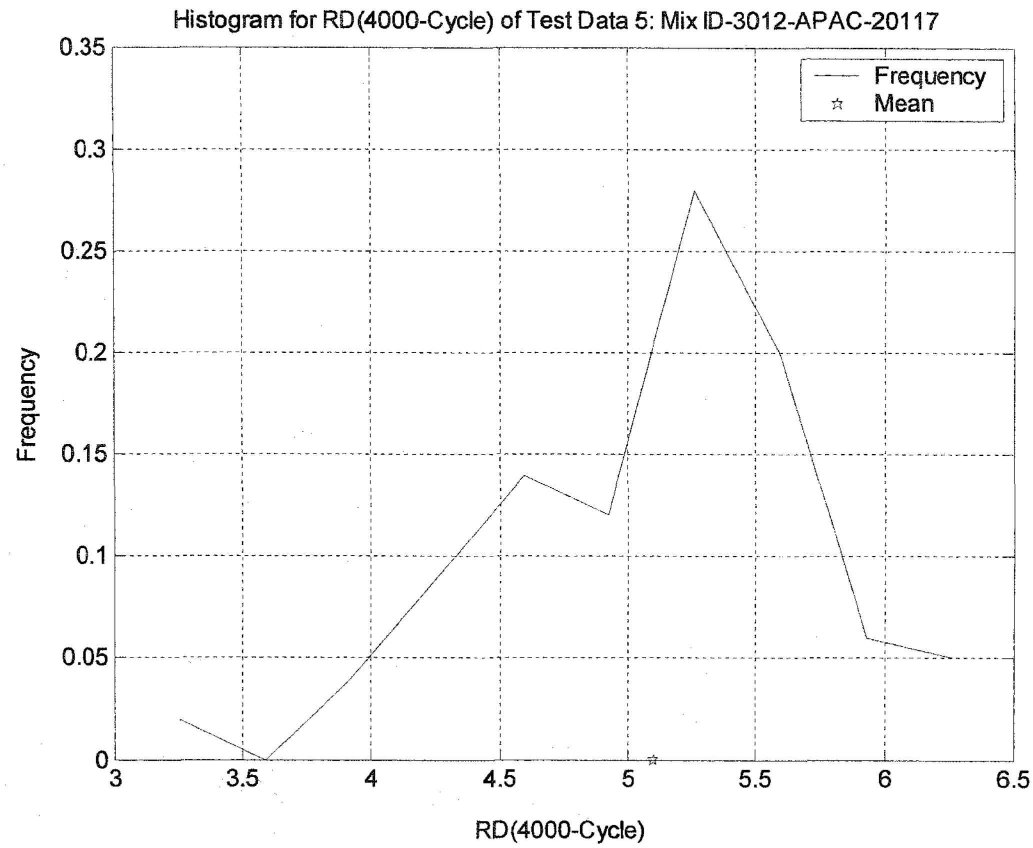

Figure 6.10(e) Histogram for RD (5) of Test Data 5

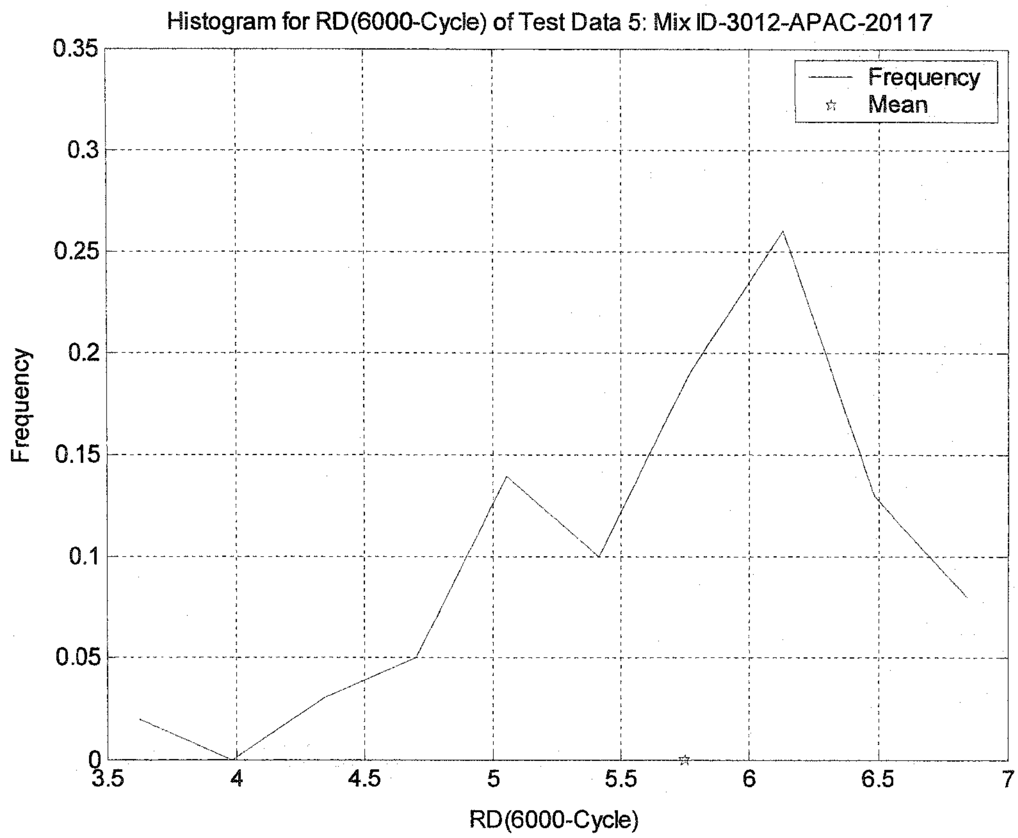

Figure 6.10(f) Histogram for RD (6) of Test Data 5

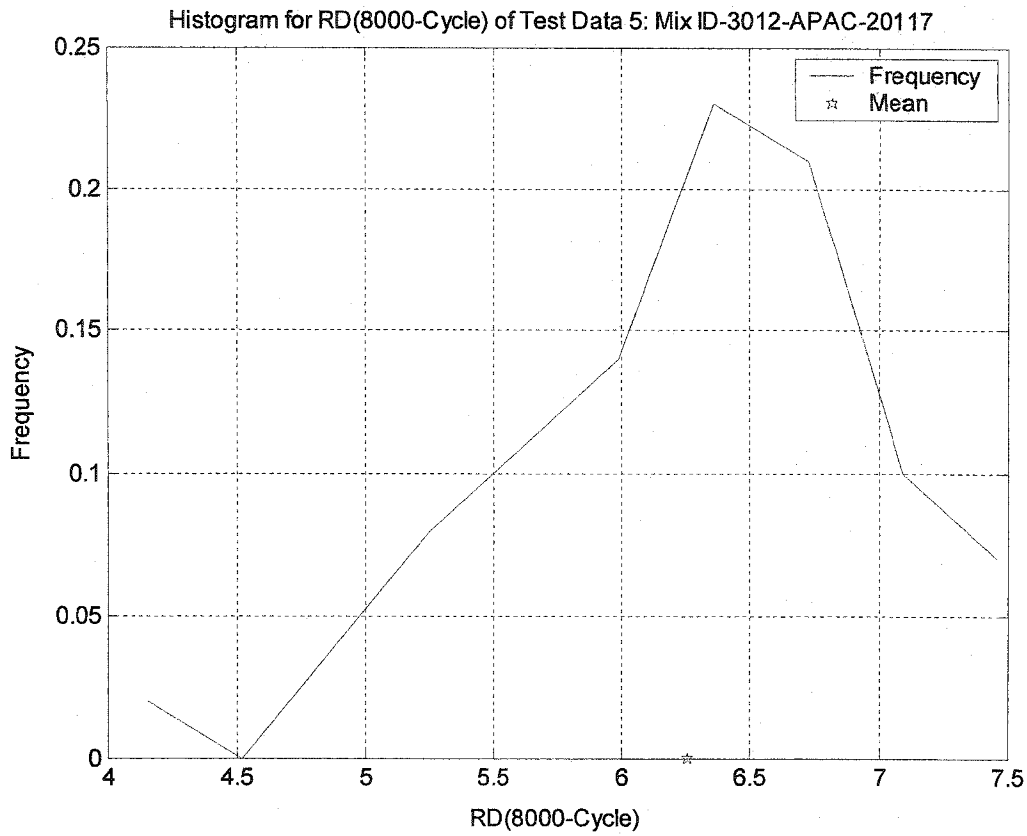

Figure 6.10(g) Histogram for RD (7) of Test Data 5

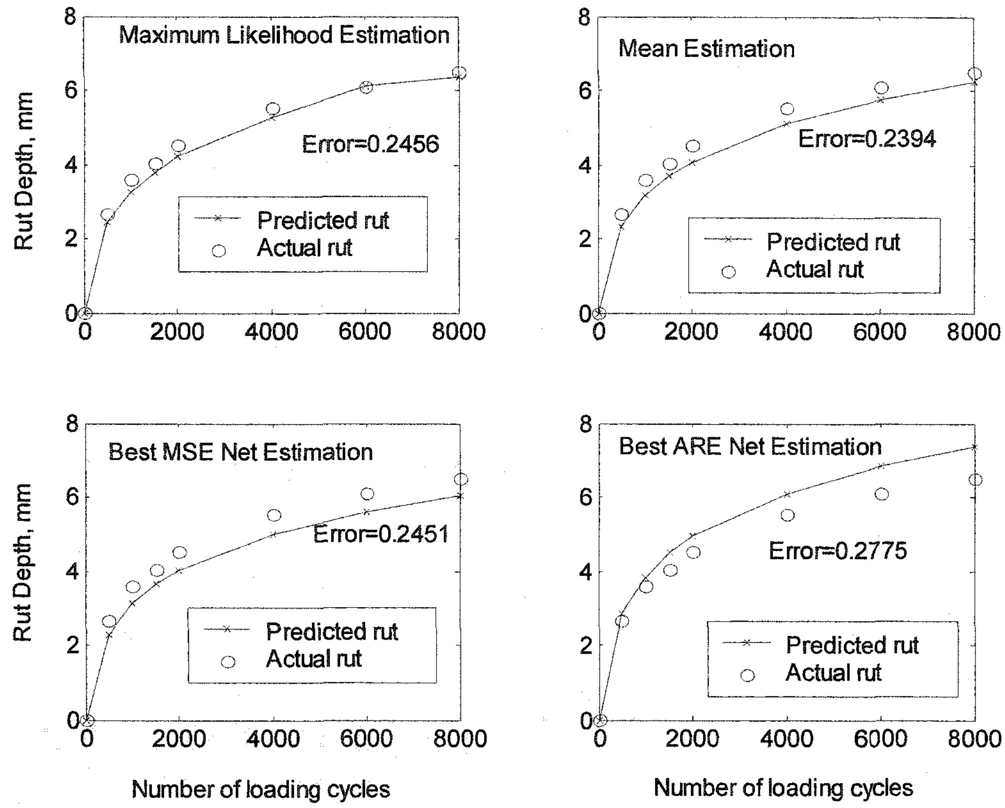

Figure 6.11 Predicted Versus Actual Rut Depths (Data Set 5)

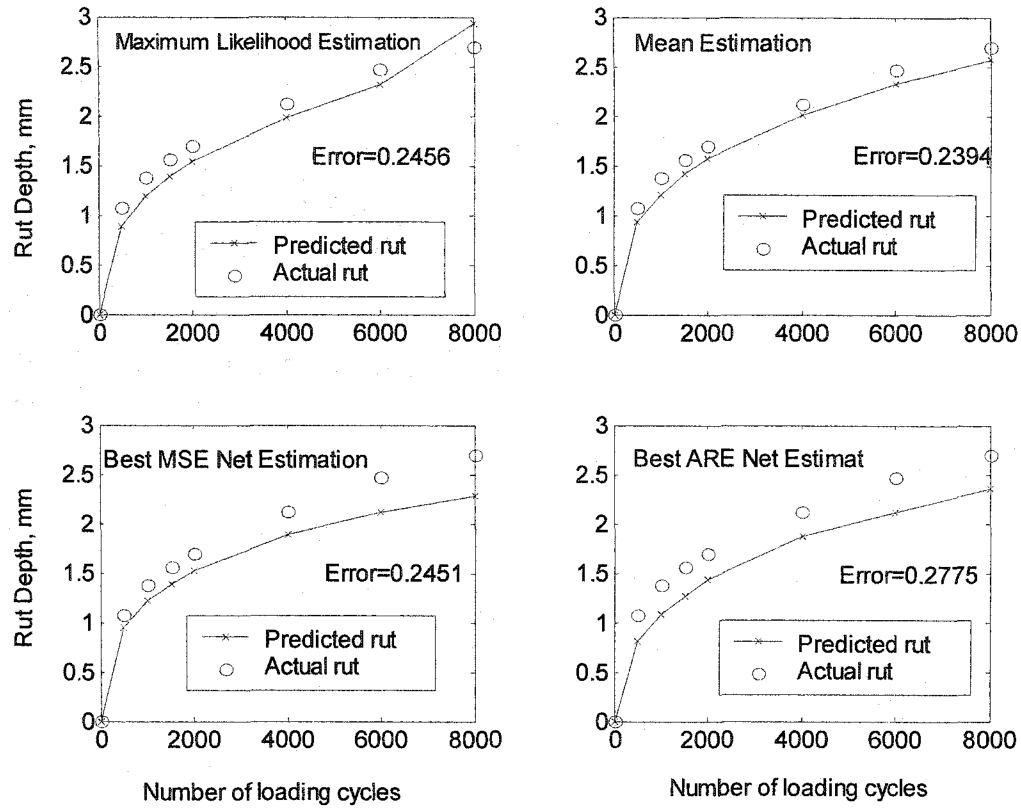

Figure 6.12 Predicted Versus Actual Rut Depths (Data Set 7)

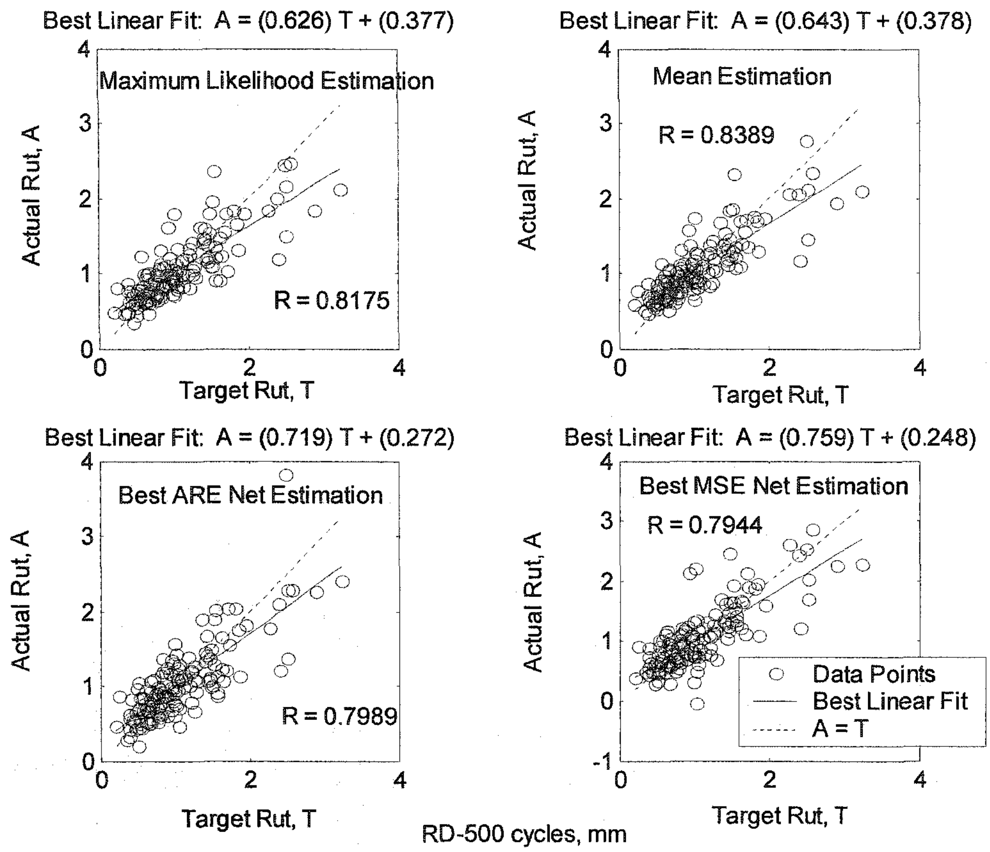

Figure 6.13 (a) Regression Plot for 500-Cycle Rut Estimation

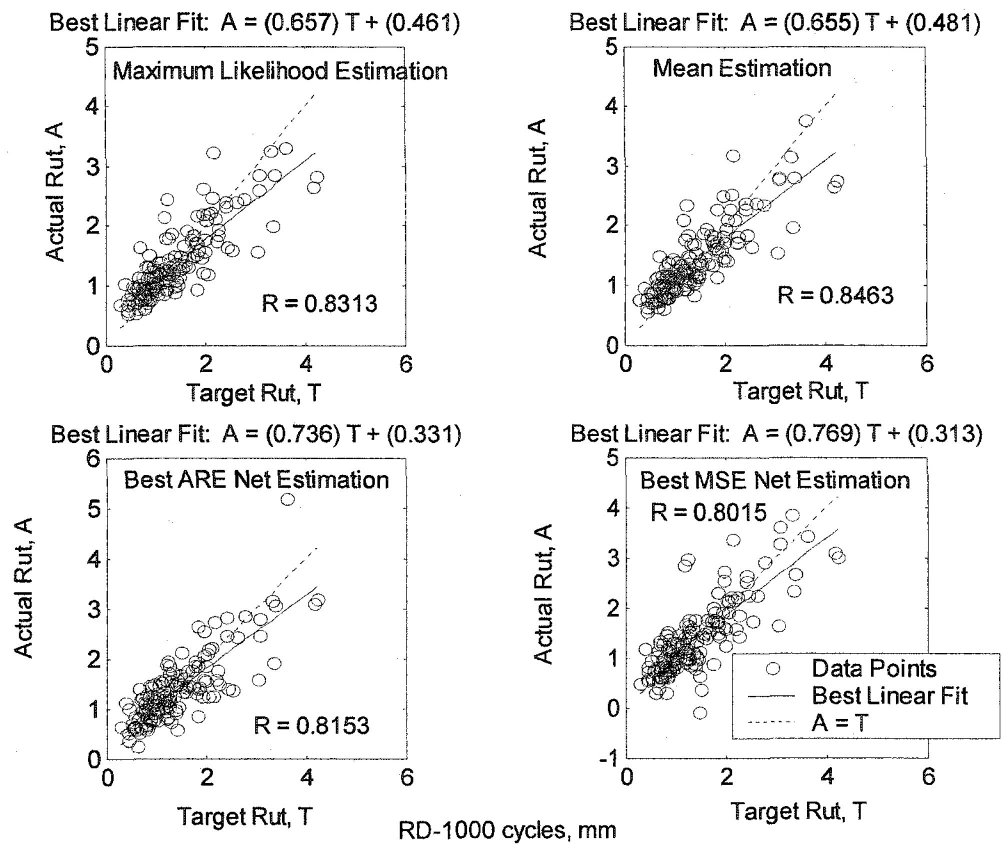

Figure 6.13 (b) Regression Plot for 1000-Cycle Rut Estimation

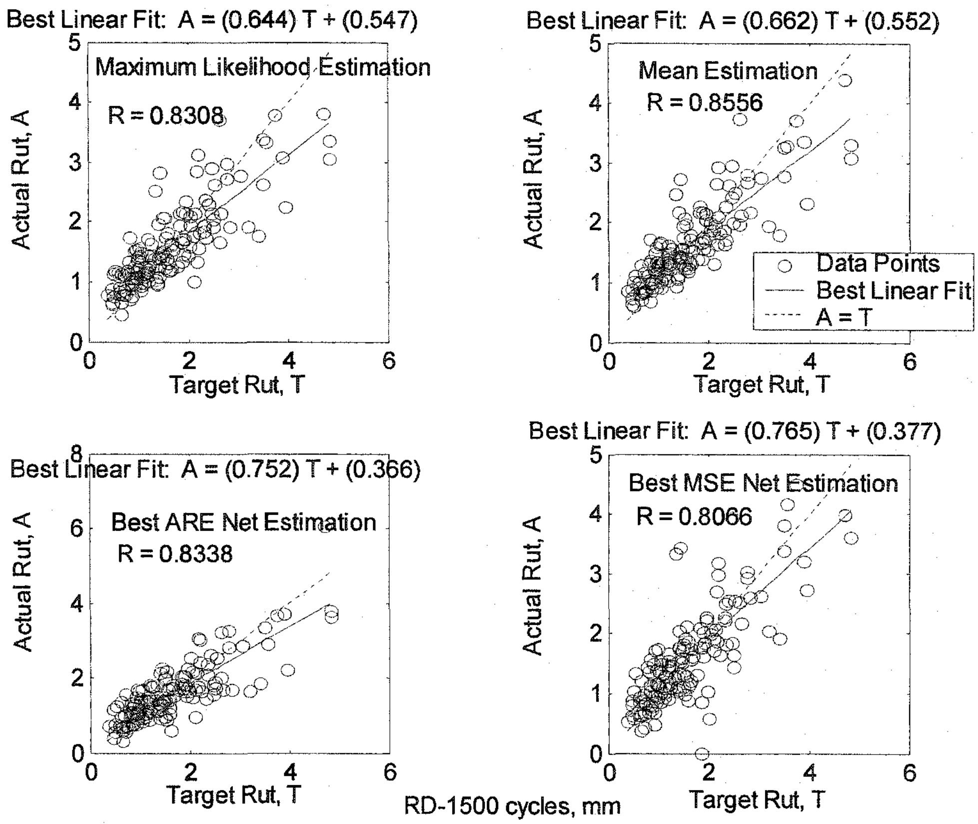

Figure 6.13 (c) Regression Plot for 1500-Cycle Rut estimation

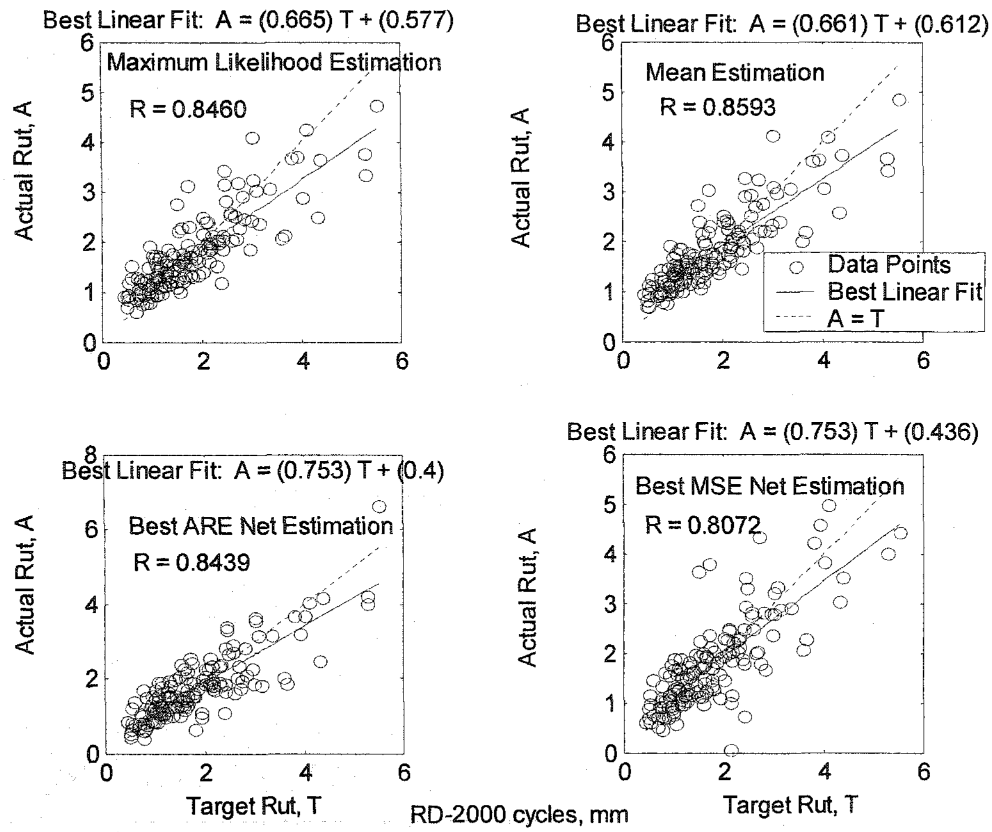

Figure 6.13 (d) Regression Plot for 2000-Cycle Rut Estimation

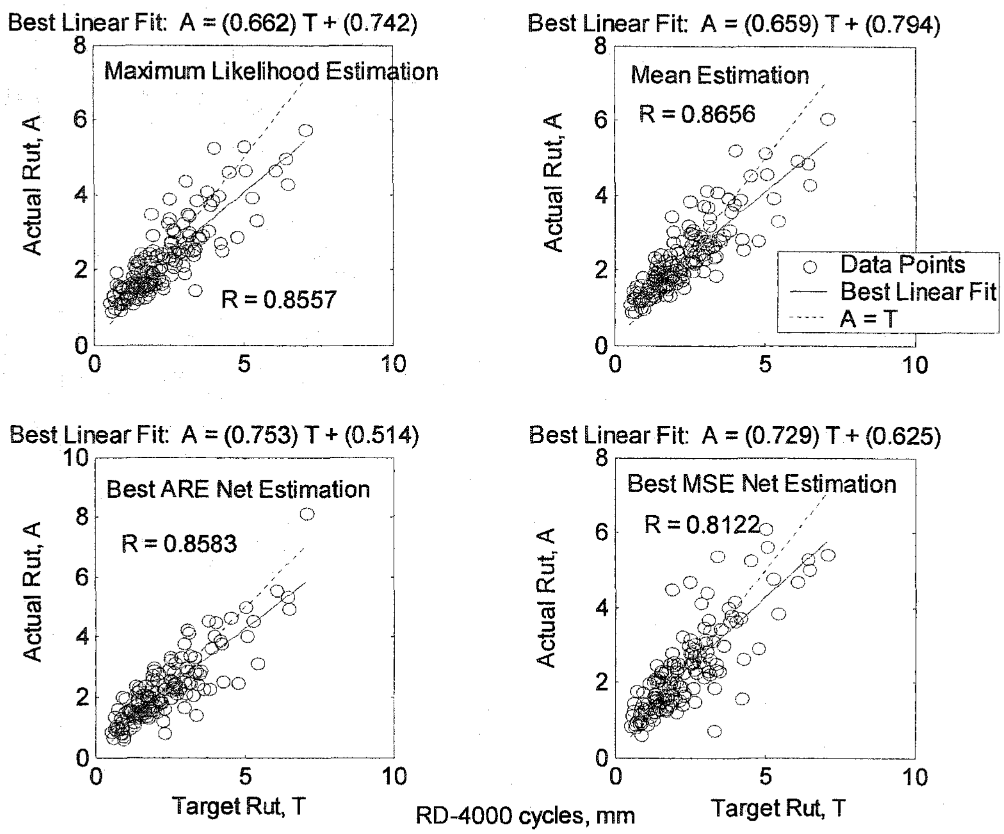

Figure 6.13 (e) Regression Plot for 4000-Cycle Rut Estimation

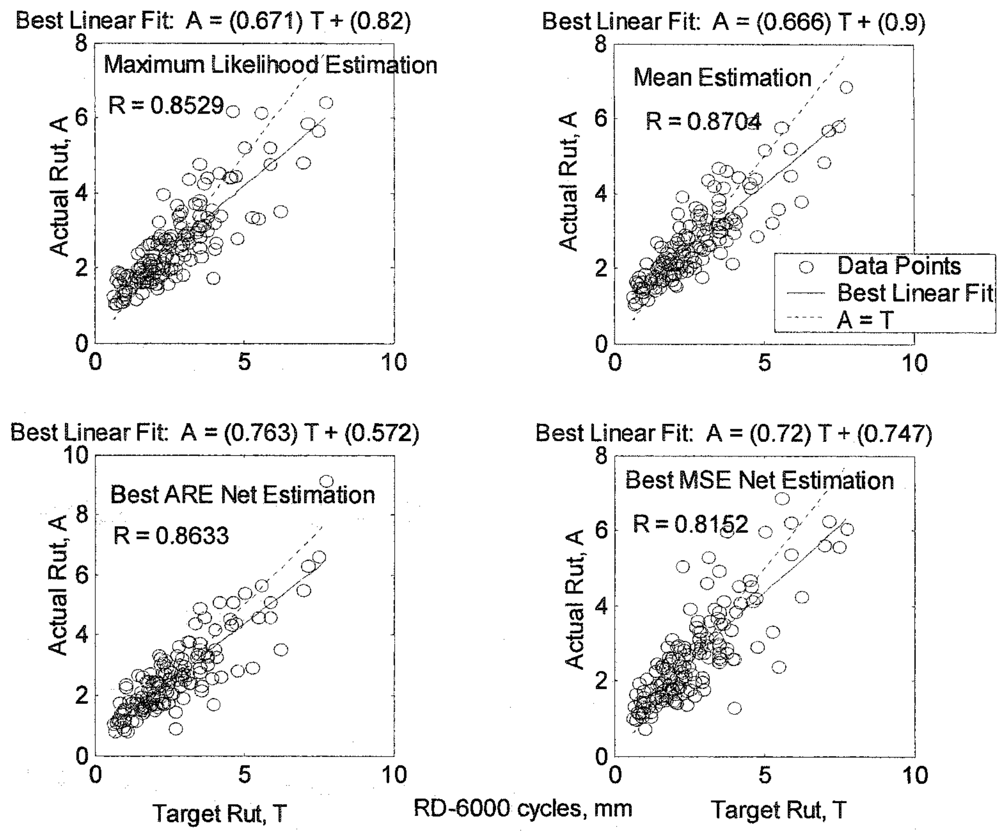

Figure 6.13 (f) Regression Plot for 6000-Cycle Rut Estimation

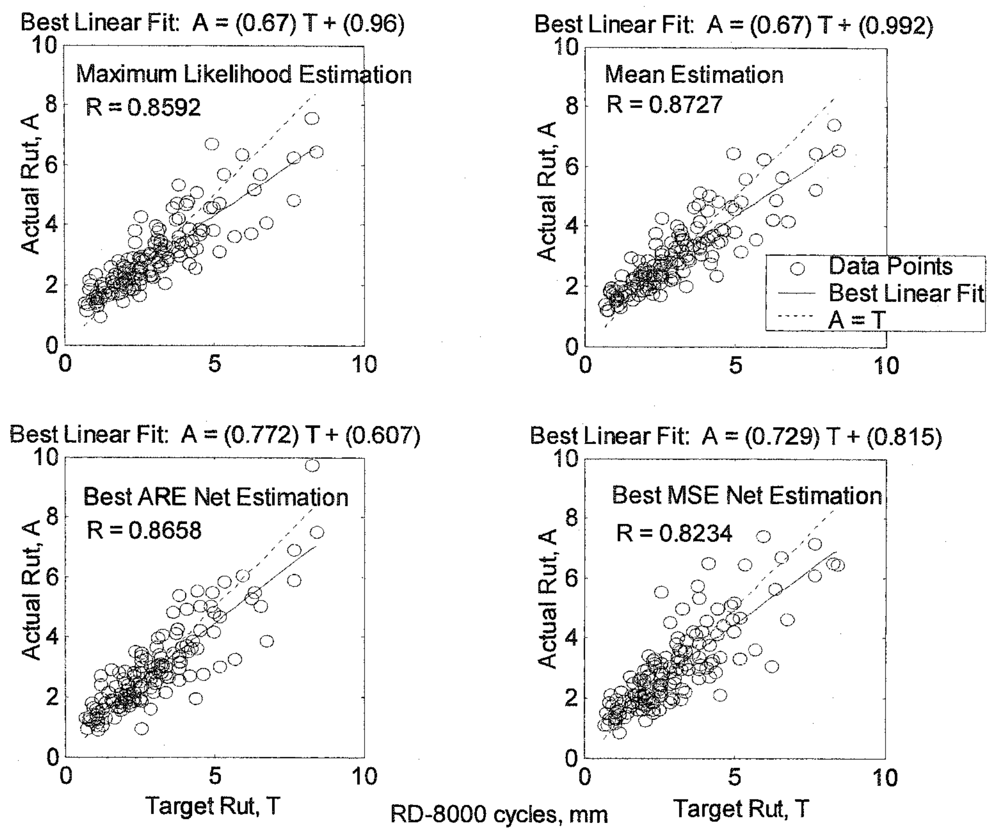

Figure 6.13 (g) Regression Plot for 8000-Cycle Rut Estimation

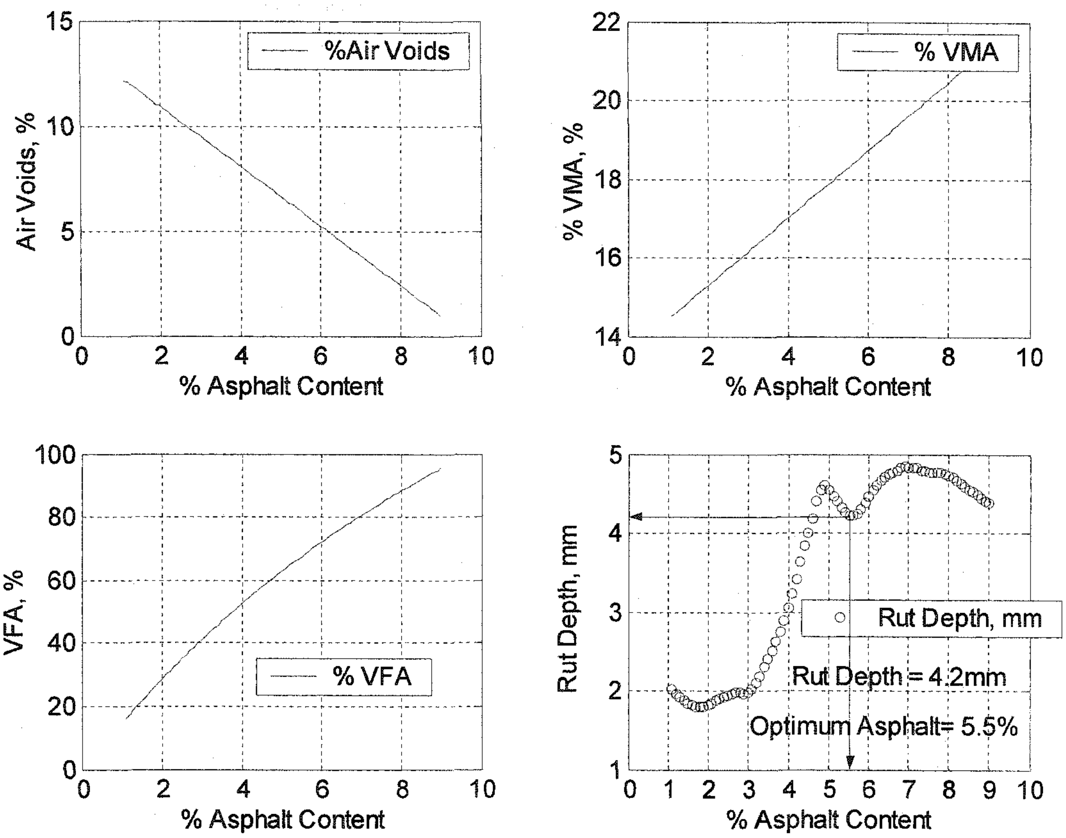

Figure 6.14 Application of NN for Optimum Asphalt Content Determination

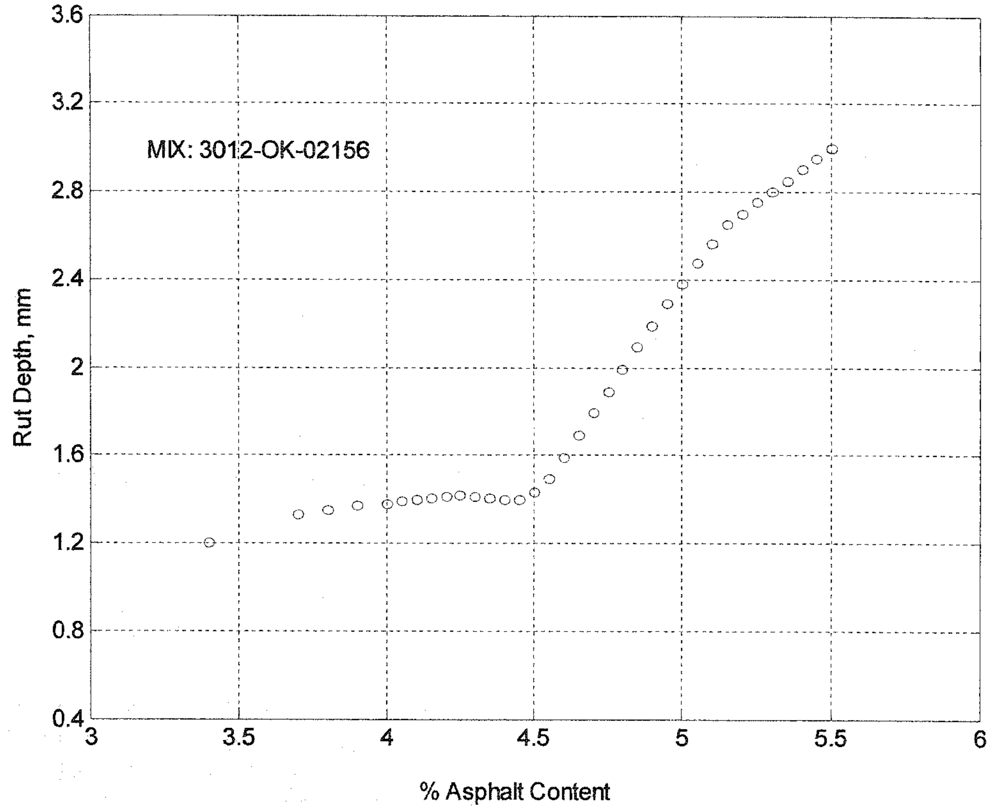

Figure 6.15 Neural Network Simulated Optimum Asphalt Content

CHAPTER 7

SUMMARY, CONCLUSIONS AND RECOMMENDATIONS

7.1 Summary

In this study, the rutting problem is introduced and followed by laboratory rut testing, mix testing, data collection and correlation of mix parameters with the rutting performance. The laboratory rut results are studied for repeatability and reproducibility. According to the Superpave method of mix design, binders are selected based on their mechanical (rut factor) and rheological properties (grade, viscosity, specific gravity) but not on the mix performance (rutting). Binders are evaluated based on their rutting performance in a mix. Thirteen different binders are studied and ranked based on the rutting criterion. Next, aggregate factors (shape, size, type), environmental factors (temperature, wet/dry conditions), mix factors (asphalt content, gradation, voids in the mineral aggregate, air voids), and load factors (wheel load, hose pressure) are correlated with rutting potential. This is followed by the analysis of correlation of rutting performance with their resilient modulus values. After determining the major rut factors, a principal component analysis is performed to ascertain the most significant factors among them. A neural network model is developed based on the most significant factors. The training algorithm used, architecture selection, and the NN design are discussed in considerable detail. Finally, the application of the proposed NN model (by simulation) is illustrated by using the model to determine the optimum asphalt content of Superpave mixes.

It is understood that rutting is contributed by many factors including mix properties, aggregate properties, binder properties, traffic loading, and environment. Each selected factor must be considered in designing the HMA mix and in examining the quality of HMA construction. For illustration, the APA rutting potential is chosen to design the HMA mix in the laboratory and to control its quality in the field. In essence, three controlled mixes are studied to investigate the effect of aggregate gradation on mix rutting. Also, the effects of air voids and asphalt content on rutting are discussed. Test results for ten different plat-produced HMA mixes are presented. These mixes are ranked based on their rut potentials. The repeatability and reproducibility of the APA testing are also examined. The mixes containing different binders are ranked based on their rutting performance. In testing plan, both modified binders and unmodified binders are incorporated. The liquid binders are tested (at Oklahoma DOT laboratory) for their properties (e.g., viscosity, shear modulus, DSR rut-factor) specified in the Superpave design requirements. Binder's rheological and mechanical properties are correlated with rutting in asphalt concrete. Two (linear and nonlinear) regression models are developed to predict rut depth incorporating binder's liquid properties in the developed nonlinear model. The effect of binder's viscosity and rut factor, $G^*/\sin\delta$ on rutting has also been investigated.

As described above, rutting of asphalt concrete is affected by many factors. These factors can be ranked based on their contributions to rutting. The statistical analysis procedure presented in Chapter 4 is developed to identify the most significant factors that affect rut potential of HMA. It is not possible to incorporate all the rutting factors together. Therefore, three test sets, each set representing a matrix whose elements are rut parameters, are employed in this study. Set A incorporates a total of seven factors. Each of these factors is investigated at two different levels. The mix design followed the Superpave method. In Set B, six factors are investigated. The mix used for Set B is a typical Hveem mixture of gravel aggregates. Different amounts of asphalt varying ±0.5% of the optimum are used as factors to be investigated. In addition, an experimental Set C with five factors is examined. All of the sets considered in this study include a partial factorial of testing program instead of a full factorial. In Chapter 5, the correlation between resilient modulus and rutting in asphalt concrete is investigated in light of the fact that the current pavement and mix design procedure seeks a simple performance test that can empirically bridge between the thickness design and mix design. A series of modulus and rut tests are conducted in the laboratory to generate data to examine if resilient modulus could be correlated with the APA rutting. Laboratory resilient modulus of asphalt concrete is determined by repeated load triaxial compression tests and cyclic indirect tensile tests. It is found that the laboratory modulus testing of asphalt concrete is complex and may suffer from variation of results due to noise. Therefore, the repeatability of resilient modulus values of asphalt concrete is investigated. The resilient modulus of asphalt content is correlated with asphalt content, temperature, and air voids.

A novel methodology is developed in this study for neural network modeling of rutting in asphalt concrete. Neural networks are considered within the context of HMA mix design to approximate the functional relationships between mix design parameters (mix properties, aggregate properties, liquid asphalt properties, traffic properties, or environmental factors) and rutting performance of asphalt concrete. The design methodology presented in this research divides the total data set into three different sets: training set, validation set and test set. The level of accuracy (average relative, MSE, and R-value) is calculated using the test data set, whereas the training set and validation set are used to train the network. Preprocessing and principal component analyses are performed, and the network trained using the Levenberg-Marquardt minimization algorithm. Improvement in the accuracy of NN performance is obtained by using different magnitudes of component variance in the principal component analysis. The selection or reduction of the descriptors among a larger pool of candidate descriptors is reported. Specifically, the developed network uses 12 neurons in the first hidden layer, 11 hidden neurons in the second hidden layer, while the output layer contains a total of 7 neurons. A sequential training algorithm based on trial-and-error is presented, which guarantees that the trained network provides minimum average relative error (maximum R^2-value) in mapping the functional relationship. Here, at each sequence, a new neural network is designed and trained to minimize the average relative error (average of 100 trials) of the previous network. The design algorithm avoids the local minima phenomenon that hampers the traditional network training, and thereby speeds up the training processes. Using a total of 21 mix factors as input, the developed model produces rut depths at 7 selected cycles (500, 1000, 1500, 2000, 4000, 6000, 8000 cycles). The time series (cycle) of rutting are recorded over 8000 cycles by an interpolation with piecewise linear element method, using network-simulated seven outputs. A total of 746 sets of data obtained from mix design information and laboratory tests are used in developing this NN model. Using randomly generated weight factors to initialize the training algorithm, histograms are compiled and outputs estimated using statistical estimators. Excellent agreement is found between the laboratory rut values and neural network predictions. A simulation study carried out on a specific Superpave mix design application demonstrates the feasibility of the proposed neural network model.

7.2 Conclusions

Based on the results presented in the preceding chapters, the following conclusions are made:

1. One of the most significant findings of this study is that it suggests a modification of the Superpave binder specification. In the current practice, rutting is taken into account using a so-called rutting factor (e.g., $G^*/\sin\delta$, where G^*= complex shear modulus of asphalt binder, δ = phase angle), which is solely dependent on the properties of the liquid asphalt binder. For rutting resistance, a high value of rut factor or G^* and a low phase angle δ are desirable. The higher the rut factor, the stiffer the asphalt and thus more resistant is the binder to rutting. However, this study found that a higher rutting factor ($G^*/\sin\delta$) alone could not ensure that a mix has a low rut potential. Binder's viscosity was found to have higher effect on rutting than other properties. A binder's ranking based on its properties does not match with the mixture performance. A binder's PG grade does not ensure the rut performance of the mixture containing the binder. Therefore, a binder satisfying the Superpave specification requirements should be evaluated by the rutting performance of the HMA mix in the APA testing.

2. Another contribution of this study is the evaluation of a number of factors that affect rutting from a rather small number of tests. Since rutting can be affected by many parameters, typically a large number of tests are needed to evaluate the effect of these parameters on rutting, as well as their relative significance. In this study, a procedure is employed to design a test matrix that includes only a small number of tests. A procedure for evaluating the test results is described. Using the developed procedure the significant factors are identified from a number of factors that affect rutting. In particular, the major rut factors identified using the developed statistical approach are:
   - Binder grade (PG 64-22 vs. PG 70-28) – This is the most significant.
   - Temperature (64°C vs. 60°C) –This is second most significant.
   - Gradation – TRZ in the gravel mixture has higher rut potential than that of BRZ in the limestone mixture.
   - Moisture of test specimens (wet vs. dry).
   - Binder content – When binder content exceeded one percent, it becomes a significant factor for the gravel mixture.
   - Specimen mold type (AVC beam vs. SGC cylinder) – If this factor is included in a test matrix, it becomes the second most significant factor among the factors that affect rutting. However, this factor (specimen type) is excluded due to difficulty in fabrication of beam specimen using the AVC.
3. The ranking of mixes can be performed based on their rutting potential. For a total of 10 different plant produced mixes, 4 excellent, 3 good, 2 fair, and 1

poor performing mixes are detected. Ranking criteria is based on mixes exhibits rut values below 2 mm (0.079 in.) are excellent, mixes exhibits rut depth more than 2 mm (0.079 in.) and less than 3 mm (0.118 in.) are good, and mixes with rut potential of 3 mm to 4 mm (0.118 in. to 0.16 in.) are fair. Any mix shows a rut depth of more 4 mm (0.16 in.) is classified as a poor mix.

4. It is found that a mix with its aggregate gradation passing through the restricted zone can have rut values lower than that of a mix with its aggregate gradation passing below or above the restricted zone. The restricted zone in the 0.45-power gradation plot does not have any significant effect on rutting. The angular aggregates show lower rut potential than the rounded aggregates. However, an angular aggregate of gradation passing through the restricted zone can have lower rutting potential than that of a rounded aggregate of gradation passing below the restricted zone. Also, asphalt content and temperature significantly affect rutting. As these factors increase, rut depth increases. However, an amount of asphalt content more than the optimum in a HMA mix increases rutting and asphalt content less than optimum reduces rutting. Also, if the air voids of laboratory-produced rut specimens are kept within 6 to 8%, then air voids play an insignificant role in the contribution to rut potential.

5. The APA rut tests are performed for 8000-cycles, and it takes about two and half hours of time for one test. If the rut value from lower cycle can be correlated with the corresponding rut from a higher cycle, it can make the APA rut testing more efficient and economical. Therefore, rut values at 500-cycle are correlated to the corresponding rut values at 8000-cycle. It is found that a

500-cycle APA rut depth can be used to predict the 8000-cycle rut depth for mixes with modified and unmodified binders, using linear and nonlinear regression models. The nonlinear model has higher R^2 value compared to that of the linear model.

6. Although rut potential of an asphalt concrete increases as the binder content increases, the correlation of modulus and asphalt content is poor. Overall, the modified binder mix (PG 70-28) shows a lower rut potential and higher triaxial resilient modulus compared to those of an unmodified binder mix (PG 64-22). The correlations between air voids with rut and resilient modulus is evident. The triaxial resilient modulus shows higher values compared to those of diametral resilient modulus. Modulus values at a lower temperature are higher than that at a higher temperature. The coefficient of variance (%error) of diametral resilient modulus testing is smaller than that in repeated load triaxial resilient modulus testing. The diametral resilient modulus test can provide a higher level of confidence, at least in an overall sense, compared to that from a triaxial resilient modulus test.

7. A study of variability is a significant component of laboratory tests results. In this study, the variability in rut values obtained from two separate laboratories is insignificant, provided the specimens are compacted to same air voids. The APA rut test results from different laboratories are relatively repeatable. The repeatability of resilient modulus testing is also investigated. It is found that the end results can be influenced by several factors. Therefore, one must be

very cautious in using laboratory resilient modulus in pavement design according to AASHTO 2000 guide.

8. It is found that a poor relationship exists between the laboratory triaxial resilient modulus and the APA rut values. When multiple regression analysis are performed based on selective descriptors (air voids, asphalt content, binder's PG), it is found that the diametral resilient modulus at 40°C has a good correlation with rutting potential compared to those at lower temperatures.

9. This study demonstrates that a neural network model can be designed and applied to determine a mapping of asphalt factors and rutting. An excellent agreement is observed between laboratory data and neural network predictions. An application of the developed NN is illustrated by estimating the optimum asphalt content for a Superpave mix. It is demonstrated that the proposed NN model can be a useful tool in the study of asphalt mix design and performance evaluation.

7.3 Recommendations

Based on the observations from this study, the following recommendations are made for future work in this area:

1. For a known gradation, the change in asphalt content changes the specific gravity of a loose mix (i.e., G_{mm}). However, G_{mm} is an input of the neural network model and it cannot be found from a closed form equation. It requires laboratory tests. Therefore, the simulation study varying the aggregate gradation

is not employed. But asphalt content of a HMA can be varied as inputs of the developed neural network and performed simulation using the NN developed in this study. If the gradation of aggregate is changed, two laboratory tests are required to find the effective and bulk specific gravity of aggregate and thereby the simulation using NN model. Therefore, a future simulation study using the developed neural network can be pursued to account for aggregate gradation using laboratory-determined bulk and effective specific gravities of aggregates.

2. Future work may study all three layers of the pavement, as actually occurring in the field pavements. A number of factors (for asphalt concrete, base, subgrade) need to be considered in neural network model to address field rutting. Such a model development work requires a large number of data sets.
3. A limited number of rut tests are performed in this study under water at 60°C. However, actual wet pavement temperature is yet to be determined and studied.
4. Laboratory tests for resilient modulus of asphalt concrete have been performed only at one frequency of loading. Frequency applied on a laboratory-tested sample represents the speed of traffic in a real pavement. In real life, the frequency of car/truck load varies. Therefore, it is necessary to perform modulus tests at several different frequencies of loading, and investigate its correlation with rutting.
5. In a neural network modeling, an effort is made to initialize the neural network with evenly distributed weights instead of uniformly distributed weights. In training procedure, the network is trained with 100 (trials) randomly generated weights and the final network weights (from each trial) are analyzed by the

histogram method. A weight vector that has the maximum likelihood probability is determined. Using the weight vector, the NN is applied to the test data sets. However, the test performance has not improved significantly. Thus, the most probable weights cannot improve network performance. Further investigation regarding finding a global solution to the NN weights can be performed.

6. Laboratory tests (cyclic triaxial and indirect tension) to measure the elastic property (resilient modulus) and the plastic property (rutting) of a HMA concrete have been conducted separately. These tests differ from each other with respect to the testing parameters such as stress level, loading time or cycle, and testing temperature. Also, durability (freeze-thaw cycles) of the HMA concrete was not addressed in the present testing program. Therefore, this study recommends a modified cyclic triaxial test including elasto-plastic deformation or strain, temperature, durability (freeze-thaw), and loading cycles. Such an experimental program test can bridge the gap between the current APA testing (rut) and cyclic triaxial or indirect tensile test that measures modulus. A modulus test with an appropriate testing protocol should be able to measure both modulus and rutting.

REFERENCES

American Association of State Highway and Transportation Officials (AASHTO), (1999). "Sieve Analysis of Fine and Coarse Aggregates," AASHTO T 27, AASHTO *Standard Specifications for Transportation Materials*, Part II, Washington, D.C.

AASHTO MP1-98, (2000). "Standard Specification for Performance Graded Asphalt Binders," *AASHTO Provisional Standards*, Washington, D.C.

AASHTO PP3-00, (1998), "Standard Practice for Superpave Volumetric Design for Hot-Mix Asphalt (HMA)," *AASHTO Provisional Standards*, Washington, D.C.

AASHTO T 166, (1999). "Bulk Specific Gravity of Compacted Bituminous Mixtures Using Saturated Surface-Dry Specimens," AASHTO *Standard Specifications for Transportation Materials*, Part II, Washington, D.C.

AASHTO T 209, (1999). "Maximum Specific Gravity of Bituminous Paving Mixtures," AASHTO *Standard Specifications for Transportation Materials*, Part II, Washington, D.C.

AASHTO T 269, (1999). "Standard Test Method for Percent Air Voids in Compacted Dense and Open Bituminous Paving Mixtures," AASHTO *Standard Specifications for Transportation Materials*, Part II, Washington, D.C.

AASHTO T 283, (1996). "Resistance of Compacted Bituminous Mix to Moisture Induced Damage," AASHTO *Standard Specifications for Transportation Materials*, Part II, Washington, D.C.

AASHTO TP1-98, (2000). "Method for Determining the Flexural Stiffness of Asphalt Binder Using the Bending Beam Rheometer (BBR)," AASHTO *Provisional Standards*, Washington, D.C.

AASHTO TP3-00, (2000). "Method for Determining the Fracture Properties of Asphalt Binder in Direct Tension (DT)," *AASHTO Provisional Standards*, Washington, D.C.

AASHTO TP5-98, (2000). "Method for Determining the Rheological Properties of Asphalt Binder Using Dynamic Shear Rheometer (DSR)," *AASHTO Provisional Standards*, Washington, D.C.

AASHTO TP7-98, (2000). "Method for Determining the Permanent Deformation and Fatigue Cracking Characteristics of Hot Mix Asphalt (HMA) Using the Simple Shear Test (SST) Device," *AASHTO Provisional Standards,* Washington, D.C.

AASHTO TP9-96, (2000). "Method for Determining the Creep Compliance and Strength of Hot Mix Asphalt (HMA) Using the Indirect Tensile Test Device," *AASHTO Provisional Standards,* Washington, D.C.

American Society for Testing and Materials (ASTM), (1999). "Standard Practice for Preparing Precision and Bias Statements for Test Methods for Construction Materials," ASTM C 670, Vol. 03.03, *Annual Book of Standards*, Philadelphia, PA.

Asphalt Institute, (2001). "Superpave Mix Design," Third Edition, The Asphalt Institute Lexington, Kentucky.

ASTM D 3381, (1998). "Standard Specification for Viscosity-Graded Asphalt Cement for use in Pavement Construction," *Annual Book of Standards*, Vol. 04.03, Philadelphia, PA.

ASTM D 946, (1998). "Standard Specification for Penetration Graded Asphalt Cement in Pavement Construction," *Annual Book of Standards*, Vol. 04.03, Philadelphia, PA.

Anderson, D.A., Christensen, D.W. and Bahia, H., (1991). "Properties of Asphalt Cement and the Development of Performance Related Specifications," Proceedings of the *Association of Asphalt Paving Technologists*, vol. 60, pp. 437-475.

Auer, P., Herbster, M., and Warmuth, M., (1996). "Exponentially Many Local Minima for Single Neurons," Advances in Neural Information Processing Systems 8, MIT Press, Cambridge, MA, 316-322.

Bahia U. H., Zhai H., Bonnetti K., and Kose. S., (1999) "Non-Linear Viscoelastic and Fatigue Properties of Asphalt Binders," Proceedings of the *Association of Asphalt Paving Technologists*, AAPT, Vol. 68, pp.1-34.

Bahia U. H., and Anderson, D.A., (1995) "The SHRP Binder Rheological Parameters: Why Are They Required and How Do They Compare to Conventional Properties," *Transportation Research Board*, Reprint Paper No. 950793.

Barksdale, R.D., (1993). "Test Device for Evaluating Rutting of Asphalt Concrete Mixes," *Transportation Research Record 1418,* National Research Council, Washington, D.C.

Barksdale, R.D, and Khosla, P., Kim, R., Lambe, P., and Rahman, M. NCHRP, (1997). "Laboratory Determination of Resilient Modulus for Flexible Pavement Design," Final Report, *NCHRP Project 1-28*, USA.

Bishop, C. (1995). "*Neural Networks for Pattern Recognition*," Oxford University Press, New York.

Bonaquist, R. F., and Witczak, M. W., (1997), "A Comprehensive Constitutive Model for Granualr Materials in Flexible Pavement Structures," *Proceedings of Eighth International Conference on Asphalt Pavements,* Vol. 1, Seattle, Washington, pp.783-802.

Brock J. D., Collins R., and Lynn C., (1999). "Performance Related Testing with Asphalt Pavement Analyzer," Technical Paper T-137, *Pavement Technology Inc.* (PTI).

Brock, Don, Ron Collins, and Cynthia Lynn. "Performance Related Testing with the Asphalt Pavement Analyzer," Technical Paper No. T-137, *Pavement Technology*, Inc., 1998.

Brown, E. R. and Cross, S. A., (1989). "A Study of In-place Rutting of Asphalt Pavements," *Proc. Association of Asphalt Paving Technologists*, Vol. 58, 1-39.

Brown, E. R., and Cross, S. A., (1992). "A National Study of Rutting in Asphalt Pavement," *Proc. of the Association of Asphalt Paving Technologists*, Vol. 61.

Brown E. R. and Foo K. Y., "Evaluation of Variability in Resilient Modulus Test Results (ASTM D 4123)," *NCAT Report No. 91-6*, USA.

Button, J. (1990). "Influence of Aggregates on Rutting in Asphalt Concrete Pavements," *Transportation Research Record 1259,* National Research Council, Washington D.C.

Carlson, D. B., (2002). "On the Reauthorization of the Federal Surface Transportation Research Program," Presented in the Committee on Environment and Public Works, United States Senate, *National Asphalt Pavement Association*, (http://www.fhwa.dot.gov/reauthorization/index.htm).

Chen, D. H., and Lin, F. (1998). "Predictive Equation for Permanent Deformation," *Texas Department of Transportation*, TX, pp. 1-26.

Christensen, D. W., Bonaquist, R., and Jack, D., (2001). "Evaluation of Triaxial Strength as a Simple Test for Asphalt Concrete Rut Resistance," Final Report, Pennsylvania DOT, *FHWA-PA-2001-010+97-04(19)*, pp. 80.

Choubane, B., Page, G. C., and Musselman, J. A., (1998). "Investigation of the Asphalt Pavement Analyzer for Predicting Pavement Rutting," *Research Report FL/DOT/SMO/98-427*, Florida Department of Transportation.

Collins, R., Watson, D.E., and Cambell, B., (1995). "Development and Use of Georgia Loaded Wheel Tester," *TRB*, No. 1492, Washington, D.C.

Cooley L. A., Kandhal, P. S., and Buchanan, M. S., (2001). "Loaded Wheel Testers in the United States: State of the Practice," *National Center for Asphalt Technology*, Auburn University, Alabama, http://www.nas.edu/trb/publications/.

Cooley, L. A. and Kandhal, P. S., (1999). "Evaluation of Density Gradients in the APA Samples," *National Center for Asphalt Technology*, Auburn University, Alabama.

Corté, J. F., Y. Brosseaud, J. P. Simoncelli, and G. Caroff. (1994) "Investigation of Rutting of Asphalt Surface Layers: Influence of Binder and Axle Load Configuration," In *Transportation Research Record 1436,* National Research Council, Washington, D.C., pp. 28-37.

Cross, S. A. and Brown, E. R. (1992). "Selection of Aggregate Properties to minimize Rutting of Heavy Duty Pavement," *ASTM Technical Publication Symposium on Effect of Aggregate and Mineral Fillers on Asphalt Mix Performance*, No. 1147, San Diego, CA.

Demuth, H. and Beale, M., (1998). *Matlab Neural Network Toolbox*, Math Works, Inc.

NCHRP, (2002). "Development of the 2002 Guide for the Design of New and Rehabilitated Pavement Structures," *NCHRP Project 1-37A*, USA.

Dougherty, M., (1995). "A Review of Neural Networks Applied to Transport," *Transportation Research*, TRB, Vol. 3, No. 4, pp. 247–260.

Engelbrecht, A. P., (2001). "Sensitive Analysis fro Selective Learning by Feedforward Neural Networks," *Fundamenta Informaticae*, IOS Press, Vol. 45, No. 1, pp. 295.

Engelbrecht, A.P., (2002). *Computational Intelligent*, John Wiley & Sons, Ltd.

Faghri, A., Martinelli, D., and Demetsky, M. J., (1997). "Neural Network Applications in Transportation Engineering," *Expert Systems and Artificial Intelligence Committee*, ASCE.

Fine, T., (1998). *Feedforward Neural Network Methodology*, Springer-Verlag, New York.

Finn, F. N., Saraf, C. L., Kulkarni, R., Nair, K., Smith, W., and Abdullah, A., (1986). "Development of Pavement Structural Subsystem," *The National Cooperative Highway Research Program* (NCHRP), Report No. 291.

Ford M. C., (1988). "Pavement Densification related to Asphalt Mix Characteristics," 67^{th} *Annual Transportation Research Board Meeting*.

Frocht, M.M., *Poroelasticity*, Vol. John Wiley and Sons, New York, 1948.

Gillespie, T.D., Karamihas, S. M., Sayers, M. W., Nasim, M. A., Hansen, W., and Ehsan, N., (1993). "Effect of Heavy-vehicle Characteristics on Pavement Response and Performance," *National Highway Cooperative Research Program*, Report 353, Transportation Research Board, National Research Council, National Academy Press, Washington, D.C.

Gramling, W. L., Suzuki, G. S., and Hunt, J. E., (1991). "Rational Approach to Cross-Profile and Rut Depth Analysis," *Transportation Research Record,* No. 1311, National Research Council, Washington, D.C., pp. 173-179.

Groenendijk, J., Vogelzang, C. H., Miradi, A., Molenaar, A. A., and Dohmen, L. J. M., (1996). "Rutting Development in Linear Tracking Test Pavements to Evaluate Shell Subgrade Strain Criterion," *Transportation Research Record 1570,* National Research Council, Washington, D.C., pp.23-29.

Hall, K. T., Correa, C. E., and Simpson, A. L., (2003). "Performance of Flexible Pavement Rehabilitation Treatments in the Long-Term Pavement Performance SPS-5 Experiment," *Transportation Research Record*, No. 1823, pp 93-101.

Hagan, M., Demuth, H., and Beale, M., (1996). *Neural Network Design*, PWS Publishing Co.

Harvey, J., Lee, T., Sousa, J., Pak, J., and Monismith, C. L., (1995). "Evaluation of Fatigue and Permanent Deformation Properties of Several Asphalt-Aggregate Field Mixes Using Strategic highway Research Program A-003A Equipment," *Transportation Research Record 1454,* National Research Council, Washington, D.C., pp.123-133.

Haykin S., (1994). *Neural Networks: A Comprehensive Foundation*, MacMillan.

Hecht N. R., (1990). *Neurocomputing*, Addison-Wesley Publishing Company, New York.

Hertz, J., Krogh, A., and Palmer, R. G., (1991). *Introduction to the Theory of Neural Computation*, Addison-Wesley Publishing Company, New York, pp. 130–141.

Hornik, K., Stinchcombe, M., and White, H. (1989). "Multilayer Feedforward Networks are Universal Approximators," *Neural Networks*, Vol. 5, pp. 359-366.

Hornik, K., Stinchcombe, M., White, H., and Auer, P., (1994). "Degree of approximation Results for Feedforward Networks Approximating Unknown Mappings and Their Derivatives," *Neural Computing*, Vol 6, pp. 1262-1275.

Hudson, S. W. and Seeds, S. B., (1988). "Evaluation of Increased Pavement Loading and Tire Pressures," *Transportation Research Record* 1207, Transportation Research Board, Washington, D.C., pp. 197-206.

Huang, Y. H., (1993). "*Pavement Analysis and Design*," Prentice Hall, Inc., NJ, USA.

Isacsson U. and Lu X., (1999). "Laboratory Investigation of Polymer Modified Bitumen," *Journal of the Association of Asphalt Paving Technologists*, AAPT, Vol. 68, pp. 35-44.

Jackson, N. M. and Ownbby, E. A., (1998). "Evaluation of Laboratory Compaction of HMA," *Transportation Center,* Final Repot, University of Tennessee.

Kandhal, P. S. and Mallick, R. B., (1999). "Evaluation of Asphalt Pavement Analyzer for HMA Mix Design," *National Center for Asphalt Technology,* Report No. 99-4, Auburn University, Alabama.

Kandhal, P. S., Cross, S. A., and Brown, E. R., (1993). "Heavy-Duty Asphalt Pavements in Pennsylvania: Evaluation for Rutting," *Transportation Research Record 1384,* National Research Council, Washington, D.C., pp. 49-58.

Kantardzic, M., (2003). *Data Mining: Concepts, Models, Methods and Algorithms*, IEEE Press, New Jersey.

Kearns, M., (1997). "A Bound on The Error of Cross Validation Using the Approximation and Estimation Rates, with Consequences for the Training-Test Split," *Neural Computation*, Vol. 9, 1143-1161.

Kennedy, J., and Eberhart, R., C., (2001). "Particle Swarm Optimization," *Proceedings of IEEE International Conferences on Neural Networks*, Vol. 4, pp. 1942-1948.

Kim, O. and C.A. Bell (1988) "Measurement and Analysis of Truck Tire Pressures in Oregon," *Transportation Research Record 1207*, Transportation Research Board, Washington, D. C., pp. 100-110.

Kyle B., (1995). "Successful Industrial Experimentation," *VCH Publishers Inc.,* ISBN 1-56081-050-5, pp. 1-131.

Lai J. S., (1996). "Development of a Simplified Test Method to Predict Rutting Characteristics of Asphalt Mixes," *Final Report*, Georgia DOT Project No. 8503.

Lai, J. S., (1986). "Evaluation of Rutting Characteristics of Asphalt Mixes Using Loaded Wheel Tester," *Project No. 8609,* Georgia Department of Transportation.

Lekarp, F., Richard, I. R., and Dawson, A. (1996). "Influences on Permanent Deformation Behavior of Unbound Granular Materials," *Transportation Research Record 1547,* National Research Council, Washington D.C. pp.68-75.

Majidzadeh, K., Bayomy, F., and Khedr, S., (1978). "Rutting evaluation of Subgrade Soil in Ohio," *Transportation Research Record,* No. 671, TRB, pp. 75-84.

Masad, E., B. Muhunthan, N. Shashidhar, and T. Harman (1999). "Quantifying Laboratory Compaction Effects on the Internal Structure of Asphalt Concrete," *Transportation Research Record: Journal of the Transportation Research Board No. 1681,* TRB, National Research Council, pp. 179-185.

MathWorks, (2002). *Neural Network Toolbox 4.0.2,* The MathWorks Inc., (http://www.mathworks.com/), USA.

Mehra, P. and Wah, B. W., (1992). *Artificial Neural Networks: Concepts and Theory*, IEEE Computer Society Press, Los Alamitos, CA, pp.1-8.

Middleton, D. R., Roberts F. L., and T. Chira-Chavala, (1986). "Measurements and Analysis of Truck Tire Pressures on Texas Highways," *Transportation Research Record* 1070, Transportation Research Board, Washington, D.C., pp. 1-8.

Miller, T., K. Ksaibati, and M. Farrar, (1995). "Utilizing the Georgia Loaded-Wheel Tester to Predict Rutting," Presented at the *74th Annual Meeting of the Transportation Research Board*, Washington, D.C.

Monismith, C. L., Harvey, J. T., Long, F., and Weissman, S. "Tests to Evaluate the Stiffness and Permanent Deformation Characteristics of Asphalt/Binder-Aggregate Mixes," A Critical Discussion, *Technical Memorandum TM-UCB PRC 2000-1*, Pavement Research Center, University of California Berkeley, pp. 86.

Monismith, C. L., (1989). "Resilient Modulus Testing: Interpretation of laboratory Results for Design Purposes," *Proceedings of the Workshop on Resilient Modulus Testing*, Oregon State University, Oregon.

Moody, J. and Darken, C., (1994). "Fast Learning in Networks of Locally-Tuned Processing Units," *Neural Computation*, Vol. 1, pp. 281–294.

Musselman, J.A., Couhaane, B., Page, G.C. and Upshaw, P.B. (1998). "Superpave Field Implementation: Florida's Early Experience," *Transportation Research Record* 1609, National Research Council, Washington D.C. pp. 51-60.

National Asphalt Pavement Association (NAPA), (1995). "An Industry Discussion on Superpave Implementation," *NAPA Special Report 174*, National Asphalt Paving Association.

Natu, G. S. and Tayebali, A. A., (1999). "Mixture Design and Accelerated Laboratory Performance Evaluation of Unmodified and Crumb Rubber Modified Mixes," *Journal of the Association of Asphalt Paving Technologists*, AAPT, Vol. 68, pp.193.

NCHRP Project 9-19, (2001). "Simple Performance Test: Test Results and Recommendations," *NCHRP Project 9-19 Task C Report*, Arizona Statue University, National Cooperative Highway Research Program.

Oklahoma Department of Transportation (ODOT), (1999). "Special Provision for Plant Mix Bituminous Bases And Surfaces," Section 708-1(a), *The Standard Specifications for Highway Construction*, 1999 Edition, Oklahoma City, Oklahoma.

ODOT, (2002). "Standard Specifications for Highway Construction," Oklahoma Highway Department, *OHD Specifications*, Oklahoma Department of Transportation, USA.

Oklahoma Highway Department (OHD), (2001). "Method of Test for Determining Rutting Susceptibility Using the Asphalt Pavement Analyzer," *Oklahoma Highway Department Laboratory Test No. 43 (OHD L 43)*, Oklahoma City, Oklahoma.

Lavin, P., (2003). "Asphalt Pavement: A Practical Guide to Design, Production and Maintenance for Engineers and Architectures," *Spon Press, Taylor & Francis Group*, NY, pp. 115.

Pidwerbesky, B.D., Steven, B.D., and Arnold, G., (1997). "Subgrade Strain Criterion for Limiting Rutting in Asphalt Pavements," *Proceedings of Eighth International Conference on Asphalt Pavements*, Vol. 2, Seattle, Washington, pp.1529-1544.

PTI, (2002). "Performance Related Testing With The Asphalt Pavement Analyzer," *Technical Paper T-137*, pp.2.

PTI, (1999). "Pavement Analyzer," *Technical Paper T-137*, Pavement Technology Inc., USA.

Press, W. H., Teukolski, W. T., Vetterling, W. T., and Flannery, B. P., (1992). *Numerical Receipe in C: the Art of Scientific Computing*; Cambridge University Press, Cambridge.

Ramsamooj, D. V., Ramadan, J., and Lin, G. S., (1998). "Model Prediction of Rutting in Asphalt Concrete," *Journal of Transportation Engineering, Vol. 124, No. 5,* American Society of Civil Engineers, pp. 448-456.

Reese, R. E. and Goodrich, J. L., (1993). "California Desert Test Road – A step Closer to Performance Based Specifications," *Association of Asphalt Pavement Technologists*, AAPT, Vol. 62, pp. 247

Roberts, F. L., Kandhal, P. S., and Brown, E. R., (1996). "Hot Mix Asphalt Materials, Mixture Design, and Construction," *NAPA Education Foundation*, Lanhamn Maryland.

Rosen B. E. and Goodwin, J. M., (1997). "Optimizing Neural Networks Using Very Fast Simulated Annealing," *Neural, Parallel and Scientific Computations*, Vol. 5, No. 3, pp. 383-392.

Rumelhart, D. E., Hinton, G. E., and McClelland, J. L., (1986). "A General Framework for Parallel Distributed Processing," *in Parallel Distributed Processing, Explorations in the Microstructure of Cognition*, Vol. 1: Foundations, MIT Press, MA, pp. 45–76.

Sherif, A., El-Samny, M. K., Zahw, M., and Halem, A. O., (1997). "Laboratory and Statistical Evaluation of the Influence of Mix parameters on Surface Rutting of Asphalt Pavement," *Proceedings of the 1997 Annual Canadian Society for Civil Engineering,* Sherbrooke, Canada, pp. 351-362.

Simpson, A.L., Daleiden, J.F. and Hadley, W.O., (1995). "Rutting Analysis From a Different Perspective," *Transportation Research Record 1473*, National Research Council, Washington, D.C., pp.9-16.

Snyman, J. A., (1983). "An Improved Version of the Original LeapFrog Dynamic Method for Unconstrained Minimization," LFOP1, *Applied Mathematical Modeling,* Vol 7, pp. 216-218.

Sousa, J. and Solaimanian, M., (1994). "Abridged Procedure to Determine Permanent Deformation of Asphalt Concrete Pavements," Presented at the *73rd Annual Meeting of the Transportation Research Board*, Washington, D. C.

Sousa, J., Weissman, W.S., Sackman, J.L., and Monismith, C.L., (1992). "Nonlinear Elastic Viscous with Damage Model to Predict Permanent Deformation of Asphalt Concrete Mixes," *Transportation Research Record 1384,* National Research Council, Washington, D.C., pp.80-93.

Stuart, K. D. and Mogawer, W. W., (2001) "Validation of Asphalt Binder and Mixture Tests that Measure Rutting Susceptibility Using the Accelerated Loading Facility," *Final Report, FHWARD- 99-204*, 348 pp.

Summers, C. J., (2001). "The Idiots Guide to Highways and Maintenance, Modified Bitumen and Bituminous Materials," Available Online at *http://www.highwaysmaintainance.com/polybitxt.htm*, visited October 22, 2001.

Tarefder, R. A., Zaman, M. M., and Hobson, K., (2003) 'A Laboratory and Statistical Evaluation of Factors Affect Rutting,' *International Journal of Pavement Engineering*, IJPE, Vol. 4, No. 1, pp. 59-68.

Tarefder, R. A., Zaman, M. M., and Hobson, K., (2002). "Laboratory Assessment of Binders' Contribution to Rutting Susceptibility," *International Journal of Pavement*, IJP, Vol. 1, No. 2, pp. 34-47.

Tarefder, R. A. and Zaman, M., (2003) "Resilient Modulus and Density Gradient Analysis of Asphalt Concrete," *Final Report*, *ORA: 125-5213,* Oklahoma DOT.

Tarefder R. A. and Zaman, M., (2002). "Evaluation of Rutting Potential of Hot Mix Asphalt Using the Asphalt Pavement Analyzer," *Final Report*, ORA: 125-6660, Oklahoma DOT.

Timoshenko, S. and Goodier, J., (1951). *Theory of Elasticity*, McGraw-Hill Book Co., Inc., New York.

Toll, D., (1996). "Artificial Intelligence Applications in Geotechnical Engineering," Journal of Geotechnical Engineering, <http://geotech.civen.okstate.edu/>, Vol. 1.

Van de Loo, P. J., (1978). "The Creep Test: A Key Tool in Asphalt Mix Design and in the Predcition of Pavement Rutting," *Proceedings, Association of Asphalt Paving Technologists*, Vol. 47, pp. 522-554.

Von Quintus, H. L., (1991). "Asphalt-Aggregate Mixture Analysis System: AAMAS," *NCHRP Report 338, Transportation Research Board,* National Research Council, Washington, D.C.

Wasserman, P. D., (1993). *Advanced Methods in Neural Computing*, Van Nostrand Reinhold, New York.

West, R. C., (1999). "A Rugged Study of the Asphalt Pavement Analyzer Rutting Test," *Memorandum to the Asphalt Pavement User Group and new APA Owners*, Georgia, Final Report.

West, R. C., Page, G. C., and K. H. Murphy (1991). “Evaluation of the Loaded Wheel Tester,” *Research Report FL/DOT/SMO/91-391*, Florida Department of Transportation, Florida.

White, H., Gallant, A. R., Hornik, K., Stinchcombe, M., and Wooldridge, J., (1992). “Artificial Neural Networks, Approximation and Learning Theory”, *Blackwell Publishers*, Cambridge.

Williams, C. R. and Prowell B. D., (1999). “Comparison of Laboratory Wheel-Tracking Test Results to West Track Performance”, Presented at the *78th Annual Meeting of the Transportation Research Board,* Washington, D.C.

Witczak, M. W., Bonaquist, R., Quintus, H. V., and Kaloush, K., (2000). "Specimen Geometry and Aggregate Size Effects in Uniaxial Compression and Constant Height Shear Tests," *Asphalt Paving Technology, Association of Asphalt Paving Technologists*, Vol. 69, pp 410.

Zaman, M. and Zhu, J. H., (1999). “Durability Effects on Resilient Moduli of Stabilized Aggregate Base,” *Transportation Research Record* 1687, TRB, pp. 29-38, USA.

Zaghloul, S. and White, T., (1994). “Use of Three Dimensional, Dynamic finite Element Program for Analysis of Flexible Pavement,” *Transportation Research Record 1388,* National Research Council, Washington D.C. pp.60-69.

APPENDIX I

'Micro-Deval Test for Evaluating Mechanical Strength Properties of Aggregate' by Tarefder, R. A., Zaman, M. M., and Hobson, K., *International Journal of Pavement*, IJP, Vol. 2, No. 2, pp. 8-20, June 2003.

MICRO-DEVAL TEST FOR EVALUATING MECHANICAL STRENGTH PROPERTIES OF AGGREGATE

Abstract: This study has evaluated mechanical strength properties of aggregates common in Oklahoma, based on aggregates' abrasion resistance and durability. Aggregates' abrasion resistance and durability were determined in a Micro-Deval apparatus and compared to their Los Angeles (L.A.) abrasion resistance and freeze-thaw soundness, respectively. A poor correlation between the L. A. abrasion and Micro-Deval abrasion was observed. The correlation between the freeze-thaw soundness and Micro-Deval loss was even poorer. A total of 18 sources of aggregates of known roadway performance were tested in the Micro-Deval apparatus. The roadway performance (wearing) was correlated with L.A. abrasion and Micro-Deval abrasion. It was found that where the L.A. abrasion is inadequate as a basis for judging aggregate quality, the Micro-Deval test could satisfactorily rank the aggregate source based on their roadway performance. The ranking of sources based on the Micro-Deval abrasion has matched the source ranking based on roadway performance. A maximum allowable limit of 25% Micro-Deval abrasion loss has been postulated to separate the poor quality aggregate from the good quality aggregates in Oklahoma. This limit necessarily eliminates the requirements of freeze-thaw soundness characteristics. In this study, an aggregate (Brechin aggregate from Canada) of known Micro-Deval loss was tested 10 times to examine the proper calibration of the Micro-Deval device. Once the calibration was found satisfactory, three sources of aggregates were tested 10 times each to examine the reproducibility of test results. The test results showed that the Micro-Deval test is highly repeatable. In this study, the effects of aggregate size, type, absorption, and clay contaminant on the Micro-Deval abrasion loss were also investigated. This study discourages the determination of maximum allowable Micro-Deval abrasion specification limit based on aggregate size and type. It is suggested that the limit should be based on aggregate applications. This study has added the use of CoreLok^{TM} device for rapid absorption of aggregate to the Micro-Deval test. The use of such absorption method will significantly reduce the Micro-Deval abrasion testing time (AASHTO T 58) and increase the use of Micro-Deval in quality control during production.

1. Background

Asphalt concrete is used to surface 96% of all paved roads in the United States [1]. Asphalt concrete is a composite material consisting of aggregate, asphalt, and air that collectively develop structural characteristics capable of supporting highway traffic. Asphalt provides the cohesive bonding for an asphalt concrete mixture and aggregate carries the traffic load. The shear force due to repeated traffic loading in asphalt pavement is resisted mainly by the frictional force acting on contacts between aggregates. Aggregate provides sufficient toughness, soundness, ductility, durability, crushing, and degradation to an asphalt pavement. The abrasion resistant property of an aggregate indicates whether it is susceptible to crushing, degradation, and disintegration when stockpiled, fed through asphalt production plant, compacted, and subjected to road traffic. If the aggregates do not have sufficient abrasion resistance, the resulting asphalt pavement can be subjected to particle wear and polishing, reduced surface friction and increased driving risk. The use of poor quality aggregate is a common cause for disintegration and particle breakdown [2]. Over time, asphalt coat on aggregate can oxidize, introducing a number of contaminants (for example, deicing salt) into the asphalt concrete, causing unwanted behavior. Good quality aggregates must be resistant to breakdown or disintegration when subjected to wetting and drying (weathering cycle) and/or freezing and thawing. The durability of the asphalt concrete is its ability to prevent weathering effects (temperature change, seasonal freeze-thaw, wet-dry cycles). Another effect of the environment is raveling. This is caused by stripping, where standing water breaks down bonds between the asphalt and aggregate, which leads to aggregate particles being lost (aggregate deterioration) from the mixture [3,4]. Thus, it is essential to use abrasion resistant and durable aggregates to maintain the integrity of the asphalt roads during service. An accurate determination of abrasion resistance and durability property of aggregates in these roads is important and, therefore, the main focus of this research.

Traditionally, aggregate abrasion resistance has been determined using Los Angeles abrasion device [5]. A study by Wu et al. indicated that 94 percent of the states use the Los Angeles abrasion test to quantify the abrasion property [6]. The L.A. abrasion is a measure of the degradation of mineral aggregates of standard grading resulting from a combination of actions including abrasion or attrition, impact, and grinding in a rotating steel drum containing a specified number of steel spheres. After the prescribed number of revolutions, the contents are removed from the drum and the aggregate portion is sieved to measure the degradation as percent lost. The majority of the states specify a maximum allowable L.A. abrasion loss of 40 to 45 percent. Oklahoma Department of Transportation (ODOT) currently uses a maximum allowable L.A. abrasion loss of 40% for aggregates to be uses in asphalt pavement. However, aggregate Los Angeles abrasion values do not show good correlation with roadway performance [7]. In Oklahoma, several aggregates (such as soft limes) showed excellent roadway performance even though their Los Angeles abrasion value is high. On the other hand, several aggregates pass the minimum Los Angeles abrasion criteria but showed poor performance [8]. Also, the L.A. abrasion test does not appear to be fully satisfactory for use with slags, cinders, and other lightweight aggregates [6]. Therefore, it is necessary to explore an alternative determination of abrasion resistance for roadway aggregates.

The durability characteristic of aggregates is generally determined using a soundness test. Both magnesium and sodium sulfate soundness tests are common methods for evaluating aggregate durability. About 53 percent of the states have a requirement for sodium sulfate soundness, 19 percent magnesium sulfate soundness, 10 percent a freeze-thaw loss requirement, 2 percent the durability index test, and 16 percent no soundness requirement (Wu, 2001). Freeze-thaw is more detrimental than wet-dry as well as other methods [9]. Water in pores or voids expands upon freezing causing a breakdown of aggregate particles. The sulfate soundness tests were developed to simulate this action and were used in lieu of freezing and thawing because of the lack of adequate refrigeration equipment. Presently, reliable and relatively inexpensive refrigeration equipment is available for durability test. In addition, the harmful expansive clay minerals in aggregates can be detected by the aggregate durability index test [10]. It is necessary to evaluate such determined durability.

Recently, Micro-Deval apparatus has simplified the task of determining both abrasion resistance and durability from a single test [11,12,13]. This gives an opportunity to evaluate abrasion resistance and durability characteristic of aggregates common in Oklahoma using a Micro-Deval test method [14]. A Micro-Deval test is basically a wet L.A. abrasion test. The Micro-Deval test measures the abrasion resistance and durability of aggregates resulting from a combination of actions including abrasion and grinding with steel balls in the presence of water. In this study, the correlation between Los Angeles abrasion loss and Micro-Deval abrasion loss has been sought to examine whether the Micro-Deval test provides a better means of establishing aggregate quality for asphalt pavements. This study has compared the Micro-Deval test results with the Freeze thaw soundness and aggregate durability index. Several other properties such as: specific gravity, absorption, size and type of aggregate were also determined in the laboratory to examine their effect on Micro-Deval abrasion loss.

2. Objectives and Scope

The main objective of the study is to test known aggregate sources using Micro-Deval apparatus and compare the test results to Los Angeles abrasion loss, freeze-thaw soundness, absorption, aggregate durability index, and bulk specific gravity of aggregate. Another objective is to rank the aggregates based on Micro-Deval loss and in-service performance. The main goal is to establish a baseline for an Oklahoma specification using the Micro-Deval abrasion test results instead of the L.A. abrasion test values and establishes a provisional specification limit. The scope of this study is to test a total of 18 different Oklahoma sources of aggregates for which the roadway performance was known previously. The aggregate types included in this study were mainly limestone and sandstone. Three of the 18 aggregate sources were tested 10 times to investigate the variability in Micro-Deval test results. The rest of the sources were tested at least twice and an average of the test results were reported in this study.

3. Sample Testing

As mentioned earlier, the abrasion resistance and durability of aggregate were assessed using the test results from AASHTO TP58 method. One thing, the study has added to the AASHTO TP58 or the Micro-Deval test method, is the use of the CoreLok™ device for water absorption [15]. A sample with standard grading is initially subjected for a rapid absorption of water using CoreLok™ vacuum technique. In this technique, 1500 grams of aggregates are sealed in a plastic bag under 99% absolute vacuum and then cut open in 2000 mL of water. The sample and water is then placed in a jar mill and an abrasive charge consisting of 5000 grams of 9.5 mm diameter steel balls. The jar, aggregate, water, and charge are revolved at 100 rpm for about 2 hours depending on aggregate gradation. The sample is then washed and oven dried. The loss is the amount of materials passing the 1.18 mm sieve expressed as a percent by mass of the original sample.

4. Calibrations and Reproducibility

In order to ensure a proper equipment setup and operation, a total of 10 Micro-Deval test were conducted on Brechin aggregate from Canada. The grading of the material was 19.00 mm to 4.75mm. The Micro-Deval loss of around 18% confirmed the proper setup with a very small variability. Next, a total of 3 aggregates of Oklahoma source were tested to examine the test variability. Test results for these aggregates are plotted in Figure 1.

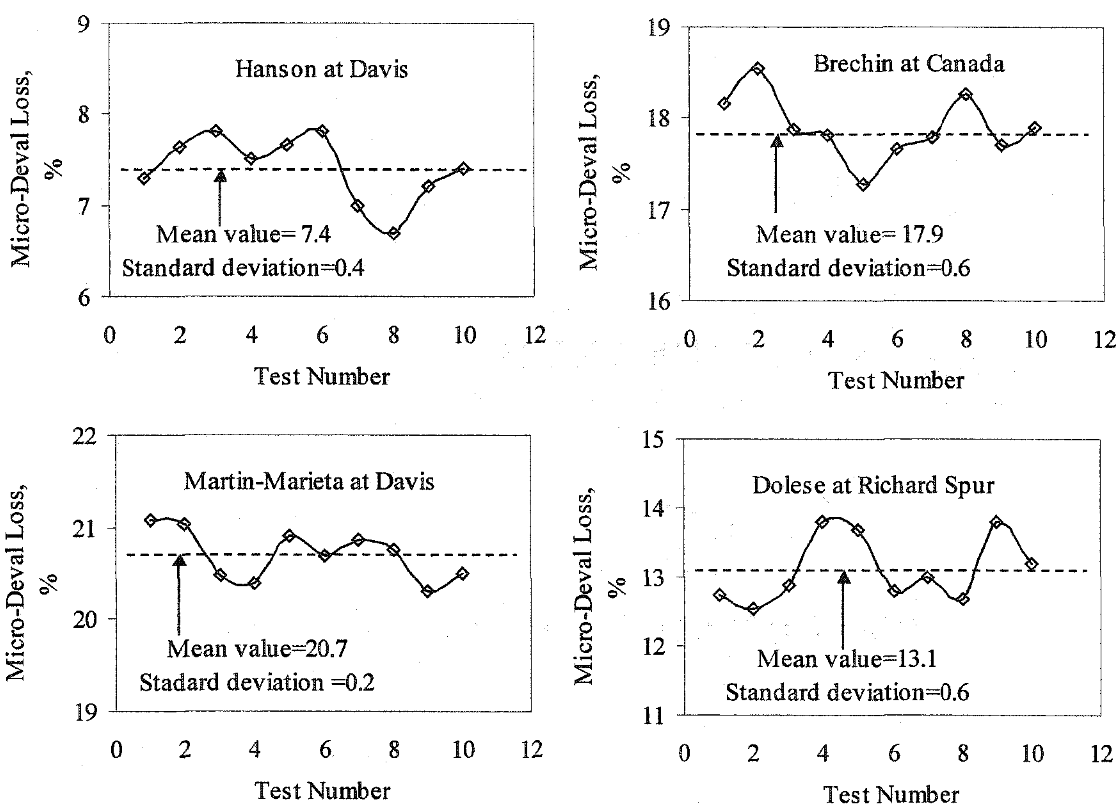

Figure 1. Mean and range of variation of Micro-Deval test values

For each source, the mean Micro-Deval loss and standard deviation are shown. The difference between two tests is in the precision limit suggested in AASHTO TP58 [14]. It is possible to establish an upper and lower limit specification for each source during aggregate quality exploration and evaluation. For the aggregate source of Hanson at Davis, the upper specification limit of Micro-Deval loss would be 7.8%, whereas the lower limit would be 7.0%. Figure 1 show that the reproducibility of the Micro-Deval test is adequate for it to be used to check the compliance of aggregates with specification that impose an upper limit on the result of the test. It may also be possible to increase the reproducibility by increasing the number of tests.

5. Test Results and Source Ranking

The Micro-Deval and Los Angeles abrasion test results of 18 aggregates with their field performances have been listed in Table 1. Typically, preliminary investigations to determine potential aggregate sources are performed during the feasibility phase, and detailed investigations are performed during the project evaluation phase prior to implementation. All sources of aggregates were ranked based on past experience and roadway performance [8]. From Table 1, it can be seen that source ranking based roadway performance matches the source ranking based on the Micro-Deval abrasion loss value. Three aggregate sources showed Micro-Deval values less than 10 and can be ranked as excellent. Eight sources showed Micro-Deval values less than 18.0 and can be ranked as good. Similarly, 5 sources can be ranked as having fair quality aggregate. Two aggregate sources showed Micro-Deval loss values above 25 and can be ranked as poor quality aggregate for use in asphalt concrete pavement.

6. Specification Limit of Micro-Deval Abrasion Loss

The determination of specification limit is a complex task. The test limit must be established based on the performance of aggregates in service pavement. The test limit has to ensure that the best locally available aggregates are used. This study has proposed a specification limit of 25 for maximum allowable Micro-Deval abrasion loss to be the best for Oklahoma source of aggregates when the Micro-Deval procedure [14] uses the CoreLok^{TM} absorption. However, the specific limit should be used with great care. It is also possible to establish a test limit for specific project based on geological diversity and the resulting rock types in an area. On some projects where, for instance, both limestone and sandstone are included in the list of sources, test limits would be required for the limestone and a slightly different test limit would be required for the sandstone. However, this study proposed an overall specification limit for all sources of aggregates.

Table 1. Abrasion loss and ranking of aggregate

Aggregate Source	Pit Number	Aggregate Type	Rank or Field Performance	L. A. Abrasion (%)	Micro-Deval Loss (%)
Stringtown MTLS at Stringtown	4301	Limestone	Excellent	19.4	6.1
Arkhola at Jennylind	7902	Sandstone	Excellent	23.9	7.5
Hanson WRP, Inc. at Davis	5008	Rhyolite	Excellent	15.1	7.4
Pryor Stone at Pryor Ledge	4901	Limestone	Good	21.3	10.2
Dolese Co. at Cooperton	3801	Limestone	Good	25.7	10.3
Martin-Matrieta at Troy	3503	Dolomite	Good	23.3	10.5
Quapaw at Drumright	1901	Dolomite	Good	21.5	12.2
Dolese Co. at Richard Spur	1601	Limestone	Good	23.2	13.1
Dolese Co. at Davis	5002	Limestone	Good	23.5	14.9
Bellco No.7 at Dewey	7404	Limestone	Good	23.0	15.2
Arkhola Sand & Gravel at OK	7302	Limestone	Good	17.1	17.4
Arkhola Sand & Gravel at Zeb	1102	Limestone	Fair	25.2	19.5
Apac-Oklahoma at Vinia	1802	Limestone	Fair	27.3	20.2
Martin-Matrieta at Davis	5005	Limestone	Fair	27.2	20.7
Light Weight Aggregate at Zeb	4485	Limestone	Fair	28.0	22.0
Pryor Stone at Pryor	4904	Limestone	Fair	24.6	23.7
Tiger Ind. Sys at Haskell	3101	Sandstone	Poor	34.7	33.0
Stiggler Stone at Haskell	3102	Sandstone	Poor	32.3	36.2

7. Comparison of Aggregate Properties

7.1 Correlation of Micro-Deval Loss with Los Angeles Abrasion

Figure 2 shows the overall correlation of Micro-Deval abrasion loss with the L. A. abrasion loss. The value of correlation square, R^2 = 0.633. The Micro-Deval abrasion loss data shows greater spread than that of the Los Angeles abrasion data, which implies that the field performance of aggregate can be more reflective to the Micro-Deval abrasion value. Majority of the 18 sources showed a Micro-Deval value below 25.0. In this study, a Micro-Deval loss of 25.0 has been proposed as the maximum limiting value of an aggregate to be used in the State of Oklahoma. Figure 2 shows that none of the aggregate tested can be rejected based on the L.A. abrasion test; however, two aggregates tested have been rejected based on the Micro-Deval test results. The field performance of pavements using these two aggregate were known to be unsatisfactory [8].

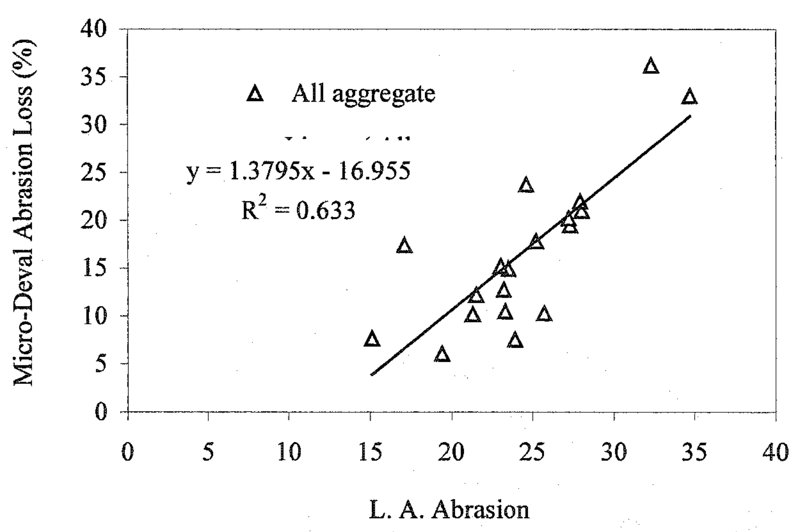

Figure 2 Correlation of Micro-Deval loss with L.A. abrasion loss

Figure 3 is the plot of Micro-Deval abrasion loss with L.A. abrasion loss for different nominal maximum size (NMS) of aggregates. From Figure 3, it is evident that the coefficient of determination, R^2-value increases as the NMS of aggregates increase. The highest correlation obtained for 19.0 mm of nominal maximum size of aggregates. For coarse aggregates, the Micro-Deval test is close to the L.A. abrasion test values. For fine aggregates, the Los Angeles abrasion value differs from the Micro-Deval abrasion loss significantly. This is because the Los Angeles abrasion test is predominantly an impact test instead of being an abrasion test [12]. The impact causes a lower mechanical degradation on coarse aggregate when compared to the fine aggregate. Micro-Deval test, which is considered as a wet abrasion test, has shown degradation loss value close to that in Los Angeles test for fine aggregates.

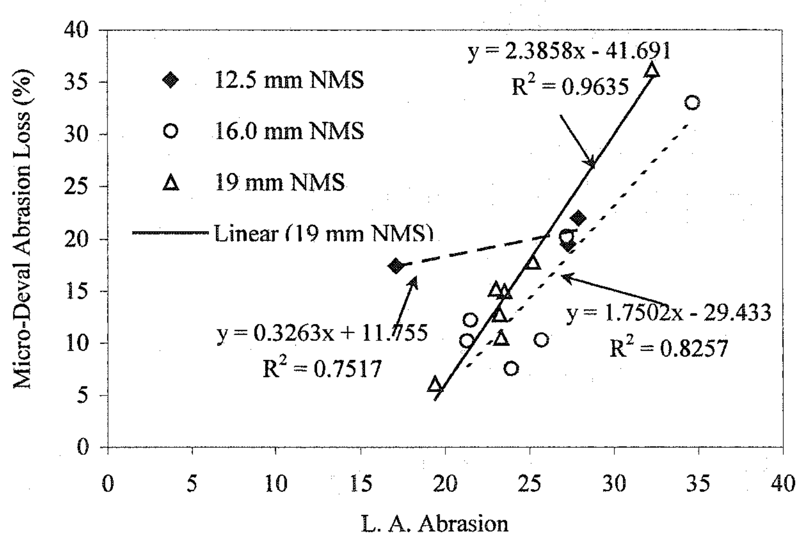

Figure 3. Correlation of Micro-Deval loss with L.A. abrasion loss by NMS

7.2 Correlation of Micro-Deval Loss with Freeze-Thaw Soundness

According to the CRD-C 144 test method, a large slab cut perpendicular to bedding or a whole large stone are subjected for freezing and thawing [16]. The test simulates the effects of a cold environment by inducing numerous cycles of freezing and thawing through a bath of water. The water in the aggregate expands and increases its volume by more than nine percent. When this water expands, it causes internal stresses in the slab, which reduces the durability of the slab. A total of 20 cycles have been selected by ODOT laboratory, to which the specimen is subjected. The number of cycles commonly exceeds 10, occasionally going to 50 or more. For small pieces wherein bedding and jointing are insignificant, a loss of 10 percent by test CRD-C 144 is of concern. Large stones and slabs losing more than 25 percent during 20 cycles were considered not to perform well in service. Large stones losing no more than 10 percent are considered as good quality aggregate. A total of three specimens are tested simultaneously in the same test bath. The effects of geological structure and other important characteristics of a material are less likely to be overlooked when an average of three values is reported in the test result. Figure 4 represents the correlation of freeze-thaw soundness with Micro-Deval abrasion loss.

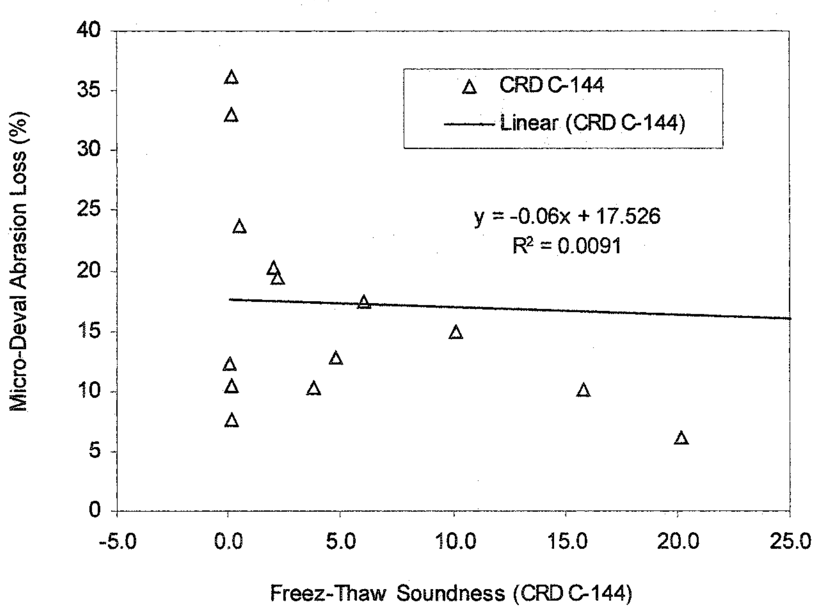

Figure 4. Micro-Deval abrasion loss versus freeze-thaw soundness

A total of 13 sources of aggregate data were plotted. From the correlation it is evident that Micro-Deval abrasion has no correlation with freeze-thaw soundness. In fact, many engineers do not believe the freezing and thawing cycles can affect aggregates used for asphalt pavement [13].

7.3 Correlation of Micro-Deval Loss with Aggregate Durability Index

The durability index is a value indicating the relative resistance of an aggregate to produce detrimental claylike fines when subjected to prescribed mechanical agitation in the presence of water. Separate and different procedures are used to evaluate coarse and fine portions of aggregate. The test assigns an empirical value to the relative amount, fineness, and character of claylike fines produced during wet degradation. It is especially suitable for basalt type aggregates containing interstitial montmorillonite [9]. The aggregate durability index test for coarse aggregates can be summarized as: a washed and dried sample of coarse aggregate is agitated in water in a mechanical washing vessel for a period of 10 minutes. The resulting wash water and passing 75 μm (No. 200 sieve) size fines are collected and mixed with stock calcium chloride solution and placed in a plastic sand equivalent cylinder. After a 20-minute sedimentation time, the level of the sediment column is read. The height of the sediment is then used to calculate the durability index of the coarse aggregate [10]. A minimum durability index value of 40 is required for use in asphalt concrete in Oklahoma. The correlation of Micro-Deval abrasion loss with aggregate durability index is shown in Figure 5. A clear trend that the Micro-Deval abrasion loss decreases as the durability index value increases can be seen.

7.4 Correlation of Micro-Deval Loss with Bulk Specific Gravity

Specific gravity of aggregates is necessary for calculating the mass of a desired volume of material. It has no clearly defined significance as a measure of suitability of material for use as asphalt concrete aggregate. Aggregates with specific gravity below 2.40 are usually suspected to be potentially unsound and, thus, not suitable for use in the exposed portions of hydraulic structures. Appropriate test methods are found in AASHTO T 84 and AASHTO T 85 [17,18]. In this paper, specific gravity characterizes only the solid components (mineralogical) of an aggregate.

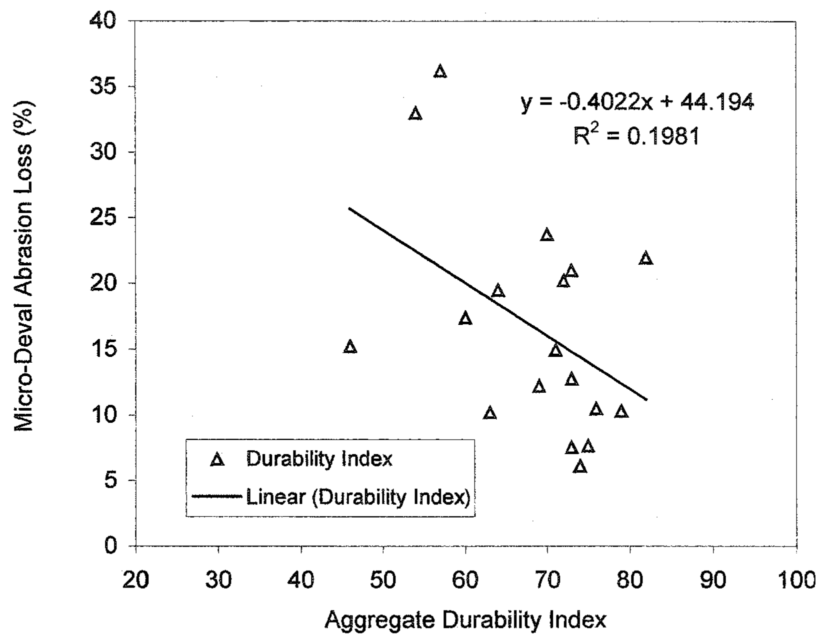

Figure 5. Micro-Deval abrasion Loss versus durability index

Figure 6 shows that Micro-Deval abrasion loss has a good correlation with bulk specific gravity of aggregate. From Figure 6, it is evident that lighter aggregates have higher Micro-Deval abrasion loss. Also from the data, low specific gravity has been indicative of poor quality in porous Stigler aggregates (pit no. 3102) having high absorption. Therefore, it may be necessary to set a limit on the permissible amount of material lighter than a given specific gravity when selecting aggregates for use in moderate or severe environment. Also, the specific gravity limit and the permissible amount lighter than the limit should be established on the basis of results of laboratory freezing-and-thawing tests as well as other tests.

7.5 Correlation of Micro-Deval Loss with Unit Weight

A more useful parameter sometimes is dry unit weight in which the important parameter of porosity is included. The overall aggregate density is conveniently characterized in terms of dry unit weight to take account of porosity as well as mineral density. Commonly used rock types range from about 140 to 160 lb/cu yd. There is a tendency for rocks with dry unit weight exceeding 160-lb/cu yd to be among the least troublesome. Toward and below the low end of the common range, the durability of an aggregate typically decreases as a reflection of increasing porosity. In this study, the unit weight of aggregates is determined following the AASHTO T 19 procedure [19]. From Figure 7, it can be seen that Micro-Deval abrasion loss has very poor correlation with the rodded unit weight of aggregate. It is a contradictory to the correlation found from saturated surface dry specific gravity in Figure 6. Actually, the rodded unit weight is an approximate measure of aggregate property and therefore, can be eliminated from aggregate quality testing.

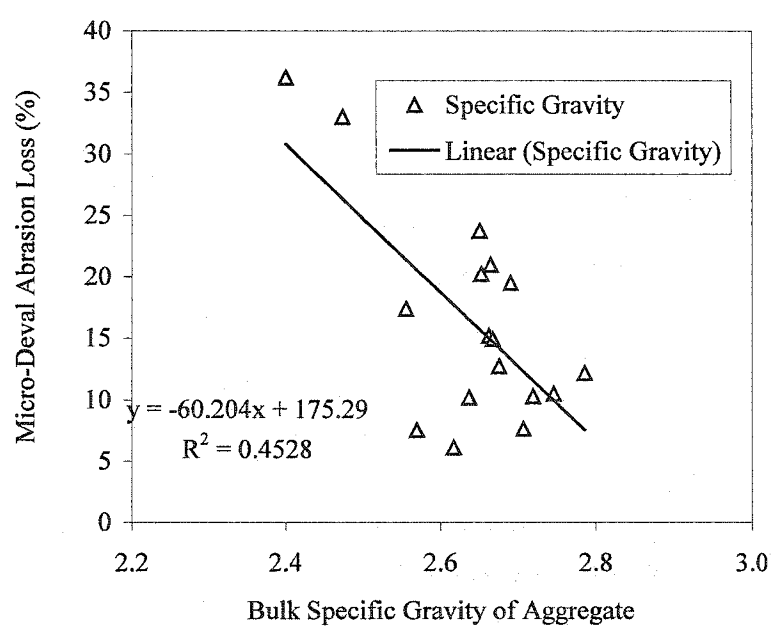

Figure 6. Micro-Deval abrasion loss versus bulk specific gravity of aggregate

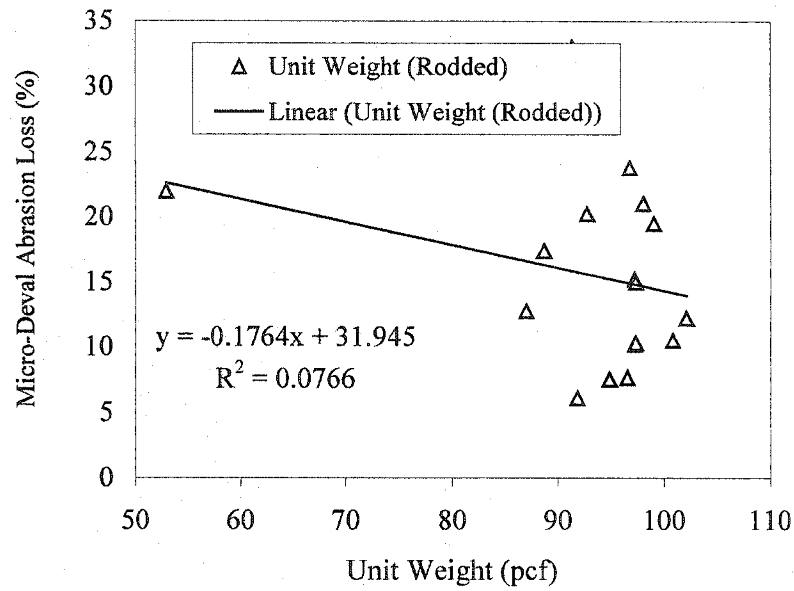

Figure 7. Micro-Deval abrasion loss versus unit weight of aggregate

7.6 Correlation of Micro-Deval Loss with Absorption

Typically, water absorption is good measure of aggregate deterioration. Absorption values exceeding two percent generally suggest potential durability problems. Values in the range from one to two percent are common among suitable and unsuitable aggregate materials. Absorption below one percent usually indicates aggregates of good quality. Absorption is determined primarily as an aid in estimating amounts of water in aggregates for laboratory, and also field control of amount of mixing water used in the asphalt concrete. In this study, water absorption was measured in accordance with the AASHTO T 84 (fine aggregate) and AASHTO T 85 (coarse aggregate) procedures. Figure 8 shows that Micro-Deval abrasion has a good correlation with absorption of aggregates. As the absorption increase, the loss in Micro-Deval increases. This is obvious as Micro-Deval measures the durability of mineral aggregates resulting from a combination of actions including abrasion and grinding with steel ball in the presence of water.

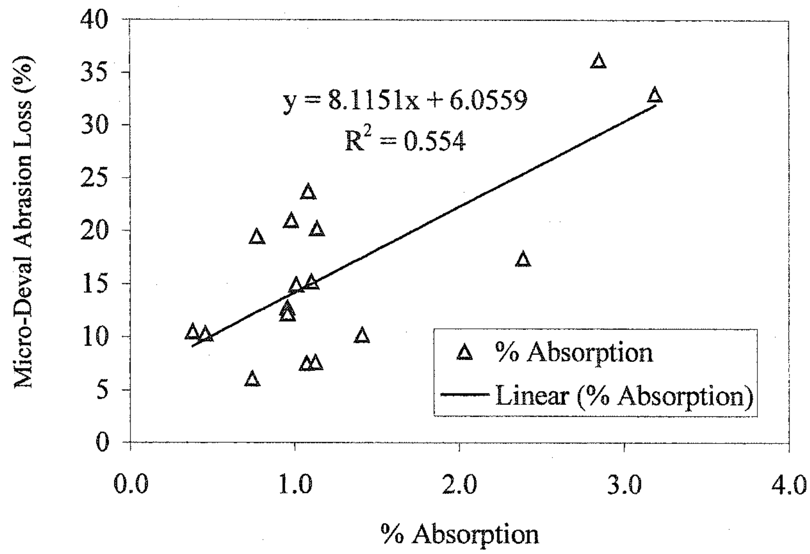

Figure 8. Micro-Deval abrasion loss versus absorption of aggregate

7.7 Micro-Deval Abrasion Loss and Aggregate Size

Nominal maximum size (NMS) is defined as one sieve size larger than the first sieve to retain more than 10 percent aggregate. Figure 9 shows the variation of Micro-Deval abrasion loss on NMS. The Micro-Deval values are scattered all over the plotted area. By a careful investigation, it can be seen that the higher the NMS the lower the Micro-Deval loss on an overall sense. In this study, Micro-Deval test has been performed on three different grading of aggregates. Type B and Type C are used in the pavement surface and Type A is used in the base coarse. Aggregate Type A consist of material passing the 19.0 mm sieve and retained on 9.5 mm sieve. Type B pass 12.5 mm sieve and retained on 4.75 mm sieve. Type C passes 9.5 mm sieve and retained 4.75 mm sieve. From Figure 10, it can be seen that Type C and Type B has higher Micro-Deval abrasion loss compared to Type A. Lane et al. (2000) requires a maximum Micro-Deval loss of 17% for regular surface coarse, 21% for binder or base coarse, 25% for granular base, and 30% for granular subbase [11]. This study specifies a maximum limit of 22% for surface and 25% for binder coarse paving.

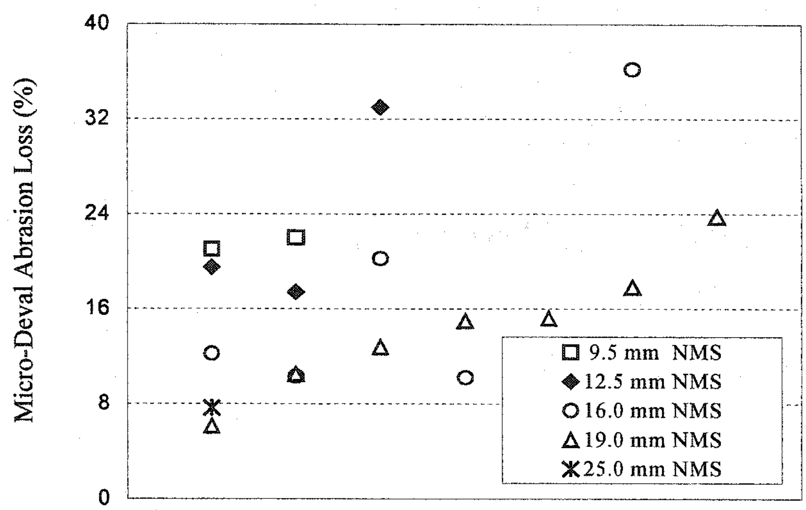

Figure 9. Micro-Deval abrasion loss by nominal maximum size

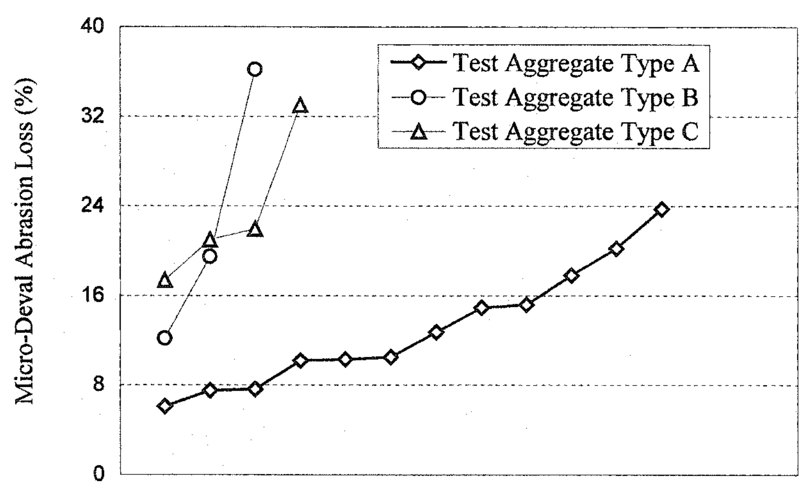

Figure 10. Micro-Deval abrasion loss by aggregate size

7.8 Micro-Deval Abrasion Loss and Aggregate Type

Micro-Deval abrasion value depends on the type of aggregate. For surface coarse aggregates, it requires a maximum Micro-Deval abrasion loss of between 10 to 15% depending on rock type, 10 for trap rock, and 15 for sandstone [11]. From Figure 11, it is evident that sand stones are more susceptible to (weak) Micro-Deval abrasion loss, whereas the Rhyolite aggregates are stronger than the limestone aggregates. Dolomitic limestone showed a lower Micro-Deval abrasion loss when compared to other limestone. In this study, a specification limit of 25 maximum Micro-Deval is chosen as best for Oklahoma source of aggregate irrespective of its type.

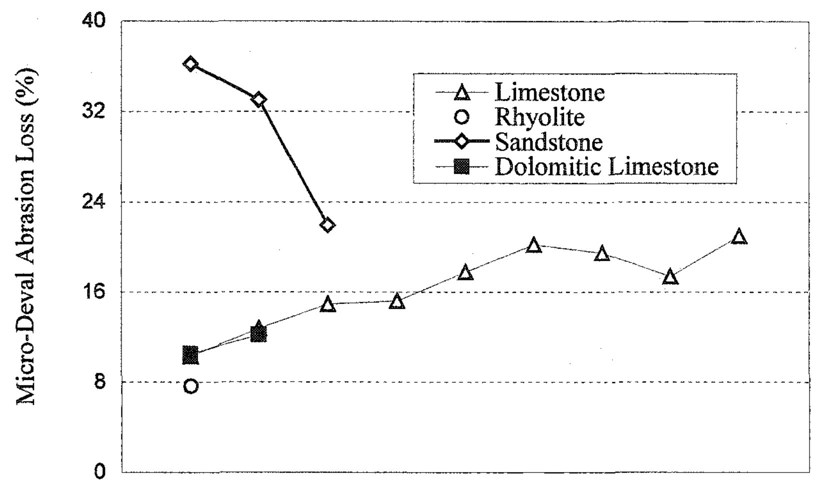

Figure 11. Micro-Deval abrasion loss by aggregate type

8. Micro-Deval Abrasion Loss in Hot Water

This study made an effort to examine aggregate degradation due to rolling in a drum mixture, especially in a hot environment by conducting Micro-Deval test in hot water instead of normal water. Three of the sources were tested using both hot (149 °C) and normal water (23.3 °C) as shown in Table 2. Its can be seen that there is no significant difference in the values between the test results. In practice, aggregates are heated and the heated aggregates have to pass a path inside the drum in a plant before mixing with asphalt and therefore, are subjected for abrasion. This study made an effort to simulate this abrasion loss using hot water in Micro-Deval.

Table 2. Effect of hot water on Micro-Deval abrasion loss

Aggregate Source	Gradation	Size (mm)	Type	Hot Water	Normal Water
Hanson WRP, Inc. at Davis	A	19	Rhyolite	7.7	7.6
Martin-Marietta at Davis	C	12.5	Limestone	26	25.9
Dolese Co. at Richard Spur	A	19	Limestone	15.2	13.7

9. Concluding Remarks

- Comparing the in service performance (field measured wear) with both the laboratory Los Angeles abrasion and Micro-Deval abrasion, it was found that the L.A. abrasion test is considered inadequate as a basis for judging the quality of the aggregates. Instead, the Micro-Deval can serve to determine the abrasion and durability of aggregate.
- Micro-Deval test is reasonably repeatable. The test can be completed in one day.
- Micro-Deval abrasion has a good correlation with water absorption of aggregate. The traditional soaking time (1 hour) can be reduced to 3 minutes using the CoreLok™ device. This study recommend the of CoreLok device for rapid absorption of Micro-Deval aggregate.
- Using a Micro-Deval test results it is possible to determine the maximum allowable loss for aggregates of a specific locality. This study found a maximum allowable loss of 25.0 % in the Micro-Deval apparatus is appropriate for Oklahoma source of aggregates..
- It is possible to rank an aggregate source based on the Micro-Deval test results.
- The correlation of Free-thaw soundness with Micro-Deval abrasion loss was very poor. Therefore, the study recommends the freeze-thaw soundness test to be conducted in conjunction with Micro-Deval test to control aggregate quality.

- The test results obtained by using hot water in the Micro-Deval test did not differ from the test result using water at room temperature (23 °C) significantly. Therefore, use of water at room temperature should be adequate.
- The maximum size of aggregate used in the Micro-Deval tests is 19.0 mm (3/4 in.), whereas aggregate up to 37.5 mm (1-1/2in.) is frequently used in asphalt concrete. In spite of its limitations, the test provides an excellent means of evaluating the relative quality of most materials and results of the test can be given prime consideration in selecting aggregate quality requirements.

Acknowledgement: The work reported herein was sponsored by the Oklahoma Department of Transportation (ODOT). The Micro-Deval device used in this study was purchased recently and installed at Material Laboratory at the Oklahoma Department of Transportation. The authors would like to express their sincere gratitude and appreciation to Reynolds Toney for providing the opportunity to work at ODOT on Micro-Deval research and use their equipments and devices. The authors thank the Geology Brach of ODOT materials division for providing information on rock quarries and their support.

Reference:

[1] Huang, Y.H. *Pavement Analysis and Design*, Prentice Hall, Inc., New Jersey, USA, 1993.

[2] Barksdale, R.D. Test Device for Evaluating Rutting of Asphalt Concrete Mixes. *Transportation Research Record 1418,* National Research Council, Washington, D.C., 1993.

[3] Hicks R.G. Moisture Damage in Asphalt Concrete. *NCHRP Synthesis of Highway Practice 175*, Transportation Research Board, Washington, D.C., 1991.

[4] Solaimanian, M., Kennedy, T. W., and Elmore W.E. Long-Term Evaluation of Stripping and Moisture Damage in Asphalt Pavements Treated with Lime and Anti-stripping Agents.

Texas Department of Transportation Report No. CTR 0-1286-1F, Center for Transportation Research, University of Texas at Austin, 1993.

[5] AASHTO T 96. Resistance to Degradation of Small-Size Coarse Aggregate by Abrasion and Impact in the Los Angeles Machine. *Standard Specifications for Transportation Materials*, American Association of State Highway and Transportation Officials (AASHTO), Part II, Washington, D.C., 2002.

[6] Wu, Y., Parker, F. Jr., and Kandhal K. Aggregate Toughness/Abrasion Resistance and Durability/Soundness Tests Related to Asphalt Concrete Performance in Pavements. *National Center for Asphalt Technology, NCAT Report No*. 98-4, 1998.

[7] Roberts, F. L., Kandhal, P. S., Brown, E. R., Lee, D., and Kennedy, T.W., *Hot Mix Asphalt Materials, Mixture Design, and Construction*. NAPA Education Foundation, Lanham Maryland, 1996.

[8] Toney, R., *Personal Communication.* Materials Division, Oklahoma DOT, 2002.

[9] Kandhal, P. S., and Parker, F. Jr. Aggregate Tests Related to Asphalt Concrete Performance in Pavements. *Final Report, National Cooperative Highway Research Program (NCHRP)*, Transportation Research Board, Washington, 1997.

[10] AASHTO T 210. Aggregate Durability Index. *Standard Specifications for Transportation Materials*, American Association of State Highway and Transportation Officials (AASHTO), Part II, Washington, D.C., 2002.

[11] Lane, B.C., Rogers, C. A., and Senior, S. A. The Micro-Deval Test for Aggregates in Asphalt Pavement. *The Eighth Annual Symposium of the International Center for Aggregate Research*, Colorado, 2000.

[12] Rogers, C. Canadian Experience with the Micro-Deval Test for Aggregates. Advances in Aggregates and Armourstone Evaluation, *Engineering Geology Special Publications-13*, Geological Society, London, pp. 139-147, 1998.

[13] Senior, S. A. and Rogers, C. A. Laboratory Tests for Predicting Coarse Aggregate Performance in Ontario. *Transportation Research Record No. 1301,* pp. 97-106, 1991.

[14] AASHTO TP58-00. Standard Test Method for Resistance of Coarse Aggregate to degradation by Abrasion in the Micro-Deval Apparatus. *Standard Specifications for Transportation Materials*, AASHTO, Part II, Washington, D.C., 2000.

[15] Tarefder R. A., and Zaman, M. Evaluation of Rutting Potential of Hot Mix Asphalt Using the Asphalt Pavement Analyzer. *Final Report, Oklahoma Department of Transportation* (ODOT), USA, October 2002.

[16] CRD C-144. *Standard Test Method for Resistance of Rock to Freezing and Thawing.* Concrete Research Division, CRD, 2001.

[17] AASHTO T 84. Determination of Specific Gravity and Absorption of Fine Aggregate. *Standard Specifications for Transportation Materials*, American Association of State Highway and Transportation Officials (AASHTO), Part II, Washington, D.C., 2001.

[18] AASHTO T 85. Determination of Specific Gravity and Absorption of Coarse Aggregate. *Standard Specifications for Transportation Materials*, American Association of State Highway and Transportation Officials (AASHTO), Part II, Washington, D.C., 2001.

[19] AASHTO T 19. Determination of Unit Weight and Voids in Aggregate. *Standard Specifications for Transportation Materials*, American Association of State Highway and Transportation Officials (AASHTO), Part II, Washington, D.C., 2001.

APPENDIX II

'Formulation of Mix Design and Asphaltic Encapsulation of Hydrocarbon Contaminated Soil' by Tarefder, R. A., Ruckgaber, M. E., Zaman, M. M., and Patton, D., ASCE Journal of Materials in Civil Engineering, Vol. 15, No. 2, pp. 166-173, ASCE, April 2003

FORMULATION OF MIX DESIGN FOR ASPHALTIC INCORPORATION OF HYDROCARBON CONTAMINATED SOIL

Abstract: This study developed a cold mix design procedure to incorporate hydrocarbon-contaminated soil as an ingredient of pavement base-product. The incorporation was achieved by asphaltic stabilization and encapsulation utilizing Cold Mix Asphalt (CMA) technology. The main focus is to maximize the soil in economically viable end products that pass the industry standards, engineering requirements, and environmental safety requirements. Mix design was performed by several trials based on bench scale parameters. Aggregate from local quarry was used as one of the ingredients of mix to reduce end product cost. Soil and aggregate, prior to incorporate, was assessed for their suitability to use in the stabilization process by bench scale tests such as particle size distribution, sand equivalent, plasticity, density, specific gravity etc. Varying amount of affected soil, aggregate, small amount of Portland cement and specified grades of emulsion were mixed, compacted and tested for resistance values and tensile strength. Leachate testing of engineered product for total hydrocarbon ensured its use in pavement base. The formulated mix design incorporated 80% of the hydrocarbon-affected soil by weight of soil-aggregate mix. The study warns that the incorporating higher percent of soil in the mix can lose the saved money for buying increased emulsion.

Key Words: Mix design, CMA, bench scale, emulsion, resistance, density, split tensile strength, hydrocarbon contaminated soil, aggregate.

Background

Over the past two decades, hydrocarbon contaminated soil has made up a continually increasing amount and significant volume of waste material (Dietz and Burns 1989). The increased waste materials impose a significant burden on landfills and disposal sites, long-term liabilities, land-ban, and increased costs for business owners and industries. Some of the major sources of the soil contamination are leaking of petroleum from underground storage tanks, drilling and treatment activities for exploration and production of hydrocarbon. In Oklahoma, contaminated soil account for about 98% of the waste generated as a one-time occurrence (Testa 1997). The soil from Cleveland County in Oklahoma, the subject of present study, was contaminated by hydrocarbon. The history of this soil dates back to 1905, when Kerr-McGee Oil Refinery Corporation began production in Cleveland County, Oklahoma (Patton 2000; Personal Communication, Surbec-ART Environmental LL.C., 3200 Marshall Avenue, Suite 200, Norman, OK 73072). Since then, the production continued until 1972. The site was then leveled, demolishing all buildings and burying all soils. This was prior to the advent of the United States Code of Federal Regulations (40 CFR Part) that currently regulates such operations (EPA 1992). One of the precepts of these regulations is cradle to grave responsibility and liability (to the owner) for materials that pose a potential threat to the environment. In the last 30 years, the constituents of concern mainly, heavy chain hydrocarbons showed a tendency to migrate into the near surface aquifer, posing a potential threat to the environment and violating the above statutes. The site owner could perform a remediation investigation and feasibility study to determine possible solutions. At the top of the list of options was no action. In other words, completely ignore all responsibilities. Next was to load, transport, and dispose the material into a landfill. The material could also be cleansed by biodegradation, either in-situ or ex-situ. Alternative more technical cleansing processes could include co-solvent extraction, soil washing, thermal desorption, incineration, vapor extraction and many others (Schaefer and Albert 1988). However, when all approved remedial options were subjected to the criteria of cost effectiveness, time efficiency, environmental correctness, and alleviation of client's liability, the preferable choice became resource recovery (Testa and Conca 1993). In other words, this option suggests that "don't throw it away or spend millions of dollars to clean it, use the material for something useful". Based on the findings of the present study, we proposed a recovery-based solution that involved using the contaminated soil as an ingredient of Cold-Mix-Asphalt (CMA) paving materials.

Hydrocarbon contaminated soil has been used as an ingredient of asphalt pavement materials since 1985 (Testa and Patton 1994). The United States Department of Transportation (DOT) in a study conducted in 1988 postulated that about 25×10^9 kg (22.8 million metric tons) of industrial waste could be recycled and consumed through the states' asphalt industry by simply incorporating 5 percent waste products in all Hot Mix Asphalt (HMA) mixes (DOT 1988). The United States Environmental Protection Agency (EPA) in 1992 identified approximately 77 permanent HMA facilities in the United States that recycle petroleum-contaminated soil into marketable products (EPA 1992). It is known that of the 6.44×10^6 km (4 million miles) of roads in the United States, about 3.7×10^6 km (2.3 million miles) of these roads are surfaced with either asphalt or concrete, of which approximately 3.5×10^6 km (2.2 million miles) or 96% are asphalt-paved. Currently, virtually any paving technique can be used with asphalt emulsions, also referred to as cold mix design. Choosing the right emulsion and application technique can yield significant economic and environmental benefits. Cold mix asphalt plants, which have the advantage of processing contaminated soil on-site and produce a wide variety of asphalt end products, are situated nationwide. There has been a continuing pressure on CMA industries to incorporate a variety of waste materials in CMA products (DOT 1993). Focusing on the relevance of the present study, Pawnee County, Oklahoma had over 725 km (450 miles) of unpaved and annually maintained roads. They had a limited budget for these operations, but much more needs. Consequently, there existed a ready market for CMA end products. As would be indicated in this paper, subsequent bench scale testing of the product samples indicated their viability for use as commercial asphalt products. From the clients' perspective and a study of the feasibility of various options, it was determined that there were a market for such CMA products. The main focus of the study was to incorporate the contaminated material as an ingredient to produce CMA product, ensure the engineering requirements needed to use the product for the fabrication of road base, meet the county needs, and enhance county's economy.

Objective

The main objective of the study was to formulate a mix design procedure to incorporate maximum possible amount of hydrocarbon affected soil-aggregate in the total volume of product. Ingredients to be suited for incorporating into a base product, their properties were determined by bench scale testing. In the design procedure, suitable amounts of ingredients were blended, encapsulated with emulsion and stabilized in a cold-processed asphalt product. Stabilization process did not change the physical properties of affected soil but it reduced the risk posed by contaminants by converting them into a less soluble and mobile form (Testa 1995). Where as, the encapsulation encompassed coating or enclosure of hydrocarbon affected soil particles and agglomerated with new substance. The end products were ensured for use by engineering and environmental tests.

Design Considerations

A design CMA mixes usually combines aggregates, affected soil, emulsion and sometimes a cement or lime additive. The characteristics of the mix ingredients are very important in obtaining good mixture properties and performance. Only soil and aggregate cannot ensure a successful product (Roberts et al. 1996). The product quality depends a lot on the mixture's properties. For an example, the optimum amount of emulsion is required to increase binding action and to increase the performance of the pavement (Jantzen 1993). Similarly, a correct amount of water is required to adequately disperse the emulsion and to achieve good mix workability. Type of emulsion must be taken into account to ensure successful coating. Adequate curing is necessary for the development of mechanical properties of binder (Mang and Leonarde 1990). The development of mix design procedure for cold mix is an art, requires several trials. In several trials, this study formulated a mix design procedure that determined the grade and percentage of emulsion, percentage of affected material, aggregate, water, cement; and such mixture properties as workability, stability and strength based on laboratory testing. Bench scale tests were also performed before the incorporation of the affected soil and local aggregate in CMA mixture.

Evaluation of Contaminated Soil

The bench scale test results of the hydrocarbon-affected soil are summarized in Table 1. Soil sample was tested for hydrocarbon contents and moisture contents (ASTM C 566 1998). Hydrocarbon content was detected above hazardous level. The field moisture content was in the range of 12% to 15%. Sampling was performed by compositing all collected soil samples. The average field moisture content of soil composite was 13.4% due to surface moisture, where as the absorption capacity of the soil was 4.8 percent. This information was used in determining the water needed for hydrating reagents and recommendation for air-drying before the application of emulsion in laboratory production. Sieve analysis was performed on the composite soil to determine the grain size distribution (AASHTO T 27 1999). The sieve analysis results showed that approximately 8% to 10% of the affected soil was coarse grained (retained on a No. 4 sieve). The sieve analysis results were used for gradation calculation of the blended mixture. Hydrometer tests were performed (AASHTO T 88 1999) to cover the size distribution of particles down to a No. 40 sieve. From hydrometer test results plotted in Fig. 1 shows that the affected soil passing a No. 200 (0.075 mm) sieve ranges from 37% to 39%, which met Oklahoma Department of Transportation's (ODOT) requirements for cold mix asphalt concrete (ODOT 1999). The soil was also tested for Liquid Limit, Plastic Limit, and Plasticity Index (AASHTO T 90 1999). Test results showed that the soil was non-plastic and medium grained. According to the United States Department of Agriculture (USDA) Classification, the contaminated soil was a sandy loam with some gravel. From experience, it was decided to use cement additive to enhance mix workability and resistance to water (MS-19 1998). The proportion of plastic materials and clay or dust in contaminated soil was determined by the Sand Equivalent (SE) test (ASTM D 2419 1999); the minimum required value of SE for successful stabilization considered being 25 (MS-14 1989). Dust, especially clay adhering to aggregate, prevents good bond between the asphalt binder and soil. The sand equivalent test result of 28 indicates that the soil is suitable for emulsion-application. It was observed that the sand equivalent value could be increased up to 39 by applying 2% Portland cement with the soil. The higher the sand equivalent values the better the soil coating. The soil was also subjected to specific gravity test (ASSHTO T 84 1999). The contaminated soil was found to be light in weight as indicated by the bulk specific gravity of 1.91. The bulk density of the soil is 1858 kg/m^3 (116 pcf). This was because of hydrocarbons were absorbed into or adhere to the surface of the soil particles. The test value was further supported by the observation of a thin layer of oily residue on the surface of the liquid when a dispersion agent called sodium hexametaphosphate was added to the soil during the hydrometer tests. The specific gravity value was used in finding the air-void content, weight-volume conversions, and in determining necessary proportions in various design mixtures.

Evaluation of Aggregate

Aggregate parameters used in the development of mix design procedure have been summarized in Table 2. Crushed aggregates were collected from a local quarry of Cleveland County to reduce cost of end products. The aggregate was subjected for quality evaluation. Gradation test was performed to determine compliance of the particle size distribution with the gradation requirements of base aggregate (ODOT

1999) and to provide necessary data for controlling gradation of blended mix containing this aggregates. The gradation test showed that a very small amount of material passed No. 40, 80, and 200 sieves. The gradation test results have been plotted on 0.45 power chart as shown in Fig. 2 (McGennis et al. 1994). Fig. 2 shows that the aggregate gradation line is passing below the maximum density line and is effective in incorporating higher percentages of affected soils as it creates a high void space to be filled by the fines. Therefore, no screen-off was performed to cut the finer portions of aggregate. The Los Angeles (L.A.) abrasion test was performed to measure toughness and abrasion characteristics of the selected aggregate (AASHTO T 96 1999). The average L.A. abrasion value for the aggregate was 27, well below ODOT's maximum requirement of 40 (ODOT 1999). For high-type HMA, the Federal Highway Administration (FHWA) recently recommended that specifications require at least 60 percent of the plus No. 4 (4.75 mm) material should have at least two mechanically induced fractured faces. Some agency specifications require that at least 75 percent or 85 percent of the coarse particles should have two crushed faces and that at least 90 percent have one crushed face (NAPA 1998). Currently there is no ASTM or ASSHTO standard test procedure for measuring the percentage of fractured faces for an aggregate. This study implemented the procedure adopted by Oklahoma Highway Department (OHD) to measure the percent fractured face (OHD L 2000). The mechanical fractured face analysis showed that 100% aggregate particles were with 2 or more fractured faces. The fine aggregate angularity, a property of blended aggregate, was measured by determining the amount of uncomplicated voids in the loose aggregate (AASHTO TP 33 2000). The higher the amount of voids the more angular the aggregate. The fine aggregate angularity was 45, which is above ODOT's minimum limit of 40 for roads designed for less than 3 millions equivalent single axle load (ODOT 1999). The average specific gravity of the aggregate was 2.7, with an absorption value around 2.2 and field moisture content of 3.6%.

Design Procedure

Once the soil and the aggregate found suitable for use in CMA, a range of soil to aggregate ratios was included in the mix design to determine a limiting percentage of soil that could be used. A number of factors including mix gradation, type and amount of emulsion, type and amount of additive, range of water content, mixing and compaction, curing, stability and tensile strength were addressed by mix design. A schematic flow-chart illustrating the steps of mix design is shown in Fig. 3. Several trials were made to develop relationships concerning porosity and packing as well as the final proportions of ingredients in blended mix. First a 50% affected-soil and 50% local-aggregate (termed as Soil to Aggregate Ratio, SAR=50/50) design was used. Design ingredients were blended and mixed with emulsion to fabricate products. End products were tested for stability, durability and workability. Test results of samples following the proportion exceeding all requirements for asphalt-stabilized base were subjected for environmental regularity criteria. Subsequently, three other designs were developed. A 60% soil and 40% aggregate (SAR=60/40) mixture was prepared and evaluated, producing similar encouraging results. As both the 50/50 and 60/40 mixtures produced satisfactory resistance values (well above the minimum), it was reasoned that a high percentage of soil could be incorporated in the mix design. Therefore, SAR=70/30 and

SAR=80/20 designs were produced. Fig. 4 represents the gradation of four design mixes on 0.45 power chart. From Fig. 4, it is evident that the gradation line deviates from the maximum density line as the percent of incorporated soil increases.

Emulsion Type

In a series of preliminary experiments, different types of asphalt emulsions such as High Float Medium Setting, HFMS-1 (anionic emulsion) and Slow Setting, SS-1 (anionic emulsion) were assessed, concerning their ability to coat the SAR = 50/50 design blend. The study found that it was not possible to achieve a uniform coat with any of these emulsions due to hydrophilic characteristics of local aggregate used. It was decided to change the electrical charge of the ions in the asphalt emulsion (MS-14 1989). Finally, application of Cationic Slow Setting (CSS-1h) emulsion appeared to coat the blended mix satisfactorily and was selected for further experiments.

Estimated Emulsion

The amount of emulsion was selected by several trials. An emulsion content was assumed as starting point emulsion. Estimated staring percentage of emulsion was then combined with damp soil-aggregate mix. The amount of water to damp the design mix was determined by the amount of water needed to darken the soil-aggregate blend without any balling of the asphalt with the fines. Mixture's coating was measured visually (OHD T 59 2000). Satisfactory coated mix was then subjected for adhesion test. If the coating showed unsatisfactory, trials were made with plus or minus one half of a percent to determine the emulsion content needed for successful coating. Coating more than 50% was considered as satisfactory for base mix. Samples passed the coating test were washed with boiling water and the amount of retained coating was visually inspected. More than 60% retained coating was considered as satisfactory.

Optimum Moisture

Samples were prepared with estimated emulsion content and compacted at different moisture contents. Density of the specimens was determined by the water displacement method (AASHTO T 166 1999). The moisture contents were plotted against density as shown in Fig. 5. It can be observed that a range of moisture contents from 6% to 7.5% by oven dry weight of mix can be used for laboratory production. Also, the mix is recommended for air drying within this range for field production. The optimum moisture content at which the sample has the highest density was 7.0% by oven-dry weight of mix.

Additive

This research selected Portland cement as additive because the soil type was sandy loam. Cement additive performs better than other additives in case of sandy soil (MS-19 1999). Soil-aggregate was mixed with 1% to 2% Portland cement followed by the addition of water for hydration and then compacted. Trials made by adding a small percent of Portland cement showed that addition of cement improved coating a very little but workability a lot.

Mixing and Compaction

Sufficient amount of dry aggregate and soil was weighted according designed proportions to obtain a compacted specimen height of 2.5 inch and mixed thoroughly after adding one third of the moisture. Portland cement was introduced in powder form and mixed thoroughly before adding the next third of water. The sample was mixed again prior to addition of last portion of water. After mixing again, the emulsion was added to the damp mixture and mixed by spoon until the emulsion was uniformly dispersed. A mechanical mixer was then used to obtain a uniform mix. Mixture was placed in compaction mold in several layers and hand compacted with bent spoon. The molded mix was then compacted using a Texas gyratory compactor (OHD L 8 2000). Compacted specimen was allowed for seating in compaction mold for minimum of one hour prior to extracting the specimen for curing.

Curing

Curing refers to the development of mechanical properties of an asphalt binder. After the emulsion molecules break down and the emulsion particles coalesce and bond to the soil-aggregate, the specimen begins to harden and gain strength (Khalid 1999). The compacted samples were subjected to early curing by placing them in a draft oven for 24 hours at $23 \pm 2.8\ ^{0}C$ before strength and stability testing. Another set of samples was subjected to for full curing to simulate the effect of prolonged exposure to subsurface water in the field. In fully curing procedure, the early cured samples were submersed under water and subject for a vacuum of 10 mm of Hg for one hour. Vacuum was then released and the specimens were allowed to soak in water for one hour before strength testing.

Strength Testing

Early cured and vacuum cured samples were tested by the Hveem procedure to determine their resistance to deformation or stability (AASHTO T246 1999). A vertical load was applied on a cured specimen while the lateral pressure exerted was measured by means of the Hveem stabilometer (Vallerga and Loverig 1985). Application of vertical load was stopped at 8900 N (2000 lb.) and turns displacement was recorded during pumping the horizontal pressure from 34.5 kPa to 689 kPa (5 psi to 100 psi). Resistance value was calculated using the values of vertical pressure, horizontal pressure and turn displacements and is tabulated in Table 3. Higher resistance values exhibit a greater chance of the mixture opposing the shear forces produced by traffic loading. A set of cured samples from similar design was tested for indirect tensile strength (AASHTO T 283 1999). A cylindrical sample was deformed diametrically at a rate of 1.65 mm per minute (0.065 inch/minute) in room temperature (23 ± 2.8 ^{0}C). Stress-strain data on various samples were recorded. Typical variation of deformations due to applied load during resistance value and split tensile tests are shown in Fig. 6 and Fig. 7, respectively.

Evaluation of Trial Designs

Table 4 summarized the bench scale testing results of all trial designs. Optimum emulsion content was established on the basis of best combination of resistance and tensile strength. For a successful design, the minimum required value of resistance was 70 for early cured sample and 78 for fully cured sample (MS-19, 1998). This study proposed the value of 172 kPa (25 psi) as a minimum tensile strength requirement for pavement base. From Table3, for SAR=50/50 design, early cured samples prepared with 4.0 % emulsion and 2% cement showed an average resistance value of 96 and tensile strength value of 310 kPa (45 psi). When these samples subjected to vacuum curing, both resistance and tensile strength decreased, the average resistance value was 89 with a tensile strength of 293 kPa (43 psi). The similar behavior was observed when percent of cement content was decreased. As the cement percentage was lowered to 1 and 0%, the average resistance values for early cured samples were found to be 93 and 90, respectively and the average tensile strengths were 255 kPa (37 psi) and 206 kPa (30 psi), respectively. In another trial, the emulsion content was increased to 4.5%. The average resistance value for early cure samples with 2% cement was 93 with an average tensile strength of 355 kPa (51 psi). The recommended optimum emulsion content for the design was made 4% of dry mix. Table 4 also shows that SAR=60/40 design, with 2% cement and 5% emulsion, showed an average resistance value of 92 and a tensile strength of 337 kPa (49 psi). Where as vacuum cured samples prepared with 2% cement plus 5% emulsion showed resistance value of 90 and the tensile strength value of 269 kPa (39 psi). When the emulsion was lowered to 4.5%, the resistance value increased to 94 and the tensile strength decreased to 255 kPa (37 psi). Vacuum cured samples of the same design gave an average resistance value of 86 with an average tensile strength of 186 kPa (27 psi). Percent emulsion contributed to tensile strength. The selected optimum asphalt content for SAR=60/40 design was kept 4.5%. From Table 4, for the case of SAR=70/30 design, samples with 1% cement and 4.5% emulsion showed an average resistance value of 91 with an average tensile strength of 179 kPa (26 psi). When cement content increased to 2%, samples showed an average resistance value of 92 with an average tensile strength of 220 kPa (32 psi). The vacuum cured sample shows an average resistance value of 84 with a tensile strength of 172 kPa (25 psi). When emulsion content increased to 5% with 2% cement early cured samples showed a resistance of 92 with 241 kPa (35 psi) of tensile strength value. At higher percentage of soil, both the increased cement content and the increased percent emulsion contributed for increased tensile strength. Table 4 also shows that for SAR=80/20 design, samples prepared with 2% cement and 5% emulsion showed an average resistance value of 90, and an average tensile strength of 186 kPa (27 psi). The vacuum cured samples show a resistance value of 83 psi with a tensile strength of 172 kPa (25 psi). When the emulsion content was lowered to 4.5%, the average value of early and vacuum samples shows resistance values of 92 and 78, respectively. The coating was not as rich as compared to the mix with 5% emulsion. When the emulsion content was increased to 5.5% the average resistance values of early and vacuum cured samples were 86 and 80. A set of samples was prepared with 1% cement and 5% emulsion, which gave an average resistance value of 90, and an average tensile strength of 158 kPa (23 psi). Average unit weights (density) ranges 2050 to 2100 kg/m^3 (128 to 131 lb/ft^3). Figure 8 is a plot of resistance versus percent emulsions for various trials for 80% soil incorporated design. From Fig. 8 optimum asphalt content was determined to be 5%, at which the vacuum cured samples have the maximum strength.

From the subsequent designs it was recommended that at least 80% soil could be incorporated into the final mix. Vacuum cured samples incorporating 80% soil met the specifications of ASB marginally. Any design incorporating more than 80% soil could not satisfy the criteria. The bench scale mix design was summarized as 80% affected soil using 5% emulsion, 2% Portland cement, 7% moisture by weight of dry soil-aggregate can be incorporated end product. However, the product had to be non-hazardous before using in the field. Subsequently, leaching tests on both grinned and intact samples were performed. The test the results confirmed the product safe to use in pavement base.

Results and Discussion

Figure 9 illustrates that the resistance value decreased as the percent of incorporated soil increased. The resistance value for the mix of 50% soil was about 96, whereas for 80% soil was 90. Similar trend was observed when tensile strength was plotted against the percent-incorporated soil as shown in Fig. 10. As percentage of soil increased, more emulsion was used in the mix for adequate binding. Again, from Table 4 it can be seen that the percentage incorporation of affected soil increases, the resistance values for the vacuum cured samples falls at a higher rate than the values of early cured samples of the same design. Study results showed as the soil percentage was increased, more emulsion was needed to produce the same results as a lower percentage soil mix with less emulsion. This is a trade off, as incorporating more soil into the mix can save money, purchasing more emulsion will lose the money. Figure 11 shows the relationship between cement percentage and resistance. The resistance values in the case of 2, 1, and

0% cement for 50% soil are 96, 93 and 90 respectively. For the 50% soil case, cement was not necessary. It increased the resistance value a little, and is too costly for it's miniscule additions. For mixtures of increased soil, however, cement was needed to improve coating and workability. Figure 12 illustrates that the tensile strength increases sharply as the percent cement is increased in a mix. It can be seen that the tensile strengths for 50% soil designed samples with 0, 1, and 2% cement were 206 kPa (30 psi), 255 kPa (37 psi), and 310 kPa (45 psi) respectively. Whereas the vales for 80% soil designed samples with 2% and 1% cement were 186 kPa (27 psi) and 158 kPa (23 psi), respectively, as shown in Table 4. The use of cement additive found to be necessary with the increasing percent soil incorporations for maintaining the mixture's tensile strength requirements above the proposed specification requirements.

Concluding Remarks

This study developed a cold mix design procedure to incorporate maximum amount of hydrocarbon-affected soil. Mix design parameters were determined by bench scale testing. Using the parameters, several designs were formulated. For each design, a mix was prepared and evaluated by engineered tests for base use. The designs, which end products met the engineering requirements, were further tested for environmental correctness. The design was finalized when the end products from it had ensured environmentally safe. The study found that 80% of the affected soil could be incorporated in a pavement base mix. The study showed that cement additive and higher percent of emulsion were necessary for the mix with higher percentage of incorporated soils. Therefore, study warns in saving the money incorporating a higher percent of soil compared to the cost of increased emulsion and cement. The study used local aggregate and CMA technology to reduce product cost. The study recommends an extensive cost-benefit analysis considering other possible options.

Acknowledgements

The research work reported here was sponsored by Surbec-ART Environmental LL.C. The authors wish to express their appreciation to Mr. Marshall Brackin, president of Surbec-ART Environmental LL.C., particularly for providing fund and support. The authors would like to thank Mr. Don Still, Mr. Emad Al Namasy, Mr. Cheong Ting Foo, Mr. Mike Smith of Broce laboratory in the University of Oklahoma

Reference

AASHTO T 27. (1999). "Sieve Analysis of Fine and Coarse Aggregates." *Standard Specifications for Transportation Materials ad Methods of Sampling and Testing Part 2,* 444 North Capitol Street, N.W., Washington, D.C. 20001.

AASHTO T 88. (1999). "Particle Size Analysis of Soils." *Standard Specifications for Transportation Materials ad Methods of Sampling and Testing Part 2,* 444 North Capitol Street, N.W., Washington, D.C. 20001.

AASHTO T 90. (1999). "Determining Plastic Limit and Plasticity Index of Soils." *Standard Specifications for Transportation Materials ad Methods of Sampling and Testing Part 2,* 444 North Capitol Street, N.W., Washington, D.C. 20001.

AASHTO T 84. (1999). "Specific Gravity and Absorption of Fine Aggregate." *Standard Specifications for Transportation Materials ad Methods of Sampling and Testing Part 2,* 444 North Capitol Street, N.W., Washington, D.C. 20001.

AASHTO T 96. (1999). "Resistance to Abrasion of Small-Sized Coarse Aggregate by Abrasion and Impact in the Los Angeles machine." *Standard Specifications for*

Transportation Materials ad Methods of Sampling and Testing Part 2, 444 North Capitol Street, N.W., Washington, D.C. 20001.

AASHTO TP 33. (2000). "Uncompacted Voids in the Loose Aggregate." *Provisional Standard Specifications for Transportation Materials,* 444 North Capitol Street, N.W., Washington, D.C. 20001.

AASHTO T 246. (1999). "Resistance to Deformation and Cohesion of Bituminous Mixtures by means of Hveem Apparatus." *Standard Specifications for Transportation Materials ad Methods of Sampling and Testing Part 2,* 444 North Capitol Street, N.W., Washington, D.C. 20001.

AASHTO T 166. (1999). "Bulk Specific Gravity of Compacted Bituminous Mixtures Using Saturated Surface-Dry Specimen." *Standard Specifications for Transportation Materials ad Methods of Sampling and Testing Part 2,* 444 North Capitol Street, N.W., Washington, D.C. 20001.

AASHTO T 283. (1999). "Resistance of Compacted Bituminous Mixtures to Moisture Induced Damaged." *Standard Specifications for Transportation Materials ad Methods of Sampling and Testing Part 2,* 444 North Capitol Street, N.W., Washington, D.C. 20001.

ASTM C 566. (1998). "Total Moisture Content of Aggregate by Drying." *Road and Paving Materials; Vehicle-Pavement Systems,* 100 Barr Drive, West Conshohocken, PA 19428.

ASTM D 2419. (1999). "Plastic Fines in Graded Aggregates and Soils by Use of the Sand Equivalent Test." *Soil and Rock,* Vol. 04.08, 100 Barr Drive, West Conshohocken, PA 19428.

Dietz, S. K., and Burns, M. E. (1989). " Quantities and Sources of Hazardous Waste." *Standard Handbook of Hazardous Waste Treatment and Disposal,* McGraw-Hill, New York.

DOT. (1988). "Selected Highway Statistics and Charts," *Federal Highway Administration (FHA).*

DOT. (1993). "A Study of the Use of Recycled Paving Material," *Report No. Federal Highway Administration, FHWA-RD-93/095 and EPA/600/R-93/095.*

EPA. (1992). "Potential Reuse of Petroleum Contaminated Soil – A Directory of Permitted Recycling Facilities." *U.S. EPA Report No. 600R-92/096.*

Jantzen, M. (1993). "Recycled Trend Means Saving for Local Governments," *Public Works*, Vol. 124, No. 10.

Khalid, H. A. (1999). "Permanent Deformation Characteristics of Bituminous Emulsion Macadams," *Transport*, vol. 135, No. 2.

Mang, T., and Leonarde, E. W. (1990). "Use of Asphalt Emulsion and Foamed Asphalt in Cold-Recycled Asphalt Paving Mixtures," *Transportation Research Record*, No 898.

MS-14. (1989). *A Basic Cold Mix Manuel*, Third Edition, Asphalt Institute Manual Series No. 19, Lexington, KY.

MS-19. (1998). *A Basic Asphalt Emulsion Manuel*, Third Edition, Asphalt Institute Manual Series No. 19, Lexington, KY.

McGennis, R. B., Anderson, R. M., Kennedy, T. W., and Solaimanian, M. (1994). "Background of Superpave Asphalt Mixture Design & Analysis," *Federal Highway Administration*, Report No. FHWA-SA-95-003.

NAPA. (1998). "Aggregate Tests Related to Asphalt Concrete Performance in Pavements," *National Cooperative Highway Research Program,* Report No. 405, National Academy Press, Washington, D.C.

ODOT. (1999). *Standards Specifications for Highway Construction.* 200 NE 21ST Street, Oklahoma City, OK 73105.

OHD L 18. (2000). "Method of Test for Percentage of Crushed Particles." *Oklahoma Highway Department Laboratory Mix Design Manuel,* 200 NE 21ST Street, Oklahoma City, OK 73105.

OHD T 59. (2000). "Method of Test for Percentage of Coating of Aggregate Particles." *Oklahoma Highway Department Laboratory Mix Design Manuel,* 200 NE 21ST Street, Oklahoma City, OK 73105.

OHD L 8. (2000). "Summary for Molding Specimen." *Oklahoma Highway Department Laboratory Mix Design Manuel,* 200 NE 21ST Street, Oklahoma City, OK 73105.

Roberts, F. L., Kandhal, P. S., Brown, E. R., Lee, D. Y. and Kennedy, T. W. (1996). "Hot Mix Asphalt Materials, Mixture Design, And Construction," *NAPA Education Foundation*, Second Edition, Lanham, Maryland.

Schaefer, C. F., and Albert, A. A. (1988). "Rotary Kilns." *Standard Handbook of Hazardous Waste Treatment and Disposal*, McGraw-Hill, New York.

Testa, S. M. (1997). *The Reuse and Recycling of Contaminated Soil,* ISBN 1-56670-188-0, Lewis Publishers, New York.

Testa, S. M. (1995). "Chemical Aspects of Cold-mix Asphalt Incorporating Contaminated Soil", *Journal of Soil Contamination*, Vol. 4, No. 2.

Testa, S., M., and Conca, J., L. (1993). "When Contaminated Soil Meets the Road." *Soils-Analysis Monitoring Remediation*, McGraw-Hill, New York.

Testa, S. M., and Patton, D. L. (1994). "Soil Remediation via Environmentally Processed Asphalt", *Process Engineering for Pollution Control and Waste Minimization*, Marcel Dekker, New York.

Vallerga, B. A., and Loverig, W. R. (1985). "Evolution of the Hveem Stabilometer Method of Designing Asphalt Paving Mixtures." *Proceedings, Association of Asphalt Paving Technologists Technical Sessions*, Vol. 54.

TABLE 1. Properties of Hydrocarbon Affected Soil

Soil Properties	Measured Values	Required Values (ODOT 1999)
Percent Moisture Content	13.4	
Percent Passing # 200 Sieve	37	10 to 50
Percent Retain # 4 Sieve	9	
Sand Equivalent Value	28	25 minimum
Liquid Limit	24	
Plastic Limit	21	
Plasticity Index	3	10 maximum
Bulk Specific Gravity	1.91	
Apparent Specific Gravity	2.11	
Percentage Absorption	4.81	
United States Department of Agriculture Classification	Sandy Loam	
Unified Classification	Sandy Organic Silt	
AASHTO Classification	A-4 (0)	

TABLE 2. Properties of Cleveland Aggregate

Aggregate Properties	Measured Values	Required Values
Sand Equivalent Value	42	40 min
Fractured Faces (FF)	100 with 2 FF	75 with 2 FF
Fine Aggregate Angularity	45	40 minimum
Los Angeles Abrasion	27	40 maximum
Percent Passing No. 200 Sieve	0.5	
Percent Passing No. 40 Sieve	3	
Bulk Specific Gravity	2.55	
Apparent Specific Gravity	2.70	
Percentage Absorption	2.2	
Percent Moisture Content	3.6	

TABLE 3. Resistance Value for Design (60/40) from Stabilometer Data

% Emulsion	4.5	4.5	4.5	4.5	4.5	4.5
% Water	7	7	7	7	7	7
% Cement	2	2	2	2	2	2
Curing	Early	Early	Early	Fully	Fully	Fully
Specimen Height, mm	66.8	69.6	69.1	60.7	64.0	71.1
Vertical Load, kg						
227	5	5.5	6	7	6.5	7
454	5.5	6.5	8	10	9.5	9
908	11	9	12	20	19	20
Final Displacement	2.94	2.71	2.86	2.85	2.95	3.31
Resistance	93	95	93	86	87	86
Corrected R-value	94	95	94	86	87	86
Average		94			86	

TABLE 4. Bench Scale Test Results of Different Designed Mixes

Design No.		50/50			60/40			70/30			80/20		
Gradation		Above Maximum Density line			Above Maximum Density line			Above Maximum Density line			Above Maximum Density line		
% Soil		50			60			70			80		
% Aggregate		50			40			30			20		
% Water		7			7			7			7		
% Coating		65	80	90	60	70	80	55	65	75	60	70	80
% Emulsion		4.0	4.5	5.0	4.0	4.5	5.0	4.0	4.5	5.0	4.5	5.0	5.5
Resistance	0% Cement	90	87	85	-	-	-	-	-	-	-	85	80
	1% Cement	93	90	88	-	-	-	-	91	92	-	90	82
	2% Cement	96 (89)	93	90	-	94 (86)	92 (90)	-	92 (84)	-	92 (78)	90 (83)	86 (80)
Tensile Strength (kPa)	0% Cement	206	159	-	-	-	-	-	-	-	-	140	190
	1% Cement	255	243	-	-	-	-	-	179	241	125	158	205
	2% Cement	310 (293)	255	-	-	255 (186)	337 (269)	-	220 (192)	-	130 (118)	186 (172)	215 (205)

Note: Values in parenthesis (-) are for fully cured samples.

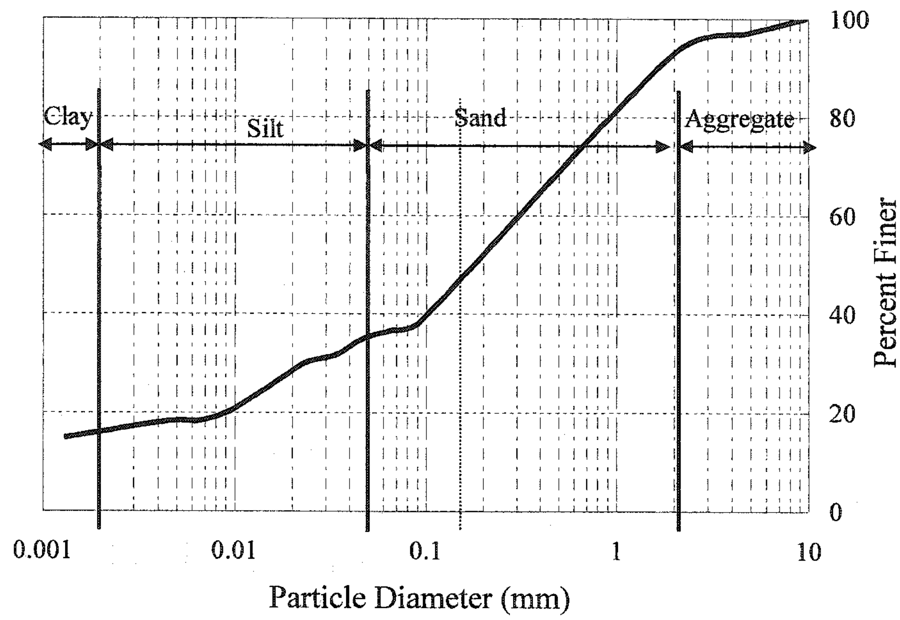

FIG. 1. Grain Size Distribution of Hydrocarbon Affected Soil

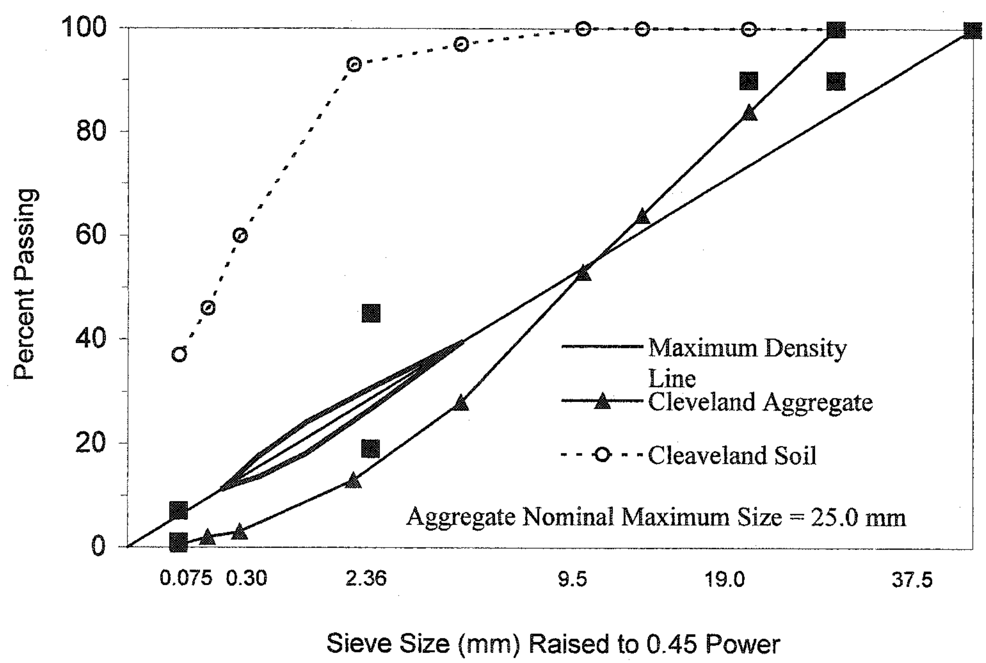

FIG. 2. Gradation of Hydrocarbon Affected Soil and Cleveland Aggregate

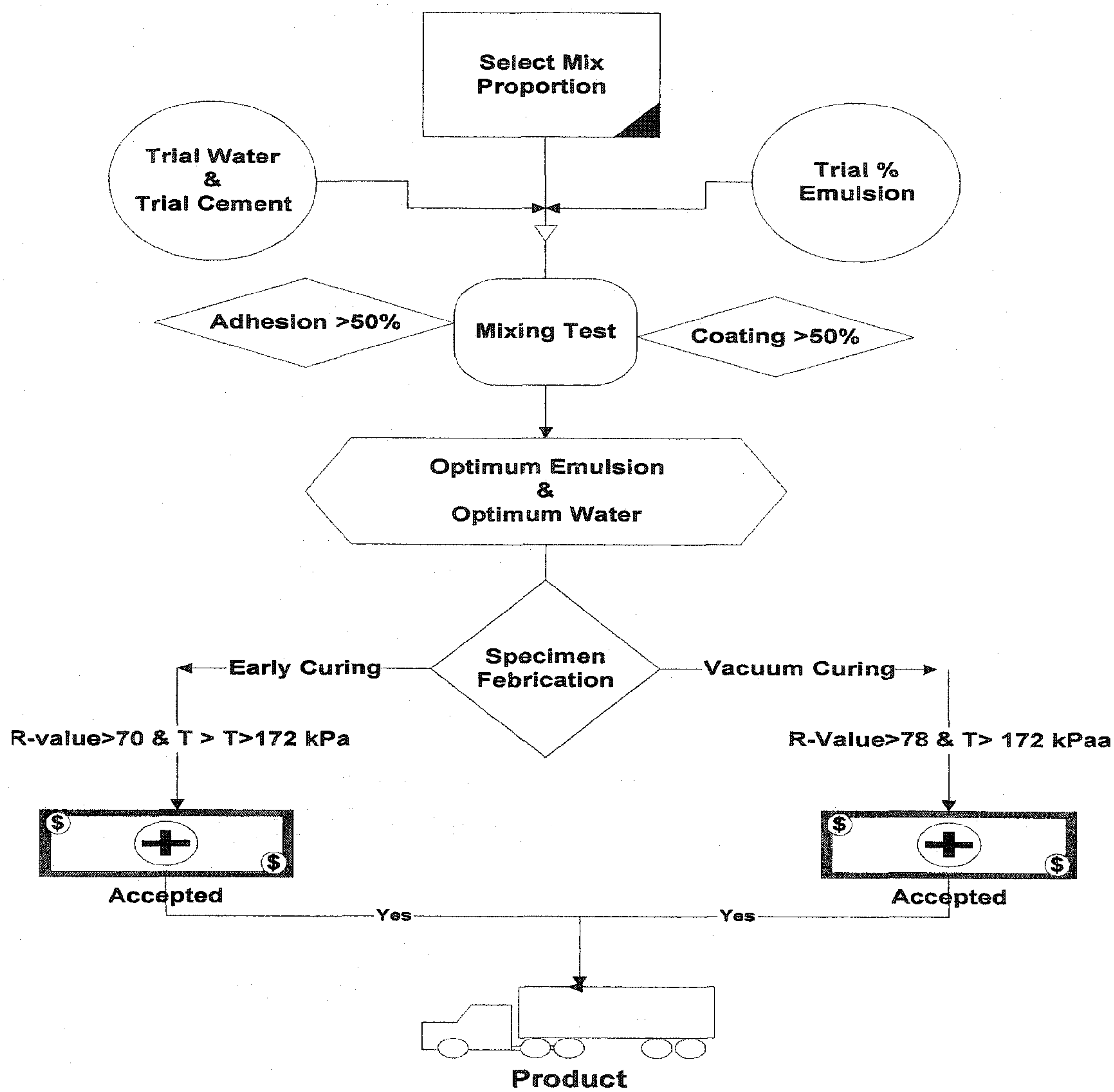

FIG. 3. Mix Design Flow Chart

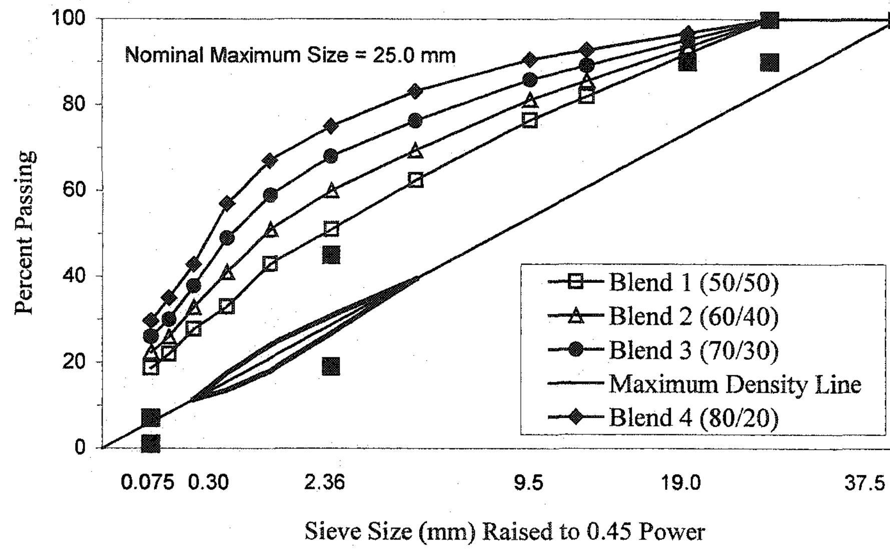

FIG. 4. Gradations of Trial Design Mixes on 0.45 Power Chart

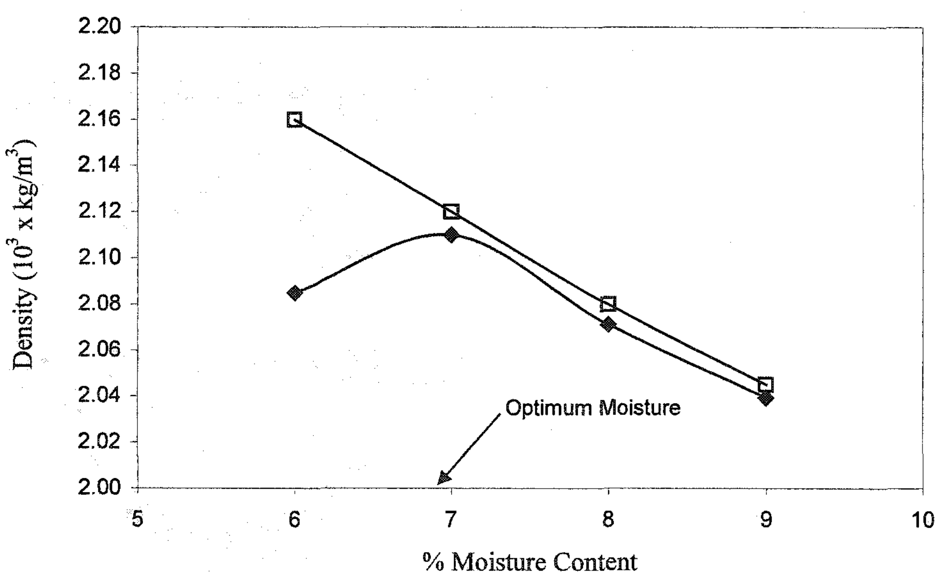

FIG. 5. Moisture-Density Relationship for Mix Design

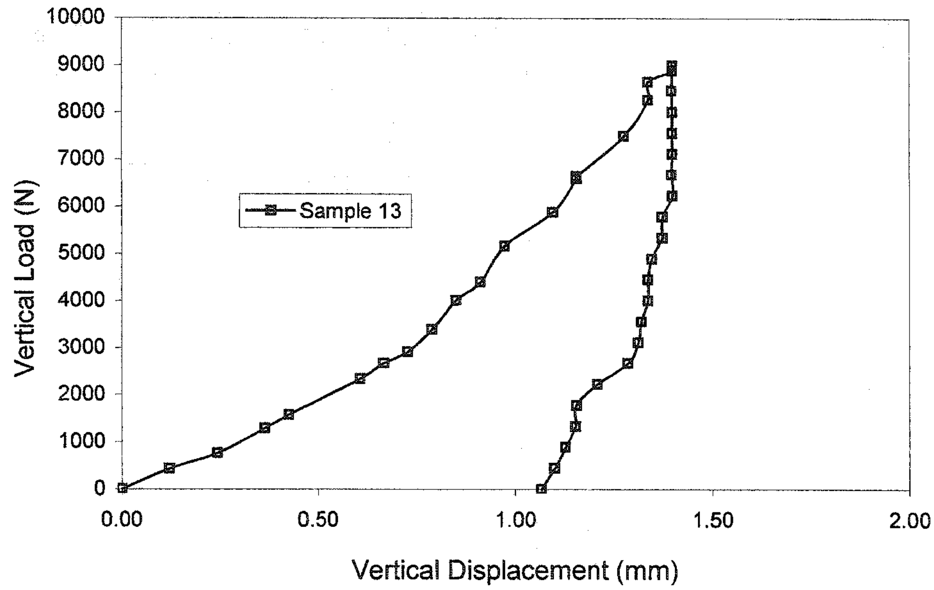

FIG. 6. Load-Displacement Diagram in Resistance Value Test

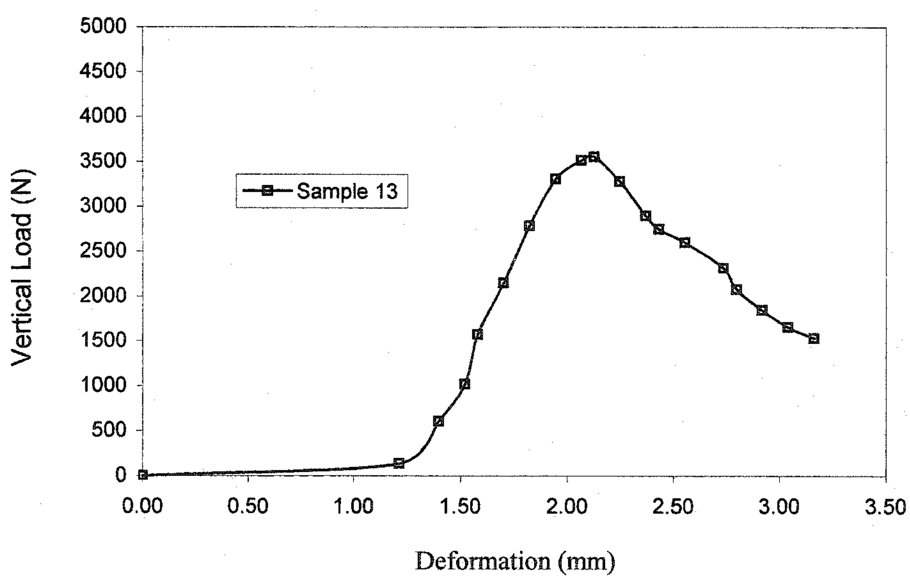

FIG. 7. Load-Deformation Diagram in Split Tensile Test

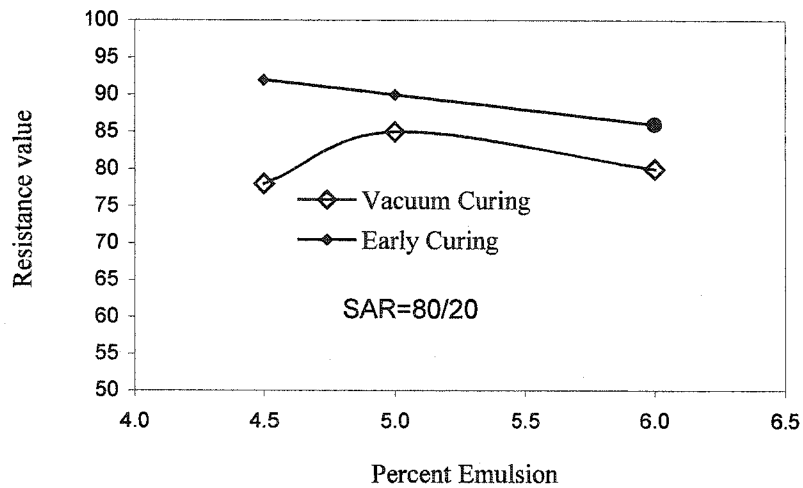

FIG. 8. Determination of Optimum Emulsion Content for SAR=80/20

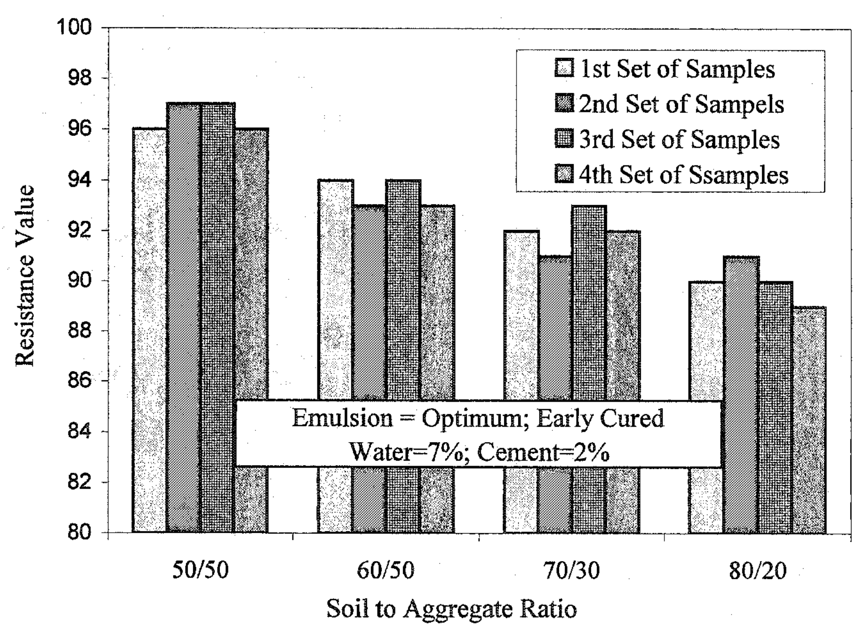

FIG. 9. Resistance Versus Soil Percentage

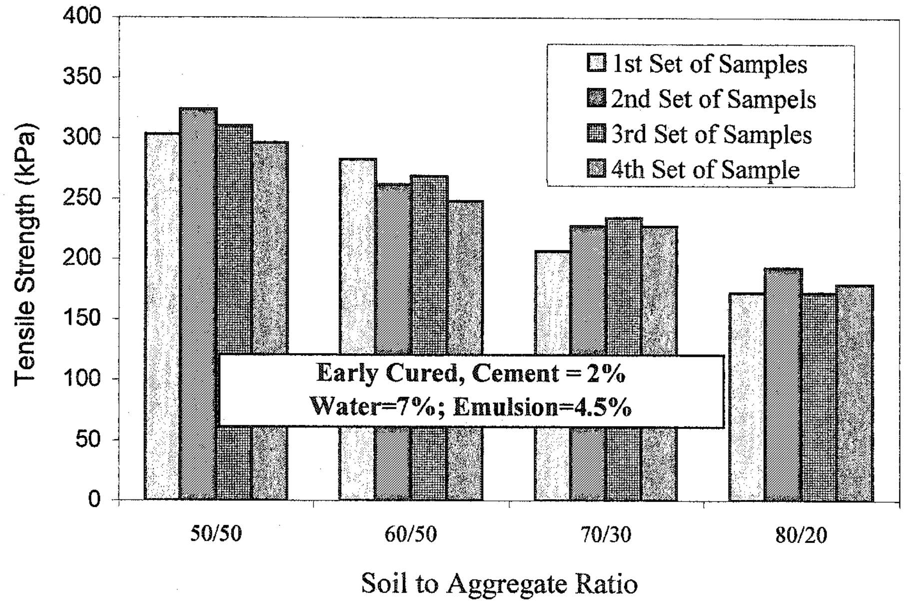

FIG. 10. Tensile Strength Versus Soil Percentage

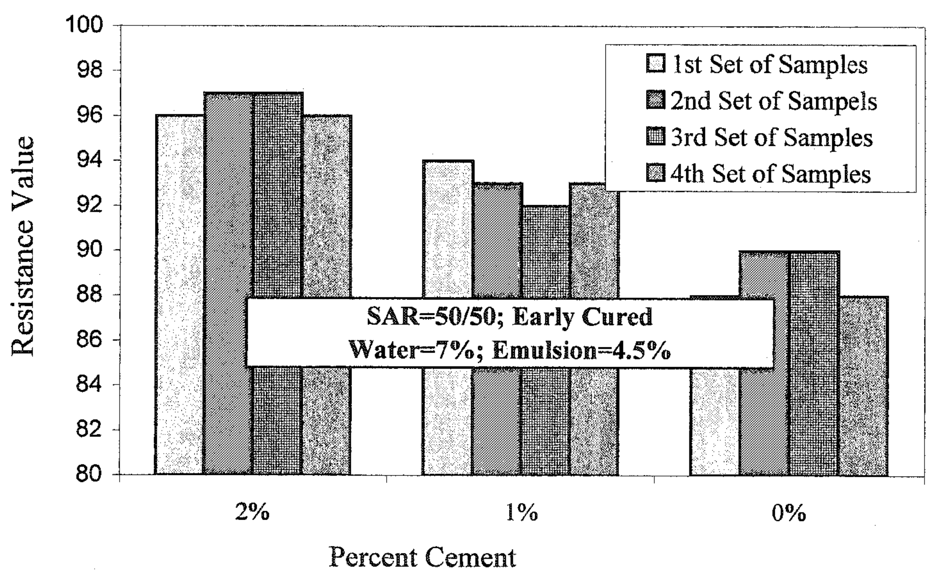

FIG. 11. Resistance Versus Cement Percentage

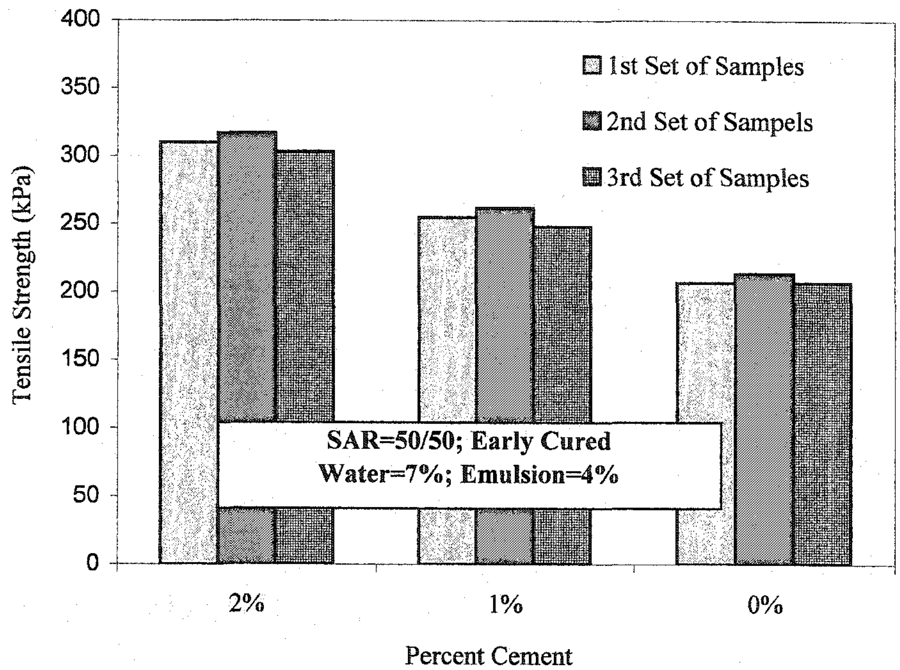

FIG. 12. Tensile Strength Versus Cement Percentage

APPENDIX III

'Evaluating the CoreLok^{TM} Measurement of Bulk Specific Gravity for Hot Mix Asphalt Samples' by Tarefder, R. A., Zaman, M. M., and Hobson, K., ASTM Journal of Testing and Evaluation, Vol. 30, No. 4, pp. 274-282, July 2002.

EVALUATING THE CORELOK^{TM} MEASUREMENT OF BULK SPECIFIC GRAVITY FOR HOT MIX ASPHALT SAMPLES

Abstract: For hot mix asphalt samples with high air voids and high absorption capacity, the saturated surface dry (SSD) method of bulk specific gravity determination yields higher values than predicted. Recently, the CoreLok^{TM} device has been found to be a simple, rapid, and nondestructive method for determining bulk specific gravity. This study evaluated CoreLok bulk specific gravity measurements by comparing its results for laboratory prepared samples and roadway cores from two types of mixture to those determined by the volumetric and the SSD methods. A linear regression analysis of the results indicated that the SSD and the CoreLok methods had significant differences from the volumetric method for determination of bulk specific gravity. It was found that for most cases, the differences in bulk specific gravity measurements were due to the combined effect of percent air voids and percent absorption. For samples with low air voids, the CoreLok and the SSD methods showed similar but not identical results. For samples with high air voids, the CoreLok method resulted in bulk specific gravity values more representative of the actual values. This study also defined a CoreLok infiltration coefficient (CIC) to evaluate the water infiltration characteristic of dense graded samples. It was shown that fine graded dense mixes had higher CIC values than the coarse graded dense mix at air void levels around 8%. The study found that water infiltration characteristics of samples with regards to CIC depend on absorption, air void content, and number of air voids.

Key Words: CoreLok^{TM}, saturated surface dry method (SSD), CoreLok infiltration coefficient (CIC), bulk specific gravity, coarse graded, fine graded, air voids, regression

Background

The bulk specific gravity of a hot mix asphalt sample is useful in calculating the air voids in it. Bulk specific gravity is the ratio of the density of a solid to the density of a reference liquid at a stated temperature. Water is usually used as a reference liquid in determining the bulk specific gravity of hot mix asphalt (HMA) sample. In CGS (centimeter, gram, second units for measuring physical dimensions) system of units, if the density of water is taken as 1.0 g/cm^3 at 25°C (77°F), the bulk specific gravity is numerically equal to its density. Bulk specific gravity is the ratio of the mass of a sample to the mass of an equal volume of water at 25°C (77°F). Mass is usually determined by a scale and has been considered accurate. The volume calculation, however, has remained a difficult task due to air voids present in the asphalt sample as well as due to its absorption characteristics. Different methods have been used (namely, volumetric method, saturated surface dry method, paraffin method, CoreLok™ method) for volume approximation [1, 2, 3]. The volume approximation of a specimen differs from one method to another, and hence there are differences in the values of bulk specific gravities. These differences can play a significant role in the design, construction, and quality control of hot mix asphalt concrete because the air voids directly depend on the measurement of bulk specific gravity. Air voids determination is an important factor that affects performance of the hot mix asphalt pavement throughout its life. It is a function of mix design and compaction of the mixture. The performance of HMA concrete in all types of laboratory testing depends highly on the air void content of a specimen [4]. Air voids of a HMA mix is related directly to its bulk specific gravity. Increased compaction, asphalt content, filler content, or any other procedure that reduces air voids can be used to achieve the required bulk specific gravity of a HMA mix. A properly designed mixture should produce a mix having adequate shear strength, while modifying it to reduce air voids (less than 3%) will produce a mixture with low shear strength having a tendency for high permanent deformation. High air voids allow moisture to penetrate a HMA pavement and can cause stripping or surface raveling. High air voids can also lead to differential rutting due to increased densification of the HMA layer under traffic loading. Low air voids in a compacted mix will not allow adequate thermal expansion of the asphalt and can cause flushing and rutting. Therefore, an efficient and accurate measurement of bulk specific gravity is an important task in characterizing HMA mixes. To this end, this study was pursued to investigate the difference in bulk specific gravities measured by three different methods, namely, the volumetric method, the saturated surface dry (SSD) method, and the CoreLok sealing method. The objective was to evaluate the CoreLok measurement of bulk specific gravity by comparing it with SSD and volumetric measurements of bulk specific gravities.

Description of Field Cores

This study investigated a total of 170 pavement cores from different locations in the state of Oklahoma. Some of these cores were from pavement surface and some of them were from pavement base. The base cores were Type A mix and Type A-recycled whereas the surface cores were Type B mix [5]. Both mix Type B and mix Type A are dense and deviate from the maximum density line (Fig. 1). Type B is a finer mix passing above the maximum density line in a 0.45 power gradation plot. Type A is a coarser mix passing below the maximum density line (Fig. 1). Type A mix has nominal maximum size (NMS) of 19 mm (3/4 in.) and Type B mix has NMS of 12.5 mm (1/2 in.). Typically, Type A-recycled mix typically contains 25% of recycled aggregate. Mix

Type A and Type B conform to the gradation requirements in Table 1. Type A or Type A-recycled mix cores had a thickness in the range of 75 mm (3 in.) to 150 mm (6 in.). Typically, Type B mix cores had thicknesses of 35 mm to 58 mm. All of these pavements were designed for a traffic level of 0.3 to 10 million equivalent single axle loads (ESALs). All the cores were cylindrical in shape, of diameter in the range of 149 mm to 150 mm.

Description of Laboratory Samples

Materials of 37 mm (1.5 in.) rocks, 19.0 mm (0.75 in.) chips, screenings, and crushed gravels were used to fabricate laboratory samples of asphalt concrete of Type A. The mix was designed for an average daily traffic of more than 3 to10 million ESALs. Performance grade (PG) asphalt cement of type PG 64-22 was used as the binder. Cylindrical samples of 150 mm diameter were prepared using a Superpave gyratory compactor (SGC). A total of 22 samples was prepared for investigation.

Experimental Methodology

At the first step, the study measured the bulk specific gravity by calculating the volume using the measurements of height and diameter of a cylindrical specimen. Height and diameter of roadway cores were determined as in ASTM D3549, "Standard Test Method for Thickness or Height of Compacted Bituminous Paving Mixture Specimens." The thickness defined in ASTM D 3549 was referenced as the diameter for diameter computation. In the case of laboratory prepared samples, mold diameter and specimen height data from the Superpave gyratory compactor (SGC) were used for the volume calculation as well as the bulk specific gravity calculation. The volumetric bulk specific gravity of an asphalt sample is calculated using the following formula,

$$G_{mb}\,(volumetric) = \frac{A}{(\frac{\pi . d^2}{4}).h.\rho_w} \tag{1}$$

where

G_{mb} = specimen bulk specific gravity at 25 °C (77 °F)

A = mass of dry specimen in air, g

d = diameter of specimen, cm

h = height of specimen, cm

ρ_w = density of water at 25°C (77°F), g/cm^3

The volumetric method assumes a perfectly smooth surface although the actual sample surface has irregularities. Therefore, this method underestimates the bulk specific gravity. However, the errors associated with the measurements of height and diameters are typically ignored [3]. The volumetric bulk specific gravity was used in calculating the theoretical air voids following the test procedure ASTM D 3203, "Standard Test Method for Percent Air Voids in Compacted Dense and Open Bituminous Paving Mixtures."

At the second step, the bulk specific gravity of the sample was determined in accordance with AASHTO T 166, "Bulk Specific Gravity of Compacted Bituminous Mixtures Using Saturated Surface-Dry Specimens." This method approximates the volume of a compacted asphalt specimen as the volume of water displaced when submerged under water. Volume of sample is calculated by using the sample's SSD weight and the weight of the sample under water. The SSD bulk specific gravity of a sample is calculated using the following formula,

$$G_{mb}(SSD) = \frac{A}{(B-C)} \qquad (2)$$

where

B = mass of saturated surface dry specimen, g

C = mass of specimen in water, g

The reliability of the water displacement method decreases with increasing depth of the surface irregularities and the presence of interconnected voids that are open to the surface of the solid [6]. Samples with high air voids can absorb readily water during submersion and drain it out quickly when removed from the tank. The lack of control over the penetration and the drainage of water in and out of the asphalt samples create a fundamental problem with the SSD method. It is difficult to consistently define the SSD condition of samples [7]. A possible solution to correct the SSD method for samples with high air voids (i.e. samples containing interconnected air voids or containing more than 10% theoretical air void and/or absorbing more than 2% of water by volume is to seal the outer surface of the specimen during submersion [8]. However, the current sealing method, namely, paraffin or parafilm, ASTM D 1188 is optimized for 100 mm (4 in.) diameter samples[2]. The method is very impractical to use effectively for 150 mm (6 inch) samples. There exists large measurement variability in the paraffin or parafilm method [7]. Besides, the method requires complete removal of paraffin wax after the completion of test, which is a difficult and time-consuming process [4].

Therefore, the present study utilized the CoreLok sealing procedure as the third step for measuring bulk specific gravity of 150 mm (6 in.) diameter roadway cores and laboratory samples. The method employed the same principle as the paraffin method except it used polymer bags with vacuum technology instead of wax for sealing [2]. The CoreLok method is highly repeatable [7]. In the CoreLok procedure, the laboratory samples and field cores were sealed completely with polymer bags, which were then evacuated. The sealed samples were weighed under water. The seals were then opened under water to allow infiltration of water and the weight measured under water. The CoreLok bulk specific gravity is calculated from the following formula,

$$G_{mb}\,(CoreLok^{TM}) = \frac{A}{(B_1 - C_1) - \frac{M_g}{G_g}} \tag{3}$$

where

B_1 = mass of sealed specimen in air, g

C_1 = mass of sealed specimen in water, g

M_g = mass of sealing bag, g

G_g = apparent specific gravity of the bag material at 25 °C (77 °F)

Air Voids Calculation

The air voids content was calculated according to the ASTM D 3203 using bulk specific gravity and theoretical maximum specific gravity. The theoretical maximum specific gravity of the asphalt mixtures was determined using the Rice method as in ASTM D 2041, "Standard Test Method for Theoretical Maximum Specific Gravity and Density of Bituminous Paving Mixtures."

Analysis of Laboratory Sample

The bulk specific gravity for laboratory samples obtained from the SSD method was compared with the CoreLok measurements (Fig. 2a). These samples had less than 10% theoretical air voids as well as less than 2% water absorption capacity. The average difference in bulk specific gravity between these two methods was 0.035 with a standard deviation of 0.023. A regression line was plotted for correlating bulk specific gravity from the SSD measurements with those from the CoreLok measurements. The R^2 value was found to be 0.97, which is a goodness-of-fit of the CoreLok data with the SSD data. That is, 97% of the SSD results can be explained or accounted for by the CoreLok measurements. The bulk specific gravities measured by the SSD and the CoreLok methods for laboratory samples with theoretical air voids less than 10% were very close but not identical. For the open graded samples (samples with high air voids), the SSD measurements, however, significantly underestimated the air voids when compared to the air voids measured by the CoreLok procedure. The test results for a few samples with more than 10% theoretical air voids are also plotted in Fig. 2b. The average overestimation of bulk specific gravity by SSD over CoreLok was found to be 0.068, with a standard deviation of 0.034 for the limited number of samples studied. The R^2 value of 0.517 reflects a relatively poor correlation between the SSD and the CoreLok methods of measurement for samples with high air voids. Fig. 3 shows a comparison of laboratory samples' bulk specific gravity by all three methods of measurement as mentioned before. Volumetric method underestimated bulk specific gravity compared to that of other two methods. From Fig. 3 it can be seen that the CoreLok measurement correlated better with the volumetric measurements. It is also evident that the difference between the SSD and the CoreLok bulk specific gravity increases with the increased theoretical air voids.

Analysis Field Core

Fig. 4 shows that the volumetric bulk specific gravity method underestimated the bulk specific gravity of specimens compared to bulk specific gravity measured by the SSD and the CoreLok methods. This is because the cores were assumed to be perfect cylinders in the volumetric method. A regression line passing through the origin was fitted for all methods and all sample data. The sample coefficient of determination R^2 for SSD was less than the R^2 value for CoreLok with respect to the volumetric method. The value of $R^2 = 0.958$ means that about 95.8% of the SSD data can be accounted for by the CoreLok method. The information also supports the use of CoreLok for dense graded mixes of low or high air voids. An attempt was made in this study to find a correlation between the bulk specific gravity by SSD and CoreLok based on two criteria. In the first criterion, when a perfect cylinder was assumed, the specimen with 10% or more theoretical air voids was considered as "open or interconnected" air voids. Fig. 5 was prepared to analyze this criterion. It was seen that CoreLok could be used with a 95.5% confidence level for roadway cores with less than 10% theoretical air voids. Fig. 5 shows that CoreLok explained 92.8% of the SSD data for cores having 10% or more theoretical air voids. The other criterion was invoked when the absorption exceeded 2%. Fig. 6 shows that CoreLok explained 96% of the SSD data when absorption was less than 2%. The confidence level drops to 93% when absorption exceeds 2%. Another investigation was sought to correlate the SSD measurement with the CoreLok measurement considering the combined effect of percentage absorption with percent theoretical air voids; results from the linear regression analyses are presented in Table 2. It can be seen that the worst correlation occurs when samples exceed the threshold values of both the percent absorption (threshold value = 2.0) and the percent theoretical air voids (threshold value = 10.0).

From Fig. 7 it is seen that Type B mix showed slightly smaller difference between the bulk specific gravity of the SSD and the CoreLok methods compared to that of Type A mix. From the analysis of data it was found that 11 samples out of 77 samples of Type A mix showed higher specific gravity by the CoreLok method compared to the SSD method; whereas 2 samples out of 93 showed higher bulk specific gravity by the CoreLok method compared to the SSD method.

CoreLok Infiltration Coefficient

A water-permeable HMA pavement suffers from poor durability. Several states have expressed concern that the Superpave mixes are more permeable than the conventional Hveem or Marshall mixes [9]. A dense graded mix with air voids above approximately 8% allows water to penetrate into the pavement, which increases potential for water damage, oxidation, raveling, and cracking [10]. A measure of moisture-induced damage potential of an HMA mix is still a debatable topic. Many states, including Oklahoma, have already applied the permeability of a mixture as a criterion for mix design and quality assurance criteria [11]. This study introduces a new property, the CoreLok infiltration coefficient (CIC) to address the damage potentials of HMA mixes as well as the durability. CIC is defined as ratio of the mass calculated from the difference between the CoreLok sealed weight and the opened weight under water to the mass of equal volume of water. Typically, air bubbles trapped within a sample occupy the void space. Water cannot flow through these air bubbles. With the application of vacuum by CoreLok, surface and interconnected air bubbles are removed. The sample seal is then opened under water. Water enters into these permeable void spaces due to the pressure gradient between the samples and the surrounding water. The opened mass of the sample under water is measured and CIC is calculated from the following formula,

$$CIC = \frac{D_1 - C_1}{(B_1 - C_1) - \frac{M_g}{G_g}} \tag{4}$$

where

D_1 = mass of sealed sample after opening under water, g

The CIC is a quantitative measurement that provides an indication of how a HMA specimen gives access to air voids through which water can pass. More specifically, CIC is believed to give an indication of the long-term permeability of a HMA mix. CIC can be very useful in determining performance of HMA mixes in the field. This study correlated CIC with bulk specific gravity, mix type, and percentage water absorption.

Fig. 8 shows that CIC did not have a good correlation with bulk specific gravity measured by the SSD and CoreLok methods. However, CIC increases as the bulk specific gravity decreases. Specimen compacted to low bulk specific gravity tends to have more and larger air voids, which increased CIC. Table 3 shows that the CIC is higher at higher air void contents. This is because at higher air void content, the chances of interconnected voids are increased.

Table 4 shows CIC dependency on mixture type as well as percent air voids. Type A-recycled mix showed the lowest CIC value. The use of recycled asphalt pavement leads to presence of excessive fines in the mix, which actually reduces the number of interconnected air voids. The CIC value increased as the percent air void increased for all types of mixes. For almost the same amount of air voids, Type B mix showed a larger CIC value than Type A-recycled mix. Overall, Type A had less CIC value compared to the CIC value of Type B mix. The possible explanation could be that for the same amount of air voids content, Type B mix has higher number of air voids than the number of air voids in Type A mix which increased the possibility of interconnected air void content. Therefore, Type A mix should perform better than Type B mix under water-induced damage. This observation suggests that Type B mixes tend to have more permeability problem at higher bulk specific gravity when compared to Type A mixes at the same bulk specific gravity level. Fig. 9 shows that percent absorption and air voids affect the CIC values to some degree. Fig. 9(a) shows that the CIC value increases as the sample becomes absorptive. Figure 9(b) shows that the CIC value increases with air voids at a higher rate, as compared to absorption.

Conclusions

The CoreLok^{TM} method showed a better estimation of bulk specific gravity compared to the SSD method, considering the volumetric method as a reference. Overall, the CoreLok bulk specific gravity showed a good correlation with the SSD bulk specific gravity for samples less than 10% theoretical air voids with less than 2% absorption capacity. The CoreLok bulk specific gravity of laboratory-prepared samples having less than 10% theoretical air voids and less than 2% absorption capacity showed better correlations with the SSD bulk specific gravity compared to the roadway cores. For samples with equal to or more than 10% theoretical air voids as well as equal to or more than 2% absorption capacity, the CoreLok measurements were more representative compared to the SSD measurements, assuming the volumetric measurement as base. Bridging of surface irregularities can always affect the sealing of a specimen by an impermeable material. However, the bulk specific gravity measurement by CoreLok based on approximating volumes of a solid with irregularly shaped surfaces is reasonably reliable. Absorption or theoretical air voids alone is not responsible for the difference in the SSD and the CoreLok measurements, rather, the difference is affected by their combined effect. Bulk specific gravity measurements by the CoreLok and the SSD methods are not affected significantly by mix type. Type B mix at certain bulk specific gravity showed a higher CIC value compared to Type A mix at the same bulk specific gravity level. Type B mix was, therefore, be considered to have the greater moisture damage potential mix when compared to the damage potential of Type A mix. The fact that CIC relates to air voids and absorption indicates its potential for permeability characterization. The CIC determined from the CoreLok measurements can be a property to identify moisture induced damage.

Acknowledgment

The authors would like to express their deep appreciation to Oklahoma Department of Transportation (ODOT) for funding this project. The authors would also like to express their appreciation and thanks to Ali Regimand, president, InstroTek Inc., for his assistance. The authors are thankful to Reynolds Toney and Eric Roberts from the ODOT for their technical assistance, support, and information.

Reference

[1] AASHTO T 166, "Bulk Specific Gravity of Compacted Bituminous Mixtures Using Saturated Surface-Dry Specimens." *Standard Specifications for Transportation Materials*, AASHTO, Part II, Washington, D.C., 1999.

[2] ASTM D 1188, "Bulk Specific Gravity of Compacted Bituminous Mixtures Using Paraffin-Coated Specimens." *Annual Book of ASTM Standards: Road and Paving Materials; Vehicle-Pavement Systems,* Vol. 04.03, 1998.

[3] CoreLok Operator's Guide, Version 8, InstroTek, Inc., 3201 Wellington Court Suite 101, Raleigh, NC 27615, USA, 2001.

[4] Sousa, J.B. and Deacon, J.A., "Effect of Laboratory Compaction Method on the Permanent Deformation Characteristics of Asphalt-Aggregate Mixtures, presented at *Annual Meeting of Association of Asphalt Paving Technologists*, 1991.

[5] Oklahoma Highway Department (OHD), *Standard Specifications for Highway Construction*, Section 708, ODOT, 1999.

[6] URL: http://www.troxlerlabs.com/3660.htm, Troxler Electronic Laboratories, Inc., 3008 Cornwallis Road, Research Triangle Park, NC 27709, USA, 2001.

[7] URL: http://www.instrotek.com/CoreLok.htm, InstroTek, Inc., 3201 Wellington Court Suite 101, Raleigh, NC 27615, USA, 2001.

[8] Harvey, J., Sousa, J.B., Deacon, J.A., and Monismith, C.L., "Effects of Sample Preparation and Air-void Measurement on Asphalt Concrete Properties," *Transportation Research Record*, No. 1317, 1991, pp. 61-67.

[9] Roberts L.F., Kandhal, P.S., and Brown, E. R., *Hot Mix Asphalt Materials, Mixture Design, and Construction,* NAPA Education Foundation, Maryland, 2nd Edition, 1996.

[10] Cooley, L.A., *Permeability of Superpave Mixtures: Evaluation of Field Permeameters,* NCAT Report No. 99-1, February 1999.

[11] OHD L-44, "Method of Test for Measurement of Water Permeability of Compacted Paving Mixtures," *Standard Specifications for Highway Construction*, ODOT, 2001.

TABLE 1 – Roadway core samples gradation

Sieve size	Passing, %	
Mixture type	A	B
37.5 mm (1 1/2 in.)	100	...
25.0 mm (1 in.)	90 - 100	...
19.0 mm (3/4 in.)	...	100
12.5 mm (1/2 in.)	70 - 90	90 - 100
9.5 mm (3/8 in.)	...	70 - 90
4.75 mm (No. 4)	40 - 65	45 - 70
2 mm (No. 10)	25 - 45	25 - 50
425 μm (No. 40)	10 - 26	12 - 30
180 μm (No. 80)	6 - 18	7 - 20
75 μm (No. 200)	2.3 - 7.8	2.8 - 9
% Asphalt cement	3.8 - 6.5	4.7 - 7.5

TABLE 2 – R^2 values of CoreLok to SSD

Theoretical air voids, %	Water absorption, %	R^2 value
< 10	< 2	0.9579
< 10	≥ 2	0.9559
≥ 10	< 2	0.9510
≥ 10	≥ 2	0.9104

TABLE 3 – Air voids and CIC relation

Air voids by CoreLok, %	CIC, %	Standard deviation
<8	5.59	1.78
>8	7.90	1.93

TABLE 4 – Influence of mixture type on CIC

Mix type	CIC, %		Air voids, %		
	CIC value	Standard deviation	SSD	CoreLok	Volumetric
A	6.43	1.32	6.58	7.12	9.06
B	6.76	2.37	7.13	7.00	9.85
A-recycled	6.02	2.62	7.60	8.18	10.03

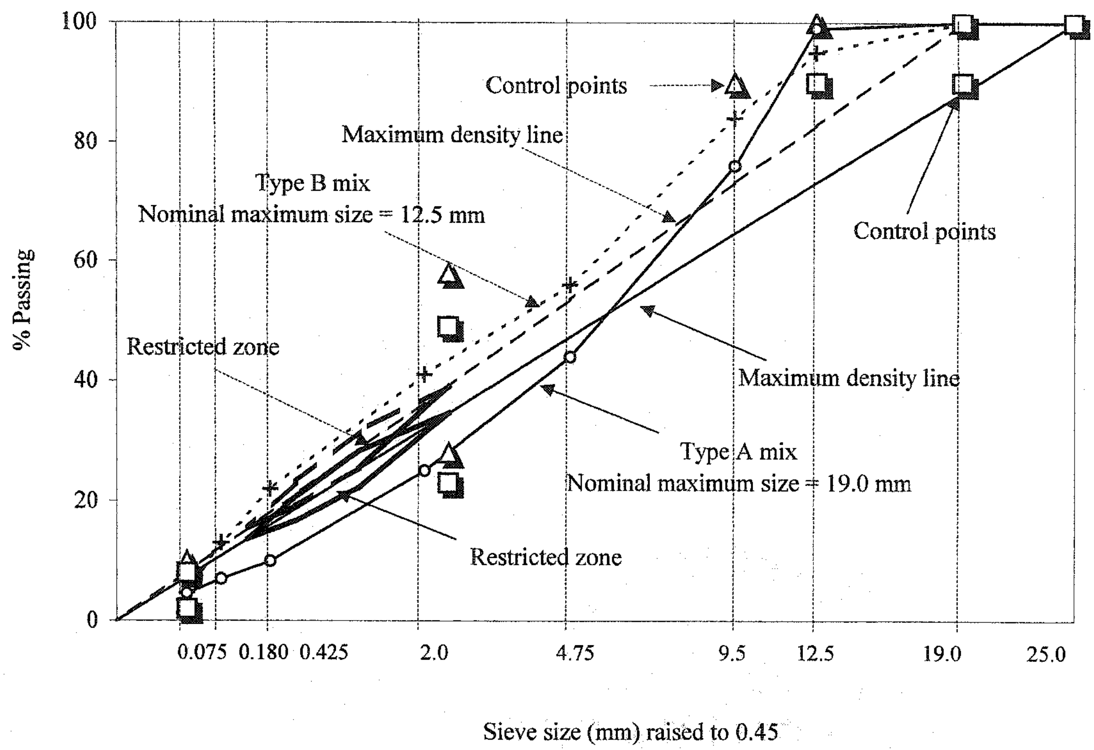

FIG. 1 – Gradation plot of roadway cores

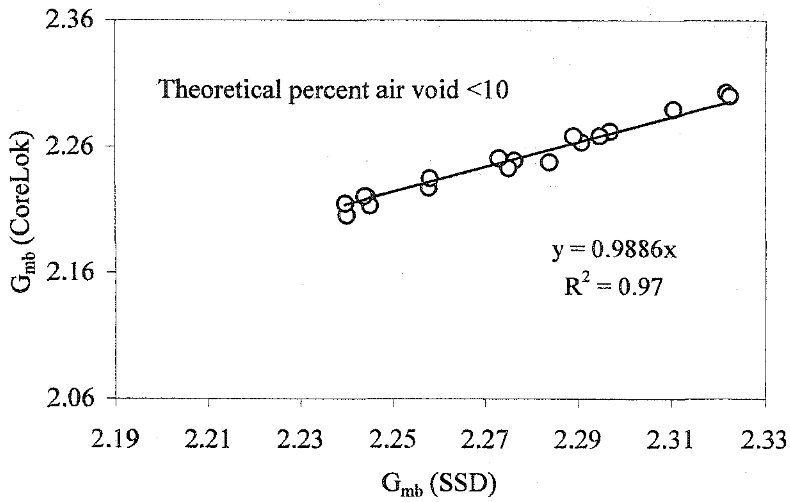

(a) Theoretical air voids < 10%

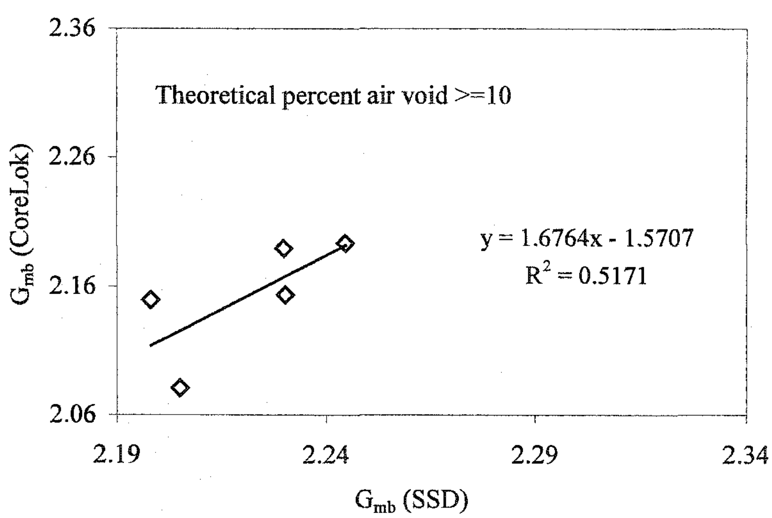

(b) Theoretical air voids ≥ 10%

FIG. 2 – CoreLok versus SSD bulk specific gravity (G_{mb}) of laboratory samples

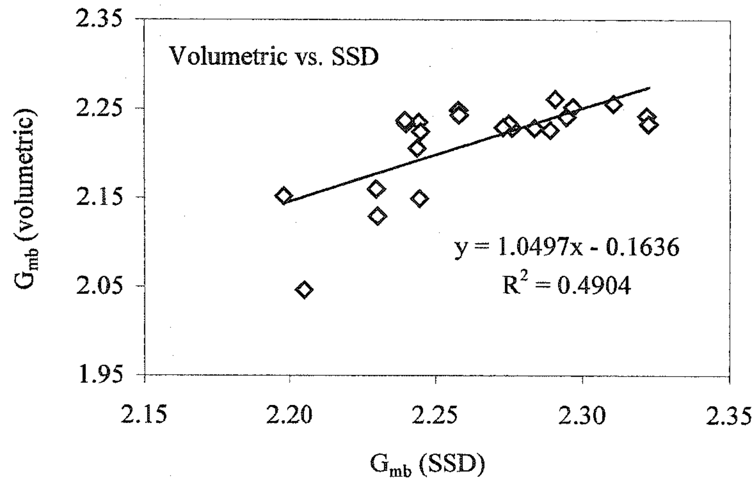

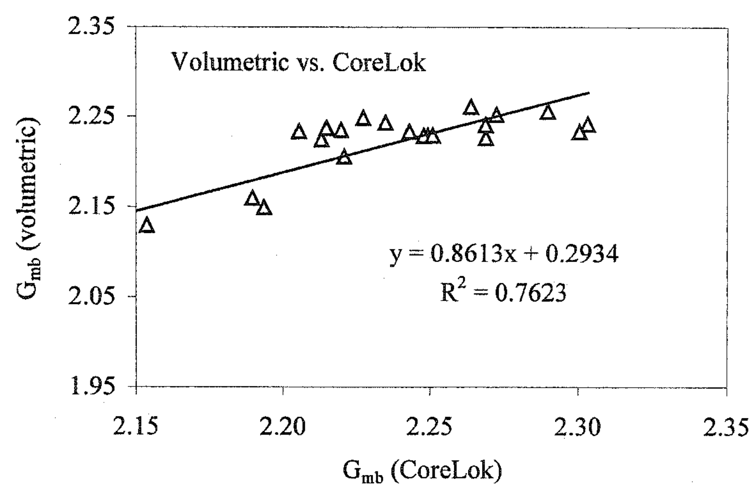

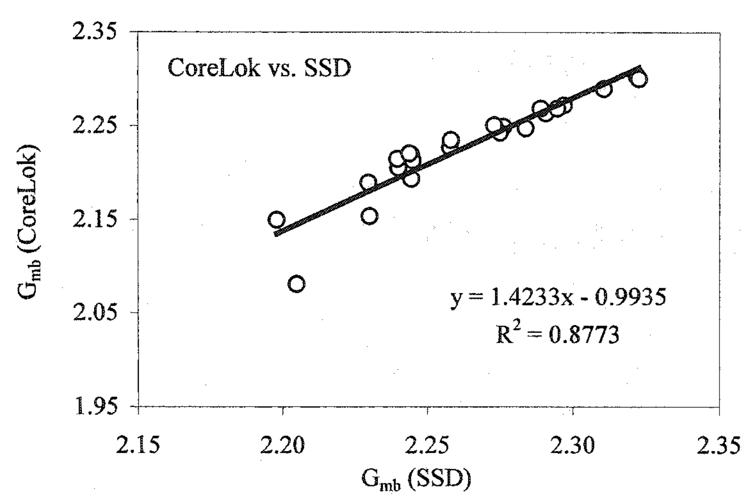

FIG. 3 – Comparison of bulk specific gravity (G_{mb}) for laboratory samples

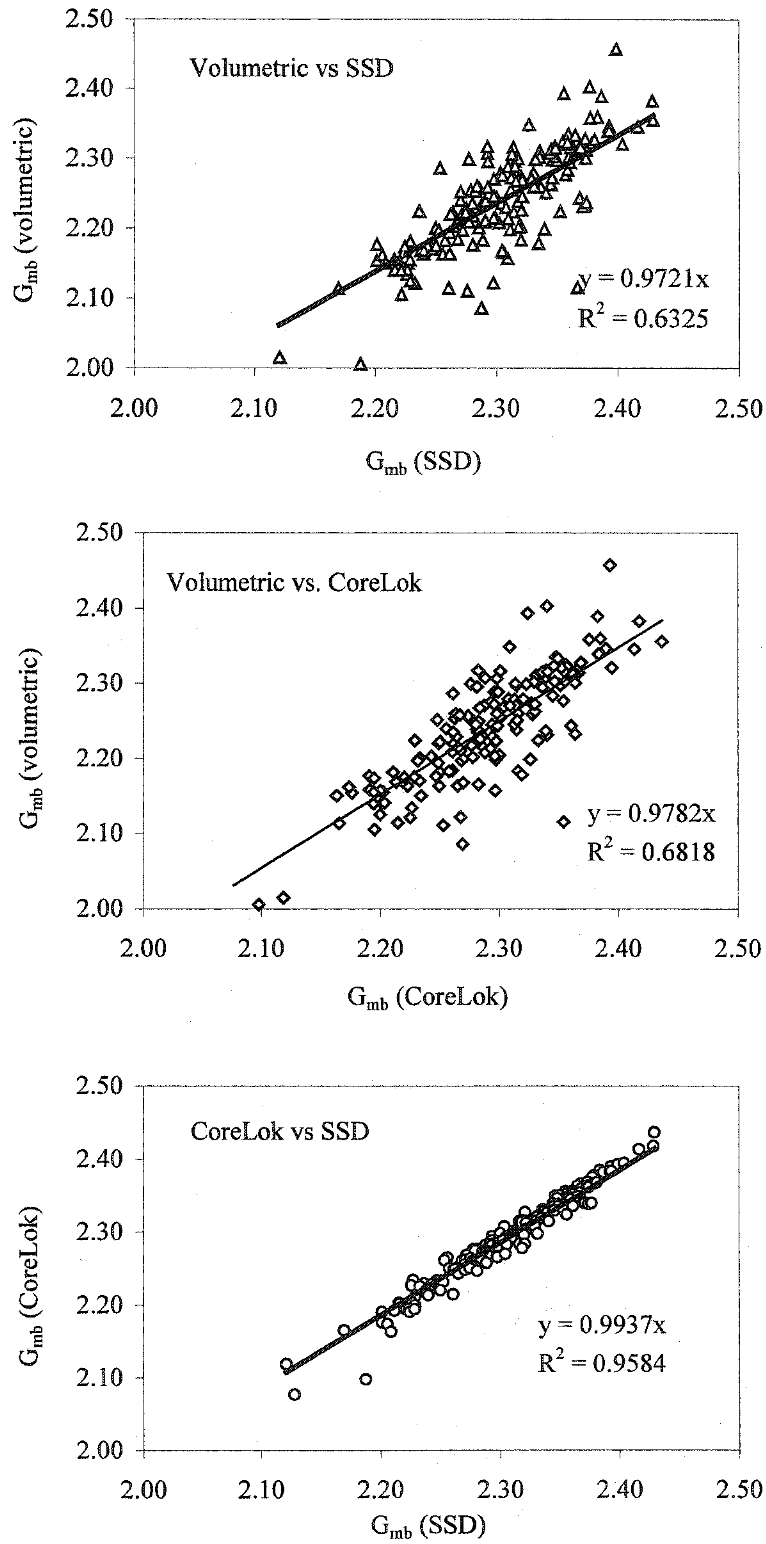

FIG. 4 – Comparison of bulk specific gravity (G_{mb}) for roadway cores

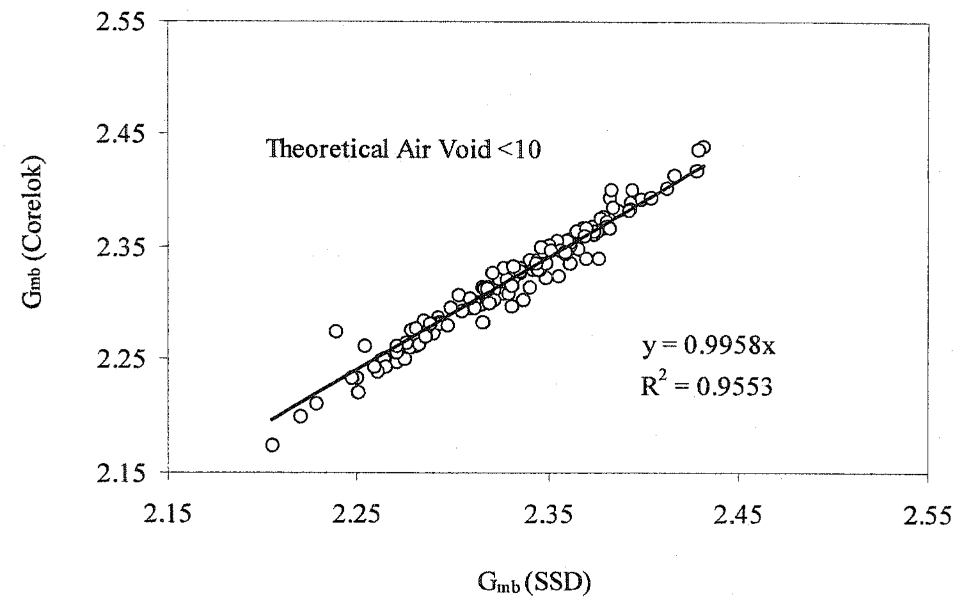

(a) Theoretical air voids < 10%

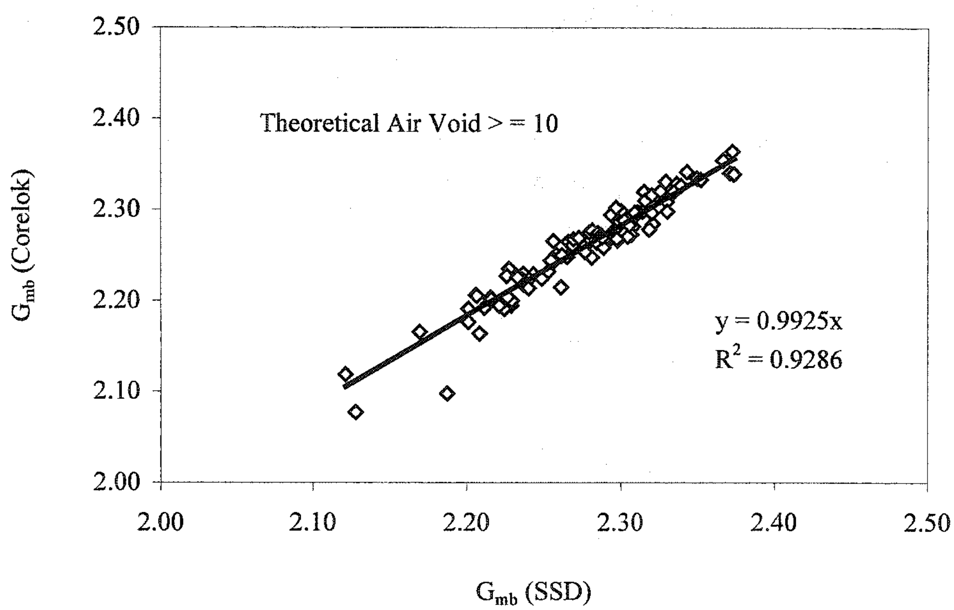

(b) Theoretical air voids ≥ 10%

FIG. 5 – Difference in bulk specific gravity (G_{mb}) of roadway cores for air voids

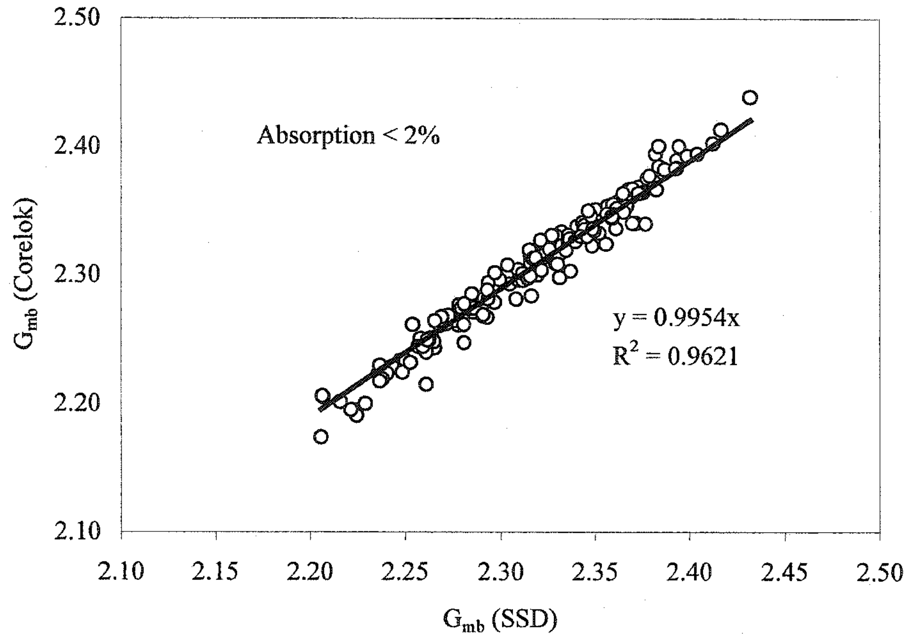

(a) Absorption < 2%

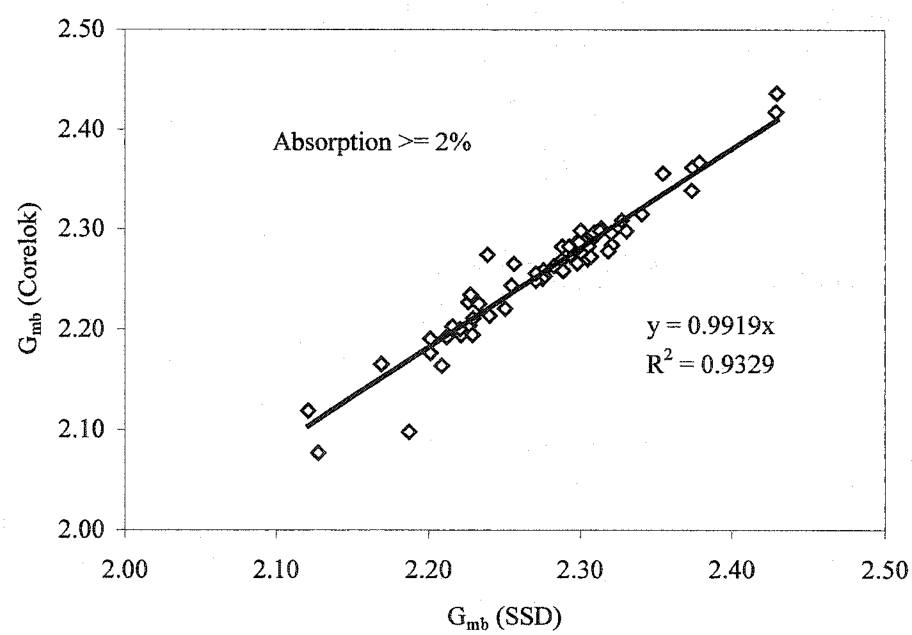

(b) Absorption ≥ 2%

FIG. 6 – Difference in Bulk specific gravity (G_{mb}) of roadway cores for absorption

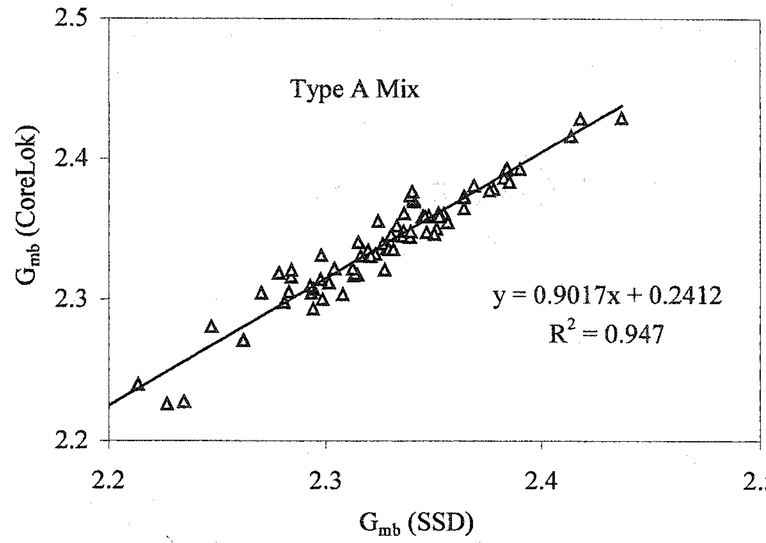

(a) Type A mix

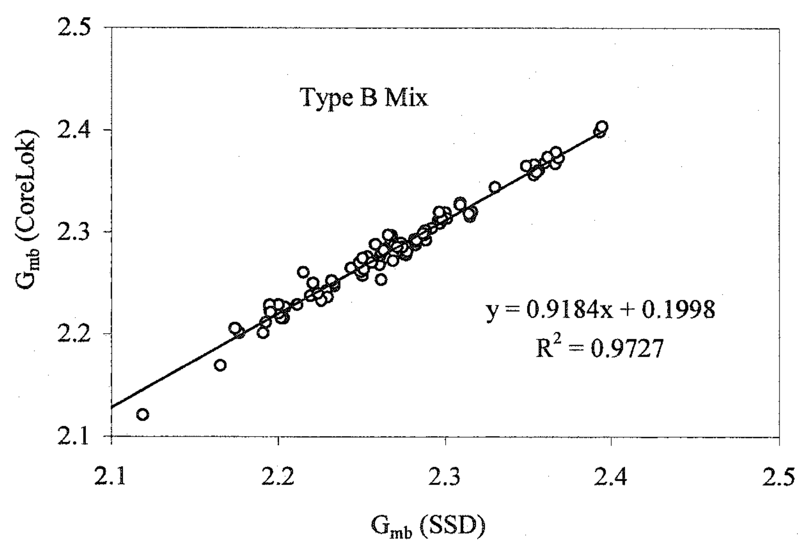

(b) Type B mix

FIG. 7 – Correlation of SSD with CoreLok bulk specific gravity (G_{mb}) by Mix Type

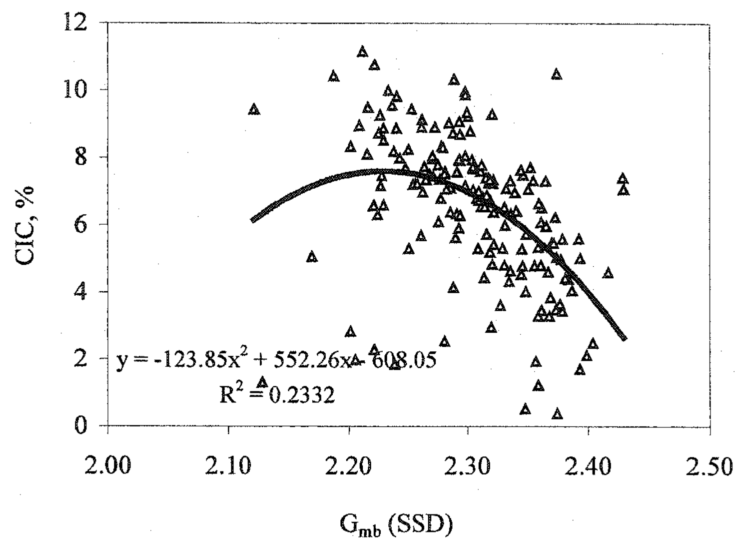

(a) CIC versus SSD

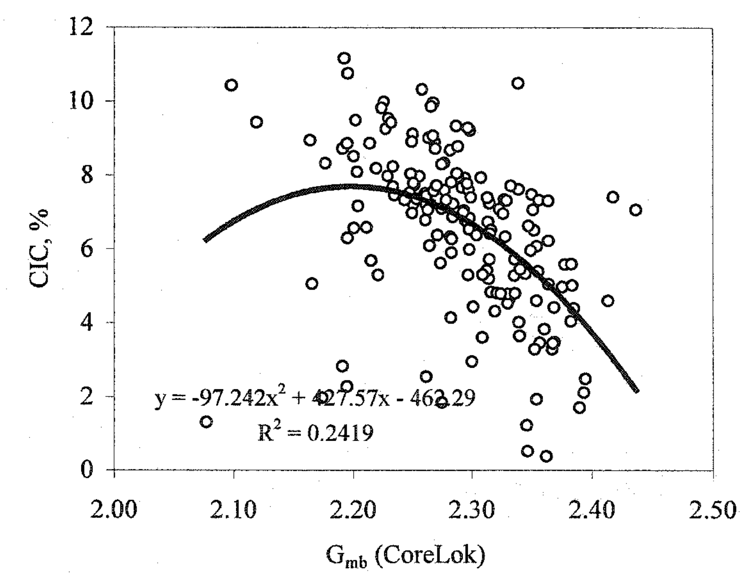

(b) CIC versus CoreLok

FIG. 8 – Variation of CIC with bulk specific gravity

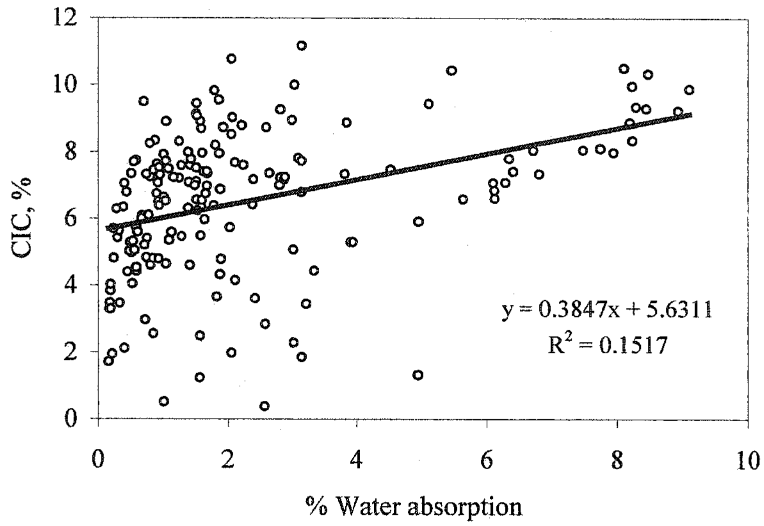

(a) CIC versus percent absorption

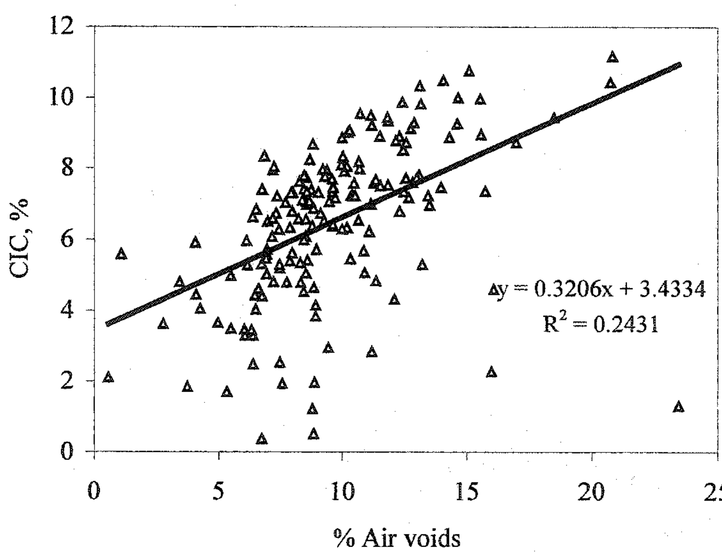

(b) CIC versus percent air voids

FIG. 9 – Variation of CIC with absorption and air voids

APPENDIX IV

Data Used for Neural Network Model Development.

Sample No.	Mix Design ID	HMA Type	Highway Name	ADT (million)	3/4 inch 19.0mm	1/2 inch 12.5mm	3/8 inch 9.5mm	No. 4 4.75 mm	No. 8 2.36 mm
1	3012-EST-01546	BH Ins	US54	3M+	100	95	83	56	43
2	3012-EST-01546	BH Ins	US54	3M+	100	95	83	56	43
3	3012-EST-01546	BH Ins	US54	3M+	100	95	83	56	43
4	3012-OK98-40473	B Ins	SH51	3M+	100	94	89	55	37
5	3012-OK98-40473	B Ins	SH51	3M+	100	94	89	55	37
6	3072-OAPA-21119	S2	various	3M+	88	71	61	41	26
7	3072-OAPA-21119	S2	various	3M+	88	71	61	41	26
8	3011-OAPA-20589	A	SH19	0.3M+	93	85	72	45	32
9	3011-OAPA-20589	A	SH19	0.3M+	93	85	72	45	32
10	3011-OAPA-20589	A	SH19	0.3M+	93	85	72	45	32
11	3074-OAPA-21107	S4	various	3M+	100	91	83	64	35
12	3074-OAPA-21107	S4	various	3M+	100	91	83	64	35
13	3074-OAPA-21107	S4	various	3M+	100	91	83	64	35
14	3073-OAPA-21106	S4	various	3M+	100	89	76	48	28
15	3073-OAPA-21106	S4	various	3M+	100	89	76	48	28
16	3073-OAPA-21106	S4	various	3M+	100	89	76	48	28
17	3012-EST-01183	B Ins	EW138	0.3M+	100	98	87	70	48
18	3012-BCC-01099	B Ins	SH1	0.3M+	100	99	89	60	37
19	3012-BCC-01098	B Bind	Various	0.3M+	100	99	90	70	51
20	3012-BCC-01098	B Bind	Various	0.3M+	100	99	90	70	51
21	3012-BCC-01101	B Bind	Various	0.3M+	100	98	89	70	52
22	3012-BCC-01102	BH Bind	US62	3M+	100	88	73	54	35
23	3012-BCC-01104	B Ins	US-83	3M+	100	92	81	60	42
24	3011-BCC-01108	A Rec	US54	3M+	82	70	66	57	47
25	3011-BCC-01109	A Rec	US-283	3M+	87	77	72	62	48
26	3011-BCC-01105	A Rec	US-283	3M+	87	77	72	62	48
27	3012-BCC-01107	B Ins	US83	3M+	100	92	81	60	42
28	3012-BCC-01110	B Ins	US183	3M+	100	97	81	58	44
29	3012-BCC-01110	B Ins	US183	3M+	100	97	81	58	44
30	3074-APKSS-00302	S4 ins	county	0.3M+	100	98	89	65	55
31	3074-APKSS-00302	S4 ins	county	0.3M+	100	98	89	65	55
32	3011-BCC-00048	A	US62	3M+	87	70	61	42	28
33	3011-BCC-00048	A	US62	3M+	87	70	61	42	28
34	3011-BCC-00048	A	US62	3M+	87	70	61	42	28
35	3012-BCC-01103	BH Ins	US62	3M+	100	90	74	54	35
36	3012-BCC-01103	BH Ins	US62	3M+	100	90	74	54	35
37	3012-BCC-01103	BH Ins	US62	3M+	100	90	74	54	35
38	3011-BCC-01111	A	US62	3M+	87	70	61	42	28
39	3011-BCC-01111	A	US62	3M+	87	70	61	42	28
40	3011-BCC-9904	A	SH1	.3M+	100	76	65	44	28
41	3011-BCC-9904	A	SH1	.3M+	100	76	65	44	28
42	3011-BCC-99024	A	US281	0.3M+	92	81	71	51	38
43	3011-BCC-99024	A	US281	0.3M+	92	81	71	51	38
44	3011-BCC-99024	A	US281	0.3M+	92	81	71	51	38
45	3012-BCC-01117	B Ins	Co RD	0.3M+	100	97	81	58	44
46	3012-BCC-01117	B Ins	Co RD	0.3M+	100	97	81	58	44
47	3012-OK97-08687	B Ins	US75	0.3M+	100	96	90	68	43
48	3012-OK97-08687	B Ins	US75	0.3M+	100	96	90	68	43
49	3011-SH00-71105	A Rec	US62	0.3M+	93	83	73	53	40
50	3011-SH00-71105	A Rec	US62	0.3M+	93	83	73	53	40
51	3012-SH01-73164	B Ins	SH99	0.3M+	100	98	90	63	38
52	3012-SH01-73164	B Ins	SH99	0.3M+	100	98	90	63	38
53	3012-APAC-20108	B Ins	Various	3M+	100	94	86	53	33
54	3012-APAC-20108	B Ins	Various	3M+	100	94	86	53	33
55	3012-APAC-20117	B	Co RD	3M+	100	93	88	60	37
56	3012-APAC-20117	B	Co RD	3M+	100	93	88	60	37
57	3012-APAC-20122	B	US75	0.3M+	100	95	86	52	35
58	3012-APAC-20122	B	US75	0.3M+	100	95	86	52	35
59	3012-APAC-20121	B	US62	3M+	100	93	84	56	37
60	3012-APAC-20121	B	Co RD	3M+	100	93	84	56	37
61	3012-APAC-20118	BH Ins	Co RD	3M+	100	92	85	56	33
62	3012-APAC-20118	BH Ins	US75	3M+	100	92	85	56	33
63	3012-APAC-20118	BH Ins	US75	3M+	100	92	85	56	33

Sample	No. 16	No. 30	No. 50	No. 100	No. 200	Asphalt			Aggregate		
No.	1.18mm	0.60mm	0.30mm	0.15 mm	0.075mm	Pb	PG	Gb	FAA	FF	G_{sb}
1	31	22	15	9	5.6	4.7	PG 76-28OK	1.0058	46.1	100	2.591
2	31	22	15	9	5.6	4.7	PG 76-28OK	1.0058	46.1	100	2.591
3	31	22	15	9	5.6	4.7	PG 76-28OK	1.0058	46.1	100	2.591
4	26	17	11	7	5.3	4.8	PG 64-22OK	1.0198	45.1	100	2.545
5	26	17	11	7	5.3	4.8	PG 70-28OK	1.0198	45.1	100	2.545
6	16	11	8	6	4.6	4.0	PG 70-28OK	1.0119	42.9	100	2.564
7	16	11	8	6	4.6	4.0	PG 64-22OK	1.0119	42.9	100	2.564
8	24	19	13	7	4.6	4.0	PG 64-22OK	1.0087	45.0	100	2.671
9	24	19	13	7	4.6	4.0	PG 64-22OK	1.0087	45.0	100	2.671
10	24	19	13	7	4.6	4.0	PG 70-28OK	1.0087	45.0	100	2.671
11	25	18	12	8	5.6	5.6	PG 70-28OK	1.0045	45.3	100	2.623
12	25	18	12	8	5.6	5.6	PG 70-28OK	1.0045	45.3	100	2.623
13	25	18	12	8	5.6	5.6	PG 64-22OK	1.0045	45.3	100	2.623
14	23	16	10	7	5.2	4.2	PG 70-28OK	1.0045	45.2	100	2.637
15	23	16	10	7	5.2	4.2	PG 70-28OK	1.0045	45.2	100	2.637
16	23	16	10	7	5.2	4.2	PG 70-28OK	1.0045	45.2	100	2.637
17	33	21	15	10	5.7	4.7	PG 70-28OK	1.0067	45.0	100	2.661
18	24	15	10	7	5.8	5.1	PG 70-28OK	1.0093	44.0	100	2.644
19	33	19	11	7	5.8	5.0	PG 70-28OK	1.0119	44.5	100	2.648
20	33	19	11	7	5.8	5.0	PG 64-22OK	1.0119	44.5	100	2.648
21	34	20	11	7	5.3	5.0	PG 64-22OK	1.0119	45.0	100	2.658
22	23	14	9	6	4.6	4.3	PG 70-28OK	1.0067	45.2	100	2.672
23	28	19	12	7	5.5	5.4	PG 64-22OK	0.9971	45.0	100	2.771
24	34	23	14	7	5.0	5.2	PG 64-22OK	1.0100	45.0	100	2.728
25	34	23	14	7	5.0	4.4	PG 64-22OK	1.0100	45.1	100	2.732
26	34	23	14	7	5.0	4.4	PG 64-22OK	1.0100	45.0	100	2.732
27	28	19	12	7	5.5	5.4	PG 64-22OK	1.0058	45.1	100	2.778
28	31	22	13	6	4.3	4.7	PG 76-28OK	1.0058	45.0	100	2.658
29	31	22	13	6	4.3	4.7	PG 64-22OK	1.0058	45.0	100	2.658
30	45	34	20	9	4.0	4.9	PG 64-22OK	0.9973	45.2	100	2.628
31	45	34	20	9	4.0	4.9	PG 64-22OK	0.9973	45.2	100	2.628
32	19	12	9	6	4.7	3.8	PG 70-28OK	1.0087	45.8	100	2.671
33	19	12	9	6	4.7	3.8	PG 76-28OK	1.0087	45.8	100	2.671
34	19	12	9	6	4.7	3.8	PG 76-28OK	1.0087	45.8	100	2.671
35	23	14	9	6	4.6	4.3	PG 76-28OK	1.0045	45.5	100	2.642
36	23	14	9	6	4.6	4.3	PG 76-28OK	1.0045	45.5	100	2.642
37	23	14	9	6	4.6	4.3	PG 64-22OK	1.0045	45.5	100	2.642
38	19	12	9	6	4.7	3.9	PG 64-22OK	1.0045	45.8	100	2.669
39	19	12	9	6	4.7	3.9	PG 64-22OK	1.0045	45.8	100	2.669
40	19	12	9	7	7.0	4.6	PG 70-28OK	1.0052	45.0	100	2.647
41	19	12	9	7	7.0	4.6	PG 70-28OK	1.0052	45.0	100	2.647
42	27	18	11	5	3.8	4.2	PG 70-28OK	1.0080	45.0	100	2.647
43	27	18	11	5	3.8	4.2	PG 70-28OK	1.0080	45.0	100	2.647
44	27	18	11	5	3.8	4.2	PG 70-28OK	1.0080	45.0	100	2.647
45	31	22	13	6	4.3	4.9	PG 70-28OK	1.0119	45.0	100	2.641
46	31	22	13	6	4.3	4.9	PG 70-28OK	1.0119	45.0	100	2.641
47	27	17	10	6	4.7	5.0	PG 64-22OK	1.0076	45.4	100	2.634
48	27	17	10	6	4.7	5.0	PG 70-28OK	1.0076	45.4	100	2.634
49	33	27	19	9	4.1	4.2	PG 70-28OK	1.0100	45.0	100	2.642
50	33	27	19	9	4.1	4.2	PG 64-22OK	1.0100	45.0	100	2.642
51	26	20	12	6	4.0	5.1	PG 64-22OK	1.0119	45.5	100	2.634
52	26	20	12	6	4.0	5.1	PG 64-22OK	1.0119	45.5	100	2.634
53	24	18	13	8	5.3	5.0	PG 64-22OK	1.0045	46.1	100	2.568
54	24	18	13	8	5.3	5.0	PG 64-22OK	1.0045	46.1	100	2.568
55	25	16	10	6	4.7	4.9	PG 64-22OK	1.0092	45.0	100	2.579
56	25	16	10	6	4.7	4.9	PG 64-22OK	1.0092	45.0	100	2.579
57	24	15	10	6	4.8	5.0	PG 70-28OK	1.0092	45.2	100	2.573
58	24	15	10	6	4.8	5.0	PG 64-22OK	1.0092	45.2	100	2.573
59	24	15	10	6	4.8	4.8	PG 64-22OK	1.0092	45.1	100	2.560
60	24	15	10	6	4.8	4.8	PG 64-22OK	1.0092	45.1	100	2.560
61	21	14	9	6	4.6	5.0	PG 64-22OK	1.0045	45.4	100	2.582
62	21	14	9	6	4.6	5.0	PG 64-22OK	1.0045	45.4	100	2.582
63	21	14	9	6	4.6	5.0	PG 64-22OK	1.0045	45.4	100	2.582

Sample	Mix		Parameters			Rut Depths (mm) at cycles						
No.	G_{mm}	G_{mb}	Wheel	Tire	Temp.	500-c	1000-c	1500-c	2000-c	4000-c	6000-c	8000-c
1	2.436	2.267	100	100	64	0.734	0.842	1.067	1.233	1.57	1.88	2.2
2	2.436	2.261	100	100	64	0.838	1.050	1.248	1.368	1.75	2.02	2.3
3	2.436	2.269	100	100	64	0.675	0.912	1.036	1.158	1.44	1.66	1.8
4	2.418	2.248	100	100	64	0.667	0.893	0.916	0.992	1.38	1.76	2.0
5	2.418	2.253	100	100	64	0.676	0.847	0.981	1.050	1.33	1.49	1.6
6	2.488	2.256	100	100	64	1.018	1.391	1.641	1.604	2.01	2.36	2.5
7	2.488	2.226	100	100	64	1.203	1.574	1.787	1.916	2.32	2.56	2.7
8	2.509	2.286	100	100	64	1.595	2.125	2.414	2.714	3.42	3.93	4.3
9	2.509	2.305	100	100	64	1.514	2.015	2.312	2.497	2.91	3.11	3.3
10	2.509	2.330	100	100	64	1.618	1.941	2.143	2.264	2.55	2.72	2.8
11	2.407	2.211	100	100	64	1.332	1.473	1.915	2.036	2.81	3.29	3.7
12	2.407	2.222	100	100	64	1.222	1.567	1.779	1.973	2.48	2.83	3.1
13	2.407	2.238	100	100	64	1.004	1.215	1.411	1.625	2.10	2.43	2.7
14	2.493	2.300	100	100	64	1.235	1.433	1.600	1.671	2.07	2.28	2.5
15	2.493	2.290	100	100	64	1.195	1.395	1.545	1.658	1.97	2.21	2.3
16	2.493	2.311	100	100	64	0.880	1.051	1.205	1.264	1.60	1.82	2.0
17	2.475	2.300	100	100	64	1.689	2.278	2.582	2.944	3.77	4.03	4.3
18	2.470	2.297	100	100	64	1.437	1.825	2.068	2.346	3.04	3.46	3.8
19	2.466	2.307	100	100	64	1.813	2.379	2.816	3.153	4.14	4.81	5.3
20	2.466	2.308	100	100	64	1.940	2.606	3.020	3.319	4.13	4.68	5.1
21	2.476	2.277	100	100	64	1.385	1.907	2.334	2.643	3.56	4.25	4.8
22	2.522	2.328	100	100	64	1.477	1.812	2.035	2.239	2.81	3.18	3.5
23	2.574	2.365	100	100	64	1.856	2.351	2.770	3.088	3.83	4.22	4.5
24	2.518	2.327	100	100	64	0.953	1.133	1.337	1.455	1.78	2.01	2.2
25	2.558	2.379	100	100	64	1.259	1.506	1.682	1.795	2.07	2.28	2.5
26	2.564	2.374	100	100	64	1.558	1.803	2.026	2.174	2.54	2.83	3.1
27	2.567	2.377	100	100	64	1.244	1.609	1.886	2.093	2.78	3.30	3.7
28	2.499	2.280	100	100	64	1.731	2.294	2.581	2.746	3.38	4.00	4.5
29	2.499	2.276	100	100	64	1.619	2.095	2.395	2.672	3.29	3.93	4.4
30	2.445	2.268	100	100	64	0.466	0.563	0.633	0.679	0.80	0.86	0.9
31	2.445	2.271	100	100	64	0.422	0.512	0.566	0.598	0.68	0.87	0.9
32	2.526	2.344	100	100	64	1.178	1.531	1.661	1.868	2.22	2.44	2.6
33	2.526	2.347	100	100	64	1.187	1.483	1.675	1.840	2.27	2.54	2.8
34	2.526	2.353	100	100	64	1.398	1.662	1.836	2.017	2.35	2.59	2.8
35	2.467	2.267	100	100	64	0.960	1.135	1.441	1.546	1.94	2.31	2.7
36	2.467	2.272	100	100	64	0.948	1.181	1.316	1.416	1.72	1.94	2.1
37	2.467	2.274	100	100	64	0.797	1.027	1.120	1.263	1.66	1.94	2.1
38	2.506	2.294	100	100	64	0.923	1.217	1.392	1.553	1.94	2.19	2.4
39	2.506	2.291	100	100	64	0.868	1.126	1.268	1.438	1.83	2.07	2.3
40	2.511	2.332	100	100	64	1.407	1.710	1.886	2.050	2.55	2.90	3.1
41	2.511	2.341	100	100	64	1.471	2.093	2.366	2.622	3.17	3.58	3.6
42	2.511	2.331	100	100	64	2.643	3.564	4.004	4.506	5.53	6.09	6.5
43	2.511	2.330	100	100	64	3.360	4.236	4.736	5.191	6.27	6.96	7.6
44	2.511	2.339	100	100	64	2.886	4.071	4.876	5.485	6.98	7.98	8.7
45	2.471	2.280	100	100	64	3.444	4.440	5.082	5.572	6.91	7.91	8.6
46	2.471	2.330	100	100	64	2.258	3.049	3.559	3.896	5.05	5.86	6.5
47	2.458	2.286	100	100	64	1.405	1.783	2.004	2.111	2.45	2.90	3.4
48	2.458	2.289	100	100	64	1.510	1.871	2.034	2.167	2.52	2.80	3.0
49	2.498	2.320	100	100	64	2.824	3.765	4.405	4.890	5.92	6.49	6.8
50	2.498	2.325	100	100	64	2.559	3.291	3.742	4.105	5.02	5.56	5.9
51	2.458	2.276	100	100	64	2.120	2.639	3.286	3.478	4.61	5.20	5.8
52	2.458	2.284	100	100	64	2.199	2.794	3.214	3.491	4.37	4.97	5.4
53	2.420	2.222	100	100	64	0.734	0.895	1.005	1.135	1.43	1.67	1.9
54	2.454	2.245	100	100	64	0.678	0.853	0.911	0.966	1.15	1.32	1.4
55	2.433	2.260	100	100	64	1.350	1.912	2.123	2.368	3.12	3.69	4.3
56	2.433	2.268	100	100	64	1.674	2.175	2.459	2.632	3.14	3.47	3.8
57	2.421	2.223	100	100	64	1.100	1.451	1.672	1.843	2.26	2.54	2.7
58	2.421	2.216	100	100	64	1.242	1.613	1.824	1.999	2.44	2.75	3.0
59	2.430	2.251	100	100	64	1.609	2.111	2.460	2.672	3.26	3.68	4.1
60	2.430	2.253	100	100	64	1.553	2.232	2.643	2.955	3.59	3.91	4.1
61	2.433	2.268	100	100	64	1.145	1.498	1.761	1.915	2.41	2.81	3.0
62	2.433	2.261	100	100	64	1.072	1.370	1.558	1.692	2.12	2.46	2.7
63	2.433	2.265	100	100	64	0.959	1.242	1.384	1.523	1.93	2.14	2.3

Sample No.	Mix Design ID	HMA Type	Highway Name	ADT (million)	3/4 inch 19.0mm	1/2 inch 12.5mm	3/8 inch 9.5mm	No. 4 4.75 mm	No. 8 2.36 mm
64	3012-APAC-20123	B Ins	US62	3M+	100	94	86	58	37
65	3012-APAC-20123	B Ins	US62	3M+	100	94	86	58	37
66	3012-APAC-20123	B Ins	SH99	3M+	100	94	86	58	37
67	3074-CCC-01003	S-4	SH99	3M+	100	91	73	57	43
68	3074-CCC-01003	S-4	Various	3M+	100	91	73	57	43
69	3074-CCC-01003	S-4	Various	3M+	100	91	73	57	43
70	3073-EST-01768	19mm rec	SH-74	0.3M+	97	87	74	61	43
71	3073-EST-01768	19mm rec	SH-74	0.3M+	97	87	74	61	43
72	3073-EST-01768	19mm rec	SH-74	0.3M+	97	87	74	61	43
73	3073-EST-01974	19mm rec	SH-75	0.3M+	97	87	74	61	43
74	3073-EST-01974	19mm rec	SH-75	0.3M+	97	87	74	61	43
75	3073-EST-01974	19mm rec	SH-75	0.3M+	97	87	74	61	43
76	3074-APAC-20125	12.5mm ins	SH-76	10M+	97	93	87	57	36
77	3074-APAC-20125	12.5mm ins	SH-77	10M+	97	93	87	57	36
78	3074-APAC-20125	12.5mm ins	SH-78	10M+	97	93	87	57	36
79	3074-APAC-20125	25mm rec	SH-51	10M+	87	76	65	36	22
80	3074-APAC-20125	25mm rec	SH-51	10M+	87	76	65	36	22
81	3074-APAC-20125	25mm rec	SH-51	10M+	87	76	65	36	22
82	3074-CCC-01005	S-4	SH-7	3M+	100	91	73	57	43
83	3074-CCC-01005	S-4	SH-7	3M+	100	91	73	57	43
84	3074-OAPA-20036	S-4	US-64	3M+	100	95	86	69	45
85	3074-OAPA-20036	S-4	US-64	3M+	100	95	86	69	45
86	3074-OAPA-20036	S-4	US-64	3M+	100	95	86	69	45
87	3073-OAPA-21139	S-3	US-64	3M+	96	87	77	59	39
88	3073-OAPA-21139	S-3	US-64	3M+	96	87	77	59	39
89	3073-OAPA-21139	S-3	US-64	3M+	96	87	77	59	39
90	3072-EST-02543	S-2 rec	US-62	3.5M	90	74	64	54	40
91	3072-EST-02543	S-2 rec	US-62	3.5M	90	74	64	54	40
92	3072-EST-02543	S-2 rec	US-62	3.5M	90	74	64	54	40
93	3073-APAC-20126	19.0 mm	SH-51	3M+	95	85	78	44	26
94	3073-APAC-20126	19.0 mm	SH-51	3M+	95	85	78	44	26
95	3073-APAC-20126	19.0 mm	SH-51	3M+	95	85	78	44	26
96	3073-APAC-20127	19.0 mm	SH-51	3M+	95	85	78	44	26
97	3073-APAC-20127	19.0 mm	SH-51	3M+	95	85	78	44	26
98	3073-APAC-20127	19.0 mm	SH-51	3M+	95	85	78	44	26
99	3012-APAC-20128	B Ins	SH 51	3M+	100	93	88	60	37
100	3012-APAC-20128	B Ins	SH 51	3M+	100	93	88	60	37
101	3073-BCC-01119	19mm	US-281	0.3M+	100	81	67	45	28
102	3073-BCC-01119	19mm	US-281	0.3M+	100	81	67	45	28
103	3073-BCC-01119	19mm	US-281	0.3M+	100	81	67	45	28
104	3073-BCC-01118	S4 binder	US-281	0.3M+	100	98	89	55	34
105	3073-BCC-01118	S4 binder	US-281	0.3M+	100	98	89	55	34
106	3074-BCC-01124	S4	US-62	3M+	100	96	81	52	35
107	3074-BCC-01124	S4	US-62	3M+	100	96	81	52	35
108	3074-BCC-01124	S4	US-62	3M+	100	96	81	52	35
109	3073-CCC-01012	S3 Inc	Varous	3M+	90	78	73	56	37
110	3073-CCC-01012	S3 Inc	Varous	3M+	90	78	73	56	37
111	3073-BCC-01126	S3	US-281	2.9M	100	81	67	45	28
112	3073-BCC-01126	S3	US-281	2.9M	100	81	67	45	28
113	3073-BCC-01126	S3	US-281	2.9M	100	81	67	45	28
114	3072-OAPA-22000	S2-rec	SH-33	3M+	90	78	70	55	42
115	3072-OAPA-22000	S2-rec	SH-33	3M+	90	78	70	55	42
116	3072-OAPA-22000	S2-rec	SH-33	3M+	90	78	70	55	42
117	3072-CCC-02007	S2-rec	various	3M+	89	69	62	38	23
118	3072-CCC-02007	S2-rec	various	3M+	89	69	62	38	23
119	3072-CCC-02007	S2-rec	various	3M+	89	69	62	38	23
120	3073-BCC-02129	S3	US-60	0.3M+	100	85	71	51	32
121	3073-BCC-02129	S3	US-60	0.3M+	100	85	71	51	32
122	3073-BCC-02129	S3	US-60	0.3M+	100	85	71	51	32
123	3073-OAPA-21253	S4	Various	3M+	100	89	79	42	25
124	3073-OAPA-21253	S4	Various	3M+	100	89	79	42	25
125	3073-OAPA-21253	S4	Various	3M+	100	89	79	42	25
126	3012-CCC-010070	B ins	Various	3M+	100	93	78	59	39

Sample	No. 16	No. 30	No. 50	No. 100	No. 200	Asphalt			Aggregate		
No.	1.18mm	0.60mm	0.30mm	0.15 mm	0.075mm	Pb	PG	Gb	FAA	FF	G_{sb}
64	28	23	16	8	4.7	4.7	PG 64-22OK	1.0092	45.0	100	2.592
65	28	23	16	8	4.7	4.7	PG 64-22OK	1.0092	45.0	100	2.592
66	28	23	16	8	4.7	4.7	PG 70-28OK	1.0092	45.0	100	2.592
67	29	21	15	6	3.7	5.5	PG 70-28OK	1.0045	47.4	100	2.507
68	29	21	15	6	3.7	5.5	PG 64-22OK	1.0045	47.4	100	2.507
69	29	21	15	6	3.7	5.5	PG 64-22OK	1.0045	47.4	100	2.507
70	31	23	16	7	4.5	3.9	PG 64-22OK	1.0100	43.7	100	2.669
71	31	23	16	7	4.5	3.9	PG 64-22OK	1.0100	43.7	100	2.669
72	31	23	16	7	4.5	3.9	PG 64-22OK	1.0100	43.7	100	2.669
73	31	23	16	7	4.5	3.9	PG 64-22OK	1.0100	43.7	100	2.669
74	31	23	16	7	4.5	3.9	PG 64-22OK	1.0100	43.7	100	2.669
75	31	23	16	7	4.5	3.9	PG 64-22OK	1.0100	43.7	100	2.669
76	23	15	9	5	4.1	5.5	PG 70-28OK	1.0092	46.0	100	2.587
77	23	15	9	5	4.1	5.5	PG 70-28OK	1.0092	46.0	100	2.587
78	23	15	9	5	4.1	5.5	PG 70-28OK	1.0092	46.0	100	2.587
79	14	9	6	4	3.1	4.3	PG 64-22OK	1.0092	46.1	100	2.597
80	14	9	6	4	3.1	4.3	PG 64-22OK	1.0092	46.1	100	2.597
81	14	9	6	4	3.1	4.3	PG 64-22OK	1.0092	46.1	100	2.597
82	29	21	15	6	3.7	5.5	PG 70-28OK	1.0067	47.4	100	2.507
83	29	21	15	6	3.7	5.5	PG 70-28OK	1.0067	47.4	100	2.507
84	30	21	14	8	5.5	4.8	PG 70-28OK	1.0045	45.4	100	2.642
85	30	21	14	8	5.5	4.8	PG 70-28OK	1.0045	45.4	100	2.642
86	30	21	14	8	5.5	4.8	PG 70-28OK	1.0045	45.4	100	2.642
87	27	20	14	8	5.1	4.3	PG 70-28OK	1.0045	45.3	100	2.661
88	27	20	14	8	5.1	4.3	PG 70-28OK	1.0045	45.3	100	2.661
89	27	20	14	8	5.1	4.3	PG 64-22OK	1.0045	45.3	100	2.661
90	30	24	16	7	4.1	3.4	PG 64-22OK	1.0100	43.6	100	2.680
91	30	24	16	7	4.1	3.4	PG 64-22OK	1.0100	43.6	100	2.680
92	30	24	16	7	4.1	3.4	PG 64-22OK	1.0100	43.6	100	2.680
93	16	11	6	4	3.3	4.4	PG 64-22OK	1.0092	45.7	100	2.597
94	16	11	6	4	3.3	4.4	PG 64-22OK	1.0092	45.7	100	2.597
95	16	11	6	4	3.3	4.4	PG 64-22OK	1.0092	45.7	100	2.597
96	16	11	6	4	3.3	4.4	PG 64-22OK	1.0058	45.7	100	2.597
97	16	11	6	4	3.3	4.4	PG 64-22OK	1.0058	45.7	100	2.597
98	16	11	6	4	3.3	4.4	PG 64-22OK	1.0058	45.7	100	2.597
99	24	16	10	6	4.7	5.0	PG 64-22OK	1.0210	45.0	100	2.613
100	24	16	10	6	4.7	5.0	PG 64-22OK	1.0210	45.0	100	2.613
101	17	11	8	5	4.2	4.7	PG 64-22OK	1.0067	45.1	100	2.644
102	17	11	8	5	4.2	4.7	PG 76-28OK	1.0067	45.1	100	2.644
103	17	11	8	5	4.2	4.7	PG 70-28OK	1.0067	45.1	100	2.644
104	21	13	9	6	4.7	5.5	PG 70-28OK	1.0067	45.5	100	2.648
105	21	13	9	6	4.7	5.5	PG 70-28OK	1.0067	45.5	100	2.648
106	22	14	9	7	5.6	5.2	PG 70-28OK	1.0210	47.0	100	2.655
107	22	14	9	7	5.6	5.2	PG 70-28OK	1.0210	47.0	100	2.655
108	22	14	9	7	5.6	5.2	PG 70-28OK	1.0210	47.0	100	2.655
109	25	19	14	6	2.8	4.5	PG 64-22OK	1.0067	45.5	100	2.689
110	25	19	14	6	2.8	4.5	PG 64-22OK	1.0067	45.5	100	2.689
111	17	11	8	5	4.2	4.7	PG 64-22OK	1.0045	45.1	100	2.644
112	17	11	8	5	4.2	4.7	PG 64-22OK	1.0045	45.1	100	2.644
113	17	11	8	5	4.2	4.7	PG 64-22OK	1.0045	45.1	100	2.644
114	26	17	10	6	4.5	4.4	PG 64-22OK	1.0100	44.4	100	2.550
115	26	17	10	6	4.5	4.4	PG 64-22OK	1.0100	44.4	100	2.550
116	26	17	10	6	4.5	4.4	PG 64-22OK	1.0100	44.4	100	2.550
117	17	14	9	4	2.2	3.8	PG 76-28OK	1.0146	41.3	100	2.669
118	17	14	9	4	2.2	3.8	PG 76-28OK	1.0146	41.3	100	2.669
119	17	14	9	4	2.2	3.8	PG 76-28OK	1.0146	41.3	100	2.669
120	25	20	10	5	3.5	4.5	PG 70-28OK	1.0059	45.5	100	2.687
121	25	20	10	5	3.5	4.5	PG 70-28OK	1.0059	45.5	100	2.687
122	25	20	10	5	3.5	4.5	PG 64-22OK	1.0059	45.5	100	2.687
123	20	16	12	9	6.6	5.0	PG 64-22OK	1.0119	47.9	91	2.572
124	20	16	12	9	6.6	5.0	PG 64-22OK	1.0119	47.9	91	2.572
125	20	16	12	9	6.6	5.0	PG 70-28OK	1.0119	47.9	91	2.572
126	29	22	16	9	4.4	4.8	PG 64-22OK	1.0067	45.5	100	2.517

Sample	Mix		Parameters			Rut Depths (mm) at cycles						
No.	G_{mm}	G_{mb}	Wheel	Tire	Temp.	500-c	1000-c	1500-c	2000-c	4000-c	6000-c	8000-c
64	2.438	2.251	100	100	64	1.145	1.498	1.761	1.915	2.41	2.81	3.0
65	2.438	2.254	100	100	64	1.072	1.370	1.558	1.692	2.12	2.46	2.7
66	2.438	2.248	100	100	64	0.959	1.242	1.384	1.523	1.93	2.14	2.3
67	2.353	2.180	100	100	64	0.572	0.764	0.802	0.968	1.22	1.27	1.4
68	2.353	2.177	100	100	64	0.776	0.969	1.068	1.178	1.41	1.56	1.7
69	2.353	2.167	100	100	64	0.698	0.841	0.915	0.986	1.23	1.39	1.5
70	2.519	2.343	100	100	64	0.995	1.344	1.549	1.766	2.11	2.37	2.5
71	2.519	2.332	100	100	64	0.812	1.057	1.215	1.332	1.76	2.07	2.3
72	2.519	2.328	100	100	64	0.998	1.338	1.983	2.068	2.34	2.53	2.6
73	2.438	2.252	100	100	64	1.869	2.504	3.039	3.313	4.15	4.64	5.0
74	2.438	2.226	100	100	64	1.953	2.498	2.854	3.109	3.70	4.17	4.5
75	2.438	2.253	100	100	64	1.205	1.636	1.909	2.105	2.69	3.06	3.3
76	2.471	2.287	100	100	64	1.464	1.713	1.952	2.099	2.64	2.83	3.2
77	2.471	2.273	100	100	64	1.426	1.833	2.016	2.201	2.62	2.82	3.0
78	2.471	2.285	100	100	64	1.056	1.256	1.407	1.561	1.81	1.94	2.1
79	2.516	2.287	100	100	64	1.100	1.511	1.854	2.094	2.79	3.38	3.8
80	2.516	2.355	100	100	64	0.876	1.263	1.636	1.954	2.93	3.49	3.9
81	2.516	2.344	100	100	64	1.117	1.362	1.558	1.681	2.08	2.53	2.9
82	2.344	2.156	100	100	64	1.307	1.669	1.944	2.162	2.76	3.17	3.5
83	2.344	2.172	100	100	64	1.115	1.571	1.970	2.290	3.13	3.60	3.9
84	2.471	2.272	100	100	64	1.219	1.509	1.808	2.115	2.72	3.19	3.4
85	2.471	2.264	100	100	64	1.394	1.876	2.240	2.524	3.35	3.83	4.2
86	2.471	2.283	100	100	64	0.965	1.256	1.472	1.642	2.08	2.35	2.5
87	2.506	2.335	100	100	64	0.826	1.157	1.239	1.456	1.60	1.72	2.0
88	2.506	2.326	100	100	64	1.021	1.338	1.537	1.712	2.16	2.49	2.7
89	2.506	2.336	100	100	64	0.855	1.090	1.224	1.402	1.70	1.93	2.1
90	2.544	2.391	100	100	64	0.834	1.169	1.511	1.719	2.65	3.48	4.3
91	2.544	2.353	100	100	64	1.112	1.634	2.080	2.404	3.42	4.07	4.6
92	2.544	2.379	100	100	64	0.917	1.386	1.793	2.169	3.37	4.36	5.0
93	2.460	2.262	100	100	64	1.174	1.499	1.659	1.743	2.19	2.53	2.8
94	2.460	2.260	100	100	64	0.991	1.189	1.361	1.439	1.85	2.11	2.3
95	2.460	2.259	100	100	64	0.950	1.158	1.291	1.398	1.72	1.90	2.0
96	2.460	2.262	100	100	64	0.510	0.623	0.698	0.772	0.84	0.99	1.2
97	2.460	2.287	100	100	64	0.984	1.138	1.211	1.277	1.45	1.60	1.7
98	2.460	2.269	100	100	64	0.689	0.765	0.877	0.917	1.02	1.12	1.2
99	2.432	2.228	100	100	64	1.137	1.681	1.830	2.022	2.68	3.06	3.5
100	2.432	2.248	100	100	64	0.999	1.236	1.384	1.505	1.85	1.94	2.1
101	2.478	2.299	100	100	64	1.636	2.144	2.528	2.804	3.52	3.94	4.3
102	2.478	2.295	100	100	64	2.558	3.352	3.806	4.208	5.16	5.85	6.4
103	2.478	2.294	100	100	64	1.747	2.287	2.650	2.975	4.06	4.78	5.3
104	2.457	2.278	100	100	64	1.828	2.180	2.409	2.584	3.08	3.51	3.8
105	2.457	2.283	100	100	64	1.359	1.715	1.927	2.071	2.62	2.93	3.3
106	2.485	2.315	100	100	64	0.863	1.134	1.403	1.421	1.84	2.06	2.3
107	2.485	2.214	100	100	64	1.101	1.244	1.413	1.489	1.73	1.90	2.0
108	2.485	2.314	100	100	64	0.889	1.215	1.341	1.558	1.99	2.25	2.5
109	2.526	2.329	100	100	64	1.167	1.881	2.403	2.766	3.60	4.08	4.4
110	2.526	2.339	100	100	64	1.609	2.094	2.395	2.550	2.91	3.31	3.6
111	2.504	2.327	100	100	64	0.514	0.658	0.960	1.307	1.89	2.18	2.5
112	2.504	2.311	100	100	64	0.338	0.512	0.653	0.779	1.07	1.31	1.5
113	2.504	2.309	100	100	64	0.469	0.774	0.946	1.104	1.43	1.69	1.9
114	2.446	2.275	100	100	64	0.753	0.867	1.157	1.114	1.57	1.47	1.7
115	2.446	2.275	100	100	64	0.626	0.794	0.912	1.091	1.32	1.60	1.8
116	2.446	2.280	100	100	64	0.810	0.945	1.026	1.159	1.36	1.68	1.9
117	2.518	2.305	100	100	64	1.066	1.589	1.663	1.706	2.29	2.21	2.8
118	2.518	2.311	100	100	64	0.845	1.074	1.281	1.437	2.13	2.68	3.0
119	2.518	2.305	100	100	64	0.941	1.157	1.303	1.418	1.81	2.12	2.3
120	2.513	2.319	100	100	64	1.516	2.219	2.619	2.926	3.50	4.06	4.4
121	2.513	2.308	100	100	64	1.318	1.710	1.976	2.201	2.85	3.38	3.8
122	2.513	2.312	100	100	64	1.176	1.556	1.774	2.001	2.46	2.86	3.2
123	2.440	2.220	100	100	64	1.340	1.403	2.107	1.884	2.46	3.02	3.1
124	2.440	2.219	100	100	64	1.250	1.514	1.722	1.851	2.26	2.55	2.7
125	2.440	2.223	100	100	64	0.785	1.022	1.224	1.345	1.83	2.09	2.4
126	2.368	2.185	100	100	64	0.954	1.192	1.227	1.424	1.87	2.26	2.5

Sample No.	Mix Design ID	HMA Type	Highway Name	ADT (million)	3/4 inch 19.0mm	1/2 inch 12.5mm	3/8 inch 9.5mm	No. 4 4.75 mm	No. 8 2.36 mm
127	3012-CCC-010070	B ins	Various	3M+	100	93	78	59	39
128	3011-APAC-20131	A	Various	0.3M+	89	75	64	43	31
129	3011-APAC-20131	A	Various	0.3M+	89	75	64	43	31
130	3011-APAC-20131	A	Various	0.3M+	89	75	64	43	31
131	3073-EST-03349	S3 Rec	US62	3.5M	97	87	74	61	43
132	3073-EST-03349	S3 Rec	US62	3.5M	97	87	74	61	43
133	3073-EST-03349	S3 Rec	US62	3.5M	97	87	74	61	43
134	3011-CCC-01009	A	HWY 70	3M+	90	76	68	52	40
135	3011-CCC-01009	A	HWY 70	3M+	90	76	68	52	40
136	3011-CCC-01009	A	HWY 70	3M+	90	76	68	52	40
137	3011-CCC-01011	A	HWY 70	3M+	90	76	68	52	40
138	3011-CCC-01011	A	HWY 70	3M+	90	76	68	52	40
139	3011-CCC-01011	A	HWY 70	3M+	90	76	68	52	40
140	3073-EST-03719	S3 Rec	US62	3.5M	98	90	79	63	43
141	3073-EST-03719	S3 Rec	US62	3.5M	98	90	79	63	43
142	3074-EST-02097	1/2" Ins	SH 51	3M+	100	91	85	64	38
143	3074-EST-02097	1/2" Ins	SH 51	3M+	100	91	85	64	38
144	3074-EST-02097	1/2" Ins	SH 51	3M+	100	91	85	64	38
145	3076-EST-03239	S6 Rec	SH 74	1.8M	100	100	100	92	66
146	3073-EST-03997	S4 Ins	US62	3.5M	100	98	86	56	37
147	3073-EST-03997	S4 Ins	US62	3.5M	100	98	86	56	37
148	3073-EST-03997	S4 Ins	US62	3.5M	100	98	86	56	37
149	3072-EST-02295	S2	US271	5.8	84	67	61	49	37
150	3072-EST-02295	S2	US271	5.8	84	67	61	49	37
151	3072-EST-02295	S2	US271	5.8	84	67	61	49	37
152	3074-CCC-02006	S-4	SH 51	3M+	100	97	85	56	31
153	3074-CCC-02006	S-4	SH 51	3M+	100	97	85	56	31
154	3074-CCC-02006	S-4	SH 51	3M+	100	97	85	56	31
155	3074-CCC-02004	S-4	US-64	3M+	100	97	87	65	50
156	3074-CCC-02004	S-4	US-64	3M+	100	97	87	65	50
157	3074-CCC-02004	S-4	US-64	3M+	100	97	87	65	50
158	3074-CCC-02002	S-4	US 64	3M+	100	97	87	65	50
159	3074-CCC-02002	S-4	US 64	3M+	100	97	87	65	50
160	3074-CCC-02002	S-4	US 64	3M+	100	97	87	65	50
161	3073-BCC-02128	S-3	US 60	0.3M+	100	85	71	51	32
162	3073-BCC-02128	S-3	US 60	0.3M+	100	85	71	51	32
163	3073-BCC-02128	S-3	US 60	0.3M+	100	85	71	51	32
164	3012-APAC-20201	B Ins	US 60	3M+	100	94	86	58	40
165	3012-APAC-20201	B Ins	US 60	3M+	100	94	86	58	40
166	3012-APAC-20201	B Ins	US 60	3M+	100	94	86	58	40
167	3073-EST-02500	S-3	US 271	5.8M	100	90	78	54	40
168	3073-EST-02500	S-3	US 271	5.8M	100	90	78	54	40
169	3073-EST-02500	S-3	US 271	5.8M	100	90	78	54	40
170	3073-EST-02300	S-3	US 271	5.8M	100	90	78	54	40
171	3073-EST-02300	S-3	US 271	5.8M	100	90	78	54	40
172	3011-APAC-20202	A Rec	US 272	3M+	91	79	67	43	31
173	3011-EST-04168	A Rec	US 54	3M+	90	80	72	57	44
174	3011-EST-04168	A Rec	US 54	3M+	90	80	72	57	44
175	3011-EST-04168	A Rec	US 54	3M+	90	80	72	57	44
176	3074-OAPA-22049	s-4	33	3M+	100	92	85	49	31
177	3074-OAPA-22049	s-4	33	3M+	100	92	85	49	31
178	3073-OAPA-22001	S-3	SH-33	3M+	98	89	79	61	47
179	3073-OAPA-22001	S-3	SH-33	3M+	98	89	79	61	47
180	3073-OAPA-22001	S-3	SH-33	3M+	98	89	79	61	47
181	3073-APAC-20204	S-3	SH-51	3M+	96	87	81	50	30
182	3073-APAC-20204	S-3	SH-51	3M+	96	87	81	50	30
183	3073-APAC-20204	S-3	SH-51	3M+	96	87	81	50	30
184	3073-APAC-20203	S-3	SH-51	3M+	96	87	81	50	30
185	3073-APAC-20203	S-3	SH-51	3M+	96	87	81	50	30
186	3073-APAC-20203	S-3	SH-51	3M+	96	87	81	50	30
187	3011-BCC-02115	A Rec	I-40	3M+	96	90	78	53	40
188	3011-BCC-02115	A Rec	I-40	3M+	96	90	78	53	40
189	3011-BCC-02115	A Rec	I-40	3M+	96	90	78	53	40

Sample	No. 16	No. 30	No. 50	No. 100	No. 200	Asphalt			Aggregate		
No.	1.18mm	0.60mm	0.30mm	0.15 mm	0.075mm	Pb	PG	Gb	FAA	FF	G_{sb}
127	29	22	16	9	4.4	4.8	PG 64-22OK	1.0067	45.5	100	2.517
128	22	15	10	7	5.3	4.1	PG 64-22OK	1.0119	45.0	100	2.580
129	22	15	10	7	5.3	4.1	PG 70-28OK	1.0119	45.0	100	2.580
130	22	15	10	7	5.3	4.1	PG 70-28OK	1.0119	45.0	100	2.580
131	31	23	16	7	4.5	4.0	PG 70-28OK	1.0100	43.2	100	2.673
132	31	23	16	7	4.5	4.0	PG 64-22OK	1.0100	43.2	100	2.673
133	31	23	16	7	4.5	4.0	PG 64-22OK	1.0100	43.2	100	2.673
134	31	25	16	8	3.5	4.7	PG 70-28OK	1.0093	45.1	100	2.554
135	31	25	16	8	3.5	4.7	PG 70-28OK	1.0093	45.1	100	2.554
136	31	25	16	8	3.5	4.7	PG 70-28OK	1.0093	45.1	100	2.554
137	31	25	16	8	3.5	4.7	PG 70-28OK	1.0119	45.0	100	2.554
138	31	25	16	8	3.5	4.7	PG 64-22OK	1.0119	45.0	100	2.554
139	31	25	16	8	3.5	4.7	PG 64-22OK	1.0119	45.0	100	2.554
140	31	23	16	8	4.6	4.2	PG 64-22OK	1.0100	45.3	100	2.681
141	31	23	16	8	4.6	4.2	PG 64-22OK	1.0100	45.3	100	2.681
142	23	14	8	5	4.1	5.1	PG 70-28OK	1.0058	45.3	100	2.561
143	23	14	8	5	4.1	5.1	PG 70-28OK	1.0058	45.3	100	2.561
144	23	14	8	5	4.1	5.1	PG 70-28OK	1.0058	45.3	100	2.561
145	47	34	24	11	6.9	5.8	PG 70-28OK	1.0100	42.7	100	2.661
146	25	18	12	5	3.3	4.8	PG 70-28OK	1.0093	45.0	100	2.662
147	25	18	12	5	3.3	4.8	PG 70-28OK	1.0093	45.0	100	2.662
148	25	18	12	5	3.3	4.8	PG 64-22OK	1.0093	45.0	100	2.662
149	30	25	17	10	5.4	3.9	PG 76-28OK	1.0219	45.6	100	2.576
150	30	25	17	10	5.4	3.9	PG 76-28OK	1.0219	45.6	100	2.576
151	30	25	17	10	5.4	3.9	PG 76-28OK	1.0219	45.6	100	2.576
152	22	18	13	6	3.7	4.7	PG 64-22OK	1.0146	45.0	100	2.650
153	22	18	13	6	3.7	4.7	PG 64-22OK	1.0146	45.0	100	2.650
154	22	18	13	6	3.7	4.7	PG 64-22OK	1.0146	45.0	100	2.650
155	37	30	20	10	5.3	5.0	PG 64-22OK	1.0146	45.0	100	2.606
156	37	30	20	10	5.3	5.0	PG 64-22OK	1.0146	45.0	100	2.606
157	37	30	20	10	5.3	5.0	PG 64-22OK	1.0146	45.0	100	2.606
158	37	30	20	10	5.3	5.0	PG 64-22OK	1.0067	45.0	100	2.606
159	37	30	20	10	5.3	5.0	PG 64-22OK	1.0067	45.0	100	2.606
160	37	30	20	10	5.3	5.0	PG 64-22OK	1.0067	45.0	100	2.606
161	25	20	10	5	3.5	5.4	PG 64-22OK	1.0087	44.7	100	2.690
162	25	20	10	5	3.5	5.4	PG 70-28OK	1.0087	44.7	100	2.690
163	25	20	10	5	3.5	5.4	PG 70-28OK	1.0087	44.7	100	2.690
164	30	23	16	8	5.1	4.7	PG 70-28OK	1.0104	45.0	100	2.618
165	30	23	16	8	5.1	4.7	PG 64-22OK	1.0104	45.0	100	2.618
166	30	23	16	8	5.1	4.7	PG 64-22OK	1.0104	45.0	100	2.618
167	33	27	18	10	5.4	4.2	PG 64-22OK	1.0253	45.1	100	2.586
168	33	27	18	10	5.4	4.2	PG 70-28OK	1.0253	45.1	100	2.586
169	33	27	18	10	5.4	4.2	PG 70-28OK	1.0253	45.1	100	2.586
170	33	27	18	10	5.4	4.2	PG 70-28OK	1.0209	45.1	100	2.586
171	33	27	18	10	5.4	4.2	PG 76-28OK	1.0209	45.1	100	2.586
172	25	21	14	6	4.7	4.0	PG 76-28OK	1.0104	45.0	100	2.617
173	32	23	15	9	4.8	4.2	PG 76-28OK	1.0100	45.6	100	2.644
174	32	23	15	9	4.8	4.2	PG 64-22OK	1.0100	45.6	100	2.644
175	32	23	15	9	4.8	4.2	PG 70-28OK	1.0100	45.6	100	2.644
176	19	12	8	5	4.4	5.6	PG 70-28OK	1.0209	46.1	100	2.562
177	19	12	8	5	4.4	5.6	PG 70-28OK	1.0209	46.1	100	2.562
178	28	18	10	6	4.1	5.0	PG 70-28OK	1.0100	44.9	100	2.554
179	28	18	10	6	4.1	5.0	PG 64-22OK	1.0100	44.9	100	2.554
180	28	18	10	6	4.1	5.0	PG 64-22OK	1.0100	44.9	100	2.554
181	20	12	7	5	3.7	4.8	PG 64-22OK	1.0119	45.2	100	2.600
182	20	12	7	5	3.7	4.8	PG 64-22OK	1.0119	45.2	100	2.600
183	20	12	7	5	3.7	4.8	PG 70-28OK	1.0119	45.2	100	2.600
184	20	12	7	5	3.7	4.8	PG 70-28OK	1.0147	45.2	100	2.600
185	20	12	7	5	3.7	4.8	PG 70-28OK	1.0147	45.2	100	2.600
186	20	12	7	5	3.7	4.8	PG 70-28OK	1.0147	45.2	100	2.600
187	30	22	16	10	4.5	3.8	PG 70-28OK	1.0100	46.1	100	2.653
188	30	22	16	10	4.5	3.8	PG 70-28OK	1.0100	46.1	100	2.653
189	30	22	16	10	4.5	3.8	PG 76-28OK	1.0100	46.1	100	2.653

Sample	Mix		Parameters			Rut Depths (mm) at cycles						
No.	G_{mm}	G_{mb}	Wheel	Tire	Temp.	500-c	1000-c	1500-c	2000-c	4000-c	6000-c	8000-c
127	2.368	2.184	100	100	64	0.844	1.076	1.219	1.344	1.78	2.17	2.5
128	2.465	2.272	100	100	64	0.910	1.235	1.608	1.548	2.06	2.22	2.4
129	2.465	2.282	100	100	64	1.072	1.389	1.588	1.753	2.09	2.32	2.5
130	2.465	2.275	100	100	64	1.248	1.637	1.875	2.093	2.59	2.89	3.1
131	2.514	2.314	100	100	64	1.715	2.310	2.715	2.914	3.67	4.18	4.5
132	2.514	2.299	100	100	64	2.425	3.129	3.599	3.987	4.99	5.74	6.3
133	2.514	2.318	100	100	64	1.956	2.838	3.364	3.727	4.67	5.29	5.8
134	2.403	2.223	100	100	64	0.995	1.304	1.546	1.830	2.41	2.71	2.9
135	2.403	2.211	100	100	64	1.073	1.278	1.388	1.505	1.76	1.94	2.1
136	2.403	2.226	100	100	64	0.803	0.942	1.040	1.110	1.29	1.41	1.5
137	2.396	2.207	100	100	64	1.481	1.986	2.213	2.544	3.29	3.74	4.2
138	2.396	2.212	100	100	64	1.585	2.400	2.882	3.323	4.26	4.76	5.1
139	2.396	2.195	100	100	64	1.444	2.184	2.557	2.871	3.66	4.16	4.4
140	2.529	2.368	100	100	64	0.663	0.835	1.034	1.093	1.40	1.63	1.9
141	2.529	2.381	100	100	64	0.623	0.832	0.942	1.058	1.43	1.63	1.7
142	2.412	2.231	100	100	64	0.879	1.069	1.213	1.335	1.73	1.96	2.2
143	2.412	2.272	100	100	64	0.912	1.146	1.293	1.417	1.67	1.87	2.0
144	2.412	2.238	100	100	64	0.900	1.193	1.295	1.414	1.82	2.08	2.4
145	2.456	2.291	100	100	64	1.241	1.825	2.274	2.679	4.13	4.88	5.3
146	2.478	2.317	100	100	64	0.606	0.795	0.902	0.993	1.37	1.77	2.3
147	2.478	2.305	100	100	64	1.009	1.189	1.279	1.398	1.73	1.80	2.0
148	2.478	2.318	100	100	64	0.854	1.052	1.139	1.227	1.53	1.74	1.9
149	2.448	2.304	100	100	64	0.769	0.948	1.022	1.096	1.28	1.43	1.6
150	2.448	2.304	100	100	64	1.208	1.426	1.574	1.633	1.96	2.15	2.3
151	2.448	2.289	100	100	64	0.937	1.076	1.150	1.299	1.60	1.78	2.0
152	2.491	2.293	100	100	64	1.171	1.421	1.736	1.928	2.35	2.94	3.0
153	2.491	2.299	100	100	64	0.989	1.343	1.568	1.876	2.88	3.51	3.9
154	2.491	2.296	100	100	64	0.865	1.084	1.292	1.458	1.95	2.33	2.6
155	2.450	2.268	100	100	64	0.821	1.116	1.626	1.606	2.14	2.64	3.3
156	2.450	2.272	100	100	64	1.079	1.448	1.765	1.986	2.59	2.95	3.3
157	2.450	2.273	100	100	64	0.981	1.431	1.737	2.020	2.73	3.12	3.4
158	2.451	2.285	100	100	64	1.072	1.385	1.535	1.540	2.34	2.28	2.4
159	2.451	2.279	100	100	64	0.923	1.372	1.705	1.907	2.43	2.73	3.0
160	2.451	2.267	100	100	64	2.508	3.327	3.928	4.299	5.39	6.19	6.7
161	2.511	2.322	100	100	64	1.823	2.129	2.215	2.419	3.28	3.78	4.3
162	2.511	2.331	100	100	64	1.353	1.667	1.702	1.816	2.49	2.93	3.3
163	2.511	2.326	100	100	64	1.781	2.295	2.310	2.590	3.26	3.64	3.9
164	2.438	2.268	100	100	64	2.543	3.542	3.942	4.435	5.41	5.85	6.3
165	2.438	2.282	100	100	64	2.355	3.151	3.688	4.175	5.59	6.53	7.4
166	2.438	2.270	100	100	64	2.889	4.157	4.826	5.284	6.44	6.96	7.6
167	2.442	2.278	100	100	64	0.890	1.154	1.712	1.536	1.87	2.15	2.3
168	2.442	2.263	100	100	64	1.289	1.720	1.998	2.214	2.84	3.24	3.6
169	2.442	2.272	100	100	64	0.737	0.968	1.116	1.259	1.72	2.22	2.7
170	2.442	2.265	100	100	64	1.133	1.388	1.648	1.745	1.88	2.25	2.6
171	2.442	2.272	100	100	64	0.688	0.819	1.032	1.402	1.83	2.20	2.5
172	2.487	2.285	100	100	64	4.862	5.450	5.898	6.169	6.78	7.12	7.4
173	2.478	2.312	100	100	64	1.010	1.216	1.383	1.486	1.86	2.22	2.6
174	2.478	2.283	100	100	64	0.815	0.982	1.092	1.157	1.42	1.59	1.7
175	2.478	2.316	100	100	64	1.041	1.286	1.386	1.548	1.89	2.13	2.3
176	2.408	2.209	100	100	64	1.053	1.372	1.576	1.590	2.03	2.41	2.3
177	2.408	2.217	100	100	64	0.758	0.954	1.096	1.193	1.47	1.65	1.8
178	2.423	2.246	100	100	64	1.024	1.081	1.333	1.346	1.61	1.86	1.8
179	2.423	2.248	100	100	64	0.592	0.708	0.771	0.838	0.98	1.13	1.2
180	2.423	2.249	100	100	64	0.992	1.186	1.396	1.477	1.74	1.95	2.1
181	2.443	2.243	100	100	64	0.845	1.076	1.021	0.909	1.06	1.21	1.5
182	2.443	2.259	100	100	64	0.673	0.779	0.847	0.899	1.04	1.11	1.2
183	2.443	2.260	100	100	64	0.796	0.918	0.999	1.029	1.16	1.25	1.3
184	2.443	2.248	100	100	64	0.824	1.033	1.152	1.217	1.38	1.87	2.2
185	2.443	2.236	100	100	64	0.595	0.717	0.793	0.868	1.00	1.10	1.2
186	2.443	2.250	100	100	64	0.846	1.085	1.189	1.262	1.55	1.78	2.0
187	2.487	2.319	100	100	64	0.471	0.614	0.695	0.739	0.82	0.97	1.0
188	2.487	2.324	100	100	64	0.542	0.576	0.610	0.656	0.80	0.87	1.0
189	2.487	2.330	100	100	64	0.546	0.620	0.671	0.697	0.82	0.93	1.0

Sample No.	Mix Design ID	HMA Type	Highway Name	ADT (million)	3/4 inch 19.0mm	1/2 inch 12.5mm	3/8 inch 9.5mm	No. 4 4.75 mm	No. 8 2.36 mm
190	3074-BCC-02130	S-4	US-60	2.2M	100	96	84	54	35
191	3074-BCC-02130	S-4	US-60	2.2M	100	96	84	54	35
192	3074-BCC-02130	S-4	US-60	2.2M	100	96	84	54	35
193	3074-APAC-20205	S-4	Various	3M+	97	94	90	57	34
194	3074-APAC-20205	S-4	Various	3M+	97	94	90	57	34
195	3074-APAC-20205	S-4	Various	3M+	97	94	90	57	34
196	3073-OAPA-22005	S-3	SH-33	13.9M	98	89	79	61	47
197	3073-OAPA-22005	S-3	SH-33	13.9M	98	89	79	61	47
198	3073-OAPA-22005	S-3	SH-33	13.9M	98	89	79	61	47
199	3072-CCC-02009	s-2 Rec	US-64	3M+	89	67	59	38	22
200	3072-CCC-02009	s-2 Rec	US-64	3M+	89	67	59	38	22
201	3072-CCC-02009	s-2 Rec	US-64	3M+	89	67	59	38	22
202	3072-CCC-02008	S-2 Rec	US-64	3M+	89	67	59	38	22
203	3072-CCC-02008	S-2 Rec	US-64	3M+	89	67	59	38	22
204	3073-EST-04516	S-3	SH-9	6.1M	99	88	81	67	47
205	3073-EST-04516	S-3	SH-9	6.1M	99	88	81	67	47
206	3074-OAPA-22059	S-4	SH-9	3M+	100	95	77	51	32
207	3074-OAPA-22059	S-4	SH-9	3M+	100	95	77	51	32
208	3074-EST-04914	S-4 Ins	SH74	1.8	100	98	87	65	54
209	3074-EST-04914	S-4 Ins	SH74	1.8	100	98	87	65	54
210	3012-AL02-83207	B inc	Varous	0.3M+	100	98	84	55	42
211	3012-AL02-83207	B inc	Varous	0.3M+	100	98	84	55	42
212	3012-AL02-83207	B inc	Varous	0.3M+	100	98	84	55	42
213	3074-OAPA-22043	S-4 Ins	SH-51	9.5	100	99	89	57	34
214	3074-OAPA-22043	S-4 Ins	SH-51	9.5	100	99	89	57	34
215	3074-OAPA-22043	S-4 Ins	SH-51	9.5	100	99	89	57	34
216	3074-HH02-93105	S4	US-270	0.7	100	98	89	63	42
217	3074-HH02-93105	S4	US-270	0.7	100	98	89	63	42
218	3072-EST-04923	S2 rec	US-281	6.9	90	77	71	61	42
219	3072-EST-04923	S2 rec	US-281	6.9	90	77	71	61	42
220	3072-EST-04923	S2 rec	US-281	6.9	90	77	71	61	42
221	3073-EST-04944	S3 rec	US-77	3.1	100	89	80	59	43
222	3073-EST-04944	S3 rec	US-77	3.1	100	89	80	59	43
223	3073-EST-04944	S3 rec	US-77	3.1	100	89	80	59	43
224	3073-EST-04975	S3	US-69	29.1	96	87	77	54	40
225	3073-EST-04975	S3	US-69	29.1	96	87	77	54	40
226	3073-EST-04975	S3	US-69	29.1	96	87	77	54	40
227	3073-EST-04948	S3 rec	US-77	3.1	100	89	80	59	43
228	3073-EST-04948	S3 rec	US-77	3.1	100	89	80	59	43
229	3073-EST-04948	S3 rec	US-77	3.1	100	89	80	59	43
230	3013-BCC-02134	C inc	various	0.3M+	100	100	98	71	48
231	3013-BCC-02134	C inc	various	0.3M+	100	100	98	71	48
232	3073-EST-05075	S-3 Rec	I40	56.34	95	86	77	51	37
233	3073-EST-05075	S-3 Rec	I40	56.34	95	86	77	51	37
234	3073-EST-05076	S-3 Rec	I-40	56.34	95	86	77	51	37
235	3073-EST-05076	S-3 Rec	I-40	56.34	95	86	77	51	37
236	3072-EST-05072	S-2 Rec	I-40	56.3	88	71	62	43	32
237	3072-EST-05072	S-2 Rec	I-40	56.3	88	71	62	43	32
238	3074-EST-05077	S-4 Rec	I-40	56.3	100	96	88	60	43
239	3074-EST-05077	S-4 Rec	I-40	56.3	100	96	88	60	43
240	3074-EST-05077	S-4 Rec	I-40	56.3	100	96	88	60	43
241	3074-EST-05074	S-4 Rec	I-40	56.3	100	96	88	60	43
242	3074-EST-05074	S-4 Rec	I-40	56.3	100	96	88	60	43
243	3074-EST-05074	S-4 Rec	I-40	56.3	100	96	88	60	43
244	3072-EST-05458	S-2 Rec	SH-33	6.7	87	68	62	51	38
245	3072-EST-05458	S-2 Rec	SH-33	6.7	87	68	62	51	38
246	3072-EST-05458	S-2 Rec	SH-33	6.7	87	68	62	51	38
247	3074-EST-05073	S-4 Ins	I-40	56.3	100	99	88	60	33
248	3074-EST-05073	S-4 Ins	I-40	56.3	100	99	88	60	33
249	3074-EST-05073	S-4 Ins	I-40	56.3	100	99	88	60	33
250	3012-BCC-02113	BH inc	I 40	3M+	100	95	82	55	40
251	3012-BCC-02113	BH inc	I 40	3M+	100	95	82	55	40
252	3012-BCC-02113	BH inc	I 40	3M+	100	95	82	55	40

Sample	No. 16	No. 30	No. 50	No. 100	No. 200	Asphalt			Aggregate		
No.	1.18mm	0.60mm	0.30mm	0.15 mm	0.075mm	Pb	PG	Gb	FAA	FF	G_{sb}
190	23	16	11	8	6.0	5.3	PG 64-22OK	1.0032	48.0	100	2.648
191	23	16	11	8	6.0	5.3	PG 64-22OK	1.0032	48.0	100	2.648
192	23	16	11	8	6.0	5.3	PG 64-22OK	1.0032	48.0	100	2.648
193	23	15	9	6	4.8	5.2	PG 64-22OK	1.0147	45.2	100	2.589
194	23	15	9	6	4.8	5.2	PG 64-22OK	1.0147	45.2	100	2.589
195	23	15	9	6	4.8	5.2	PG 64-22OK	1.0147	45.2	100	2.589
196	28	31	10	6	4.1	5.0	PG 64-22OK	1.0100	44.4	100	2.551
197	28	31	10	6	4.1	5.0	PG 64-22OK	1.0100	44.4	100	2.551
198	28	31	10	6	4.1	5.0	PG 64-22OK	1.0100	44.4	100	2.551
199	15	12	8	6	4.5	3.8	PG 64-22OK	1.0146	44.2	100	2.669
200	15	12	8	6	4.5	3.8	PG 70-28OK	1.0146	44.2	100	2.669
201	15	12	8	6	4.5	3.8	PG 76-28OK	1.0146	44.2	100	2.669
202	15	12	8	6	4.5	3.8	PG 76-28OK	1.0087	44.2	100	2.669
203	15	12	8	6	4.5	3.8	PG 76-28OK	1.0087	44.2	100	2.669
204	33	25	18	10	4.9	4.1	PG 70-28OK	1.0119	45.0	100	2.661
205	33	25	18	10	4.9	4.1	PG 70-28OK	1.0119	45.0	100	2.661
206	23	16	11	7	5.5	5.2	PG 64-22OK	1.0209	47.1	100	2.591
207	23	16	11	7	5.5	5.2	PG 64-22OK	1.0209	47.1	100	2.591
208	39	28	18	7	4.0	4.5	PG 76-28OK	1.0209	44.0	100	2.661
209	39	28	18	7	4.0	4.5	PG 76-28OK	1.0209	44.0	100	2.661
210	33	27	19	11	5.8	5.0	PG 76-28OK	1.0277	47.1	100	2.596
211	33	27	19	11	5.8	5.0	PG 64-22OK	1.0277	47.1	100	2.596
212	33	27	19	11	5.8	5.0	PG 70-28OK	1.0277	47.1	100	2.596
213	23	18	13	8	5.5	5.3	PG 70-28OK	1.0146	45.0	100	2.672
214	23	18	13	8	5.5	5.3	PG 64-22OK	1.0146	45.0	100	2.672
215	23	18	13	8	5.5	5.3	PG 70-28OK	1.0146	45.0	100	2.672
216	32	27	21	10	5.1	4.6	PG 70-28OK	1.0104	46.1	100	2.663
217	32	27	21	10	5.1	4.6	PG 70-28OK	1.0104	46.1	100	2.663
218	28	19	12	5	3.4	3.7	PG 76-28OK	1.0100	44.0	100	2.666
219	28	19	12	5	3.4	3.7	PG 76-28OK	1.0100	44.0	100	2.666
220	28	19	12	5	3.4	3.7	PG 76-28OK	1.0100	44.0	100	2.666
221	30	22	15	9	5.4	4.0	PG 64-22OK	1.0100	45.2	100	2.667
222	30	22	15	9	5.4	4.0	PG 64-22OK	1.0100	45.2	100	2.667
223	30	22	15	9	5.4	4.0	PG 64-22OK	1.0100	45.2	100	2.667
224	30	23	14	10	5.5	4.5	PG 64-22OK	1.0104	45.2	100	2.523
225	30	23	14	10	5.5	4.5	PG 76-28OK	1.0104	45.2	100	2.523
226	30	23	14	10	5.5	4.5	PG 76-28OK	1.0104	45.2	100	2.523
227	30	22	15	9	5.4	4.0	PG 76-28OK	1.0100	45.2	100	2.668
228	30	22	15	9	5.4	4.0	PG 64-22OK	1.0100	45.2	100	2.668
229	30	22	15	9	5.4	4.0	PG 64-22OK	1.0100	45.2	100	2.668
230	32	20	12	7	5.0	5.2	PG 64-22OK	1.0087	45.3	100	2.632
231	32	20	12	7	5.0	5.2	PG 64-22OK	1.0087	45.3	100	2.632
232	28	22	17	12	4.6	4.3	PG 64-22OK	1.0100	45.1	100	2.658
233	28	22	17	12	4.6	4.3	PG 64-22OK	1.0100	45.1	100	2.658
234	28	22	17	12	4.6	4.3	PG 70-28OK	1.0100	45.1	100	2.658
235	28	22	17	12	4.6	4.3	PG 70-28OK	1.0100	45.1	100	2.658
236	25	20	15	11	4.1	3.8	PG 70-28OK	1.0100	45.1	100	2.662
237	25	20	15	11	4.1	3.8	PG 70-28OK	1.0100	45.1	100	2.662
238	32	24	18	13	5.4	4.5	PG 70-28OK	1.0100	45.1	100	2.657
239	32	24	18	13	5.4	4.5	PG 70-28OK	1.0100	45.1	100	2.657
240	32	24	18	13	5.4	4.5	PG 70-28OK	1.0100	45.1	100	2.657
241	32	24	18	13	5.4	4.5	PG 70-28OK	1.0100	45.1	100	2.657
242	32	24	18	13	5.4	4.5	PG 64-22OK	1.0100	45.1	100	2.657
243	32	24	18	13	5.4	4.5	PG 64-22OK	1.0100	45.1	100	2.657
244	29	23	16	9	4.9	3.7	PG 76-28OK	1.0100	45.6	100	2.722
245	29	23	16	9	4.9	3.7	PG 76-28OK	1.0100	45.6	100	2.722
246	29	23	16	9	4.9	3.7	PG 76-28OK	1.0100	45.6	100	2.722
247	20	13	10	6	4.6	4.9	PG 76-28OK	1.0209	46.1	100	2.651
248	20	13	10	6	4.6	4.9	PG 70-28OK	1.0209	46.1	100	2.651
249	20	13	10	6	4.6	4.9	PG 70-28OK	1.0209	46.1	100	2.651
250	29	20	14	9	3.3	4.5	PG 70-28OK	1.0087	45.7	100	2.639
251	29	20	14	9	3.3	4.5	PG 70-28OK	1.0087	45.7	100	2.639
252	29	20	14	9	3.3	4.5	PG 70-28OK	1.0087	45.7	100	2.639

Sample	Mix		Parameters			Rut Depths (mm) at cycles						
No.	G_{mm}	G_{mb}	Wheel	Tire	Temp.	500-c	1000-c	1500-c	2000-c	4000-c	6000-c	8000-c
190	2.487	2.314	100	100	64	0.759	1.002	1.192	1.322	1.63	1.87	2.0
191	2.487	2.312	100	100	64	0.685	0.821	1.044	1.109	1.49	1.73	1.9
192	2.487	2.313	100	100	64	0.671	0.836	0.973	1.080	1.44	1.85	2.1
193	2.425	2.236	100	100	64	1.580	1.875	2.231	2.521	3.19	3.70	4.0
194	2.425	2.244	100	100	64	2.769	3.789	4.229	4.636	5.48	6.07	6.5
195	2.425	2.249	100	100	64	2.938	3.685	4.141	4.468	5.20	5.75	6.2
196	2.419	2.226	100	100	64	0.496	0.705	0.779	0.873	1.05	1.19	2.0
197	2.419	2.231	100	100	64	0.516	0.658	0.728	0.797	1.04	1.21	1.3
198	2.419	2.228	100	100	64	0.707	0.866	0.944	1.012	1.12	1.28	1.4
199	2.520	2.308	100	100	64	0.858	1.089	1.309	1.410	1.82	2.27	2.6
200	2.520	2.284	100	100	64	0.740	0.902	1.005	1.046	1.34	1.49	1.7
201	2.520	2.309	100	100	64	0.918	1.074	1.150	1.282	1.56	1.77	1.9
202	2.519	2.294	100	100	64	0.003	1.123	1.287	1.370	1.71	1.93	2.1
203	2.519	2.283	100	100	64	1.026	1.462	1.809	2.182	3.19	3.74	3.0
204	2.512	2.347	100	100	64	0.543	0.662	0.756	0.837	1.00	1.28	1.5
205	2.512	2.340	100	100	64	0.701	0.845	0.911	0.987	1.18	1.32	1.4
206	2.418	2.210	100	100	64	0.888	1.277	1.513	1.899	2.21	2.66	2.8
207	2.418	2.235	100	100	64	0.756	1.014	1.284	1.346	1.68	1.88	2.2
208	2.489	2.305	100	100	64	1.003	1.502	1.940	2.266	2.89	3.29	3.5
209	2.489	2.312	100	100	64	0.943	1.306	1.609	1.819	2.42	2.74	3.0
210	2.424	2.269	100	100	64	1.456	1.979	2.345	2.663	3.35	3.73	4.2
211	2.424	2.274	100	100	64	1.258	1.681	1.998	2.221	2.06	3.30	3.7
212	2.424	2.272	100	100	64	1.403	2.064	2.423	2.718	3.49	3.99	4.4
213	2.482	2.299	100	100	64	1.013	1.340	1.577	1.710	2.26	2.70	2.9
214	2.482	2.299	100	100	64	0.761	1.044	1.272	1.478	2.00	2.44	2.7
215	2.482	2.293	100	100	64	0.974	1.300	1.648	1.739	2.30	2.67	3.0
216	2.494	2.302	100	100	64	1.564	2.042	2.315	2.380	2.99	3.17	3.4
217	2.494	2.309	100	100	64	1.114	1.433	1.635	1.800	2.23	2.50	2.7
218	2.532	2.360	100	100	64	0.533	0.738	0.892	0.986	1.27	1.57	1.7
219	2.532	2.367	100	100	64	0.569	0.762	0.870	0.963	1.32	1.58	1.8
220	2.532	2.365	100	100	64	0.708	0.888	0.971	1.111	1.41	1.71	1.9
221	2.515	2.330	100	100	64	0.929	1.017	1.270	1.314	1.76	2.22	2.9
222	2.515	2.333	100	100	64	0.796	0.916	1.045	1.145	1.56	1.89	2.3
223	2.515	2.324	100	100	64	0.845	1.150	1.341	1.474	1.83	2.19	2.5
224	2.378	2.156	100	100	64	1.840	2.548	2.998	3.353	4.11	4.56	4.8
225	2.378	2.187	100	100	64	1.732	2.325	2.725	3.009	3.89	4.47	5.0
226	2.378	2.165	100	100	64	1.790	2.390	2.758	3.015	3.74	4.15	4.4
227	2.509	2.325	100	100	64	0.858	1.044	1.076	1.277	1.47	1.54	1.6
228	2.509	2.324	100	100	64	0.713	0.873	0.932	1.076	1.28	1.38	1.6
229	2.509	2.331	100	100	64	0.593	0.741	0.809	0.893	1.09	1.21	1.3
230	2.431	2.278	100	100	64	1.450	1.820	2.101	2.298	2.80	3.10	3.3
231	2.431	2.281	100	100	64	0.955	1.280	1.549	1.697	2.12	2.38	2.6
232	2.504	2.405	100	100	64	0.592	0.739	0.795	0.872	1.02	1.13	1.2
233	2.504	2.430	100	100	64	1.014	1.348	1.636	1.814	2.49	2.92	3.2
234	2.504	2.373	100	100	64	1.179	1.492	1.730	1.934	2.45	2.73	3.0
235	2.504	2.358	100	100	64	0.598	0.735	0.798	0.895	1.02	1.09	1.2
236	2.524	2.347	100	100	64	0.499	0.606	0.633	0.747	0.92	1.04	1.2
237	2.524	2.364	100	100	64	0.491	0.611	0.632	0.689	0.93	1.13	1.2
238	2.484	2.312	100	100	64	0.335	0.394	0.378	0.427	0.53	0.62	0.7
239	2.484	2.278	100	100	64	0.382	0.379	0.385	0.438	0.50	0.56	0.6
240	2.484	2.249	100	100	64	0.673	0.759	0.823	0.870	0.97	1.13	1.2
241	2.487	2.330	100	100	64	0.531	0.761	0.787	0.850	1.00	1.03	1.1
242	2.487	2.336	100	100	64	0.605	0.739	0.786	0.840	0.97	1.09	1.1
243	2.487	2.329	100	100	64	0.512	0.670	0.747	0.773	0.94	1.04	1.1
244	2.591	2.420	100	100	64	0.921	1.283	1.510	1.663	2.22	2.73	3.2
245	2.591	2.431	100	100	64	0.956	1.241	1.481	1.613	2.14	2.53	2.9
246	2.591	2.419	100	100	64	0.803	1.077	1.257	1.393	1.86	2.18	2.5
247	2.471	2.302	100	100	64	0.612	0.808	0.900	1.053	1.40	1.72	2.0
248	2.471	2.308	100	100	64	0.495	0.673	0.734	0.810	0.98	1.18	1.3
249	2.471	2.300	100	100	64	0.469	0.585	0.643	0.683	0.86	0.97	1.1
250	2.460	2.301	100	100	64	1.402	1.806	2.022	2.317	2.96	3.44	3.9
251	2.460	2.306	100	100	64	1.411	1.865	2.093	2.275	2.77	3.08	3.3
252	2.460	2.305	100	100	64	0.992	1.278	1.449	1.592	1.97	2.27	2.5

Sample No.	Mix Design ID	HMA Type	Highway Name	ADT (million)	3/4 inch 19.0mm	1/2 inch 12.5mm	3/8 inch 9.5mm	No. 4 4.75 mm	No. 8 2.36 mm
253	3012-OAPA-21108	B inc	SH-11	0.3M+	100	93	86	61	40
254	3012-OAPA-21108	B inc	SH-11	0.3M+	100	93	86	61	40
255	3012-OAPA-21108C	B inc	SH-11	0.3M+	100	93	86	61	40
256	3012-OAPA-21108C	B inc	SH-11	0.3M+	100	93	86	61	40
257	3074-EST-06368	S-4 Ins	US-281	6.9	100	98	89	66	49
258	3074-EST-06368	S-4 Ins	US-281	6.9	100	98	89	66	49
259	3074-EST-06368	S-4 Ins	US-281	6.9	100	98	89	66	49
260	3075-EST-06062	S-5 Ins	SH-53	0.3M+	100	100	100	89	62
261	3075-EST-06062	S-5 Ins	SH-53	0.3M+	100	100	100	89	62
262	3075-EST-06062	S-5 Ins	SH-53	0.3M+	100	100	100	89	62
263	3074-EST-06084	S-4 Ins	SH-53	0.3M+	100	97	81	48	34
264	3074-EST-06084	S-4 Ins	SH-53	0.3M+	100	97	81	48	34
265	3074-EST-06084	S-4 Ins	SH-53	0.3M+	100	97	81	48	34
266	3073-EST-05719	S-3 Rec	I-35	54.8	96	81	71	61	39
267	3073-EST-05719	S-3 Rec	I-35	54.8	96	81	71	61	39
268	3073-EST-05719	S-3 Rec	I-35	54.8	96	81	71	61	39
269	3074-EST-05702	S-4 Rec	I-35	54	100	97	87	66	42
270	3074-EST-05702	S-4 Rec	I-35	54	100	97	87	66	42
271	3074-EST-05702	S-4 Rec	I-35	54	100	97	87	66	42
272	3072-EST-05016	S-2 Rec	Various	3M+	90	74	67	52	34
273	3072-EST-05016	S-2 Rec	Various	3M+	90	74	67	52	34
274	3073-EST-04977	S-3	Various	3M+	100	87	73	52	39
275	3073-EST-04977	S-3	Various	3M+	100	87	73	52	39
276	3073-EST-04977	S-3	Various	3M+	100	87	73	52	39
277	3074-EST-04976	S-4 Bnd	Various	3M+	100	94	90	60	42
278	3074-EST-04976	S-4 Bnd	Various	3M+	100	94	90	60	42
279	3074-EST-04976	S-4 Bnd	Various	3M+	100	94	90	60	42
280	3074-EST-04970	S-4 Ins	Various	3M+	100	93	86	58	41
281	3074-EST-04970	S-4 Ins	Various	3M+	100	93	86	58	41
282	3074-EST-04970	S-4 Ins	Various	3M+	100	93	86	58	41
283	3073-EST-05461	S-3 Rec	SH-33	6.7	94	83	73	57	42
284	3073-EST-05461	S-3 Rec	SH-33	6.7	94	83	73	57	42
285	3074-EST-05456	S-4 Rec	SH-33	6.7	100	97	85	65	46
286	3074-EST-05456	S-4 Rec	SH-33	6.7	100	97	85	65	46
287	3074-EST-05456	S-4 Rec	SH-33	6.7	100	97	85	65	46
288	3073-EST-05460	S-3 Rec	SH-33	6.7	94	83	73	57	42
289	3073-EST-05460	S-3 Rec	SH-33	6.7	94	83	73	57	42
290	3073-EST-05460	S-3 Rec	SH-33	6.7	94	83	73	57	42
291	3074-EST-05457	S-4 Ins	SH-33	6.7	100	97	86	64	44
292	3074-EST-05457	S-4 Ins	SH-33	6.7	100	97	86	64	44
293	3074-EST-05457	S-4 Ins	SH-33	6.7	100	97	86	64	44
294	3073-OAPA-22092	S-3 Rec	SH-51	4.7	99	85	75	48	29
295	3073-OAPA-22092	S-3 Rec	SH-51	4.7	99	85	75	48	29
296	3073-OAPA-22092	S-3 Rec	SH-51	4.7	99	85	75	48	29
297	3072-OAPA-22077	S-2 Rec	SH-51	4.7	89	79	74	46	24
298	3072-OAPA-22077	S-2 Rec	SH-51	4.7	89	79	74	46	24
299	3072-OAPA-22077	S-2 Rec	SH-51	4.7	89	79	74	46	24
300	3073-OAPA-22091	S-3 Rec	SH-51	4.7	99	85	75	48	29
301	3073-OAPA-22091	S-3 Rec	SH-51	4.7	99	85	75	48	29
302	3073-OAPA-22091	S-3 Rec	SH-51	4.7	99	85	75	48	29
303	3074-OAPA-22093	S-4	SH-51	3M+	100	94	90	64	34
304	3074-OAPA-22093	S-4	SH-51	3M+	100	94	90	64	34
305	3074-OAPA-22093	S-4	SH-51	3M+	100	94	90	64	34
306	3074-OAPA-22094	S-4	SH-51	4.7	100	93	87	63	31
307	3074-OAPA-22094	S-4	SH-51	4.7	100	93	87	63	31
308	3074-OAPA-22094	S-4	SH-51	4.7	100	93	87	63	31
309	3072-OAPA-22122	S-2 Rec	SH-51	4.7	87	79	74	43	23
310	3072-OAPA-22122	S-2 Rec	SH-51	4.7	87	79	74	43	23
311	3072-OAPA-22122	S-2 Rec	SH-51	4.7	87	79	74	43	23
312	3074-EST-05622	S-4 Ins	SH-29	1.2	100	97	84	59	44
313	3074-EST-05622	S-4 Ins	SH-29	1.2	100	97	84	59	44
314	3074-EST-05622	S-4 Ins	SH-29	1.2	100	97	84	59	44
315	3074-EST-06060	S-4 Ins	SH-76	0.9	100	98	88	59	44

Sample	No. 16	No. 30	No. 50	No. 100	No. 200	Asphalt			Aggregate		
No.	1.18mm	0.60mm	0.30mm	0.15 mm	0.075mm	Pb	PG	Gb	FAA	FF	G_{sb}
253	28	19	12	7	5.2	5.0	PG 70-28OK	1.0092	45.7	100	2.614
254	28	19	12	7	5.2	5.0	PG 70-28OK	1.0092	45.7	100	2.614
255	28	19	12	7	5.2	5.0	PG 70-28OK	1.0092	45.6	100	2.614
256	28	19	12	7	5.2	5.0	PG 70-28OK	1.0092	45.6	100	2.614
257	33	26	21	8	4.2	4.7	PG 70-28OK	1.0209	46.0	100	2.648
258	33	26	21	8	4.2	4.7	PG 64-22OK	1.0209	46.0	100	2.648
259	33	26	21	8	4.2	4.7	PG 64-22OK	1.0209	46.0	100	2.648
260	42	31	21	11	6.7	5.9	PG 64-22OK	1.0128	45.0	100	2.645
261	42	31	21	11	6.7	5.9	PG 64-22OK	1.0128	45.0	100	2.645
262	42	31	21	11	6.7	5.9	PG 64-22OK	1.0128	45.0	100	2.645
263	23	18	13	7	3.7	4.9	PG 64-22OK	1.0128	43.2	100	2.660
264	23	18	13	7	3.7	4.9	PG 64-22OK	1.0128	43.2	100	2.660
265	23	18	13	7	3.7	4.9	PG 64-22OK	1.0128	43.2	100	2.660
266	30	24	18	9	4.8	4.4	PG 64-22OK	1.0100	45.2	100	2.669
267	30	24	18	9	4.8	4.4	PG 64-22OK	1.0100	45.2	100	2.669
268	30	24	18	9	4.8	4.4	PG 64-22OK	1.0100	45.2	100	2.669
269	33	26	20	10	5.3	5.0	PG 70-28OK	1.0100	45.6	100	2.662
270	33	26	20	10	5.3	5.0	PG 70-28OK	1.0100	45.6	100	2.662
271	33	26	20	10	5.3	5.0	PG 70-28OK	1.0100	45.6	100	2.662
272	27	22	17	8	4.7	4.1	PG 64-22OK	1.0100	46.1	100	2.678
273	27	22	17	8	4.7	4.1	PG 64-22OK	1.0100	46.1	100	2.678
274	30	24	19	11	6.0	4.0	PG 64-22OK	1.0253	45.2	100	2.654
275	30	24	19	11	6.0	4.0	PG 64-22OK	1.0253	45.2	100	2.654
276	30	24	19	11	6.0	4.0	PG 70-28OK	1.0253	45.2	100	2.654
277	32	25	19	12	6.4	4.6	PG 76-28OK	1.0253	45.4	100	2.653
278	32	25	19	12	6.4	4.6	PG 76-28OK	1.0253	45.4	100	2.653
279	32	25	19	12	6.4	4.6	PG 64-22OK	1.0253	45.4	100	2.653
280	32	25	19	12	6.3	4.6	PG 64-22OK	1.0209	45.9	100	2.636
281	32	25	19	12	6.3	4.6	PG 76-28OK	1.0209	45.9	100	2.636
282	32	25	19	12	6.3	4.6	PG 76-28OK	1.0209	45.9	100	2.636
283	32	25	17	9	5.2	3.9	PG 76-28OK	1.0100	45.6	100	2.685
284	32	25	17	9	5.2	3.9	PG 64-22OK	1.0100	45.6	100	2.685
285	34	26	19	11	6.4	5.0	PG 64-22OK	1.0100	45.3	100	2.659
286	34	26	19	11	6.4	5.0	PG 64-22OK	1.0100	45.3	100	2.659
287	34	26	19	11	6.4	5.0	PG 64-22OK	1.0100	45.3	100	2.659
288	32	25	17	9	5.2	3.9	PG 64-22OK	1.0100	45.6	100	2.685
289	32	25	17	9	5.2	3.9	PG 64-22OK	1.0100	45.6	100	2.685
290	32	25	17	9	5.2	3.9	PG 64-22OK	1.0100	45.6	100	2.685
291	33	25	18	10	4.8	4.9	PG 64-22OK	1.0209	45.3	100	2.659
292	33	25	18	10	4.8	4.9	PG 76-28OK	1.0209	45.3	100	2.659
293	33	25	18	10	4.8	4.9	PG 76-28OK	1.0209	45.3	100	2.659
294	19	12	7	5	3.7	4.7	PG 76-28OK	1.0100	49.3	100	2.563
295	19	12	7	5	3.7	4.7	PG 64-22OK	1.0100	49.3	100	2.563
296	19	12	7	5	3.7	4.7	PG 64-22OK	1.0100	49.3	100	2.563
297	16	10	6	4	3.3	4.7	PG 64-22OK	1.0100	44.8	100	2.542
298	16	10	6	4	3.3	4.7	PG 64-22OK	1.0100	44.8	100	2.542
299	16	10	6	4	3.3	4.7	PG 64-22OK	1.0100	44.8	100	2.542
300	19	12	7	5	3.7	4.7	PG 64-22OK	1.0100	49.3	100	2.563
301	19	12	7	5	3.7	4.7	PG 64-22OK	1.0100	49.3	100	2.563
302	19	12	7	5	3.7	4.7	PG 64-22OK	1.0100	49.3	100	2.563
303	21	14	8	5	4.1	5.4	PG 64-22OK	1.0104	46.4	100	2.546
304	21	14	8	5	4.1	5.4	PG 70-28OK	1.0104	46.4	100	2.546
305	21	14	8	5	4.1	5.4	PG 70-28OK	1.0104	46.4	100	2.546
306	18	11	7	5	3.8	5.6	PG 70-28OK	1.0104	46.1	100	2.545
307	18	11	7	5	3.8	5.6	PG 64-22OK	1.0104	46.1	100	2.545
308	18	11	7	5	3.8	5.6	PG 64-22OK	1.0104	46.1	100	2.545
309	15	10	7	5	3.7	4.5	PG 64-22OK	1.0100	46.2	100	2.544
310	15	10	7	5	3.7	4.5	PG 64-22OK	1.0100	46.2	100	2.544
311	15	10	7	5	3.7	4.5	PG 64-22OK	1.0100	46.2	100	2.544
312	34	27	17	8	4.7	4.9	PG 64-22OK	1.0168	46.2	100	2.656
313	34	27	17	8	4.7	4.9	PG 76-28OK	1.0168	46.2	100	2.656
314	34	27	17	8	4.7	4.9	PG 76-28OK	1.0168	46.2	100	2.656
315	33	25	17	8	4.9	4.8	PG 76-28OK	1.0193	45.2	100	2.646

Sample	Mix		Parameters			Rut Depths (mm) at cycles						
No.	G_{mm}	G_{mb}	Wheel	Tire	Temp.	500-c	1000-c	1500-c	2000-c	4000-c	6000-c	8000-c
253	2.447	2.280	100	100	64	2.004	2.899	3.244	3.542	4.34	4.90	5.2
254	2.447	2.283	100	100	64	1.533	2.356	2.789	3.076	3.82	4.38	4.8
255	2.415	2.253	100	100	64	1.568	2.124	2.489	2.746	3.49	3.99	4.4
256	2.415	2.257	100	100	64	1.361	1.815	2.138	2.422	3.09	3.63	4.0
257	2.476	2.307	100	100	64	0.841	1.118	1.343	1.483	2.03	2.34	2.6
258	2.476	2.305	100	100	64	0.765	1.061	1.294	1.499	2.17	2.56	2.9
259	2.476	2.312	100	100	64	0.544	0.740	0.920	1.162	1.64	1.82	2.0
260	2.437	2.227	100	100	64	1.695	2.766	3.491	4.010	5.24	5.85	6.3
261	2.437	2.239	100	100	64	1.671	2.357	2.785	3.115	3.90	4.40	4.7
262	2.437	2.237	100	100	64	1.497	2.264	2.895	3.403	4.62	5.20	5.6
263	2.470	2.288	100	100	64	1.811	3.182	4.266	4.993	6.31	6.91	7.3
264	2.470	2.295	100	100	64	1.322	1.884	2.288	2.551	3.26	3.74	4.1
265	2.470	2.291	100	100	64	1.719	2.969	3.922	4.518	5.74	6.51	7.0
266	2.504	2.344	100	100	64	0.430	0.509	0.575	0.575	0.69	0.78	0.8
267	2.504	2.338	100	100	64	0.563	0.640	0.717	0.765	0.88	0.97	1.0
268	2.504	2.362	100	100	64	0.313	0.360	0.395	0.472	0.54	0.60	0.7
269	2.479	2.318	100	100	64	0.364	0.438	0.442	0.487	0.60	0.70	0.8
270	2.479	2.296	100	100	64	0.379	0.413	0.468	0.487	0.58	0.63	0.7
271	2.479	2.286	100	100	64	0.353	0.365	0.376	0.396	0.46	0.55	0.6
272	2.432	2.336	100	100	64	1.376	1.869	2.204	2.475	3.36	4.00	4.5
273	2.432	2.331	100	100	64	1.191	1.604	1.930	2.194	2.96	3.41	3.7
274	2.502	2.287	100	100	64	0.850	1.097	1.125	1.212	1.53	1.79	1.9
275	2.502	2.301	100	100	64	0.552	0.701	0.767	0.854	0.96	1.09	1.2
276	2.502	2.297	100	100	64	0.650	0.746	0.831	0.898	1.07	1.22	1.3
277	2.489	2.311	100	100	64	0.649	0.759	0.913	0.960	1.12	1.30	1.4
278	2.489	2.317	100	100	64	0.551	0.662	0.742	0.794	0.98	1.08	1.2
279	2.489	2.302	100	100	64	0.559	0.709	0.817	0.915	1.14	1.31	1.5
280	2.472	2.274	100	100	64	0.740	0.806	0.861	0.969	1.18	1.34	1.4
281	2.472	2.276	100	100	64	0.609	0.697	0.732	0.799	0.90	1.00	1.1
282	2.472	2.275	100	100	64	0.559	0.661	0.742	0.784	0.96	1.04	1.1
283	2.533	2.355	100	100	64	0.997	1.414	1.737	2.048	3.11	4.03	4.7
284	2.533	2.333	100	100	64	1.951	2.414	2.792	3.074	3.82	4.32	4.7
285	2.488	2.334	100	100	64	0.524	0.727	0.772	0.847	1.17	1.44	1.7
286	2.488	2.341	100	100	64	0.781	0.915	1.042	1.139	1.46	1.74	2.0
287	2.488	2.343	100	100	64	0.547	0.716	0.909	0.982	1.30	1.68	2.0
288	2.533	2.375	100	100	64	0.676	0.834	0.991	1.102	1.47	1.87	2.2
289	2.533	2.368	100	100	64	0.760	0.952	1.127	1.272	1.72	2.16	2.7
290	2.533	2.386	100	100	64	0.521	0.655	0.770	0.827	1.13	1.36	1.6
291	2.491	2.320	100	100	64	0.650	0.874	0.971	1.094	1.44	1.70	2.0
292	2.491	2.312	100	100	64	0.870	1.074	1.246	1.404	1.80	2.16	2.5
293	2.491	2.312	100	100	64	0.672	0.928	1.123	1.239	1.71	2.07	2.4
294	2.432	2.256	100	100	64	1.628	2.017	2.285	2.446	2.94	3.36	3.5
295	2.432	2.256	100	100	64	0.810	1.025	1.165	1.273	1.58	1.77	1.9
296	2.432	2.255	100	100	64	0.827	1.041	1.188	1.301	1.67	1.91	2.1
297	2.445	2.262	100	100	64	0.800	1.086	1.253	1.502	2.07	2.71	3.0
298	2.445	2.260	100	100	64	0.913	1.054	1.227	1.354	1.78	2.30	2.7
299	2.445	2.259	100	100	64	0.688	0.756	0.863	0.952	1.35	1.64	1.8
300	2.432	2.226	100	100	64	0.409	0.423	0.460	0.527	0.62	0.96	1.2
301	2.432	2.231	100	100	64	0.578	0.755	0.819	0.871	1.08	1.21	1.4
302	2.432	2.225	100	100	64	0.631	0.859	0.941	0.998	1.20	1.35	1.5
303	2.404	2.214	100	100	64	2.057	2.703	3.165	3.529	4.06	4.50	4.9
304	2.404	2.217	100	100	64	1.639	2.293	2.674	2.958	3.69	4.08	4.4
305	2.404	2.216	100	100	64	1.744	2.352	2.790	3.054	3.85	4.38	4.7
306	2.404	2.206	100	100	64	1.855	2.236	2.495	2.714	3.14	3.50	3.8
307	2.404	2.209	100	100	64	1.259	1.600	1.780	1.890	2.27	2.54	2.7
308	2.404	2.213	100	100	64	1.400	1.962	2.339	2.615	3.42	3.79	4.2
309	2.433	2.247	100	100	64	1.025	1.328	1.561	1.769	2.46	2.89	3.2
310	2.433	2.252	100	100	64	0.902	1.195	1.408	1.619	2.16	2.56	2.8
311	2.433	2.251	100	100	64	0.742	0.919	1.021	1.160	1.41	1.58	1.7
312	2.488	2.300	100	100	64	0.622	0.729	0.799	0.931	1.13	1.26	1.4
313	2.488	2.298	100	100	64	0.534	0.679	0.752	0.860	1.07	1.21	1.3
314	2.488	2.295	100	100	64	0.727	0.869	0.961	1.052	1.23	1.34	1.5
315	2.481	2.315	100	100	64	0.461	0.579	0.663	0.710	0.93	1.04	1.1

Sample No.	Mix Design ID	HMA Type	Highway Name	ADT (million)	3/4 inch 19.0mm	1/2 inch 12.5mm	3/8 inch 9.5mm	No. 4 4.75 mm	No. 8 2.36 mm
316	3074-EST-06060	S-4 Ins	SH-76	0.9	100	98	88	59	44
317	3074-EST-06060	S-4 Ins	SH-76	0.9	100	98	88	59	44
318	3075-EST-06061	S-5 Ins	SH-76	0.9	100	100	99	80	55
319	3075-EST-06061	S-5 Ins	SH-76	0.9	100	100	99	80	55
320	3075-EST-06061	S-5 Ins	SH-76	0.9	100	100	99	80	55
321	3073-EST-06369	S3 rec	SH-76	0.9	97	82	73	53	38
322	3073-EST-06369	S3 rec	SH-76	0.9	97	82	73	53	38
323	3073-EST-06369	S3 rec	SH-76	0.9	97	82	73	53	38
324	3075-EST-06216	S5 inc	I 44	13.67	100	100	100	86	66
325	3075-EST-06216	S5 inc	I 44	13.67	100	100	100	86	66
326	3075-EST-06216	S5 inc	I 44	13.67	100	100	100	86	66
327	3074-EST-06215	S4 inc	I 44	13.67	100	98	87	66	52
328	3074-EST-06215	S4 inc	I 44	13.67	100	98	87	66	52
329	3074-EST-06215	S4 inc	I 44	13.67	100	98	87	66	52
330	3073-EST-05579	S3 rec	SH-4	4.5	98	90	79	63	43
331	3073-EST-05579	S3 rec	SH-4	4.5	98	90	79	63	43
332	3073-EST-05579	S3 rec	SH-4	4.5	98	90	79	63	43
333	3073-EST-05546	S3 rec	I 40	76.72	99	88	80	62	45
334	3073-EST-05546	S3 rec	I 40	76.72	99	88	80	62	45
335	3073-EST-05546	S3 rec	I 40	76.72	99	88	80	62	45
336	3074-EST-05578	S4 inc	I 40	76.72	100	97	86	62	47
337	3074-EST-05578	S4 inc	I 40	76.72	100	97	86	62	47
338	3074-EST-05578	S4 inc	I 40	76.72	100	97	86	62	47
339	3074-EST-05551	S4 inc	SH-4	4.5	100	98	88	75	50
340	3074-EST-05551	S4 inc	SH-4	4.5	100	98	88	75	50
341	3074-EST-05551	S4 inc	SH-4	4.5	100	98	88	75	50
342	3074-EST-06314	S4 inc	county	1.7	100	99	90	67	48
343	3074-EST-06314	S4 inc	county	1.7	100	99	90	67	48
344	3074-EST-05413	S4 inc	SH-2	3M+	100	93	85	75	55
345	3074-EST-05413	S4 inc	SH-2	3M+	100	93	85	75	55
346	3074-EST-05413	S4 inc	SH-2	3M+	100	93	85	75	55
347	3073-CCC-01012	S3 Inc	Varous	3M+	90	78	73	56	37
348	3073-CCC-01012	S3 Inc	Varous	3M+	90	78	73	56	37
349	3074-EST-05850	S4 inc	I 40	50.7	100	93	84	75	56
350	3074-EST-05850	S4 inc	I 40	50.7	100	93	84	75	56
351	3074-EST-05851	S4 inc	I 40	50.7	100	93	84	75	56
352	3074-EST-05851	S4 inc	I 40	50.7	100	93	84	75	56
353	3074-EST-05851	S4 inc	I 40	50.7	100	93	84	75	56
354	3073-EST-05852	S3	I-40	50.7	100	87	72	58	45
355	3073-EST-05852	S3	I-40	50.7	100	87	72	58	45
356	3073-EST-05852	S3	I-40	50.7	100	87	72	58	45
357	3074-AL02-83128	S4 ins	county	0.9	100	97	86	61	46
358	3074-AL02-83128	S4 ins	county	0.9	100	97	86	61	46
359	3074-AL02-83128	S4 ins	county	0.9	100	97	86	61	46
360	3073-EST-05852	S3	US60	4.31	100	87	75	44	28
361	3073-EST-05852	S3	US60	4.31	100	87	75	44	28
362	3073-EST-05852	S3	US60	4.31	100	87	75	44	28
363	3073-EST-05852	S3	US60	4.31	100	87	75	44	28
364	3073-EST-05852	S3	US60	4.31	100	87	75	44	28
365	3073-EST-05852	S3	US60	4.31	100	87	75	44	28
366	3074-EST-05821	S4 rec	US60	4.3	100	94	86	47	32
367	3074-EST-05821	S4 rec	US60	4.3	100	94	86	47	32
368	3074-EST-05821	S4 rec	US60	4.3	100	94	86	47	32
369	3074-EST-06234	S3 rec	I 40	3	99	86	78	63	46
370	3074-EST-06234	S3 rec	I 40	3	99	86	78	63	46
371	3074-EST-06234	S3 rec	I 40	3	99	86	78	63	46
372	3074-EST-06233	S4 Ins	I 40	3	100	98	89	66	48
373	3074-EST-06233	S4 Ins	I 40	3	100	98	89	66	48
374	3074-EST-06233	S4 Ins	I 40	3	100	98	89	66	48
375	30072-CCC-02033	25 mm	SH-3	3	89	81	74	50	29
376	30072-CCC-02033	25 mm	SH-3	3	89	81	74	50	29
377	30072-CCC-02033	25 mm	SH-3	3	89	81	74	50	29
378	3073-CCC-02034	19 mm Inc	SH-3	3	97	90	86	57	33

Sample	No. 16	No. 30	No. 50	No. 100	No. 200	Asphalt			Aggregate		
No.	1.18mm	0.60mm	0.30mm	0.15 mm	0.075mm	Pb	PG	Gb	FAA	FF	G_{sb}
316	33	25	17	8	4.9	4.8	PG 76-28OK	1.0193	45.2	100	2.646
317	33	25	17	8	4.9	4.8	PG 76-28OK	1.0193	45.2	100	2.646
318	43	30	21	8	5.2	5.6	PG 76-28OK	1.0193	45.0	100	2.638
319	43	30	21	8	5.2	5.6	PG 64-22OK	1.0193	45.0	100	2.638
320	43	30	21	8	5.2	5.6	PG 64-22OK	1.0193	45.0	100	2.638
321	29	23	16	8	5.0	4.1	PG 64-22OK	1.0100	44.8	100	2.629
322	29	23	16	8	5.0	4.1	PG 64-22OK	1.0100	44.8	100	2.629
323	29	23	16	8	5.0	4.1	PG 64-22OK	1.0100	44.8	100	2.629
324	45	31	20	9	5.8	5.9	PG 64-22OK	1.0295	45.3	100	2.650
325	45	31	20	9	5.8	5.9	PG 64-22OK	1.0295	45.3	100	2.650
326	45	31	20	9	5.8	5.9	PG 64-22OK	1.0295	45.3	100	2.650
327	36	26	17	7	4.3	4.9	PG 64-22OK	1.0295	45.2	100	2.649
328	36	26	17	7	4.3	4.9	PG 64-22OK	1.0295	45.2	100	2.649
329	36	26	17	7	4.3	4.9	PG 64-22OK	1.0295	45.2	100	2.649
330	31	23	16	8	4.6	4.2	PG 70-28OK	1.0100	45.3	100	2.681
331	31	23	16	8	4.6	4.2	PG 70-28OK	1.0100	45.3	100	2.681
332	31	23	16	8	4.6	4.2	PG 70-28OK	1.0100	45.3	100	2.681
333	31	23	17	11	5.5	4.0	PG 64-22OK	1.0100	45.5	100	2.674
334	31	23	17	11	5.5	4.0	PG 64-22OK	1.0100	45.5	100	2.674
335	31	23	17	11	5.5	4.0	PG 64-22OK	1.0100	45.5	100	2.674
336	33	24	18	11	4.6	4.6	PG 64-22OK	1.0100	45.4	100	2.667
337	33	24	18	11	4.6	4.6	PG 64-22OK	1.0100	45.4	100	2.667
338	33	24	18	11	4.6	4.6	PG 64-22OK	1.0100	45.4	100	2.667
339	33	24	16	8	5.1	4.7	PG 64-22OK	1.0032	45.4	100	2.653
340	33	24	16	8	5.1	4.7	PG 64-22OK	1.0032	45.4	100	2.653
341	33	24	16	8	5.1	4.7	PG 70-28OK	1.0032	45.4	100	2.653
342	33	24	18	7	4.2	4.7	PG 70-28OK	1.0151	44.1	100	2.653
343	33	24	18	7	4.2	4.7	PG 70-28OK	1.0151	44.1	100	2.653
344	42	32	19	10	6.7	5.2	PG 70-28OK	1.0209	45.0	100	2.509
345	42	32	19	10	6.7	5.2	PG 70-28OK	1.0209	45.0	100	2.509
346	42	32	19	10	6.7	5.2	PG 70-28OK	1.0209	45.0	100	2.509
347	25	19	14	6	2.8	4.5	PG 70-28OK	1.0093	45.5	100	2.689
348	25	19	14	6	2.8	4.5	PG 64-22OK	1.0093	45.5	100	2.689
349	42	32	19	10	6.9	5.1	PG 64-22OK	1.0253	45.3	100	2.512
350	42	32	19	10	6.9	5.1	PG 64-22OK	1.0253	45.3	100	2.512
351	42	32	19	10	6.9	5.1	PG 70-28OK	1.0253	45.3	100	2.512
352	42	32	19	10	6.9	5.1	PG 64-22OK	1.0253	45.3	100	2.512
353	42	32	19	10	6.9	5.1	PG 64-22OK	1.0253	45.3	100	2.512
354	34	26	16	9	5.8	4.7	PG 64-22OK	1.0253	45.0	100	2.517
355	34	26	16	9	5.8	4.7	PG 70-28OK	1.0253	45.0	100	2.517
356	34	26	16	9	5.8	4.7	PG 70-28OK	1.0253	45.0	100	2.517
357	35	27	18	11	6.9	4.5	PG 70-28OK	1.0087	43.8	100	2.640
358	35	27	18	11	6.9	4.5	PG 70-28OK	1.0087	43.8	100	2.640
359	35	27	18	11	6.9	4.5	PG 70-28OK	1.0087	43.8	100	2.640
360	20	14	11	7	5.9	4.4	PG 64-22OK	1.0146	45.2	100	2.660
361	20	14	11	7	5.9	4.4	PG 64-22OK	1.0146	45.2	100	2.660
362	20	14	11	7	5.9	4.4	PG 64-22OK	1.0146	45.2	100	2.660
363	20	14	11	7	5.9	4.4	PG 64-22OK	1.0147	45.2	100	2.660
364	20	14	11	7	5.9	4.4	PG 64-22OK	1.0147	45.2	100	2.660
365	20	14	11	7	5.9	4.4	PG 64-22OK	1.0147	45.2	100	2.660
366	24	18	13	8	5.0	4.6	PG 64-22OK	1.0100	45.1	100	2.653
367	24	18	13	8	5.0	4.6	PG 64-22OK	1.0100	45.1	100	2.653
368	24	18	13	8	5.0	4.6	PG 64-22OK	1.0100	45.1	100	2.653
369	31	23	18	11	5.9	4.1	PG 64-22OK	1.0100	45.3	100	2.663
370	31	23	18	11	5.9	4.1	PG 64-22OK	1.0100	45.3	100	2.663
371	31	23	18	11	5.9	4.1	PG 70-28OK	1.0100	45.3	100	2.663
372	33	24	18	7	4.2	4.8	PG 70-28OK	1.0295	45.1	100	2.648
373	33	24	18	7	4.2	4.8	PG 70-28OK	1.0295	45.1	100	2.648
374	33	24	18	7	4.2	4.8	PG 64-22OK	1.0295	45.1	100	2.648
375	22	19	16	8	5.0	3.9	PG 64-22OK	1.0087	46.4	100	2.668
376	22	19	16	8	5.0	3.9	PG 64-22OK	1.0087	46.4	100	2.668
377	22	19	16	8	5.0	3.9	PG 64-22OK	1.0087	46.4	100	2.668
378	25	22	19	9	5.4	4.5	PG 64-22OK	1.0087	46.5	100	2.645

Sample	Mix		Parameters			Rut Depths (mm) at cycles						
No.	G_{mm}	G_{mb}	Wheel	Tire	Temp.	500-c	1000-c	1500-c	2000-c	4000-c	6000-c	8000-c
316	2.481	2.310	100	100	64	0.616	0.812	0.951	1.067	1.44	1.72	1.9
317	2.481	2.314	100	100	64	0.900	1.131	1.312	1.451	1.85	2.15	2.4
318	2.454	2.290	100	100	64	0.746	0.929	1.034	1.162	1.50	1.73	2.0
319	2.454	2.282	100	100	64	0.677	0.832	0.938	1.051	1.42	1.67	2.0
320	2.454	2.287	100	100	64	0.645	0.782	0.916	1.000	1.32	1.58	1.8
321	2.478	2.321	100	110	64	0.597	0.774	0.899	1.012	1.30	1.55	1.8
322	2.478	2.318	100	100	64	0.636	0.804	0.918	1.011	1.28	1.47	1.6
323	2.478	2.314	100	100	64	0.740	0.833	0.978	1.093	1.45	1.78	2.0
324	2.438	2.263	100	100	64	0.752	0.906	1.027	1.090	1.28	1.44	1.6
325	2.438	2.261	100	110	64	0.604	0.709	0.779	0.807	0.97	1.08	1.3
326	2.438	2.255	100	100	64	0.495	0.613	0.666	0.736	0.85	0.98	1.0
327	2.468	2.302	100	100	64	0.672	0.817	0.922	1.004	1.24	1.42	1.6
328	2.468	2.237	100	100	64	0.575	0.715	0.804	0.897	1.12	1.23	1.4
329	2.468	2.291	100	110	64	0.788	0.961	1.073	1.182	1.42	1.64	1.8
330	2.494	2.339	100	100	64	0.667	0.857	0.945	1.054	1.40	1.58	1.8
331	2.494	2.337	100	100	64	0.687	0.852	0.962	1.089	1.42	1.80	2.2
332	2.494	2.336	100	100	64	0.818	1.005	1.133	1.216	1.61	1.87	2.1
333	2.521	2.311	100	110	64	0.574	0.741	0.846	0.935	1.20	1.40	1.6
334	2.521	2.313	100	100	64	0.804	1.000	1.130	1.283	1.56	1.80	2.0
335	2.521	2.318	100	100	64	0.475	0.607	0.704	0.770	1.02	1.19	1.3
336	2.491	2.368	100	110	64	0.375	0.434	0.478	0.521	0.63	0.71	0.8
337	2.491	2.363	100	100	64	0.462	0.539	0.563	0.600	0.71	0.77	0.8
338	2.491	2.322	100	100	64	0.353	0.351	0.401	0.452	0.56	0.63	0.8
339	2.481	2.294	100	100	64	0.702	0.900	1.004	1.155	1.51	1.76	2.1
340	2.481	2.299	100	110	64	0.757	0.956	1.078	1.216	1.58	1.83	2.0
341	2.481	2.292	100	100	64	0.513	0.677	0.792	0.886	1.21	1.39	1.6
342	2.478	2.314	100	100	64	1.364	2.328	3.133	3.578	4.58	5.04	5.3
343	2.478	2.319	100	100	64	0.752	1.823	2.452	2.802	3.65	4.02	4.5
344	2.366	2.223	100	100	64	0.403	0.457	0.413	0.449	0.60	0.61	0.7
345	2.366	2.196	100	100	64	0.434	0.512	0.560	0.608	0.72	0.80	0.9
346	2.366	2.191	100	100	64	0.346	0.436	0.450	0.484	0.53	0.61	0.6
347	2.520	2.340	110	100	64	1.056	1.414	1.731	1.750	2.31	2.70	2.9
348	2.520	2.339	100	100	64	0.674	0.842	1.001	1.231	1.61	1.80	2.0
349	2.367	2.220	100	100	64	1.116	1.470	1.696	1.856	2.27	2.51	2.7
350	2.367	2.223	100	100	64	1.109	1.583	1.916	2.153	2.76	3.08	3.3
351	2.339	2.202	110	100	64	0.504	0.659	0.752	0.845	1.10	1.26	1.4
352	2.339	2.188	100	100	64	0.571	0.765	0.865	0.989	1.30	1.53	1.8
353	2.339	2.186	100	100	64	0.519	0.645	0.743	0.820	1.09	1.32	1.5
354	2.383	2.236	100	100	64	0.616	0.751	0.854	0.888	1.15	1.30	1.4
355	2.383	2.210	100	110	64	0.492	0.615	0.710	0.787	0.93	1.08	1.2
356	2.383	2.240	100	100	64	0.378	0.471	0.471	0.504	0.61	0.73	0.8
357	2.449	2.283	100	100	64	1.964	2.840	3.215	3.535	4.24	4.65	4.9
358	2.449	2.289	100	100	64	2.236	2.883	3.279	3.543	4.21	4.67	5.1
359	2.449	2.296	100	110	64	1.385	1.886	2.239	2.448	3.09	3.50	3.8
360	2.483	2.309	110	110	64	0.543	0.648	0.708	0.751	0.90	0.97	1.0
361	2.483	2.297	100	100	64	0.499	0.593	0.693	0.695	0.82	0.90	1.0
362	2.483	2.322	100	100	64	0.449	0.595	0.710	0.775	0.99	1.19	1.3
363	2.492	2.337	100	100	64	1.108	1.463	1.734	1.974	2.72	3.32	3.7
364	2.492	2.320	110	110	64	0.978	1.310	1.575	1.809	2.44	2.91	3.3
365	2.492	2.329	100	100	64	1.003	1.343	1.578	1.756	2.31	2.67	2.9
366	2.483	2.297	100	100	64	0.533	0.723	0.866	1.011	1.50	1.81	2.1
367	2.483	2.301	100	100	64	0.636	0.769	0.916	0.993	1.24	1.37	1.5
368	2.483	2.304	100	100	64	0.671	0.835	0.945	1.036	1.37	1.54	1.7
369	2.509	2.342	100	100	64	0.930	1.236	1.444	1.668	2.31	2.77	3.1
370	2.509	2.347	100	100	64	0.830	1.144	1.375	1.592	2.29	2.92	3.3
371	2.509	2.345	100	100	64	0.236	0.509	0.745	1.040	1.95	2.34	2.8
372	2.472	2.305	100	100	64	0.732	0.919	1.016	1.106	1.40	1.60	1.7
373	2.472	2.298	100	100	64	0.645	0.807	0.886	0.988	1.23	1.35	1.4
374	2.472	2.299	100	100	64	0.181	0.357	0.432	0.554	0.89	1.15	1.2
375	2.516	2.320	100	100	64	0.800	1.038	1.222	1.342	1.92	2.40	3.0
376	2.516	2.309	100	100	64	1.283	1.715	1.959	2.166	2.61	2.96	3.2
377	2.516	2.311	100	100	64	0.971	1.288	1.602	1.817	2.66	3.19	3.6
378	2.489	2.297	100	100	64	0.803	1.319	1.630	1.998	2.56	2.75	3.0

Sample No.	Mix Design ID	HMA Type	Highway Name	ADT (million)	3/4 inch 19.0mm	1/2 inch 12.5mm	3/8 inch 9.5mm	No. 4 4.75 mm	No. 8 2.36 mm
379	3073-CCC-02034	19 mm Inc	SH-3	3	97	90	86	57	33
380	3073-CCC-02034	19 mm Inc	SH-3	3	97	90	86	57	33
381	3073-CC-02035	19 mm Inc	SH-3	3	97	90	86	57	33
382	3073-CC-02035	19 mm Inc	SH-3	3	97	90	86	57	33
383	3073-CC-02035	19 mm Inc	SH-3	3	97	90	86	57	33
384	3074-CCC-02065	S4 Inc	Int. Rd	1.6	100	97	82	57	42
385	3074-CCC-02065	S4 Inc	Int. Rd	1.6	100	97	82	57	42
386	3073-CCC-02047	S3 rec	I-40	86.3	96	85	80	53	33
387	3073-CCC-02047	S3 rec	I-40	86.3	96	85	80	53	33
388	3073-CCC-02039	S3 rec	I-40	86.3	96	85	80	52	29
389	3073-CCC-02039	S3 rec	I-40	86.3	96	85	80	52	29
390	3073-CCC-02060	S3 rec	I-40	86.3	95	81	74	36	25
391	3073-CCC-02060	S3 rec	I-40	86.3	95	81	74	36	25
392	3073-CCC-02060	S3 rec	I-40	86.3	95	81	74	36	25
393	3073-CCC-02057	S3 rec	I-40	30M+	95	82	76	38	26
394	3073-CCC-02057	S3 rec	I-40	30M+	95	82	76	38	26
395	3074-CCC-02048	S4 rec	I-40	86.3	100	98	87	52	29
396	3074-CCC-02048	S4 rec	I-40	86.3	100	98	87	52	29
397	3074-CCC-02048	S4 rec	I-40	86.3	100	98	87	52	29
398	3074-CCC-02049	S4 rec	I-40	86.3	100	98	87	52	29
399	3074-CCC-02049	S4 rec	I-40	86.3	100	98	87	52	29
400	3074-CCC-02049	S4 rec	I-40	86.3	100	98	87	52	29
401	3074-CCC-02055	S4 Ins	I-40	30M+	100	99	82	52	32
402	3074-CCC-02055	S4 Ins	I-40	30M+	100	99	82	52	32
403	3074-CCC-02055	S4 Ins	I-40	30M+	100	99	82	52	32
404	3074-CCC-02059	S4 Ins	I-40	0.1	100	92	83	57	51
405	3074-CCC-02069	S4 Ins	US60	3M+	100	97	87	65	50
406	3074-CCC-02069	S4 Ins	US60	3M+	100	97	87	65	50
407	3074-CCC-02069	S4 Ins	US60	3M+	100	97	87	65	50
408	3074-OAPA-22117	S4	SH-9	3M+	100	95	77	51	32
409	3074-OAPA-22117	S4	SH-9	3M+	100	95	77	51	32
410	3074-OAPA-22117	S4	SH-9	3M+	100	95	77	51	32
411	3073-OAPA-22116	S3	SH-6	5.1	93	76	65	40	25
412	3073-OAPA-22116	S3	SH-6	5.1	93	76	65	40	25
413	3073-OAPA-22116	S3	SH-6	5.1	93	76	65	40	25
414	3073-OAPA-22118	S3	SH-6	3M+	93	76	65	40	25
415	3073-OAPA-22118	S3	SH-6	3M+	93	76	65	40	25
416	3073-OAPA-22118	S3	SH-6	3M+	93	76	65	40	25
417	3074-OAPA-22145	S4 inc	Int. Rd	1.6	100	98	89	60	34
418	3074-OAPA-22145	S4 inc	Int. Rd	1.6	100	98	89	60	34
419	3074-BCC-02154	S4 Inc	I-40B	1.8	100	97	79	48	31
420	3074-BCC-02154	S4 Inc	I-40B	1.8	100	97	79	48	31
421	3074-BCC-02150	S4 Inc	I-40B	0.3M+	100	97	79	48	31
422	3074-BCC-02150	S4 Inc	I-40B	0.3M+	100	97	79	48	31
423	3074-BCC-02150	S4 Inc	I-40B	0.3M+	100	97	79	48	31
424	3013-BCC-02141	C inc	US-62	3M+	100	100	97	77	50
425	3013-BCC-02141	C inc	US-62	3M+	100	100	97	77	50
426	3013-BCC-02141	C inc	US-62	3M+	100	100	97	77	50
427	3012-BCC-02135	C inc	various	0.3M+	100	100	98	70	48
428	3012-BCC-02135	C inc	various	0.3M+	100	100	98	70	48
429	3074-BCC-02127	S4 binder	US-281	2.9	100	97	78	45	31
430	3074-BCC-02127	S4 binder	US-281	2.9	100	97	78	45	31
431	3074-BCC-02144	S4	I-35	30M+	100	96	80	55	38
432	3074-BCC-02144	S4	I-35	30M+	100	96	80	55	38
433	3074-BCC-02144	S4	I-35	30M+	100	96	80	55	38
434	3074-BCC-02143	S4	SH-39	3	100	98	90	57	40
435	3074-BCC-02143	S4	SH-39	3	100	98	90	57	40
436	3074-BCC-02143	S4	SH-39	3	100	98	90	57	40
437	3074-BCC-02142	S4 inc	SH-39	3	100	94	77	48	33
438	3074-BCC-02142	S4 inc	SH-39	3	100	94	77	48	33
439	3074-BCC-02142	S4 inc	SH-39	3	100	94	77	48	33
440	3074-BCC-02145	S4 Inc	various	0.3M+	100	96	84	54	35
441	3074-BCC-02145	S4 Inc	various	0.3M+	100	96	84	54	35

Sample	No. 16	No. 30	No. 50	No. 100	No. 200	Asphalt			Aggregate		
No.	1.18mm	0.60mm	0.30mm	0.15 mm	0.075mm	Pb	PG	Gb	FAA	FF	G_{sb}
379	25	22	19	9	5.4	4.5	PG 64-22OK	1.0087	46.5	100	2.645
380	25	22	19	9	5.4	4.5	PG 64-22OK	1.0087	46.5	100	2.645
381	25	22	19	9	5.4	4.5	PG 64-22OK	1.0146	46.5	100	2.645
382	25	22	19	9	5.4	4.5	PG 64-22OK	1.0146	46.5	100	2.645
383	25	22	19	9	5.4	4.5	PG 76-28OK	1.0146	46.5	100	2.645
384	32	25	18	9	4.4	4.9	PG 76-28OK	1.0151	45.9	100	2.641
385	32	25	18	9	4.4	4.9	PG 76-28OK	1.0151	45.9	100	2.641
386	23	17	12	8	5.6	4.1	PG 76-28OK	1.0253	45.1	100	2.705
387	23	17	12	8	5.6	4.1	PG 76-28OK	1.0253	45.1	100	2.705
388	19	15	11	7	4.7	4.0	PG 76-28OK	1.0087	45.0	100	2.705
389	19	15	11	7	4.7	4.0	PG 64-22OK	1.0087	45.0	100	2.705
390	18	14	10	6	4.4	4.0	PG 64-22OK	1.0100	45.7	100	2.705
391	18	14	10	6	4.4	4.0	PG 64-22OK	1.0100	45.7	100	2.705
392	18	14	10	6	4.4	4.0	PG 76-28OK	1.0100	45.7	100	2.705
393	19	14	11	7	4.6	4.0	PG 76-28OK	1.0100	45.7	100	2.705
394	19	14	11	7	4.6	4.0	PG 76-28OK	1.0100	45.7	100	2.705
395	20	15	11	7	4.6	4.7	PG 76-28OK	1.0100	45.0	100	2.701
396	20	15	11	7	4.6	4.7	PG 76-28OK	1.0100	45.0	100	2.701
397	20	15	11	7	4.6	4.7	PG 76-28OK	1.0100	45.0	100	2.701
398	20	15	11	7	4.6	4.8	PG 70-28OK	1.0100	45.0	100	2.701
399	20	15	11	7	4.6	4.8	PG 70-28OK	1.0100	45.0	100	2.701
400	20	15	11	7	4.6	4.8	PG 70-28OK	1.0100	45.0	100	2.701
401	21	14	10	7	5.0	4.8	PG 64-22OK	1.0100	48.3	100	2.663
402	21	14	10	7	5.0	4.8	PG 64-22OK	1.0100	48.3	100	2.663
403	21	14	10	7	5.0	4.8	PG 70-28OK	1.0100	48.3	100	2.663
404	41	31	21	10	5.3	4.7	PG 70-28OK	1.0193	45.1	100	2.562
405	37	30	20	10	5.3	5.0	PG 70-28OK	1.0201	45.0	100	2.630
406	37	30	20	10	5.3	5.0	PG 70-28OK	1.0201	45.0	100	2.630
407	37	30	20	10	5.3	5.0	PG 70-28OK	1.0201	45.0	100	2.630
408	23	16	11	7	5.5	5.2	PG 64-22OK	1.0087	46.6	100	2.591
409	23	16	11	7	5.5	5.2	PG 64-22OK	1.0087	46.6	100	2.591
410	23	16	11	7	5.5	5.2	PG 76-28OK	1.0087	46.6	100	2.591
411	20	16	11	6	4.2	4.5	PG 76-28OK	1.0087	47.4	100	2.589
412	20	16	11	6	4.2	4.5	PG 76-28OK	1.0087	47.4	100	2.589
413	20	16	11	6	4.2	4.5	PG 76-28OK	1.0087	47.4	100	2.589
414	20	16	11	6	4.2	4.6	PG 76-28OK	1.0209	47.4	100	2.589
415	20	16	11	6	4.2	4.6	PG 76-28OK	1.0209	47.4	100	2.589
416	20	16	11	6	4.2	4.6	PG 64-22OK	1.0209	47.4	100	2.589
417	24	18	13	8	5.6	5.4	PG 64-22OK	1.0104	45.0	100	2.672
418	24	18	13	8	5.6	5.4	PG 64-22OK	1.0104	45.0	100	2.672
419	22	16	11	7	4.7	5.4	PG 70-28OK	1.0087	45.4	100	2.664
420	22	16	11	7	4.7	5.4	PG 70-28OK	1.0087	45.4	100	2.664
421	22	16	11	7	4.8	5.2	PG 70-28OK	1.0209	45.4	100	2.664
422	22	16	11	7	4.8	5.2	PG 64-22OK	1.0209	45.4	100	2.664
423	22	16	11	7	4.8	5.2	PG 64-22OK	1.0209	45.4	100	2.664
424	32	20	12	8	6.4	5.3	PG 64-22OK	1.0253	42.3	100	2.632
425	32	20	12	8	6.4	5.3	PG 64-22OK	1.0253	42.3	100	2.632
426	32	20	12	8	6.4	5.3	PG 64-22OK	1.0253	42.3	100	2.632
427	32	21	13	9	6.3	5.6	PG 64-22OK	1.0253	45.4	100	2.618
428	32	21	13	9	6.3	5.6	PG 76-28OK	1.0253	45.4	100	2.618
429	20	13	9	6	4.9	5.5	PG 76-28OK	1.0146	47.6	100	2.636
430	20	13	9	6	4.9	5.5	PG 76-28OK	1.0146	47.6	100	2.636
431	24	17	10	6	4.6	4.9	PG 76-28OK	1.0253	45.0	100	2.674
432	24	17	10	6	4.6	4.9	PG 76-28OK	1.0253	45.0	100	2.674
433	24	17	10	6	4.6	4.9	PG 76-28OK	1.0253	45.0	100	2.674
434	22	13	9	6	4.9	5.4	PG 64-22OK	1.0087	45.1	100	2.621
435	22	13	9	6	4.9	5.4	PG 64-22OK	1.0087	45.1	100	2.621
436	22	13	9	6	4.9	5.4	PG 64-22OK	1.0087	45.1	100	2.621
437	20	12	8	6	4.6	5.0	PG 64-22OK	1.0032	48.2	100	2.692
438	20	12	8	6	4.6	5.0	PG 64-22OK	1.0032	48.2	100	2.692
439	20	12	8	6	4.6	5.0	PG 64-22OK	1.0032	48.2	100	2.692
440	23	16	11	8	6.0	5.1	PG 70-28OK	1.0059	48.0	100	2.648
441	23	16	11	8	6.0	5.1	PG 70-28OK	1.0059	48.0	100	2.648

Sample	Mix		Parameters			Rut Depths (mm) at cycles						
No.	G_{mm}	G_{mb}	Wheel	Tire	Temp.	500-c	1000-c	1500-c	2000-c	4000-c	6000-c	8000-c
379	2.489	2.305	100	100	64	0.606	0.780	0.903	1.021	1.25	1.44	1.6
380	2.489	2.302	100	100	64	0.667	0.844	0.974	1.053	1.34	1.58	1.8
381	2.488	2.313	100	100	64	1.172	1.374	1.725	1.794	2.35	2.70	3.1
382	2.488	2.300	100	100	64	0.703	0.846	0.978	1.027	1.23	1.39	1.5
383	2.488	2.340	100	100	64	0.597	0.734	0.825	0.895	1.10	1.20	1.3
384	2.477	2.286	100	100	64	2.751	3.933	4.494	4.856	5.71	6.27	6.7
385	2.477	2.289	100	100	64	2.630	3.479	3.953	4.203	5.10	5.56	6.1
386	2.445	2.262	100	100	64	0.550	0.750	0.850	0.900	1.10	1.35	1.6
387	2.445	2.262	100	100	64	0.550	0.750	0.850	0.900	1.10	1.35	1.6
388	2.522	2.312	100	100	64	0.425	0.591	0.688	0.743	0.91	1.09	1.2
389	2.522	2.342	100	100	64	0.362	0.485	0.572	0.641	0.82	1.00	1.2
390	2.550	2.332	100	100	64	1.039	1.247	1.443	1.549	2.02	2.30	2.5
391	2.550	2.329	100	100	64	0.713	0.900	1.040	1.195	1.66	1.99	2.2
392	2.550	2.335	100	100	64	0.700	0.895	0.971	1.158	1.47	1.66	1.8
393	2.548	2.335	100	100	64	0.534	0.617	0.655	0.701	0.86	0.97	1.0
394	2.548	2.325	100	100	64	0.480	0.546	0.600	0.671	0.83	0.94	1.0
395	2.479	2.318	100	100	64	1.021	1.537	1.886	2.249	2.88	3.29	3.6
396	2.479	2.306	100	100	64	0.774	1.135	1.458	1.754	2.66	3.15	3.4
397	2.479	2.286	100	100	64	0.703	0.970	1.214	1.464	2.28	2.88	3.2
398	2.521	2.323	100	100	64	0.667	0.768	0.896	0.959	1.19	1.28	1.4
399	2.521	2.325	100	100	64	0.718	0.848	0.947	1.055	1.26	1.41	1.6
400	2.521	2.327	100	100	64	0.445	0.551	0.713	0.723	0.85	0.98	1.1
401	2.480	2.297	100	100	64	0.582	0.732	0.800	0.868	1.04	1.20	1.3
402	2.480	2.277	100	100	64	0.661	0.822	0.949	1.016	1.28	1.46	1.6
403	2.480	2.284	100	100	64	0.440	0.562	0.646	0.756	0.90	1.12	1.2
404	2.405	2.217	100	100	64	0.490	0.804	1.114	1.254	1.68	1.91	2.1
405	2.461	2.289	100	100	64	0.583	0.707	0.797	0.879	1.06	1.20	1.3
406	2.461	2.281	100	100	64	0.436	0.528	0.612	0.653	0.81	0.93	1.0
407	2.461	2.284	100	100	64	0.278	0.373	0.483	0.538	0.93	1.08	1.2
408	2.415	2.246	100	100	64	1.654	2.330	2.773	3.031	3.78	4.11	4.3
409	2.415	2.230	100	100	64	1.640	2.030	2.340	2.528	3.14	3.63	4.0
410	2.415	2.240	100	100	64	1.465	1.997	2.335	2.536	3.15	3.47	3.7
411	2.450	2.236	100	100	64	1.534	1.960	2.156	2.351	2.88	3.26	3.6
412	2.450	2.245	100	100	64	1.108	1.387	1.623	1.845	2.25	2.60	2.8
413	2.450	2.242	100	100	64	1.621	2.303	2.739	3.085	3.96	4.48	4.9
414	2.453	2.255	100	100	64	0.773	1.063	1.265	1.385	1.94	2.37	2.7
415	2.453	2.262	100	100	64	0.821	1.096	1.286	1.452	1.95	2.30	2.5
416	2.453	2.255	100	100	64	0.761	0.994	1.152	1.255	1.74	2.15	2.5
417	2.477	2.288	100	100	64	1.370	1.952	2.456	2.871	3.97	4.66	5.1
418	2.477	2.291	100	100	64	1.357	1.881	2.316	2.624	3.44	3.90	4.2
419	2.462	2.278	100	100	64	1.742	2.281	2.583	2.843	4.05	4.73	5.3
420	2.462	2.259	100	100	64	1.841	2.400	2.745	3.060	3.94	4.52	4.8
421	2.474	2.282	100	100	64	1.138	1.454	1.641	1.797	2.17	2.41	2.6
422	2.474	2.284	100	100	64	1.083	1.556	1.870	2.101	2.68	2.98	3.1
423	2.474	2.290	100	100	64	1.113	1.394	1.565	1.694	2.15	2.49	2.7
424	2.447	2.281	100	100	64	0.691	0.838	0.916	1.034	1.25	1.43	1.6
425	2.447	2.280	100	100	64	0.634	0.820	0.929	1.000	1.26	1.44	1.6
426	2.447	2.280	100	100	64	0.613	0.753	0.836	0.950	1.15	1.41	1.5
427	2.436	2.267	100	100	64	0.651	0.752	0.821	1.003	1.17	1.29	1.5
428	2.436	2.266	100	100	64	0.671	0.848	0.947	1.095	1.39	1.60	1.8
429	2.466	2.295	100	100	64	0.799	1.060	1.210	1.425	2.02	2.59	3.1
430	2.466	2.292	100	100	64	0.725	0.929	1.107	1.264	1.88	2.43	2.9
431	2.511	2.314	100	100	64	0.620	0.762	0.832	0.889	1.11	1.20	1.4
432	2.511	2.318	100	100	64	0.674	0.802	0.881	0.933	1.16	1.26	1.4
433	2.511	2.324	100	100	64	0.426	0.592	0.644	0.697	0.91	1.10	1.3
434	2.462	2.280	100	100	64	1.138	1.561	1.838	2.020	2.59	3.00	3.4
435	2.462	2.285	100	100	64	1.427	1.909	2.123	2.288	2.74	3.02	3.3
436	2.462	2.289	100	100	64	1.262	1.598	1.805	2.004	2.43	2.75	3.0
437	2.489	2.291	100	100	64	0.774	0.976	1.105	1.232	1.52	1.76	1.9
438	2.489	2.289	100	100	64	0.581	0.744	0.852	0.952	1.26	1.54	1.8
439	2.489	2.292	100	100	64	0.466	0.658	0.743	0.778	1.00	1.07	1.2
440	2.463	2.275	100	100	64	0.195	0.284	0.359	0.438	0.66	0.83	1.0
441	2.463	2.275	100	100	64	0.262	0.477	0.645	0.761	1.15	1.48	1.7

Sample No.	Mix Design ID	HMA Type	Highway Name	ADT (million)	3/4 inch 19.0mm	1/2 inch 12.5mm	3/8 inch 9.5mm	No. 4 4.75 mm	No. 8 2.36 mm
442	3074-BCC-02145	S4 Inc	various	0.3M+	100	96	84	54	35
443	3012-BCC-02153	BH Ins	SH-7	3M+	100	100	93	75	53
444	3012-BCC-02153	BH Ins	SH-7	3M+	100	100	93	75	53
445	3012-BCC-02153	BH Ins	SH-7	3M+	100	100	93	75	53
446	3013-BCC-02159	C inc	US-412	0.3M+	100	100	93	60	40
447	3013-BCC-02159	C inc	US-412	0.3M+	100	100	93	60	40
448	3013-BCC-02159	C inc	US-412	0.3M+	100	100	93	60	40
449	3012-BCC-02146	BH rec	SH-7	3M+	100	93	83	55	39
450	3012-BCC-02146	BH rec	SH-7	3M+	100	93	83	55	39
451	3012-BCC-02146	BH rec	SH-7	3M+	100	93	83	55	39
452	3072-BCC-02140	S2	US-70	3M+	90	77	72	54	40
453	3072-BCC-02140	S2	US-70	3M+	90	77	72	54	40
454	3072-BCC-02140	S2	US-70	3M+	90	77	72	54	40
455	3073-BCC-02138	S3 rec	SH-76	3.6	97	89	73	45	31
456	3073-BCC-02138	S3 rec	SH-76	3.6	97	89	73	45	31
457	3073-BCC-02148	S3 rec	SH-76	3.6	97	89	73	45	34
458	3073-BCC-02148	S3 rec	SH-76	3.6	97	89	73	45	34
459	3073-BCC-02148	S3 rec	SH-76	3.6	97	89	73	45	34
460	3012-BCC-02136	B binder	I-40	0.3M-	100	97	90	61	38
461	3074-BCC-02137	S4	US-70	3M+	100	94	77	47	33
462	3074-BCC-02137	S4	US-70	3M+	100	94	77	47	33
463	3074-BCC-02137	S4	US-70	3M+	100	94	77	47	33
464	3073-EST-05816	S3 rec	SH 51	4.7	99	86	77	50	32
465	3073-EST-05816	S3 rec	SH 51	4.7	99	86	77	50	32
466	3073-EST-05427	S3 rec	various	3M+	100	90	80	52	31
467	3073-EST-05427	S3 rec	various	3M+	100	90	80	52	31
468	3073-EST-05427	S3 rec	various	3M+	100	90	80	52	31
469	3074-EST-05430	S4 Inc	various	3M+	100	91	80	59	37
470	3074-EST-05430	S4 Inc	various	3M+	100	91	80	59	37
471	3074-EST-05829	S4 Inc	various	0.3M-	100	97	90	68	47
472	3074-EST-05829	S4 Inc	various	0.3M-	100	97	90	68	47
473	3074-EST-05829	S4 Inc	various	0.3M-	100	97	90	68	47
474	3073-SH02-72109	S3 rec	SH-99	16.7	99	90	82	56	34
475	3073-SH02-72109	S3 rec	SH-99	16.7	99	90	82	56	34
476	3073-SH02-73312	S4 Inc	SH-99	16.7	100	98	88	58	39
477	3073-SH02-73312	S4 Inc	SH-99	16.7	100	98	88	58	39
478	3073-SH02-73312	S4 Inc	SH-99	16.7	100	98	88	58	39
479	3072-SH02-71108	S2 rec	US-377	16.7	90	78	71	49	32
480	3072-SH02-71108	S2 rec	US-377	16.7	90	78	71	49	32
481	3072-SH02-71108	S2 rec	US-377	16.7	90	78	71	49	32
482	3073-SH02-72310	S3 rec	SH-99	16.7	99	90	82	56	34
483	3073-SH02-72310	S3 rec	SH-99	16.7	99	90	82	56	34
484	3073-SH02-72310	S3 rec	SH-99	16.7	99	90	82	56	34
485	3074-ARKH-02001	S-4	various	3M+	100	92	78	59	37
486	3074-ARKH-02001	S-4	various	3M+	100	92	78	59	37
487	3074-ARKH-02001	S-4	various	3M+	100	92	78	59	37
488	3073-ARKH-02002	S-3	various	0.3M+	100	85	74	52	31
489	3073-ARKH-02002	S-3	various	0.3M+	100	85	74	52	31
490	3073-ARKH-02002	S-3	various	0.3M+	100	85	74	52	31
491	3012-HH02-93117	B rec	various	3M+	100	98	81	52	32
492	3012-HH02-93117	B rec	various	3M+	100	98	81	52	32
493	3012-HH02-93117	B rec	various	3M+	100	98	81	52	32
494	3073-HH02-92323	S3	Hwy-177	16.7	100	88	77	51	31
495	3073-HH02-92323	S3	Hwy-177	16.7	100	88	77	51	31
496	3073-HH02-92323	S3	Hwy-177	16.7	100	88	77	51	31
497	3074-OAPA-22130	S4 inc	SH-51	4.7	100	92	86	50	30
498	3074-OAPA-22130	S4 inc	SH-51	4.7	100	92	86	50	30
499	3074-OAPA-22130	S4 inc	SH-51	4.7	100	92	86	50	30
500	3073-OAPA-22163	S3 rec	US-169	32.3	98	88	79	43	34
501	3073-OAPA-22163	S3 rec	US-169	32.3	98	88	79	43	34
502	3073-OAPA-22163	S3 rec	US-169	32.3	98	88	79	43	34
503	3013-APAC-20219	C binder	various	3M+	100	100	98	71	45
504	3013-APAC-20219	C binder	various	3M+	100	100	98	71	45

Sample	No. 16	No. 30	No. 50	No. 100	No. 200	Asphalt			Aggregate		
No.	1.18mm	0.60mm	0.30mm	0.15 mm	0.075mm	Pb	PG	Gb	FAA	FF	G_{sb}
442	23	16	11	8	6.0	5.1	PG 70-28OK	1.0059	48.0	100	2.648
443	41	33	21	10	6.0	4.3	PG 64-22OK	1.0160	46.0	100	2.670
444	41	33	21	10	6.0	4.3	PG 64-22OK	1.0160	46.0	100	2.670
445	41	33	21	10	6.0	4.3	PG 76-28OK	1.0160	46.0	100	2.670
446	27	18	11	7	5.3	6.8	PG 76-28OK	1.0209	45.0	100	2.797
447	27	18	11	7	5.3	6.8	PG 64-22OK	1.0209	45.0	100	2.797
448	27	18	11	7	5.3	6.8	PG 64-22OK	1.0209	45.0	100	2.797
449	27	18	12	8	5.3	4.3	PG 64-22OK	1.0100	45.1	100	2.651
450	27	18	12	8	5.3	4.3	PG 64-22OK	1.0100	45.1	100	2.651
451	27	18	12	8	5.3	4.3	PG 64-22OK	1.0100	45.1	100	2.651
452	28	20	15	8	4.6	4.8	PG 76-28OK	1.0151	44.2	100	2.641
453	28	20	15	8	4.6	4.8	PG 76-28OK	1.0151	44.2	100	2.641
454	28	20	15	8	4.6	4.8	PG 64-22OK	1.0151	44.2	100	2.641
455	21	15	10	7	3.0	4.5	PG 64-22OK	1.0100	45.5	100	2.641
456	21	15	10	7	3.0	4.5	PG 64-22OK	1.0100	45.5	100	2.641
457	25	17	11	7	3.5	4.5	PG 76-28OK	1.0100	45.5	100	2.640
458	25	17	11	7	3.5	4.5	PG 76-28OK	1.0100	45.5	100	2.640
459	25	17	11	7	3.5	4.5	PG 76-28OK	1.0100	45.5	100	2.640
460	24	15	10	6	4.6	5.6	PG 76-28OK	1.0087	46.2	100	2.668
461	19	12	7	5	3.9	5.1	PG 76-28OK	1.0151	47.2	100	2.675
462	19	12	7	5	3.9	5.1	PG 76-28OK	1.0151	47.2	100	2.675
463	19	12	7	5	3.9	5.1	PG 64-22OK	1.0151	47.2	100	2.675
464	19	13	9	5	3.6	4.5	PG 76-28OK	1.0100	45.4	100	2.567
465	19	13	9	5	3.6	4.5	PG 76-28OK	1.0100	45.4	100	2.567
466	21	14	10	7	4.9	4.3	PG 76-28OK	1.0209	45.5	100	2.578
467	21	14	10	7	4.9	4.3	PG 64-22OK	1.0209	45.5	100	2.578
468	21	14	10	7	4.9	4.3	PG 64-22OK	1.0209	45.5	100	2.578
469	25	17	11	8	5.6	5.0	PG 64-22OK	1.0211	45.7	100	2.518
470	25	17	11	8	5.6	5.0	PG 64-22OK	1.0211	45.7	100	2.518
471	36	27	17	9	4.9	5.8	PG 64-22OK	1.0253	45.3	100	2.523
472	36	27	17	9	4.9	5.8	PG 64-22OK	1.0253	45.3	100	2.523
473	36	27	17	9	4.9	5.8	PG 70-28OK	1.0253	45.3	100	2.523
474	22	14	9	5	3.0	4.7	PG 70-28OK	1.0100	45.1	100	2.691
475	22	14	9	5	3.0	4.7	PG 70-28OK	1.0100	45.1	100	2.691
476	26	18	13	6	2.9	4.8	PG 64-22OK	1.0100	45.4	100	2.693
477	26	18	13	6	2.9	4.8	PG 64-22OK	1.0100	45.4	100	2.693
478	26	18	13	6	2.9	4.8	PG 64-22OK	1.0100	45.4	100	2.693
479	20	14	10	6	4.2	3.6	PG 64-22OK	1.0100	45.4	100	2.675
480	20	14	10	6	4.2	3.6	PG 70-28OK	1.0100	45.4	100	2.675
481	20	14	10	6	4.2	3.6	PG 70-28OK	1.0100	45.4	100	2.675
482	22	14	9	5	3.0	4.5	PG 70-28OK	1.0100	45.1	100	2.691
483	22	14	9	5	3.0	4.5	PG 76-28OK	1.0100	45.1	100	2.691
484	22	14	9	5	3.0	4.5	PG 76-28OK	1.0100	45.1	100	2.691
485	25	17	11	8	5.5	6.3	PG 76-28OK	1.0253	43.1	100	2.519
486	25	17	11	8	5.5	6.3	PG 76-28OK	1.0253	43.1	100	2.519
487	25	17	11	8	5.5	6.3	PG 76-28OK	1.0253	43.1	100	2.519
488	21	14	10	7	5.0	5.9	PG 70-28OK	1.0253	43.7	100	2.602
489	21	14	10	7	5.0	5.9	PG 70-28OK	1.0253	43.7	100	2.602
490	21	14	10	7	5.0	5.9	PG 76-28OK	1.0253	43.7	100	2.602
491	17	7	3	6	3.1	4.7	PG 76-28OK	1.0100	45.8	100	2.676
492	17	7	3	6	3.1	4.7	PG 76-28OK	1.0100	45.8	100	2.676
493	17	7	3	6	3.1	4.7	PG 64-22OK	1.0100	45.8	100	2.676
494	20	14	11	7	4.6	4.1	PG 64-22OK	1.0100	45.5	100	2.652
495	20	14	11	7	4.6	4.1	PG 64-22OK	1.0100	45.5	100	2.652
496	20	14	11	7	4.6	4.1	PG 70-28OK	1.0100	45.5	100	2.652
497	19	13	10	7	5.2	5.7	PG 70-28OK	1.0253	46.0	100	2.596
498	19	13	10	7	5.2	5.7	PG 70-28OK	1.0253	46.0	100	2.596
499	19	13	10	7	5.2	5.7	PG 64-22OK	1.0253	46.0	100	2.596
500	17	13	7	4	3.7	3.9	PG 64-22OK	1.0100	45.0	100	2.600
501	17	13	7	4	3.7	3.9	PG 64-22OK	1.0100	45.0	100	2.600
502	17	13	7	4	3.7	3.9	PG 76-28OK	1.0100	45.0	100	2.600
503	30	20	12	8	6.1	5.4	PG 76-28OK	1.0147	45.0	100	2.556
504	30	20	12	8	6.1	5.4	PG 76-28OK	1.0147	45.0	100	2.556

Sample	Mix		Parameters			Rut Depths (mm) at cycles						
No.	G_{mm}	G_{mb}	Wheel	Tire	Temp.	500-c	1000-c	1500-c	2000-c	4000-c	6000-c	8000-c
442	2.463	2.274	100	100	64	0.370	0.616	0.798	1.012	1.68	2.16	2.5
443	2.496	2.308	100	100	64	0.709	0.792	0.853	0.927	1.09	1.22	1.3
444	2.496	2.309	100	100	64	0.504	0.604	0.688	0.715	0.91	1.02	1.1
445	2.496	2.305	100	100	64	0.513	0.577	0.629	0.642	0.86	0.95	1.0
446	2.452	2.321	100	100	64	1.102	1.563	1.882	2.143	2.65	2.99	3.2
447	2.452	2.319	100	100	64	1.005	1.453	1.861	2.154	2.75	3.06	3.3
448	2.452	2.320	100	100	64	0.967	1.424	1.794	2.063	2.66	2.92	3.1
449	2.496	2.309	100	100	64	0.514	0.625	0.694	0.771	0.94	1.03	1.1
450	2.496	2.315	100	100	64	0.527	0.654	0.701	0.765	0.86	0.95	1.0
451	2.496	2.310	100	100	64	0.434	0.512	0.652	0.709	0.84	0.97	1.1
452	2.493	2.277	100	100	64	1.400	2.004	2.416	2.771	3.64	4.07	4.4
453	2.493	2.290	100	100	64	1.119	1.590	1.921	2.219	2.95	3.32	3.6
454	2.493	2.295	100	100	64	0.659	1.072	1.350	1.560	2.01	2.17	2.3
455	2.504	2.305	100	100	64	1.125	1.499	1.741	1.879	2.37	2.63	2.9
456	2.504	2.295	100	100	64	1.035	1.362	1.552	1.700	2.23	2.55	2.8
457	2.499	2.290	100	100	64	0.757	1.013	1.185	1.327	1.87	2.25	2.5
458	2.499	2.287	100	100	64	0.707	0.913	1.063	1.207	1.61	1.86	2.1
459	2.499	2.292	100	100	64	0.346	0.553	0.736	0.875	1.13	1.33	1.3
460	2.473	2.304	100	100	64	1.643	2.429	2.823	3.128	3.77	4.21	4.6
461	2.495	2.305	100	100	64	1.092	1.561	2.027	2.363	2.55	2.73	3.0
462	2.495	2.301	100	100	64	0.960	1.400	1.811	2.079	2.65	2.90	3.1
463	2.495	2.304	100	100	64	0.887	1.192	1.380	1.526	1.83	2.06	2.3
464	2.429	2.288	100	100	64	2.388	3.326	3.845	4.198	5.17	5.73	6.2
465	2.429	2.286	100	100	64	2.071	3.372	4.035	4.457	5.26	5.83	6.1
466	2.427	2.288	100	100	64	1.012	1.366	1.345	1.550	1.81	2.02	2.2
467	2.427	2.271	100	100	64	0.797	0.996	1.124	1.203	1.43	1.54	1.6
468	2.427	2.277	100	100	64	0.631	0.763	0.929	0.971	1.18	1.41	1.6
469	2.366	2.199	100	100	64	0.542	0.652	0.722	0.794	0.92	1.05	1.1
470	2.366	2.183	100	100	64	0.601	0.812	0.921	0.983	1.25	1.22	1.3
471	2.480	2.243	100	100	64	0.542	0.691	0.800	0.881	1.11	1.37	1.6
472	2.480	2.240	100	100	64	0.614	0.796	0.906	1.015	1.31	1.57	1.8
473	2.480	2.246	100	100	64	0.501	0.624	0.710	0.783	1.06	1.26	1.4
474	2.527	2.371	100	100	64	1.178	1.461	1.803	2.218	3.27	3.92	4.3
475	2.527	2.373	100	100	64	1.179	1.910	2.390	2.746	3.56	4.02	4.4
476	2.502	2.328	100	100	64	1.190	1.511	1.672	1.846	2.27	2.47	2.6
477	2.502	2.335	100	100	64	1.156	1.473	1.717	1.912	2.40	2.71	3.0
478	2.502	2.335	100	100	64	1.114	1.542	1.850	2.094	2.70	3.11	3.4
479	2.542	2.370	100	100	64	0.742	1.032	1.069	1.186	1.44	1.70	2.0
480	2.542	2.378	100	100	64	0.567	0.721	0.829	1.000	1.33	1.60	1.8
481	2.542	2.380	100	100	64	0.507	0.636	0.771	0.823	1.12	1.32	1.5
482	2.521	2.338	100	100	64	0.629	0.705	0.839	0.851	1.05	1.22	1.3
483	2.521	2.332	100	100	64	0.728	0.903	0.997	1.095	1.34	1.61	1.7
484	2.521	2.333	100	100	64	0.532	0.646	0.748	0.789	1.06	1.20	1.3
485	2.384	2.208	100	100	64	1.005	1.318	1.582	1.837	2.69	3.34	3.9
486	2.384	2.202	100	100	64	0.674	0.857	0.991	1.152	1.82	2.46	3.0
487	2.384	2.207	100	100	64	0.713	0.915	1.098	1.257	1.76	2.25	2.6
488	2.460	2.237	100	100	64	2.119	3.087	3.742	4.207	5.35	5.97	6.4
489	2.460	2.238	100	100	64	2.076	2.765	3.183	3.529	4.43	5.03	5.4
490	2.460	2.237	100	100	64	1.512	1.942	2.177	2.430	3.03	3.50	3.8
491	2.488	2.351	100	100	64	1.273	1.804	2.012	2.342	3.16	3.61	3.8
492	2.488	2.346	100	100	64	0.921	1.132	1.309	1.437	1.83	2.14	2.4
493	2.488	2.343	100	100	64	1.059	1.393	1.641	1.851	2.33	2.69	3.0
494	2.532	2.364	100	100	64	0.511	0.568	0.676	0.678	0.82	0.93	1.0
495	2.532	2.367	100	100	64	0.478	0.552	0.612	0.630	0.76	0.86	0.9
496	2.532	2.367	100	100	64	0.499	0.650	0.645	0.780	0.86	0.93	1.1
497	2.395	2.215	100	100	64	0.586	0.751	0.855	0.968	1.29	1.57	1.8
498	2.395	2.216	100	100	64	0.842	1.026	1.155	1.291	1.61	1.85	2.1
499	2.395	2.217	100	100	64	0.494	0.635	0.758	0.818	1.05	1.30	1.5
500	2.459	2.276	100	100	64	0.233	0.349	0.502	0.574	0.72	0.79	0.9
501	2.459	2.261	100	100	64	0.398	0.444	0.514	0.535	0.64	0.69	0.7
502	2.459	2.258	100	100	64	0.292	0.434	0.470	0.521	0.73	0.82	0.9
503	2.388	2.195	100	100	64	0.849	1.143	1.382	1.612	2.35	2.88	3.3
504	2.388	2.194	100	100	64	1.036	1.452	1.775	2.084	2.87	3.36	3.8

Sample No.	Mix Design ID	HMA Type	Highway Name	ADT (million)	3/4 inch 19.0mm	1/2 inch 12.5mm	3/8 inch 9.5mm	No. 4 4.75 mm	No. 8 2.36 mm
505	3013-APAC-20219	C binder	various	3M+	100	100	98	71	45
506	3073-APAc-20209	S3	various	3M+	97	86	81	53	30
507	3073-APAc-20209	S3	various	3M+	97	86	81	53	30
508	3074-APAC-20226	S4	Various	3M+	100	91	85	64	38
509	3074-APAC-20226	S4	Various	3M+	100	91	85	64	38
510	3074-APAC-20226	S4	Various	3M+	100	91	85	64	38
511	3012-APAC-20225	B ins	Various	3M+	100	92	84	61	40
512	3012-APAC-20225	B ins	Various	3M+	100	92	84	61	40
513	3012-APAC-20225	B ins	Various	3M+	100	92	84	61	40
514	3012-APAC-20235	B binder	various	3M+	100	93	84	56	38
515	3012-APAC-20235	B binder	various	3M+	100	93	84	56	38
516	3012-APAC-20235	B binder	various	3M+	100	93	84	56	38
517	3074-APAC-20231	S-4 Bnd	Various	3M+	100	94	86	56	35
518	3074-APAC-20231	S-4 Bnd	Various	3M+	100	94	86	56	35
519	3074-APAC-20231	S-4 Bnd	Various	3M+	100	94	86	56	35
520	3012-APAC-20234	B Ins	Various	0.3M+	100	92	84	61	39
521	3012-APAC-20234	B Ins	Various	0.3M+	100	92	84	61	39
522	3012-APAC-20234	B Ins	Various	0.3M+	100	92	84	61	39
523	3074-APAC-20232	S-4 Ins	Various	3M+	100	94	86	60	36
524	3074-APAC-20232	S-4 Ins	Various	3M+	100	94	86	60	36
525	3074-APAC-20232	S-4 Ins	Various	3M+	100	94	86	60	36
526	3011-APAC-20206	A	Various	3M+	92	83	75	59	41
527	3011-APAC-20206	A	Various	3M+	92	83	75	59	41
528	3011-APAC-20206	A	Various	3M+	92	83	75	59	41
529	3072-APAC-20210	S-2 Rec	Various	3M+	86	76	67	38	23
530	3072-APAC-20210	S-2 Rec	Various	3M+	86	76	67	38	23
531	3072-APAC-20210	S-2 Rec	Various	3M+	86	76	67	38	23
532	3074-APAC-20212	S-4 Ins	US-69	20.7	100	91	85	64	38
533	3074-APAC-20212	S-4 Ins	US-69	20.7	100	91	85	64	38
534	3074-APAC-20212	S-4 Ins	US-69	20.7	100	91	85	64	38
535	3074-APAC-20221	S-4	Various	3M+	97	93	87	54	32
536	3074-APAC-20221	S-4	Various	3M+	97	93	87	54	32
537	3074-APAC-20221	S-4	Various	3M+	97	93	87	54	32
538	3073-APAC-20224	S-3	I-44	25.5M	96	84	79	51	30
539	3073-APAC-20224	S-3	I-44	25.5M	96	84	79	51	30
540	3073-APAC-20224	S-3	I-44	25.5M	96	84	79	51	30
541	3011-APAC-20222	A	Various	3M+	92	82	74	57	39
542	3011-APAC-20222	A	Various	3M+	92	82	74	57	39
543	3011-APAC-20222	A	Various	3M+	92	82	74	57	39
544	3011-APAC-20216	A	Various	3M+	92	82	74	57	39
545	3011-APAC-20216	A	Various	3M+	92	82	74	57	39
546	3011-APAC-20216	A	Various	3M+	92	82	74	57	39
547	3011-APAC-20223	A	Various	3M+	92	82	74	57	39
548	3011-APAC-20223	A	Various	3M+	92	82	74	57	39
549	3011-APAC-20223	A	Various	3M+	92	82	74	57	39
550	3074-APAC-20220	S-4	US-69	20.7	100	93	87	54	32
551	3074-APAC-20220	S-4	US-69	20.7	100	93	87	54	32
552	3074-APAC-20220	S-4	US-69	20.7	100	93	87	54	32
553	3012-APAC-20218	B inc	various	3M+	100	94	86	61	39
554	3012-APAC-20218	B inc	various	3M+	100	94	86	61	39
555	3012-APAC-20218	B inc	various	3M+	100	94	86	61	39
556	3074-APAC-20221	S4	variuus	3M+	100	93	87	54	32
557	3074-APAC-20221	S4	variuus	3M+	100	93	87	54	32
558	3074-APAC-20221	S4	variuus	3M+	100	93	87	54	32
559	3012-APAC-20215	B ins	variuus	0.3M+	100	92	84	61	39
560	3012-APAC-20215	B ins	variuus	0.3M+	100	92	84	61	39
561	3012-APAC-20214	B Binder	various	3M+	100	93	84	56	38
562	3012-APAC-20214	B Binder	various	3M+	100	93	84	56	38
563	3012-APAC-20214	B Binder	various	3M+	100	93	84	56	38
564	3012-APAC-20236	S4 inc	county	0.4	100	92	85	58	35
565	3012-APAC-20236	S4 inc	county	0.4	100	92	85	58	35
566	3074-HH02-93324	S4 ins	I-35	54	100	99	90	53	29
567	3074-HH02-93324	S4 ins	I-35	54	100	99	90	53	29

Sample	No. 16	No. 30	No. 50	No. 100	No. 200	Asphalt			Aggregate		
No.	1.18mm	0.60mm	0.30mm	0.15 mm	0.075mm	Pb	PG	Gb	FAA	FF	G_{sb}
505	30	20	12	8	6.1	5.4	PG 70-28OK	1.0147	45.0	100	2.556
506	19	11	8	6	4.4	5.0	PG 70-28OK	1.0147	47.2	100	2.601
507	19	11	8	6	4.4	5.0	PG 70-28OK	1.0147	47.2	100	2.601
508	23	14	8	5	4.1	5.1	PG 76-28OK	1.0146	45.3	100	2.561
509	23	14	8	5	4.1	5.1	PG 76-28OK	1.0146	45.3	100	2.561
510	23	14	8	5	4.1	5.1	PG 76-28OK	1.0146	45.3	100	2.561
511	26	17	10	6	4.8	5.3	PG 64-22OK	1.0209	45.0	100	2.571
512	26	17	10	6	4.8	5.3	PG 64-22OK	1.0209	45.0	100	2.571
513	26	17	10	6	4.8	5.3	PG 64-22OK	1.0209	45.0	100	2.571
514	26	17	11	6	4.9	5.1	PG 64-22OK	1.0104	45.1	100	2.571
515	26	17	11	6	4.9	5.1	PG 64-22OK	1.0104	45.1	100	2.571
516	26	17	11	6	4.9	5.1	PG 70-28OK	1.0104	45.1	100	2.571
517	23	16	10	6	4.7	5.2	PG 70-28OK	1.0147	45.0	100	2.563
518	23	16	10	6	4.7	5.2	PG 70-28OK	1.0147	45.0	100	2.563
519	23	16	10	6	4.7	5.2	PG 64-22OK	1.0147	45.0	100	2.563
520	26	17	10	6	4.7	5.4	PG 64-22OK	1.0104	45.0	100	2.543
521	26	17	10	6	4.7	5.4	PG 64-22OK	1.0104	45.0	100	2.543
522	26	17	10	6	4.7	5.4	PG 64-22OK	1.0104	45.0	100	2.543
523	24	16	9	6	4.3	5.8	PG 76-28OK	1.0146	45.1	100	2.558
524	24	16	9	6	4.3	5.8	PG 76-28OK	1.0146	45.1	100	2.558
525	24	16	9	6	4.3	5.8	PG 70-28OK	1.0146	45.1	100	2.558
526	27	17	10	6	4.9	3.9	PG 70-28OK	1.0147	45.0	100	2.622
527	27	17	10	6	4.9	3.9	PG 70-28OK	1.0147	45.0	100	2.622
528	27	17	10	6	4.9	3.9	PG 70-28OK	1.0147	45.0	100	2.622
529	15	11	7	5	4.0	4.3	PG 70-28OK	1.0147	44.3	100	2.594
530	15	11	7	5	4.0	4.3	PG 64-22OK	1.0147	44.3	100	2.594
531	15	11	7	5	4.0	4.3	PG 64-22OK	1.0147	44.3	100	2.594
532	23	14	8	5	4.1	5.1	PG 64-22OK	1.0253	45.3	100	2.561
533	23	14	8	5	4.1	5.1	PG 64-22OK	1.0253	45.3	100	2.561
534	23	14	8	5	4.1	5.1	PG 64-22OK	1.0253	45.3	100	2.561
535	21	13	8	5	4.2	4.8	PG 76-28OK	1.0146	45.0	100	2.602
536	21	13	8	5	4.2	4.8	PG 76-28OK	1.0146	45.0	100	2.602
537	21	13	8	5	4.2	4.8	PG 76-28OK	1.0146	45.0	100	2.602
538	20	14	9	6	4.5	4.8	PG 64-22OK	1.0146	45.0	100	2.593
539	20	14	9	6	4.5	4.8	PG 64-22OK	1.0146	45.0	100	2.593
540	20	14	9	6	4.5	4.8	PG 64-22OK	1.0146	45.0	100	2.593
541	27	18	11	6	4.9	4.4	PG 76-28OK	1.0209	45.0	100	2.542
542	27	18	11	6	4.9	4.4	PG 76-28OK	1.0209	45.0	100	2.542
543	27	18	11	6	4.9	4.4	PG 76-28OK	1.0209	45.0	100	2.542
544	27	18	11	6	4.9	4.4	PG 64-22OK	1.0147	45.0	100	2.542
545	27	18	11	6	4.9	4.4	PG 64-22OK	1.0147	45.0	100	2.542
546	27	18	11	6	4.9	4.4	PG 64-22OK	1.0147	45.0	100	2.542
547	27	18	11	6	4.9	4.4	PG 64-22OK	1.0104	45.0	100	2.542
548	27	18	11	6	4.9	4.4	PG 64-22OK	1.0104	45.0	100	2.542
549	27	18	11	6	4.9	4.4	PG 64-22OK	1.0104	45.0	100	2.542
550	21	13	8	5	4.2	4.8	PG 64-22OK	1.0147	45.0	100	2.602
551	21	13	8	5	4.2	4.8	PG 64-22OK	1.0147	45.0	100	2.602
552	21	13	8	5	4.2	4.8	PG 64-22OK	1.0147	45.0	100	2.602
553	26	17	10	6	4.9	5.3	PG 76-28OK	1.0146	45.2	100	2.551
554	26	17	10	6	4.9	5.3	PG 76-28OK	1.0146	45.2	100	2.551
555	26	17	10	6	4.9	5.3	PG 76-28OK	1.0146	45.2	100	2.551
556	21	13	8	5	4.2	4.8	PG 76-28OK	1.0146	45.0	100	2.602
557	21	13	8	5	4.2	4.8	PG 76-28OK	1.0146	45.0	100	2.602
558	21	13	8	5	4.2	4.8	PG 76-28OK	1.0146	45.0	100	2.602
559	26	17	10	6	4.7	5.4	PG 76-28OK	1.0147	45.1	100	2.542
560	26	17	10	6	4.7	5.4	PG 76-28OK	1.0147	45.1	100	2.542
561	26	17	11	6	4.9	5.1	PG 76-28OK	1.0147	45.1	100	2.546
562	26	17	11	6	4.9	5.1	PG 64-22OK	1.0147	45.1	100	2.546
563	26	17	11	6	4.9	5.1	PG 64-22OK	1.0147	45.1	100	2.546
564	24	14	9	6	4.5	5.2	PG 64-22OK	1.0147	42.9	100	2.592
565	24	14	9	6	4.5	5.2	PG 64-22OK	1.0147	42.9	100	2.592
566	21	17	14	7	3.0	4.9	PG 64-22OK	1.0253	45.6	100	2.651
567	21	17	14	7	3.0	4.9	PG 70-28OK	1.0253	45.6	100	2.651

Sample	Mix		Parameters			Rut Depths (mm) at cycles						
No.	G_{mm}	G_{mb}	Wheel	Tire	Temp.	500-c	1000-c	1500-c	2000-c	4000-c	6000-c	8000-c
505	2.388	2.189	100	100	64	0.903	1.126	1.274	1.356	1.73	1.87	2.1
506	2.445	2.264	100	100	64	0.912	1.251	1.568	1.795	2.48	2.83	3.0
507	2.445	2.255	100	100	64	0.938	1.227	1.449	1.602	2.04	2.42	2.7
508	2.411	2.233	100	100	64	0.485	0.729	0.932	1.144	1.62	2.00	2.3
509	2.411	2.206	100	100	64	0.722	0.860	0.995	1.111	1.36	1.50	1.6
510	2.411	2.234	100	100	64	0.635	0.812	0.976	1.121	1.51	1.86	2.1
511	2.398	2.210	100	100	64	0.886	1.356	1.376	1.392	1.33	1.35	2.2
512	2.398	2.216	100	100	64	0.833	0.942	1.067	1.308	1.87	2.37	2.7
513	2.398	2.219	100	100	64	1.234	1.664	2.094	2.276	2.98	3.41	3.7
514	2.400	2.224	100	100	64	0.724	0.942	1.095	1.223	1.62	1.90	2.2
515	2.400	2.232	100	100	64	0.926	1.126	1.281	1.366	1.64	1.82	2.0
516	2.400	2.234	100	100	64	1.167	1.746	2.107	2.280	3.02	3.39	3.6
517	2.394	2.222	100	100	64	0.770	1.123	1.365	1.593	2.04	2.29	2.5
518	2.394	2.220	100	100	64	0.753	0.951	1.110	1.221	1.54	1.73	1.9
519	2.394	2.222	100	100	64	0.531	0.758	0.903	1.053	1.54	1.70	1.8
520	2.389	2.215	100	100	64	2.402	3.039	3.389	3.584	4.22	4.75	5.2
521	2.389	2.221	100	100	64	0.852	1.033	1.163	1.237	1.44	1.59	1.7
522	2.389	2.202	100	100	64	1.442	2.261	2.786	3.157	3.89	4.30	4.5
523	2.383	2.195	100	100	64	0.549	0.722	0.833	0.898	1.11	1.23	1.3
524	2.383	2.201	100	100	64	0.675	0.898	1.108	1.267	1.65	1.89	2.0
525	2.383	2.191	100	100	64	0.442	0.704	0.941	1.100	1.33	1.48	1.5
526	2.478	2.287	100	100	64	1.714	1.937	2.172	2.440	2.83	3.06	3.2
527	2.478	2.280	100	100	64	2.194	2.709	2.990	3.226	3.81	4.19	4.4
528	2.478	2.286	100	100	64	1.324	2.034	2.480	2.762	3.37	3.72	4.0
529	2.461	2.264	100	100	64	0.973	1.251	1.351	1.541	2.17	2.50	2.7
530	2.461	2.267	100	100	64	0.781	0.986	1.175	1.264	1.64	1.80	2.0
531	2.461	2.235	100	100	64	1.281	1.617	1.789	1.894	2.26	2.50	2.7
532	2.419	2.222	100	100	64	0.836	1.068	1.241	1.365	1.75	2.04	2.4
533	2.419	2.224	100	100	64	0.866	1.125	1.229	1.342	1.73	1.97	2.2
534	2.419	2.227	100	100	64	0.849	1.133	1.281	1.427	1.87	2.22	2.5
535	2.440	2.269	100	100	64	0.910	1.287	1.635	2.007	2.71	3.09	3.3
536	2.440	2.269	100	100	64	0.647	1.015	1.182	1.372	1.92	2.28	2.5
537	2.440	2.245	100	100	64	0.641	0.842	1.028	1.211	1.62	1.92	2.2
538	2.464	2.282	100	100	64	0.469	0.548	0.580	0.621	0.72	0.80	0.9
539	2.464	2.258	100	100	64	0.465	0.551	0.607	0.659	0.75	0.84	0.9
540	2.464	2.282	100	100	64	0.456	0.554	0.612	0.706	0.83	0.90	1.0
541	2.420	2.228	100	100	64	0.704	0.932	1.070	1.249	1.91	2.40	2.8
542	2.420	2.235	100	100	64	0.721	0.859	1.004	1.099	1.41	1.66	1.9
543	2.420	2.242	100	100	64	0.766	0.932	1.062	1.189	1.40	1.54	1.7
544	2.419	2.233	100	100	64	0.676	1.101	1.353	1.529	2.21	2.76	3.2
545	2.419	2.227	100	100	64	0.507	0.794	1.009	1.245	1.70	1.99	2.2
546	2.419	2.224	100	100	64	0.383	0.622	0.780	0.918	1.28	1.60	1.8
547	2.417	2.229	100	100	64	0.641	0.813	0.902	1.024	1.28	1.43	1.6
548	2.417	2.238	100	100	64	0.940	1.267	1.503	1.697	2.20	2.51	2.7
549	2.417	2.240	100	100	64	0.883	1.116	1.334	1.518	2.09	2.47	2.8
550	2.440	2.251	100	100	64	1.265	1.898	2.314	2.571	3.21	3.54	3.8
551	2.440	2.259	100	100	64	1.038	1.543	1.975	2.234	2.77	3.04	3.3
552	2.440	2.270	100	100	64	0.625	0.757	0.928	1.079	1.44	1.74	1.9
553	2.371	2.215	100	100	64	1.061	1.479	1.795	2.017	2.67	3.09	3.4
554	2.371	2.215	100	100	64	1.050	1.577	2.001	2.363	3.08	3.44	3.7
555	2.371	2.213	100	100	64	1.115	1.496	1.633	1.869	2.38	2.74	3.0
556	2.440	2.243	100	100	64	0.694	0.878	0.982	1.083	1.29	1.45	1.6
557	2.440	2.242	100	100	64	0.990	1.291	1.504	1.697	2.15	2.47	2.7
558	2.440	2.242	100	100	64	0.653	0.830	0.973	1.124	1.40	1.57	1.8
559	2.390	2.200	100	100	64	1.373	1.777	2.006	2.185	2.67	2.93	3.1
560	2.390	2.214	100	100	64	1.051	1.313	1.493	1.582	1.92	2.17	2.3
561	2.413	2.217	100	100	64	2.176	2.844	3.154	3.445	4.00	4.39	4.7
562	2.413	2.220	100	100	64	1.251	1.668	1.955	2.179	2.77	3.13	3.4
563	2.413	2.224	100	100	64	1.581	2.187	2.447	2.669	3.11	3.45	3.7
564	2.426	2.243	100	100	64	3.291	4.282	4.828	5.267	6.35	6.92	7.4
565	2.426	2.229	100	100	64	2.919	3.866	4.570	5.104	6.66	7.73	8.6
566	2.477	2.317	100	100	64	0.636	0.795	0.930	1.054	1.34	1.53	1.7
567	2.477	2.318	100	100	64	0.619	0.790	0.916	1.046	1.28	1.47	1.7

Sample No.	Mix Design ID	HMA Type	Highway Name	ADT (million)	3/4 inch 19.0mm	1/2 inch 12.5mm	3/8 inch 9.5mm	No. 4 4.75 mm	No. 8 2.36 mm
568	3074-SH02-73230	S4 ins	SH-48	15.9	100	98	88	58	39
569	3074-SH02-73230	S4 ins	SH-48	15.9	100	98	88	58	39
570	3074-SH02-73230	S4 ins	SH-48	15.9	100	98	88	58	39
571	3074-HH02-93324	S4 ins	I-35	54	100	96	87	53	29
572	3074-HH02-93324	S4 ins	I-35	54	100	96	87	53	29
Field Core Sample No.	**Mix Design ID**	**HMA Type**	**Highway Name**	**ADT (million)**	**3/4 inch 19.0mm**	**1/2 inch 12.5mm**	**3/8 inch 9.5mm**	**No. 4 4.75 mm**	**No. 8 2.36 mm**
573	3011-BCC-01105	A Rec	US-283	3M+	87	77	72	62	48
574	3011-SH00-71105	A-rec	US62	0.3M+	93	83	73	53	40
575	3011-OAPA-20588	A-rec	SH19	0.3M+	93	85	72	45	32
576	3011-OAPA-20588	A-rec	SH19	0.3M+	93	85	72	45	32
577	3073-OAPA-21099	19-mm	SH-3	3M+	96	82	71	54	41
578	3011-Est-01726	A-rec	US77	3M+	89	75	69	56	43
579	3011-OK98-32976	A-rec	SH1/SH63	3M+	92	82	69	43	31
580	3073-OAPA-21099	19.0mm	SH3	3M+	96	82	71	54	41
581	3031-92042	A-rec	SH102	0.3M+	92	81	72	54	39
582	3011-Est02330	A-rec	US54	3M+	93	84	76	60	46
583	3012-OVR-1121	B-ins	US177	0.3M	100	96	86	64	45
584	3011-EST-02406	A	SH9	3M+	89	77	65	40	34
585	3011-EST-01725	A-rec	I35	3M+	89	75	69	56	43
586	3012-OAPA-98389	B-ins	SH1/SH63	3M+	100	90	79	52	34
587	3011-91822	A	SH66	0.3M+	93	84	74	54	40
Plant Sample No.	**Mix Design ID**	**HMA Type**	**Highway Name**	**ADT (million)**	**3/4 inch 19.0mm**	**1/2 inch 12.5mm**	**3/8 inch 9.5mm**	**No. 4 4.75 mm**	**No. 8 2.36 mm**
588	3011-56875	A Res	N/A	0.3M+	92	84	76	60	39
589	3011-56875	A Res	N/A	0.3M+	92	84	76	60	39
590	3011-56875	A Res	N/A	0.3M+	92	84	76	60	39
591	3012-OAPA-99048	B Ins	N/A	3M-	100	98	85	54	34
592	3012-OAPA-99048	B Ins	N/A	3M-	100	98	85	54	34
593	3012-OAPA-99048	B Ins	N/A	3M-	100	98	85	54	34
594	3012-OAPA-20095	B ins	N/A	3M+	100	90	75	50	39
595	3012-OAPA-20095	B ins	N/A	3M+	100	90	75	50	39
596	3012-OAPA-20095	B ins	N/A	3M+	100	90	75	50	39
597	3012-OAPA-20095	B ins	N/A	3M+	100	90	75	50	39
598	3012-OAPA-20095	B ins	N/A	3M+	100	90	75	50	39
599	3012-OAPA-20095	B ins	N/A	3M+	100	90	75	50	39
600	3012-APAC-99018	B ins	N/A	3M+	100	95	86	50	35
601	3012-APAC-99018	B ins	N/A	3M+	100	95	86	50	35
602	3012-APAC-99018	B ins	N/A	3M+	100	95	86	50	35
603	3012-APAC-99018	B ins	N/A	3M+	100	95	86	50	35
604	3012-APAC-99018	B ins	N/A	3M+	100	95	86	50	35
605	3012-APAC-99018	B ins	N/A	3M+	100	95	86	50	35
606	3011-OAPA-20048	A Res	N/A	3M+	88	76	69	54	42
607	3011-OAPA-20048	A Res	N/A	3M+	88	76	69	54	42
608	3011-OAPA-20048	A Res	N/A	3M+	88	76	69	54	42
609	3012-OAPA-20049	B ins	N/A	3M+	100	99	86	60	47
610	3012-OAPA-20049	B ins	N/A	3M+	100	99	86	60	47
611	3012-OAPA-20049	B ins	N/A	3M+	100	99	86	60	47
612	3012-OAPA-20049	B ins	N/A	3M+	100	99	86	60	47
613	3012-OAPA-20049	B ins	N/A	3M+	100	99	86	60	47
614	3012-OAPA-20049	B ins	N/A	3M+	100	99	86	60	47
615	3011-OAPA-20090	A Rec	N/A	3M+	92	82	75	61	40
616	3011-OAPA-20090	A Rec	N/A	3M+	92	82	75	61	40
617	3011-OAPA-20090	A Rec	N/A	3M+	92	82	75	61	40
618	3011-OAPA-20090	A Rec	N/A	3M+	92	82	75	61	40
619	3011-OAPA-20090	A Rec	N/A	3M+	92	82	75	61	40
620	3011-OAPA-20090	A Rec	N/A	3M+	92	82	75	61	40
621	3013-OAPA-20225	C Ins	N/A	0.3M+	100	100	95	66	48
622	3013-OAPA-20225	C Ins	N/A	0.3M+	100	100	95	66	48
623	3013-OAPA-20225	C Ins	N/A	0.3M+	100	100	95	66	48
624	3013-OAPA-20225	C Ins	N/A	0.3M+	100	100	95	66	48
625	3013-OAPA-20225	C Ins	N/A	0.3M+	100	100	95	66	48
626	3013-OAPA-20225	C Ins	N/A	0.3M+	100	100	95	66	48

Sample	No. 16	No. 30	No. 50	No. 100	No. 200	Asphalt			Aggregate		
No.	1.18mm	0.60mm	0.30mm	0.15 mm	0.075mm	Pb	PG	Gb	FAA	FF	G_{sb}
568	26	18	13	6	2.9	4.5	PG 70-28OK	1.0209	45.4	100	2.693
569	26	18	13	6	2.9	4.5	PG 70-28OK	1.0209	45.4	100	2.693
570	26	18	13	6	2.9	4.5	PG 70-28OK	1.0209	45.4	100	2.693
571	21	17	14	7	3.0	4.9	PG 70-28OK	1.0253	45.6	100	2.651
572	21	17	14	7	3.0	4.9	PG 70-28OK	1.0253	45.6	100	2.651
Field Core	**No. 16**	**No. 30**	**No. 50**	**No. 100**	**No. 200**	**Asphalt**					
Sample No.	**1.18mm**	**0.60mm**	**0.30mm**	**0.15 mm**	**0.075mm**	**Pb**	**PG**	**Gb**	**FAA**	**FF**	**GSB**
573	34	23	14	7	5.0	4.4	PG 64-22OK	1.0100	45.0	100	2.732
574	33	27	19	9	4.1	4.2	PG 64-22OK	1.0100	45.2	100	2.642
575	24	19	13	7	4.6	4.0	PG 64-22OK	1.0052	45.3	100	2.647
576	24	19	13	7	4.6	4.0	PG 64-22OK	1.0052	45.1	100	2.647
577	29	22	18	8	4.7	4.9	PG 64-22OK	1.0150	45.1	100	2.483
578	32	26	17	9	4.9	4.0	PG 64-22OK	1.0100	45.1	100	2.654
579	23	19	12	8	4.7	3.9	PG 64-22OK	1.0198	42.9	100	2.648
580	29	22	18	8	4.7	4.9	PG 64-22OK	1.0150	42.9	100	2.483
581	30	23	16	9	4.2	4.2	PG 64-22OK	1.0100	45.1	100	2.643
582	33	24	15	9	4.9	4.3	PG 70-28OK	1.0100	45.6	100	2.668
583	30	18	11	7	5.7	5.6	PG 70-28OK	1.0087	45.3	100	2.727
584	28	22	16	10	5.3	4.3	PG 70-28OK	1.0210	45.1	100	2.519
585	32	25	17	9	4.9	4.0	PG 64-22OK	1.0100	45.4	100	2.656
586	25	19	14	9	5.1	4.7	PG 64-22OK	1.0198	45.3	100	2.637
587	31	25	17	9	4.7	4.0	PG 64-22OK	1.0220	45.4	100	2.781
Plant	**No. 16**	**No. 30**	**No. 50**	**No. 100**	**No. 200**	**Asphalt**					
Sample No.	**1.18mm**	**0.60mm**	**0.30mm**	**0.15 mm**	**0.075mm**	**Pb**	**PG**	**Gb**	**FAA**	**FF**	**GSB**
588	29	22	15	8	4.5	4.6	PG 64-22OK	1.0100	45.7	100	2.654
589	29	22	15	8	4.5	4.6	PG 64-22OK	1.0100	45.7	100	2.654
590	29	22	15	8	4.5	4.6	PG 64-22OK	1.0100	45.7	100	2.654
591	25	19	12	6	4.2	4.8	PG 76-28OK	1.0201	45.7	100	2.658
592	25	19	12	6	4.2	4.8	PG 76-28OK	1.0201	45.7	100	2.658
593	25	19	12	6	4.2	4.8	PG 76-28OK	1.0201	45.7	100	2.658
594	31	24	17	10	5.7	5.6	PG 70-28OK	1.0119	45.3	100	2.529
595	31	24	17	10	5.7	5.6	PG 70-28OK	1.0119	45.3	100	2.529
596	31	24	17	10	5.7	5.6	PG 70-28OK	1.0119	45.3	100	2.529
597	31	24	17	10	5.7	5.6	PG 70-28OK	1.0119	45.3	100	2.529
598	31	24	17	10	5.7	5.6	PG 70-28OK	1.0119	45.3	100	2.529
599	31	24	17	10	5.7	5.6	PG 70-28OK	1.0119	45.3	100	2.529
600	27	22	15	7	4.7	4.9	PG 70-28OK	1.0198	45.3	100	2.580
601	27	22	15	7	4.7	4.9	PG 70-28OK	1.0198	45.3	100	2.580
602	27	22	15	7	4.7	4.9	PG 70-28OK	1.0198	45.3	100	2.580
603	27	22	15	7	4.7	4.9	PG 64-22OK	1.0198	45.3	100	2.580
604	27	22	15	7	4.7	4.9	PG 64-22OK	1.0198	45.3	100	2.580
605	27	22	15	7	4.7	4.9	PG 64-22OK	1.0198	45.3	100	2.580
606	32	23	15	8	4.7	3.8	PG 64-22OK	1.0100	45.3	100	2.638
607	32	23	15	8	4.7	3.8	PG 64-22OK	1.0100	45.3	100	2.638
608	32	23	15	8	4.7	3.8	PG 64-22OK	1.0100	45.3	100	2.638
609	35	26	16	8	4.6	4.7	PG 64-22OK	1.0232	45.1	100	2.603
610	35	26	16	8	4.6	4.7	PG 64-22OK	1.0232	45.1	100	2.603
611	35	26	16	8	4.6	4.7	PG 64-22OK	1.0232	45.1	100	2.603
612	35	26	16	8	4.6	4.7	PG 70-28OK	1.0232	45.1	100	2.603
613	35	26	16	8	4.6	4.7	PG 70-28OK	1.0232	45.1	100	2.603
614	35	26	16	8	4.6	4.7	PG 70-28OK	1.0232	45.1	100	2.603
615	31	25	18	9	4.7	4.1	PG 70-28OK	1.0100	45.1	100	2.640
616	31	25	18	9	4.7	4.1	PG 70-28OK	1.0100	45.1	100	2.640
617	31	25	18	9	4.7	4.1	PG 70-28OK	1.0100	45.1	100	2.640
618	31	25	18	9	4.7	4.1	PG 64-22OK	1.0100	45.1	100	2.640
619	31	25	18	9	4.7	4.1	PG 64-22OK	1.0100	45.1	100	2.640
620	31	25	18	9	4.7	4.1	PG 64-22OK	1.0100	45.1	100	2.640
621	33	22	14	9	6.7	6.3	PG 64-22OK	0.9943	45.4	100	2.812
622	33	22	14	9	6.7	6.3	PG 64-22OK	0.9943	45.4	100	2.812
623	33	22	14	9	6.7	6.3	PG 64-22OK	0.9943	45.4	100	2.812
624	33	22	14	9	6.7	6.3	PG 64-22OK	0.9943	45.4	100	2.812
625	33	22	14	9	6.7	6.3	PG 76-28OK	0.9943	45.4	100	2.812
626	33	22	14	9	6.7	6.3	PG 76-28OK	0.9943	45.4	100	2.812

Sample	Mix		Parameters			Rut Depths (mm) at cycles						
No.	G_{mm}	G_{mb}	Wheel	Tire	Temp.	500-c	1000-c	1500-c	2000-c	4000-c	6000-c	8000-c
568	2.510	2.332	100	100	64	0.790	0.999	1.178	1.329	1.79	2.23	2.6
569	2.510	2.331	100	100	64	0.723	0.978	1.141	1.269	1.76	2.19	2.5
570	2.510	2.340	100	100	64	0.689	0.915	1.121	1.257	1.77	2.24	2.5
571	2.480	2.321	100	100	64	0.630	0.741	0.825	0.862	1.06	1.20	1.3
572	2.480	2.321	100	100	64	0.594	0.707	0.786	0.856	1.02	1.12	1.2
Field Core	**Mix**		**Testing parameters**			**APA rut values**						
Sample No.	**Gmm**	**Gmb**	**Load**	**Pres.**	**Temp.**	**500-cyc**	**1000-cyc**	**1500-cyc**	**2000-cyc**	**4000-cyc**	**6000-cyc**	**8000-cyc**
573	2.564	2.374	100	100	64	1.558	1.803	2.026	2.174	2.54	2.83	3.1
574	2.529	2.327	100	100	64	2.361	3.092	3.579	3.921	4.84	5.42	5.7
575	2.517	2.385	100	100	64	5.425	6.700	7.371	7.782	8.67	9.24	9.8
576	2.517	2.388	100	100	64	2.482	3.615	4.684	5.516	7.06	7.73	8.2
577	2.387	2.221	100	100	64	3.656	4.753	5.374	5.805	6.61	7.04	7.3
578	2.531	2.390	100	100	64	2.299	2.992	3.348	3.621	4.35	4.74	5.1
579	2.508	2.311	100	100	64	1.743	2.166	2.414	2.631	3.13	3.45	3.7
580	2.372	2.184	100	100	64	1.387	1.752	1.941	2.092	2.49	2.79	3.1
581	2.530	2.395	100	100	64	2.551	3.345	3.887	4.130	4.84	5.42	5.9
582	2.495	2.360	100	100	64	1.352	1.826	2.010	2.089	2.53	2.83	2.9
583	2.491	2.285	100	100	64	0.655	0.760	0.845	0.906	1.17	1.25	1.4
584	2.388	2.190	100	100	64	1.496	1.855	2.098	2.287	2.65	2.86	3.0
585	2.524	2.375	100	100	64	1.260	1.654	1.925	2.107	2.69	3.09	3.4
586	2.469	2.206	100	100	64	1.056	1.394	1.619	1.785	2.26	2.68	2.5
587	2.607	2.484	100	100	64	1.840	2.618	3.109	3.522	4.67	5.35	5.6
Plant	**Mix**		**Testing parameters**			**APA rut values**						
Sample No.	**Gmm**	**Gmb**	**Load**	**Pres.**	**Temp.**	**500-cyc**	**1000-cyc**	**1500-cyc**	**2000-cyc**	**4000-cyc**	**6000-cyc**	**8000-cyc**
588	2.513	2.362	100	100	64	0.647	0.812	1.019	1.120	1.52	1.93	2.3
589	2.513	2.350	100	100	64	0.581	0.770	0.910	1.086	1.81	2.32	2.6
590	2.513	2.274	100	100	64	0.557	0.652	0.818	0.954	1.53	2.14	2.8
591	2.464	2.331	100	100	64	0.494	0.583	0.650	0.610	0.93	0.95	1.1
592	2.464	2.240	100	100	64	0.570	0.629	0.742	0.722	1.14	1.32	1.7
593	2.464	2.292	100	100	64	0.615	0.732	0.807	0.809	1.02	1.17	1.2
594	2.348	2.219	100	100	64	0.767	1.050	1.297	1.525	2.25	2.86	3.3
595	2.348	2.219	100	100	64	0.887	1.206	1.469	1.728	2.59	3.15	3.5
596	2.348	2.217	100	100	64	1.493	2.513	3.183	3.626	4.72	5.25	5.6
597	2.348	2.190	100	100	64	1.333	2.098	2.661	3.120	4.12	4.72	5.1
598	2.348	2.187	100	100	64	1.017	1.689	2.472	2.998	4.03	4.55	4.9
599	2.348	2.179	100	100	64	1.083	1.580	2.097	2.571	3.97	4.66	5.1
600	2.435	2.267	100	100	64	0.772	0.944	1.094	1.150	1.48	1.88	2.3
601	2.435	2.291	100	100	64	0.466	0.589	0.678	0.675	0.90	1.06	1.2
602	2.435	2.284	100	100	64	0.650	0.786	0.878	0.854	1.12	1.26	1.4
603	2.435	2.274	100	100	64	0.680	1.004	1.012	1.291	1.63	2.10	2.5
604	2.435	2.273	100	100	64	0.591	0.718	0.886	0.969	1.28	1.57	1.8
605	2.435	2.254	100	100	64	0.709	0.943	1.146	1.205	1.56	1.67	2.0
606	2.526	2.344	100	100	64	0.999	1.247	1.472	1.651	2.14	2.55	2.9
607	2.526	2.350	100	100	64	0.914	1.117	1.241	1.331	1.63	1.85	2.0
608	2.526	2.345	100	100	64	0.470	0.622	0.712	0.819	1.09	1.34	1.5
609	2.479	2.382	100	100	64	0.635	0.824	0.958	1.040	1.34	1.59	1.8
610	2.479	2.313	100	100	64	0.984	1.219	1.369	1.500	1.72	1.94	2.1
611	2.479	2.296	100	100	64	1.175	1.445	1.636	1.737	2.14	2.53	2.8
612	2.479	2.311	100	100	64	0.429	0.498	0.584	0.655	0.81	0.98	1.1
613	2.479	2.307	100	100	64	0.770	0.957	1.104	1.188	1.39	1.70	1.9
614	2.479	2.301	100	100	64	0.942	1.124	1.293	1.413	1.67	1.93	2.1
615	2.525	2.346	100	100	64	1.204	1.446	1.550	1.667	1.92	2.07	2.2
616	2.525	2.331	100	100	64	0.765	0.906	0.959	1.081	1.26	1.43	1.6
617	2.525	2.328	100	100	64	0.986	1.179	1.297	1.372	1.55	1.72	1.9
618	2.525	2.355	100	100	64	0.756	0.948	1.017	1.080	1.40	1.69	1.9
619	2.525	2.350	100	100	64	0.420	0.526	0.583	0.628	0.77	0.87	0.9
620	2.525	2.350	100	100	64	0.583	0.752	0.925	1.063	1.27	1.51	1.7
621	2.563	2.399	100	100	64	0.816	0.994	1.172	1.313	1.92	2.59	3.2
622	2.563	2.389	100	100	64	0.603	0.707	0.804	0.866	1.18	1.73	2.4
623	2.563	2.366	100	100	64	0.408	0.515	0.650	0.719	1.15	1.70	2.2
624	2.563	2.383	100	100	64	0.621	1.030	1.278	1.542	2.35	3.01	3.6
625	2.563	2.377	100	100	64	0.773	1.188	1.473	1.758	2.53	3.07	3.5
626	2.563	2.364	100	100	64	0.760	1.199	1.494	1.895	2.95	3.55	4.1

Sample No.	Mix Design ID	HMA Type	Highway Name	ADT (million)	3/4 inch 19.0mm	1/2 inch 12.5mm	3/8 inch 9.5mm	No. 4 4.75 mm	No. 8 2.36 mm
627	3012-OAPA-20095	B ins	N/A	3M+	100	99	89	62	47
628	3012-OAPA-20095	B ins	N/A	3M+	100	99	89	62	47
629	3012-OAPA-20095	B ins	N/A	3M+	100	99	89	62	47
630	3012-OAPA-20095	B ins	N/A	3M+	100	99	89	62	47
631	3012-OAPA-20095	B ins	N/A	3M+	100	99	89	62	47
632	3012-OAPA-20095	B ins	N/A	3M+	100	99	89	62	47
633	3012-OAPA-20033	BH ins	N/A	3M+	100	89	73	57	43
634	3012-OAPA-20033	BH ins	N/A	3M+	100	89	73	57	43
635	3012-OAPA-20033	BH ins	N/A	3M+	100	89	73	57	43
Control Sample No.	**Mix Design ID**	**HMA Type**	**Highway Name**	**ADT (million)**	**3/4 inch 19.0mm**	**1/2 inch 12.5mm**	**3/8 inch 9.5mm**	**No. 4 4.75 mm**	**No. 8 2.36 mm**
636	3012-OAPA-99037	B ins	US54	3M+	100	90	81	55	43
637	3012-OAPA-99037	B ins	US54	3M+	100	90	81	55	43
638	3012-OAPA-99037	B ins	US54	3M+	100	90	81	55	43
639	3012-OAPA-99037	B ins	US54	3M+	100	90	81	55	43
640	3012-OAPA-99037	B ins	US54	3M+	100	90	81	55	43
641	3012-OAPA-99037	B ins	US54	3M+	100	90	81	55	43
642	3012-OAPA-99037	B ins	US54	3M+	100	90	81	55	43
643	3012-OAPA-99037	B ins	US54	3M+	100	90	81	55	43
644	3012-OAPA-99037	B ins	US54	3M+	100	90	81	55	43
645	3012-OAPA-99037	B ins	US54	3M+	100	90	81	55	43
646	3012-OAPA-99037	B ins	US54	3M+	100	90	81	55	43
647	3012-OAPA-99037	B ins	US54	3M+	100	90	81	55	43
648	3012-OAPA-99037	B ins	US54	3M+	100	90	81	55	43
649	3012-OAPA-99037	B ins	US54	3M+	100	90	81	55	43
650	3012-OAPA-99037	B ins	US54	3M+	100	90	81	55	43
651	3012-OAPA-99037	B ins	US54	3M+	100	90	81	55	43
652	3012-OAPA-99037	B ins	US54	3M+	100	90	81	55	43
653	3012-OAPA-99037	B ins	US54	3M+	100	90	81	55	43
654	3012-OAPA-99037	B ins	US54	3M+	100	90	81	55	43
655	3012-OAPA-99037	B ins	US54	3M+	100	90	81	55	43
656	3012-OAPA-63071	A-type	US54	3M+	100	78	68	49	32
657	3012-OAPA-63071	A-type	US54	3M+	100	78	68	49	32
658	3012-OAPA-63071	A-type	US54	3M+	100	78	68	49	32
659	3012-OAPA-63071	A-type	US54	3M+	100	78	68	49	32
660	3012-OAPA-63071	A-type	US54	3M+	100	78	68	49	32
661	3012-OAPA-63071	A-type	US54	3M+	100	78	68	49	32
662	3012-OAPA-63071	A-type	US54	3M+	100	78	68	49	32
663	3012-OAPA-63071	A-type	US54	3M+	100	78	68	49	32
664	3012-OAPA-63071	A-type	US54	3M+	100	78	68	49	32
665	3012-OAPA-63071	A-type	US54	3M+	100	78	68	49	32
666	3012-OAPA-63071	A-type	US54	3M+	100	78	68	49	32
667	3012-OAPA-63071	A-type	US54	3M+	100	78	68	49	32
668	3012-OAPA-63070	A-type	US54	3M+	92	81	71	51	28
669	3012-OAPA-63070	A-type	US54	3M+	92	81	71	51	28
670	3012-OAPA-63070	A-type	US54	3M+	92	81	71	51	28
671	3012-OAPA-63070	A-type	US54	3M+	92	81	71	51	28
672	3012-OAPA-63070	A-type	US54	3M+	92	81	71	51	28
673	3012-OAPA-63070	A-type	US54	3M+	92	81	71	51	28
674	3012-OAPA-63070	A-type	US54	3M+	92	81	71	51	28
Lab Mix Sample No.	**Mix Design ID**	**HMA Type**	**Highway Name**	**ADT (million)**	**3/4 inch 19.0mm**	**1/2 inch 12.5mm**	**3/8 inch 9.5mm**	**No. 4 4.75 mm**	**No. 8 2.36 mm**
675	Total, Ardmore	B ins	N/A	3M+	98	88	81	68	43
676	Lion Oi, Muskogee	B ins	N/A	3M+	98	88	81	68	43
677	Royal Co.	B ins	N/A	3M+	98	88	81	68	43
678	Total, Ardmore	B ins	N/A	3M+	98	88	81	68	43
679	Frontier, Muskogee	B ins	N/A	3M+	98	88	81	68	43
680	Royal Trading	B ins	N/A	3M+	98	88	81	68	43
681	Lion oil, Aldorado	B ins	N/A	3M+	98	88	81	68	43
682	Gary.W, Wynewood	B ins	N/A	3M+	98	88	81	68	43
683	Royal Co.	B ins	N/A	3M+	98	88	81	68	43
684	Sinclair	B ins	N/A	3M+	98	88	81	68	43
685	Total, Ardmore	B ins	N/A	3M+	98	88	81	68	43

Sample	No. 16	No. 30	No. 50	No. 100	No. 200	Asphalt			Aggregate		
No.	1.18mm	0.60mm	0.30mm	0.15 mm	0.075mm	Pb	PG	Gb	FAA	FF	G_{sb}
627	36	28	19	10	5.4	5.2	PG 70-28OK	1.0128	45.4	100	2.650
628	36	28	19	10	5.4	5.2	PG 70-28OK	1.0128	45.4	100	2.650
629	36	28	19	10	5.4	5.2	PG 70-28OK	1.0128	45.4	100	2.650
630	36	28	19	10	5.4	5.2	PG 76-28OK	1.0128	45.4	100	2.650
631	36	28	19	10	5.4	5.2	PG 76-28OK	1.0128	45.4	100	2.650
632	36	28	19	10	5.4	5.2	PG 64-22OK	1.0128	45.4	100	2.650
633	32	23	15	9	5.3	4.5	PG 64-22OK	1.0245	45.4	100	2.609
634	32	23	15	9	5.3	4.5	PG 64-22OK	1.0245	45.4	100	2.609
635	32	23	15	9	5.3	4.5	PG 64-22OK	1.0245	45.4	100	2.609
Control	**No. 16**	**No. 30**	**No. 50**	**No. 100**	**No. 200**	**Asphalt**					
Sample No.	**1.18mm**	**0.60mm**	**0.30mm**	**0.15 mm**	**0.075mm**	**Pb**	**PG**	**Gb**	**FAA**	**FF**	**GSB**
636	31	22	15	9	4.5	5.5	PG 64-22OK	1.0177	45.1	83	2.635
637	31	22	15	9	4.5	5.8	PG 64-22OK	1.0177	45.1	83	2.635
638	31	22	15	9	4.5	4.8	PG 64-22OK	1.0177	45.1	83	2.635
639	31	22	15	9	4.5	5.8	PG 64-22OK	1.0177	45.1	83	2.635
640	31	22	15	9	4.5	5.8	PG 64-22OK	1.0177	45.1	83	2.635
641	31	22	15	9	4.5	5.3	PG 64-22OK	1.0177	45.1	83	2.635
642	31	22	15	9	4.5	4.5	PG 64-22OK	1.0177	45.1	83	2.635
643	31	22	15	9	4.5	5.5	PG 64-22OK	1.0177	45.1	83	2.635
644	31	22	15	9	4.5	5.5	PG 70-28OK	1.0177	45.1	83	2.635
645	31	22	15	9	4.5	5.5	PG 70-28OK	1.0177	45.1	83	2.635
646	31	22	15	9	4.5	5.0	PG 70-28OK	1.0177	45.1	83	2.635
647	31	22	15	9	4.5	5.0	PG 70-28OK	1.0177	45.1	83	2.635
648	31	22	15	9	4.5	5.0	PG 70-28OK	1.0177	45.1	83	2.635
649	31	22	15	9	4.5	6.0	PG 70-28OK	1.0177	45.1	83	2.635
650	31	22	15	9	4.5	6.0	PG 70-28OK	1.0177	45.1	83	2.635
651	31	22	15	9	4.5	6.0	PG 70-28OK	1.0177	45.1	83	2.635
652	31	22	15	9	4.5	6.0	PG 70-28OK	1.0177	45.1	83	2.635
653	31	22	15	9	4.5	6.0	PG 76-28OK	1.0177	45.1	83	2.635
654	31	22	15	9	4.5	6.0	PG 76-28OK	1.0177	45.1	83	2.635
655	31	22	15	9	4.5	6.0	PG 76-28OK	1.0177	45.1	83	2.635
656	23	17	12	8	5.5	4.3	PG 76-28OK	1.0078	45.2	79.1	2.620
657	23	17	12	8	5.5	5.3	PG 76-28OK	1.0078	45.2	79.1	2.620
658	23	17	12	8	5.5	4.3	PG 76-28OK	1.0078	45.2	79.1	2.620
659	23	17	12	8	5.5	5.3	PG 70-28OK	1.0078	45.2	79.1	2.620
660	23	17	12	8	5.5	4.3	PG 70-28OK	1.0078	45.2	79.1	2.620
661	23	17	12	8	5.5	4.3	PG 70-28OK	1.0078	45.2	79.1	2.620
662	23	17	12	8	5.5	4.3	PG 70-28OK	1.0078	45.2	79.1	2.620
663	23	17	12	8	5.5	4.5	PG 70-28OK	1.0078	45.2	79.1	2.620
664	23	17	12	8	5.5	4.8	PG 70-28OK	1.0078	45.2	79.1	2.620
665	23	17	12	8	5.5	5.0	PG 64-22OK	1.0078	45.2	79.1	2.620
666	23	17	12	8	5.5	4.5	PG 64-22OK	1.0078	45.2	79.1	2.620
667	23	17	12	8	5.5	5.3	PG 64-22OK	1.0078	45.2	79.1	2.620
668	19	14	10	7	4.7	4.8	PG 64-22OK	1.0078	45.4	83	2.606
669	19	14	10	7	4.7	4.3	PG 64-22OK	1.0078	45.4	83	2.606
670	19	14	10	7	4.7	5.5	PG 64-22OK	1.0078	45.4	83	2.606
671	19	14	10	7	4.7	4.5	PG 70-28OK	1.0078	45.4	83	2.606
672	19	14	10	7	4.7	5.0	PG 70-28OK	1.0078	45.4	83	2.606
673	19	14	10	7	4.7	5.0	PG 70-28OK	1.0078	45.4	83	2.606
674	19	14	10	7	4.7	4.5	PG 70-28OK	1.0078	45.4	83	2.606
Lab Mix	**No. 16**	**No. 30**	**No. 50**	**No. 100**	**No. 200**	**Asphalt**					
Sample No.	**1.18mm**	**0.60mm**	**0.30mm**	**0.15 mm**	**0.075mm**	**Pb**	**PG**	**Gb**	**FAA**	**FF**	**GSB**
675	30	22	15	9	5.6	4.4	PG 70-28OK	1.0110	45.2	100	2.639
676	30	22	15	9	5.6	4.4	PG 70-28OK	1.0254	45.2	100	2.639
677	30	22	15	9	5.6	4.4	PG 70-28OK	1.0122	45.2	100	2.642
678	30	22	15	9	5.6	4.4	PG 70-28OK	1.0160	45.2	100	2.639
679	30	22	15	9	5.6	4.4	PG 70-28OK	1.0152	45.2	100	2.639
680	30	22	15	9	5.6	4.4	PG 64-22OK	1.0258	45.2	100	2.642
681	30	22	15	9	5.6	4.4	PG 64-22OK	1.0315	45.2	100	2.639
682	30	22	15	9	5.6	4.4	PG 64-22OK	1.0076	45.2	100	2.639
683	30	22	15	9	5.6	4.4	PG 64-22OK	1.0150	45.2	100	2.642
684	30	22	15	9	5.6	4.4	PG 64-22OK	1.0159	45.2	100	2.639
685	30	22	15	9	5.6	4.4	PG 64-22OK	1.0087	45.2	100	2.639

Sample	Mix		Parameters			Rut Depths (mm) at cycles						
No.	G_{mm}	G_{mb}	Wheel	Tire	Temp.	500-c	1000-c	1500-c	2000-c	4000-c	6000-c	8000-c
627	2.482	2.328	100	100	64	0.118	0.218	0.246	0.321	0.49	0.63	0.7
628	2.482	2.296	100	100	64	0.251	0.347	0.367	0.391	0.54	0.59	0.7
629	2.482	2.291	100	100	64	0.063	0.088	0.116	0.132	0.19	0.20	0.3
630	2.482	2.310	100	100	64	0.660	0.863	1.028	1.178	1.66	2.06	2.5
631	2.482	2.307	100	100	64	1.516	1.927	2.098	2.254	2.88	3.34	3.8
632	2.482	2.282	100	100	64	0.851	1.136	1.341	1.533	2.41	3.37	4.1
633	2.476	2.409	100	100	64	0.746	0.899	1.029	1.071	1.37	1.55	1.8
634	2.476	2.372	100	100	64	0.951	1.079	1.213	1.299	1.60	1.84	2.1
635	2.476	2.362	100	100	64	0.756	0.888	1.052	1.159	1.51	1.80	2.1
Control	**Mix**		**Testing parameters**			**APA rut values**						
Sample No.	**Gmm**	**Gmb**	**Load**	**Pres.**	**Temp.**	**500-cyc**	**1000-cyc**	**1500-cyc**	**2000-cyc**	**4000-cyc**	**6000-cyc**	**8000-cyc**
636	2.441	2.356	100	100	64	0.992	1.486	1.990	2.381	4.20	5.44	6.2
637	2.432	2.366	100	100	64	0.816	1.196	1.640	1.921	3.58	5.05	6.4
638	2.468	2.370	100	100	64	0.589	0.847	0.996	1.122	1.89	2.70	3.5
639	2.432	2.333	100	100	64	0.834	1.139	1.353	1.553	2.45	3.71	5.3
640	2.432	2.364	100	100	64	0.802	1.145	1.457	1.646	2.46	3.63	5.0
641	2.450	2.372	100	100	64	0.717	1.016	1.278	1.472	2.07	2.87	4.0
642	2.477	2.382	100	100	64	1.144	1.600	1.869	2.075	3.01	4.18	5.8
643	2.450	2.262	100	100	64	0.934	1.091	1.121	1.168	1.39	1.69	2.0
644	2.450	2.262	100	100	64	0.508	0.596	0.670	0.742	0.80	1.01	1.0
645	2.450	2.262	100	100	64	0.724	0.759	0.821	1.022	1.11	1.37	1.5
646	2.459	2.326	100	100	64	0.661	0.774	0.919	1.027	1.45	2.06	3.0
647	2.459	2.270	100	100	64	0.526	0.581	0.735	0.777	1.09	1.49	2.0
648	2.459	2.320	100	100	64	0.727	0.801	0.910	1.063	1.32	1.74	2.1
649	2.423	2.298	100	100	64	0.560	0.633	0.687	0.714	0.93	1.15	1.4
650	2.423	2.283	100	100	64	0.620	0.745	0.857	0.941	1.27	1.59	1.9
651	2.423	2.268	100	100	64	0.582	0.738	0.756	0.799	1.01	1.38	1.6
652	2.423	2.267	100	100	64	0.715	0.913	1.156	1.357	2.64	3.45	4.5
653	2.423	2.325	100	100	64	1.017	1.453	1.735	2.075	3.39	4.69	5.6
654	2.423	2.278	100	100	64	1.128	1.564	1.900	2.271	3.89	5.15	6.0
655	2.557	2.382	100	100	64	1.144	1.600	1.869	2.075	3.01	4.18	5.8
656	2.478	2.385	100	100	64	1.038	1.467	1.837	2.134	3.29	3.99	4.5
657	2.442	2.376	100	100	64	0.737	1.039	1.314	1.600	2.61	3.38	4.0
658	2.439	2.253	100	100	64	1.671	2.147	2.594	2.905	3.63	4.15	4.5
659	2.421	2.237	100	100	64	1.517	1.962	2.252	2.483	3.03	3.37	3.6
660	2.442	2.243	100	100	64	3.234	4.202	4.814	5.284	6.43	7.11	7.6
661	2.439	2.180	100	100	64	2.266	2.948	3.403	3.784	5.03	6.16	7.1
662	2.476	2.333	100	100	64	0.713	1.046	1.377	1.701	3.11	4.09	4.8
663	2.439	2.180	100	100	64	2.468	2.327	3.403	3.784	5.03	6.16	7.1
664	2.439	2.180	100	100	64	2.459	2.373	3.403	3.784	5.03	6.16	7.1
665	2.439	2.180	100	100	64	2.450	2.388	3.403	3.784	5.03	6.16	7.1
666	2.478	2.385	100	100	64	1.038	1.467	1.837	2.134	3.29	3.99	4.5
667	2.442	2.376	100	100	64	0.737	1.039	1.314	1.600	2.61	3.38	4.0
668	2.457	2.227	100	100	64	1.247	1.747	2.143	2.423	3.64	4.54	5.3
669	2.476	2.285	100	100	64	2.035	2.547	2.760	2.958	3.69	4.58	5.5
670	2.468	2.264	100	100	64	2.515	3.373	3.889	4.358	6.04	7.46	8.4
671	2.439	2.215	100	100	64	2.200	2.915	3.474	4.109	6.14	7.83	9.2
672	2.421	2.181	100	100	64	3.593	5.207	6.395	7.283	10.07	12.00	13.5
673	2.439	2.187	100	100	64	2.759	4.587	5.085	5.201	7.81	9.32	11.1
674	2.457	2.190	100	100	64	2.865	3.210	4.562	5.201	7.10	9.02	10.3
Lab Mix	**Mix**		**Testing parameters**			**APA rut values**						
Sample No.	**Gmm**	**Gmb**	**Load**	**Pres.**	**Temp.**	**500-cyc**	**1000-cyc**	**1500-cyc**	**2000-cyc**	**4000-cyc**	**6000-cyc**	**8000-cyc**
675	2.526	2.338	100	100	64	1.148	1.706	2.101	2.417	3.56	4.09	4.5
676	2.534	2.312	100	100	64	1.476	2.133	2.440	2.690	3.36	3.74	4.1
677	2.525	2.355	100	100	64	0.420	0.531	0.645	0.715	0.90	0.97	1.1
678	2.527	2.339	100	100	64	0.764	1.079	1.318	1.473	2.38	3.10	3.6
679	2.527	2.318	100	100	64	0.471	0.670	0.899	1.054	1.62	2.10	2.4
680	2.527	2.354	100	100	64	0.483	0.711	0.614	0.806	0.95	1.03	1.1
681	2.536	2.321	100	100	64	2.620	3.792	4.397	4.730	5.56	6.09	6.4
682	2.525	2.343	100	100	61	2.011	2.693	3.134	3.396	4.06	4.45	4.8
683	2.525	2.349	100	100	61	0.667	0.930	0.858	0.983	1.21	1.39	1.6
684	2.527	2.318	100	100	61	1.387	2.040	2.519	2.904	3.77	4.18	4.6
685	2.523	2.352	100	100	64	0.683	0.873	1.002	1.176	1.81	2.36	2.8

Sample No.	Mix Design ID	HMA Type	Highway Name	ADT (million)	3/4 inch 19.0mm	1/2 inch 12.5mm	3/8 inch 9.5mm	No. 4 4.75 mm	No. 8 2.36 mm
686	Royal Co.	B ins	N/A	3M+	98	88	81	68	43
687	Trumbull	B ins	N/A	3M+	98	88	81	68	43
688	Total, Ardmore	B ins	N/A	3M+	98	88	81	68	43
689	Lion Oi, Muskogee	B ins	N/A	3M+	98	88	81	68	43
690	Royal Co.	B ins	N/A	3M+	98	88	81	68	43
691	Total, Ardmore	B ins	N/A	3M+	98	88	81	68	43
692	Frontier, Muskogee	B ins	N/A	3M+	98	88	81	68	43
693	Royal Trading	B ins	N/A	3M+	98	88	81	68	43
694	Lion oil, Aldorado	B ins	N/A	3M+	98	88	81	68	43
695	Gary.W, Wynewood	B ins	N/A	3M+	98	88	81	68	43
696	Royal Co.	B ins	N/A	3M+	98	88	81	68	43
697	Sinclair	B ins	N/A	3M+	98	88	81	68	43
698	Total, Ardmore	B ins	N/A	3M+	98	88	81	68	43
699	Royal Co.	B ins	N/A	3M+	98	88	81	68	43
700	Trumbull	B ins	N/A	3M+	98	88	81	68	43
701	Total, Ardmore	B ins	N/A	3M+	98	88	81	68	43
702	LionOil,Muskogee	B ins	N/A	3M+	98	88	81	68	43
703	Royal Trading, Tulsa	B ins	N/A	3M+	98	88	81	68	43
704	Total, Ardmore	B ins	N/A	3M+	98	88	81	68	43
705	Frontier, Muskogee	B ins	N/A	3M+	98	88	81	68	43
706	Royal Trading	B ins	N/A	3M+	98	88	81	68	43
707	Sinclair	B ins	N/A	3M+	98	88	81	68	43
708	Total, Ardmore	B ins	N/A	3M+	98	88	81	68	43
709	Royal Trading	B ins	N/A	3M+	98	88	81	68	43
710	Trumbull	B ins	N/A	3M+	98	88	81	68	43
711	Total, Ardmore	B ins	N/A	3M+	98	88	81	68	43
712	Lion Oi, Muskogee	B ins	N/A	3M+	98	88	81	68	43
713	Royal Trading, Tulsa	B ins	N/A	3M+	98	88	81	68	43
714	Total, Ardmore	B ins	N/A	3M+	98	88	81	68	43
715	Frontier, Muskogee	B ins	N/A	3M+	98	88	81	68	43
716	Royal Trading	B ins	N/A	3M+	98	88	81	68	43
717	Royal Co.	B ins	N/A	3M+	98	88	81	68	43
718	Royal Co.	B ins	N/A	3M+	98	88	81	68	43
719	Frontier	B ins	N/A	3M+	98	88	81	68	43
720	Frontier	B ins	N/A	3M+	98	88	81	68	43
721	Royal Co.	B ins	N/A	3M+	98	88	81	68	43
722	Royal Co.	B ins	N/A	3M+	98	88	81	68	43
723	Royal	B ins	N/A	3M+	98	88	81	68	43
724	Royal	B ins	N/A	3M+	98	88	81	68	43
725	Royal	B ins	N/A	3M+	98	88	81	68	43
726	Royal	B ins	N/A	3M+	98	88	81	68	43
727	Frontier	B ins	N/A	3M+	98	88	81	68	43
728	Frontier	B ins	N/A	3M+	98	88	81	68	43
729	Royal	B ins	N/A	3M+	98	88	81	68	43
730	Royal	B ins	N/A	3M+	98	88	81	68	43
731	Frontier	B ins	N/A	3M+	98	88	81	68	43
732	Frontier	B ins	N/A	3M+	98	88	81	68	43
733	Frontier	B ins	N/A	3M+	98	88	81	68	43
734	Frontier	B ins	N/A	3M+	98	88	81	68	43
735	Royal	B ins	N/A	3M+	98	88	81	68	43
736	Royal	B ins	N/A	3M+	98	88	81	68	43
737	Royal	B ins	N/A	3M+	98	88	81	68	43
738	Royal	B ins	N/A	3M+	98	88	81	68	43
739	Royal Trading	B ins	N/A	3M+	98	88	81	68	43
740	Royal Trading	B ins	N/A	3M+	98	88	81	68	43
741	Lion Oi, Muskogee	B ins	N/A	3M+	98	88	81	68	43
742	Lion Oi, Muskogee	B ins	N/A	3M+	98	88	81	68	43
743	Royal Co.	B ins	N/A	3M+	98	88	81	68	43
744	Royal Co.	B ins	N/A	3M+	98	88	81	68	43

Sample	No. 16	No. 30	No. 50	No. 100	No. 200	Asphalt			Aggregate		
No.	1.18mm	0.60mm	0.30mm	0.15 mm	0.075mm	Pb	PG	Gb	FAA	FF	G_{sb}
686	30	22	15	9	5.6	4.4	PG 64-22OK	1.0151	45.2	100	2.642
687	30	22	15	9	5.6	4.4	PG 64-22OK	1.0103	45.2	100	2.639
688	30	22	15	9	5.6	5.4	PG 64-22OK	1.0110	45.2	100	2.639
689	30	22	15	9	5.6	5.4	PG 64-22OK	1.0254	45.2	100	2.639
690	30	22	15	9	5.6	5.4	PG 64-22OK	1.0122	45.2	100	2.642
691	30	22	15	9	5.6	5.4	PG 64-22OK	1.0160	45.2	100	2.639
692	30	22	15	9	5.6	5.4	PG 64-22OK	1.0152	45.2	100	2.639
693	30	22	15	9	5.6	5.4	PG 64-22OK	1.0258	45.2	100	2.642
694	30	22	15	9	5.6	5.4	PG 64-22OK	1.0315	45.2	100	2.639
695	30	22	15	9	5.6	5.4	PG 70-28OK	1.0076	45.2	100	2.639
696	30	22	15	9	5.6	5.4	PG 70-28OK	1.0150	45.2	100	2.642
697	30	22	15	9	5.6	5.4	PG 70-28OK	1.0159	45.2	100	2.639
698	30	22	15	9	5.6	5.4	PG 70-28OK	1.0087	45.2	100	2.639
699	30	22	15	9	5.6	5.4	PG 70-28OK	1.0151	45.2	100	2.642
700	30	22	15	9	5.6	5.4	PG 64-22OK	1.0103	45.2	100	2.639
701	30	22	15	9	5.6	5.4	PG 64-22OK	1.0110	45.2	100	2.639
702	30	22	15	9	5.6	5.4	PG 64-22OK	1.0254	45.2	100	2.639
703	30	22	15	9	5.6	5.4	PG 64-22OK	1.0122	45.2	100	2.642
704	30	22	15	9	5.6	5.4	PG 64-22OK	1.0160	45.2	100	2.639
705	30	22	15	9	5.6	5.4	PG 64-22OK	1.0152	45.2	100	2.639
706	30	22	15	9	5.6	5.4	PG 64-22OK	1.0258	45.2	100	2.642
707	30	22	15	9	5.6	5.4	PG 64-22OK	1.0159	45.2	100	2.639
708	30	22	15	9	5.6	5.4	PG 64-22OK	1.0087	45.2	100	2.639
709	30	22	15	9	5.6	5.4	PG 64-22OK	1.0150	45.2	100	2.642
710	30	22	15	9	5.6	5.4	PG 64-22OK	1.0103	45.2	100	2.639
711	30	22	15	9	5.6	5.4	PG 64-22OK	1.0110	45.2	100	2.639
712	30	22	15	9	5.6	5.4	PG 64-22OK	1.0254	45.2	100	2.639
713	30	22	15	9	5.6	5.4	PG 64-22OK	1.0122	45.2	100	2.642
714	30	22	15	9	5.6	5.4	PG 64-22OK	1.0160	45.2	100	2.639
715	30	22	15	9	5.6	5.4	PG 64-22OK	1.0152	45.2	100	2.639
716	30	22	15	9	5.6	5.4	PG 64-22OK	1.0258	45.2	100	2.642
717	30	22	15	9	5.6	4.9	PG 64-22OK	1.0122	45.2	100	2.686
718	30	22	15	9	5.6	4.9	PG 64-22OK	1.0122	45.2	100	2.686
719	30	22	15	9	5.6	5.1	PG 64-22OK	1.0152	45.2	100	2.688
720	30	22	15	9	5.6	5.1	PG 64-22OK	1.0152	45.2	100	2.688
721	30	22	15	9	5.6	4.9	PG 64-22OK	1.0122	45.2	100	2.686
722	30	22	15	9	5.6	4.9	PG 70-28OK	1.0122	45.2	100	2.686
723	30	22	15	9	5.6	5.1	PG 64-22OK	1.0151	45.2	100	2.688
724	30	22	15	9	5.6	5.1	PG 70-28OK	1.0151	45.2	100	2.688
725	30	22	15	9	5.6	5.4	PG 70-28OK	1.0150	45.2	100	2.686
726	30	22	15	9	5.6	5.4	PG 64-22OK	1.0150	45.2	100	2.686
727	30	22	15	9	5.6	5.1	PG 64-22OK	1.0152	45.2	100	2.688
728	30	22	15	9	5.6	5.1	PG 70-28OK	1.0152	45.2	100	2.688
729	30	22	15	9	5.6	5.4	PG 70-28OK	1.0150	45.2	100	2.686
730	30	22	15	9	5.6	5.4	PG 76-28OK	1.0150	45.2	100	2.686
731	30	22	15	9	5.6	5.1	PG 70-28OK	1.0152	45.2	100	2.688
732	30	22	15	9	5.6	5.1	PG 64-22OK	1.0152	45.2	100	2.688
733	30	22	15	9	5.6	5.4	PG 64-22OK	1.0152	45.2	100	2.688
734	30	22	15	9	5.6	5.4	PG 64-22OK	1.0152	45.2	100	2.688
735	30	22	15	9	5.6	5.1	PG 76-28OK	1.0122	45.2	100	2.686
736	30	22	15	9	5.6	5.1	PG 70-28OK	1.0122	45.2	100	2.686
737	30	22	15	9	5.6	4.9	PG 70-28OK	1.0122	45.2	100	2.686
738	30	22	15	9	5.6	4.9	PG 70-28OK	1.0122	45.2	100	2.686
739	30	22	15	9	5.6	5.1	PG 70-28OK	1.0258	45.2	100	2.685
740	30	22	15	9	5.6	5.1	PG 70-28OK	1.0258	45.2	100	2.685
741	30	22	15	9	5.6	5.4	PG 70-28OK	1.0254	45.2	100	2.693
742	30	22	15	9	5.6	5.4	PG 70-28OK	1.0254	45.2	100	2.693
743	30	22	15	9	5.6	4.9	PG 70-28OK	1.0122	45.2	100	2.686
744	30	22	15	9	5.6	4.9	PG 70-28OK	1.0122	45.2	100	2.686

Sample	Mix		Parameters			Rut Depths (mm) at cycles						
No.	G_{mm}	G_{mb}	Wheel	Tire	Temp.	500-c	1000-c	1500-c	2000-c	4000-c	6000-c	8000-c
686	2.527	2.330	100	100	64	1.221	1.955	2.495	2.828	3.45	3.76	4.0
687	2.526	2.334	100	100	64	1.354	1.939	2.334	2.790	3.68	4.23	4.6
688	2.487	2.224	100	100	60	1.210	1.998	2.524	2.743	3.47	3.97	4.3
689	2.496	2.273	100	100	60	1.818	2.776	3.422	3.768	4.88	5.80	6.4
690	2.486	2.268	100	100	60	1.012	1.217	1.433	1.686	2.46	3.14	3.8
691	2.489	2.213	100	100	64	1.639	2.019	2.343	2.560	3.34	3.88	4.3
692	2.488	2.226	100	100	64	1.459	1.825	2.179	2.465	3.48	4.38	5.0
693	2.488	2.226	100	100	64	0.857	1.126	1.294	1.417	1.75	2.00	2.3
694	2.489	2.291	100	100	64	2.146	2.859	3.213	3.423	3.92	4.22	4.4
695	2.486	2.295	100	100	64	2.497	3.250	3.736	4.052	4.63	5.00	5.2
696	2.487	2.269	100	100	64	0.935	1.152	1.320	1.474	1.85	2.29	2.5
697	2.489	2.317	100	100	64	1.323	2.014	2.430	2.796	3.50	3.89	4.1
698	2.484	2.267	100	100	64	2.501	3.568	4.131	4.506	5.35	5.86	6.2
699	2.488	2.317	100	100	64	2.496	3.674	4.296	4.718	5.64	6.10	6.3
700	2.487	2.261	100	100	64	2.392	3.060	3.480	3.773	4.50	5.00	5.3
701	2.487	2.254	100	100	64	2.401	3.279	3.813	4.131	5.10	5.78	6.1
702	2.496	2.229	100	100	64	1.792	2.244	2.477	2.730	3.20	3.51	3.7
703	2.486	2.325	100	100	64	0.907	1.246	1.468	1.651	2.33	2.68	2.8
704	2.489	2.270	100	100	64	2.167	2.715	2.995	3.270	4.01	4.48	4.7
705	2.486	2.371	100	100	62	2.957	4.016	4.490	4.960	6.17	7.03	7.7
706	2.486	2.337	100	100	62	0.851	1.044	1.196	1.309	1.75	2.09	2.5
707	2.489	2.314	100	100	64	1.973	3.263	4.125	4.740	6.09	6.74	7.4
708	2.484	2.321	100	100	64	1.129	1.577	1.906	2.172	3.10	3.83	4.3
709	2.488	2.300	100	100	64	1.540	2.137	2.612	3.003	3.98	4.60	4.9
710	2.487	2.332	100	100	64	1.540	2.137	2.612	3.003	3.98	4.60	4.9
711	2.487	2.310	100	100	64	2.050	3.296	3.850	4.304	5.06	5.50	5.7
712	2.496	2.313	100	100	64	2.090	3.217	3.652	3.979	4.76	5.15	5.5
713	2.486	2.333	100	100	64	1.015	1.504	1.835	2.154	2.99	3.68	4.2
714	2.489	2.274	100	100	64	1.984	2.673	3.118	3.390	3.99	4.32	4.6
715	2.488	2.268	100	100	64	2.599	3.306	3.735	3.975	4.69	5.09	5.6
716	2.488	2.268	100	100	64	1.255	1.814	2.079	2.360	3.32	3.92	4.4
717	2.505	2.338	100	100	64	1.102	1.498	1.724	1.994	2.65	3.31	3.8
718	2.505	2.341	100	100	64	1.102	1.498	1.724	1.994	2.65	3.31	3.8
719	2.500	2.315	100	100	64	1.410	2.017	2.513	2.789	3.83	4.53	5.0
720	2.500	2.312	100	100	64	1.410	2.017	2.513	2.789	3.83	4.53	5.0
721	2.505	2.371	100	100	64	0.738	1.089	1.235	1.344	1.72	2.13	2.4
722	2.505	2.334	100	100	64	0.738	1.089	1.235	1.344	1.72	2.13	2.4
723	2.500	2.291	100	100	64	2.598	3.403	3.886	4.232	5.00	5.61	6.0
724	2.500	2.267	100	100	64	2.598	3.403	3.886	4.232	5.00	5.61	6.0
725	2.487	2.330	100	100	64	1.211	1.552	1.818	1.990	2.53	2.90	3.2
726	2.487	2.331	100	100	64	1.211	1.552	1.818	1.990	2.53	2.90	3.2
727	2.500	2.353	100	100	64	2.897	4.161	5.055	5.655	6.95	7.71	8.2
728	2.500	2.302	100	100	64	2.897	4.161	5.055	5.655	6.95	7.71	8.2
729	2.487	2.329	100	100	64	0.978	1.224	1.418	1.576	2.03	2.33	2.7
730	2.487	2.335	100	100	64	0.978	1.224	1.418	1.576	2.03	2.33	2.7
731	2.500	2.326	100	100	64	2.602	3.608	4.146	4.588	5.81	6.52	7.0
732	2.500	2.325	100	100	64	2.602	3.608	4.146	4.588	5.81	6.52	7.0
733	2.488	2.320	100	100	64	3.502	4.890	5.579	5.933	7.01	7.72	8.4
734	2.488	2.323	100	100	64	3.502	4.890	5.579	5.933	7.01	7.72	8.4
735	2.497	2.327	100	100	64	1.435	1.853	2.212	2.390	3.08	3.47	3.8
736	2.497	2.351	100	100	64	1.435	1.853	2.212	2.390	3.08	3.47	3.8
737	2.505	2.313	100	100	64	3.063	3.853	4.287	4.625	5.60	6.32	6.9
738	2.505	2.316	100	100	64	3.063	3.853	4.287	4.625	5.60	6.32	6.9
739	2.501	2.328	110	110	64	0.785	0.990	1.086	1.237	1.65	2.01	2.3
740	2.501	2.361	110	110	64	0.785	0.990	1.086	1.237	1.65	2.01	2.3
741	2.496	2.328	100	100	64	2.293	3.405	4.119	4.562	5.83	6.68	7.1
742	2.496	2.336	100	100	64	2.293	3.405	4.119	4.562	5.83	6.68	7.1
743	2.505	2.366	110	110	64	0.926	1.193	1.381	1.463	2.28	2.83	3.5
744	2.505	2.370	110	110	64	0.926	1.193	1.381	1.463	2.28	2.83	3.5